UNIVERSITY OF SOUTHERN QUEENSLAND

AN INVESTIGATION INTO THE FEASIBILITY AND APPLICATION OF FIBRE COMPOSITES TO FLATBED SEMI-TRAILERS

A DISSERTATION SUBMITTED BY

Rick A. Coker
B Eng (Mech.) (Hons I)

for the award of

DOCTOR OF PHILOSOPHY

2003

ABSTRACT

The highly competitive nature of the transportation industry has produced significant demand for increased equipment efficiency. This has been manifested in attempts to increase carrying capacity whilst lowering running costs. While these factors remain at the forefront of trailer design, the dependence on steel as the primary material has limited the extent to which these goals are realised.

The advantages associated with the use of fibre composite materials in automotive applications have been well documented, demonstrating that the substitution of steel with fibre composite materials greatly increases the scope for tare mass reduction. However, to fully utilise the advantages produced through the use of fibre composites, it is necessary to formulate a design philosophy that incorporates the selection of materials and the definition of acceptable performance of both the material and the trailer. This dissertation addresses this broad subject.

Within this greater context, this study addresses the incorporation of fibre composite materials into semi-trailers, with the significant issues being divided into two areas:

- The development of a design philosophy, intended specifically to address the application of fibre composites to semi-trailers.
- The design, analysis and experimental validation of a new type of fibre composite trailer chassis, utilising the aforementioned design philosophy.

This PhD project is a foundational study on the suitability of fibre composite materials in the heavy transportation industry, primarily focusing on a practical assessment of the potential for tare mass reduction. The work presented in this dissertation is seen to provide a basis for fibre composite trailer design, in addition to a foundation upon which further investigation into this field can be made.

The major outcomes of this project include, amongst others:

- The definition of significant load cases and trailer classifications
- The development of a design philosophy suited specifically to FRP semi-trailers
- The establishment of selection criteria which identifies appropriate FRP materials for use in this application
- The development of a new type of FRP chassis for a flatbed semi-trailer
- Validation of the design philosophy through experimental testing
- Affirmation of the potential of FRPs in application to flatbed semi-trailers

CERTIFICATION OF DISSERTATION

I certify that the ideas, experimental work, results, analyses, software and conclusions reported in this dissertation are entirely my own effort, except where otherwise acknowledged. I also certify that the work is original and has not been previously submitted for any other award, except where otherwise acknowledged.

_____ _____

Signature of Candidate Date

ENDORSEMENT

_____ _____

Signature of Supervisor/s Date

_____ _____

ASSOCIATED PUBLICATIONS

Coker RA, Van Erp GM. Development of a small scale fibre composite semi trailer. Proceedings of the 16th Australasian Conference on the Mechanics of Structures and Materials; 1999 Dec 8-10; UNSW, Sydney, Australia.

Coker RA, Van Erp GM. The development of a fibre composite semi-trailer. Proceedings of the ACUN-2 International Composites Conference; Volume 1; 2000 Feb 14-18; UNSW, Sydney, Australia.

Note: This research was conducted through the financial support of an industry partner. As a result, publication of results has been delayed for commercial reasons.

ACKNOWLEDGEMENTS

The undertaking and completion of this study would not have been possible without the assistance of a number of significant persons, to whom I wish to express my sincere gratitude.

To my principal supervisor, Prof. Gerard Van Erp – Thankyou for first recognising my potential as an undergraduate, for providing me with invaluable insight and assistance in many areas of this work, and for your patience and guidance in producing this document.

To my secondary supervisor, Prof. Malcolm McKay – Thankyou for sharing with me your knowledge and support, and giving of your time to edit and review this work.

To my wife, Debbie – Thankyou so much for your love and support through the ups and downs, and for allowing me to pursue this goal. Thankyou also for the countless hours you gave up with me so that I could finish this, and for all of the broken deadlines that you overlooked. I acknowledge and thankyou for your sacrifice. I could not have done it without you.

To the FCDD team – Thankyou for teaching me the skills I needed to produce the experimental specimens for my study. Your assistance and advice saved me many hours, and I gratefully acknowledge your part in this work. Thanks especially to my fellow postgraduates, who have provided support and friendship throughout the years, and reminded me that life doesn't always have to be serious.

To my family – Thankyou for your constant support and interest in this project, and for giving me the opportunity and motivation to become an engineer.

To God – through whom all things are possible.

To all others who have had a part to play in this work, regardless of the size of their contribution, I offer my thanks.

TABLE OF CONTENTS

CHAPTER 3 AN OVERVIEW OF STEEL AND FRP TRAILERS

CHAPTER 4 A DESIGN PHILOSOPHY FOR FRP SEMI-TRAILERS

CHAPTER 5 SELECTION OF MATERIALS

CHAPTER 6 CONCEPTUAL DESIGN

CHAPTER 7 APPLICATION OF THE DESIGN PHILOSOPHY TO THE FINAL CONCEPT

LIST OF TABLES

CHAPTER 5

SELECTION OF MATERIALS

CHAPTER 6

CONCEPTUAL DESIGN

CHAPTER 7

APPLICATION OF THE DESIGN PHILOSOPHY TO THE FINAL CONCEPT

LIST OF FIGURES

CHAPTER 4

A DESIGN PHILOSOPHY FOR FRP SEMI-TRAILERS

CHAPTER 5

SELECTION OF MATERIALS

CHAPTER 6

CONCEPTUAL DESIGN

CHAPTER 7

APPLICATION OF THE DESIGN PHILOSOPHY TO THE FINAL CONCEPT

CHAPTER 8

AN INVESTIGATION INTO THE FATIGUE PERFORMANCE OF AN FRP CHASSIS RAIL

Chapter 1 Introduction

1.1 Background

The need for transportation has always been present in society. The transition from the use of animals to machinery with the advent of the steam engine in the 1830's represented an enormous shift in scale, dramatically increasing the volume of goods transported in a single movement.

However the introduction of the motor vehicle at the end of the 19th century heralded the beginning of a mode of transport, which offered unprecedented convenience and freedom from the limitations associated with the steam engine and the horse and cart. Adaptation of the passenger vehicle, initiated by those requiring a greater carrying capacity, saw the introduction of the first generation of solid-body trucks.

The addition of trailers resulted in further increases in vehicle carrying capacity, which grew in response to increases in engine horsepower. As the automotive industry expanded, variations of trailer configuration evolved in response to demands for the transportation of diverse payloads. Since these beginnings, road transportation experienced significant growth throughout the 20th century, and the proliferation of the road network throughout the country has assured the continuation of this mode of transportation in the 21st century.

The movement by road of goods and produce plays a large part in the Australian economy. The exceptionally low population density of this country and the broad distribution of the population over a large proportion of the coastline necessitates the perpetual movement of materials over long distances.

In general, coverage of the rail network and shipping industry is limited to major cities and restricted to large quantities of material only. Road transportation is therefore responsible for distribution to areas not served by rail or sea, and consequently the dependence of other transport industries on road transportation is significant. A survey of the transportation industry for 1998-1999 showed that within Australia there are more than 13,000 transportation firms, comprising 406,000 freight heavy vehicles, which transport more than 1.3 billion tonnes of produce and materials each year [1,2].

Competition between transportation firms is extremely high, demonstrated by the operating procedures adopted by some companies, including overloading [3,4]. Overloading of trailers to increase profits has been well documented. A report by the National Road Transport Commission (NRTC) states that "in grouping all AUSTROADS Class 8 and above vehicle types, from over 5.6 million individual heavy vehicle observations, 0.16 per cent (9344 heavy vehicles or 1 in 609) were overloaded more than 30 per cent of their GVM limit. Furthermore, 0.01 per cent (771 heavy vehicles or 1 in 7374) were overloaded more than 50 per cent of their GVM limit." [5]

As an additional consequence of industry competition, drivers have been compelled to increase the number of hours spent behind the wheel. To minimise the associated driver fatigue, legislation restricting driving hours was introduced in Australia, and is summarised in [6]. The compulsory completion of log books which record the drivers activities are also enforced in Australia, while the UK and Europe have introduced the mandatory fitting of tachographs to all heavy vehicles. These recording devices automatically register time, speed, distance and driving hours.

Manufacturers of heavy vehicles have invested significant amounts of time to improve driver comfort, ease of operation, and safety in order to increase productivity and encourage drivers to maximise their driving time (refer Section 4.3.1).

Since the introduction of Gross Vehicle Mass (GVM) limits in 1975, which were implemented to protect the various components of the road from overloading, the significance of the tare mass of a trailer has been realised. The reduction of the tare mass of a trailer allows a greater payload to be carried without exceeding the GVM limits. It would appear that the total mass of goods transported over the duration of the trailer's life is directly related to its tare mass. However, a report prepared by the National Road Transport Commission (NRTC), indicates that on average, 25% of travel by 6 axle articulated trucks is performed unladen, while the maximum payload is transported only

50% of the total travel time [1]. So it seems that the advantages of a reduced tare mass are only partially utilised in practice. However other benefits do become apparent for a partially loaded trailer. These include:

1. **Fuel savings -** The quantity of fuel used is dependent on a number of factors, including aerodynamic characteristics and engine efficiency. However the dominant factor determining fuel consumption is the GVM of the vehicle. Performance figures were obtained from Wagners Transport Pty Ltd. pertaining to fuel usage for truck-trailer combinations with varying GVMs. This data indicates that, neglecting conditional differences such as head wind and tyre pressure, a 2000 kg reduction of trailer tare mass could potentially yield a fuel saving of $8.84 per 1000 kilometres travelled. While the trailers surveyed travel approximately 160,000 kilometres per annum, fuel saving would only be realised whilst partially loaded, which approximates to 50% of all kilometres travelled as previously mentioned. Neglecting rises in fuel prices as a conservative estimate, the savings in fuel for a partially loaded trailer could potentially be as high as $700 each year, or $10,500 over a 15-year lifespan.

2. **Reduced wear -** Just as fuel consumption is proportional to the GVM of the trailer, wear on the tyres, suspension components and the hitch is similarly dependent on the load imposed on these components. For each journey a lightweight trailer does not support the maximum payload, each of these components experience a load of lower magnitude when compared with a trailer of greater tare mass carrying the same payload. The increasing popularity of air bag suspension systems has been accompanied by the introduction of retractable axles. The load placed on the triaxle group determines the number of axles necessary, such that a sufficiently low load on the trailer initiates the retraction of one or two axles. A lighter trailer would encourage this retraction more frequently, thereby reducing the total amount of wear on the tyres and suspension components of the axle group.

The significance of tare mass reduction has consequently been recognised by the industry, and subsequent attempts to reduce the tare mass of various trailers are discussed in Chapter 3. The attention of the industry is justified considering that freight costing provided by Wagners Pty Ltd suggest that a reduction in tare mass of 1000 kg corresponds to a saving of $50,000 throughout the life of the trailer. This is based on the price per kilogram of freight transported between capital cities by Wagners Pty Ltd, and an estimate of an additional 500 kg of payload per trip, assuming that the trailer is full for 50% of the total travel time. For express transportation companies which charge higher freight prices, the

potential for additional profit is estimated at over $250,000 for every 1000 kg reduction in tare mass. Additionally, discussion with various operators of transportation companies by the author and [7] revealed that an increase of $20,000 to $25,000 in capital costs would be considered justifiable in exchange for a reduction in trailer tare mass of 1000 kg.

While is it possible to approach the reduction of trailer tare mass from a number of perspectives, the utilisation of alternative materials of lower density would appear to offer the greatest potential.

"Lighter vehicles offer the possibility of reducing consumption of energy and materials. To reduce the weight of a given structural component, a designer can search for the minimum weight design of the component by using an optimisation technique. To further reduce weight, however, he must search for optimal designs with ***feasible alternate materials****."* [12]

Extensive optimisation within the industry throughout the past decade would seem to indicate that the scope for further optimisation of steel trailers is relatively low, and the search for a feasible alternate material points to the use of FRPs.

1.2 Fibre Reinforced Polymers

Fibre reinforced polymers, or FRPs, have been utilised in a vast range of applications, the primary focus of which involves either mass reduction or resistance to corrosive environments. Consequently the aerospace, motor sport and boating industries have dominated FRP usage. However more recent research has been instrumental in initiating significant growth of FRPs in mainstream engineering applications, examples of which can be seen in [8,9,10]. These would indicate that FRPs possess substantial potential for the production of structures which are not only low in mass, but are practical, cost competitive alternatives to more traditional materials.

While steel has dominated material usage in the manufacture of trailers, the physical properties of FRPs would indicate that substantial reductions in tare mass are possible through the use of composite materials.

It can be seen from Table 1.1 that composite materials provide several advantages, as they can withstand greater magnitudes of stress than common grades of steel, will not plastically deform (fully elastic), and have significantly larger failure strains. However, the most significant advantage that FRPs possess in relation to applications to trailers is exceptionally high strength-to-weight and stiffness-to-weight ratios. The data in Table 1.1 was taken from various literary sources, and is indicative only.

Table 1.1 A Comparison of Representative Material Properties

System Type (Orientation)	Density (kg/m^3)	Tensile Strength (MPa)	Tensile Modulus (GPa)	Max. Elastic Strain (%)	Specific Tensile Strength (Ult.) ($MPa/kg/m^3$)	Specific Tensile Modulus ($Mpa/kg/m^3$)
Carbon/Epoxy *Fibres at 0°*	1750	1000 (UTS)	100	1.0	0.57	57
E-glass/Epoxy *Fibres at 0°*	2540	700 (UTS)	40	1.75	0.28	16
Steel *Grade 350*	7850	350 (Yield) 480 (UTS)	200	0.18 -	- 0.06	25
Aluminium *Grade 6063-T5*	2800	110 (Yield) 151 (UTS)	69	0.16 -	- 0.05	25

Notes:

1. 0° represents unidirectional fibre orientation
2. Properties may vary depending on fibre content and consolidation technique

In particular, the specific tensile strength, $\sigma T/\rho$, (Tensile strength per unit mass per unit volume), and specific modulus, E/ρ, (Modulus per unit mass per unit volume) are substantially higher for FRPs than those of metals. The potential for mass reduction in various applications is therefore evident.

Initially, it may appear that the lower moduli of FRPs present a disadvantage in applications where the stiffness of an FRP structure must be comparable with that of a steel counterpart. However in such cases, this is overcome by using a greater volume of composite material to provide the required rigidity. The substantially lower density of FRPs enables the part or structure to retain a lower mass than the steel structure, despite an increase in material quantity. The mechanical properties of FRPs will be discussed in more detail in Chapters 2 and 5.

The primary disadvantage associated with FRPs is that of relative cost. Per unit volume, steel is significantly less expensive, as shown by Simpson et al [11]. However, through intelligent design and efficient use of the material, this cost can be minimised to produce a structure whose slight increase in capital cost is justified by the savings gained throughout the service life of the structure

Therefore, it was with the apparent advantages associated with the high specific strength and stiffness of FRPs that research into the application of FRPs to semi-trailers was undertaken.

1.3 Aims and Objectives

It is the general aim of this project to investigate the feasibility and assess the potential of FRPs in application to semi-trailers, the primary objective being the reduction of tare mass. Within this aim, more specific objectives were adopted and are listed as follows:

a) **Establish a selection criteria which identifies appropriate FRP materials for use in this application**

While a large range of fibre composite materials is available, not all are suitable for application to trailers. Hence, selection criteria will be established which address all relevant aspects of material performance and expectations. Material testing will be used to verify material properties where possible.

b) **Conduct a critical analysis and evaluation of current steel and FRP trailers in order to identify any points of design applicable to this research**

A literature survey will be conducted of current design standards and any relevant research on such topics as (1) the development of FRP or other alternative trailer types, and (2) research which focuses on vehicle dynamics that specifically quantify the loads imposed on trailers during service.

Finite element analysis of current trailers will also be performed in order to identify the design difficulties or shortcomings responsible for any failure that may take place.

c) **Develop conceptual designs for an FRP trailer and, through the identification of key selection parameters, distinguish the concept most suitable for further investigation**

Based on the information gained from objectives (a) and (b), a number of concepts utilising various materials and configurations will be generated. Each concept will be assessed in relation to parameters in keeping with the aims of the project and the practicalities of manufacture, repair and service. The most suitable concept will hence be ascertained, and further research focused on this concept.

d) **Produce a design philosophy which outlines considerations necessary for the successful development of an FRP trailer**

The definition of design criteria for FRP trailers forms an integral part in determining the feasibility of FRPs in this application. The primary design constraints including deflection, strength and fatigue performance will be addressed, along with the formulation of critical load cases and failure modes.

e) **Formulate and execute an experimental and analytical program, with the express purpose of providing validation to the design philosophy**

The identification of possible failure modes within the conceptual design will be addressed individually through experiments designed to specifically target each mode. These tests will be both static and dynamic in nature, and will be calibrated and compared with accompanying finite element analysis where appropriate.

f) **Consolidate the design philosophy through the evaluation of the experimental testing results, and thereby assess the feasibility and potential of FRPs in application to semi-trailers**

The assumptions made and conclusions reached during the formulation of the design philosophy will be directly compared with experimental results. The anticipated failure modes will be assessed in light of these results, and conclusions drawn in relation to the accuracy of the analytical predictions. The degree of success achieved in determining the behaviour of the structure under the prescribed conditions will be used as a measure of the suitability of FRPs to semi-trailers.

1.4 Scope and Limitations

A number of limitations were adopted to provide sufficient focus for this research. These are as follows:

a) The design philosophy developed in this thesis is not intended to be exhaustive in its contents. The infancy of this area of research dictates that this investigation be preliminary in nature. As such, a large number of areas are investigated with limited detail. Indeed many of these areas could, in themselves, constitute entire doctoral studies. This broader approach was taken in order that the essential fundamentals could be soundly established, providing a base from which further research could continue.

b) The design philosophy developed in this thesis is intended solely for application to fibre composite, flat bed semi-trailers. The combinations of structural layout, loading conditions and typical operating environment considered herein are unique to this specific trailer configuration.

c) Extensive numerical and computational investigation of the dynamic behaviour of this type of trailer was intentionally excluded from this research. It was decided this type of investigation could not realistically be included considering the already broad scope. Hence the response of the trailer to steering or braking inputs, or extreme conditions such as overturning or the effects of a crash impact, was not considered.

d) While fatigue of the main chassis rails is considered in some detail, the shear fatigue capacity of the shear reinforcement was not considered. Insufficient time and resources to investigate this phenomenon has prevented the inclusion of this into the design philosophy. Additional factors of safety were added to prevent the occurrence of damage due to shear fatigue in any experimental fatigue testing.

e) The torsional rigidity of the trailer was not considered, as it was not possible to experimentally verify or contradict any predictions made by analytical models with the available testing infrastructure. Therefore, comparisons of an analytical model of an FRP trailer with a steel trailer were not considered, as the accuracy of such a comparison would be questionable.

f) Details concerning the attachment of suspension components or the skid plate assembly were not addressed in this investigation. The project sponsor is currently conducting research in this area. However, it was decided that any conceptual design produced herein should be capable of accommodating standard suspension and skid plate attachment with a minimum of alteration.

g) All other limitations and exclusions are defined in the appropriate places within the text.

1.5 Structure of Thesis

Chapter 2 provides a brief overview of fibre-reinforced plastics (FRPs). Various reinforcements and matrix materials and their mechanical properties are presented in summarised form.

Chapter 3 outlines the current position of the trailer industry, primarily within Australia. An overview of various types of trailers currently in service in Australia is provided. The current uses of FRPs within the automotive industry are summarised, with particular focus on previous attempts to apply FRPs to trailers.

The evaluation of research performed on trailers is summarised in a literature review in Chapter 4. This is followed by an assessment of steel trailer design techniques provided during discussion with trailer manufacturers. Significant load cases are defined, and moment and shear envelopes are produced for application in fibre composite, flat bed trailer design. A comparison of design constraints between steel and FRP trailers is made, and the dominant criteria are identified for consideration in FRP trailer design.

Chapter 5 addresses the selection of materials. The core material, reinforcement and matrix are all considered individually, and the results of the corresponding materials testing are presented.

Chapter 6 outlines the various conceptual designs produced during the course of this research, and shows in greater detail the concept chosen for further examination. Each of the possible failure modes relevant to the concept chosen are listed and discussed in some detail.

Chapter 7 includes the analysis and experimental testing undertaken in consideration of these modes of failure presented in the previous chapter, with the exception of fatigue.

The fatigue performance of the trailer chassis is considered in Chapter 8. Fatigue testing on both an elemental and structural scale is considered, and results from testing are presented. This chapter also details the influence of the fatigue performance on the design philosophy.

Chapter 9 provides a summary of the results of the previous chapters, presenting the major outcomes and key findings of the research conducted. Several key topics are also identified for further research and application.

References

[1] National Road Transport Commission (NRTC). Survey of truck use and loading patterns: results. ISBN 0 642 22218 5; October 1994; Working Paper 15.

[2] Australian Bureau of Statistics. Survey of motor vehicle use; Australia; 1999 (9208.0); Yearbook 2000 (1303.0).

[3] Henderson J. Are plastics the answer to trucking's tough questions? In: Machine Design; 1998; 70(19): 74-6.

[4] Design of an ultra-lightweight composite semi-trailer [online] 1996 [cited 1998 September 18]. Available from: http://www.clc.tno.nl/projects/recent/trailer.html.

[5] Koniditsiotis C. Incidence of grossly overloaded heavy vehicles. ARRB Transport Research; ISBN - 0 642 54400 X; April 1998.

[6] National Road Transport Commission (NRTC). Amalgamation of truck and bus driving hours regulations. Regulatory Impact Statement; October 1997.

[7] McKay M. Personal Communication. Toowoomba: University of Southern Queensland; 1999 August 19.

[8] Davey SW, Van Erp GM, Marsh R. Fibre composite bridge decks – an alternative approach. Proceedings of the ACUN-2 International Composites Conference; Volume 1; 2000 Feb 14-18; UNSW, Sydney, Australia.

[9] Maxwell J. Plastics in the automotive industry. SAE international; Cambridge, England: Woodhead Publishing Ltd; 1994.

[10] Humphreys MF, Van Erp GM, Tranberg CH, Structural behaviour of monocoque fibre composite trusses. Proceedings of the 16th Australasian Conference on the Mechanics of Structures and Materials; 1999 Dec 8-10; UNSW, Sydney, Australia.

[11] Simpson P, Van Erp GM, 1999, Composite materials? The 3000 MPa question. Proceedings of the 16th Australasian Conference on the Mechanics of Structures and Materials; 1999 Dec 8-10; UNSW, Sydney, Australia.

[12] Chang DC. Optimal designs with alternate materials suitable for high volume production. Warren, Michigan: Society of Automotive Engineers; 1979.

Chapter 2 Fibre Composites in Brief

2.1 Introduction

Until recently, fibre reinforced polymers had experienced a relatively small percentage of application within engineering structures. While the aerospace and marine industries have utilised fibre composite materials for many years, penetration into mainstream engineering applications has not been widespread. In addition to high material costs, the relatively complex nature of composite materials in comparison with steel, combined with an absence of relevant design codes has fuelled uncertainty and hesitation within the engineering community, thereby limiting the opportunities in which FRPs are considered as a viable material alternative.

This chapter examines FRPs more closely, defining the characteristics and capabilities of these materials. It provides a brief overview of fibre composite materials and the most common methods of manufacture, in addition to a number of design considerations unique to fibre composite materials. It should be noted that this was not compiled so as to represent an extensive study or literature survey, but is intended rather as a basic synopsis that is included to assist readers with little exposure to fibre composite technology and terminology.

A composite material is defined as a material system comprised of two or more distinct constituents which differ in form and/or material composition. The purpose of this combination is to produce a material that possesses physical properties superior to either constituent. Examples of common composite materials include reinforced concrete, consisting of aggregate, a cement mix and steel reinforcing bars, as well as mud bricks, which utilise straw as reinforcement in a mud matrix. Fibre reinforced polymers (FRPs)

utilise high strength fibrous reinforcement set within a comparatively weak polymer matrix, which acts to contain the fibres and provide a bulk form. This combination provides a material that possesses both high strength and a resistance to abrasive, environmental and chemical attack. While it could be said that the anisotropic nature of composites complicates the design process, the stacking of reinforcing layers to form a laminate enables the user to tailor strength requirements in various directions as necessary by altering the orientation of each layer. The ability to mould polymers into complex shapes also provides advantages over more traditional materials such as steel by part simplification and assembly time reduction.

The following sections will examine in greater detail the constituents of FRPs and the variations in reinforcing and matrix materials that are available. Manufacturing methods and design techniques applicable to FRPs are also briefly discussed in this section.

2.2 Reinforcing Fibres

2.2.1 Introduction

The use of fibres in composite material stems from the advantages that fibres provide over their respective bulk materials. These advantages include a reduction in the overall material density (when the fibres are combined with the matrix), in addition to the flexibility of shape that accompanies the fibrous form. However, an increase in mechanical properties is also observed when the form of the material is changed from monolithic to fibrous. For example, the tensile modulus and tensile strength of carbon in monolithic form are 10 GPa and 20 MPa respectively [1]. However in fibrous form, the modulus and strength increase to approximately 290 GPa and 3100 MPa respectively. The cause of this phenomenon is dependent on the material in question. With respect to aramid and carbon fibres, the observed improvements in properties result from the improved alignment of the polymeric molecules along the axis of the fibre. As for E-Glass fibres, the substantial increase in material strength is due to a reduction in the quantity and size of surface flaws and stress concentrators present in the material resulting from the production of fibre reinforcement, the diameters of which range from 0.003 to 0.01 mm. That is, the transformation of a material into a fibrous form effectively eliminates many of the microscopic flaws and irregularities associated with the bulk material, thereby reducing the number of potential sites at which failure may initiate.

Of the wide range of reinforcing fibres that are currently produced, only the more commonly used fibres will be examined here. Discussion of other fibre types not mentioned within this chapter can be found in [1,2,3,4]. A comparison of various fibre types and their typical properties is given at the conclusion of this section.

2.2.2 Glass Fibres

Glass fibres possess all typical properties normally associated with glass including inertness, hardness and corrosion resistance. Additionally they possess flexibility, a relatively low density and are inexpensive in comparison with other fibre types. Hence they have become the most widely used of all reinforcing fibres for most industrial applications. Various grades of glass fibres are in existence, which vary in mechanical properties and cost, the two most common being E-Glass and S2-Glass. E-Glass (E is an abbreviation for electrical) is the most common form of glass reinforcement due to its low

cost. E-Glass is based on the CaO-Al_2O_3-SiO_2 system, and is formed by passing molten glass through an orifice under gravity. A coating, known as a sizing, is applied to the fibres to protect them from surface damage and promote adhesion to the matrix. Glass reinforcement is compatible with all common resin types.

Greater stiffness and strength as well as higher operating temperatures can be gained using S2-Glass, which is based on the SiO_2-Al_2O_3-MgO system. However greater difficulty in drawing the fibres due to a limited working temperature range greatly increases the cost of S2-Glass, which is three to four times more expensive than E-Glass [1].

The disadvantages of glass fibres include a relatively low tensile modulus and poor fatigue performance (in comparison with carbon) and susceptibility to a reduction in strength under long-term static loading, known as static fatigue.

2.2.3 Carbon Fibres

Carbon fibres are characterised by high strength, high stiffness, and low density, and are the predominant reinforcing fibre used in 'high performance' applications. A wide variation of strength and stiffness is achievable through controlled variations in the manufacturing process. All carbon fibres are produced through pyrolysis of one of three precursor fibres within an inert atmosphere. The precursors commonly used in the production of carbon fibre reinforcement include polyacrylonitrile (PAN), pitch, and rayon, which are listed in descending order of current usage [4]. The mechanical properties obtained are dependent on both the precursor and the degree of heat treatment during and post- carbonisation. A comparison between various carbon reinforcement types can be found in reference [2]. Within Australia the most commonly available carbon reinforcement type is a low cost, high strength (LHS) carbon denoted as T-300 (by Toray and BP Amoco) and AS4 (by Hexcel). Several other grades of carbon reinforcement are shown in Table 2.1 (refer page 18).

In addition to a higher specific modulus and stiffness, the fatigue performance of carbon is superior to that of glass fibres, since the higher modulus of carbon fibres reduces the amount of strain variation produced with the matrix for a given load. The preservation of the matrix reduces the potential for micro cracking, debonding and delamination. Carbon is not susceptible to static fatigue, and possesses a very low coefficient of thermal expansion. However, despite these advantages, carbon fibre consumption has been relatively low in comparison with E-glass. The principal reason for this is the high cost of carbon fibre.

While this has dropped significantly in recent years due to an increase in demand, prices in excess of $100 per kilogram are not uncommon (within Australia) when purchased in small quantities. Additionally, carbon fibre is incompatible with some matrix systems, and is typically combined with more expensive epoxy and high-performance vinylester resin systems. Despite this, usage of carbon fibre is continuing to increase, thereby encouraging lower prices through increased production.

2.2.4 Aramid Fibres

The term 'aramid' fibre is the generic name for aromatic polyamide fibres, which have undergone significant development since the 1960s. They possess the lowest density, highest specific strength and highest specific modulus of current reinforcing fibres. However aramid fibres are more widely known for application in ballistics, due to exceptionally high energy absorption characteristics and non-linear compressive behaviour. The manufacture of aramid fibres is summarised as follows. The polymers are created by adding a diacid chloride to a cool amine solution. The polymer is then formed into fibres by extrusion from spinnerets at an elevated temperature, and is finally washed and dried. Aramid fibres are available under a number of trade names, including Kevlar (by DuPont), Twaron (by Akzo Nobel) and Technora (by Teijin). As with carbon fibres, a variety of properties can be achieved through the inclusion of solvent additives, or by varying the spinning conditions and heat treatment. Various aramid fibre types are compared more closely in references [3,4].

Generally, aramid fibres possess excellent tensile strength and stiffness characteristics without the brittle nature of glass and carbon. As previously mentioned, they also possess exceptional toughness and resistance to impact and dynamic loading. However a number of disadvantages also exist. Poor coupling of resin matrices to the fibres acts to significantly reduce compressive strength, rendering them primarily useful in tension dominated applications [2]. Aramid fibres also have the tendency to absorb moisture, degrade under UV light, and creep under sustained static loading.

2.2.5 Other Fibres

A number of other fibres are available in limited quantities, however high costs have retarded the use of the majority of these in most applications. These include boron, silicon carbide, polyethylene, nylon, and a large range of ceramic fibres.

Table 2.1 Typical Mechanical Properties of Various Reinforcing Fibres

[Source: 1 - 4,14,15]

	Density (kg/m^3)	Modulus (GPa)	Tensile Strength (MPa)	Elongation (%)	Poisson's Ratio
Glass					
E-glass	2580	75	3500	4	0.23
S-glass	2460	85	4500	5.5	0.22
Carbon - PAN					
T-300 (Toray)	1750	235	3200	1.4	0.25
AS4 (Hexcel)	1700	240	3800	1.6	0.25
Carbon - Pitch					
P55 (BP Amoco)	2000	380	2000	0.5	0.25
P100 (BP Amoco)	2150	725	2100	0.32	0.25
Aramid					
Kevlar 29 (DuPont)	1440	65	2800	4	0.34
Kevlar 49 (DuPont)	1440	130	3500	2.3	0.35

2.3 Common Fibre Forms and Orientations

2.3.1 Introduction

The physical forms of fibrous reinforcement utilised in practice are many. The arrangement of the reinforcing fibres within the matrix is the single largest determinant of laminate properties, since it is by the fibres that the load is carried. Fibre orientations are commercially available in one-, two-, and three-dimensional forms, with numerous variations in weave patterns and directional bias. Each of these forms will be briefly discussed in the following sections.

2.3.2 One-dimensional Reinforcement

The simplest form of reinforcement involves the placement of all reinforcing fibres in a single direction. The orientation of the reinforcement would typically be dictated by the direction in which the greatest strength is required. The properties of such a laminate would be orthotropic, dominated by direction of the reinforcement. This form of reinforcement is referred to as *uni-directional* reinforcement. Whilst technically, uni-directional reinforcement is required to possess a minimum of 70% of the fibres in a singular direction, the volume of reinforcement which does not lie in the dominant direction is typically small enough to be neglected in any calculations. In order to achieve greater mechanical properties in various directions, stacking of uni-directional lamina at various angles is often performed, as this offers greater flexibility in tailoring the laminate properties than that provided by standard multi-directional fabrics.

2.3.3 Two-dimensional Reinforcement

Two-dimensional or multi-axial reinforcements are comprised of two or more layers of fibres of varying directions which are stitched, woven or bonded together to form a single fabric. While this removes the freedom of precise directional placement of the reinforcement to some degree, it provides the user with a single fabric ready for matrix impregnation that would otherwise be comprised of several individual layers.

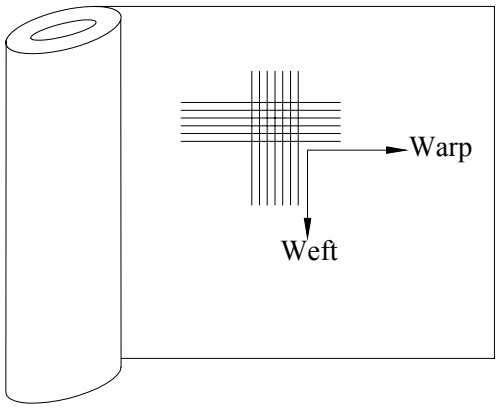

Figure 2.1 Denotation of Fibre Orientations

Fibres oriented in the longitudinal direction of the reinforcement are known as the warp fibres, while those that traverse the reinforcement at 90 degrees are referred to as the weft. Warp threads are also often referred to as 'ends', and weft threads as 'picks.' Common multi-axial reinforcements include the following:

Plain Weave fabric consists of ends and picks that are weaved in an alternating 'over-and-under' fashion, perpendicular to each other. A number of variations to this weave pattern also exist which alter the pliability and strength of the fabric to varying degrees.

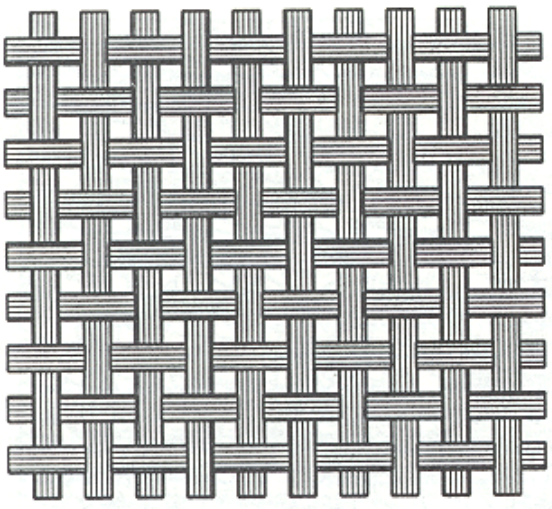

Figure 2.2 Plain Weave Fabric

Biaxial reinforcement is similar to plain weave, except that the two directional layers are overlaid on each other and stitched together at 0^0 and 90^0, rather than woven.

Double Bias (DB) fabric is denoted by two layers of uni-directional fibres which are stitched or bonded together at $+45^0$ and -45^0. This form of reinforcement is often used to carry shear loading, as the fibres are generally oriented in the directions of principal stress in such a case.

Triaxial reinforcement combines fibres at 0^0, $+45^0$ and -45^0 or similarly at 90^0, $+45^0$ and -45^0.

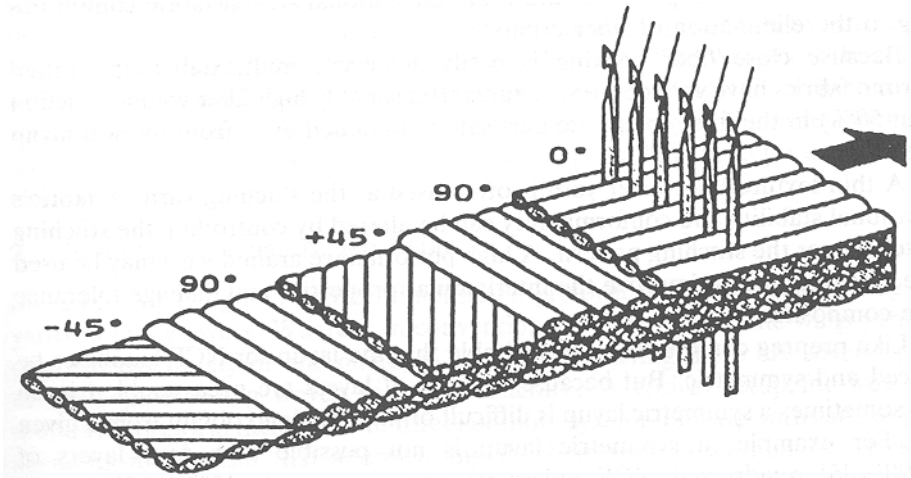

Figure 2.3 Stitched Multi-axial Fabric (Source [4])

Quadraxial fabric contains a layer of fibres in each of the aforementioned directions, namely 0^0, $+45^0$, -45^0 and 90^0. The ratio of fibres in each direction of triaxial and quadraxial fabrics is typically equal, and this fabric often includes a thin layer of chopped strand matting which covers each face of the fabric.

Chopped Strand Mat (CSM) is a two-dimensional reinforcement comprised of randomly oriented non-continuous filaments that are held in place by a binder (adhesive). Consequently, while the in-plane properties of CSM are essentially isotropic when set within a matrix, they are significantly lower than for a quadraxial laminate of equivalent fibre mass. This form of reinforcement is used in low strength applications or where isotropic material properties are desired.

Both the unidirectional reinforcement and the two-dimensional fabrics mentioned here are commonly available in a range of fabric weights, being largely dependent on the reinforcement material. Fabric weight denotes the mass of reinforcement per unit area, and is expressed in either kg/m^2 or g/m^2.

2.3.4 Three-dimensional Reinforcement

While two-dimensional laminates possess high in-plane strength, the matrix is the sole contributor to the strength of the laminate perpendicular to the plane. However on occasion an increased value of strength is required in this direction. Hence three-dimensional fabrics have been developed to accommodate such instances. These fabrics are essentially comprised of a number of stacked layers of biaxial fabric, through which a series of interlinking yarns are inter-woven, as illustrated in Figure 2.4. Few fabrics are available, typically utilising a limited dispersion of high performance fibres in the z-direction. As such fabrics present greater difficulties in manufacture, they are expensive when compared with other fabric forms, and as such are rarely utilised. Greater detail on three-dimensional fabrics can be found in Mallick [4].

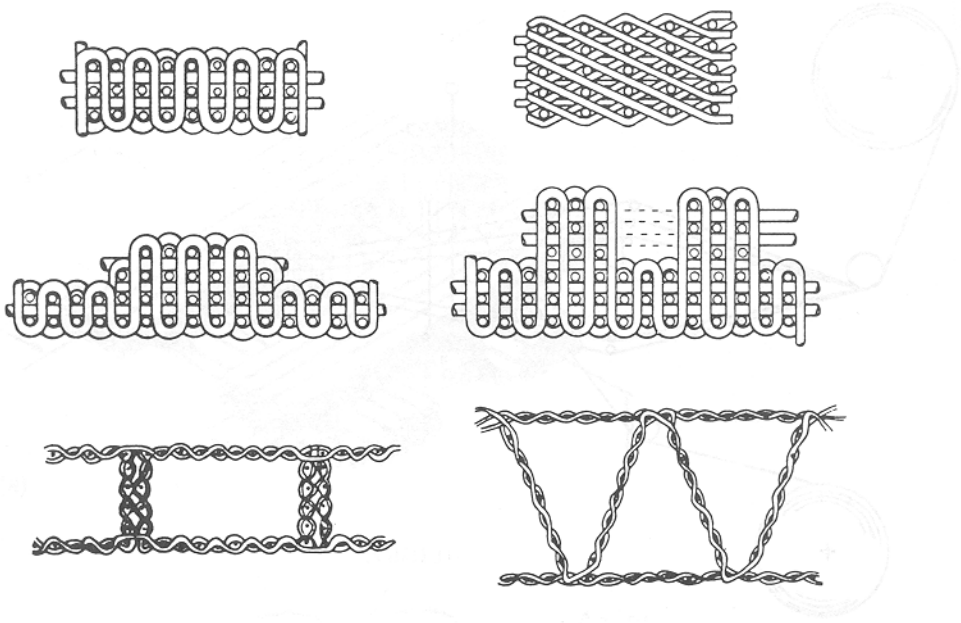

Figure 2.4 Structural Geometry of Various 3D Woven Fabrics (Source [4])

2.4 Polymer Matrix Resins

2.4.1 Introduction

The matrix plays a vital role within a fibre composite laminate. While the reinforcing fibres dominate the bulk laminar strength and stiffness characteristics, the resin matrix acts as a binder that confines the fibres and provides a bulk form, and also distributes the load between adjacent fibres. Additionally, the selected resin largely determines characteristics such as inter-laminar shear strength, corrosion resistance, flammability, and working temperature range [4]. Properties such as ductility, electrical conductivity, and laminate toughness are also affected by the characteristics of the resin.

Polymer matrices can be divided into two classifications: thermoplastic and thermosetting. Thermoplastic resins are formed by the reaction of small monomeric molecules to produce molecules of very high molecular weight [4]. Cross linking of polymeric chains does not occur within these materials, rather they are connected by the entanglement of the long polymeric chains. Therefore since no chemical reaction takes place, it is possible to repeatedly reshape thermoplastic resins through a process of melting and cooling within a mould. Common examples of thermoplastic resins include nylon, polystyrene, and polyethylene.

While the use of thermoplastic resins typically increase laminate toughness and damage tolerance, processing difficulties represent the primary obstacle to more widespread use of thermoplastics. The high temperatures and pressures that are required to induce flow of the polymer present great difficulties in comparison to thermosetting resins, despite vastly shorter processing cycle times. As they maintain a relatively high viscosity at high temperatures, satisfactory wetting of continuous fibre reinforcement is inhibited [4]. The limited processing methods and low stiffness and strength of thermoplastic resins excludes them from many applications, and hence they will not be discussed any further in this chapter. Additional information on various types of thermoplastic resins can be found in references such as [1,5,9].

A thermosetting matrix is characterised by extensive cross-linking between polymer chains of low molecular weight, in a permanent and irreversible reaction. This is facilitated by a catalyst or hardener, which forms part of the chemical reaction. The catalyst can be modified to alter the rate of reaction, and consequently the working time. Thermosetting resins are substantially more brittle than thermoplastic resins, suffer from shrinkage and

exothermic problems, and cannot be reshaped through the application of heat. Despite this, thermosetting resins are more widely used as they provide significant processing advantages, are comparatively inexpensive, and possess superior strength characteristics due to the cross-linking of the polymer chains. Additionally, thermosetting resins can be processed and cured at room temperature, and provide higher working temperatures, better creep performance, and greater resistance to chemical corrosion when cured. Of the plethora of thermosetting resins available, the three most widely available resins, namely polyester, vinylester and epoxy resins, will be discussed in the following section. A comparison of typical resin properties is provided at the conclusion of this discussion.

2.4.2 Polyester Resins

A polyester matrix consists of unsaturated linear polyesters that are dissolved in a reactive monomer such as vinyl acetate or, more commonly, styrene. An organic peroxide is typically used to initiate the reaction, which takes place between the unsaturated polymer and unsaturated monomer to form a three-dimensional cross-linked network [1,5]. Polyester resins are comprised of two main categories – Orthophthalic and Isophthalic.

Orthophthalic polyesters, also known as General Purpose (GP) resins, are the least expensive of the polyesters. However, this resin group possesses comparatively poor mechanical properties and corrosion resistance. These polyesters use the anhydride form of orthophthalic acid, phthalic anhydride, as the saturated acid.

By comparison, isophthalic polyesters are more expensive than orthophthalic polyesters, and possess improved mechanical properties and corrosion resistance. The heat distortion temperature of isophthalic resins is also superior to orthophthalic polyesters.

It should be noted that these categorisations have been made due to difference in the modifying acid used in the formulation. However Ayers [9] suggest that other constituents such as the glycol component actually dominate resin performance, and hence proposes a performance based categorisation, rather than one based on chemical composition.

Generally, polyesters possess adequate mechanical properties for a large range of applications, and are the least expensive of all thermosetting resins. Consequently they are the most widely used matrix, particularly in marine applications. Polyesters can be formulated to resist ultra violet attack and exposure to the elements for extended periods of

time. It is also possible to formulate polyesters that are inherently fire retardant or resistant to chemical erosion. However, volumetric shrinkage exceeding 8% during cure reduces dimensional stability, and therefore excludes polyesters from applications requiring close tolerances. Further discussion regarding polyester resins can be found in greater detail in references [3, 4, 9].

2.4.3 Vinylester Resins

Vinlyesters are often included as a subset of the polyester resin family due to the similarities in basic structure. Both consist of unsaturated polymer backbones dissolved in styrene, and are cured by similar catalyst systems. However vinylesters possess a number of chemical characteristics, particularly in the backbone structure, which set them apart from polyesters in general. Essentially, vinylesters are comprised of epoxy resins that are cured like polyesters through reaction with acrylic or methylacrylic acids [9]. The primary distinction between vinylesters and polyesters therefore, is that the epoxy molecule does not possess the weak chemical link which makes polyesters potentially vulnerable to chemical corrosion. Additionally, the insaturation is limited to two sites at the end of each vinylester molecule, which results in superior mechanical properties, fatigue performance, and resistance to impact damage [4]. However, as with polyester resins, some shrinkage does occur which is dependent on the particular formulation. Generally, shrinkage in vinylesters is greater than epoxies, but less than polyesters.

The epoxy component of a vinylester matrix allows for a wide range of modifications to be made to the resin, which affects the matrix performance. Increases in fire retardant and heat distortion temperatures are possible through the addition of brominated bis A epoxies and methacrylated novolac epoxies respectively. High elongation vinylesters are also achievable, primarily through the addition of rubber particles to the matrix.

The effective combination of polyesters and epoxies manifested in vinylester resins has generally resulted in a matrix that provides a transition in material properties and cost between the two. A large number of vinylester formulations are available, and are discussed in further detail in references [3, 4, 9].

2.4.4 Epoxy Resins

Epoxy resins consist essentially of epoxy groups or rings, which are comprised of one oxygen and two carbon atoms. The structure of this ring is such that it is particularly

reactive with a wide range of acids and bases, including amines and anhydrides, which cause the ring to open. In the case of a reaction with amine, by way of example, the epoxy chemical group reacts with the active hydrogen molecules of the amine to form a linear chain. Cross-linking of these chains occurs if the epoxy or amine molecule contains a functionality that is higher than two. Various epoxy molecule configurations and the chemical process involved in the polymerisation of epoxies are described in more detail in references [3,4,6,7,9].

Epoxies possess mechanical properties that are superior to both polyesters and vinylesters. High corrosion resistance, low shrinkage, and good electrical insulation properties are also inherent in epoxy matrices, and they are generally less susceptible to moisture and heat [5]. Variations in formulation are also numerous for epoxy systems. As well as the use of common additives such as tougheners, epoxy resins can be modified for use as a casting resin, or applied to resin transfer moulding (refer section 2.6.6). It is also possible to utilise epoxy resin systems in a number of alternative ways. These include prepregs (reinforcement pre-impregnated with resin: refer section 2.6.5) and adhesive films, which use modified epoxies to extend cure times.

While epoxy resins are clearly superior to other resin types in regard to mechanical properties and versatility, extensive use by all industries is prevented due to cost. As shown in Table 2.2, epoxy resins are significantly more expensive than both polyesters and vinylesters, and consequently have been adopted primarily for high performance applications such as aerospace and motor racing components, as well as racing yachts.

2.4.5 Other Resins

While the aforementioned matrices may be described as 'general purpose' resins, a large number of other resins are available, primarily formulated as specialty matrices for specific purposes. Phenolic resins are utilised in applications where low flammability and low smoke production are required, while polyimides are often utilised in high service temperature environments [1]. Polybutadiene resins are formulated for use in resin transfer and injection moulding applications, which will be described further in section 2.6.

The vast array of resin formulations and systems has not been exhausted in this discussion, however the most commonly used resin systems have been outlined. The wide variations in matrix performance denoted in Table 2.2 demonstrate that suitable resin systems are

available to suit a wide range of application, with the level of performance predominantly dictated by cost.

Table 2.2 Typical Mechanical Properties Of Various Resins [Source: 4,6,14,15]

	Density (kg/m3)	Tensile Modulus (GPa)	Tensile Strength (MPa)	Compress. Strength (MPa)	Tensile Elongation (%)	Flexural Modulus (GPa)	Flexural Strength (MPa)	Poisson's Ratio	Approx. Cost (AUD$/kg)
Polyester	1100-1460	2.8-3.4	40-80	100-120	1.5-3.5	2.5-3.2	80-110	0.38	3.00-4.00
Vinylester	1000-1200	3.2-3.6	70-90	105-125	5.0-6.0	2.8-3.4	100-145	0.38	6.00-8.00
Epoxy	1000-1300	2.4-6.0	55-100	90-115	5.0-8.0	2.9	95-125	0.36	10.00-12.00

2.5 Sandwich Panels and Core Materials

Due to the extensive use of sandwich panels in the chassis rails of the proposed FRP trailer concept (refer Chapter 6), this section provides a brief summary of sandwich panels, focussing particularly on the common core materials used in sandwich panel applications.

2.5.1 Sandwich Panels

Efficient use of composite materials within a structure is essential in order to minimise the quantity of laminates required to provide a particular stiffness or moment capacity, and to maintain competition with conventional, less expensive materials. This requires strategic placement of the reinforcement in order to maximise the high strength characteristics for which fibre composites are used. One method of achieving this placement is through the use of sandwich structures. Essentially this involves two thin, strong facings separated by a thick, lightweight and inexpensive core material which carries the shear load. The high strength and inherently thin nature of laminated composites has resulted in widespread use of FRPs in sandwich panel construction, particularly in marine and aerospace applications. A brief glance at the fundamentals of section properties clearly demonstrates the increase in stiffness achieved by the spacing of the load carrying flanges, given that flexural stiffness is proportional to the cube of the panel thickness. Essentially a sandwich panel is similar in principle to an I-beam. The skins or facings act as the flanges of the I-beam, and the core material takes on the role of the web. Chapters 7 and 8 detail the use of sandwich panels within this project.

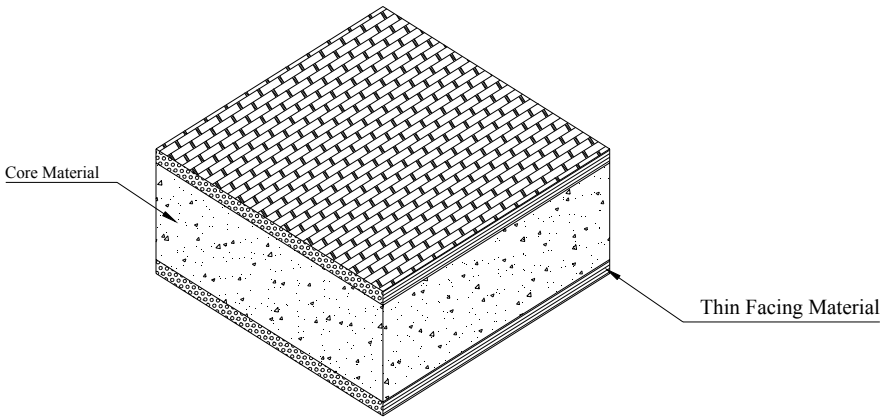

Figure 2.5 Representation of an FRP Sandwich Panel

2.5.2 Core Materials

The core material is responsible for a number of functions. Apart from providing a spacing for the laminates and resisting the shear loading, the core must also withstand out-of-plane compressive loading and prevent the skins from local buckling or wrinkling, which would lead to ultimate failure of the panel.

Various core materials have been developed and employed in sandwich structures, and the more common materials are outlined in the following discussion. A comparison of core material properties is provided at the conclusion of this section.

Timber is perhaps the oldest of core materials used in sandwich panel construction. Microscopically it is similar in cross sectional shape to synthetic honeycomb cores, and therefore generally the grain of the timber is placed perpendicular to the plane of the skins. The use of cedar as a core material has found application primarily in marine structures where weight is of secondary importance. End-grain balsa is the timber core most commonly used, due to its low weight, low relative cost, and high compressive strength in the direction of the grain. Balsa also possesses good thermal insulation and acoustic absorption, and is easily shaped and joined. However, it is susceptible to moisture and dry rot, and will absorb large volumes of resin during sandwich panel fabrication unless sealed. Despite this, balsa has been employed in a large range of applications including boat hulls and decks, automotive panelling (such as the floor of later models (2000) of the Chevrolet Corvette), large tanks, and various components in aircraft.

Foam has been used as a structural core for some time, and extensive development of various foam types has established this material as the most widely used of all cores. As with resins, a wide variation in properties is available through differences in base materials and formulation, and the mechanical properties of foams are generally proportional to cost. Additional costs are also associated with the production techniques required to achieve uniform properties throughout foam products, which are inherently difficult to achieve.

Foams are manufactured from a range of synthetic polymers including more common types such as polyvinyl chloride (PVC), polystyrene (PS), polyurethane (PU) and styreneacroylonitrile (SAN). Foam densities typically range from 30 kg/m^3 to 300 kg/m^3, and are generally available in thicknesses between 5 mm and 50 mm.

PS Foams represent the low end of the foam range in terms of performance. While they are extremely inexpensive to produce and are easily shaped, low material properties exclude them from a large number of structural applications. The use of this foam is further limited by an incompatibility with polyester resins, since polystyrene foams dissolve in styrene.

PU Foams have likewise experienced limited usage in many structural components. While they possess reasonable mechanical properties, they have been disregarded for most structural applications due to a tendency of the core/skin interface to deteriorate with age, leading to delamination. Consequently, use of polyurethane foams has been relegated to lightly loaded panels and the production of void formers.

PVC Foams are one of the most commonly used core materials in high performance applications. They possess good mechanical properties both statically and dynamically, and their closed-cell structure is resistant to water absorption. PVC foams are available in two forms: crosslinked or uncrosslinked. As with the resin systems previously discussed, cross-linking provides increased material strength and operating temperatures. While uncrosslinked or linear PVC foams have lower mechanical properties, they possess greater toughness and are inherently less brittle.

Toughened PVC foams have also been developed in recent years by a number of companies, which combine the strength of crosslinked foams with the toughness of linear foams.

The primary disadvantage of PVC foams is cost, as they are one of the most expensive foams available. They are also inherently flammable, and therefore require particular fire resistant grades in fire critical applications.

SAN Foams possess properties that have much in common with the properties of toughened crosslinked PVC foams. While the static properties of SAN foams are slightly lower than those of PVC foams, they possess greater inherent toughness and impact resistance than any PVC foam. Additionally, this toughness is inherent within the polymer, and does not require plasticisers as used in PVC foams. Hence, the toughness properties do not degrade with age. As a result, SAN foams are replacing PVC foams in a number of applications. However, only a limited range of densities is available which restricts usage in some applications.

Honeycomb cores were developed primarily for the aerospace industry specifically for the maximum reduction in weight. These cores are constructed from a large range of materials, the choice of which is dependent on application. Paper or cardboard honeycombs represent the oldest form of this type of core. Due to the low strength of the card used, these cores are often dipped in resin to improve properties. However as they possess the lowest strength of any honeycomb in use, they are generally utilised in only low strength, non-structural applications.

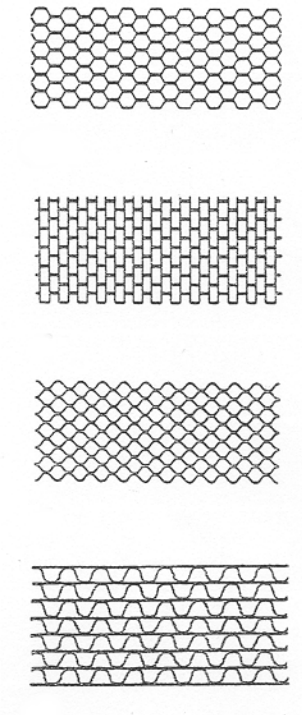

Figure 2.6 Typical Honeycomb Sections

Aluminium honeycombs are possibly the most popular of all honeycombs, as they provide one of the highest strength/weight and strength/cost ratios available. A number of alloys are available, intended for specific applications such as corrosive environments or for use at elevated temperatures, and variations in foil gauge expand the range of achievable mechanical properties. There are however two distinct disadvantages suffered by aluminium honeycomb. Aluminium is susceptible to aggressive corrosive environments, particularly when in contact with conductive carbon skins, which can assist galvanic corrosion. Additionally, any local deformation experienced by aluminium honeycomb due to impact incidents is plastic and permanent, which can result in skin debonding.

Aramid paper honeycombs are available in applications requiring a higher impact resistance or damage tolerance. Aramid cores such as 'Nomex' honeycomb, produced by DuPont, consist of a synthetic paper based on Kevlar™, which is typically covered in a phenolic resin to increase fire resistance. While mechanical properties are inferior to those of the aluminium counterpart, aramid paper honeycombs possess the ability to withstand localised overloading without permanent damage. However application of this type of core is limited primarily to aircraft structures due to high costs.

The cross sectional shape of the honeycomb structure is responsible for the high compressive and shear properties achievable at such a reduced weight. Variations in cell shape are readily available which, apart from the material choice, most readily influence the anisotropic properties of the core. Variations in cell size are also available, however this has only a secondary effect on the majority of mechanical properties.

The manufacture of honeycomb cores is conditional on the material in question and further details on manufacturing processes and honeycomb material properties can be found in reference [3].

Particulate Filled Resins (PFRs) have played an increasing part in core materials in recent years. PFR consists simply of a matrix, typically vinylester or epoxy, combined with a second-phase filler material. This bond between the matrix and the filler is mechanical, rather than chemical, and the properties of the filled resin are heavily dependent on the type and quantity of the filler present in the matrix. Researchers at USQ have undertaken extensive investigation of this type of core material, and typical findings can be seen in papers such as [8 and 9]. PFRs possess exceptionally high strength compared with other core materials, and remove the necessity of hard point placement within sandwich cores. Depending on the combination of matrix and filler, a wide range of properties and densities are achievable.

Flexibility of shape also represents a significant advantage for PFR. Following the combination of the uncured resin with the filler, the mixture can be poured into a mould prior to cure. PFR also possesses exceptional wear resistance and durability, and is damage tolerant.

However due to a relatively high density, current market penetration of PFRs has generally been limited to civil structures. In such applications, an ability to carry concentrated

compressive loads and withstand incidental damage is preferred over low density and major reductions in structural mass.

Casting resins have also been utilised in PFR mixtures. These resins are specifically formulated to enable casting in thick sections, particularly in conjunction with short fibres or other fillers, which increase strength.

Table 2.3 Typical Mechanical Properties of Various Core Materials

[Source: Manufacturers Data and USQ Test Data]

	Density (kg/m3)	Tensile Strength (MPa)	Compress. Modulus (MPa)	Compress. Strength (MPa)	Shear Modulus (MPa)	Shear Strength (MPa)
Balsa						
Along grain	96-250	9.5-31	110-380	1.1-3.6	2250-8000	3.5-20
Across grain		0.5-1.5	-	-	35-380	0.34-1.36
Honeycomb						
5052 Alloy Hexagonal Aluminium 1/8-5052-0.002	130	-	2400	10.1	930	5
Polyurethane Foam	20-400	0.1-8.96	-	0.1-13.8	1.56-103.5	0.14-3.1
PVC Partially Crosslinked Foam (H Series from DIAB)	30-250	0.8-8.8	20-400	0.3-5.8	10-108	0.35-4.5
SAN Foam (Corecell from ATL)	50-200	1.0-6.8	22.8-86.0	0.4-3.44	11.7-45.2	0.66-1.97
PFR Glass Microspheres 40% K15 filler by volume from 3M	650	25	2050	47	-	-

2.6 Manufacturing of FRP Laminates

2.6.1 Introduction

The cost of production of FRPs is primarily dependent on the method of manufacture. While the work within this project utilised the wet layup technique exclusively, it is envisaged that alternate methods, more suited to large volume production, would be used for commercial trailer construction. Hence, this section outlines a number of methods that may have be applied in the production of one or more trailer components.

The manufacture of FRPs is essentially completed within a three-stage process. Firstly, the reinforcements are stacked, and the fibres oriented as required. Secondly, the fibres are impregnated with the matrix and then cured through polymerisation that may be assisted by the application of heat and pressure. Finally, the product is demoulded and trimmed as necessary. A large range of consolidation techniques are available, the more common of which are discussed in this section. The choice of manufacturing process is dependent on a number of variables that the designer must consider. These include the type of matrix and fibre to be consolidated, the quantity and quality of parts to be produced, and the cost effectiveness of the process [5].

2.6.2 Wet Layup

The wet layup technique, also known as contact moulding, is the simplest and most widely used process in the manufacture of FRPs. This can be performed in two basic ways: hand layup and spray-up moulding.

Hand layup is performed by placing the reinforcing fibres into a prepared mould, or draping the fibres over a former. The reinforcement is then saturated with resin, and brushed or rolled to completely impregnate the resin, compress the laminates, and remove any air trapped between layers. The part is then cured at room temperature, and subsequently post cured at elevated temperatures (where required) to ensure complete polymerisation.

Spray-up moulding, a form of wet layup, differs in that continuous reinforcing fibres are chopped into short strands and sprayed onto the mould along with a precatalysed resin through a 'chopper' gun. Laminate thickness is essentially constant throughout the part,

and is determined by the amount of material sprayed by the operator. This technique is useful only for parts that do not require specific orientation of the reinforcement.

While capital equipment costs are extremely low and a large degree of flexibility is afforded by this method of manufacture, the hand layup process is labour-intensive, produces only low product volumes, and makes it difficult to maintain product uniformity. It is therefore best suited to prototyping and pre-production, or to low performance applications that require little quality assurance.

2.6.3 Vacuum Bag Moulding

Bag moulding techniques form an extension of the hand layup process. This technique utilises a vacuum to remove excess resin and air voids, and atmospheric pressure to compress the laminate onto the mould during cure. The initial stages of vacuum bag lamination are identical to those of the standard wet layup process. However when the lamination is completed, a flexible diaphragm or bag is placed over the laminate and sealed along all edges. The air within the bag is evacuated using a vacuum pump and the part left to cure. A combination of a 'breather' and a 'bleeder' cloth is often placed between the part and the diaphragm, which aid in evacuation of air and the absorption of excess resin.

This process is often utilised in large or complex parts, particularly when the shape of the part is not suitable for consolidation by closed moulding techniques. Vacuum bagging also possesses the shaping versatility of hand layup processing, and is limited only by the size of the mould and the evacuating capacity of the pump. Tooling costs are negligible in comparison to other pressure-cure processes.

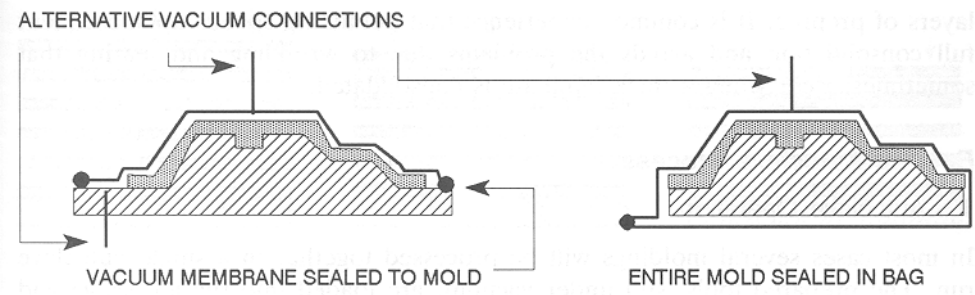

Figure 2.7 Typical Vacuum Bagging Configurations (Source [14])

Vacuum bagging is more labour intensive than the hand layup process, and is therefore suited to low-volume production only. Product quality is largely dependent on the operator, and product cycle times are low.

2.6.4 Autoclave Production

Laminate consolidation through autoclave processing is a further extension of vacuum bagging. Following hand layup and bagging of the laminate, a partial or full vacuum is drawn within the bag. The laminate is then placed within a pressure vessel at elevated temperatures and cured. This additional pressure, typically between 345 and 690 MPa [2], is achieved by either high capacity compressors or nitrogen. Production autoclaves are typically cylindrical in shape, and vary between 1 and 8 metres in diameter.

Autoclave processing produces parts that are superior to vacuum bagged products, as the higher temperatures and pressures minimise porosity and void content, and more closely control laminate thickness. This process is able to accommodate a wide range of product geometry and sizes, and it is this flexibility which has maintained this method as one of the most cost effective for low to medium volume production of high quality laminates [4].

Labour content is marginally higher than for vacuum bagging, whilst capital costs are substantially greater. The autoclave also requires large quantities of energy and material, including industrial gases and consumables such as bagging. Cure cycle time is very high, and exceptionally thick laminates must be put through the cure cycle several times to complete the cure in optimum conditions.

2.6.5 Prepreg Layup

The term 'Prepreg' is used to describe reinforcement pre-impregnated with a thermosetting matrix (usually epoxy), which has partially cured. Since the resin polymerisation has begun, the prepreg is stored at low temperatures to retard the reaction for a limited time. When ready for use, the prepreg is placed into the appropriate mould and heated to complete full cure.

Prepregs typically contain lower volume fractions of resin, and therefore are used primarily in high performance parts where weight reduction is important. They are generally expensive however, and labour content is high since the process is difficult to automate.

2.6.6 Resin Transfer Moulding

Resin transfer moulding (RTM) is one of a number of production techniques developed for high production volumes. RTM uses a closed mould, into which the dry reinforcement is placed. The matrix (resin) is then introduced into the mould through inlet ports, and the air is allowed to escape. When the mould has been filled, all ports are sealed and the mould is heated until cure is completed.

The primary advantage provided by this process is found in the relatively low cure cycle times, combined with the ability to place continuous fibrous reinforcement in any desired orientation. Additionally, RTM does not require a moulding press and produces products that are very low in porosity and void content.

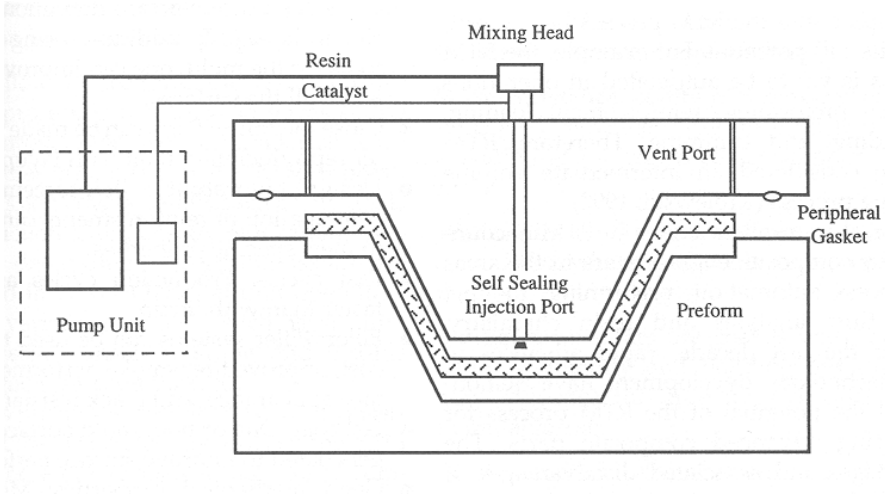

Figure 2.8 Schematic Representation of RTM Process (Source [14])

However as with all closed moulding processes, parts require machining and trimming following cure. The capital costs associated with tooling and machinery set up are reasonably high, although substantially lower than autoclaving. Little flexibility in part geometry and size is available, and consequently, this process is suitable only for high volume production.

2.6.7 Filament Winding

This process involves the winding of a continuous, resin impregnated roving or tow (a grouping of untwisted fibres) around a rotating or stationary mandrel. The reinforcement, typically glass, is fed via a resin bath which impregnates the tow. It is then drawn through a delivery eye, which controls the angle at which the fibres are wrapped around the

mandrel. Depending on the capacity of the machine, fibres can be placed at orientations between 5^0 and 90^0 to the axis of rotation. Rotational speed and fibre placement is typically computer controlled, with the delivery head free to move with as many as six degrees of freedom.

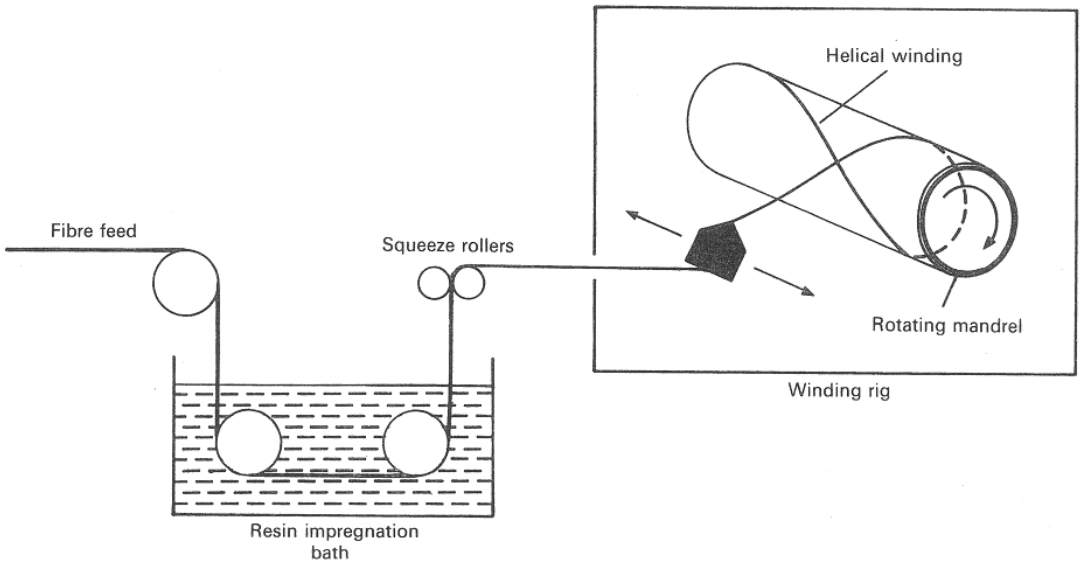

Figure 2.9 Filament Winding Process (Source [1])

This form of laminating is ideally suited to applications in which large volumes of reinforcement are required, as it is possible to process between 50 and 350 kilograms of reinforcement per hour at a relatively low cost per part [1]. Computer control and the automated nature of filament winding improve repeatability and quality control, and also reduces labour costs. The use of continuous reinforcement eliminates joints and stress concentrations, and the process easily accommodates the orientation of the fibres in the directions of principal stress.

However filament winding is limited in a number of ways. The component shape must allow removal of the mandrel. Hence, production is generally limited to long tubular or hollow shapes that must possess a taper. While the cross sectional shape need not be circular, product shapes are generally cylindrical, conical or geodesic. Capital costs for the winding machine and mandrel are usually high, and the external surface finish is typically poor.

Applications include rocket motor casings, golf club shafts, windmill rotors, light poles and pressure vessels.

2.6.8 Pultrusion

Pultrusion is a continuous manufacturing process capable of producing FRP members with constant cross sectional shape of any length. The pultrusion process was initially developed as a high volume manufacturing technique used to produce solid sections reinforced with unidirectional fibres. However pultrusion is now capable of producing a vast range of solid and hollow profiles available in lengths which are not possible through other techniques.

The pultrusion process involves the drawing of continuous rovings through a resin bath for impregnation with the matrix. The matrix must be stable and only slightly reactive at room temperature. Following resin saturation, the fibres are drawn into a heated die. The die shapes the fibres into the desired cross section, and is heated sufficiently to initiate and complete cure of the resin before it exits the die. The material is then cooled by natural or forced convection, beyond which point the pulling device is employed. A moving cut off saw is then able to cut the product to length.

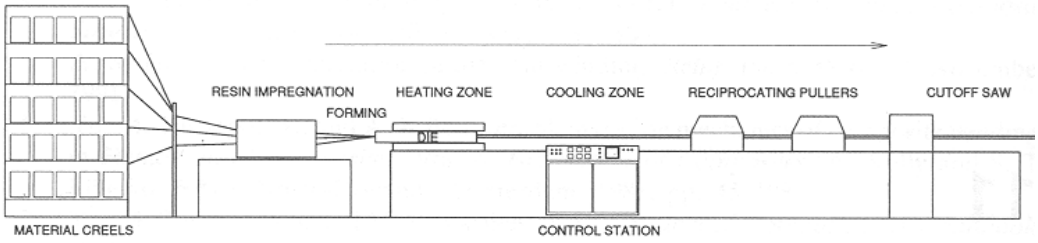

Figure 2.10 Basic Pultrusion Process

The primary advantage of the pultrusion process is found in the low cost, high volume production of continuous sections. In comparison with other techniques, pultrusion is capable of producing substantially less expensive parts within this context. Significant variations in reinforcement types and orientations are also available, which greatly increases the versatility of this process. Glass, aramid, and carbon fibres can be used in combination with polyester, vinylester and epoxy resins. Current production rates are as high as 6 metres per minute [3], and labour costs and material wastage are low when compared with most other production methods.

A number of limitations exist with this manufacturing technique. Applications are limited since the cross sectional shape must be constant, and the inclusion of inserts or hard points for joining at specific locations cannot be accommodated. While operational costs are low,

capital equipment costs including dies and the guidance system are high. Short production runs are therefore uneconomical, particularly for non-standard sections. Fibre fraction is often low, and fillers are often required to reduce resin costs. Wall sections are limited to approximately 12 mm due to standard heater capacities, and some constraints exist regarding fibre orientation and content [5].

2.6.9 Matched Die Moulding (SMC and BMC)

Matched die moulding involves the curing of a material enclosed within a mould to which the material has conformed. This form of manufacture is required in applications where part tolerances and quality repeatability are necessary, such as in the automotive industry. While the matched die moulding process includes a plethora of process variations, the two most common moulding compounds and their associated manufacturing techniques will be discussed here.

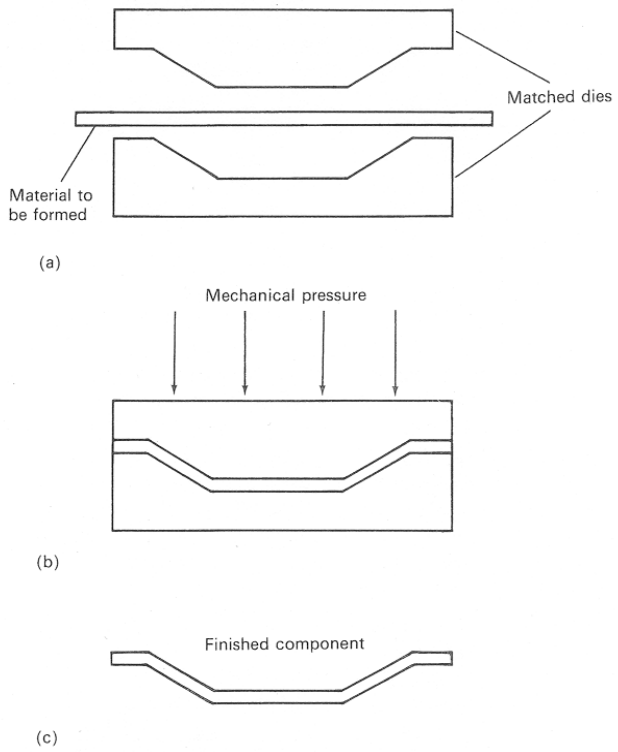

Figure 2.11 Matched Die Moulding Process (Source [14])

Sheet moulding compound (SMC) is a composite material consisting of reinforcing fibres pre-impregnated with a thermosetting resin. SMC differs from prepregs however, in that the reinforcement usually consists of short, discontinuous, random fibres, and the fibre volume fraction is low, at approximately 30%. A combination of fillers including wood flower, cellulose and particulate minerals are often added, and the pre-cured product

possesses a dry, pasty consistency. The SMC is produced in sheets that can be cut or punched to shape before placement in the mould. The heated mould is then closed and the resin cured while subjected to 7 to 14 MPa of pressure. Polyester or vinylester resins are usually used since they are inexpensive and provide a low cure cycle time.

Bulk moulding compound (BMC) is similar to SMC in composition and processing techniques. The primary differences involve the form of the material, as BMC is supplied in bulk rather than sheet form, is available only with discontinuous CSM (refer section 2.3.3), and generally possesses a lower fibre volume fraction. The fibre length of reinforcement is also shorter, and is cured in a heated mould under 3 to 4 MPa of pressure [4].

SMC and BMC parts are most commonly used in the production of automotive body panels, and are available with a range of mechanical properties that are determined by the filler type and content.

2.7 General Laminate Characteristics

2.7.1 Introduction

The mechanical properties of FRPs vary greatly in response to the material type, laminate construction, and loading condition. The orthotropic and highly variable nature of fibre composites further complicates the description of these materials, such that a number of terms used to characterise isotropic materials are inadequate in describing those of FRPs. This section briefly describes the general design considerations applicable in the context of this thesis, in particular the failure characteristics of FRPs. The reader is directed to chapter 6 for a separate detailed discussion regarding the physical properties of the FRP materials used during the course of this research.

2.7.2 Stress and Strain Characteristics of FRP Laminates

As the fibrous reinforcement carries the majority of the load within a laminate, the modulus and strength of a laminate varies with the direction of loading. For the purposes of this discussion, it is assumed within this section that all loading is performed upon unidirectional laminates at the angle 0°. This assumption is also forms the basis for laminate design in later chapters.

The stress-strain relationship for tensile loading of unidirectional laminates is generally linear up to the point of failure. Figure 2.12 compares the stress-strain characteristics of various materials. The most obvious point to note is the comparatively high elastic strain of FRPs to common metals. This has a significant effect on design constraints in applications governed by deflection, and this will be discussed in section 2.7.4. While both steel and aluminium possess significant strain capacity before failure, the majority of this occurs during plastic deformation. As design of structures is generally concerned only with elastic deformation, the stress-strain characteristics beyond yield of steel and aluminium are not shown in the figure.

Yielding does not occur before ultimate failure as in metallic structures, but rather failure is initiated through individual fibre breakage at various isolated locations. This produces a number of reactions within the laminate, which culminate in complete failure. The failure modes that contribute to this final failure include:

(1) Fibre-matrix debonding which occurs when a weak interface between the two constituents exist or when the ultimate failure strain of the fibres are relatively high,

(2) Transverse matrix cracking which occurs when the matrix is brittle and there is a strong interface between the two constituents, or

(3) Conical shear fracture when the matrix is ductile and the interface is strong [4]. Hence, the dominant failure mode is dependent on the particular combination of reinforcement and matrix used. For example, a glass/epoxy laminate will tend to fail through fibre matrix debonding due to the high failure strains of the glass reinforcement.

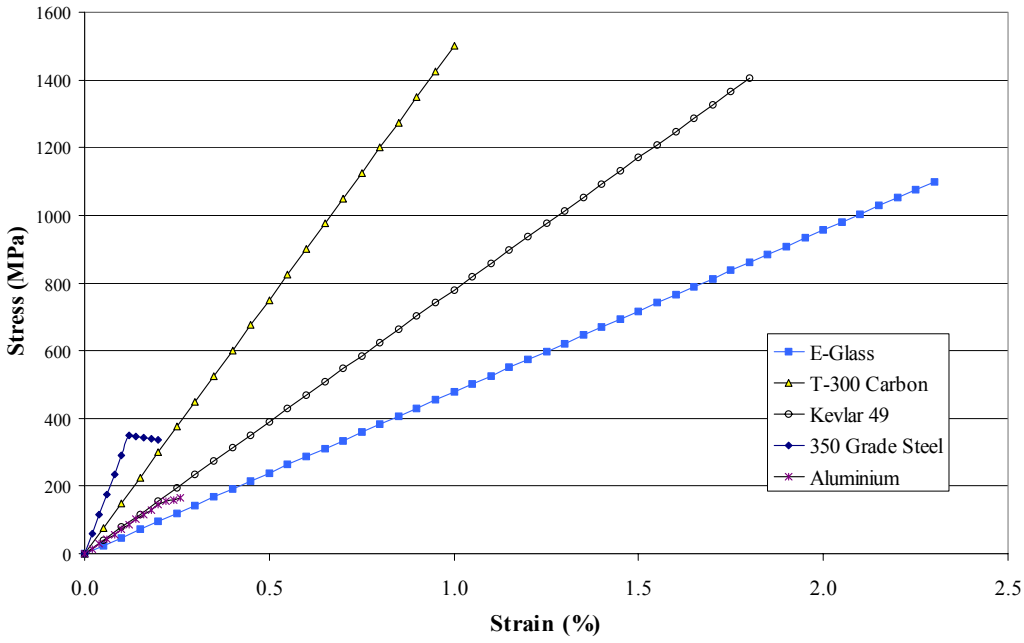

Figure 2.12 Typical Elastic Stress-Strain Characteristics of Various Materials

2.7.3 FRPs: Brittle or Ductile

Fibre reinforced plastics have long been cited as examples of brittle materials. This perception continues to be upheld due to the fact that, as shown in Figure 2.12, no yield point is observed, and failure of the laminate is not preceded by plastic deformation, strain hardening or any of the other phenomenon observed prior to reaching the ultimate strength of the steel. It is therefore argued that due to the sudden and catastrophic nature of FRP laminate failure, structures that rely on FRPs in a strength capacity ought to be designed with greater factors of safety in order to minimise the risk of unexpected failure.

However FRPs are not, by definition, brittle materials. While brittle materials are characterised by the absence of a yield point and plastic deformation, they are also characterised by low strains at failure [10]. However, the strain-at-failure of FRP materials is significantly higher than the strain at the yielding point of steel. This does not account for differences in the serviceability limits applicable to each material, which is not considered here. The effects of serviceability limits on FRPs, particularly in trailer design, are contained in Section 4.8.

The appeal of ductility through yielding and plastic deformation is found in the warnings these phenomena provide regarding impending material failure. However, a distinction must be made between material and structural ductility. Van Erp [11] discusses this distinction, demonstrating that a structure constructed from ductile materials such as steel and reinforced concrete does not guarantee a ductile structural failure.

The principles established by Van Erp can also be applied within the context of trailer chassis design. That is to say that the failure of a semi-trailer constructed from steel members is not necessarily ductile, particularly if a substantially overloaded trailer encounters difficult terrain or sudden evasive manoeuvring. A steel or aluminium trailer, which may have already begun to plastically deform under the static load, may suddenly fail catastrophically once subjected to the difficult terrain or evasive manoeuvring. By contrast, a trailer constructed from FRPs would potentially withstand identical conditions without any permanent damage or structural failure, due to the purely elastic nature and high ultimate strain characteristics of the material. Further discussion on the failure modes of steel and FRP trailers are found in Chapters 4, 6 and 7.

Warning of failure and/or progressive failure can be achieved through exploitation of the different ultimate failure strains of different fibre types. Through use of hybrid laminates, a combination of two or more types of reinforcing fibre, pseudo-ductile behaviour may be achieved. For example, consider a hybrid laminate that consists of carbon and glass unidirectional reinforcement set within a matrix. The stress-strain curve for such a laminate would appear similar to that shown in Figure 2.13. Due to the difference in ultimate strain capacity, the carbon fibres would fail first, with the load carried by the carbon reinforcement being transferred to the glass reinforcement. The effective laminate modulus would consequently drop, and hence a 'knee' would become evident. This effect was successfully demonstrated by Mr. Paul Simpson as part of current research at the University of Southern Queensland, by using a hybrid laminate on a FRP beam. Simpson showed that this 'yield' point occurred reliably at the ultimate strain capacity of the carbon,

the value of which was determined through experimental testing of carbon laminate specimens. Hence, the use of pseudo-ductile laminates could be specifically allowed for in design. The reader is directed to [12] for further discussion on pseudo-ductile performance of hybrid laminates.

Hence, while the brittle nature of FRPs is arguably inherent on a material basis, this does not necessarily imply that FRP structures are brittle and unpredictable. Additionally, traditional building materials such as steel and reinforced concrete, which display ductile behaviour on a material level, do not always result in a ductile behaviour at a 'systems level'.

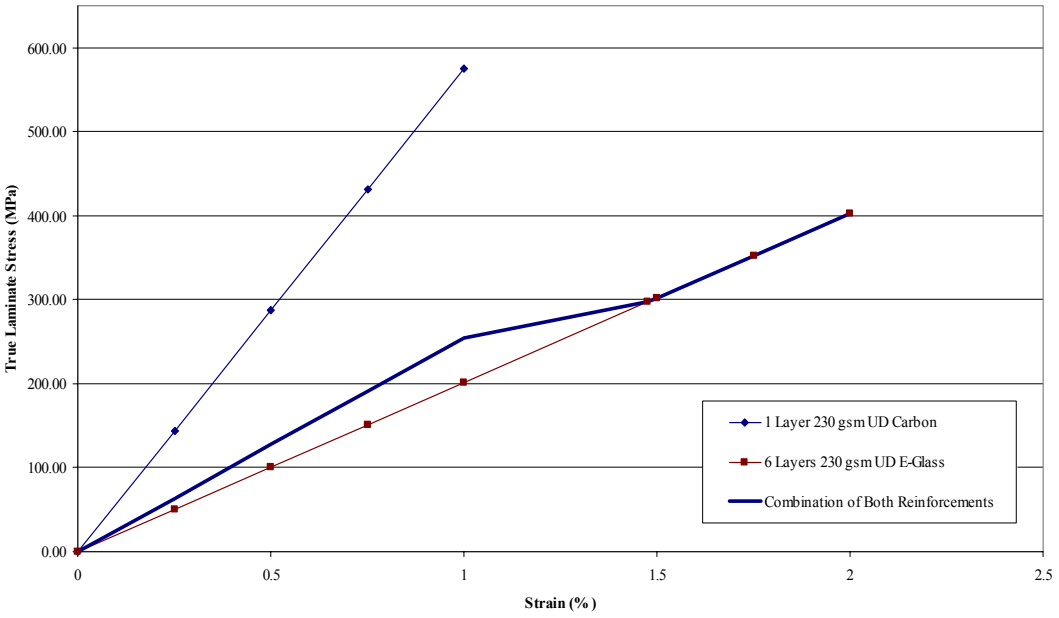

Figure 2.13 Pseudo-ductile Behaviour of Hybrid Laminate

2.7.4 Laminate Characterisation of FRPs

Typically, the determination of characteristic mechanical properties for more common engineering materials is accomplished by examination of data tables provided by the relevant manufacturer. However with respect to FRPs, this is not necessarily possible, as the final properties often depend significantly on the manufacturing method.

A survey of the literature regarding unidirectional laminates, reveals significant variations in the measured mechanical properties (refer Table 2.4). However, as indicated by Van Erp et al [12], this variation is largely the result of the use of a stress-based characterisation approach. Instead, Van Erp et al suggest that FRP materials characterisation, which

includes the amount of reinforcement fibres as the dominant factor, results in significantly improved consistency in the data. Hence, while the use of traditional descriptors for material characterisation such as Ultimate Tensile Stress and Tensile Modulus are adequate for isotropic materials, the utilisation of alternate descriptors may be necessary to better represent materials such as unidirectional FRP laminates.

Ayers [9] and Van Erp and Ayers [18,19] observed that the ultimate loads carried by specimens of varying resin content (but with identical reinforcement) appeared to exhibit good consistency. Additionally, it was found that the corresponding strain values at which the loads were carried were also consistent. However, substantial differences were observed in the values of Ultimate Tensile Stress and Tensile Modulus yielded by these tests, caused by variances in laminate thicknesses. A comparison of the values obtained by the author's testing clearly shows that the resin content of the author's test specimens was significantly higher than the resin content of the specimens used by others.

Table 2.4 Typical Unidirectional Laminate Properties

	Ultimate Tensile Stress (MPa)	Ultimate Tensile Modulus (GPa)	Source
E-Glass/Epoxy	750	42	Matthews et al [1]
E-Glass/Epoxy	965	39	Schwartz [15]
E-Glass/Epoxy	1062	39	Mallick [4]
E-Glass/Epoxy	500	29	Authors Testing (refer Chapter 5)
T-300 Carbon/Epoxy	1524	141	Peters [14]
T-300 Carbon/Epoxy	1758	138	Toray [16]
T-300 Carbon/Epoxy	1500	181	Mallick [4]
T-300 Carbon/Epoxy	726	65	Authors Testing (refer Chapter 5)

Ayers [9] and Van Erp and Ayers [18,19] have also shown that the correlation between material thickness and load capacity inherent in isotropic materials does not necessarily hold true for FRP laminates. Rather, it was proposed that an appropriate characterisation of unidirectional lamina strength should instead incorporate the mass of reinforcement

present within a laminate, as the tensile strength of the laminate is dominated by the reinforcement. Hence, the elimination of thickness as an influential parameter in respect to strength characterisation is possible by replacing stress with a normalised load-per-layer laminate specification. That is, if the thickness of a laminate is replaced by 'unit mass of reinforcement', the strength characterisation of the laminate is no longer denoted by stress (force per unit cross sectional area) but rather by *normalised unit strength* (force per unit width per unit mass of reinforcement). Similarly, the Modulus of Elasticity (N/mm^2) may be replaced with a *normalised unit modulus* (N/mm width per kg/m^2 of reinforcement). This was demonstrated to provide reliable and uniform results in quantifying the strength and stiffness properties of a laminate. The reader is directed to [9,18,19] for further reference.

While the description of the ultimate strength of a laminate can be quantified through a normalised unit strength value, this applies essentially to the determination of the ultimate laminate capacity and is useful in determining factors of safety for direct application in design. However, for the purposes of quantifying the load experienced by a given laminate at a specified point relative to the ultimate capacity of the laminate, the normalised unit strength value is somewhat impractical. The use of strain, rather than stress, as a description of the magnitude of laminate loading is a far more useful tool. As strain is non-dimensional, it is independent of thickness, and is directly proportional to deflection. Additionally, it can be easily measured during the course of experimental testing using strain gauges. The benefits associated with the use of strain have been recognised for some time, and a number of failure criteria based on strain have been developed for FRPs, although universal adoption of a single criteria has not yet taken place.

It is with these factors in mind that the characterisation of ultimate laminate strength by normalised unit strength was adopted, in conjunction with the use of strain as a measurement of the instantaneous load placed on the laminate. Consequently, all material testing data presented within this thesis is represented by these descriptors.

2.8 Conclusion

Fibre composites form a group of materials that are unique in many ways. While composite materials have been ever present in various natural forms, FRPs provide an alternative to traditional engineering materials such as steel with significant advantages in some applications. The vast range of reinforcement, matrix, and core types provide an extensive variation in properties, which can be tailored to suit the intended application. The manufacturing processes available for the production of FRPs are also numerous, the product quality of which is primarily dependant on cost.

Due to the orthotropic, non-homogeneous, nature of FRPs, the description of laminate strength must be considered in a different manner to materials that are isotropic and homogeneous. The use of normalised unit strength and stiffness, in addition to laminate strain have been adopted within this project to eliminate the dependence of strength measurements upon laminate thickness.

Cost and public perception remain the two greatest obstacles in the attempt to adopt FRPs into mainstream engineering. It is anticipated that these perceptions will change over time and enable FRPs to compete more closely with steel and concrete.

References

[1] Matthews FL, Rawlings RD. Composite materials: engineering and science. London: Chapman and Hall; 1994.

[2] Schwartz MM. Composite materials handbook. New York: McGraw-Hill; 1984

[3] Lubin G, editor. Handbook of composites. New York; Van Nostrand Reinhold; 1982.

[4] Mallick PK, editor. Composites engineering handbook. New York: Marcel Dekker; 1997.

[5] Barbero EJ. Introduction to composite materials design. Philadelphia: Taylor & Francis; 1998.

[6] May CA, editor. Epoxy resins, chemistry and technology. 2nd ed. New York: Marcel Dekker; 1988.

[7] Lee H, Neville K. Handbook of epoxies. New York: McGraw-Hill; 1982.

[8] Ayers SR, Van Erp GM. Development of a new structural core material for composites in civil engineering. Proceedings of the 16th Australasian Conference on the Mechanics of Structures and Materials; 1999 Dec 8-10; UNSW, Sydney, Australia.

[9] Ayers SR. 2001, Material foundations for the application of fibre composite materials in civil and structural engineering [PhD dissertation]. Toowoomba, Queensland: University of Southern Queensland; 2001.

[10] Beer FP, Johnston ER Jnr. Mechanics of materials. London: McGraw Hill; 1992

[11] Van Erp GM. Flexural behaviour and robustness of fibre composite beams. Proceedings of 2nd International Conference on Mechanics of Structures, Materials and Systems; 2001 Feb 14-16; University of Wollongong: Sydney, Australia.

[12] Van Erp GM, Ayers SR, Simpson PE. Design of fibre composite structures in a civil engineering environment. Proceedings of the ACUN-2 International Composites Conference; Volume 1; 2000 Feb 14-18; UNSW, Sydney, Australia.

[13] Simpson P, Van Erp GM, 1999, Composite materials? The 3000 MPa question. Proceedings of the 16th Australasian Conference on the Mechanics of Structures and Materials; 1999 Dec 8-10; UNSW, Sydney, Australia.

[14] Peters ST, editor. Handbook of composites, 2nd ed. Cambridge: Chapman and Hall; 1998.

[15] Schwartz MM. Composite materials, volume 1: properties, non-destructive testing and repair. New Jersey: Prentice Hall; 1997; ISBN 0-13-300039-7.

[16] Toray. Carbon fibre prepreg [online]. 1998 [cited 1999 July30]. Available from:- http//: www.toray.com/carbon/html/prepreg.html

[17] Abraham D, Matthews S, McIlhagger R. A comparison of physical properties of glass fibre epoxy composites produced by wet lay up with autoclave consolidation and resin transfer moulding. Composites Part A; Applied Science and Manufacturing 1998; 29A:795-801

[18] Van Erp GM, Ayers SR. An alternative system for the structural characterisation of unidirectional fibre reinforced laminae in civil and structural engineering. In: E. Pereloma and K. Raviprasad, eds. Proceedings of Engineering Materials 2001 Conference. Melbourne: The Institute of Materials Engineering, Australasia; 2001.

[19] Van Erp GM, Ayers SR. Development of an australian code of practice for the structural design of fibre composites. In: J.C. Teng, ed. FRP Composites in Civil Engineering. London: Elsevier Science Ltd; 2001.

Chapter 3 An Overview of Steel and FRP Trailers

3.1 Introduction

Technology, innovation and adaptation have all contributed to the diverse range of trailers presently in operation. This chapter outlines the contemporary position of trailer design and manufacture within Australia, by presenting an overview of the various types of steel trailers currently in service. The contemporary uses of FRPs within the automotive industry are also summarised, with particular focus on existing FRP trailers.

3.2 Steel Trailers

The predominance of steel within the context of automotive structures was well established in the 20th century, including application to semi-trailers. This material choice is founded in the availability, predictability, strength, low cost, and manufacturing versatility provided by steel. In addition to these, repair and modifications are easily accommodated, and welding or bolting facilitates assembly.

An extensive variety of trailer configurations have been initiated in order to accommodate payloads of various forms and quantities. The evolution of road regulations governing the size and capacity of trailers has also exerted significant influence in the modification and diversification of trailer types, this being particularly evident when comparing trailers

produced in differing countries. Within Australia, a significant number of steel trailer types exist, the more predominant of which are discussed briefly in this section.

3.2.1 Flat bed Trailers

The flat bed trailer, shown in Figure 3.1, is the most prolific trailer type within Australia at present. The simplicity of these trailers has been the primary contributor to their popularity, as a vast array of payload types and forms are transported by these trailers. This versatility has been responsible for the domination of flat bed trailers in most transportation firms thus far. Under current national road regulations, a flat bed trailer may possess between 31 and 34 m^2 over which the payload can be distributed, depending on the suspension type and number of axles employed.

Figure 3.1 Typical Flat bed Trailer

The chassis layout is generally characterised as a '*ladder frame*'. The two longitudinal members, known as chassis rails, facilitate the primary load carrying. Transverse loading is accommodated by cross members, which connect the chassis rails through perpendicular intersection. A decking is then placed over the frame to provide a continuous loading surface and enable the distribution of point loads. This layout affords comparatively simple construction, and is consequently inexpensive to manufacture. The chassis rails typically take the form of an I-beam, however the beam section does not remain constant. Rather, the web is shaped to produce a reduction in the beam depth at the forward end of the member, enabling a lower centre of gravity of the payload whilst maintaining clearance

between the rear wheels of the prime mover and the trailer. These rails are profile cut from plate steel and welded together while fixed to a jig in order to produce the desired precamber. The cross members typically comprise of standard I-beam sections.

The expected loads upon a trailer determine the number of axles fitted. Both dual and tri-axle groups are fitted to flat bed trailers, with tri-axle groups often incorporating lift-axles.

Greater detail regarding member sizes and capacities is contained in Chapter 4.

3.2.2 Low Loader and Drop Deck Trailers

While flat bed trailers are extremely versatile in the accommodation of various payloads, they are limited predominantly by axle loading and vehicle dimensional constraints. Hence, it is not possible to legally transport payloads that are exceptionally large or high in mass using a standard flat bed trailer. In such circumstances, low loader and drop deck trailers are employed. These trailers possess a lower centre of gravity, thereby increasing cornering stability and decreasing the overturning moment of the trailer. The lower platform also reduces the probability of interference from low bridges or overpasses, and allows equipment to be driven onto the trailer more easily. Extendable platforms are also incorporated into some low loaders to accommodate exceptionally wide payloads.

In order to avoid overloading of the various component of the road, a greater number of axle groups (up to eight) are often employed to distribute the higher loads.

The basic layout of a low loader is similar to that of a flat bed trailer, the primary difference being the addition of a '*gooseneck*' to enable the inclusion of a lower deck height. The chassis rails and cross members are also typically larger to provide additional strength, and wheel diameters are generally smaller to minimise intrusion into the lowered deck.

Construction expenses associated with these trailers are marginally higher as a result of labour costs associated with an increase in chassis complexity. Capital costs are also increased due to the installation of platform extension systems and additional axle groups, in addition to the utilisation of high strength alloys for improved strength.

Figure 3.2 Typical Low Loader

Some inefficiency is inherent in this trailer type, as the presence of the gooseneck significantly reduces the continuous floor space available for payload placement. Additionally, as lift axles are generally impractical due to the lowered floor, increased tyre wear is common due to 'scrubbing' of the outer axle groups during cornering, thereby increasing running costs when the trailer is unladen.

3.2.3 Tanker Trailers

Tanker trailers, as shown in Figure 3.3 facilitate the transportation of liquid or powdered substances. The transportation of gases is achieved by tank pressurisation, so as to compress the gas into a liquid state. Strength to withstand high internal pressure is also required in the unloading of some powered substances, such as cement powder. In such instances, payload deposition is facilitated by pressurisation of the tanker, which induces flow of the product into the appropriate receptacle.

The construction of tanker trailers varies in complexity. Those designed to contain liquids such as petroleum and liquid petroleum gas (LPG) are essentially cylindrical in shape with domed or hemispherical ends. The cylinder is self-supporting, and requires only small sub-frames from which the suspension system, kingpin and skid plate are mounted. Internal baffles are often required to reduce excessive wave motion. Tankers which transport

powderous substances, are often more complicated in structural layout as illustrated in Figure 3.3. The addition of conical outlets on the underside of the cylinder are necessary to assist in the removal of the powder, as the combination of gravity and cylinder pressurisation is insufficient to unload the payload from a single outlet.

Figure 3.3 Tanker Used to Transport Cement Powder

The complex shapes and performance requirements of pressure vessels and the associated quality control all contribute to the high cost of this type of trailer, as do the inclusion of inlet/outlet fittings and high maintenance costs.

Triaxle groups, incorporating the lift axles, are generally used for these trailers.

3.2.4 Tipping Trailers

Tipping trailers are utilised for the transportation of bulk granular materials, including sand or other aggregates and raw produce such as grains and seeds. The rapid deposition of the payload, particularly of aggregates in the genre of road construction, is essential in increasing procedural efficiency. Whilst loading of the trailer is facilitated by heavy machinery such as backhoes, excavators and tippers, or via direct feeding from silos or hoppers, the unloading of the trailer cannot be performed by such means. Due to the

tendency of some granular payloads to resist flow, tipping is necessary to increase the fall angle and ensure complete deposition of the payload.

Initial efforts in tipping containers involved '*solid body*' trucks, which combine the prime mover and trailer into a single unit. More recently, full-length semi-trailers have been employed in this way, and are commonly known as '*tip-over-axle*' trailers.

These trailers possess a sub-frame to which the kingpin, suspension, and the lower end of the hydraulic ram are attached. The container is pivoted about the rear axle, and the upper end of the ram attached to a reinforced section at the front of the trailer, as illustrated in Figure 3.4.

The structural layout of end-tipping trailers is quite efficient. Whilst the tub contains the load, it also provides the majority of the strength and stiffness to the structure. Sub-frames of varying structural capacities are utilised, the construction of which is dependent on the tipping mechanism. Figure 3.4 depicts a split sub-frame, which allows the front section to pivot and provide stabilisation and additional lift to the trailer. Alternately, a rigid sub-frame can also be utilised, which prevents the rear axle group from rotating. Additional length to the lifting hydraulic actuator is then required to produce the correct tipping angle.

Figure 3.4 Tip-over-axle Trailer

The predominant criticism of end-tipping trailers however, concerns the low deposition height of the payload. This necessitates the gradual movement of the trailer in a forward direction during unloading to enable the complete deposition of the payload. In response to this, side-tipping trailers have been developed.

These trailers comprise a flexible metallic bowl mounted on a skeletal steel chassis, as shown in Figure 3.5. In this case, the chassis provides strength to the trailer, and remains stationary throughout the tipping process. The flexible bowl is rotated via hydraulic rams at either end, and rests on the side of the chassis in such a way that the lower edge of the bowl is deformed, forming an angle of approximately 50 degrees to the horizontal at full rotation. The deformation of the bowl and the angle of tipping are such that the payload can be deposited whilst maintaining stability of the trailer at all times.

The rate of deposition is controllable by the angle of rotation. The deposition length and height above ground of this trailer type enables the complete discharge of the payload without repositioning the vehicle.

Tipping trailers generally incur significant expense because of high labour costs associated with the complex chassis and inclusion of the hydraulic lifting system.

Figure 3.5 Side-tipping Trailer

3.2.5 Livestock Trailers

The transportation of livestock is a difficult proposition. The safe restraint of a large number of beasts in a dynamic environment without harm or injury is a formidable task. The complete utilisation of all available space allowed by legislation resulted in the addition of a second floor to these trailers, thereby doubling the number of livestock transported in a single delivery.

The variations in livestock trailers are many, examples of which are summarised in [1]. The trailer shown in Figure 3.6 utilises an independent chassis, which supports a removable crate structure. Other trailer configurations include those which rely on truss structures or shear panels, which form part of the crate walls, to provide strength to the trailer. In such cases, a series of cross members connect the two walls, and support a timber, aluminium or steel floor.

Figure 3.6 Crate-on-Chassis Livestock Trailer [1]

These trailers demand relatively large quantities of labour, and consume a substantial volume of material. It is this high material, in addition to the allowance of volume loading rather than axle-loading limitation for livestock trailers, which has been responsible for the significantly high tare weights of these trailers, some of which exceed 16,000 kg.

The livestock enter the trailer via loading ramps, with the size of both beast and trailer generally determining the number of beasts transported. In essence, the volume of livestock loaded is such that the movement of any one beast is almost entirely restricted by

surrounding livestock. This acts to protect the livestock, preventing falls or injury as a result of trailer movement.

3.2.6 Other Steel Trailers

A number of other less common trailer configurations exist which have not been mentioned here. These include container trailers, designed exclusively to transport shipping containers, or volatile or hazardous materials such as radioactive waste. Refrigerated trailers have been intentionally omitted within this section, as they are discussed in section 3.4.4.

3.3 Tare Weight Reduction of Steel Trailers

Efforts by the heavy vehicle industry to reduce trailer tare weight have been focused in two distinct areas: improved design and structural efficiency, and the use of alternative materials. To increase the clarity of the discussion, the following sections are directly related to flat bed trailers. However, similar observations can be equally made in relation to other trailer types.

3.3.1 Improved Design

Designers of steel trailers have, throughout the last 50 years, learned to optimise their designs by trial and error [2]. This optimisation has been primarily focused on the two chassis rails of the trailer, as they represent the predominant contributors to tare mass. Incremental adjustments to web and flange thicknesses in addition to minor evolutionary changes in chassis rail profiles have been effected over time, however these have yielded relatively meagre reductions in vehicle mass. The difficulties associated with eliminating failures due to fatigue would also appear to have inhibited innovation to some degree.

Perhaps the greatest scope for mass reduction exists in the utilisation of alternate structural configurations, as demonstrated by [1] in the genre of livestock trailers. However, it would appear that there exists reluctance within the industry to investigate the possibility of such alternatives. This is evidenced by the apparent absence of structural innovation within the design of flat bed trailers observed on the roads today. Discussion with trailer manufacturers confirms this assumption. The process involved in the design of 'new' trailers consists of little more than a revision of the previous model and the modification of design faults reported by customers. Further discussion on this is contained in section 4.4.

It would therefore seem that the reduction of the tare mass of steel flat bed trailers through design improvements has been largely abandoned, apart from continuing improvements achieved in an incremental fashion. One would assume this cessation in innovation would indicate that steel trailers, in their current form and configuration, could be considered highly optimised.

3.3.2 Utilisation of Alternate Materials

In conjunction with the iterative process of refinement, the selection of suitable materials has undergone significant investigation. Initial efforts involved the utilisation of high strength steel and selected metal alloys. The increase in material strength enabled a reduction in the size of the load carrying members, thereby decreasing the structural mass. However while the ultimate strength of the trailer remained the same throughout these changes, the use of smaller members reduced trailer stiffness, increasing the effects of fatigue on the structure. Additionally, the materials used are also inherently more expensive than standard grades of steel. Consequently, in order to keep the increased cost in proportion to the magnitude of the mass reduction, only modest improvements in tare weight reduction have been realised in this way.

Similarly the use of metals possessing a significantly lower density than steel in order to reduce tare mass is largely restricted due to economic constraints. However, the use of aluminium as a structural alternative has provided the potential to greatly reduce tare mass without excessive financial penalties, although this has produced varied success. In the United States it has enjoyed application in almost every type of trailer, including flat beds, end tippers, tankers and other specialty trailers. While its comparatively poor fatigue resistance and low modulus excludes it from use in heavy-duty applications such as low loaders, it has provided acceptable performance in lighter-weight equipment hauling trailers. Within the automotive industry, high-strength aluminium, whilst highly priced, has enjoyed extensive use in items such as wheels, doors, hoods bumpers and frames [3].

This success has not been reproduced within Australia however, partially due to differences in operational conditions. The exceptional coverage and condition of the road network across the United States provides relatively few occasions of exposure to poor road surfaces in comparison with trailers in this country. However, such a well-maintained road network does not exist in Australia; consequently the large majority of Australian trailers experience harsh service conditions for the majority of their working life, particularly in remote regions. Additionally, the unsuccessful application of aluminium to trailers can often be attributed to the direct substitution of steel for aluminium, with no modification to the design to allow for inherent differences in their characteristics. The resulting poor performance of these trailers has significantly eroded market confidence in the use of aluminium. Poor fatigue resistance, welding difficulties, higher maintenance and expensive repair have also contributed to the decline of aluminium usage in trailers, such that only end tippers and some tankers remain in production within this country.

The investigation of low density, high strength materials suitable for use in trailers has resulted in the investigation of non-metallic materials such as FRPs.

3.4 FRP Trailers

3.4.1 Introduction

FRPs have experienced extensive application as an alternative material within the automotive context. They provide considerable benefits, particularly in relation to mass reduction, part consolidation, and corrosion resistance. The more significant developments involving the incorporation of FRPs to the automotive and heavy transport industries are outlined within this section.

3.4.2 FRPs in the Automotive Industry

The automotive industry has adopted FRPs to varying degrees since 1950. Initially the reduction of vehicle weight in the interest of reducing fuel consumption was of minimal importance in vehicle design, and FRP usage was confined to external body panelling. However since the oil crisis in 1973, fuel consumption has attracted increasing attention. The continually increasing usage of plastics and FRPs in minor vehicle parts such as fuel tanks and battery boxes has brought some savings in production and weight [4]. FRP leaf springs, cross members, brakes, and drive shafts have been successfully developed, and many other applications are outlined in [4,5,6,7].

Perhaps the most significant application of FRPs within an automotive context is that of the use of carbon fibre in the construction of vehicle chassis' used in competitive motor sport. The high specific stiffness of carbon yields an extremely light yet stiff frame, which is highly resistant to fatigue. Additionally, the use of carbon fibre, particularly in the driver cockpit, has seen a great increase in crashworthiness. The progressive collapse of the composite frame, due to delamination, provides an increase in energy absorption, thereby lessening the impact on the driver [6].

The application of FRPs to mass-produced vehicles is demonstrated in examples such as the Chevrolet Corvette. From its conception in 1953, FRPs were used to form the body panels of the Corvette, which contributed to the high power-to-weight ratio of the vehicle. Until the mid-1960s, the FRP was laid up by hand. SMC (refer to section 2.6.9) replaced this

time-consuming method, and has been used successfully to this day. Further examples of FRP use in passenger vehicles are discussed in [4].

3.4.3 Prime Movers

The application of composites to prime movers has existed for some time. Chopped strand matting in conjunction with a gel-coat, has been used extensively as paneling for prime movers. The stiffness of the CSM panel is comparable to the equivalent steel panel at a reduced weight. The gel-coat, a resin rich layer at the surface of the laminate, provides a cosmetic appearance comparable to a sheet steel equivalent. However apart from external paneling, the prime mover has not undergone any major investigation with respect to mass reduction. This is because a reduction in the mass of the prime mover would primarily reduce the load on only the front axle, and hence would not reduce the load on any of the axle groups supporting the payload. While minor savings may be realised through a slight reduction in fuel consumption, reduced load on the front axle may lessen the steering and handling stability of a fully laden vehicle. The potential for significant weight saving therefore rests with improvement of the trailer.

3.4.4 Refrigerated Trailers

FRPs have experienced extensive use in refrigerated trailers for a number of years. The high specific strength of FRPs, combined with the excellent insulation characteristics of sandwich panel construction, has been the primary contributor to the success of this type of trailer.

The structural layout of a typical refrigerated trailer consists of four FRP sandwich panels connected along their edges to form a hollow box section. The joints consist of extruded aluminium sections, which are riveted to the panels. This box section construction provides excellent structural efficiency, thereby eliminating the need for a steel supporting chassis. However as with end-tipping trailers, a small steel sub-frame is typically utilised to attach the skid plate and suspension system to the trailer.

A typical wall cross-section usually consists of polyurethane foam, combined with E-glass in the form of a double-bias weave and CSM. The foam acts as an excellent insulator, and the structural efficiency of the box section requires only thin laminates, thereby allowing the use of a relatively low strength, low cost CSM reinforcement without substantial increases in mass.

However, investigation into the reduction in tare mass of refrigerated trailers has been undertaken. A refrigerated trailer was developed by the Dutch trade organisation for the coach building industry (FOCWA). A prototype, shown in figure 3.7, was built by 'Burg Carrosseriebouw' (located in Pijnacker, the Netherlands), and was released in February, 1996 [8]. This project aimed to reduce the tare mass of the trailer by 30% through utilisation of a number of techniques and materials that had not yet been applied to refrigerated trailers. Aramid and carbon fibres were used in preference to E-glass, and high strength PVC foam was used as a core material. A lowered floor increased the depth of the box section, improving strength. This trailer also substituted a number of steel members for carbon fibre members, further reducing tare mass. The economic viability of this trailer was investigated, and it was shown that the extra purchase cost could realistically be regained after 2.5 to 4 years of service. The 2.5-year estimate allowed for large-scale production techniques. Upon completion, the mass of this prototype was measured to be 6,490 kg, a reduction of 2,700 kg (30%) in the tare weight of a typical refrigerated trailer.

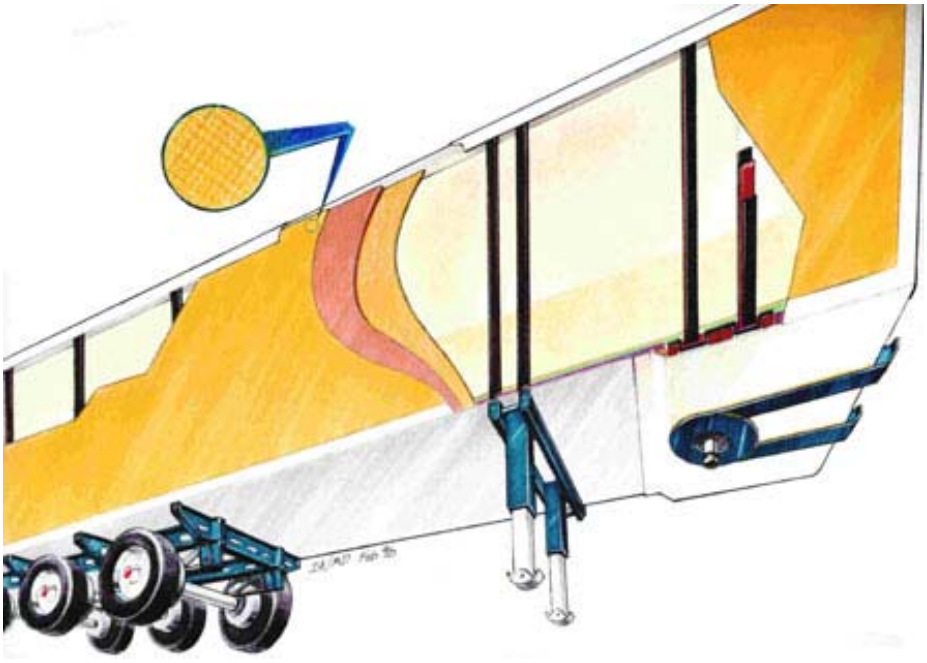

Figure 3.7 Cut away of FRP Refrigerated Trailer (Source: [8])

3.4.5 Flat bed Trailers

The widespread popularity of flat bed trailers has encouraged the application of lightweight materials, with the promise of a substantial market share to the successful developer.

Within the United States, a number of 'composite' flat bed trailers have been commercially produced. Many of these 'composite' trailers are in fact metal hybrid trailers, constructed from steel and aluminium, such as those produced by East Manufacturing. This particular company produces a hybrid flat bed trailer which consists of an aluminium hollow core deck extrusion mounted on bi-metal chassis rails, and tubular cross members.

However, flat bed trailers that comprise of FRPs have also seen commercial reality within the United States. Since the mid-1990's, Trail King, in conjunction with TPI Composites, have produced two different versions of a 48-foot FRP flat bed trailer. The first trailer, a steel/FRP hybrid, retained a steel frame and used FRPs for decking, skirting and various other items, reducing the tare mass by a relatively small percentage. This trailer represented a more conservative approach, as steel members facilitated the primary load carrying.

The second trailer, shown in Figure 3.8, involved the removal of all remaining steel members from the trailer chassis, yielding a trailer consisting entirely of FRPs, with the deck and beam grid impregnated with resin in a single process. The trailer used E-glass, S-glass and carbon fibre reinforcement set in vinylester resin, being supported by Baltek (balsa) and Nida (polypropylene honeycomb) core materials. Further structural and design details were unavailable due to issues of confidentiality.

However, the author was made aware of various failures of this second trailer. The nature of these failures appeared to be punching shear of the balsa core in the decking. More detailed information was unavailable, as only a limited number of these trailers were commercially produced. The magnitude of the tare reduction achieved through this design was not disclosed.

Figure 3.8 Trail King Trailer (Source [10])

3.4.6 Tanker Trailers

Another successful application of FRP to trailers can be found in tanker trailers. A market of substantial size exists for the transportation of fluids, including chemicals, waste substances, bulk materials such as fly ash, and various foods and liquids for human consumption. However, FRPs were not initially introduced to reduce tare mass, but rather to improve chemical resistance. Hence while the strength of FRPs enables an economical yet comparably strong structure, it also provides a product which is impervious to most chemical attack. These tankers are filament wound (see section 2.6.7), as their shape is essentially cylindrical.

There are currently a large number of FRP tankers in operation throughout the world. These tankers are typically constructed from E-glass and vinylester or epoxy resins. Efforts to reduce tare weight of these trailers have also been undertaken through the use of alternate reinforcement types. In 1994, Boerman Transport (the Netherlands) in conjunction with Akzo Nobel produced a FRP tanker based on an aramid fibre reinforced vinylester resin, as shown in Figure 3.9.

The use of FRPs in the tank section of this trailer reduced the mass of the previous tank by 25%, and produced a total tare mass saving of 400 kg. The tank of the trailer was supported during transportation by a steel chassis and cradle, and only during unloading was the tank required to support itself, as demonstrated in Figure 3.9. The experimental testing performed during commission of this trailer is discussed in section 4.3.2.

Figure 3.9 Twaron Reinforced Tanker

3.4.7 Tipping Trailers

FRP end tippers have also been constructed, with the first of its kind designed and built in Australia several years ago. The tipper, shown in Figure 3.10, utilised the tub to provide structural strength and stiffness, and was complemented by a steel sub-frame to which the suspension, kingpin and lifting ram were attached. A closed cell foam core, approximately 27 mm in thickness, was covered on each side by a single layer of quad-axial E-glass. Additional reinforcement was placed around the area of the lifting ram.

Unfortunately, this particular trailer failed catastrophically during initial testing. Discussion with the designers suggested that the incorrect conveyance of information resulted in the reduction of the sidewall height without the inclusion of additional reinforcement to compensate the loss in wall strength. The consequent failure of the trailer resulted in the abandonment of the project through a lack of sponsor confidence.

3.4.8 Other FRP Trailers

Stevens of Lokeren, Belgium, have developed a number of composite trailers, including a potato carrier; a high volume trailer with moving floor, and a platform trailer, designed to carry felled timber. The platform trailer was constructed using pultruded beams, with the glass reinforced isophthalic sections being bonded together using epoxy adhesives [9]. Road testing of each of the trailers was apparently successful, however large deflections were observed during testing of the platform trailer, and will be discussed further in Chapter 4. Further detailed information regarding these trailers was unavailable due to confidentiality.

Figure 3.10 FRP End Tipper

3.5 A Small-Scale FRP Semi-Trailer

As part of the initial investigation by the author into FRPs and their potential in transportation, the design, manufacture and testing of a small-scale, flat bed trailer was undertaken. The small scale of the trailer reduced the cost of the exercise, while providing insight into potential advantages and disadvantages. This was initiated as a learning exercise, designed to provide a greater appreciation of the practical application of fibre composites.

In order to gain maximum insight from the prototype, the trailer configuration was designed to replicate a steel, flat bed trailer to the greatest extent possible. A trailer approximately equivalent in dimensions to a standard car trailer was chosen, as this was judged large enough to enable sufficiently high loads to be applied to the structure without difficulty, whilst reducing the financial costs.

In addition to the minimisation of tare mass, one of the primary objectives of this trailer involved the elimination of mechanical fasteners required for assembly. Due to the sensitivity of FRPs to stress concentrations caused by the insertion of fasteners through the laminate (refer section 7.7), a structure that is independent of mechanical fasteners renders these characteristics inconsequential.

3.5.1 Beam Profile

It is widely recognised that an I-beam cross section provides exceptional characteristics in relation to structural efficiency. However, the utilisation of FRP I-beams in this application was neither economically nor practically feasible. Such members require manufacturing methods such as pultrusion, which is not viable on such a small production scale. However, the fundamental principle of an I-beam was maintained by an alternative method of construction.

The beam developed for this trailer is illustrated in Figure 3.11. Each beam comprised a sandwich panel subjected to in-plane loading. This panel was employed to perform the role of the beam web, separating the flanges and providing shear strength. Balsa wood and double bias E-glass were used as the core material and web reinforcement respectively.

The flexural strength of the beam was accommodated by the addition of 'end caps'. These caps were manufactured by draping unidirectional E-glass over the ends of the panel, with the reinforcement aligned longitudinally with the beam axis.

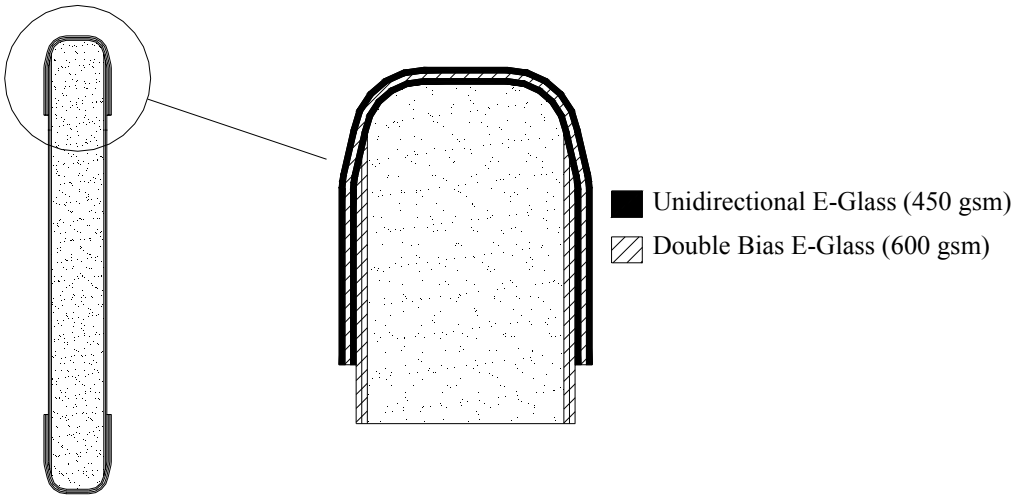

Figure 3.11 Beam Construction of Small-Scale FRP Trailer

A reduction in beam depth, denoted as the beam '*neck*' (refer section 6.3), was incorporated into the chassis rails in replication of a steel counterpart. Additional reinforcement was placed in this region to reduce the effects of resulting stress concentrations.

The effective elimination of mechanical fasteners was realised by the adoption of a modular approach. The modular construction involved removing sections of the web from the chassis rail to accommodate the insertion of the cross members. Notches were cut into the top flange of the cross members (see Figure 3.12) to allow location and partial restraint of the member. Connection of the cross members to the chassis rails was accomplished by insertion through the gap in the chassis rails in a diagonal manner. The cross members were then rotated to an upright position, providing a semi-stable structure. The remaining gaps in the web of the chassis rails were then filled by the insertion and adhesive bonding of a sandwich panel of identical construction to the web, thereby fixing the cross members in place.

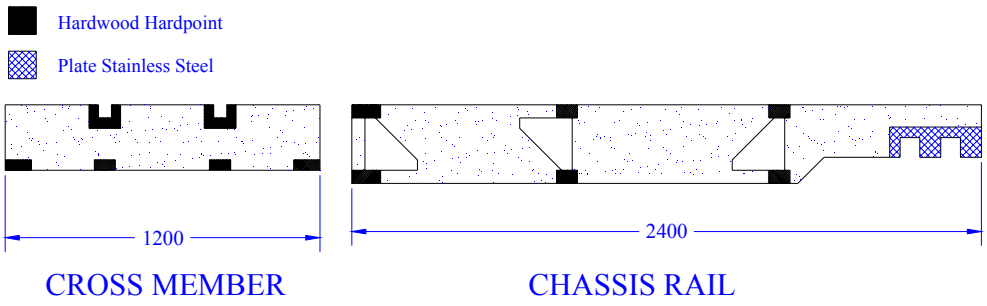

Figure 3.12 Member layout with hard point placement

Hardwood hard points were inserted into the balsa core at each bearing point, as illustrated in Figure 3.12. Two stainless steel plates, 5 millimetres in thickness, were also inserted between the core and shear laminates on the chassis rails at the front end of the trailer. These plates were introduced in the region of the hitch connection point to aid in the transfer of the load from the chassis to the hitch.

The trailer deck comprised a balsa core (10 mm in thickness), reinforced with a single layer of double bias E-glass and epoxy resin on each side. This deck was adhesively bonded to the chassis. Identical panels were bonded to the sides of the trailer to protect the ends of the chassis rails and improve the aesthetic appearance.

In order to prevent racking (the relative movement of the chassis rails in a longitudinal direction), additional panels were bonded in place as shown by the shaded regions in Figure 3.13.

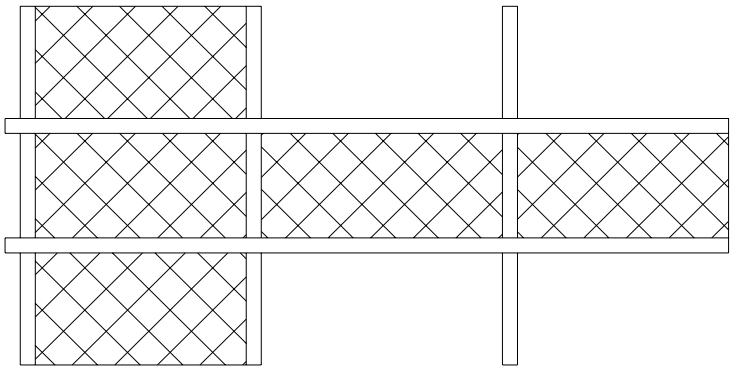

Figure 3.13 Placement of Diaphragm Panels in Completed Frame

After assembling the trailer, the frame was weighed and found to have a mass of 60 kg.

3.5.2 Suspension and Hitch

Due to the small scale of the trailer, it was not possible to replicate the suspension systems employed on a steel semi-trailer. As no suitable suspension of an appropriate scale was available, a leaf spring suspension system was selected, as is typically found on box trailers of this size. Stability dictated that the suspension be mounted at the outer most ends of the cross members, rather than directly beneath the chassis rails as found on semi-trailers. This was achieved using purpose built spring hangers.

As the trailer was to be towed by a passenger vehicle fitted with a standard tow ball, the use of a skid plate and kingpin was impractical for articulated connection. Consequently, a hitch and dolly constructed from mild steel were designed to provide towing characteristics similar to that of a semi-trailer. This link was designed to allow rotational freedoms similar to those provided by a standard king pin and skid plate attachment. The hitch point was adhesively bonded to the chassis rails.

3.5.3 Validation of Structural Characteristics

Subsequent to initial design calculations, a finite element representation of the trailer was created in order to assess structural performance. Direct comparison between the characteristics of the model and the structure would also provide insight into the validity of the model construction.

However, this analysis was solely intended to be preliminary in nature, as this trailer was not representative of any proposed full size trailer. Consequently, only a limited amount of detail on the analysis is presented. Two-dimensional layered plate elements were used in representation of the structure as illustrated in Figure 3.14 and 3.15. Linear-static analysis was performed using STRAND v6.1, with material properties taken from specimen testing results generated internally at the USQ.

The loading scenario chosen to validate the finite element model is represented in Figure 3.16. The load was applied through a horizontally positioned beam placed midspan, and while this load case represents a worst-case scenario, it enabled simplification of the testing procedure. A load of 20 kN was placed on the trailer, as this is representative of 100% of the static load capacity (800 kg) with a dynamic load multiplication factor of 2.5.

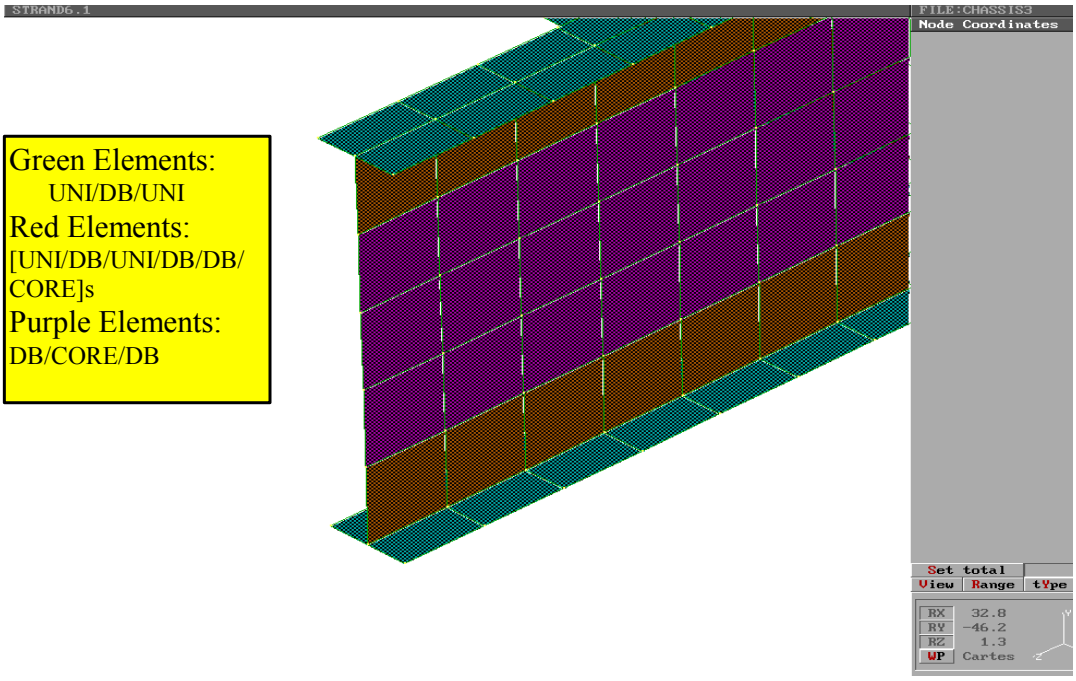

Figure 3.14 Beam Representation with 2-D Layered Elements

The suspension was removed and replaced with a beam, pivoted about the midpoint to ensure load sharing between cross members.

A comparison of the experimental results and the finite element analysis can be seen in Figure 3.17. The discrepancy between the calculated and observed values of deflection observed is reasonable, due to the stiffening effect of the deck and diaphragm panels, which were not included in the finite element analysis. The increased deviations observed at the rear of the trailer occurred due to flexure of the supporting beams.

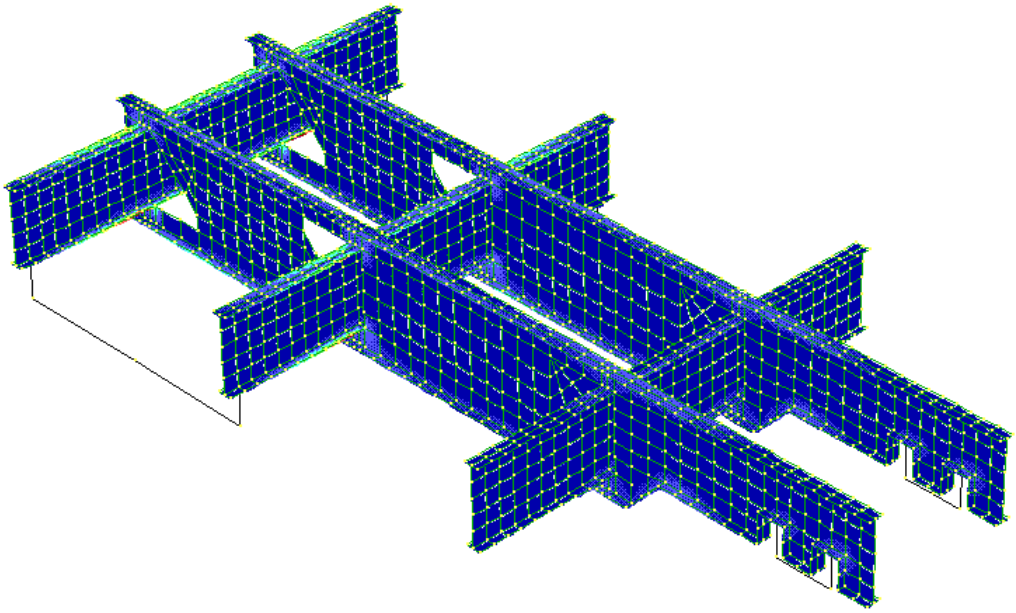

Figure 3.15 Finite Element Representation of Small-Scale Trailer

3.5.4 Dynamic Field Testing

The loading of the trailer in a dynamic environment represented the final method of structural evaluation. This was undertaken by towing the trailer over a series of obstacles and sections of harsh terrain whilst loaded to prescribed percentages of the maximum load capacity.

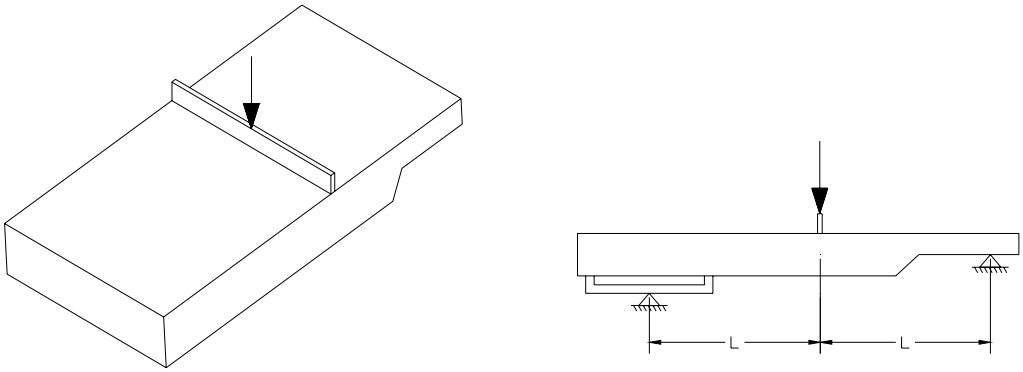

Figure 3.16 Experimental Test Configuration of Small-Scale Trailer

The trailer was initially loaded to 100% of its 800 kg (maximum) load capacity, and led through a designated course at speeds that maintained load stability. Visual inspection following this test detected no indications of laminate damage or failure.

This test was then repeated whilst loaded to 125% of the load capacity. This also proved successful, as the trailer withstood all testing without any signs of excessive strain.

Increasing the payload further for subsequent testing was not possible due to the limited capacity of the suspension system.

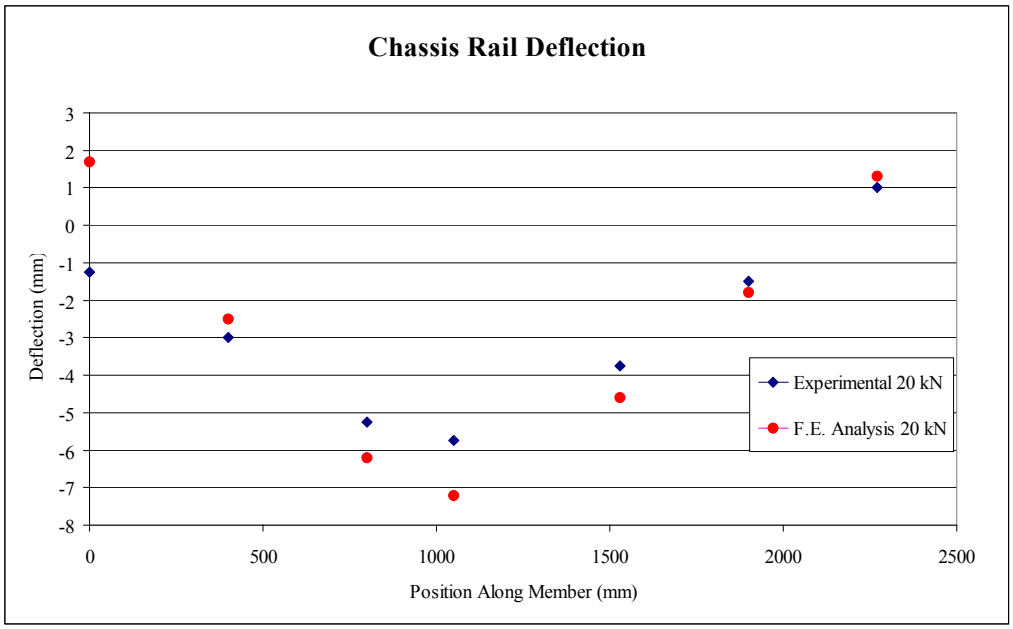

Figure 3.17 Comparison of Predicted and Experimental Structural Characteristics of Small-Scale Trailer

3.5.5 Conclusions

This trailer represented the first step in this investigation towards the evaluation of fibre composites within transportation. The minimisation of tare mass was successfully achieved, and the elimination of mechanical fasteners was completed by utilisation of an interlocking design approach. This trailer demonstrated the potential of the modular approach, which warranted further consideration in the conceptual design phase described in Chapter 6.

The use of end-grain balsa as a core material provided an extremely lightweight and efficient structure. However the primary shortcoming of balsa resided in a low transverse compressive strength. This necessitated the use of hard points to spread concentrated loads, thereby introducing additional manufacturing difficulties. Additionally, the balsa proved vulnerable to impact and bearing damage. This was highlighted in the deck of the

trailer, which was accidentally damaged on a number of occasions by relatively insignificant incidents.

These shortcomings highlight the need for a core material possessing a greater resistance to crushing under concentrated loads without a substantial increase in material density. The selection of a suitable core material is discussed further in Chapter 5.

The inclusion of a simplified beam neck highlighted the need for further detailed design in this area. The layout of this neck however, would be essentially dependent on the conceptual design chosen for further investigation. The analysis and experimental testing of these neck sections are discussed in Chapter 7.

Despite the shortcomings and difficulties associated with this initial trailer, the potential of FRPs to produce a low weight trailer was successfully demonstrated. With a mass of 60 kg and a payload capacity of 800 kg, this trailer provided the impetus for further research into FRP trailers.

3.6 Selection of Trailer Type

This research initially intended to investigate the feasibility of a FRP side-tipping or tanker trailer. Wagners Transport Pty. Ltd., sponsor to the project, expressed great interest in the specific development in this direction, as these two trailer types offered the greatest financial advantage for the company.

However after careful consideration, it was decided that a flat bed trailer would form the focus of this research. The elementary layout of a flat bed trailer provides the greatest opportunity to establish the fundamental elements of trailer design. With so little known about the use of FRPs as major structural components within the transportation industry and with so few examples to learn from, it follows that the most basic and fundamental design should form the initial attempt. The widespread use of flat bed trailers also ensures that the philosophy established by this research is of greatest benefit to the industry.

References

[1] Hall D, Walsh P, Lapworth J, Roufaeil Dr. O. Low tare weight livestock trailers. Final Research Report to Meat Research Corporation; December, 1993; Project DAQ.60.

[2] Harris MN, Nawrocki PE. Design analysis for heavy duty vehicles – today and tomorrow. Int. J. of Vehicle Design 1984; 5.

[3] Mabley ET. Truck design for the 1990s (Truck Engineering Supplement) Automotive Engineering; Society of Automotive Engineers; Nov 1989; 97(11); pTE9(9).

[4] Maxwell J. Plastics in the automotive industry. SAE international; Cambridge, England: Woodhead Publishing Ltd; 1994.

[5] Mallick PK, editor. Composites engineering handbook. New York: Marcel Dekker Inc; 1997.

[6] Strong AB. Fundamentals of composites manufacturing: materials, methods, and applications. Society of Manufacturing Engineers; Michigan: Publications Development Department; 1989.

[7] Swanson SR. Introduction to design and analysis with advanced composite materials. Upper Saddle River, New Jersey: Prentice Hall; 1997.

[8] Design of an ultra-lightweight composite semi-trailer [online] 1996 [cited 1998 September 18]. Available from: http://www.clc.tno.nl/projects/recent/trailer.html.

[9] Truck's composite chassis takes the load. Reinforced Plastics; 2000 March: 58,59.

[10] Flat bed trailer wins SPI honours. Reinforced Plastics; 1993 April: 26-30.

Chapter 4 A Design Philosophy for FRP Semi-Trailers

4.1 Introduction

Design philosophies, methodologies and standards form the foundation of many engineering applications. However, in contrast to the design processes used in civil or aeronautical engineering fields, the design of semi-trailers has relied primarily on experience and trial-and-error. The conspicuous absence of design criteria in this application resulted in the evaluation of research performed in regard to the design of semi-trailers and attempts to describe their behaviour when subjected to varying conditions. A review of the literature is summarised in this chapter, in an attempt to quantify current knowledge in relation to trailer design. This is followed by an assessment of steel trailer design techniques provided by discussion with trailer manufacturers. Significant load cases are defined, and moment and shear envelopes are produced for application in fibre composite, flat bed trailer design. A comparison of design criteria between steel and FRP trailers is made, and the dominant criteria are identified for consideration in FRP trailer design.

4.2 Industry Design Standards

While the heavy transportation industry in Australia has existed for decades, it may reasonably be considered relatively embryonic with regard to formal engineering development. This is reflected in the low number of structural design standards relating to trailers, both in Australia and throughout the world.

Australian Standards (AS) which address heavy vehicle design include AS 4235-1994 [1] which makes provision for the attachment of the kingpin and skid-plate, while Australian Design Rules such as ADR 42 and 43 [2] address the standing legs and axles. Standards that directly relate to the chassis of the trailer, such as ADR 13 and 42 [2], simply state the position of marking lamps, and establish the general dimensions of the trailer. However apart from the aforementioned guidelines, there exist no standards that dictate strength or load capacity requirements for any trailer type.

Extensive investigation by the author failed to identify any equivalent standards or guidelines in place throughout the United States or Europe. However a number of specialised standards do exist, formulated to address specific trailer types which demanded attention due to the nature of the payload. One standard developed for the design of pressurised tanker trailers in the United States borrows from the American Society of Manufacturing Engineers (ASME) standard Section VIII Division 1 [3] which provides pressure vessel specifications. Perhaps the most significant standard suitable for application in this research was developed for the highway transport of weight-concentrated radioactive loads by the American National Standard Institute. This standard, ANSI N14.30-1992, explicitly defines both the strength capacities and dynamic design factors (DDF) to be incorporated into the design process. Specifically, the standard states that all structural members should be designed to withstand a static load of 2.5 times the maximum load of any load case, or the product of a cyclic fatigue factor (1.2 as a minimum) and DDF (1.7) multiplied by the static load: which ever is the greater [4].

The existence of this single design standard, which addresses the strength capacity of a single specific trailer type, highlights the sparsity of engineering development in this area. Unfortunately, this standard is somewhat insufficient for use in the context of this research due to the specific application considered in this thesis. More specifically, it fails to address the definition of load cases to which the specified loading factors must be applied, and does not specify the required stiffness of the trailer.

The apparent absence of standards relevant to flat bed trailer specification compelled the author to seek alternative assistance in design. Assistance was therefore pursued from sources outlined in the following sections in order to identify design parameters suitable to FRP flat bed semi-trailers.

4.3 Literature Review

A review of available literature regarding heavy vehicles was undertaken in order to ascertain an accurate assessment of current knowledge regarding the structural characteristics and behaviour of semi-trailers in general. In particular, it was anticipated that simulations of heavy vehicle systems would provide quantification of the loads imposed on the trailer during typical service conditions, particularly the effects of the maximum stresses imposed on the trailer by dynamic loading. The definition of these loading conditions would hence provide a foundation for the establishment of trailer design load capacities.

The research community has endeavoured to mathematically describe the behaviour of most of the major aspects of trailers. The complex nature of a dynamic system such as an articulated vehicle demands investigation of a plethora of characteristics, both individually and collectively. Each of the aspects on which data has been published is addressed below to provide an overview of the current state of understanding with regard to trailer behaviour.

4.3.1 Vehicle Dynamics

This section outlines the predominantly theoretical research describing the dynamic behaviour of articulated vehicles. Experimental testing programs are discussed separately.

The investigation of vehicle dynamics presents great difficulties. It involves the use and manipulation of complex models with many degrees of freedom. System non-linearity further increases solution difficulty. While linearisation of some problems may lower the degree of difficulty somewhat, this simplification is not widely accepted as an accurate means of obtaining reliable results.

Bernard, Vanderploeg and Shannan [5] and Shaw [6] have carried out extensive literature reviews of advances in vehicle dynamics since the 1960's. A noticeable increase was observed in the latter review in the focus on areas such as suspension, road roughness and tyre modelling throughout the last decade.

Ellis [7], Gillespie [8] and others have derived a number of simple equations describing vehicle dynamics, and many similar equations have been available for some time. Such equations are simplified however, and restrict the model to only a few degrees of freedom

and small displacements. More complex equations of motion require computer assistance because of the large matrix manipulation required to cater for the number of degrees of freedom. The majority of research conducted into the dynamics of heavy vehicles revolves around five distinct areas:

1. The static and dynamic simulation and optimisation of chassis frames, typically utilising finite element techniques.
2. The prediction of a truck-trailer response to driver inputs such as braking and cornering.
3. The assessment of ride quality and its effects on driver fatigue and performance.
4. Estimation and prediction of the effects of heavy vehicles on road surfaces and bridges.
5. Modelling of heavy vehicle components, particularly suspension systems and tyres.

Each of these areas is addressed separately, with the relevance to this research highlighted at the conclusion of each section.

Static and Dynamic Simulation and Optimisation

A small volume of information exists regarding the analysis of several types of vehicle frames subject to various static and dynamic conditions. It was anticipated that this area would contain the most directly applicable data for design, as the focus of the work in this area primarily centres around the design and evaluation of efficient chassis structures.

Beermann [9] presents a hybrid analysis method, combining analytical and finite element techniques, in an examination of ladder frame joints. The rigid connection of open section beams and the prediction of the joint flexibility is analysed with this method and compared with experimental results.

Mills and Johnson [10] describe the creation of a finite element idealisation of a solid-body truck frame. Deflections experienced by the actual structure, when subjected to various static loading conditions were compared with this model. Good agreement was observed for out-of-plane and torsional loads, however in-plane loads produced significant discrepancies due to the exclusion of elastic buckling in the side members.

Mills and Sayer [11] conducted similar analysis on an integral construction, light van body. Static tests including torsion and bending were performed on the van body, and

compared with two half-structure finite element models, the second possessing greater refinement and providing greater agreement. The van body was also dynamically excited in order to expose the first 10 natural frequencies. While the second finite element model again predicted the mode shapes of the van more accurately, both models were shown to over-estimate the stiffness of the structure.

Using an equivalent linearisation technique, El Madany [12] investigated the dynamic interaction between an articulated vehicle and an irregular road surface. A number of effects influencing ride comfort and road safety were evaluated, including road characteristics, load condition, and vehicle speed.

Gadala et al. [13] compare an analytical and finite element model of a articulated heavy vehicle traversing a random road surface. Stationary Gaussian random excitations were used to describe the road surface. This paper compared the results from two separate models. An analytical model was developed, approximating the trailer as a rigid body with equivalent mass and inertia properties positioned at its centre of gravity. The finite element method was composed of three-noded isoparametric elements, and represented the trailer as a flexible beam with lumped masses at several discrete intermediate points. A difference of 8% was observed in the natural frequencies of the two systems, each representative of an unladen trailer. The mode shapes determined by the finite element model were also presented.

Besselink and Van Asperen [14] describe the optimisation of the linear dynamic behaviour of commercial vehicles. The presented technique was designed to identify suitable values for specific constraints that would produce an optimum solution in relation to a specified objective. The example presented considered the impact of a number of variables on driver comfort. A sensitivity analysis, using LaGrange multipliers, was also presented.

Sharman [15] and Megson [16] have investigated the torsional performances of trailer chassis. Sharman considers the effect of cross-sectional shape variations on two simplified chassis models. Four types of torsional loading were defined, and addressed with respect to weight minimisation and maintenance of acceptable stress levels. Megson proposes a method for the determination of torsional stiffness of a semi-trailer chassis. Both open and closed section cross members are addressed in connection with open section chassis rails. Good correlation was shown in the prediction of stresses and displacements.

Unfortunately, none of the aforementioned studies address the implications of dynamic loading on the levels of stress within the respective chassis'. While the dynamic response of various chassis frames was addressed, these studies focused on ulterior issues such as natural frequency response and driver comfort.

Prediction of Truck-Trailer Response to Driver Input

The dynamic behaviour of articulated heavy vehicles has attracted much attention, predominantly from a safety viewpoint. In particular, the prediction and control of heavy vehicles subjected to various conditions has undergone significant investigation. A selected portion of literature published on this subject is presented in this section, as this subject is of some relevance to the research topic (refer to Section 1.4). Further references can be found in [6], [17], [23], and [25].

Starr [18] presents a design system used in the prediction of lateral stability of towed heavy vehicles. This paper considers the ability of the tow vehicle to recover from various braking conditions in a stable manner.

Tabarrok and Zhang [19] have developed a full non-linear yaw-roll-pitch model of the dynamics of log hauling trucks, based on Kane's equations. Similarly, Ali Attia [20] presents the transient dynamic analysis of a vehicle model. A two step transformation is used to form the equations of motion, and the results of the simulation reveal the simple and general nature of the equation formulation.

Hecker et al. [21] presents the Vehicle Dynamics Control (VDC) for commercial vehicles developed by BOSCH. They demonstrate the use and effectiveness of VDC for commercial vehicles in different critical driving situations.

Sayers and Riley [22] describe popular numeric multi-body programs such as ADAMS and AUTOSIM. Such software is capable of simulating the dynamic response of various articulated vehicles in response to steering and braking manoeuvres, and is used to evaluate the stability of a vehicle combination in collision avoidance scenarios.

Many passenger vehicle manufacturers have also developed their own software, capable of detailed analysis of vehicle dynamics. However, these programs are neither publicly or commercially available.

Due to the focus on the stability and directional response of the vehicles, this area of research yielded little relevant information in regard to the design of heavy vehicle chassis'.

Ride Quality Assessment and Driver Fatigue

The study of the dynamic behaviour of articulated heavy vehicles with respect to driver comfort appear to have been undertaken in an attempt to improve productivity and alleviate driver fatigue associated with poor ride quality.

Wang and Hu [23] present an analytical model for the evaluation of ride quality of an articulated heavy vehicle moving over an irregular road surface. The vehicle model possessed nine degrees-of-freedom, and a stationary ergodic Gaussian random road profile provided the displacement input. The frequency response was determined at the driver's seat, and the ride quality compared with the relevant international standard. The ride quality experienced by the payload was also briefly addressed.

Similarly, the longitudinal, vertical and pitching motions of an articulated heavy vehicle were described by computer simulation by Dokainish and ElMadany [24]. A 'man-seat' model was incorporated into the simulation, and the response of this when subjected to various road conditions is also compared to the ISO riding comfort standard. Both laden and unladen conditions are considered, and the simulation indicated that an uncomfortable ride would result from the vehicle model in all conditions.

Further simulations of driver ride quality include a 17 degree-of-freedom model presented by Zhou [25], which utilises a statistical linearisation technique.

It was hoped that this area of research would include further information on the role of the payload, including the effects on the payload due to the dynamic response of the trailer. However, there did not appear to be any significant attention given to payload response, and no data was found to be applicable to trailer chassis design.

Effects of Heavy Vehicles on Roads and Bridges

The investigation into effects of heavy vehicles on road surfaces was primarily initiated by road authorities, to enable the determination and assessment of axle load limits and to assist in the reduction of road surface damage and repair. It was hoped that this area of research would include some information on the effects of wheel loadings on the trailer chassis.

El-Gindy [26] presents a set of performance measures in relation to vehicle safety in order to control the dynamic quality of heavy vehicles on an individual basis. A proposal involving the marriage of particular truck-trailer combinations is suggested, based on the matching of dynamic characteristics of both vehicles.

The estimation of wheel loads has been observed and addressed by a number of authors. Karamihas and Gillespie [27] presented a pitch-plane model for articulated heavy vehicles with emphasis on suspension and tyre modelling. The dynamic loads resulting from road roughness inputs were evaluated and transformed into stress values imposed on the surface of pavement structural modes.

Potter et al. [28] presents a similar paper, focusing on the damage caused to road surfaces from measured dynamic tyre forces.

de Pont [29], presented an assessment of 'road-friendly' suspension systems, through the use of two-post, servo-hydraulic facility. A series of tests were performed on a full trailer fitted with multi-leaf spring suspension. The same vehicle was then fitted with airbag suspension and the tests repeated, thereby providing a direct comparison between the two suspension systems.

Sweatman [30-32] has completed much of the initial research within Australia involving the impacts of various axle, suspension and tyre configurations on road surfaces. Continuing investigation in this area has resulted from the increased usage of airbag suspension systems. Reports produced by the National Road Transport Commission (NTRC) [33], the Australian Road Research Board (ARRB) [34] and Roaduser International Pty. Ltd. [35,36] have comprehensively investigated the effects of trailers fitted with airbag suspension on road surface in comparison with spring suspension. The results of this research have resulted in the increasing of axle load limits for 'road friendly' suspension (refer to Section 4.5.1) introduced recently within Australia.

The impact of heavy vehicles on bridges has been investigated by Miller [37]. An analytical model was developed for the description of the dynamic behaviour of a bridge-vehicle system in both two and three dimensions. The model was compared with field tests which involved an in-service bridge and a heavy vehicle under controlled conditions.

Weissmann and Harrison [38] discuss the impact of a 44 tonne tri-axle semitrailer truck on bridges in the urban and rural U.S. interstate system. Li et al [39] present a model for analysis of bridge vibration and impact due to vehicles moving on irregular bridge decks.

Although this is not a comprehensive review of research in this field, none of the studies reviewed in this section address the implications of dynamic wheel loading on the levels of stress within the chassis, as the focus remained on the force imposed by the tyre to the road or bridge. These studies did not provide adequate information regarding the configuration of the trailer and suspension system to be useful in determining the loads on the trailer, and hence they provided no assistance in regard to chassis design.

Suspension and Tyre Modelling

The accurate dynamic description of any vehicle system is predominantly determined by the accuracy of the suspension system representation. While the research field would appear to hold minor significance in the determination of a dynamic design factor (DDF), it was addressed in search of information regarding the transfer of dynamic loading from the road surface to the trailer chassis. More complete reviews of suspension and tyre models can be found in other references including [6] and [37].

It appears that the wide variation in the configuration of suspension systems currently found on commercial vehicles has provided some difficulty for those investigating the performance of heavy vehicle suspension systems. This diversity, illustrated by Sweatman [31,32], has hindered the concentration upon any one particular suspension configuration by the research community. As a result, there appears to be no accepted method of analysis of a given suspension system, nor is there any single set of standard equations which has been adopted to reliably model the behaviour of a given suspension configuration.

Page [40] investigated the dynamic loading and behaviour of a single axle vehicle suspension using a quarter truck model. A non-linear spring stiffness was included, and the model was analysed in the time domain using a Runge-Kutta technique. Reasonably good correlation was found between theoretical and experimental results, and the tyre stiffness was shown to dominate the severity of initial peak dynamic loads experienced as the vehicle negotiated an irregularity. A number of steel spring suspension configurations were modelled by Sayers and Gillespie [41,42]. The leaf springs were linearly approximated, however the loading and unloading curves were described by differing stiffness values. A

time domain analysis was used, and the results provided reasonable agreement with experimental data.

A comparison between the linear and non-linear representation of leaf springs is presented by Kunjamboo and O'Connor [43]. Both linear and non-linear models were used to describe the behaviour of a steel spring and tyre. This experiment was performed on a spring comprising a main spring of fourteen leaves, and an auxiliary spring of four leaves, and was included in a simplified two-mass system, which represented a suspension spring and tyre system. Load-deflection curves of the spring and the tyre were devised through experimental testing, and polynomial equations were fitted to the resulting loading and unloading curves. These equations were used to represent a non-linear model of the system. These polynomials were then simplified to a linear approximation. A comparison of the two models revealed that the non-linear models for both the spring and tyre provided good correlation with experimental behaviour. While linearisation of the tyre characteristics was shown to provide only slightly less satisfactory results, the linear representation of the spring resulted in significant degeneration in accuracy.

The loss of accuracy resulting from linearisation of suspension systems is also reported by Dohrmann and Carne [44]. A method was presented which was used in the estimation of unknown parameters in models involving transient response. A linear, three degree-of-freedom model of an articulated heavy vehicle was analysed using this method, the results of which indicated that the linear model was inadequate in response to both high and low amplitude input.

Shaw [6] developed a generalised approach to the modelling of truck suspension systems. Specifically, Shaw focussed on linked, multi-axle suspension systems such as linked spring suspension systems. Air suspension was ignored in this study, as this suspension type had not become widespread at the time of publication. The model incorporated realistic spring and tyre models, and assumed large displacements. Both static and dynamic analyses were conducted on the non-linear model, and a method for obtaining suspension data from a heavy vehicle in a laboratory was presented. The chassis included in the model was assumed to be rigid. Only the portion of the chassis connected to the suspension was considered in the model.

Kamar et al. [45] employed a new technique for the description of complex suspension systems. The technique was based on Newton's second law and employs the finite element method as an analytical tool. A comparison of linear and non-linear models of pitch angle

curves is made in response to a square bump excitation, showing reasonably large differences between the two. The harmonic excitation of a tanker trailer provided a comparison between experimental results and 2- and 3-dimensional theoretical models. Poor correlation was shown at velocities below 4.5m/s.

The most popular model of a typical heavy vehicle pneumatic tyre is the model presented by Pacejka and Bakker [46]. It is commonly called 'The Magic Tyre Formula', and is a semi-empirical tyre model which has some success at predicting tyre behaviour.

Zegelaar and Pacejka [47] and Gipser et al. [48] present analysis on the behaviour of tyres on uneven roads. Zegelarr et al. use a flexible ring model, which is dependant on the deflection of the sidewalls. Gipser et al. take a different approach, using a rigid ring-shell fixed to the rim by massless elements with elastic and damping properties. Both papers draw conclusions regarding the influence of the frequency of the forces transmitted to the axle.

Despite the variety of approaches to various aspects of the suspension and wheels of heavy vehicles, the literature reviewed did not include any significant information with respect to chassis response. Typically, the chassis was assumed to be a rigid body [6, 40], and therefore effects on the chassis due to the transfer of dynamic loading from the road surface were not considered.

4.3.2 Characteristic Determination through Experimental Testing

The absence of data applicable to the design of semi-trailer chassis' within the anlaytical research (reviewed in the previous section), led to the investigation of an alternative area of research. Rather than using mathematical modelling of a dynamic system to determine the dynamic characteristics of the vehicle, a variety of research has utilised experimental means on existing trailers to determine the magnitude and frequency of dynamic loading to which a trailer is subjected. A significant amount of experimental research has also been conducted to determine a number of parameters in both vehicles and the structures, such as bridges, with which the vehicles interact. Such work involving bridge-vehicle interaction will not be considered here, as these investigations focus on the response of the bridge to variations in vehicle types and configurations, and the events immediately preceding the contact between the two systems. Further information on this type of experimental work can be found in [37].

Weiblen and Oelmann [49] discuss the importance of load determination in vehicle design. Wheel force transducers were used to measure lateral, braking and vertical forces on the wheels of a passenger vehicle during cornering and braking manoeuvres. The passenger vehicle was then placed in a test rig, and subjecting to a series of loads consistent with the forces measured by the transducers. This enabled the measurement of the forces to which the vehicle was subjected in a controlled environment. The results of the testing were applied to the design of various suspension components. Due to the focus on passenger vehicle suspension systems, this work did not provide any information relevant to trailer chassis design.

Willing [50] describes the experimental testing of an aramid fibre tanker trailer. As the tank was not designed to be self-supporting during transportation (refer section 3.4.6), the worst-case loading scenarios were identified as occurring whilst the trailer was stationary. Strain gauges were placed in critical positions to verify the performance of the tanker trailer subjected to loading scenarios including overpressure, loading, unloading and tipping of the tank. A number of driving tests were also performed, however the strains on the tank were not recorded due to the assumption that the steel chassis, rather than the tank, was responsible for the absorption of dynamic road loads. Hence, the dynamic loading effects on the tank or chassis were not recorded.

There have been a number of experiments conducted involving the placement of strain gauges at particular points of interest on a semi-trailer chassis in order to determine the magnitude of static and dynamic loading.

Woodley and Piggott [51] measured the fluctuating stresses on a high capacity, low loader trailer, carrying a 300 tonne payload over a typical delivery route. The static stresses were measured and compared favourably with design calculations. Strain (and hence stress) readings were then taken during the course of 'typical' operational conditions to evaluate the effect of dynamic loading. They found that, due to the low speeds of travel necessary for such a high payload, the fluctuating strains recorded during the course of the test were remarkably low in comparison with the high mean static strains. Hence, as the operating conditions of this trailer were vastly different from a standard flat bed trailer (particularly vehicle speed), it could not be assumed that dynamic loading of a similar magnitude would necessarily be induced in a standard trailer.

Taylor [52] briefly describes the static and dynamic testing performed on a high capacity, low loader trailer, designed for the specific transportation of spent radioactive fuel casks. The static testing involved the placement of a load equivalent to twice the cask weight for two hours, as per ANSI N14.30. Strain gauges were connected to the trailer in positions at which the highest stresses were predicted to occur. The observed strains throughout the loading sequence were recorded and compared with the predicted and threshold values of the material. These results reportedly found good correlation with the predicted results. The trailer was visually inspected and displayed no signs of overloading. A dynamic road test was also performed, in accordance with ANSI N14.30 requirements. The trailer was driven over a prescribed test route, which included a defined set of manoeuvres designed to replicate a 'typical' journey specific to this trailer type. Strain gauges and accelerometers were used to record the response of the chassis throughout the test. The values obtained from these tests were made available to the author, but are confidential and therefore cannot be reproduced. However, it can be stated that the results proved similar to those presented by Woodley and Piggot, and consequently the value of such results is somewhat limited. The specific and unique nature of the payloads for which these trailers were designed further diminishes the significance of these results, particularly in relation to flat bed semi-trailers, which experience a wide range of loading scenarios.

Hall et al [53] describes the instrumentation and testing of a livestock trailer. Four accelerometers and two strain gauges were attached to the trailer, which was subsequently towed over a series of road surfaces typical of the service conditions of the trailer.

Difficulties were encountered however, with regard to data quality. The strain gauge data allegedly acquired an unknown DC bias, which eliminated the possibility of quantitative analysis.

Cole and Cebon [54] present the results of a series of tests performed on an articulated vehicle which measured the dynamic tyre forces and sprung mass accelerations. These results were then compared with a 21 degree-of-freedom model of the vehicle in order to validate the accuracy of the model. The results from the experimental tests did show good correlation with the proposed model. Included in the experimental testing was the measurement of the trailer 'bending' acceleration response at 13 m/s and 22 m/s whilst half laden and fully laden. A decrease in the resonant frequency from 9-10 Hz to 7 Hz was observed due to the increase in the trailer sprung mass. The significance of trailer bending was greatly diminished due to the concentration of the payload at the two ends of the trailer, and consequently the results did not provide and significant insight into the dynamic loading experienced by the chassis under a worst-case loading scenario.

Sharman [55] describes an experiment in which the dynamic strain was recorded at a number of positions of maximum stress on a 16 tonne GVM semi-trailer. The purpose of this test was to identify DDFs through statistical analysis, and subsequently determine the maximum stresses imposed and the corresponding fatigue life. A static load test identified the location of the maximum stress points, and several accelerometers were also put in place to measure dynamic vertical accelerations in specific positions. The vehicle was driven at speeds between 40 and 60 km/h over various surfaces and the strains recorded. Table 4.1 shows the distributions of exceedences for various stress levels on given road surfaces.

Assuming a Gaussian distribution of signal, a design factor was derived. This factor was a numerical value greater than one, which was multiplied by the static load case (1g) to provide a load for design and analysis. The dynamic design factor was given as

$$DDF = (1+3S)/h_{mean}$$

Where S represents the standard deviation and h_{mean} is the static or mean stress. Table 4.2 shows the DDFs given for various road conditions.

Table 4.1 Distributions of Stress Level Exceedences in Chassis Rail for Various Road Surfaces (Source [55])

Road Condition	Stress Level (MPa)	No. of Exceedences
Smooth Tarmac	115	4
	112	12
	109	20
	107	48
	104	112
	101	120
	99	132
Coarse Tarmac	120	43
	117	8
	115	12
	112	25
	109	40
	107	88
	104	155
	101	180
	99	205
Ride & Handling Track	146	3
	136	8
	130	12
	125	17
	120	29
	115	84
	109	144
	104	195
	99	250
Pave Track	185	4
	173	27
	160	72
	148	100
	136	150
	123	188
	110	208
	99	208

Table 4.2 shows that for typical smooth highway operation, a DDF of 1.2 is sufficient. However 'rough' roads with continuously harsh undulations warrant a dynamic design factor of 2.4. A number of limitations were highlighted by Sharman, due to difficulties encountered during the recording of the data. The application of this data must also be selectively applied, when it is considered that the span of the trailer chassis rails tested here is significantly smaller than a 30 tonne GVM trailer. Additionally, the distribution of the payload was not specified by Sharman, further limiting a wide application of these design

factors. Despite these factors, this paper did provide the specific design guidelines for application to flat bed semitrailers, and the contribution of this data to the design philosophy is discussed in section 4.4.4.

Table 4.2 Design Factors for Chassis Rails Derived From (1 + 3S) Criterion (Source[55])

Road Condition	Design Factor
Smooth Tarmac	1.20
Coarse Tarmac	1.25
Ride & Handling Track	1.60
Short Bumps on R&H Track	1.90
Long Waves on R&H Track	1.40
Level Crossing	2.20
Pave Surface	2.40

Alternate DDFs have been suggested which, although limited in their scope, are mentioned here for completeness. Fenton [56] briefly states that measurement of the dynamic loads on vehicles have yielded a maximum value of three times the static load. Garrett [57] suggests a factor of safety of 1.5 be applied to this 3g load, resulting in a total design factor of 4.5. However the 3g acceleration is the estimated force acting on the tyre, and does not take into account the retardation afforded by the suspension system or flexure of the chassis.

4.3.3 Summary of Vehicle Dynamics Literature

A review of available literature regarding the structural and behavioural characteristics of heavy vehicles was performed. This review was conducted in anticipation of finding design data that is presently lacking, in the form of standards or codes within the heavy vehicle industry. Specifically, it was anticipated that simulations of heavy vehicle systems would provide quantification of the loads imposed on the trailer during typical service conditions, including the effects of the maximum bending stresses on the chassis resulting from dynamic flexural loading and payload bounce.

The static and dynamic simulation and optimisation of heavy vehicle systems yielded little relevant information regarding trailer design. The use of lumped mass models and the assumption of rigid trailer elements were present in all but one paper reviewed. However while Gadala et al [13] considered flexure of the trailer chassis, this was purely with

respect to the identification of the natural frequencies and mode shapes of an unloaded trailer.

Research into the assessment of ride quality similarly utilises lumped mass models, particularly with respect to the trailer. This is reasonable however, as the vibration and accelerations experienced by the driver represent the focus of such investigations.

The investigation of bridge-vehicle interaction and the quantification of wheel loading on road surfaces are of limited value in this context. These studies focus on the impact upon the road surfaces or structures, and little information is revealed regarding the transfer of forces to the suspension system or, more importantly, to the chassis.

The accurate modelling of the suspension systems of heavy vehicles represents a significant aspect of accurate vehicle simulation. It can not, however, provide any insight with respect to the dynamic loading sustained by a trailer without the combination of such suspension models with complimentary models of the trailer and prime mover.

The use of experimentation through instrumentation of heavy vehicles provided some assistance. In particular, Sharman identified the design factors for flat bed semi-trailers travelling over a number of surfaces. Limitations associated with this data must be considered however, particularly with respect to the accuracy of the figures provided.

The apparent lack of relevant information provided through dynamic analysis, and the inconsistencies observed in the suggested design factors warrants further investigation into trailer design factors through alternative avenues.

4.4 Current Trailer Capacities

4.4.1 Evolutionary Trailer Design

In response to the absence of relevant standards or applicable data which adequately defines the criteria by which trailers should be designed, an investigation was undertaken to determine the load capacities of current trailers.

The design and manufacture of trailers has always been accomplished through use of little more than prior experience. Structural loads and design criteria are traceable to infrequent but harsh operating conditions experienced during the life of a vehicle. However the identification and quantification of these conditions and the loading they inflict upon the structure is, at the very least, difficult. Hence, a comparison to an existing (successful) design is a common method of dynamic evaluation [58].

In general, the layout of a typical flat bed trailer has experienced relatively minor change with respect to the global structural configuration. However, evolution of trailer specifications has taken place, resulting in increased structural efficiency. Such evolution is often prompted by the failure of a trailer, on both a minor and a catastrophic scale. Figure 4.1 depicts the repairs made to a flat bed trailer, which failed catastrophically in September 2000. This failure was initiated by poor weld placement, which occurred during the welding of an additional flange plate to the bottom flange of the chassis rail. Under fatigue loading, this defect produced a stress concentration of sufficient severity to initiate a crack, which proceeded through the bottom flange and web of the chassis rail and resulted in failure.

Discussion with the owner of this particular trailer revealed that while catastrophic failures such as this are not considered common, he was able to recount two similar incidents reported to him by industry associates within the previous 12 months.

The presence of significant structural failures in current trailers suggests that the process of optimisation is ongoing, and that the determination of the typical operational conditions to which a trailer is subjected remains difficult despite continuous incremental evolution.

The significance of attention to the design of small details to the long-term performance of a trailer is also noteworthy. The example illustrated in Figure 4.1 serves as a typical example of this. Insufficient moment capacity was not the origin of this particular failure,

but rather poor weld placement. Failures of this nature were also reported to the author by Road Users International (RUI) Pty. Ltd (refer Section 4.4.3). Stress concentrations and the degradation of material properties through incorrect weld placement or techniques were cited as typical contributors to failures of various magnitudes.

Figure 4.1 Repairs Made to Failed Neck of Flat Bed Trailer

4.4.2 Estimation and Comparison of Trailer Capacities

An estimation of the initial load cases and static capacities used in the design process was sought through the identification of the ultimate capacities of several existing trailers. Measurements of the web and flange sizes used in the construction of the chassis rails and cross members were recorded, and the moment capacity of each member calculated. The dimensions of the trailers investigated are shown in full detail in Appendix A. Various trailer manufacturers and a range of trailer ages were included in this study as it was anticipated that this cross section would highlight any changes to trailer design throughout the last two decades. However, the limited number of trailers available for measurement restricts the generalisation of any such trends with respect to the entire trailer industry.

The results of the assessment of the aforementioned trailer capacities are summarised in Figure 4.2. This comparison reveals the significant magnitude of variation in trailer capacities present in this sample. In particular, the figure suggests an increase in the moment capacity of trailers of all makes, particularly from 1987 onwards. This is supported by the increase in the strength of Haulmark trailers by over 30% within a ten year time period. The high strength of Loughlin trailers is well noted within the industry, and was confirmed as typical to the author by several sources familiar with trailers in general.

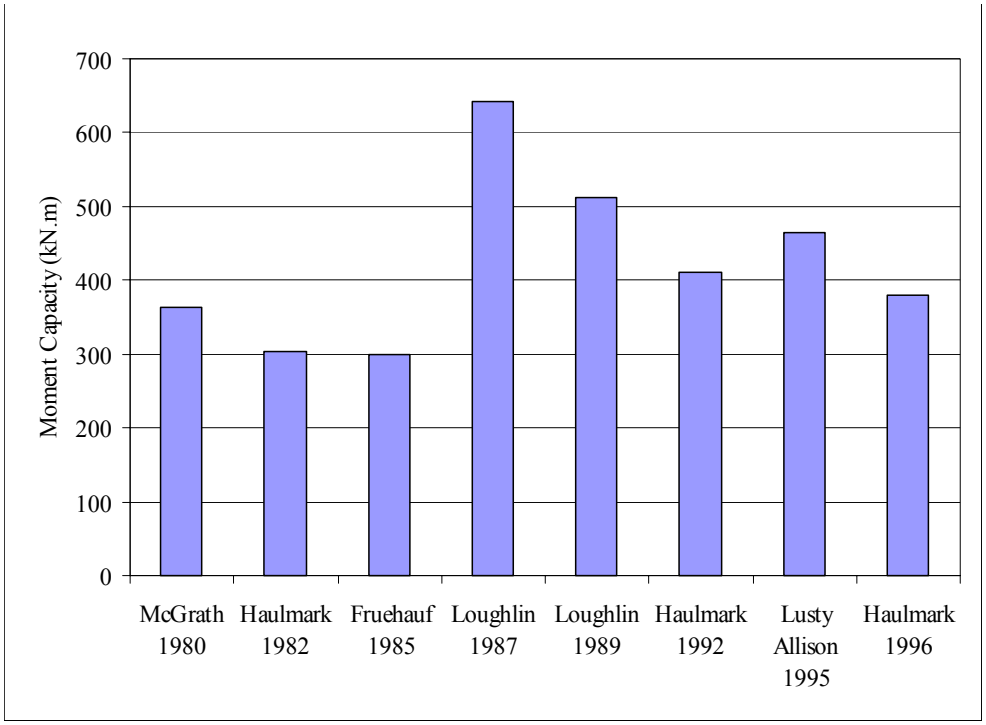

Figure 4.2 Moment Capacity (at yield) of Various Flat bed Trailers

The large range of trailer capacities, which are all 'rated' to carry the same loads under the same conditions, demonstrates a lack of uniformity in acceptable factors of safety. This emphasises the necessity for design standards within the industry, and demonstrates the infancy of trailer design from an engineering viewpoint. This variation also suggests that the experience possessed by each manufacturer with respect to flat bed trailers is proportional to the number of iterations that have taken place throughout the lifespan of that particular design. Hence the extent of structural optimisation varies with each manufacturer, in addition to the differences in design techniques used by the respective companies.

4.4.3 Industry Design Techniques

Following the identification of the moment capacities of steel trailers, the author conducted a number of interviews with various manufacturers from Australia, the US, and the Netherlands to gain further insight regarding design techniques. Each interviewee was asked to specify, where confidentiality restrictions would permit, the DDFs and loading scenarios used in trailer design. A summary of their responses is given below.

Haulmark Trailers are a recognised leader in the design and construction of flat bed and specialty trailers in Australia. They are respected by the industry, as their trailers are regarded as reliable yet reasonably lightweight and cost competitive. Haulmark claim to use a DDF that varies between 2.5 and 3.0, depending on the application and life expectancy of the trailer. The load case to which this factor applies is determined by the usage of the trailer specified by the customer.

RoadUser International Pty Ltd are a consultancy company which specialises in the dynamic analysis of trailers and their directional response, as well as the impact of trailers on roads. RUI is led by Peter Sweatman, a recognised leader in the field of trailer dynamics. RUI claim to use a DDF of between 2.2 and 2.5 for flatbed trailers, which is applied to an undisclosed worst-case loading scenario.

Two of the many flatbed trailer manufacturers in the US include Wabash International and East Manufacturing. A DDF of 2.5 is employed by Wabash Intl., which is applied to a loading scenario dependant on the application of the trailer. East MFG also uses a DDF between 2.0 and 3.0, which is applied to the worst case legal concentrated loads. The specific details of such loading conditions were not made known to the author.

Refrigerated vans are designed in a similar manner, with a DDF of 3.0 being applied by Fibreglass Transport Equipment (FTE) and the makers of 'Coldfeather' lightweight refrigerated trailers in the Netherlands (refer section 3.4.4). A higher DDF is typically used for refrigerated vans due to the unconstrained nature of the payload. Since chains or straps cannot restrain the load, it behaves as a 'live load', and is able to leave contact with the trailer under dynamic conditions.

Further discussion with manufacturers revealed that trailers are typically designed for explicit uses. Consequently, trailers specifically designed for the application of concentrated loads (eg. Heavy machinery) or travel on rough terrain will be stronger and

heavier than those designed for the application of uniformly distributed loads (eg. Pallets) or travel on main highways. However the confidential nature of the loading scenarios used in design by commercial companies leave much to be defined with respect to trailer design in general.

This 'made-to-order' approach would appear to collaborate with the obvious discrepancies observed between the various trailer types in Figure 4.2. However this approach does present a number of difficulties, which are addressed in Section 4.6.

4.4.4 Design Factor Selection

The determination of an appropriate DDF proved a considerable task. The ANSI standard suggested that a value of 2.5 be adopted, which shows reasonable agreement with the value of 2.4 presented by Sharman. The current trends in trailer design apparent from the survey would appear to concur with these figures, indicating the use of DDFs between 2.0 and 3.0. Consequently, it was decided that a DDF of 2.5 would be adopted in the design of this trailer. This factor would be applied to the worst-case loading scenario as a requirement of sufficient structural strength. This factor was adopted on the assumption that the trailer would subsequently be capable of sustaining the dynamic loading effects imposed during typical operation.

4.5 Load Case Definition

4.5.1 Introduction

In addition to DDFs, it is necessary to define realistic loading scenarios to which the design factors must be applied. The distribution of the payload over the deck of the trailer is the primary contributor to the stresses induced within the chassis rail, particularly with respect to dynamic loading. The determination of relevant load cases is the responsibility of the designer, and is performed by analysis of the expected operational process [59].

The mass limits for axle loadings by heavy vehicles within Australia, as defined by the state road authorities, restrict the load imposed on the road surface in accordance with the number of axles within the 'axle group'. These limits were revised in 2000, allowing an increase in the mass limits of axle groups comprised of 'road-friendly' suspension systems. These changes were initiated in response to reports from RUI, the NRTC and ARRB [30-36], which suggested that the impact on road surfaces was lessened through the use of airbag suspension in comparison with equivalent steel spring suspension systems. Figure 4.3 illustrates the mass limits imposed on a typical 6-axle heavy articulated vehicle. The figures shown in the parenthesis denote the mass limits applicable to any suspension system not considered 'road-friendly'.

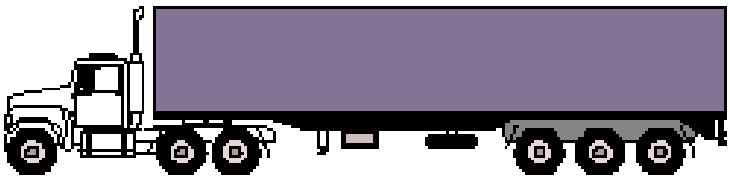

Maximum Mass Limit (tonnes) **45.5 (42.5)**

Steer Axle = **6 tonne (no change)**

Tandem Axle = **17 tonne (16.5)**

Triple axle = **22.5 tonne (20.0)**

Figure 4.3 Mass Limits For a Six-axle Articulated Vehicle

(Source: http://www.nrtc.gov.au/place/hv-masslimits.htm)

In consideration of the benefits supplied by the increased mass limits with respect to payload capacities, it was assumed that the adoption of airbag suspension would be mandatory in application to a lightweight trailer. The GVM of the truck-trailer combination should therefore not exceed 45.5 tonnes. Subtracting the mass of the prime

mover and other ancillaries, the estimation of the trailer payload capacity is determined as follows:

Table 4.3 Payload Limits on Typical Flat bed Trailer

		Mass (kg)
Mass Limit (Fig. 4.3)	Tandem Axle	17000
Subtract	Portion of Prime Mover Mass on Tandem	4200
	Payload Capacity of Tandem Axle	12800
Mass Limit (Fig. 4.3)	Triple Axle	22500
Subtract	Trailer Chassis and Ancillaries	2000
	Triaxle Airbag Suspension System	2500
	Payload Capacity of Triple Axle	18000
	TOTAL PAYLOAD CAPACITY OF TRAILER	30800

The distribution of this payload may be facilitated in a number of ways. The following sections describe the loading scenarios developed for use in the design of the FRP trailer. These load cases were defined by considering the spatial form of various types of payloads, and the restrictions they impose on their respective distribution over the trailer deck. The load cases are presented in an order based solely on the author's discretion. Each scenario assumes the application of the maximum payload to the trailer. The values shown in the bending moment and shear diagrams in the following section represent the effects of the maximum payload on the chassis rails when shared evenly between the two. Due to the assumption of symmetry, the diagrams illustrate the moments and shear forces imposed on either one of the chassis rails. The program used to generate the bending moment and shear force diagrams used the positive sign convention (United States convention).

The load cases described below consider only the longitudinal distribution of the payload. Hence, neither the contribution of the load to cornering stability nor the effects of variations in lateral load spread will be addressed.

4.5.2 Load Case One

This load case, illustrated in Figure 4.4 (a), denotes the uniform distribution of the payload over the trailer. This loading scenario is commonly observed in transportation of both continuous and discrete payloads, which are typically low in density and require the entire surface area of the loading platform. Examples of continuous payloads include long lengths of steel section or piping, while goods that can be stacked onto pallets would be considered

discrete, able to be separated and rearranged. The uniform distribution of the payload does misrepresent reality to a small degree, since a rear load bias must exist to achieve the mass limit requirements. However, for the purposes of this analysis, a uniform distribution is assumed.

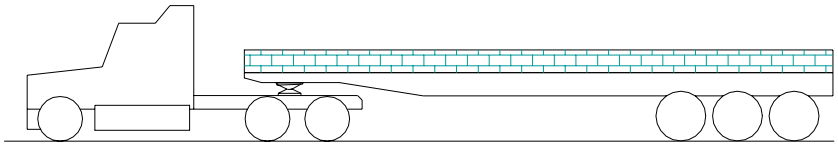

Figure 4.4 (a) Load Case One

The bending moments and shear forces imposed on a single chassis rail are presented in Figure 4.4 (b). A comparison of these values is shown in section 4.6.

The values presented should be considered only as indicative, as variations in chassis rail profiles and spring stiffness will cause minor variations in load sharing and distribution. Additionally, the ability of the tri-axle suspension group to equally share the load will significantly influence the shear forces imposed on the chassis rail.

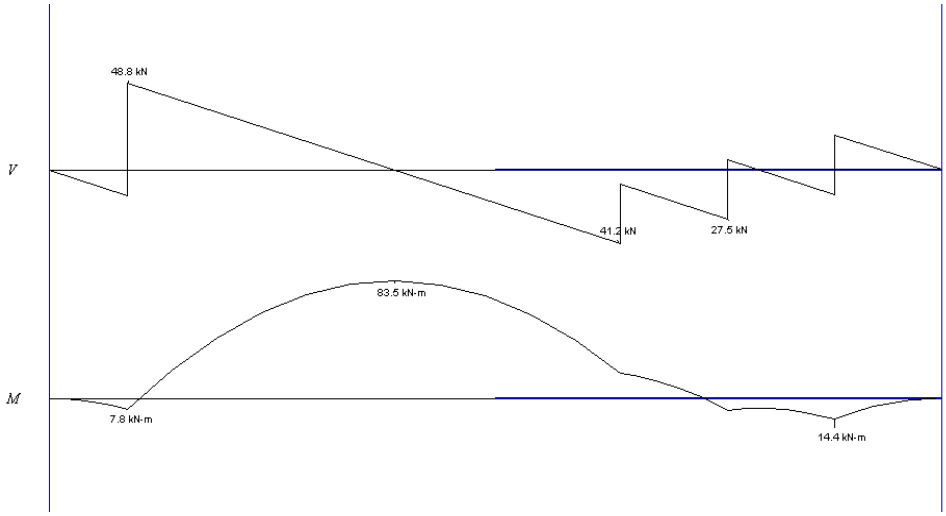

Figure 4.4 (b) Shear Force and Bending Moment Diagram – Load Case One

4.5.3 Load Case Two

The second load case considered is shown in Figure 4.5 (a). The deposition of the payload directly above the suspension groups is frequently observed in cases where a discrete

payload of high density is transported. Operators often prefer this method of loading, as the correct distribution of the payload between each axle group is greatly simplified. This loading pattern is also utilised when the trailer is partially loaded.

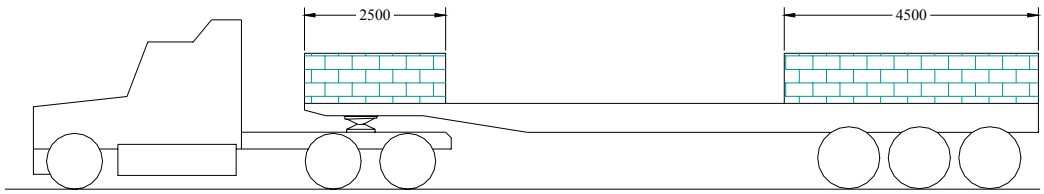

Figure 4.5 (a) Load Case Two

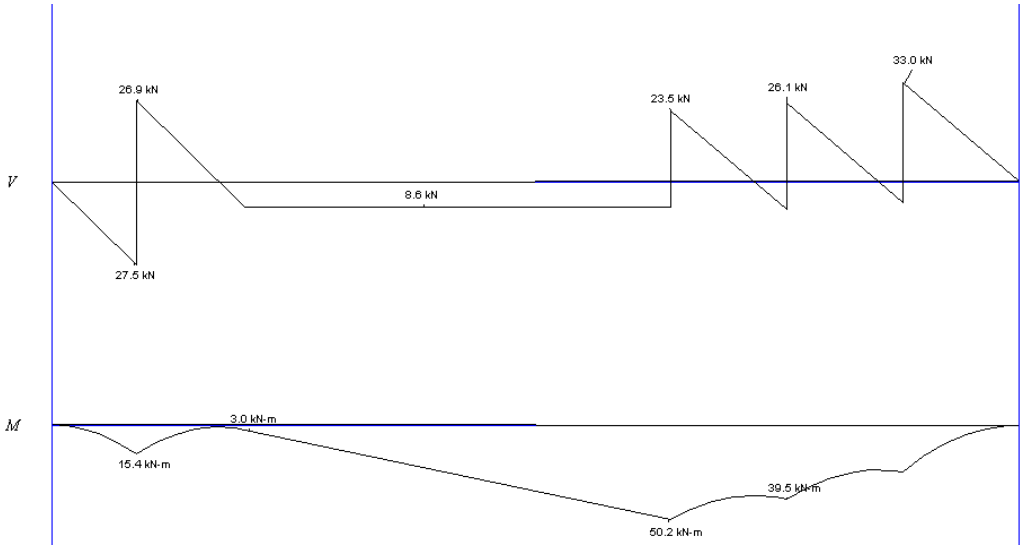

Figure 4.5 (b) Shear Force and Bending Moment Diagram – Load Case Two

4.5.4 Load Case Three

The third load case represents the transportation of a continuous payload with a reduced span. The payload must be positioned such that the load is distributed to the axle groups in the correct proportions. Payloads of this nature would include items such as shipping containers and machinery or other cargo of significant size and density. Figure 4.6 (a) illustrates the distribution of a payload over a six-metre span, which was chosen to represent this payload.

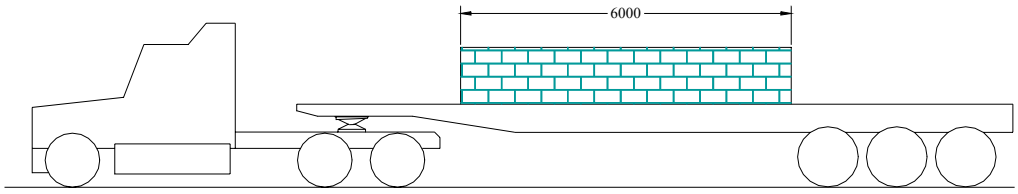

Figure 4.6 (a) Load Case Three

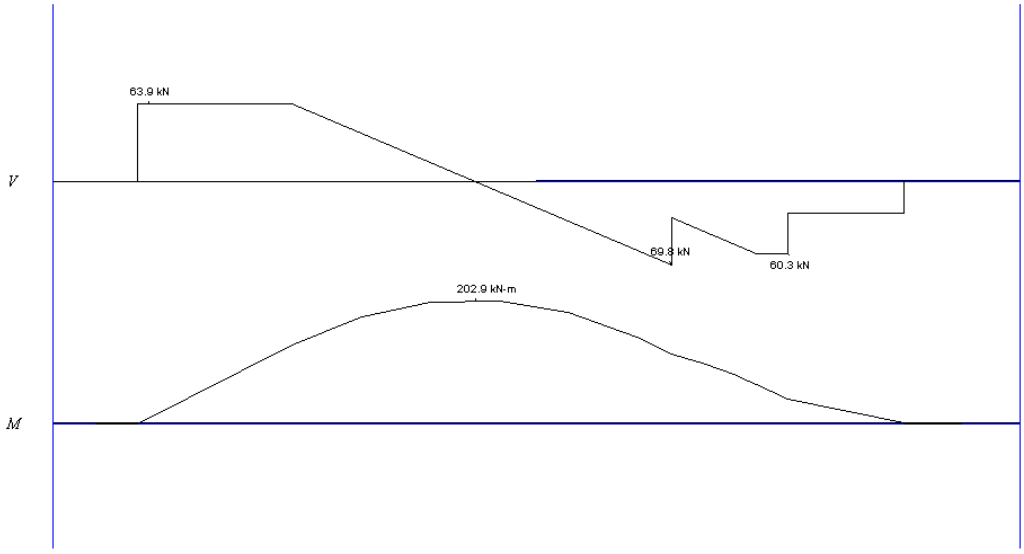

Figure 4.6 (b) Shear Force and Bending Moment Diagram – Load Case Three

4.5.5 Load Case Four

Load case four denotes a more severe scenario, in which the load spread was reduced from six to three metres. This distribution is characteristic of a more compact load, such as a large cable coil or a transformer. While in reality this type of payload would suggest the use of a low loader or drop deck trailer to increase load stability, this load case was included as representative of the worst practical loading case experienced by this type of trailer.

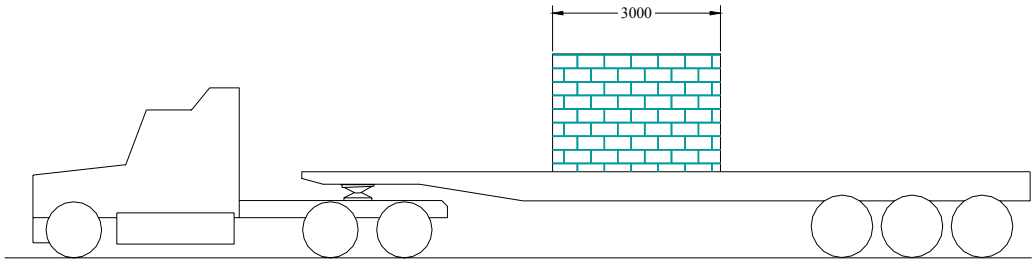

Figure 4.7 (a) Load Case Four

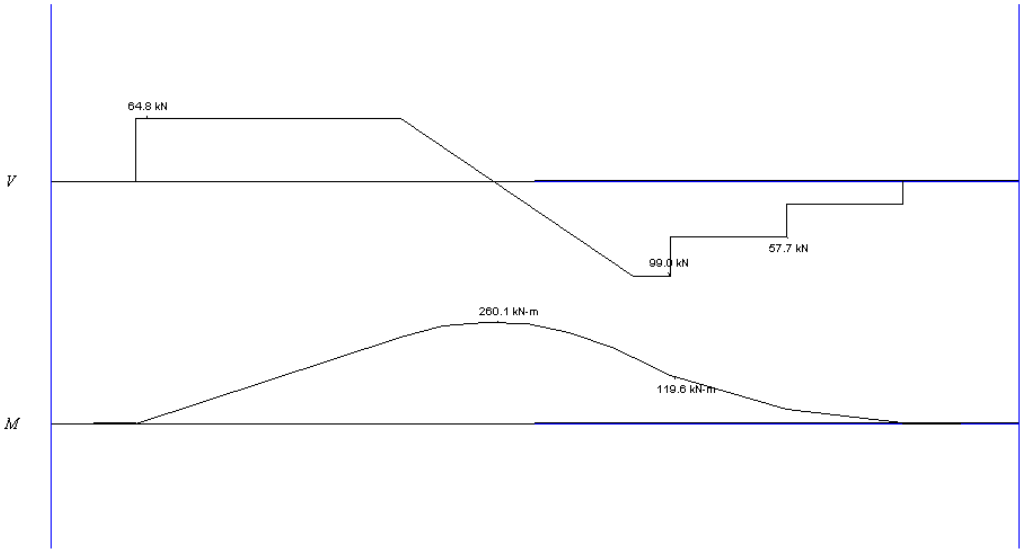

Figure 4.7 (b) Shear Force and Bending Moment Diagram – Load Case Four

4.5.6 Load Case Five

In addition to the load case described in 4.5.5, the transportation of heavy machinery and earth moving equipment is often facilitated by low loaders and specialised trailers, particularly when the machinery possesses a high centre of gravity. However standard flat bed trailers are occasionally used in the transportation of heavy machinery despite the risks associated with trailer damage or load instability. Figure 4.8 (a) represents the loading of a two-axle heavy vehicle, placed such that the load is distributed correctly between the front and rear axle groups.

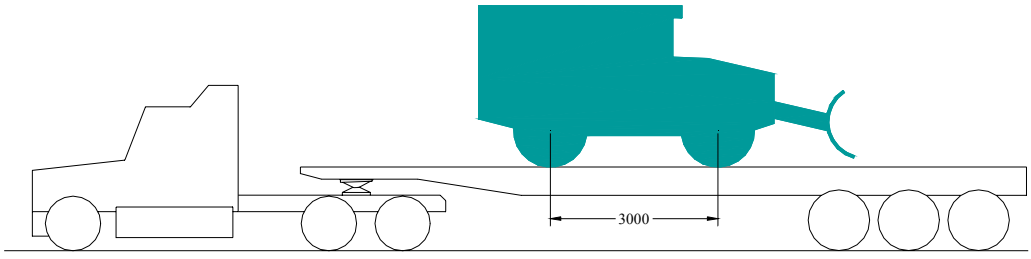

Figure 4.8 (a) Load Case Five

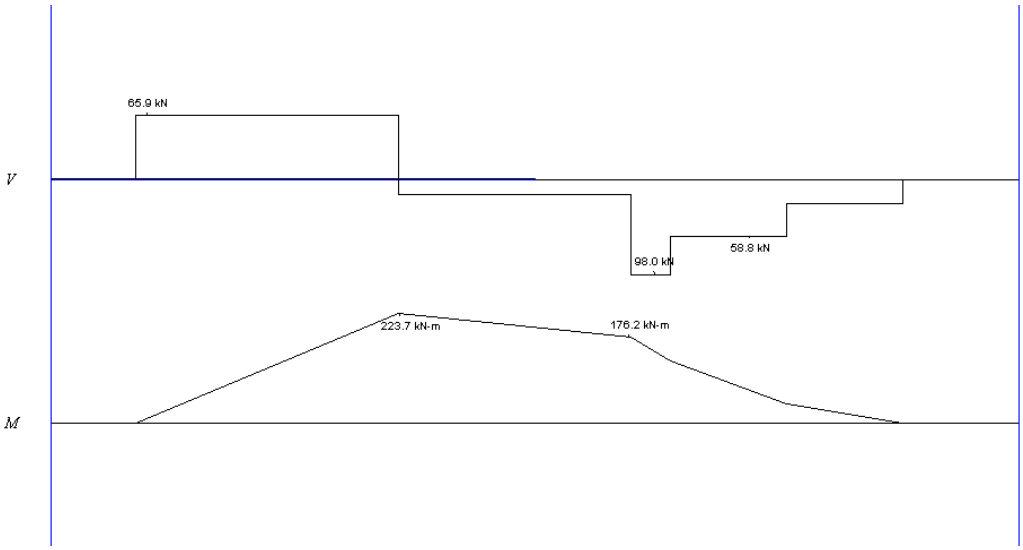

Figure 4.8 (b) Shear Force and Bending Moment Diagram – Load Case Five

4.5.7 Load Case Six

Load combinations as shown in Figure 4.9 (a) are common, and represent a mixed payload. The load case defined here denotes the transportation of two, ten-tonne vehicles in combination with a spread load included to maximise the payload.

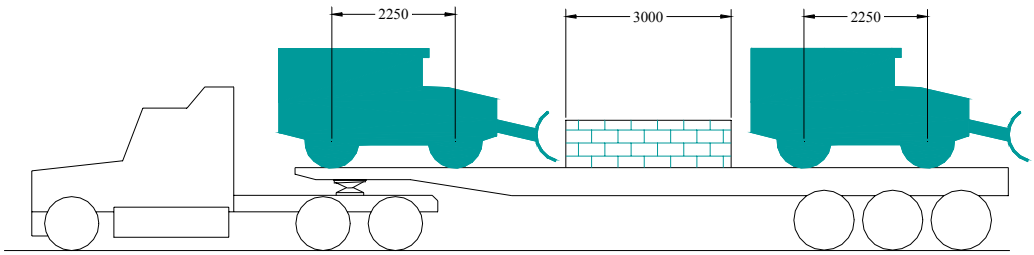

Figure 4.9 (a) Load Case Six

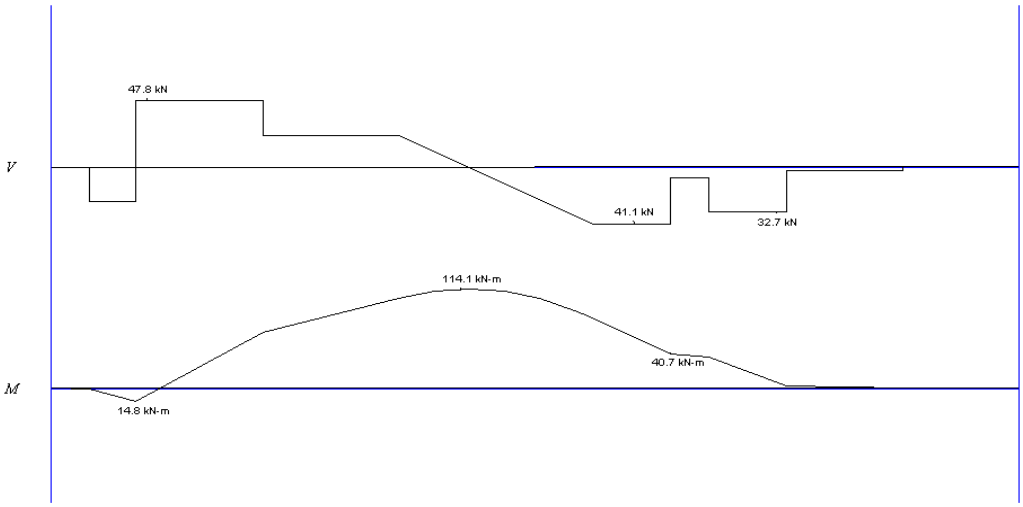

Figure 4.9 (b) Shear Force and Bending Moment Diagram – Load Case Six

4.5.8 Comparison and Summary of Loading Conditions

Having defined a spectrum of loading scenarios to which a typical flat bed trailer is subjected, moment and shear capacity envelopes were produced. These two envelopes, shown in Figures 4.10 and 4.11, provide a direct comparison of the loads imposed on a trailer in response to each load case. The dotted lines represent the upper limit of the moment and shear loads at any given point along the chassis rail.

These figures clearly show the variance in the loads imposed on the chassis rail by each loading scenario, particularly with respect to the bending moment at the trailer midspan. This highlights the influence of the choice of load case to which the DDF is applied, and the significance of the variations in the moment capacity of existing steel trailers.

In order to gain an indication of the load cases considered in the design of the aforementioned steel trailers, the maximum static moment capacity of each trailer was determined and compared with the bending moment envelope shown in Figure 4.10.

Table 4.4 Current Trailer Capacities

Trailer Make	Ulimate Moment Capacity (kNm)	Static Design Moment (kNm)	Capable of Carrying Load Case Number
McGrath 1980	364	146	1,2,6
Haulmark 1982	309	124	1,2,6
Fruehauf 1985	304	122	1,2,6
Loughlin 1987	641	256	1-3,5,6
Loughlin 1989	512	205	1-3,6
Haulmark 1992	411	164	1,2,6
Lusty Allison 1995	482	193	1,2,6
Haulmark 1996	421	169	1,2,6

The Table 4.4 would appear to indicate that, in general, steel flat bed trailers are designed to primarily accommodate uniformly distributed or split loads, as shown in load cases one, two and six. As previously mentioned, Loughlin trailers have maintained a reputation of high strength, albeit at the expense of tare mass.

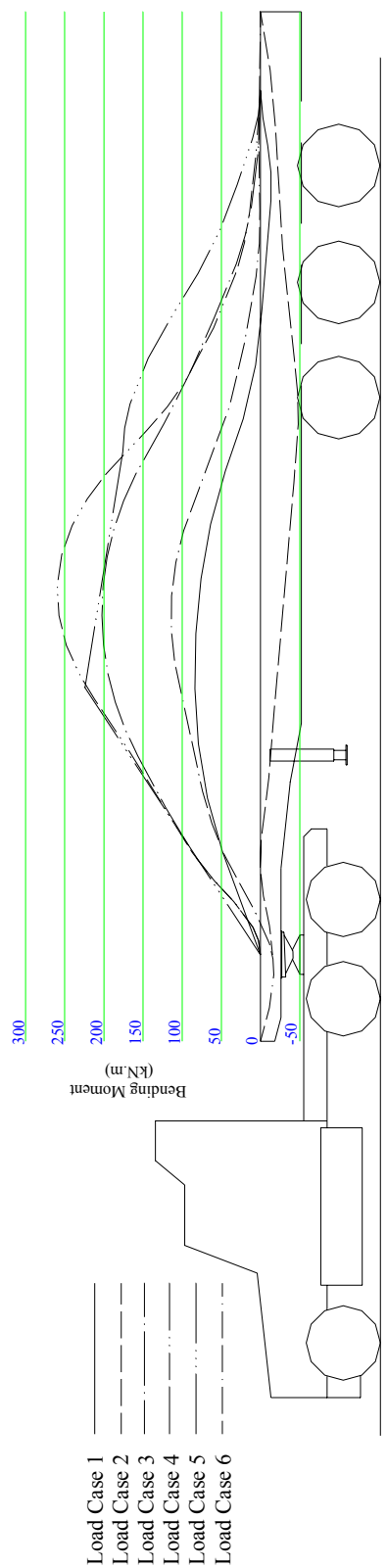

Figure 4.10 Moment Distribution Over Typical Trailer

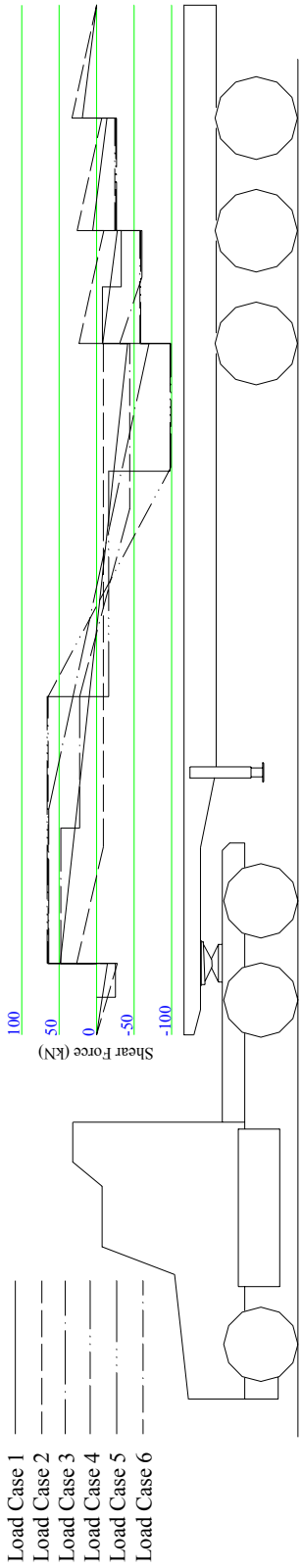

Figure 4.11 Shear Force Distribution Over Typical Trailer

4.6 Trailer Classification by Capacity

The adoption of the load cases defined in the previous section for use in trailer design, allow the introduction of trailer classifications. The concept of trailer specifications is presented by El-Gindy [26], particularly with respect to the dynamic performance of a given truck-trailer combination. He suggests that a 'marriage certificate' plaque be fitted to all prime movers and trailers, indicating which vehicle units should be *married* together for optimised performance. A similar concept is presented here with respect to loading capacity.

The classification of flat bed trailers with respect to the allowable loading scenarios is required due to the shortcomings of current design techniques. As discussed in section 4.4.3, trailers are currently 'made-to-order', with the expected operational conditions specified by the estimations of the customer. However this method of load estimation increases the probability of overloading the trailer. For example, consider a trailer that is designed, at the request of the customer, to withstand only light loading conditions such as load cases one and two. Should this trailer be sold at a later date, the purchaser may be unaware of the operational conditions for which the trailer was designed. Hence, the potential for failure of this trailer is greatly increased should the new owner subject the trailer to any of the other specified load cases. However, the introduction of trailer classifications, detailed in the following sections, would eliminate such potential by the fitting of a trailer classification plate to each trailer. This plate would define the conditions of use by clearly indicating the allowable loading conditions.

The bending moment and shear force diagrams in the previous section have been summarised in Table 4.5. These load cases were grouped into three broad categories as discussed in the following section.

Table 4.5 Static Loads On Each Chassis Rail

	Max. Moment (kNm)	Max. Shear at Kingpin (kN)	Max. Shear at Triaxle (kN)
Load Case 1	84	49	41
Load Case 2	50	28	33
Load Case 3	203	64	70
Load Case 4	260	65	100
Load Case 5	224	65	100
Load Case 6	114	48	41

4.6.1 Light Duty Trailers

This category represents those trailers typically used for the transportation of low-density loads spread over a large area. This classification would therefore incorporate load cases one, two and six. A maximum static bending moment of 150 kNm was set for this classification, necessitating that the payload be distributed over a length no less than nine metres when fully loaded. A static shear capacity of 50 kN at the kingpin, and 45 kN at the tri-axle, should also be applied to this trailer type.

Assuming identification plaques were fitted to each trailer as suggest by El-Gindy, any trailer displaying this classification symbol would not legally be able to transport a full payload unless it was distributed over a length greater than nine metres.

4.6.2 Medium Duty Trailers

The medium classification enables the safe transportation of all typical loading scenarios imposed on a flat bed semi-trailer. This category includes load cases one, two, three and six. A maximum static bending moment of 200 kNm was defined for this category, allowing a load spread of no less than six metres at full payload capacity. A static shear capacity of 65 kN at the kingpin, and 70 kN at the tri-axle, should also be applied to this trailer type.

Any trailer displaying the medium classification symbol would not legally be able to transport a full payload unless it was distributed over a length greater than six metres.

4.6.3 Heavy Duty Trailers

As previously discussed, loading scenarios as illustrated in load cases four and five are rarely imposed on flat top trailers, as such payloads are typically accommodated by low loader trailers. However, the tendency of some transport firms to overload trailers to varying degrees (refer to section 1.1) must not be overlooked. While the introduction of trailer classifications does not prevent the overloading of trailers, it provides guidelines for the safe operation of trailers and more clearly defines the limitations of the trailer.

Heavy trailers should withstand a maximum static bending moment of up to 260 kNm, thereby restricting the distribution of the load to no less than three metres. The static

shear capacity of the chassis rail at the kingpin should exceed 65 kN, while a shear capacity of 100 kN should be present at the tri-axle.

4.7 Implications of Classification to Tare Weight and Cost

The primary aim of this project is to reduce the tare weight of a flat bed semi-trailer through the use of alternate materials and an effective design philosophy. However this must be balanced with respect to the capital cost of the trailer. While a trailer possessing a substantially lower tare mass may provide outstanding financial incentives to the owner, section 1.1 points out that heavy vehicle operators are likely to accept only a proportionally small increase in the capital cost of the trailer.

The suggested classification of trailer capacities has a direct influence on both the capital cost and tare mass of the trailer. Assuming an identical manufacturing process and chassis configuration is used for all trailer classifications, a heavy-duty trailer would require additional fibrous reinforcement to sustain a high bending moment compared to a light or medium duty trailer, and may also require a stronger deck and cross members. Each of these additions would directly contribute to an increase in the total quantity of material and labour required in the manufacture of the trailer, thereby inflating the capital cost to the customer. Similarly, a trailer of higher classification would incur mass penalties due to the additional material required. This would appear to diminish the viability of a lightweight trailer of a higher strength classification, as the increased flexibility with respect to payload distribution would reduce the benefits of tare mass reduction of the trailer. Additionally, the extra material used to provide greater strength would result in an increase in the capital cost.

It should also be noted that the trailer capacities as specified in Table 4.5 assume that no overloading would occur. While the DDF (when applied to the capacities recommended in section 4.6) is intended to account for the dynamic flexure of the trailer due to various road conditions, it is assumed that the load mass and distribution is within the specified limits. In accordance with the designer's discretion, overloading incidents can be accounted for by increasing the static loads tabled in Table 4.5. The reader is referred to section 1.1 and reference [5] of Chapter 1 for details regarding the overloading of heavy vehicles.

4.8 Design Criteria for FRP Trailers

4.8.1 Introduction

The previous sections of this chapter have established the applicable load cases to which a trailer is subjected, in addition to the quantification of appropriate DDFs. However this information forms only a portion of the design philosophy of FRP trailers.

This section examines the design criteria applied to steel trailers, and consequently defines a number of criteria for consideration in the design of FRP trailers. A comparison of these constraints is performed to determine the presence of a single dominant design constraint. However the design methodology presented here does not address every aspect of flatbed trailer design. Rather, it highlights the key components of the design process, and establishes the fundamental principals with respect to chassis design. It should be noted that a number of assumptions with regard to the specifications and requirements of the trailer were made within the course of this discussion, to enable the use of an example. In reality, these assumptions would be primarily dependent on the requirements specified by the customer and the preferences of the designer.

4.8.2 Considerations in Steel Trailer Design

The definition of design constraints relevant to FRP trailers was initiated by examining those appropriate to steel trailers. Discussion with trailer manufacturers and a review of available literature revealed that the design criteria used in steel trailer design include the assessment of both the strength and fatigue performance.

Assuming that, for steel trailers, flexural strength is more critical than the shear capacity or deflection, the moment capacity of the trailer represents the primary constraint considered by a designer. After establishing the critical load case, a trailer is typically designed to accommodate the corresponding bending moment, the magnitude of which is modified by the designated DDF. The flange and web thicknesses are selected from an array of standard steel sizes, and the beam depth adjusted to provide the appropriate section properties.

Consideration of fatigue in steel trailer design is far less prevalent, particularly in relation to more common trailer types such as flat beds. This is generally attributed to the fact that

the majority of flat bed trailers are not designed from first principles, as previously mentioned in section 4.4. However, specialty trailers which are specifically designed for the transportation of a particular payload (even if this is a 'once only' event), require more detailed fatigue analysis, as no predecessor is typically available to allow the manipulation of a similar design. This is demonstrated by the specifications set out in ANSI N14.30 for the analysis of fatigue performance of high-level radioactive waste carrying trailers.

Analysis of the fatigue performance of steel trailers is facilitated by clearly defined fatigue life data and established analysis techniques, which are available for most grades of steel. The reliability of this data ensures that fatigue failure should not occur in the portions of the chassis rail subjected to the highest stresses. However, as discussed in section 4.4.1, fatigue damage is most likely to occur in areas where stress concentrations are present.

4.8.3 Strength Capacity of FRP Trailers

As with steel trailers, adequate moment capacity is required to accommodate the critical load case and the associated effects of dynamic loading. However unlike the manufacturing process utilised in steel trailer construction, the formation of an I-beam comprised of prefabricated FRP sections of standard sizes is not possible. Consequently each aspect of the member sizing remains completely at the discretion of the designer, including the dimensions and quantity of reinforcing laminates required in each direction. The absence of reliable material data necessitates the testing of the selected laminate to determine the specific material characteristics and enable laminate optimisation.

The yield point of a steel component holds great significance with respect to design in general, as this phenomenon represents the reference point and design limit of the material. However as FRPs exhibit essentially linear elastic behaviour until failure, such a point of reference does not exist (refer section 2.7.3). In response to this, material capacity reductions factors have been suggested, which take into account variations in material types, manufacturing methods, and load types. The reduction factor applied to the laminate provides an upper limit for strength design in a similar manner to the yield point of steel. The critical load case and associated dynamic allowances are then combined with the modified laminate capacity to provide the complete spectrum of data necessary to establish a suitable trailer classification, and determine the required strength capacity.

The application of capacity reduction factors, such as those presented by Karbhari [60], is examined in greater detail in section 4.8.6.

4.8.4 Fatigue Capacity of FRP Trailers

In contrast to the limited investigation of fatigue performance observed in steel trailer design, the assessment of the fatigue performance forms an integral part in the design process of FRP trailers. While the fatigue performance of commonly used steels is well documented and is suitable for design, the variability present in FRP laminates prevents the establishment of similarly applicable fatigue data. As discussed in Chapter 8, variations in the orientation of a laminate can greatly affect fatigue performance. This sensitivity is compounded by the fact that various reinforcement materials and matrix types respond differently to fatigue. For example, while carbon fibres possess exceptional fatigue performance, aramid fibres are particularly sensitive to compressive fatigue loading. The individualistic nature of the response of FRP materials to fatigue loading typically necessitates specific testing of the respective laminate or the use of appropriate reduction factors to ensure a sufficient fatigue life.

The characteristic of fatigue damage observed in FRPs emphasises the proper consideration of FRP fatigue life. While fatigue cracks in steel can generally be repaired or the section replaced with comparatively little effort, fatigue damage in FRPs manifests itself in delamination and micro cracking throughout all layers of the laminate. As these forms of damage are impossible to repair, the reduction or elimination of fatigue damage is of paramount importance. Chapters 5 and 8 address fatigue in greater detail.

4.8.5 Deflection Constraints on FRP Trailers

The third design constraint requiring consideration with respect to FRP trailers is deflection. The limitation of deflection is more commonly observed in relation to civil structures rather than vehicle design, and forms no part of the design process of steel trailers. However, the comparatively low elastic modulus and high strain-to-failure characteristics of FRP materials yield structures that, although maintaining an equivalent strength capacity, possess significantly lower stiffness. This section examines the effects of large deflections on trailer performance, and presents deflection constraints applicable for FRP trailer design.

Public opinion plays a large part in the *perceived* success of civil structures. For instance, a pedestrian bridge that is perceived by the public to deflect excessively will not be considered a safe structure. Hence, the sensation of uneasiness experienced by the user

forms an important part of the design, despite the existence of adequate strength in the aforementioned bridge. Whilst the deflection limits which now form a significant part in the design of civil structures were introduced to avoid structural phenomenon (such as resonance at natural frequencies and crack control of concrete), they also serve to satisfy public perception of structural soundness. This perception is highly subjective, and is dependent on the sensitivity and awareness of the individual. However, current design standards ensure that deflection limits remain sufficiently low so as to reassure the public.

Inadvertently, public perception plays a similar role in the design of steel flat bed trailers. Negative deflection, or 'bowing', of a loaded trailer is often perceived as indicative of insufficient strength, much like the aforementioned pedestrian bridge. Conversely a positive deflection, known as 'arching', instils confidence in both the public and the user. Hence a loaded trailer that visually maintains an arched appearance is perceived to possess adequate strength. Manufacturers of flat bed trailers have acknowledged this phenomenon by introducing a precamber into the chassis rails. The magnitude of the precamber is prescribed by the customer, with a maximum of 75 mm being made available by most manufacturers. Further precamber is unnecessary, since the deflection of a typical steel trailer under the worst case loading case would not exceed 75 mm. Consequently, arching would continue to remain apparent and the perception of strength maintained even if the trailer was grossly overloaded and nearing failure.

A perception of adequate strength by the user and the driving public is essential to the successful integration of FRP trailers into mainstream transportation. This is emphasised by the inevitable comparison of the *perceived* strength of FRP trailers with that of steel trailers. Discussion with a number of heavy vehicle operators revealed substantial scepticism in regard to the concept of FRP trailers. This hesitation was characterised by a distinct lack of confidence in the strength of FRPs, and a generally pessimistic attitude with respect to the aims of this project.

The significance of deflection limitation is further accentuated by considering the implications of the comparatively high strain-to-failure characteristics of FRPs. As presented in Chapter 2, the ultimate strain capacity of glass fibres is approximately 2%, while carbon typically fails between 0.5 and 1.5% strain, depending on the type of precursor used (refer section 2.2). Hence, an overloaded FRP trailer (without deflection constraints) would potentially experience ultimate failure at a midspan deflection value between 250 to 400 mm, depending on the reinforcement type. Apart from the alarm experienced by the motoring public, potential damage to the suspension system or contact between the

standing legs and the road surface under such circumstances reinforce the need for deflection constraints.

The limitation of deflection therefore, is necessary to ensure that public confidence in FRP trailers is developed in a similar manner to any civil structure. This confidence would be established by public observation of FRP trailers possessing stiffness comparable to steel trailers, thereby implying comparable 'perceived strength.' Hence in order to win the approval of the industry and the driving public, deflection limits which compare with those of steel trailers should be enforced.

In addition to issues of public perception, the deflection of FRP trailers must be constrained due to possible difficulties associated with payload geometry. Payload distributions defined by load cases two, five and six would be relatively unaffected by large midspan deflections. However particular distributions of the payload, specifically load cases one and three, may require that the load remain straight and/or fully supported. A relatively flexible payload, corrugated iron sheeting for example, may span the length of the trailer. Throughout the duration of transportation, excessive deflection of the trailer under the payload may induce permanent deformation in the sheeting, thereby damaging the product. Alternatively a rigid payload, which is typically fully supported on a flat surface, will become supported by only two edges when subjected to excessive flexure of the trailer. This would effectively alter the payload distribution from that of load cases three or four to a distribution equivalent to load case five. Consequently, damage or failure of the decking may result from the highly concentrated loading. Similarly, damage may occur to the payload if it is structurally incapable of self-support on these two edges.

Considering the above discussion, it is appropriate to ensure that FRP flat bed trailers retain a value of structural stiffness similar to the steel equivalent. Three variables must therefore be defined, namely: 1) the amount of precamber set into the FRP chassis rails, 2) the maximum deflection allowable, and 3) the definition of the load case at which the designated maximum deflection should take place.

The designated magnitude of the precamber will largely determine the required stiffness of the trailer. A high precamber can sustain greater flexure whilst maintaining the 'arched' appearance. However excessive precamber is neither visually reassuring nor practical from the viewpoint of loading. For example, too much precamber will interfere with the loading of long, stiff items such as shipping containers, and would influence the load-sharing performance of the suspension.

The measurement of the precamber imposed on a given trailer may be performed from two distinct reference points. During the design and manufacture of a steel trailer, each end of the chassis rails act as reference points. However, subsequent to trailer assembly, a second datum can be set, as shown in Figure 4.12. This datum crosses the pivot point at the kingpin, and the centre axle position of the rear axle group, which are subsequently referred to as the support points. As shown in the figure, the magnitude of the *effective* precamber is substantially lower than the total precamber. The significance of the *effective* precamber is found in those load cases that distribute the payload between the support points, namely: load cases three, four and five. As these load cases induce a greater deflection than those load cases that are distributed along the entire length of the trailer, they require greater amounts of precamber be set in the trailer. Hence, it follows that the deflection of the chassis rails should be measured with respect to the support points, rather than the ends of the trailer.

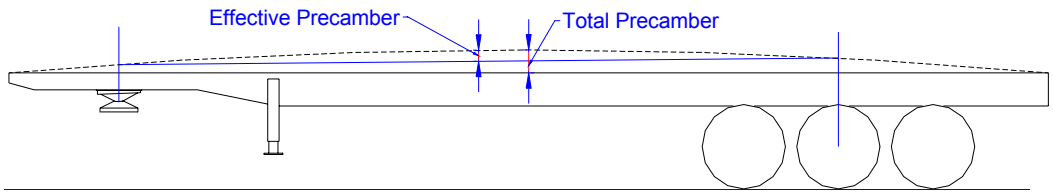

Figure 4.12 Total and Effective Precamber

While the maximum amount of precamber used for steel trailers is 75 mm, this should not necessarily represent the bound for FRP trailers. Due to the high stiffness of steel, typical *effective* mid-span deflection under dynamic loading conditions is approximately 35 mm (under load case one). Hence in order to maintain an arch, a total precamber of 75 mm would be required, as shown in Table 4.6.

Table 4.6 Comparison of Total and Effective Precamber for a 9.5 metre Span

Total Precamber (mm)	Effective Precamber (mm)
75	36
100	49
125	60
150	72

The limitations on precamber set by visual inspection are completely subjective, and can only provide limited assistance in setting a precamber. As with most issues in steel trailers, time and experience have yielded this value. Limitations of practicality can, in general, only be assessed on a case-by-case basis. Consequently, it is hard to judge whether or not a precamber of 200 mm would be visually offensive, or if it would present difficulties in the insertion of gates and the loading of the payload. A greater precamber, which would allow a lower structural stiffness, would result in lower material usage and cost, in addition to a reduction in tare weight. Hence, the use of a higher value of precamber is ideal in this application, as an FRP trailer possessing identical stiffness to that of a steel trailer would require a considerably large quantity of material due to the significantly lower stiffness of FRPs with respect to steel. However, in order to provide a FRP trailer that compares reasonably with a steel trailer, it was decided that a total precamber of 125 mm was suitable (for the purposes of this discussion), yielding an *effective* precamber of 60 mm. This precamber was set under the assumption that the distance between the kingpin and the centre of the rear axle group would be 9.5 metres, as denoted by ADR 43/04 6.1.2.1 [63]. While this value of precamber is substantially higher than that of a steel trailer, it was judged not to be excessive with respect to visual assessment, and would maintain practicality with respect to payload loading. With respect to suspension performance, lift axles would be required to minimise the effects of the high precamber when the trailer was lightly loaded. The insertion and removal of gates could be accommodated, if necessary, by alterations to the connection points.

Having defined the allowable precamber, and the significance of maintaining an arched appearance, it was necessary to define a load case at which the chassis rail should experience the designated maximum deflection. Of the load cases presented in section 4.5, the fourth and fifth have been clearly shown to impose the greatest moment and associated deflection. However, these load cases represent the extreme for flat bed trailers. As previously mentioned, low loaders would typically accommodate such payloads, which would rarely be imposed upon a standard flat bed trailer. Load case three more realistically represents the upper bounds of payload distribution to which a typical flat bed is subjected, and was therefore chosen as the defining load case, thereby classifying the trailer considered in this research project as a 'Medium Duty Trailer'.

Hence the deflection of the FRP trailer should, as a maximum, equal the effective precamber under the static load of load case three. Data presented in Table 4.2 suggests that the dynamic loading induced by typical road surfaces does not exceed 1.25 times that of the static load. Therefore, chassis flexure in response to dynamic loading would only

momentarily impose a small value of negative bowing on the trailer when subjected to this load case. Consequently, any payload distribution less severe than load case three would allow the maintenance of arching under typical operational conditions.

Loading of the trailer in a manner more severe than this limiting load case would produce bowing, even in a static context. This would provide a visual warning to the operator, indicating that the payload distribution has exceeded the design load, and that an alternative trailer of higher capacity should be utilised. However in the event that an operator should ignore such a warning, the trailer would possess sufficient strength capacity to safely transport the load, albeit with substantially noticeable bowing.

4.8.6 Identification of Dominant Design Constraint

The constraints imposed by three separate design parameters were presented in the previous sections. However, each parameter imposes differing constraints on the design of the trailer. The process by which these constraints were compared is described within this section, with the objective of this comparison being the identification of the dominant or critical constraint.

Of the three design constraints mentioned in the previous section, only strength and deflection constraints will be compared here. The complex nature of fatigue damage and the establishment of an associated design capacity are discussed separately in Chapters 5 and 8.

In order to compare the various constraints in a consistent manner, allowable strain limits are used (refer section 2.7.3). Each constraint is defined by a maximum allowable strain limit, set by the respective reduction factors placed on the material. The maximum allowable strain for the strength constraint is determined using material capacity reduction factors. Similarly, the maximum allowable strain for the deflection constraint is determined by assessing the relationship between the laminate strain, the slenderness of the beam, and the allowable beam deflection. These reduction factors are applied to the ultimate laminate capacity to determine acceptable levels of strain in relation to the nature of loading. Hence, the dominant constraint will be determined by identification of the lowest maximum allowable strain. For example, if the deflection limits of the chassis required a lower maximum allowable strain than that required for strength, then deflection would be considered the critical or dominant design criteria. So whilst a moment capacity must still be established, the strain limits placed on the reinforcement would be set by deflection

constraints, rather than those applicable for strength. Identical loads (and DDFs) are applied in consideration of both of these constraints, and it was therefore assumed that the magnitude of the load did not contribute to the determination the dominant constraint.

To demonstrate, consider the FRP chassis rail illustrated in Figure 4.13. For simplicity, the beam is of uniform cross section. It is assumed that carbon fibre reinforcement is used to carry the bending moment, and E-glass double bias reinforcement carries the shear loading (refer section 5.5.1). It is also assumed that the core is of zero stiffness, and that shear deflection is negligible. This method is equally valid regardless of the beam shape or reinforcement type used.

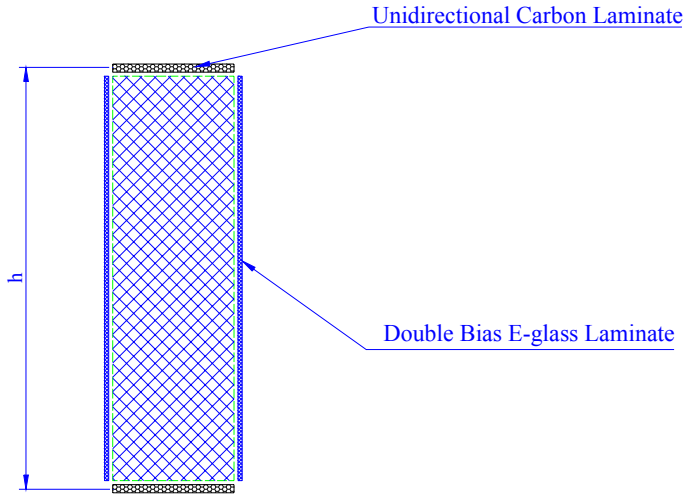

Figure 4.13 Simplified FRP Chassis Rail

Strength Constraints

In order to determine the material capacity reduction factor of the carbon fibre reinforcement, the approach used by Karbhari [60] was adopted. This approach has been widely accepted by the structural engineering community in the design of composite structures, and is used in an abridged form in this section.

Karbhari proposes the use of a material capacity reduction factor, derived on the basis of variables related to materials and processing which directly influence laminate properties. This approach proposes that the design value for a material can be determined as

$$F_d = \square F_k$$

where F_k is the characteristic value. It is proposed that, at the ultimate state, the Material Capacity Reduction Factor for strength, Φ, is defined as

$$\Phi = \Phi_{mat} \cdot \Phi_{proc} \cdot [(\Phi_{cure} + \Phi_{loc})/2] \cdot \Phi_{degr} \qquad (4.1)$$

where Φ_{mat} addresses the variation in material properties determined by different methods (refer Table 4.7), Φ_{proc} accounts for property deviation due to the manufacturing method used (refer Table 4.8), Φ_{cure} denotes the variation in properties resulting from the degree of cure achieved (refer Table 4.9), Φ_{loc} accounts for the uncertainty associated with the manufacturing environment and location (refer Table 4.10), and Φ_{degr} addresses changes in material properties which occur over time and in response to environmental effects (refer Table 4.11).

Table 4.7 Values for Factor Based on Derivation of Material Properties (Φ_{mat})

Source: [60]

Value	Description
0.50 - 0.80	Properties based on constituent material test data Lamina and laminate properties derived from theory
0.67 - 0.90	Properties based on individual plies derived from tests Laminate properties derived from theory
0.85 - 0.97	Properties derived from laminate or structural tests

Table 4.8 Values for Factor Based on Processing Method Used (Φ_{proc}) Source: [60]

Value	Description
0.95 - 1.0	Prepreg based autoclave cure
0.95 - 1.0	Prepreg based filament winding
0.85 - 0.95	Wet-winding
0.75 - 0.80	Wet lay-up of Fabric (Vacuum Bag)
0.60 - 0.75	Wet Lay-up of Fabric (Unbagged and w/o vacuum)
0.70 - 0.95	Pultrusion
0.75 - 0.87	Resin Transfer Moulding (RTM)
0.70 - 0.85	Resin Infusion
0.60 - 0.65	Spray-up

Table 4.9 Values for Factor Based on Type of Cure Applied (Φ_{cure}) Source: [60]

Value	Description
1	Autoclave cure
0.90 - 1.0	Elevated temperature controlled cure process
0.80 - 0.95	Ambient cure

Table 4.10 Values for Factor Based on Location of Manufacturing/Construction (Φ_{loc})

Source: [60]

Value	Description
1	Controlled factory environment
0.90 - 0.95	Uncontrolled field environment within an enclosure
0.80 - 0.90	Field environment without an enclosure

Table 4.11 Values for Factor Based on Material Degradation/Aging (Φ_{degr})

Source: [60]

Material System	Short-term	Long-term
E-Glass Composite	0.60 - 0.80	0.30 - 0.50
S-Glass Composite	0.75 - 0.90	0.55 - 0.80
Carbon Composite	0.95 - 1.00	0.70 - 0.90

In determination of the reduction factor in this example, the following assumptions were made:

- Material properties were derived from laminate tests (refer Chapter 5)
- Manufacturing is performed by wet lay-up with a vacuum bag
- The product is subjected to a controlled cure at an elevated temperature following manufacture in a climate controlled facility
- The carbon fibre reinforcement used would be subject to long term loading of an intermittent nature - ie. Periodic fatigue loading is assumed, and creep effects are negligible

Hence, the capacity reduction factor was found to be:

$$\Phi = 0.91 \text{ x } 0.775 \text{ x } [(0.95 \text{ x } 1.0)/2] \text{ x } 0.8$$
$$= 0.55$$

The reduced material properties of the carbon can therefore be found. Assuming a failure strain of approximately 8700 με (refer section 5.6.6), the reduced material capacity equals

$$\varepsilon_{Reduced} = \Phi \text{ x } \varepsilon_{Ult.} \qquad (4.2)$$
$$= 0.55 \text{ x } 8700 \text{ με}$$
$$= 4785 \text{ με}$$

Dividing this number by the DDF of 2.5, the allowable strain under the static load of load case three is equal to 1914 με. However, Karbhari [60] states that, in general, LHS carbon such as T-300 should not be subjected to strains in excess of 3000 με for typical service loads, and 4500 με for the ultimate load experienced by the laminate under any service condition. These limits were founded on the basis of issues of durability and long-term performance, taking into account possible changes in loading conditions and the operating environment throughout the life of the trailer. Adopting these recommendations, the maximum allowable strain established by equation (4.2) was reduced from 4785 με to 4500 με. The allowable strain under the static load of load case three is therefore reduced to 1800 με.

It should be noted at this point, that there exist significant differences in the compressive and tensile capacities of FRP laminates. This phenomenon (discussed further in section 5.6.6) is largely dependent on the reinforcement and matrix types, in addition to the buckling restraint provided to the laminate. Although tests conducted by the author yielded compressive failure strains almost identical to the tensile failure strains, a review of the literature would suggest that the compressive properties and performance of a laminate are, in general, approximately 10 – 20% lower than the tensile properties. This is often due to buckling of the fibres in compression, particularly when there is a low resin content. However, based on the test results, it was decided not to distinguish between tensile and compressive performance, consequently the allowable ultimate strain capacity with respect to both tension and compression was taken to be identical.

An additional point to note is that a comparative increase or decrease in the quantity of reinforcement contained within the compressive laminate would effectively shift the neutral axis either closer to the compressive and tensile reinforcements respectively. This enables the modification of the failure mode, as the strain imposed on a either laminate is directly related to the distance from the neutral axis.

It should also be noted that the material capacity reduction factors proposed by Karbhari were developed specifically for common LHS carbon reinforcements such as T-300 and AS4 (refer section 2.2.3), and should therefore only be applied to this type of carbon reinforcement. As mentioned in Chapter 2, the ultimate tensile strain capacity of various carbon fibre types ranges from 0.5% to over 1.5%. Clearly, the maximum allowable strain due to service loads of 4500 με is not appropriate for a carbon fibre whose ultimate strain capacity is barely 500 με greater than that seen in service. It would therefore be appropriate to review the material capacity reduction factors should an alternate carbon fibre reinforcement type be selected for application in this context.

Having established the design moment (from the applicable load case), in addition to the maximum allowable strain in the laminate during typical and ultimate service conditions, the subsequent number of layers required to carry the imposed moment can be calculated. An example of this method of design, using the techniques discussed here, is shown in Chapter 7.

Deflection Constraints

The evaluation of the strain levels resulting from the deflection characteristics of the trailer can be performed by assessing the relationship between the laminate strain, the depth of the beam, and the allowable beam deflection. Fundamentally, for a predetermined deflection and beam span, the strain within the laminates is directly related to the beam depth. Hence, the range of possible chassis rail depths available to the designer allows a measure of flexibility in setting the laminate strain levels. Having previously defined the allowable static deflection, and the worst-case payload distribution, the relationship between beam depth and laminate strain can then be calculated. Consideration of various beam depths and the corresponding strains within the laminate should then yield an optimum solution with respect to beam depth.

To demonstrate, the example introduced in the previous section will be expanded upon. It is assumed that a 125 mm total precamber is in place, and that the distance between the kingpin and the centre of the rear axle group is equal to the maximum allowable distance of 9.5 metres. For the purposes of this example, the rear axle group was considered as a single pinned support at the centre of the axle group, as a simplified method of representing of the load sharing characteristics of the suspension system. Having loaded the chassis rail in accordance with load case three (the worst load case for the Medium Duty Trailer), the allowable strain in the top and bottom laminates were determined as shown below:

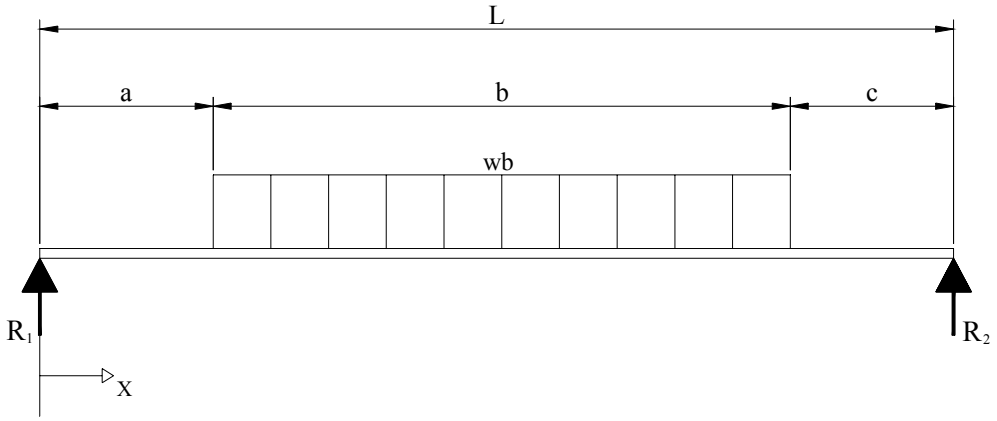

Figure 4.14 Simplified Chassis Rail Subjected to Load Case Three

The known parameters are:

Beam Span, L = 9.5 m

Payload Length, b = 6.0 m

Force Imposed by the Payload, wb = 154 kN (half of the maximum payload as defined by section 4.5.1)

Similarly, in keeping with the maximum allowable wheel loads (refer section 4.5.1), the reactions at the centre of each axle group are:

$$R_1 = 59 \text{ kN}$$
$$R_2 = 95 \text{ kN}$$

Now it can be shown that

$$c = [(2R_1L/wb) - b]/2 \quad (4.3)$$
$$c = 0.64 \text{ m}$$

Therefore,

$$a = 2.86 \text{ m}$$

In order to determine the maximum strain within the top and bottom flanges of the beam, it is necessary to identify the position along the beam, x, at which the greatest deflection occurred. Now when $a \leq x \leq (a+b)$, it can be shown that:

$$\Delta_x = (w/24EI)\{(x-a)^4 + [b(b+2c)x/L][-2x^2 + 2a(2L-a) + b(b+2c)]\} \quad (4.4)$$

Substituting Δ_x = 60 mm (effective precamber – refer Table 4.6), and unity for EI, the equation is solved to find a maximum value for x

This yields

$$\Delta_{max} \text{ at } x = 4.88 \text{ m}$$

Now, using Hooke's law,

$$E = \sigma\varepsilon$$
$$= My/I\varepsilon$$
$$= Mh/2\varepsilon I \quad (4.5)$$

Where the term, h, denotes the beam depth.

Hence, equation 4.4 becomes

$$\Delta_x = (w\varepsilon/12M_xh)\{(x-a)^4 + [b(b+2c)x/L][-2x^2 + 2a(2L-a) + b(b+2c)]\} \quad (4.6)$$

If $$M_x\ (a<x<(a+b)) = R_1 x - 0.5w(x-a)^2 \qquad (4.7)$$

$$M_{x=4.88} = 235.55 \text{ kNm}$$

Hence, at $x = 4.88$ m, $\Delta_x = 60$ mm, equation 4.4 can be resolved in terms of h and ε
This yields

$$\varepsilon/h = 3.304 \qquad (4.8)$$

The constant in this linear relationship between laminate strain and beam depth is unique to this load case, and hence the investigation of any alternate loading scenarios would necessitate the determination of the respective constant.

A report by the National Road Transport Commission (NRTC) [61] emphasises the significance of the reduction of the centre of gravity of the laden vehicle with respect to the rollover threshold. Specifically, this report recommends the introduction of regulations that would require all new trailers to be able to withstand a minimum lateral acceleration of 0.35g. This is significant as Fancher et al [62] and Winkler [63] state that some trailers are able to withstand no greater than 0.2g in lateral acceleration.

The selection of beam depth must therefore be considered with regard to the effects of beam depth on the centre of gravity of a fully laden vehicle. It was observed that both the clearance between the trailer chassis and the rear of the prime mover, and between the trailer chassis and ground level remained relatively constant, regardless of the depth of the chassis rail. That is, an increase in chassis rail depth resulted in a greater deck height, this being attributable to the uniformity of the tri-axle suspension size and wheel diameters. (Further discussion regarding the clearance between the trailer chassis and the prime mover are contained within Chapter 7.) As observed by the survey of steel trailers presented previously in section 4.4, it would appear that the depth of chassis rails of steel trailers do not, in general, exceed 600 mm. Indeed, it is anticipated that those trailers possessing greater chassis rail beam depths are those that have a greater susceptibility to rollover. Conversely, a beam depth of less than 400 mm is not observed in steel trailers, as this necessitates a significant increase in the flange thickness required to maintain flexural stiffness. The minimisation of beam depth is particularly uneconomical with respect to the use of carbon fibres, which possess a lower modulus than that of steel. It was therefore decided, as a general limit, to replicate these outer bounds with respect to the depth of the FRP chassis rails, with the anticipation that the optimum solution would lie closer to the

middle value. It should also be noted that the reduction of tare weight of an FRP trailer effectively increases the height of the centre of gravity of a laden trailer.

This range of chassis rail depth allows some flexibility in the adjustment of strain limits, as the strain in the outer fibres of a beam will vary in accordance with both beam depth and deflection. Having predetermined the allowable deflection of the chassis, the strain remains proportional to beam depth. The variations in allowable strain in relation to chassis rail height are tabulated in Table 4.12, which shows that the strain induced by the maximum deflection varies substantially depending on the beam depth chosen. The greater beam depths enable the more efficient utilisation of the carbon reinforcement, thereby reducing the volume of reinforcement required to sustain the load within the deflection limits. Provided inexpensive core material is used, significant economic advantages result from chassis rails of greater depth.

Table 4.12 Maximum Allowable Strain Due to Static Deflection Constraints

Chassis Rail Depth, h (mm)	Maximum Allowable Strain (με)
400	1322
450	1487
500	1652
550	1817
600	1982

Comparison of Constraints

The capacity reduction factor with respect to laminate strength has been determined, and was shown to yield a static strain limit of 1800 με. This represents the maximum allowable strain imposed by constraints on the strength of the laminate. By comparison, the magnitude of the strains imposed by the deflection criteria was dependent on the chassis depth. As shown in Table 4.12, the maximum allowable strain, as determined by deflection constraints, yields values that are both above and below that set by laminate strength constraints due to variations in beam depth.

Consequently, the critical or dominant constraint applicable in design is primarily dependent on the beam depth. As shown in Figure 4.15, deflection constraints become dominant when the beam depth is on the lower bound of the range of allowable depth.

Conversely, strength constraints become dominant when the beam depth approaches the upper bound. Also included in Figure 4.15 are the trendlines resulting from alternate choices in total chassis rail precamber. The figure illustrates that those values of total precamber of approximately 110mm or lower result in the elimination of laminate strength considerations as a design constraint for any allowable beam depth. Conversely, total precamber values of approximately 200 mm or greater, would result in the elimination of deflection criteria as a design constraint.

From the figure, it was concluded that, based on a total precamber of 125 mm, the dominant constraint is determined by the beam depth. Ideally, strength would be utilised in the establishment of design constraints, as this enables the utilisation of the reinforcement to the maximum allowable strain value. However, this must be weighed against the concerns of rollover threshold previously discussed. Hence, it would appear that the optimum solution lies in the intersection of the two lines describing the two constraints. With respect to this simplified beam utilising a total precamber of 125 mm as previously established, the optimum solution lies at a beam depth of approximately 545 mm.

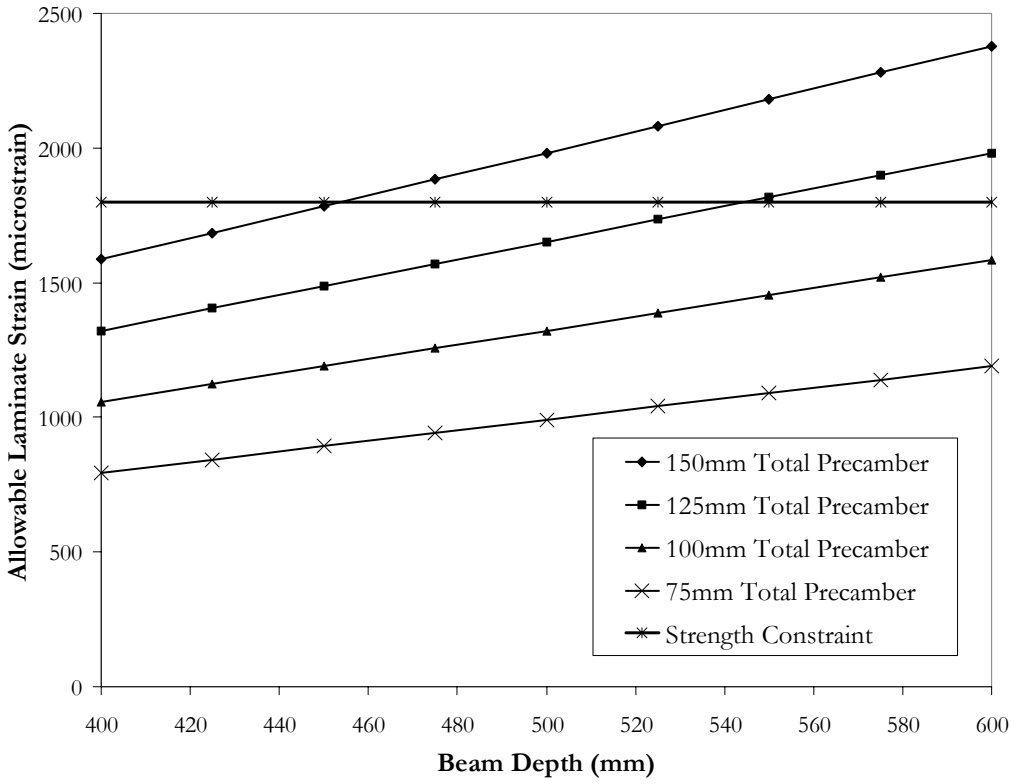

Figure 4.15 Comparison of Strength and Deflection Constraints on Chassis Rail Depth

This example has demonstrated that, for a given value of precamber, the optimum solution with respect to beam depth is not found by the identification of a singular dominant constraint. That is, neither deflection nor strength constraints should be used exclusively in the determination of the chassis rail capacity. Rather, maximum utilisation of both the material and the structural characteristics is achieved by the identification of the configuration at which the two constraints are each fully exploited.

Figure 4.15 also demonstrates that the selection of a lower value of precamber (say 75mm), would not enable the maximisation of the strength constraint whilst maintaining a sensible chassis rail depth. Conversely, the selection of a higher value of precamber (say 175mm), would require an extremely small chassis rail depth to enable the maximisation of the deflection constraints. Hence, in the context of this example, it would appear that only values of precamber ranging from approximately 115mm to 160mm would enable the greatest utilisation of both constraints.

A FRP trailer which possesses higher precamber and lower stiffness than a steel trailer would require careful selection of an appropriate suspension system. Parameters such as the load sharing characteristics of the system under dynamic conditions would need particular attention, to ensure that a fully laden FRP trailer maintained an evenly distributed load to the chassis, and to the road.

The significance of fatigue as a design constraint has not been addressed within this chapter. A comparison of the constraints governing deflection, strength, and fatigue characteristics is presented in Chapter 8.

4.9 Conclusions

This chapter has discussed a number of issues. The extent of published research into vehicle dynamics has been investigated, revealing a clear focus on the prediction of the dynamic response and behaviour of semi-trailers, as well as the impact of heavy vehicles on roads. There would appear to remain a significant volume of research yet to be performed in order to establish national design standards that can be agreed upon with respect to safety and economic viability. It seems that a distinct absence of research exists regarding the effects of dynamic loading on the stresses imposed on the chassis rail.

The overview of current industry practice highlighted the need for industry guidelines in design. The substantial variations in the structural capacity of flat bed semi-trailers did not enable the immediate selection of the most efficient structural characteristics. These variations highlighted the independent nature of trailer design, in which each manufacturer determines it's own design in accordance with experience.

The designation of a dynamic design factor (DDF) included data extracted from both research and industry sources. A common factor of 2.5 was identified and adopted for use in further analysis within this project.

The definition of significant load cases was performed, and implications to the classification of trailers by variations in load distribution were suggested to assist in design optimisation and the reduction of trailer overloading caused by incorrect payload distribution.

A number of design constraints pertinent to FRP trailers were presented, and compared in order to determine the critical or dominant constraint. The constraints on deflection and strength were shown to be necessary in terms of public perception and the preservation of acceptable factors of safety with respect to the FRP. For a prescribed range of precamber values (75 – 150 mm), it was shown that an optimum value could be identified which utilised the upper limits of each constraint. In the example given, for a precamber of 125mm, the optimum solution was identified at a beam depth of 545mm, with a maximum laminate strain of 1800 με. Outside the prescribed range of precamber values, the deflection constraint was shown to be dominant for lower values of precamber, while the laminate strength constraints were shown to dominate when the values of precamber were high.

References

[1] Articulated vehicles – design criteria for fifth wheel skidplates: AS 4235-1994. Homebush NSW: Standards Association of Australia; 1994.

[2] Australia design rules for motor vehicles and trailers. 3rd edition. Canberra, ACT: Department of Transport and Regional Services; 1989.

[3] Boiler and pressure vessel code – section VIII division 1: rules for construction of pressure vessels. The American Society of Mechanical Engineers; 1998; ISBN#: 0791825140.

[4] Semi-trailers employed in the highway transport of weight-concentrated radioactive loads – design, fabrication, and maintenance: ANSI N14.30-1992. New York: American National Standards Institute; 1992.

[5] Bernard J, Vanderploeg M, Shannan, J. Recent developments in vehicle dynamics. Shock and Vibration Digest 1987 April; 19(4): 10-16.

[6] Shaw PA. Static analysis and dynamic simulation of linked multi-axle truck suspension units [PhD dissertation]. Brisbane, Queensland: University of Queensland; 1993.

[7] Ellis JR. Vehicle dynamics. London: London Business Books; 1969.

[8] Gillespie TD. Fundamentals of vehicle dynamics. Warrendale, PA: Society of Automotive Engineers; 1992.

[9] Beermann HJ. Static analysis of commercial vehicle frames: a hybrid – finite element and analytical – method. Int. J. of Vehicle Design 1984; 5(½).

[10] Mills B, Johnson PF. Static analysis of a light truck frame using the finite element method. IEEE Conference Record of Annual Conference of Electrical Engineering Problems in the Rubber and Plastics Industries, Inst. of Phys, Stress Anal Group, Annual Conference, Stress, Vibration and Noise Analysis in Vehicles 1975; Birmingham, England; New York: John Wiley and Sons; 1975: 47-73.

[11] Mills B, Sayer J. Static and dynamic analysis of a light van body using the finite element method. IEEE Conference Record of Annual Conference of Electrical Engineering Problems in the Rubber and Plastics Industries, Inst. of Phys, Stress Anal Group, Annual Conference, Stress, Vibration and Noise Analysis in Vehicles 1975; Birmingham, England; New York: John Wiley and Sons; 1975: 283-312

[12] ElMadany MM. Nonlinear ride analysis of heavy trucks. Computers and Structures 1987; 24 (1): 69-82.

[13] Gadala ME, ElMadany MM, Gadala MS. Finite element and analytical modelling of a tractor-semitrailer vehicle. Computers and Structures 1986; 23 (6): 831-836.

[14] Besselink I, Van Asperen F. Numerical optimisation and linear dynamic behaviour of commercial vehicles. Vehicle System Dynamics 1994; 23: 53-70.

[15] Sharman PW. Torsional design aspects of long wheelbase vehicles. IEEE Conference Record of Annual Conference of Electrical Engineering Problems in the Rubber and Plastics Industries, Inst. of Phys, Stress Anal Group, Annual Conference, Stress, Vibration and Noise Analysis in Vehicles 1975; Birmingham, England; New York: John Wiley and Sons; 1975: 123-148.

[16] Megson THG. Analysis of semi-trailer chassis subjected to torsion. Institution of Mechanical Engineers 1984; C176/84

[17] Nalecz AG, Genin J. Dynamic stability of heavy articulated vehicles. Int. J. of Vehicle Design 1984; 5 (4).

[18] Starr PJ. A personal computer-based CAD system for investigating lateral stability of vehicle-dolly-trailer combinations. Int. J. of Vehicle Design 1993; 14 (2/3).

[19] Tabarrok B, Zhang DJ. On nonlinear yaw-roll-pitch model of the dynamics of log hauling trucks. Heavy Vehicle Systems; Int. J. of Vehicle Design 1998; 5 (3-4): 181-207.

[20] Ali Attia H. Computer simulation of vehicle dynamics. Transactions of the Canadian Society for Mechanical Engineering 1998; 22 (2): 127-142

[21] Hecker F, Hummel S, Jundt O, Leimbach KD, Faye I, Schramm H. Vehicle dynamics control for commercial vehicles; SAE Special Publications 1997 Nov; 1307: 59-66.

[22] Sayers MW, Riley SM. Modelling assumptions for realistic multibody simulations of the yaw and roll behaviour of heavy trucks. SAE paper 960173; Warrendale, PA: Society of Automotive Engineers; 1996.

[23] Wang B, Hu P. The assessment of the ride quality of a truck-full trailer combination. Heavy Vehicle Systems; Int. J. of Vehicle Design 1998; 5 (¾): 208-235.

[24] Dokainish MA, ElMadany MM. Random Response of Tractor-Semitrailer system. Vehicle System Dynamics 1980; 9: 87-112.

[25] Zhou J. Ride simulation of a nonlinear tractor-trailer combination using the improved linearisation technique. Heavy Vehicle Systems; Int. J. of Vehicle Design 1998; 5 (2): 149-166.

[26] El-Gindy M. The use of heavy vehicle performance measures for design and regulation. DSC- Systems: ASME; 1992; 44.

[27] Karamihas SM, Gillespie TD. Characterising trucks for dynamic load prediction. Heavy Vehicle Systems; Int. J. of Vehicle Design 1993; 1 (1).

[28] Potter TEC, Cebon D, Cole DJ, Collop AC. Road damage due to dynamic tyre forces measured on a public roads. Heavy Vehicle Systems; Int. J. of Vehicle Design 1996; 3 (4): 346-362.

[29] de Pont JJ. Experiences with simulating on-road heavy vehicle suspension behaviour using servo-hydraulics. Heavy Vehicle Systems; Int. J. of Vehicle Design 1996; 3 (1-4).

[30] Sweatman PF. Dynamic performance and traffic impacts of road trains. Vermont South, Victoria: Australian Road Research Board; 1991.

[31] Sweatman PF. Effect of heavy vehicle suspensions on dynamic road loading. Vermont South, Victoria: Australian Road Research Board; 1980.

[32] Sweatman PF. A study of dynamic wheel forces in axle group suspensions of heavy vehicles. Vermont South, Victoria: Australian Road Research Board; 1983.

[33] National Road Transport Commission (NRTC). Evaluation of in-service compliance of road friendly suspensions. Final Report. Melbourne National Road Transport Commission; 2000 Aug.

[34] Starrs MM Pty Ltd, Ian Wright and Associates & ARRB Transport Research Ltd. Evaluation of in-service compliance of road friendly suspensions. Draft for Comment. Melbourne: National Road Transport Commission; 2000 Mar.

[35] Roaduser International Pty Ltd, 1999, "Investigation in the Specification of Heavy Trucks and Consequent Effects on Truck Dynamics and Drivers" Draft Final Report, Department of Transport and Regional Services, November 1999

[36] Roaduser International Pty Ltd. In-service assessment of road friendly suspensions. Melbourne: National Road Transport Commission; 2000 Jan.

[37] Miller CW. On the Dynamic Behaviour of a Bridge-Vehicle System [PhD Dissertation]. Brisbane, Queensland: University of Queensland; 1984.

[38] Weissmann J, Harrison R. Impact Of 44000 kg (97,000-lb) six-axle semitrailer trucks on bridges on rural and urban U.S. interstate system. Transportation Research Record; Univ of Texas at San Antonio, San Antonio, TX; 1998 Sep; 624: 180-183.

[39] Li CY, Fafitis A. Bridge vibration and impact under moving vehicles. Vauhn & Melton Consulting Engineers, Asheville, NC: American Society of Mechanical Engineers, Petroleum Division 1996; 81 (9): 17-23.

[40] Page J. Dynamic behaviour of a single-axle vehicle suspension: a theoretical study. Corwthorne (UK): Department of Environment; Transport and Road Research Laboratory; 1973; TRRL Report 580.

[41] Sayers M, Gillespie TD. Dynamic pavement/wheel loading for trucks with tandem suspensions. Vehicle Systems Dynamics 1983; 12 (1-3): 171-172.

[42] Sayers M, Gillespie TD. Dynamic pavement/wheel loading for trucks with tandem suspensions. Proceedings of the 8th IAVSD Symposium on the Dynamics of Vehicles on Roads and Tracks; Link\ping (Sweden): Swets and Zeitlinger; 1983: 517-533.

[43] Kunjamboo KK, O'Connor C. Truck suspension models. Brisbane, Queensland: Department of Civil Engineering, University of Queensland; 1981; Research Report No. CE 21.

[44] Dohrmann CR, Carne TG. Model refinement using transient response. Proceedings of the International Modal Analysis Conference (IMAC); Bethel, CT, USA; 1998; 1: 630-636.

[45] Kamar EA, El-Zafarany A, Cookson RA. Simulation of suspension systems by the finite element methods. Int. J. of Vehicle Design 1988; 9 (4/5): 447 – 459.

[46] Pacejka HB, Bakker E. The magic formula tyre model, tyre models for vehicle dynamics. Proceedings of the 1st International Colloquium on Tyre Models for Vehicle Dynamic Analysis; 1991 Oct; Delft, Netherlands: Swets & Zeitlinger, Amsterdam; 1993.

[47] Zegelaar PWA, Pacejka HB. The in-plane dynamics of tyres on uneven roads. Vehicle System Dynamics Supplement 25; 1996: 714-730.

[48] Gisper M, Hofer R, Lugner P. Dynamical tyre forces response to road unevennesses. Vehicle System Dynamics Supplement 27; 1997: 94-108.

[49] Weiblen W, Oelmann B. Measurement of multiaxial wheel forces and application of the results for the fatigue life evaluation of vehicles. Warrendale, PA: Society of Automotive Engineers; 1996; SAE Paper 962564.

[50] Willing J. Development of an aramid fiber reinforced road tanker with increased loading capacity. Warrendale, PA: Society of Automotive Engineers; 1995; SAE Paper 952624.

[51] Woodley CC, Piggott BR. Design data for heavy vehicles. IEEE Conference Record of Annual Conference of Electrical Engineering Problems in the Rubber and Plastics Industries, Inst. of Phys, Stress Anal Group, Annual Conference, Stress, Vibration and Noise Analysis in Vehicles 1975; Birmingham, England; New York: John Wiley and Sons; 1975: 473-481.

[52] Taylor C. Fabrication and testing of high-strength, high capacity, weight optimised trailers. Proceeding of the 5th Annual International Conference on High Level Radioactive Waste Management; 1994 May; Las Vegas, Nevada; 2: 931-933.

[53] Hall D, Walsh P, Lapworth J, Roufaeil Dr. O. Low tare weight livestock trailers. Final Research Report to Meat Research Corporation; December, 1993; Project DAQ.60.

[54] Cole DJ, Cebon D. Validation of an articulated vehicle simulation. Vehicle System Dynamics 1992; 21: 197-223.

[55] Sharman PW. The use of dynamic strain records to estimate the fatigue life of a semi-trailer chassis. IEEE Conference Record of Annual Conference of Electrical Engineering Problems in the Rubber and Plastics Industries, Inst. of Phys, Stress Anal Group, Annual Conference, Stress, Vibration and Noise Analysis in Vehicles 1975; Birmingham, England; New York: John Wiley and Sons; 1975: 461 – 471.

[56] Fenton J. Vehicle body layout and analysis. London: Mechanical Engineering Publications Ltd; 1980.

[57] Garrett K. Automobile dynamic loads. Automobile Engineer; 1953.

[58] Harris MN, Nawrocki PE. Design analysis for heavy duty vehicles – today and tommorow. Int. J. of Vehicle Design 1984; 5 (1/2): 104–114.

[59] Michelberger P, Keresztes A, Bokor J, Varlaki P. Modelling and identification of bus axle and frame structure dynamics. Int. J. of Vehicle Design 1988; 9 (1): 52-66.

[60] Karbhari VM. Determination of materials design values for the use of fibre reinforce polymer composites in civil infrastructure. Short Course Notes – Use of Fibre Reinforces Polymer (FRP) Composites in Civil Infrastructure; 2000 June; UNSW.

[61] National Road Transport Commission (NRTC). Definition of potential performance measures and initial standards. Discussion Paper. Melbourne, VIC; 2001 April.

[62] Fancher PS, Matthew A, Campbell K, Blower D, Winkler CB. Turner truck handling and stability properties affecting safety. Final Report. Ann Arbor: University of Michigan Transportation Research Institute; 1989; Report No. UMTRI-89-11-1; Vol 1.

[63] Winkler CB, Blower D, Ervin RD, Chalsani RM. Rollover of heavy commercial vehicles. SAE Research Report. Warrendale, PA: Society of Automotive Engineers; 2000.

[64] Australian Design Rule 43/04. Vehicle Configuration and Dimensions. Commonwealth of Australia Gazette No. P1; 1997.

Chapter 5 Selection of Materials

5.1 Introduction

As discussed in Chapter 2, there exists within the broad range of composite materials a vast array of physical properties, with the selection of the appropriate materials being the responsibility of the designer. The evaluation of material properties forms an integral part of this process, particularly in relation to laminate characteristics.

The process of evaluation and selection of the most suitable combination of matrix, reinforcement, and core materials in application to FRP flat bed trailers is described in this chapter. Specifically, the desired material characteristics and performance of each constituent of composite construction are outlined. This is performed via a combination of available literature and material testing where possible. Evaluation criteria are defined, and the most suitable materials are identified.

5.2 Characteristics of Core Materials

The primary roles of a core material are to separate the laminates within the context of sandwich panel construction, and to provide a supporting shape over which the reinforcement can be laid during cure. However, the core material is also a primary contributor to a number of other characteristics inherent within a composite structure. Each of these characteristics is outlined in the following sections in specific relation to FRP trailers. These were selected on the basis of their significance with respect to the project aims and the expected operational conditions.

5.2.1 Density

Within any large composite structure utilising sandwich panel construction, the mass of the core material represents a significant proportion of the mass of the entire structure. As the reduction of the trailer tare mass is of primary importance within this project, the core material used within the construction should possess a low density. Table 5.1 provides a summary of the densities of various core materials. It appears that the foam cores present the greatest advantage with respect to density, particularly in comparison to the particulate filled resin (PFR). Additionally, there exists a range of available densities, which allow the variation of mechanical properties. However, these low-density foams also possess relatively low values of strength.

5.2.2 Modulus and Strength

The structural performance of any core material is of great significance. Whilst the laminates provide the bending stiffness to the structure, the core material determines the shear stiffness characteristics of any given sandwich panel. Hence, a sufficiently high shear modulus is required to prevent excessive shear deflection. Sufficient shear stiffness is also desired to prevent overall buckling and skin dimpling.

The core should also contain sufficient shear strength to withstand the shear stresses applied to the member. The addition of shear reinforcement adds mass, material and labour costs, and hence significant advantages exist in using a core material with sufficient shear strength.

A high compressive strength is required to withstand the inevitable concentration of load. In such circumstances, the core must provide support to the laminate, allowing the load to be distributed by the laminate. The addition of hard points can minimise the significance of this issue, however hard points increase the structural mass, and the cost of materials and labour.

When the laminate is subjected to high compressive forces, a high compressive modulus is also required to prevent the wrinkling or localised crushing of the laminate [2]. This can occur when the core provides insufficient support to the laminate, allowing it to buckle locally in the area of highest stress.

Table 5.1 Typical Mechanical Properties of Various Core Materials

	Density (kg/m3)	Tensile Strength (MPa)	Compress. Modulus (MPa)	Compress. Strength (MPa)	Shear Modulus (MPa)	Shear Strength (MPa)
Balsa						
Along grain	96-250	9.5-31	110-380	1.1-3.6	2250-8000	3.5-20
Across grain		0.5-1.5	-	-	35-380	0.34-1.36
Honeycomb						
5052 Alloy Hexagonal Aluminium 1/8-5052-0.002	130	-	2400	10.1	930	5
Polyurethane Foam	20-400	0.1-8.96	-	0.1-13.8	1.56-103.5	0.14-3.1
PVC Partially Crosslinked Foam (H Series from DIAB)	30-250	0.8-8.8	20-400	0.3-5.8	10-108	0.35-4.5
SAN Foam (Corecell from ATL)	50-200	1.0-6.8	22.8-86.0	0.4-3.44	11.7-45.2	0.66-1.97
PFR Glass Microspheres 40% K15 filler by volume from 3M	650	25	2050	47	-	-

The comparative values of strength shown in Table 5.1 clearly indicate that the PFR exceeds the strength capacity of any of the other core materials shown. The low-density foams mentioned in the previous section display comparatively poor strength, particularly as the foam density decreases. The high strength of PFR would also suggest the removal of hard points in order to withstand load concentrations. The anisotropic nature of the balsa and honeycomb cores presents various difficulties with respect to the assessment of core performance. The multi-directional nature of loading imposed on a trailer chassis through flexure, torsion, and handling manoeuvres, in addition to the three dimensional construction of the chassis, suggests that a core material possessing isotropic mechanical characteristics would be beneficial.

5.2.3 Ultimate Strain Capacity

The core material is responsible for the support of the laminate, both during manufacture and throughout the service life of the structure. However, support of the laminate is particularly important when nearing the ultimate capacity of the laminate. Failure of the core typically occurs in regions of highest strain, which coincide with the regions of highest laminate strain. Consequently, premature failure of the core in these regions can initiate

stress concentrations in the laminate, in addition to debonding of the laminate from the core. A loss of structural integrity results in progressive collapse under sustained loading. Hence, whilst the laminates provide strength to the member, the core must possess a sufficient ultimate strain capacity in order to remain intact until after the laminates have failed.

However, the significance of this phenomenon is largely dependent on the expected strains imposed during the service life of the structure. The restrictions regarding deflection limitation in civil structures significantly reduce the maximum strain experienced at serviceability. Hence, the strains imposed on any FRP reinforcement utilised in these circumstances are extremely low in relation to the ultimate capacity.

In applications such as FRP trailers, which allow greater values of strain in service, the allowable ultimate strain capacity of the core is largely determined by the choice of reinforcement. For example, the use of carbon reinforcement will permit a substantially lower core strain capacity than that required when E-glass reinforcement is utilised.

The ultimate tensile strain capacities of various core materials are shown in Table 5.1. The tensile strain properties in the direction of strength of commercially available forms of balsa and honeycomb cores are not generally published by manufacturers, due to difficulties associated with the tensile testing of these materials.

The superior strain capacity of the foam cores is apparent, as the ultimate strain capacity of most foam types exceeds 5%. By contrast, the strain capacity of PFR is relatively low at 1.6%. Consequently, while the foam cores would be suitable for application in conjunction with E-glass, aramid, or carbon fibre reinforcement, the use of PFR as a core material in FRP trailers would prevent the E-glass reinforcement from reaching its full capacity.

5.2.4 Fatigue Performance

The service environment to which trailers are subjected is dominated by dynamic loading. Hence, the structure must be considered with respect to fatigue performance. Specifically, the core material must be capable of sustaining the strains imposed during dynamic loading in order to maintain laminate support. In a similar manner to the ultimate strain capacity discussed in the previous section, ideally the fatigue performance of the core should be equal or superior to that of the laminates. Failure of the core as a result of fatigue damage will

result in debonding of the laminate from the core, thereby destroying the structural integrity of the trailer, regardless of the fatigue performance of the laminates.

The fatigue performance of balsa- and honeycomb-cored structures has been proven through extensive use of these materials in marine and aerospace applications. Similarly, the use of SAN and PVC foams in environments of high fatigue has been well documented within marine, transportation, and aerospace applications [8,9]. The inherent ductility and toughness of these foams, in addition to a high strain capacity, would suggest these foams possess sufficient fatigue characteristics to warrant utilisation in this context. Conversely, the use of expanded polyurethane foams has been abandoned by industry in load bearing applications. This is in response to the tendency of expanded polyurethane foams to debond at the interface between the core and laminate when subjected to a sustained load or fatigue environment. As part of continuing research at USQ, Mr. Paul Simpson has demonstrated the response of PFR to low levels of fatigue loading as experienced in a civil engineering context [10]. A PFR mixture comprising ceramic microspheres and epoxy resin was used to form the core and web of a bridge girder. This girder was successfully subjected to cyclic loading, which simulated the repeated loading of the girder to the maximum serviceability limit for the duration of one million cycles. However, the strain limits imposed on the structure during the course of this testing were extremely low in comparison to those required in this context. Hence, additional fatigue testing was incorporated in this study (refer Chapter 8).

5.2.5 Cost

As discussed in section 1.1, the reduction of trailer tare mass must be considered in relation to the associated increases in capital cost. Typically, the core occupies the majority of the total material volume of a composite structure, and therefore the cost of the core material per unit volume needs to be comparatively low to offset the high cost per unit volume of the laminates. The importance of strength with respect to core performance would indicate that core materials of higher strength be employed in order to provide adequate support to the laminates. With respect to shear, an increase in core strength can enable a reduction in the core volume required to sustain the applied loads.

The significance of mass reduction outlined in section 5.2.1 dictates that the density of the core material should be at a minimum. However this must be balanced with the physical properties desired from the core. Generally, core materials possessing a higher density also possess greater physical properties.

Table 5.2 provides a number of comparisons of the relative costs of various core materials. The final column takes into account the specific cost of the core material as a function of material density and ultimate strength. This provides a complete overview of core material costs in relation to each of the areas discussed within this section.

Table 5.2 Relative Costs of Various Common Core Materials

Core Material	Density (kg/m^3)	Cost per Unit Mass ($/kg)	Cost per Unit Volume ($/$m^3$)	Relative Cost per Unit Strength ($/MPa)	Relative Cost per Unit Density per Unit Strength ($/kg/$m^3$ per MPa)
Balsa Rigid End Grain (25 mm thick)	150	12.60	1890	1.00	4.11
Honeycomb Phenolic Impregnated Paper-Honeycomb (25 mm thick)	50	32.00	1600	5.08	62.70
Polyurethane Foam Rigid Foam Closed-Cell	350	7.50	2625	1.67	2.94
PVC Crosslinked Foam (H200 Series from DIAB 30mm thick)	200	45.00	9000	12.69	39.18
SAN Foam (A200 Corecell™ by ATL Composites)	200	58.00	11600	21.65	66.84
PFR Glass Microspheres 40% K15 filler by volume from 3M in epoxy matrix	650	12.00	7800	1.05	1.00

Cost varies depending on thickness and fluctuations in exchange rates

The data from this table would suggest three of the listed core materials as being particularly attractive with respect to cost and mechanical properties. Specifically the balsa, the polyurethane foam, and the PFR core materials all provide an economic advantage over the remaining core materials listed in the table. In addition to the low relative cost of the base materials, this advantage can also be attributed to the fact that, in general, minimal effort is expended (or necessary) in the monitoring of product quality and consistency. As balsa is a natural product, variations in density and other material properties are unavoidable. Quality control of polyurethane foams is usually unnecessary, as poor long-term performance has minimised the use of PU foams in strength applications. Little effort is necessary to ensure consistent quality with respect to PFR, provided the mixing process is properly adhered to.

By contrast, honeycomb cores require a significant amount of processing and assembly in the forming of the final product. Similarly, as product consistency with respect to mechanical properties is of paramount importance for PVC and SAN foams (due to market

demand), substantial effort is exerted to ensure that the expansion of the base material is closely controlled. Consequently honeycomb cores and PVC and SAN foams constitute some of the more expensive core materials available, particularly when compared on the basis of mechanical properties.

5.2.6 Impact and Toughness Characteristics

Despite the protection provided by the laminates, the core is occasionally subject to impact loading. In the case of a semi-trailer, this will predominantly occur through dynamic loading from the suspension system, and from accidental impact to the deck or combing rail during loading or unloading. Impact damage to the core occurs indirectly, as an impact experienced by the laminate is transferred to the core material, the efficiency of which being primarily dependent on the laminate. The impact performance of the laminate is discussed later in this chapter.

Good impact performance is manifested in the resistance of material to form cracks and fracture points. A core possessing good impact performance will undergo elastic or plastic deformation in preference to crack initiation. Elastic deformation of the core is preferred, since the core is able to continue to support the laminate post-impact. While plastic deformation results in localised laminate debonding, the effects of this are typically minimal in comparison to the widespread debonding caused by cracking of the core.

Similarly, the toughness of the core material represents a characteristic of some significance. Should a crack initiate as a result of impact, defect, or fatigue damage, the inhibition of crack propagation is essential to maintain structural integrity. Crack blunting, a product of core ductility, prevents an increase in crack length by local deformation at the crack tip. This deformation absorbs the strain energy stored at the tip, thereby controlling the advance of the crack.

As is discussed further in 5.4.6, the significance of the impact and toughness characteristics of the core is primarily limited to the decking and combing rail construction. Provided sufficient fatigue capacity is present, the core should not be subjected to the possibility or presence of cracks in the majority of the chassis. Extreme events such as motor vehicle accidents are also addressed in 5.4.6.

The good impact performance of balsa has been substantiated by the marine industry. The impact of waves on the hull, particularly in high-speed vessels, has demonstrated the ability

of balsa to withstand considerable impact loading. However the toughness of this core material is relatively poor, due to the low mechanical properties perpendicular to the direction of the timber grain. Hence, a crack that acts to separate the longitudinal grains is difficult to arrest.

The impact performance of honeycomb cores is primarily dependent on the material type. Paper honeycombs are generally not used in load bearing applications due to low mechanical properties. The impact performance of paper honeycomb cores is also generally low. Comparatively, aluminium honeycomb cores possess significant impact resistance, which is typified by plastic deformation. Aramid honeycomb cores such as Nomex™ (refer section 2.5.2) possess exceptional impact performance in comparison with other types of honeycomb core. The high strength of the aramid paper is complemented by elastic deformation under impact conditions. The toughness of honeycomb cores is predominantly reliant on the adhesive bond, which exists between the individual cells in the honeycomb structure, and also between the honeycomb structure and facing material.

However, the damage tolerance of honeycomb cores with respect to that of most foam types is poor. While the homogeneous nature of foams allows for the dissipation of an impact load in three dimensions, the cellular nature of honeycomb cores confines the impact load, transmitting it directly through to the laminate on the opposite side of the panel.

A wide variation in impact performance is observed in the range of foam cores available. The resistance to crack propagation by polyurethane foams is generally satisfactory, particularly when higher densities are used. The inherent ductility and durability of polyurethane is observed to some extent in the performance of the expanded foam. However, expanded polyurethane foams do exhibit some brittleness, and are susceptible to debonding from the laminate under impact or fatigue loading.

SAN and linear PVC foams exhibit exceptional impact performance and toughness. Consequently, these foam types are extensively utilised in applications in which FRP sandwich panels are subjected to impact loading. In particular, the recent development of a high ductility grade of PVC foams by DIAB (HD series) has enjoyed extensive use in applications requiring exceptional resistance to shock loading such as the forward sections of high-speed trains and watercraft.

The high physical properties of PFR provide significant resistance to impact and accidental damage. However, the brittle nature of PFR encourages the propagation of cracks.

Consequently, the toughness of PFR is comparatively poor, and is prone to extensive delamination following the initiation of a crack. Further discussion on the toughness of PFR is found in [3,4].

5.3 Selection of Core Material

The data and discussion presented in section 5.2 is summarised in Table 5.3. Relative terms of performance were employed to provide a clear distinction between each core type in relation to the various characteristics detailed previously. Using this table, a number of assessments were made regarding the suitability of each core material type to this application, and a core material was selected for further use in this project. These assessments are summarised as follows:

- Balsa exhibits exceptional physical characteristics in all of the considered aspects within the direction of the grain. However, as end-grain balsa is actually a honeycomb structure at a micro level, the corresponding properties measured across the grain are comparatively poor. Synthetic, large celled honeycomb cores utilise a similar cellular structure, which provides the material with good performance in most categories. However, these properties are also highly directional, and are therefore not ideally suited to the multi-directional loading imposed by the trailer.
- While polyurethane foams are extremely economical and possess good material properties, the tendency of polyurethane foams to debond from the laminate under impact or fatigue loading removes the use of this foam as a viable alternative.
- PFR possess the highest mechanical properties of any of the materials considered. Additionally, PFR provides shape flexibility and excellent economic advantages. However, high specific gravity, combined with inadequate fatigue performance and toughness disqualify this core material from usage in application to lightweight FRP trailers.
- The superior performance of both SAN and PVC foams within the context of this application is clearly evident. While the modulus and strength of these foams are low in comparison to PFR, the accommodation of highly concentrated loads is accomplished through the use of hard points where required. Despite the relatively high cost of these foam types, both appear to be equally suitable for use in application to lightweight FRP trailers. Due to material availability, the H series PVC foam was selected for use in this project. A density of 200 kg/m^3, the highest available density at that time in Australia, was chosen in order to maximise the support provided to the laminate by the core.

Table 5.3 Relative Performance Comparison of Various Core Materials

	Density	Modulus and Strength	Ultimate Strain Capacity	Fatigue Performance	Cost	Impact and Toughness
Balsa						
Along grain	Good	Good	Good	Good	Excellent	Good
Across grain		Poor	Poor			
Aluminium Honeycomb	Good	Good	Excellent	Good	Fair	Poor
Polyurethane Foam	Excellent	Fair	Excellent	Poor	Excellent	Good
PVC Partially Crosslinked Foam (H Series from DIAB)	Excellent	Fair	Excellent	Excellent	Fair	Excellent
SAN Foam (Corecell from ATL)	Excellent	Fair	Excellent	Excellent	Poor	Excellent
PFR Glass Microspheres 40% K15 filler by volume from 3M	Poor	Excellent	Fair	Poor	Excellent	Poor

5.4 Reinforcement Characteristics

The variations of both reinforcement and matrix types outlined in Chapter 2 provide an overview of the available properties and characteristics. The significance of each of these characteristics within the context of an FRP trailer is discussed in this section. All comparisons and recommendations as to the most suitable reinforcement type are contained within section 5.5. Also, due to product availability, only E-glass, carbon (T300), and aramid fibres are considered here as viable alternatives. Any reference to carbon fibre reinforcement is made with respect to T300 carbon fibre unless otherwise specified.

5.4.1 Density

The contribution of the laminates to the mass of the structure is dependent on the relative mass of the core material. Assuming the use of a low-density core material (100-200 kg/m^3), the influence of laminate density on the total mass of the trailer is significant, despite the relatively small volume occupied by the laminate within the structure.

The densities of carbon, E-glass, and aramid fibres have been previously presented in Table 2.1, section 2.2.5. While a direct comparison between reinforcement types may be made with respect to density, evaluation without regard to the material strength and stiffness is misleading due to the differing mechanical properties of each reinforcement types.

5.4.2 Modulus and Strength

As discussed in Section 2.7.3, the quantification of the material strength of FRPs is performed using *normalised unit strength* (force per unit width per unit mass of reinforcement) in addition to the use of strain in preference to stress.

However, while laminate strength is of some significance, the dominance of deflection as a design criterion (refer section 4.8.6) dictates that the elastic modulus of the reinforcement is of primary importance. Therefore a comparison on the basis of reinforcement stiffness provides a more relevant assessment with respect to the present application. The inclusion of density provides an additional insight into the efficiency of the material with respect to stiffness. Table 5.4 presents the specific strength and stiffness of various reinforcement types with respect to density. The properties of all reinforcements are shown without combination with a matrix material.

Table 5.4 Specific Stiffness and Strength of Various Reinforcements

	Dry Fibre Density (kg/m^3)	Specific Tensile Modulus ($MPa/(kg/m^3)$)	Tensile Strength ($N/mm\ width/(kg/m^2)$)	Specific Tensile Strength ($N/mm\ width/(kg/m^2)/(kg/m^3)$)
Glass				
E-glass	2580	29.1	700 - 800	0.27 - 0.31
Carbon				
T300	1750	134	1000 - 1200	0.57 - 0.69
Aramid				
Kevlar49	1440	90	900 - 1200	0.63 - 0.83

Note: Properties may vary depending on data source

The low specific stiffness of E-glass suggests that it is less suitable for applications governed by high stiffness and low structural mass. While aramid fibres exhibit particularly high specific strength, the corresponding modulus is significantly lower than that of carbon fibre. The constraints of trailer deflection in addition to the minimisation of structural mass discussed in Chapter 4 indicate that a reinforcement of higher specific stiffness will provide a more efficient structure. Consequently, carbon fibres were chosen as the most suitable choice of reinforcement with respect to these considerations.

5.4.3 Fatigue Performance

Due to the dynamic environment under which the trailer operates, the fatigue performance of the reinforcement is of particular importance. While the fatigue performance of a trailer is often determined by detail design (eg connection of members), the material must also possess resistance to fatigue loading. As observed in the fatigue behaviour of metals, the static strength of FRPs is significantly greater than the strength of the material subjected to a cyclic or repeated load.

This section does not address the determination of the fatigue performance of specific laminate configurations, nor does it specify the actual fatigue performance requirements for this application. Rather, the typical fatigue performance of unidirectional FRPs is presented with respect to the identification of the reinforcement type with the greatest fatigue performance. Detailed discussion on fatigue and the laminate requirements is presented in Chapter 8.

Figure 5.1 presents a summary of the general fatigue performance of various unidirectional reinforcement types in the form of an S-N diagram.

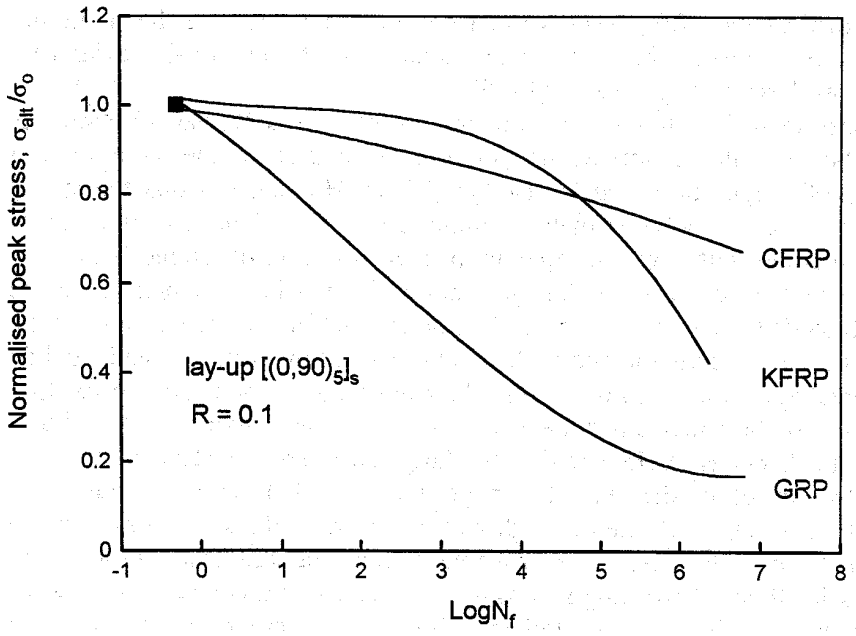

Figure 5.1 Comparison of Stress/Life Curves of Various Fibre Types in Epoxy Resin

Source [3]

The ratio of fatigue strength at 10^6 cycles to the initial static strength illustrates the variations in strength retention of each reinforcement type. The degradation of strength of aramid fibres occurs quickly after 10^4 cycles in relation to both E-glass and carbon fibres, however the ratio of fatigue strength to static strength for both aramid and E-glass fibres is similar at 10^7 cycles. The material capacity reduction factor with respect to fatigue is less severe for carbon fibres, with higher values attributed relative to the other fibre types represented. Carbon fibre possesses superior fatigue performance, particularly when the number of cycles exceeds 10^5.

5.4.4 Cost

The predominant contributor to the material costs associated with a typical composite structure is that associated with the laminates, the cost of which is largely dependent on the type of reinforcing fibre. Table 5.5 shows the typical costs of various uni-directional reinforcement types per unit mass. The prices shown are based on the cost of commercially available woven and stitched fabrics.

This table indicates that both carbon and aramid fibres are relatively expensive in comparison with E-glass. The cost of carbon fibres within Australia has remained relatively high when compared with the United States. However increased usage has allowed a reduction in the cost of carbon in recent years, and it is anticipated that this

decline will continue. Similarly, the cost per unit mass of aramid fibres has remained high due to a limited demand. The absence of facilities which manufacture either carbon or aramid fibres within Australia add to the increased costs. The relatively low cost of E-glass stems from the widespread use of this reinforcement in the manufacture of the majority of FRP applications. The marine industry utilises E-glass (in the form of chopped strand mat [CSM]) in most applications, and the versatility of open mould spraying of chopped fibres is utilised in the production of a vast array of domestic and commercial products.

The dominance of stiffness in this application demands that a comparison of cost be performed on this basis. The specific cost, with respect to modulus, is also shown in Table 5.5. Despite possessing a comparatively low modulus, E-glass compares favourably with both carbon and aramid reinforcement because of its low cost.

Table 5.5 Comparative Specific Costs of Various Reinforcement Types

	Cost per Unit Mass ($/kg)	Cost per unit Modulus per unit Mass ($/GPa/kg)	Cost per unit Strength ($/N/mm width/kg)
E-glass	16	0.21	0.02
T300 (48K)	88	0.37	0.08
Kevlar49	83	0.64	0.08

Note: Properties may vary depending on data source

5.4.5 Damage Tolerance and Impact Resistance

Section 5.2.6 addressed the impact loading experienced by the deck and combing rails. However, the chassis rails and cross members are also subjected to impact damage. This damage would be incurred as a result of two main types of impact.

The most extreme form of impact loading would occur during a motor vehicle accident. For example, significant impact damage would result to the chassis rail should a vehicle strike the side of the trailer. However, the damage tolerance of the laminate does not primarily determine the response of the structure to loading of this form and magnitude.

More commonly, damage occurs as a result of projectiles of various sizes impacting upon the underside of the chassis rails and cross members. These projectiles originate from the tread of the tyres, in which small pieces of aggregate become embedded. This is partially

reduced by the addition of wheel covers and 'mudflaps', however an inspection of the underside of most trailers reveals that a significant quantity of projectiles continue to make contact with the underside of the trailer. Unlike the core material, impact damage to the reinforcement will predominantly occur directly without any buffer or protection. This exposure to potential damage would suggest that a laminate possessing good impact tolerance is necessary for structural durability.

The damage tolerance of any given laminate is determined by a number of parameters. The primary factor influencing the impact energy absorbed by a laminate is the fibre type. The absorption of impact energy is directly related to the ultimate strain capacity of the reinforcement. Hence, fibres possessing low ultimate strain capacities, such as carbon, are more susceptible to impact damage than fibre types possessing higher strain capacities, such as aramid and glass fibres.

The adhesion of the matrix to the fibres is also influential in the impact response of a laminate. Specifically, higher levels of adhesion promote brittle failure between the fibre and matrix, resulting in relatively minor releases of energy. However, poor adhesion of the matrix to the fibre allows delamination without significant fibre failure [4].

Various techniques are employed to counter the poor impact performance of carbon fibre. The use of hybrid laminates, which combine two or more fibre types in a single laminate, allows for the inclusion of glass and aramid reinforcements in a laminate predominantly constructed from carbon fibre reinforcement. Mallick and Broutman [5] have demonstrated that a hybrid laminate comprising carbon (GY-70) and E-glass reinforcements possesses an impact energy 35 times greater than a laminate consisting purely of GY-70.

Hence, while glass and aramid fibres possess superior impact performance and damage tolerance, the appropriate combination of these fibre types with carbon would provide a more acceptable level of impact performance to a carbon laminate. Further discussion regarding trailer durability is presented in Chapter 7.

5.5 Selection of Reinforcement and Matrix

5.5.1 Reinforcement Selection

The data and discussion presented in section 5.4 is summarised in Table 5.6. Relative terms of performance were employed to provide a clear distinction between each reinforcement type in relation to the various characteristics detailed previously. Using this table, a number of assessments were made regarding the suitability of each fibre type to this application, culminating in the identification of the reinforcement types recommended for use in FRP trailers. These assessments are summarised as follows:

- While the mechanical properties of E-glass are significantly lower than other reinforcement types, this disadvantage is partially offset by the inexpensive nature of E-glass. However, due to a low specific modulus and relatively poor fatigue performance, the use of E-glass as the primary load carrying reinforcement is not feasible in this application. E-glass should be suitable for application as shear reinforcement, as it is expected that the shear deflection of the chassis rail would be minimal in comparison with the deflection due to the imposed bending moment. Although glass fibres possess a relatively high specific density, the volume of reinforcement required to accommodate the shear loading is expected to be significantly less than the reinforcement used to contain the bending moment. Double bias fabric is most efficient at carrying shear loads due to alignment of the fibres with the principal shear stresses. However, limited availability of double bias fabric in carbon and aramid fibres also suggests that E-glass would be most practical. Hence, E-glass, in the form of a double bias fabric, was chosen to accommodate the shear-loading component within the chassis.

Table 5.6 Relative Performance Comparison of Various Reinforcing Fibres

	Density	Specific Modulus	Specific Strength	Fatigue Performance	Cost	Damage Tolerance
E-glass	Poor	Fair	Fair	Poor	Low	Good
T300 (48K)	Good	Excellent	Good	Excellent	High	Poor
Kevlar49	Excellent	Good	Excellent	Fair	High	Excellent

- Aramid fibres display excellent physical properties, particularly in relation to specific modulus and strength. A relatively high strain capacity and excellent toughness and impact resistance complements these, despite a relatively high cost, particularly with respect to modulus. However, the primary disadvantage of aramid fibres in relation to this application is that of fatigue performance. The significant degradation of the strength of aramid fibres as illustrated in Figure 5.1 suggest that this fibre type is unsuited to applications involving high fatigue loading, particularly in comparison with carbon fibres. Consequently, aramid fibres were not selected for use in load carrying applications associated with this trailer.

- Carbon fibres displayed a clear dominance in relation to the majority of the characteristics considered. In particular, the high specific modulus of carbon fibres suggests the use of this reinforcement for structures governed by stiffness constraints. Carbon also displayed superior fatigue performance with respect to both E-glass and aramid fibres, and is clearly best suited to accommodate the dynamic bending moments imposed on the trailer during service. While the poor impact and toughness performance of carbon is of some concern, the hybridisation of the carbon laminate with E-glass has been shown to significantly increase damage tolerance. The installation of protective coatings in the appropriate areas will also decrease the probability of exposure to severe impact. Therefore, carbon fibre reinforcement was selected to provide flexural stiffness to the trailer, supporting the appropriate bending moments imposed on the chassis. Due to issues of availability and cost, T300 carbon fibres were used throughout this project.

5.5.2 Matrix Selection

The use of carbon fibre reinforcement eliminates the use of polyester resins, due to the relatively poor properties exhibited by this resin type when used with carbon. Additionally, there exists an absence of a suitable fibre sizing that would allow adequate matrix-fibre adhesion.

A number of vinylester resins possess properties sufficient to provide a carbon fibre laminate with performance adequate for this application. And while vinylester resins have been successfully used in combination with carbon fibre (coated in a specific sizing) in various applications, the majority of carbon reinforcement commonly available within Australia is not compatible with vinylester resins.

Since both the polyester and vinylester resins available for use in this study are unsuitable in for use in conjunction with the available carbon reinforcement, an epoxy resin was selected for use in this project. Consequently, a relative performance comparison of each resin type (as performed in relation to the reinforcement in Table 5.6) was not necessary. Epoxy resins represent the most common matrix used in conjunction with carbon fibre reinforcement, as they are considered to be a 'high performance' matrix. An epoxy resin, supplied by ATL Composites Pty Ltd was used as the matrix for use in all subsequent laminates. This resin, ADR246TX, is a formulated laminating resin, which consists of a DGEBA (Diglycidyl ether of bisphenol A) based epoxy blend with the addition of a Bisphenol F epoxide [1]. This resin also contains a diluent for viscosity modification and a thixotropic additive. The resin was combined with ADH160 hardener, which is a proprietary amine blend, produced by ATL Composites.

5.6 Determination of Laminate Properties

5.6.1 Introduction

The wide variation observed in the plethora of laminate property data presents significant difficulties to the designer. The accuracy of such data is of paramount importance, as it is to these values that capacity reduction factors are applied. Any uncertainty or inaccuracy contained in the material property data directly affects the performance of the structure.

In the context of this project, it was decided that all reinforcement types used during the course of this research would be subjected to material testing, to determine the basic physical characteristics. In this way, confidence in the predicability of the material performance would be established. This would also remove any discrepancies resulting from variations in manufacturing techniques and associated quality observed in the relevant literature (refer section 2.7.3), particularly with respect to laminate performance.

The data produced by material testing was then available for use in the design and analysis of subsequent structures and components, which were constructed for testing purposes during the course of this research.

5.6.2 Experimental Program

The aim of this experimental program was to determine the basic mechanical properties of carbon fibre and E-glass laminates, in order to obtain properties on which subsequent design would be based.

The following factors were identified as necessary for the establishment of sufficient design data for the unidirectional carbon reinforcement:

- Tensile modulus (MPa)
- Tensile strength (N/mm width of reinforcement)
- Ultimate tensile Strain
- Poisson's ratio
- Compressive modulus (MPa)
- Compressive strength (N/mm width)
- Ultimate compressive strain

The following factors were identified as necessary for the establishment of sufficient design data for the double-bias E-glass reinforcement:

- Shear modulus (MPa)
- Shear Strength (MPa)

As previously discussed in section 2.7, the characterisation of the physical properties of a FRP laminate requires the consideration of several descriptors unique to fibre composite materials. Particularly, the tensile and compressive strengths of the laminates were measured with respect to force per unit width of reinforcement.

5.6.3 Materials Investigated

Following the decisions established in section 5.5, three types of reinforcement were considered:

- T300 carbon fibre unidirectional reinforcement in combination with a matrix comprising an epoxy resin of ADR246TX and ADH160. This was supplied by Hexcel Composites in the form of a heat-set stitched unidirectional fabric, possessing a density of 230 g/m^2.
- E-glass fibre double bias reinforcement in combination with a matrix comprising an epoxy resin of ADR246TX and ADH160. The double bias stitched fabric possessed a density of 600g/m^2, and was supplied by ATL Composites.
- E-glass fibre unidirectional reinforcement in combination with a matrix comprising an epoxy resin of ADR246TX and ADH160. The unidirectional heat set tape possessed a density of 460 g/m^2, and was supplied by Colan Pty Ltd.

Evaluation of the properties of the shear reinforcement was performed in two ways. Firstly, specimens using double bias reinforcement were prepared and tested in accordance with ISO 14129. These results (refer section 5.6.6) were to be utilised in all hand calculations for the determination of the initial quantities of shear reinforcement required. The accuracy of the typical properties provided by this simplified representation was assumed sufficiently accurate for this purpose. However, it is acknowledged that strict representation of a double-bias fabric should include two separate layers of unidirectional reinforcement at +45° and −45° respectively to account for the highly directional properties of double bias reinforcement, in addition to coupling effects which occur with a non-symmetrical laminate sequence. Hence, unidirectional laminates oriented (at ±45°) were used to represent the double-bias reinforcement in all finite element analysis (refer section 5.6.6). It was therefore necessary to determine the properties of unidirectional E-glass

reinforcement. This is explained in further detail at the end of section 5.6.6. The reader is also directed to Chapter 7, which includes several comparisons between the hand calculations and finite element analysis using the property values obtained through each method. It should also be noted that the author was not the sole contributor to the testing of these laminates. Acknowledgment of the respective contributors is noted where appropriate.

5.6.4 Specimen Preparation

All laminates, measuring approximately 400x400 mm, were produced by hand layup. Following consolidation of the matrix with the reinforcement, a layer of peel ply was applied to both sides of the uncured laminate to ensure an even and uniform surface finish. Excess resin was forced out of the laminate through the application of pressure by a squeegee. The laminates were allowed to cure at room temperature for the duration of 48 hours, after which the laminates were post-cured at 80^0C for the duration of eight hours.

5.6.5 Mechanical Testing

All carbon tensile specimens were prepared in accordance with ISO 527:1993 [6], measuring approximately 15 mm in width, 1.2 mm in thickness, and 300 mm in length, and consisting of 3 layers of carbon reinforcement. The tensile unidirectional and double bias E-glass specimens were also prepared in accordance with ISO 527:1993, measuring approximately 25 mm in width, 1.8 mm in thickness, and 300 mm in length, and comprising 4 layers of E-glass reinforcement. A total of 7 specimens (in accordance with the standard) were tested in each of the characteristic tests, at a constant displacement rate of 2 mm/minute. Strains were measured using an extensometer, and the specimen ends were gripped over a length of 50 mm. An example of the test configuration is shown in Figure 5.2.

The compressive specimens, including both carbon and E-glass unidirectional laminates, were prepared in accordance with ASTM D3410 [7], measuring approximately 6.3 mm in width, 2.0 mm and 1.8 mm in thickness respectively, and 140 mm in length. The specimens were tested using a modified Celanese compressive test fixture in compliance with ASTM D3410, and a total of 5 specimens (in accordance with standard) were tested for each reinforcement type over a 'gauge' (or unsupported) length of approximately 12 mm. An extensometer was used to measure strain, at a constant displacement rate of 2 mm/minute.

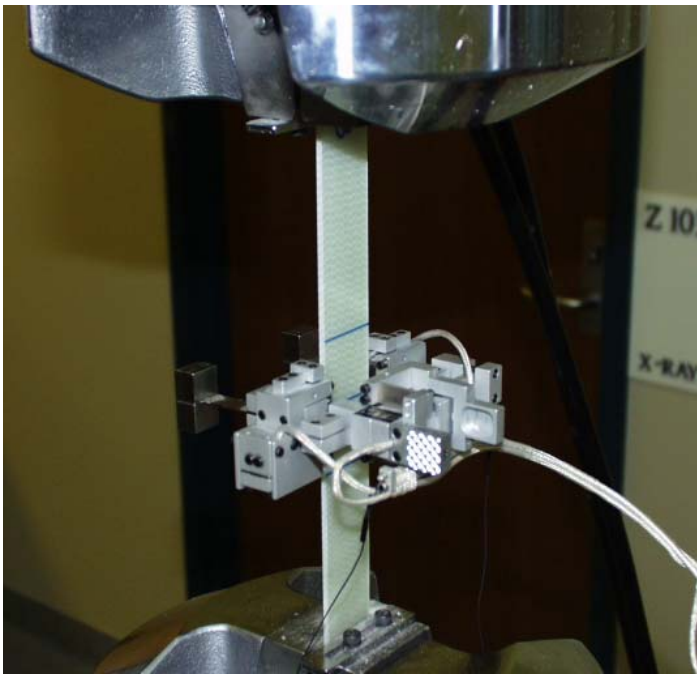

Figure 5.2 Tensile Test of Unidirectional E-glass (with Extensometer)

5.6.6 Results

Carbon Unidirectional Laminate Properties - Tension

The preparation and testing of the tensile carbon laminates was performed by a fellow research associate at the University of Southern Queensland, Mr. Paul Simpson. The results of the tensile tests are summarised in Table 5.7. A 95% confidence interval was used to provide a statistically valid measure of the test data. The results and subsequent design values are valid only with respect to the particular reinforcement type tested, and was not intended to be applicable to all commercially available carbon reinforcement denoted as T300.

Table 5.7 Tensile Properties of Unidirectional Carbon

Test Method: Determination of Tensile Properties (ISO 527)
Sample ID. TEN-0-CFEP-3-01-160999

Specimen No.	Width (mm)	Thickness (mm)	Area (mm2)	Peak Load (N)	Peak Stress (MPa)	Axial Strain at Peak (%)	Tensile Modulus (MPa)
1	15.08	1.2	18.1	13691	756.6	1.11	64680
2	15.14	1.21	18.3	11783	643.2	0.963	63800
3	15.13	1.15	17.4	14548	836.1	1.158	70400
4	15.09	1.19	18	13315	741.5	1.029	68370
5	15.13	1.27	19.2	11816	614.9	0.971	60620
6	15.11	1.22	18.4	14316	776.6	1.153	63210
7	15.11	1.21	18.3	14767	807.7	1.181	63730
95% C.I.	**15.092**	**1.207**	**18.2**	**12316**	**726**	**0.996**	**64973**

The use of stress in the software program utilised in these tests highlights the inconsistent nature of this descriptor when compared with typical material properties quoted in literature (refer Chapter 2). In order to determine the strength of the reinforcement in relation to force per unit width, the peak load was transformed in relation to the specimen width and the number of layers within the laminate. This was generalised to accommodate all fabric weights by providing values for a fabric weight of 1 g/m^2. Hence this gives:

Maximum Force per unit width per gram of reinforcement

= Peak load (N) / Specimen Width (mm)/ No. of Layers/ Fabric Weight (g/m^2) (5.1)

= 12316 / 15.092 / 3 / 230

= 1.18 N/mm width/gram of reinforcement

Assuming the influence of the matrix is negligible (by comparison of modulus), the strength of a unidirectional carbon fabric of any weight can be calculated, the value of which being independent of the method of manufacture. Hence, the tensile force carried by a carbon laminate at any given value of laminate strain can be determined by the following equation:

F_{tc} = [Strain (%) / 0.996] x 1.18 x Laminate Width (mm) x Fabric Weight (g/m^2) x No. of layers

= 1.19 x Strain (%) x Laminate Width (mm) x Fabric Weight (g/m^2) x No. of layers (5.2)

Equation 5.2 was subsequently adopted for use in the design of all structures within this project. This technique is applicable to all reinforcement types, and is useful in determining the true tensile strength of unidirectional laminates.

Carbon Unidirectional Laminate Properties – Compression

Within the relevant literature, the typical properties represented are the tensile properties of the material. However, the exclusive use of this data for use in both tension and compression is not advised, due to the anisotropic nature of FRPs. Consequently, the compressive characteristics of the carbon reinforcement were also investigated in order to determine the magnitude of any differences in properties. Table 5.8 presents the results of compressive testing performed using a modified Celanese method.

Table 5.8 Compressive Properties of Unidirectional Carbon

Test Method: Determination of Compressive Properties (ASTM D3410)
Sample ID. USQI-00-058-C

Specimen No.	Width (mm)	Thickness (mm)	Area (mm2)	Peak Load (N)	Peak Stress (MPa)	Max. Linear Strain (%)	Compressive Modulus (MPa)
1	6.32	1.99	12.59	7722	613.29	0.67	73481
2	6.28	2.10	13.21	9285	702.93	0.83	65954
3	6.29	2.04	12.81	8984	701.27	0.97	66984
4	6.29	2.00	12.61	8793	697.42	1.02	62206
5	6.29	2.08	13.08	8955	684.8	0.98	71383
95% CI	**6.29**	**2.04**	**12.81**	**8649**	**674**	**0.87**	**67262**

Despite relatively uniform values of peak load, some question remains with regard to data reliability, as buckling dominated the failure mode of these specimens. The maximum linear strain represents the highest value of strain achieved before specimen buckling was observed. Although application of the confidence interval to this data provided a particularly conservative estimate of the laminate capacity, it was not possible to extrapolate the linear data to predict a purely compressive failure. Consequently, this data was adopted for use in the design and analysis contained within this research. The particularly low buckling load observed in specimen one strongly suggested an incorrect restraint of the specimen, and this specimen was therefore eliminated from the sample in the calculation of the confidence interval with respect to the maximum linear strain.

In order to determine the compressive strength of this reinforcement in relation to force per unit width, the peak load was transformed in relation to the specimen width and the number of layers within the laminate. This was generalised to accommodate all fabric weights by providing values for a fabric weight of 1 g/m^2. Hence, substituting into equation 5.1, this gives:

Maximum Force per unit width per gram of reinforcement

= Peak load (N) / Specimen Width (mm)/ No. of Layers/ Fabric Weight (g/m^2)

= 8649 / 6.29 / 6 / 230

= 0.996 N/mm width/gram of reinforcement

Assuming the function of the matrix is only to prevent fibre buckling, and accounting for it's comparatively low modulus, the influence of the matrix is assumed negligible. Hence, the strength of a unidirectional carbon fabric of any weight can be calculated, the value of

which being independent of the method of manufacture. Hence, the compressive force carried by a carbon laminate at any given value of laminate strain can be determined by the following equation:

$$F_{cc} = [\text{Strain (\%)} / 0.87] \times 0.996 \times \text{Laminate Width (mm)} \times \text{Fabric Weight (g/m}^2\text{)} \times \text{No. of layers}$$
$$= 1.14 \times \text{Strain (\%)} \times \text{Laminate Width (mm)} \times \text{Fabric Weight (g/m}^2\text{)} \times \text{No. of layers} \quad (5.3)$$

The results and subsequent design values presented here are valid only with respect to the particular reinforcement type and manufacturing method as tested.

E-glass Double Bias Laminate Properties

E-glass, in the form of a double bias fabric, was chosen in section 5.5 to accommodate the shear loading placed on the chassis of the trailer, as the ±45° orientation of the fibres in this fabric coincide with the direction of principal stress/strain. The specific material properties of the double bias laminate were investigated, including the maximum shear stress and the shear modulus of double bias laminates. Additionally, the tensile modulus and strength of the $\pm 45^0$ laminate were investigated, in order to estimate the contribution of the shear reinforcement to the flexural stiffness and strength characteristics of the chassis. The author was assisted in specimen preparation and testing by Mr. Peter Girgenti, an engineer with Wagners Transport Pty Ltd.

The results of the tests relating to the laminate shear properties are summarised in Table 5.9. A 95% confidence interval was again used to obtain a statistically reliable summary of the results. The first sample was removed from the data set due to difficulties encountered with the gripping of the specimen.

The test was terminated prior to ultimate laminate failure in order to avoid damaging the dual extensometer. Hence, the peak shear stress data presented is not representative of the ultimate capacity of the laminate. However, a plot of shear strain versus shear stress indicated that non-linear, plastic deformation was initiated at a compressive strain value of 1.01%. Therefore, this point was designated as the ultimate allowable shear stress for the purposes of design within this project.

Table 5.9 Shear Properties of DB E-glass

Test Method: Determination of Shear Properties (ISO 14129)
Sample ID. USQI-00-061-SM

Specimen No.	Width (mm)	Thickness (mm)	Area (mm2)	Peak Load (N)	Peak Shear Stress (MPa)	Axial Strain at Peak (%)	Shear Strain at Peak (%)	Shear Modulus (MPa)
1	25.49	2.38	60.67	2174	17.95	0.37	0.6	2932
2	25.44	2.38	60.55	3066	25.36	0.6	1.02	2982
3	25.26	2.38	60.12	3045	25.32	0.6	1.01	2977
4	25.26	2.37	59.87	3072	25.7	0.6	1.03	3018
5	25.24	2.38	60.07	3070	25.52	0.6	1.02	3018
6	25.25	2.34	59.09	2980	25.22	0.6	1.01	2972
7	25.24	2.35	59.31	3035	25.59	0.6	1.02	3000
95% CI	**25.29**	**2.37**	**59.86**	**2866**	**25**	**0.6**	**1.02**	**2986**

Due to the simplifying assumptions made regarding the double-bias reinforcement in section 5.6.3, no attempt was made to characterise the shear strength results in terms of load per layer. The tensile properties of the double bias laminate were also determined in accordance with ISO 527, and the results are summarised in Table 5.10.

Table 5.10 Tensile Properties of DB E-glass

Test Method: Determination of Tensile Properties (ISO 527)
Sample ID. USQI-00-061-(+-45)- T

Specimen No.	Width (mm)	Thickness (mm)	Area (mm2)	Peak Load (N)	Peak Stress (MPa)	Axial Strain at Peak (%)	Tensile Modulus (MPa)
1	25.49	2.38	60.67	6609	109	9.84	9973
2	25.44	2.38	60.55	6893	114	12.08	10127
3	25.26	2.38	60.12	6776	113	13.77	10194
4	25.26	2.37	59.87	6974	117	10.16	10247
5	25.24	2.38	60.07	6948	115	10.62	10425
6	25.25	2.34	59.09	7208	122	14.91	10016
7	25.24	2.35	59.31	6843	115	12.28	10392
95% CI	**25.29**	**2.36**	**59.86**	**6862**	**114**	**11.64**	**10168**

The values observed from this test, in particular the elastic modulus, were included in the calculation of chassis stiffness presented in Chapter 7.

E-glass Unidirectional Laminate Properties for Use in FE Analysis

As stated in previous sections, the simplified approach to determining the properties of the double bias reinforcement was adopted in order to provide values for hand calculations and initial estimation of the required quantities of shear reinforcement. However, the use of finite element analysis allows a multi-directional laminate be defined by the properties of

each individual layer. As this represents a more accurate representation of the laminate than the simplified approach (presented previously), the modelling of all double bias reinforcement in subsequent finite element analysis utilised this technique. Hence, in order to specify the input properties in the process of analysis, it was necessary to determine the properties of unidirectional glass reinforcement.

The unidirectional, heat-set E-glass fabric obtained from Hexcel Composites was chosen because of the absence of weft fibres. This effectively eliminated any influence of the cross-reinforcement present in most unidirectional reinforcements on the tensile properties.

The results of the tensile and compressive laminate tests are shown in Tables 5.11 and 5.12 respectively.

Table 5.11 Tensile Properties of Unidirectional E-glass

Test Method: Determination of Tensile Properties (ISO 527)
Sample ID. USQI-00-055-(0)-T

Specimen No.	Width (mm)	Thickness (mm)	Area (mm2)	Peak Load (N)	Peak Stress (MPa)	Axial Strain at Peak (%)	Tensile Modulus (MPa)	Poisson's Ratio (mm/mm)
1	25.31	1.83	46.32	19209	414	1.4	29352	0.318
2	25.29	1.82	46.03	24733	536	1.81	30034	0.355
3	25.34	1.81	45.87	25780	562	2.06	27945	0.325
4	25.43	1.91	48.57	29136	599	2.2	27242	0.331
5	25.33	1.91	48.38	19036	394	1.34	29024	0.319
6	25.26	1.83	46.23	25238	547	1.98	28794	0.32
7	25.37	1.79	45.41	24460	540	1.91	29043	0.302
95% CI	**25.32**	**1.83**	**46.48**	**23341**	**500**	**1.76**	**28624**	**0.322**

Specimens one and five experienced significant slippage in the jaws, which prompted a higher clamping pressure. Unfortunately, this initiated premature specimen failure in the region of the jaws. Consequently, these specimens were removed from the data set in the determination of appropriate values according to the 95% confidence interval.

In order to determine the strength of the unidirectional E-glass reinforcement in relation to force per unit width, the peak load was transformed in relation to the specimen width and the number of layers within the laminate. This was generalised to accommodate all fabric weights by providing values for a fabric weight of 1 g/m^2. Hence, substituting into equation 5.1, this gives:

Maximum Force per unit width per gram of reinforcement

= Peak load (N) / Specimen Width (mm)/ No. of Layers/ Fabric Weight (g/m^2)

= 23942 / 25.33 / 4 / 460

= 0.51 N/mm width/gram of reinforcement

Assuming the influence of the matrix is negligible (by comparison of modulus), the strength of a unidirectional carbon fabric of any weight can be calculated, the value of which being independent of the method of manufacture. Hence, the tensile force carried by an E-glass laminate at any given value of laminate strain can be determined by the following equation:

F_{tg} = [Strain (%) / 1.992] x 0.51 x Laminate Width (mm) x Fabric Weight (g/m²) x No. of layers

= 0.256 x Strain (%) x Laminate Width (mm) x Fabric Weight (g/m²) x No. of layers (5.4)

Table 5.12 Compressive Properties of Unidirectional E-glass

Test Method: Determination of Compressive Properties (ASTM D3410)
Sample ID. USQI-00-059-C

Specimen No.	Width (mm)	Thickness (mm)	Area (mm2)	Peak Load (N)	Peak Stress (MPa)	Max. Linear Strain (%)	Compressive Modulus (MPa)
1	6.28	1.85	11.60	5910	509.62	1.50	30250
2	6.28	1.85	11.60	5860	505.32	1.41	28011
3	6.30	1.84	11.60	5461	470.82	1.48	25971
4	6.29	1.82	11.43	5701	498.93	1.68	28945
5	6.27	1.82	11.41	5939	520.69	1.43	27774
6	6.25	1.84	11.52	5654	490.81	1.37	31044
95% CI	**6.28**	**1.83**	**11.51**	**5724**	**497**	**1.46**	**28359**

Specimen buckling was also encountered during the testing of this sample. Hence the maximum linear strain was adopted for use in the design and analysis contained within this research.

In order to determine the compressive strength of this reinforcement in relation to force per unit width, the peak load was transformed in relation to the specimen width and the number of layers within the laminate. This was generalised to accommodate all fabric weights by providing values for a fabric weight of 1 g/m². Hence, substituting into equation 5.1, this gives:

Maximum Force per unit width per gram of reinforcement

= Peak load (N)/ Specimen Width (mm)/ No. of Layers/ Fabric Weight (g/m²)

= 5724 / 6.28 / 4 / 460

= 0.495 N/mm width/gram of reinforcement

Assuming the function of the matrix is only to prevent fibre buckling, and accounting for it's comparatively low modulus, the influence of the matrix is assumed negligible. Hence, the strength of a unidirectional E-glass fabric of any weight can be calculated, the value of which being independent of the method of manufacture. Hence, the compressive force carried by an E-glass laminate at any given value of laminate strain can be determined by the following equation:

$$F_{cg} = [\text{Strain (\%)} / 1.46] \times 0.495 \times \text{Laminate Width (mm)} \times \text{Fabric Weight (g/m}^2\text{)} \times \text{No. of layers}$$
$$= 0.339 \times \text{Strain (\%)} \times \text{Laminate Width (mm)} \times \text{Fabric Weight (g/m}^2\text{)} \times \text{No. of layers} \qquad (5.5)$$

The results and subsequent design values presented here are valid only with respect to the particular reinforcement type and manufacturing method as tested.

5.7 Conclusion

This chapter addressed the evaluation and selection of the most suitable combination of matrix, reinforcement, and core materials in application to FRP flat bed trailers. The desired material characteristics were selected on the basis of their significance with respect to the project aims and the expected operational conditions.

A number of core materials, as listed in Chapter 2, were considered with respect to several critical material characteristics. The selection process identified two suitable core materials. These included a partially cross-linked PVC foam core, available from Divinycell, and a SAN foam core, available from ATL Composites Pty Ltd. These materials exhibited similar material characteristics, and were deemed equally suitable for this application. Due to material availability, the H200 PVC foam was selected, possessing a density of 200 kg/m^3.

Three commonly available fibre types were considered, namely: E-glass, carbon, and aramid fibres. These fibres were also subjected to a comparison with respect to several key characteristics relevant to reinforcement properties. Carbon fibre reinforcement was shown to exhibit superior performance in almost every category, and was subsequently selected as the primary reinforcement type. The low cost and availability of E-glass double bias fabric were the primary factors in the selection of this form of reinforcement for the accommodation of the shear loads to which the chassis is subjected. It was also anticipated that the inclusion of E-glass would improve the damage tolerance of the carbon laminates. A readily available epoxy matrix was chosen for application to the trailer and all aspects of testing associated with this research.

The uncertainty associated with published laminate properties prompted the limited testing of each of the reinforcement types used within this research. Specifically, the tensile and compressive properties of the unidirectional carbon laminates used within this project were established, in addition to the proposal of a general equation designed to provide an accurate estimation of the strength characteristics and capacity of a unidirectional carbon laminate.

With respect to the E-glass reinforcement, the shear properties and tensile modulus of a double bias laminate were presented for application in hand calculations and initial estimation of required quantities of shear reinforcement. To enable a more accurate representation of double bias laminates within finite element analysis, the tensile and compressive properties of a unidirectional E-glass laminate were also presented.

References

[1] Ayers SR, Van Erp GM. Development of a new core material for composites in primary structural applications. Proceedings of the ACUN-2 International Composites Conference; Volume 1; 2000 Feb 14-18; UNSW, Sydney, Australia.

[2] Mallick PK, editor. Composites engineering handbook. New York: Marcel Dekker; 1997.

[3] Cardon AH, editor. Durability analysis of structural composites systems. Rotterdam: A.A. Balkema; 1996.

[4] Schwartz MM. Composite materials, volume 1: properties, non-destructive testing and repair. New Jersey: Prentice Hall; 1997; ISBN 0-13-300039-7.

[5] Mallick PK, Broutman LJ. The effect of glass-resin interface strength on the impact strength of fibre reinforced plastics. Polym. Eng. Sci. 1978; 18.

[6] ISO 527-1:1993. Plastics – Determination of Tensile Properties – Part 1: General Principals. Geneve: International Organisation for Standardisation

[7] ASTM D3410:1987. Standard test method for compressive properties of unidirectional or crossply fibre-resin composites. Philadelphia, PA: American Society for Testing and Materials.

[8] Danielsson M, Olsson K. Rigid foam core material for design of tough sandwich structures. Journees Europeennes des Composites; Paris; 1996.

[9] Introduction to core materials [online]. 1997 [cited February 12 2000]. Available from: http://www.spsystems.com

[10] Simpon PE. "The application of fibre composite materials to Australian bridge elements." [PhD dissertation in progress]. Toowoomba, Queensland: University of Southern Queensland; 2003.

Chapter 6 Conceptual Design

6.1 Introduction

As discussed in Chapter 3, the ladder frame construction utilised in steel flatbed trailers, having undergone significant refinement, represents a most economical and practical layout with respect to this material. However, similar advantages are not necessarily inferred with respect to FRP materials. The significant differences in physical properties and, in particular, the flexibility of shape inherent in FRPs suggested that the investigation of alternative trailer layouts is warranted.

Generally, trailer manufacturers have been reluctant to experiment with alternate flatbed designs, this being evidenced by an observed absence of trailer layouts deviating from the traditional ladder frame. However, the presence of an ever-increasing number of specialty trailers (eg. Side Tippers) would indicate that such innovation is currently focused in other directions. It would appear too, that the flatbed trailers developed by Trail King and Stevens Transport (refer section 3.4) adopted the traditional layout of a flat bed. Additionally, the Stevens trailer utilised pultruded beam sections, which mimicked the steel equivalents.

While the continued adoption of the ladder frame layout in FRP trailers is not inherently indicative of insufficient conceptualisation, the investigation of alternative structural configurations was considered worthwhile. This chapter outlines the various conceptual designs produced during the course of this research, including monocoque and ladder frame chassis layouts. The range of conceptual designs presented here is not intended to be

exhaustive, but rather represents a demonstrative sample of possible structural configurations possible through the use of FRP materials.

The selection process used to identify a single concept for further examination is described. The possible failure modes associated with the final concept are investigated, with those modes considered critical referred to Chapter 7 for further investigation.

6.2 General Conceptualisation

A number of broad considerations were made prior to the generation of conceptual designs. The use of pultruded beams in application to chassis rails were not considered viable due to the restriction of a constant cross-sectional shape implied by this method. Variations in beam depth are required to maximise structural efficiency and minimise the centre of gravity. Therefore, due to time restrictions and the difficulties associated with member stiffness (in light of the deflection constraints presented in Chapter 4), pultruded sections did not receive any further consideration.

Two chassis configurations were considered during conceptual design: ladder frame and monocoque construction. The use of ladder frames excluded the consideration of perimeter frame chassis', as this frame type requires significantly larger cross members, yielding a greater tare mass. Additionally, supplementary sub frames are necessary to enable the attachment of a standard suspension system and kingpin. The investigation of monocoque structures was initiated by the potential of PFR for use as a core material. These concepts originated during a period of time in which PFR was the subject of extensive investigation by researchers at the University of Southern Queensland. As the full capability of this material had not yet been established, a complete assessment of the suitability of PFR in application to FRP trailers is not yet complete. Consequently, the comparison of the various concepts presented in this chapter was performed independently of considerations of the material characteristics discussed in Chapter 5. Concepts Two, Three and Four discuss various concepts that utilise PFR in some capacity.

Estimations of trailer tare mass are presented in section 6.8, and are based on initial estimates of the required material volume, assuming that an identical quantity of carbon reinforcement is required for each concept. Hence, the comparison of tare mass is predominantly based on variations in the mass of the core and shear reinforcement.

Each of these concepts was developed with the intention of utilising existing suspension systems and other ancillaries, which are currently attached to steel trailers. However minor modifications to the attachment plates are assumed necessary, as these cannot be welded into place.

6.3 Concept One

The initial concept considered for development was based on the structural configuration of the small-scale FRP trailer discussed in section 3.5, and is illustrated in Figure 6.1(a) and (b). The chassis rail construction consists of a solid balsa or foam core, and the placement of reinforcement on the sides and ends of the beam to accommodate the shear and bending moments respectively. The aspect ratio of the chassis rail cross section was decreased (in relation to the small-scale FRP trailer) to reduce the possibility of member buckling and to more easily accommodate the suspension system.

The chassis assembly would be accomplished by inserting the cross member through preformed slots in the web of the chassis rail. Following the adhesive bonding of the cross member to the chassis rail, placement tabs could then be bonded as shown in Figure 6.1(a) to ensure a rigid connection. The addition of shear panels to prevent racking (as required in the small-scale trailer) may be necessary, depending on the rigidity of the connection and the out-of-plane flexural stiffness of the cross members.

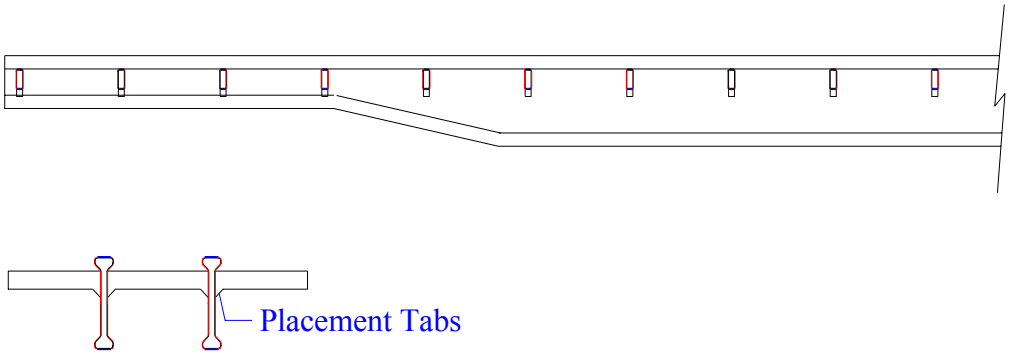

Figure 6.1 (a) Basic Chassis Layout of Concept One

Member fabrication would consist of applying the reinforcement to an appropriately shaped core, as illustrated in Figure 6.1 (b). A deck comprising a sandwich panel of appropriate strength would be bonded to the top of the frame, and the connecting plates of the skid plate and suspension system modified to accommodate the bonding or bolting of the ancillaries to the chassis.

One of the failure modes common to all concepts is illustrated in Figure 6.2. The tensile force placed on the reinforcement located on the underside of the chassis rail encourages the

straightening of the fibres, resulting in delamination of the reinforcement from the core. The probability of this form of failure, demonstrated in Section 7.5, is primarily dependent on the angle of change, the removal of stress concentrators from the region, and the presence of confining reinforcement, sufficiently attached to the chassis to restrain the tensile reinforcement from this behaviour. The shape of the lower flange of the chassis rail presented in this first concept is conducive to the restraint of the tensile reinforcement in the region of the beam neck, as demonstrated in Figure 6.1 (b).

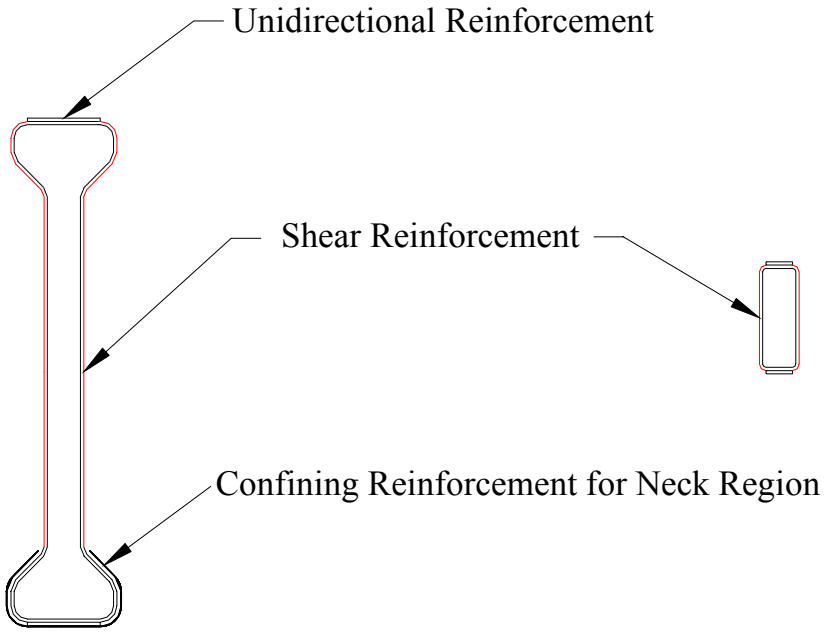

Figure 6.1 (b) Cross Section of Chassis Rail and Cross Member

While this structure possesses a low tare mass and presents little difficulties in construction, a number of potential shortcomings are apparent with this design. According to a number of industry sources, web buckling has been observed in steel trailers during an overloading event, with the instability of the relatively thin web resulting in catastrophic failure. The slenderness ratio of the FRP chassis rails must therefore be low enough to avoid this failure mode. Additionally, significant out-of-plane loads are imposed on the chassis when the prime mover is attempting to pull the trailer perpendicular to the longitudinal axis. Particularly, the reaction from the suspension during this manoeuvre acts to transversely distort the lower half of the chassis rail. Consequently, the web stiffness must be sufficient to withstand these loads. An increase in core thickness is necessary to achieve this, however this greatly increases the volume, mass and cost of core

material required. An increase in reinforcement, in addition to that required for shear, is therefore also necessary.

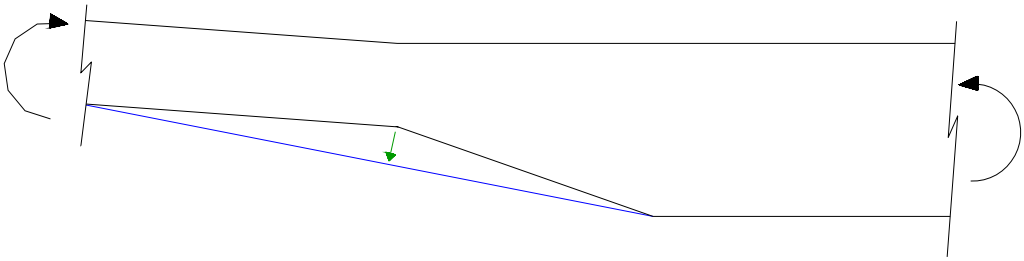

Figure 6.2 Delamination of Tensile Reinforcement in Neck Section

In general, this beam is uneconomical in the use of the core material, particularly in the upper and lower sections that act in support of the unidirectional reinforcement. The shape of the flanges also suggests that these sections are predominantly dependent on the performance of the core material when the section is subjected to vertical loading, such as would occur when the payload was placed directly above a support point. This is largely undesirable due to the relatively low strength of typical core materials. While the use of PFR would significantly increase the strength in this area, this would result in a large increase in the mass of the trailer, due to the large volume of core material required. An estimation of the trailer mass using various core materials is provided in section 6.8.

6.4 Concept Two

This concept comprises a monocoque structure, primarily of PFR. Two similar variations are illustrated in Figure 6.3 (a) and (b).

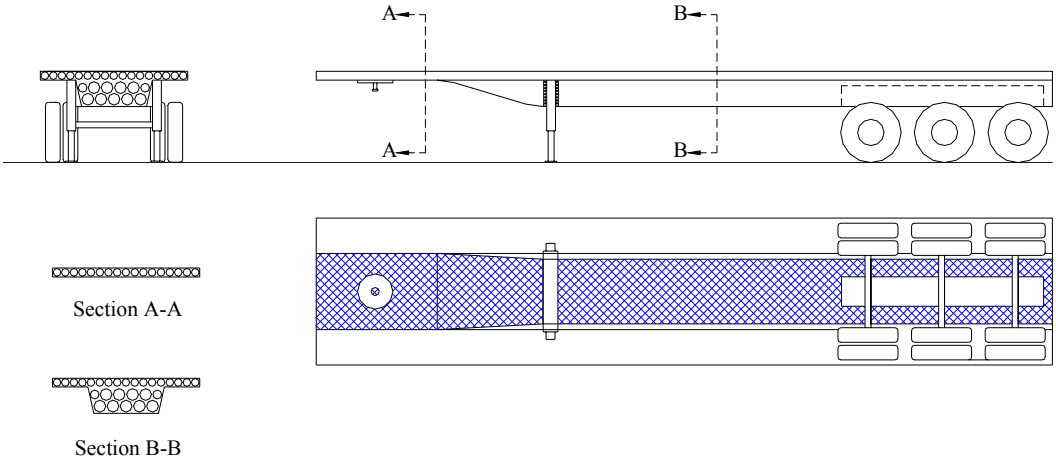

Figure 6.3(a) Basic Chassis Layout of Concept Two

Figure 6.3 (a) shows the initial configuration of the trailer. The circular shapes shown in the figure represent sections of PVC piping, which were inserted as a sacrificial void former within the core material to reduce the weight and cost of the PFR. Details of this type of void forming are discussed in papers by Van Erp [1,2] and Davey et al. [3].

Figure 6.3 (b) illustrates a similar configuration, with a greater focus on reducing the amount of PFR used. The PVC pipes have been replaced with larger voids, which were created by wrapping E-glass around low-cost, sacrificial forming foam. Each of these trailers would facilitate construction in an open mould, with the voids placed in the mould prior to the pouring of the PFR.

The cavity created under the rear axles would accommodate the air reservoir and associated equipment necessary for the air suspension and brakes. The addition of shear reinforcement would be significantly reduced, due to the high shear strength of PFR. The high compressive strength would eliminate the inclusion of hard points. The shaded area in the figure denotes the bottom layer of reinforcement employed to carry the bending moment. The top reinforcement is spread across the entire width of the deck, giving a total equivalent 'flange' width of 2500 mm. A protective layer of some description (possibly PFR) would be necessary to protect the top laminate, particularly from damage inflicted by

the payload. The suspension, hitch and standing legs would be adhesively bonded or bolted to the chassis.

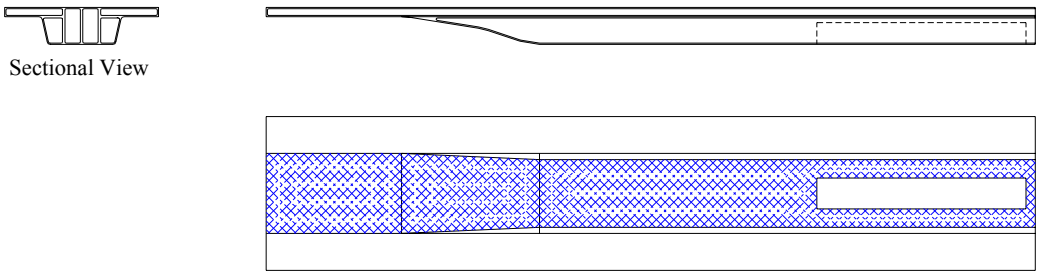

Figure 6.3 (b) Alternate Chassis Layout of Concept Two

6.5 Concept Three

This concept represents a further evolution of concept two, and is similar in cross section to some large span bridges. Void formation would be accommodated by sacrificial piping or a solid piece of foam acting as the former, this being wrapped in a single layer of double bias E-glass (refer Figure 6.4). This concept further reduces the chassis mass by removing a significant volume of the core from the centre of the structure. A central support, shown in the figure, may be necessary to partially support the deck.

Manufacture of this trailer would be performed in two phases. The bottom section would be manufactured separately in a closed mould, following which this section would be placed into a second mould. The decking pipes would then be placed around the upper portion of the sides, and the decking PFR poured directly around the upper sides of the lower section. A cavity over the rear axle group would again be necessary, and the suspension and associated equipment would be attached in a similar manner to concept two.

The structures represented by concepts two and three present several advantages. The closed section inherent in the chassis structure provides high torsional rigidity, and eliminates the need for shear diaphragms as required in concept one. The incorporation of the deck and cross members increases load-sharing efficiency, thereby reducing the effects of concentrated loads. Significant advantages are also present with respect to manufacturing. The monocoque nature of the chassis eliminates the need for section connections, and the large flat areas over which the reinforcement would be placed, would allow the use of higher weight fabrics and the automation of the laminating process. The high shear and compressive strength of PFR would significantly reduce the need for shear reinforcement and hard points respectively.

However, a number of distinct difficulties are associated with the monocoque construction utilised in concepts two and three. While the monocoque nature of these concepts presents some advantages with respect to manufacture and load distribution, the materials used are inherently difficult to repair. The fibre splitting, delamination, and matrix cracking associated with the failure of the reinforcement necessitates the removal the affected reinforcement, without inciting further damage to the surrounding laminate. The grafting of additional reinforcement must then be accomplished, ensuring adequate overlap is provided and a suitable surface finish and secondary bond are achieved. However, it is not possible to reliably repair PFR that contains significant cracking, as the high rate of crack propagation inherent in PFR rapidly transmits the crack throughout the structure,

particularly under dynamic loading conditions. Hence, this suggests that any event which initiated substantial cracking or damage of the structure, particularly the PFR core, would result in the effective failure of the entire structure.

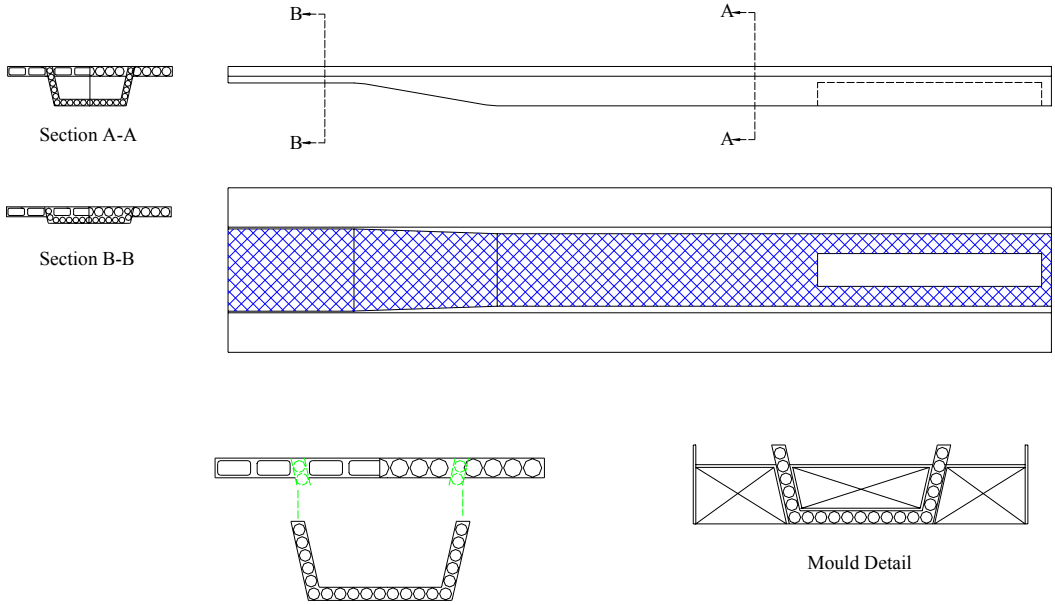

Figure 6.4 Basic Layout of Concept Three

The restraint of the tensile reinforcement throughout the neck section of the chassis also presents a number of difficulties with respect to these concepts. The configuration of these concepts is not conducive to the incorporation of confining reinforcement to restrain the tensile laminate, thereby presenting significant difficulties with regard to this failure mode.

The necessity of a precamber has already been established in Chapter 4. This precamber forms an integral part of the allowable deflection of the chassis, and maintains the appearance of structural strength through 'arching.' However, the incorporation of the precamber into the trailer chassis presented in concepts two and three would present a number of complications. In addition to the difficulties and expense associated with the incorporation of the required precamber into the bottom surface of such a large scale mold, the viscosity of the PFR mixture prior to cure would ensure a level upper surface. Hence, the precamber required on the top surface of the chassis could only be accomplished through the use of a closed mould, or by increasing the mould height and manually removing excess core material through abrasion or cutting.

Perhaps the most significant contributor to the estimated poor performance of these concepts is that of a high tare mass. The high density of PFR combined with the substantial volume of core material required, particularly with respect to the combination of

the cross members and the deck, resulted in a relatively high trailer tare mass. An estimation of the trailer mass of concepts two and three is provided in section 6.8.

6.6 Concept Four

The disadvantages associated with the monocoque structures presented in concepts two and three suggest that a modular, ladder frame configuration would provide an improvement in tare mass reduction and reduce the probability of the failure of the entire structure due to localised damage.

This concept continues the use of PFR as the core material, but reverts to a ladder frame chassis configuration. Figure 6.5 illustrates the modular nature of the chassis with respect to assembly, which facilitates assembly following the production of all components.

The figure illustrates the insertion of the cross members into the chassis rail, which would subsequently be adhesively bonded into place. The addition of placement tabs, as in section 6.3, is also possible. Following the insertion of all cross members, the reinforcement would be laid over the top and bottom of the chassis rails, followed by the bonding of the decking to the top of the chassis.

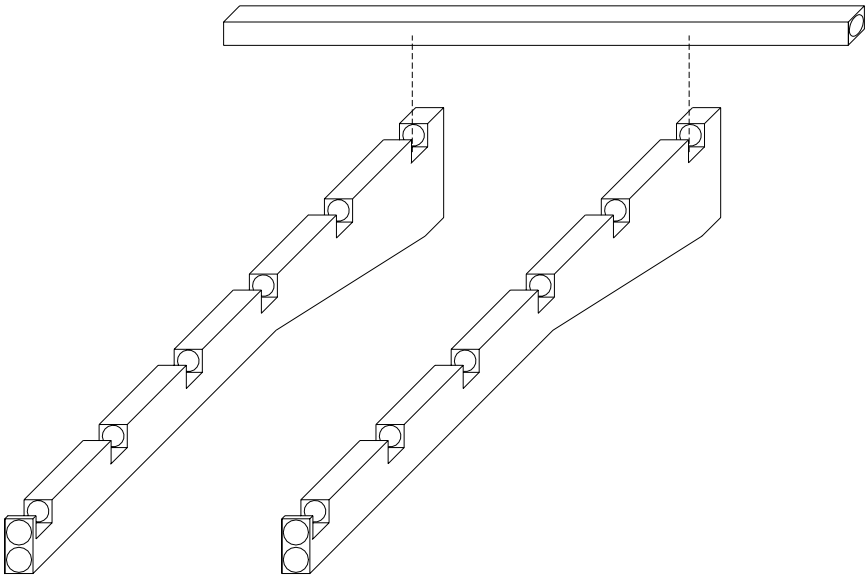

Figure 6.5 Section of Concept Four Chassis without Deck or Reinforcement

The beam cross-sections, illustrated in Figure 6.6, also utilise sacrificial piping to reduce the mass of PFR required. These beams require shear reinforcement to provide sufficient shear capacity. While this reinforcement is applied externally to the chassis rail, the shear reinforcement required for the cross members can be wrapped around the pipe contained within the beam.

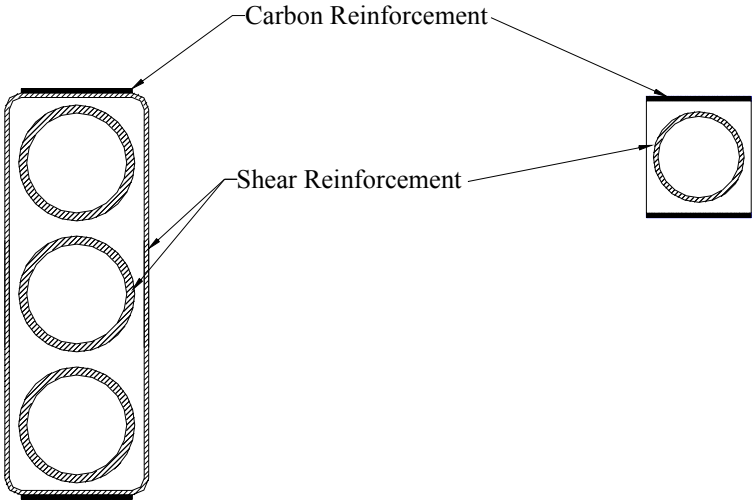

Figure 6.6 Cross Sections of Chassis Rail and Cross Member of Concept Four

The structure represented by this concept possesses a number of advantages. As previously mentioned, this concept would provide a significantly lower tare mass than the monocoque structures presented in section 6.4 and 6.5. Additionally, comparatively simple moulding would accommodate the manufacture of this chassis, and the inclusion of a precamber would be possible by constructing the mold such that the core of the beam would be manufactured whilst laying it on its side. The restraint of the neck reinforcement would be accomplished by the addition of a wrapping reinforcement, as illustrated in Figure 6.7, which would be applied following the insertion of the cross members and the consolidation of the carbon reinforcement.

However, the primary disadvantage of this configuration resides in the absence of a completely modular structure. Whilst construction of the chassis is inherently modular with respect to the piecewise construction, the consolidation of the compressive reinforcement and the reinforcement employed to restrain the tensile reinforcement in the neck region removes the possibility of removing damaged cross members without disturbing these laminates. Consequently, the failure of a cross member would necessitate the local removal of the compressive reinforcement, and the joining and repair of this laminate following the insertion of a new cross member.

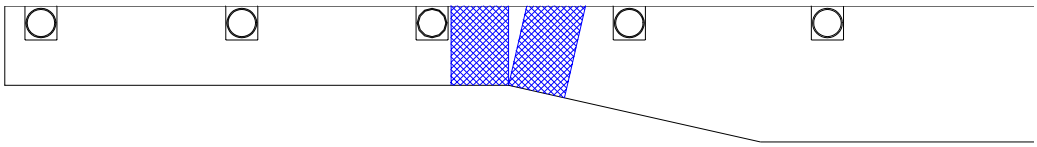

Figure 6.7 Restraint of Tensile Reinforcement in Beam Neck

Despite this difficulty, concept four exhibits a significant advantage over concepts two and three, particularly with respect to tare mass. The problems associated with this configuration are addressed within the context of concept five.

6.7 Concept Five

The final concept to be considered was initiated as a result of the apparent advantages provided by the ladder frame structures contained within concepts one and four. Specifically, the minimisation of tare weight provided by the inclusion of a low density core material as demonstrated in concept one was combined with the sectional stability of concept four, to produce the structure illustrated in Figure 6.8. The rectangular cross section of this trailer largely eliminates the possibility of lateral torsional buckling associated with an I-section. The wall stiffness, in combination with the inclusion of laminates on the inner wall of the chassis rail, ensures that compressive loads imposed on the section are sufficiently accommodated.

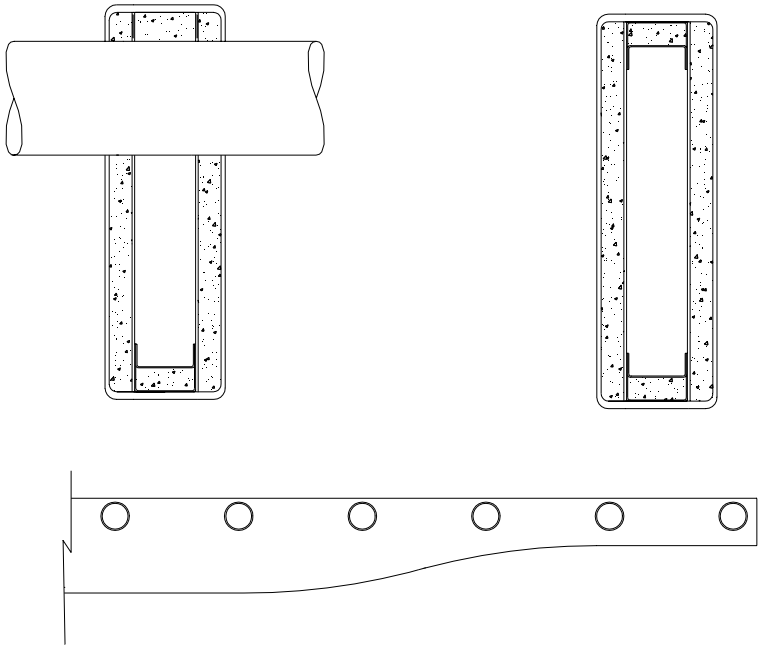

Figure 6.8 Basic Structural Configuration of Concept Five

This concept utilises tubular cross members, connected to the chassis rails in a similar fashion as presented in concept one. The circular shape was adopted for two reasons. Primarily, this shape enables more practical insertion and removal of cross members, particularly with respect to cutting. Hence, both the creation of the circular shape within the chassis rail, and the removal of a damaged or failed cross member, would be facilitated by a rotary cutting tool. Secondly, the circular shape minimises the inclusion of any stress

concentrations associated with the cross member insertion and the disturbance of the shear reinforcement.

The cross members comprise a number of layers of reinforcement wrapped around a former, such as a PVC pipe. The reinforcement consists of a combination of unidirectional and double bias reinforcement, accommodating the bending moment and shear loading respectively, and the absence of a core material within the cross member construction reduces the cost and mass of the components.

As this type of beam does not utilise PFR as a core material, the manufacture of the beam requires none of the associated moulding. The beam essentially consists of four individual sandwich panels, bonded together to form a rectangular hollow section. Hence, the core requires minimal shaping or preparation, substantially reducing manufacturing complexity.

This concept provides an extremely lightweight structure, primarily due to the substitution of PFR with a core material substantially less dense. The configuration of the chassis could also be considered modular, as the replacement of any damaged cross members would be facilitated by cutting off the extending ends of the failed beam, and the removal of the remaining laminate within the chassis rail through the use of an abrasive wheel. After completing the appropriate surface preparation, the new member could then be glued into place. The confining of the tensile reinforcement in the neck region of the chassis rails would be achieved in a similar manner to that described in concept four.

Minor disadvantages associated with this concept include the necessity of hard point insertion. In particular, the high compressive loading associated with the bolting of ancillaries and the region directly beneath the cross members would require a core material possessing sufficient compressive strength. While this concept would arguably possess less durability and resistance to incidental damage than an equivalent structure utilising PFR as a core material, the significance of this could be diminished by the addition of protective coatings (such as polyurethane) in the appropriate areas.

6.8 Selection of a Single Concept for Further Investigation

6.8.1 Discussion

To facilitate a more detailed investigation of the potential of the application of FRPs to flatbed semitrailers, the selection of a single concept from those presented in the previous section was required. Following the initial examination of each concept with respect to apparent advantages and disadvantages, a direct comparison of each possible configuration was performed and is summarised in Table 6.1. Each concept was assessed on a comparative scale with the exception of tare mass.

An evaluation of the tare mass of each concept demonstrates the magnitude of the contribution of the core to the structural mass. In particular, the substitution of PFR with a foam core (H200 PVC) provides a reduction of approximately 30% to the tare mass of the chassis, as observed between concepts four and five. Each of the monocoque structures possess substantially higher tare masses, due to the incorporation of the cross members and deck into a single, continuous, form in addition to the relatively large volume of core material present throughout the centre of the structure.

Comparison with respect to structural stability reveals that the closed-section, monocoque structures provide exceptional high torsional and sectional stability, whereas the open-section, ladder frame configuration is inherently less stable. In particular, the thin-webbed chassis rail section illustrated in concept one displays a relatively high susceptibility to buckling and crushing in comparison with the closed section chassis rails of concepts four and five.

The fundamental premise of monocoque construction involves the reduction of parts and the elimination of piece-wise assembly. However, implications exist with respect to repair and maintenance, as localised damage cannot be repaired through the replacement of the affected part or area. Rather, repair of the material is necessary. However, while the repair of FRPs is substantially more difficult than that of steel, it is not feasible to repair cracking of the PFR, particularly if the cracking occurs beneath the load carrying reinforcement. Conversely, the modular construction inherent in concepts one and five allow the replacement of damaged sections with minimal influence on the surrounding structure.

The circular shape of the cross members present in the latter concept provides additional benefits with respect to the removal of damaged cross members.

Examination of the relative cost of each concept reveals that, with the exception of concept two, the cost of materials is essentially similar. While the H200 foam used in concepts one and five is significantly more expensive per unit volume than PFR (refer section 5.2.5), this is offset by the substantially larger volumes of PFR required in the monocoque construction. The primary distinction associated with cost therefore relates to manufacturing expenses. While concept 4 requires comparatively small moulding, concepts two and three require moulds capable of casting the entire chassis core in a single pour. By comparison, manufacture of concepts one and five would occur by shaping and bonding prefabricated material. These concepts also avoid the costs associated with the preparation and placement of sacrificial piping, however they do require the addition of large amounts of shear reinforcement to the outer surfaces of the chassis rails.

As previously discussed, the confinement of the tensile reinforcement is more complicated in the case of the monocoque chassis configurations presented here, due to the absence of suitable wrap positioning. The absence of confinement can be compensated through an increase in the quantity of tensile reinforcement in this area. This would result in a reduction in the magnitude of the tensile force within the laminate in addition to an increase the total laminate stiffness, thereby reducing the tendency of the fibres to straighten. However, this decreases structural efficiency, and increases the cost and mass of the beam. Conversely, those concepts utilising a ladder frame construction allow the constraint of the tensile reinforcement through the encapsulation of the entire beam section with reinforcement, as demonstrated in Figure 6.7. Structural efficiency is maintained by the utilisation of the shear reinforcement to perform this function.

Each of the concepts presented was considered capable of accommodating standard suspension and skid plate assemblies with a minimum of modification. This would be achieved through a combination of adhesive bonding and bolting. However the low compressive strength of the foam cores would necessitate the inclusion of hard points in the regions immediately surrounding any mechanical fasteners.

The type of facilities, production volumes, and the level of available technology, would all influence the ease of manufacture of each concept. In addition to these factors, a comparison with respect to the ease of manufacture should consider the method of construction. The inclusion of a large volume of sacrificial void forming, required for concepts two and three,

demand significant attention with respect to preparation and three-dimensional placement within the mould prior to casting. The complexities associated with the installation of a precamber also increase the difficulty of manufacture. The large volume of PFR would also necessitate the control of exothermic reactions through continuous cooling of the mould. The manufacture of concept three would present further complication, as the moulding of the core is performed in two separate casting processes. While concept four would also require the preparation of void formers, this would occur in two dimensions in a comparatively simple mould capable of accommodating the required precamber. The piece-wise construction of this concept also significantly reduces problems associated with exothermic heat dissipation by reducing the volume of PFR contained within any single casting. The use of foam cores significantly simplifies the manufacturing process. By contrast, the chassis configuration presented in concept one would appear to provide the simplest manufacturing, particularly in relation to core preparation. Similarly, the chassis rails of concept five essentially consist of several sandwich panels bonded together, and connected by cross members of tubular shape. While the latter presents a slightly greater degree of complexity, the degree of difficulty associated with manufacture would appear to be substantially lower than those concepts utilising PFR.

Table 6.1 Comparative Summary of Conceptual Designs

	Approximate Tare Mass# (kg)	Relative Structural Stability	Relative Repairability	Estimated Relative Cost	Confinement of Tensile Reinforcement	Able to Attach Standard Ancillaries	Hard Point Insertion Required	Estimated Relative Ease of Manufacture	Overall Rating
Concept 1	750	Poor	Good	Low	Good	Yes	Yes	Excellent	3rd
Concept 2	2300 (a)* 1900 (b)*	Excellent Excellent	Poor Poor	High High	Poor Poor	Yes Yes	No No	Fair Fair	6th 5th
Concept 3	1230*	Excellent	Poor	Medium	Poor	Yes	No	Poor	4th
Concept 4	1090*	Good	Fair	Low	Good	Yes	No	Good	2nd
Concept 5	700	Good	Excellent	Low	Good	Yes	Yes	Good	1st
Steel Trailer	3500	Excellent	Excellent	Low	Excellent	Yes	No	Excellent	-

Includes complete chassis and deck, but excludes suspension, wheels, and other ancillaries

* Assuming 40% by vol. 3M-K15 filler in Epoxy

6.8.2 Conclusion

An assessment of the data, presented in Table 6.1, clearly suggests that concept five possesses characteristics that are best suited to this application. This is particularly evident with respect to tare mass. While, in general, the use of PFR provides excellent structural stability and accommodation of concentrated loads, the high relative density of PFR substantially increases the tare mass of the structure. As the reduction of tare mass forms an integral part of the aim of this research, the use of PFR in significant quantities should be avoided in favour of lower density core materials. While the selection process described above was performed independently of the discussion presented in section 5.2, the use of structural foam in preference to PFR as a core material was confirmed. Concept five was therefore adopted for further investigation. An experimental investigation of this concept is described in Chapters 7 and 8.

6.9 Identification of Possible Failure Modes

6.9.1 Introduction

The selection of a single concept was necessary to provide a focal point for further investigation into the potential of FRPs in application to semi-trailers. This investigation involves the application of the design philosophy and constraints outlined previously in Chapter 4, in addition to the verification of the performance of the selected structural configuration. Thus, the identification of all relevant failure modes associated with the chosen concept was necessary to enable a full evaluation.

This section outlines the primary failure modes associated with the particular structural configuration selected previously. Specifically, the failure modes relevant to the chassis rail were considered separately to those identified in relation to the cross members. The modes considered were limited exclusively to the chassis, and hence did not include issues relating to the decking, combing rail or other components not directly related to the performance of the chassis. Figures 6.9 and 6.10 present a summary of the failure modes considered with respect to the chassis rail and cross members respectively. The following sections briefly address each of the modes presented within the appropriate figure. As noted within the text, Chapters 7 and 8 will address a number of these modes of failure in further detail.

6.9.2 Failure Modes of Chassis Rail

Modes 1 – 3 The first three failure modes listed in Figure 6.9 are relevant to the basic design process with respect to beam strength. The material data presented in Chapter 5 provides sufficient information to allow the designer to calculate the required volume of reinforcement, given the moment capacity specified by the classification of trailer chosen from Chapter 4. Failure of the tensile reinforcement would result in catastrophic and complete member failure, as the shear reinforcement and core would not be capable of providing any significant contribution to the load carrying capacity of the beam. Conversely, while the failure of the compressive or shear reinforcement would necessitate the replacement of the beam, catastrophic failure would not be anticipated. A compressive failure would be contained to some degree by a combination of the core material and shear reinforcement, thereby inducing a substantial loss in stiffness and providing immediate warning to the operator.

Similarly, the core material would accommodate failure of the shear reinforcement, which would also be characterised by a significant increase in beam deflection.

Mode 4 Failure mode four addresses the connection of the shear reinforcement with the tensile and compressive laminates, which is necessary for the adequate transfer of the shear forces into tensile and compressive reinforcement. Typical steel beam sections possess a continuous connection between the web and the flanges that facilitates this. However, as is common to most FRP structures, the beam of the particular form considered here allows significant flexibility in the placement of reinforcement. Hence, sufficient care must be taken to ensure that the transfer of the shear forces is performed via this connection, rather than through the core material. This will be addressed in further detail in Chapter 7.

Modes 5 - 7 Failure modes five, six, and seven also relate to the basic design process of the chassis rail, in particular the application of suitable reduction factors that allow for the influences of fatigue. Additionally, attention to stress concentrations and regions of complex geometry that are particularly susceptible to fatigue is necessary to avoid the types of failures observed in steel trailers. Further discussion on the fatigue performance of the chassis rails can be found in Chapter 8.

Modes 8 and 9 The modes of failure denoted by eight and nine concern complications associated with the change in cross section, which occurs at the neck region of the chassis rail. As previously mentioned in section 6.3, the tensile force placed on the reinforcement located on the underside of the chassis rail encourages the straightening of the fibres, resulting in delamination of the reinforcement from the core. Additionally, failure to prevent the introduction of stress concentrations to the tensile reinforcement may induce a substantial localised increase in the laminate strain, resulting in premature failure of the member. Each of these failure modes is addressed in further detail in Chapter 7.

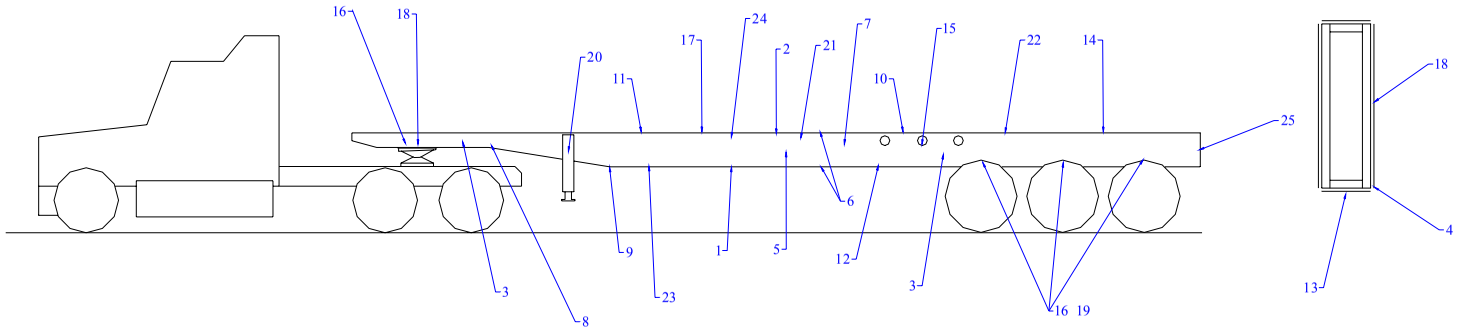

1 Tensile failure of laminate (insufficient moment capacity)
2 Compressive failure of laminate (insufficient moment capacity)
3 Shear failure of laminate (insufficient shear strength)
4 Inadequate shear connection betweeen shear reinforcement and laminates
5 Fatigue failure of core (tension/compression/shear)
6 Fatigue failure of laminates (tensile/comp)
7 Fatigue failure of shear reinforcement (shear fatigue)
8 Pull out of fibres in tension in neck region

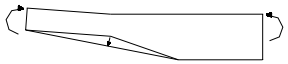

9 Stress concentration - tensile failure in neck region

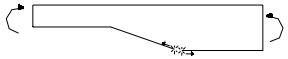

10 Crinkling of laminates under compression

11 Shear crimping

12 Excessive Deflection (insufficient stiffness)
13 Splitting and delamination of unidirectional laminates due to insufficient cross reinforcement and edge effects

14 Crushing/buckling of section

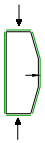

15 Crushing under X-member

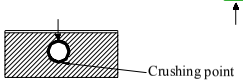

16 Vertical Crushing under skidplate and suspension
17 Localised crushing under point loads from payload
- laminate
- core
18 Bolt Pullout under lateral loading
19 Pullout of bolts due to braking loads
20 Twisting or crushing at leg attachment
21 Lateral Torsional Buckling due to Overloading
22 Torsional failure - insufficient stiffness
23 Impact damage to laminates (stone chips)
24 Harmonic vibration - natural frequencies
25 Major impact during a motor vehicle accident

Figure 6.9 Possible Failure Modes of FRP Chassis Rail

Modes 10 and 11 The compressive properties of the upper sandwich panel are directly related to failure modes ten and eleven. Laminate buckling occurs in sandwich panel construction as a result of insufficient compressive or tensile modulus with respect to the core [1]. A low core modulus is unable to provide sufficient support to the laminate whilst under high compressive loading, and hence the selection of a core material that possesses a sufficiently high modulus is particularly significant. Similarly, shear crimping occurs as a result of an insufficient core shear modulus. Compressive loading placed on the sandwich panel may induce destabilisation, should the shear rigidity of the core be too low. However this is minimised not only by an increase in the core shear modulus, but also by adequate external support of the panel. A brief investigation of these particular modes of failure with respect to the selected beam dimensions is included in Chapter 7.

Mode 12 Failure mode twelve refers to the deflection constraints defined in Chapter 4, and is associated with the dynamic behaviour of the trailer. Although excessive deflection may not in fact initiate structural damage, insufficient stiffness observed by the operator may indicate the presence of undetected damage, or alternatively indicate inherently deficient member stiffness. While excessive deflection resulting from undetected damage would warn of imminent failure, the latter indication would result in the exceeding of the strain limits established with respect to the tensile and compressive reinforcement. Even if this does not produce immediate member failure, the continued exceedence of the prescribed strain limits may induce failure through fatigue.

Mode 13 Failure mode thirteen exists primarily in non-homogeneous laminated materials such as FRPs. Laminates characterised by highly directional properties, such as unidirectional laminates, are susceptible to longitudinal splitting as a result of insufficient transverse strength. A unidirectional laminate relies predominantly on the matrix when subjected to transverse or out-of-plane loading. In the context of the chassis rail, the compressive and tensile laminates on the upper and lower surfaces of the beam should contain a proportion of cross reinforcement sufficient to prevent the occurrence of laminate splitting [2]. Additionally, FRP laminates are susceptible to delamination initiated at free edges [2]. Consequently all free edges, particularly in regions of high loading, should be avoided in order to maintain structural integrity. The techniques applied in avoidance of these phenomena are presented in Chapter 7.

Mode 14 Conditions inducing failure mode fourteen would occur in the regions of high vertical compression of the chassis rail. Specifically, a payload distribution similar to Load Case 2 (refer section 4.5.3) effectively imparts direct vertical compression to the cross

section of the chassis rail in combination with the reaction force presented by the suspension system. Consequently, insufficient wall stiffness and strength would promote buckling of the wall sections and localised beam failure. The avoidance of this form of failure is discussed in greater detail in Chapter 7.

Mode 15 Failure mode fifteen denotes the localised failure of the chassis rail in relation to connection with the cross member. The vertical forces placed on the cross member during the course of typical operation are transferred to the chassis rail. The laminate and core directly beneath the cross member are the primary recipients of the vertical loading component. Inadequate strength in this region would lead to delamination and crushing of the core, thereby destroying the integrity of the joint. The effective connection of the cross member and chassis rails is therefore paramount in maintaining structural integrity. The design and testing of this connection is described in detail in Chapter 7.

Mode 16 Regions of the chassis rail susceptible to localised crushing include those directly in contact with the high compressive forces imposed by the suspension and skid plate attachments. This mode of failure would result from insufficient compressive strength, particularly from the core material. Inadequate foundational support by the core would allow the plastic deformation of the laminates, thereby inducing delamination, fibre splitting, and other stress concentrators, which would act to further locally degrade the laminate. Inherent in the avoidance of this failure mode would be the adequate distribution of all concentrated loads to ensure the minimisation of compressive stress.

Mode 17 In a similar fashion, a concentrated distribution of the payload positioned over the chassis rail would induce high compressive stresses on both the decking and the compressive laminate of the beam. Sufficiently high loading would initiate damage to both the laminate and the underlying core, thereby increasing the possibility of failure of the compressive reinforcement in a fatigue environment. However, the application of a load of the required magnitude would result in a failure of the deck through punching shear, and it is assumed that this would alert the operator to remove or redistribute the payload. As the probability of this type of failure is relatively low, this was not considered in any further detail within this research.

Modes 18 – 20 These failure modes address the attachment of ancillaries to the chassis rail. High longitudinal and vertical loading is particularly present in the regions of the skid plate, suspension attachments, and standing legs. The use of mechanical fasteners and adhesives to facilitate attachment of these components attracts the possibility of localised

stress concentrations and debonding respectively. However, the combination of the two methods of attachment ensures a measure of redundancy, enabling the avoidance of catastrophic failure resulting from the disengaging of one or more of the primary ancillary attachments previously mentioned. While the author did not investigate the attachment of these ancillaries, the results of an initial investigation conducted by a fellow researcher are summarised in the following chapter.

Mode 21 As previously mentioned in section 6.3, lateral torsional buckling has been observed in the failure of the chassis rails of steel trailers. This is predominantly due to the relatively thin web used in the I-beam construction of these members. However, the rectangular cross section of the proposed FRP trailer should possess significantly greater resistance to lateral torsional buckling. Additionally, it is anticipated that the large diameter of the proposed cross member should provide further lateral support to the lower flange of the chassis rail. Given the limited time available and the unlikelihood of this phenomenon, this mode of failure was not investigated by the author, and will not be addressed further. It is recommended that this area be considered for subsequent research into FRP trailers of this type.

Mode 22 This mode includes considerations of the chassis' performance in response to conditions which induce torsional loading. This loading is induced by several factors, including ground plane twist, asymmetric load distribution, lateral acceleration due to cornering and static turning forces. Ideally, the suspension is capable of accommodating the majority of terrain irregularities experienced by the trailer. However torsional stiffness is essential to withstand the loads imposed by the remaining loading conditions of those previously mentioned. Sharman [3] demonstrates that the use of chassis rails with rectangular cross sections, in combination with circular cross members, produces the greatest torsional resistance in a ladder frame chassis. However, given the limited time available, and the unlikelihood of this phenomenon, this mode of failure was not investigated by the author, and will not be addressed further. It is recommended that this area be considered for subsequent research into FRP trailers of this type.

Mode 23 The subject of durability has been outlined previously in section 5.4.5. The laminate material inherently determines the results of impact of road debris on exposed laminates. However, the continual and abrasive nature of these incidents would suggest that protective coatings or shields be employed in the affected regions to eliminate the erosion of the laminates. The prevention of laminate abrasion is particularly significant, as the regions more commonly affected include the tensile reinforcement located in the neck

region. Degradation of these laminates would greatly increase the probability of catastrophic tensile failure, and should therefore be avoided. This is discussed further in Chapter 7.

Mode 24 The dynamic nature of the road environment continually subjects the trailer to vibration of various frequencies. This mode of failure describes the excessive deflection experienced by the chassis when excited at or near the natural frequency of the structure. The natural frequency is not only determined by the characteristics of the chassis, but also by those of the suspension systems of the trailer and the prime mover. Additionally, the distribution of any payload present will substantially contribute to the response of the trailer as a whole [4]. With respect to the chassis, vibrational response is primarily determined by the stiffness and mass distribution characteristics of the trailer, which are themselves dependent on the dimensional aspects and connection details selected by the designer. Shaw [5] provides general estimates for the natural frequencies possessed by various components of the trailer system. However the chassis' represented by these figures are relevant only for steel, and should not be adopted for use in the genre of FRP materials. Determination of the natural frequencies and mode shapes of any given trailer must be performed on an individual basis, due to the unique characteristics resulting from variations in design specifications. Additionally, the suspension characteristics would greatly influence the natural frequency, as it would need to be adjusted to account for the change in stiffness and greater deflection (refer Section 4.8.5). It is not within the scope of this thesis to investigate the range of natural frequencies to be expected in relation to the large number of variables resulting from differences in structural or suspension detail, and hence this topic was not considered further by the author.

Mode 25 The final failure mode considered in relation to the chassis rails is that which occurs as a result of contact with another vehicle or solid object, or the overturning of the trailer due to unsafe manoeuvring. Depending on the severity and circumstances of a collision and the size and position of the payload, this may result in partial or total failure of the chassis. With respect to an overturning of the trailer, the possibility of partial or complete member failure also exists. To the author's knowledge, investigation into the crashworthiness of flatbed semitrailers has not yet been undertaken, and no attempt has been made within this research to address this topic.

6.9.3 Failure Modes of Cross Members

Modes 26 – 28 The first three failure modes listed in Figure 6.10 are relevant to the basic design process with respect to cross member strength. The material data presented in Chapter 5 provides sufficient information to allow the designer to calculate the required volume of reinforcement, given a specified moment capacity and deflection limit as defined in Chapter 4. Failure of the cross member due to insufficient tensile, compressive or shear strength would produce only localised effects, and would result in transference of the load to adjoining cross members, provided the deck remained structurally intact. Failure of a single cross member in isolation would not indicate the presence of an overloaded trailer, but instead would result purely from the excessive concentration of load above the respective member. While failure of any type would necessitate the replacement of the cross member, the immediate effect on the performance of the trailer should remain minimal.

Modes 29 – 31 These failure modes also relate to the basic design process of the cross member, in particular the application of suitable reduction factors which allow for the influences of fatigue. It is anticipated that the type of connection used to join the cross member to the chassis rail would have a significant effect on the fatigue performance, specifically with respect to the introduction of stress concentrations at the outer points of connection. Further discussion on the fatigue performance of the cross members can be found in Chapter 8.

Mode 32 In addition to the compressive failure of the laminate, the tendency of thin-shelled structures to buckling or 'crinkle' in compression has been widely documented. Mode 10 addressed the influence of the core material on the buckling strength of a laminate. In this case however, the member consists purely of a laminate formed over a mandrel. Hence, it is expected that the probability of local laminate buckling is relatively high. The consequence of this type of failure would be similar to that of a compressive laminate failure, necessitating the replacement of the member. The local inclusion of a supporting core material or the use of a sacrificial mandrel may be employed to provide the laminate with buckling restraint, thus allowing failure to occur in a manner more predictable. The performance of the member with respect to compressive performance is demonstrated in Chapter 7.

26 Tensile failure of reinforcement
27 Compressive failure of reinforcement
28 Shear failure
29 Fatigue failure in tension
30 Fatigue failure in compression
31 Fatigue failure in shear
32 Crinkling/buckling of reinforcement in comp
33 Crushing/deformation of section shape
34 Impact damage (stones, tyres)
35 Torsional failure due to torsional flexure of chassis

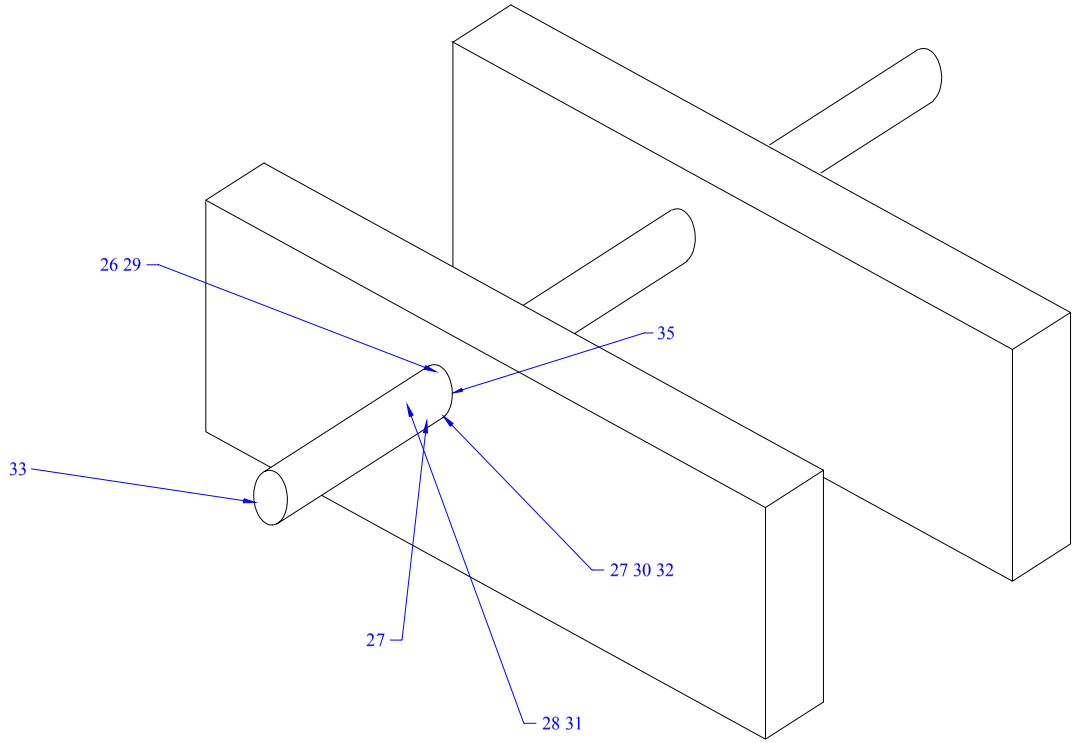

Figure 6.10 Possible Failure Modes of FRP Cross Member

Mode 33 The particularly open section of the cross members increases the susceptibility of the member to sectional deformation under compressive loading. The load transferred to the cross members by the deck acts to compress the section, thereby locally deforming it. This induces stress in these regions, and increases the likelihood of failure. While the restraint provided by the connection to the chassis rail would prevent the local deformation of the cross member immediately surrounding the joint, the outer end possesses no such restraint. Consequently, to avoid this deformation at the free ends, a solid connection to the combing rail must be made. This would provide a resistance to deformation similar to that provided by the bond to the chassis rail. The investigation of cross members in Chapter 7 includes an alternative method to preventing this deformation.

Mode 34 As previously mentioned in mode 23, resistance to impact from various object should be primarily accommodated by protective surfaces, thereby reducing the frequency and severity of impact to the exposed laminates. In a similar manner to the chassis rails, erosion of the laminate through the continual impact of road debris would result in member failure. However the prevention of laminate abrasion is of lesser significance in relation to the cross members, as the failure of the exposed compressive laminate would require only the replacement of the affected beam.

Mode 35 The torsional loading imposed on the chassis, as described in mode 22, relies primarily on the torsional capacities of the members, and the rigidity of the connection between them. Assuming a rigid connection, the loads induced on the laminate of the cross member must be accommodated by the shear reinforcement. Failure of cross members due to torsional loading of the chassis would not be catastrophic, provided sufficient torsional stiffness remained to ensure the adequate support and restraint of the load. As previously mentioned, the consideration of torsional loading lies outside the scope of this thesis, and will therefore not be considered further. A number of initial observations of the effects of joint rigidity on torsional performance are outlined in Chapter 7.

6.10 Conclusion

This chapter outlined a number of possible conceptual designs of FRP flatbed semitrailers that were considered during the course of this research, and summarised the process of comparison and selection of a suitable design. The identification of a single concept enabled the continuation of research with increased focus into the practical feasibility of FRPs in this application.

The various concepts considered comprised monocoque and ladder frame configurations, the latter of which being essentially modular. The presented range of conceptual designs was intended as representative, rather than exhaustive, of the structural configurations possible through the use of FRP materials. All monocoque structures, in addition to one of the ladder frame structures, utilised the casting nature of PFR for use as a high strength core. The use of a structural foam core, in addition to the lower material volume provided by the ladder frame configuration, provided large reductions in tare mass to concepts one and five in comparison with the monocoque structures consisting of PFR. Of all concepts considered, the fifth concept was selected due to superior performance in the majority of the defined criteria.

The possible failure modes associated with the final concept were briefly summarised, being separated into those applicable to the chassis rail or cross members. Within the context of this thesis, only those associated with the chassis were considered, with the critical modes referred to Chapters 7 and 8 for further investigation.

References

[1] Lubin G, editor. Handbook of composites. New York; Van Nostrand Reinhold; 1982.

[2] Mallick PK, editor. Composites engineering handbook. New York: Marcel Dekker; 1997.

[3] Sharman PW. Torsional design aspects of long wheelbase vehicles. IEEE Conference Record of Annual Conference of Electrical Engineering Problems in the Rubber and Plastics Industries, Inst. of Phys, Stress Anal Group, Annual Conference, Stress, Vibration and Noise Analysis in Vehicles 1975; Birmingham, England; New York: John Wiley and Sons; 1975: 123-148.

[4] Cole DJ, Cebon D. Validation of an articulated vehicle simulation. Vehicle System Dynamics 1992; 21: 197-223.

[5] Shaw PA. Static analysis and dynamic simulation of linked multi-axle truck suspension units [PhD dissertation]. Brisbane, Queensland: University of Queensland; 1993.

Chapter 7 Application of the Design Philosophy to the Final Concept

7.1 Introduction

Chapter 4 established a design philosophy suitable for FRP flatbed semi trailers, while Chapter 5 identified the materials best suited to this application. The discussion of various conceptual designs presented in Chapter 6 culminated in the selection of a single concept, which possessed superior performance characteristics in relation to relevant criteria. The predicted modes of failure relevant to this concept were then identified in order to provide an increased focus to the practical feasibility of FRPs in this application.

This chapter addresses the application of the design philosophy to the selected concept, allowing the practical assessment of the potential of both the material and the chassis configuration. It should be noted however, that this investigation addresses only the fundamental characteristics of this concept, as the examination of manufacturing details necessary for complete prototype production does not form part of the objectives of this thesis. Rather, the basic design process is described, and several of the significant modes of failure introduced in the previous chapter are addressed in detail.

It is acknowledged that this chapter contains a substantial quantity of data and information relating to the experimental program undertaken as part of this study. However, this data was included in detail to ensure that sufficient guidance and information was available for future research.

7.2 A More Detailed Analysis of Existing Steel Trailers

As the concept selected in the previous chapter comprises a ladder frame similar in configuration to that of existing steel trailers, further investigation was undertaken into the structural behaviour of steel trailers in order to highlight those portions of the chassis that should be considered critical. While the location of these critical points may not necessarily coincide with those on an FRP trailer, it was anticipated that this would provide an indication as to the nature and general cause of these local phenomenon.

Two trailers were chosen from the sample presented in Chapter 4, namely the 1992 Haulmark and 1995 Lusty Allison trailers. These trailers appeared to possess similar load carrying capacity with respect to ultimate strength, although the chassis rail profile of each contains marked differences with respect to the other. Consequently, it was anticipated that a comparative analysis of the two configurations would indicate the significance of the chassis rail profile on the actual capacity of the trailer.

7.2.1 Linear Elastic Finite Element Model

A finite element program, ANSYS (v. 5.7), was used to complete the numerical analysis of each model, with a 4-node shell element (SHELL 63) used throughout the analysis to represent both the web and flanges of the beams. Perfectly elastic material characteristics were assumed, and plastic deformation was not considered.

The analysis included only the chassis rail, as the primary purpose of this analysis was to identify the effects of section changes to the stress state within the beam. In order to simulate the effects of the suspension system, spring elements were used. These elements possessed three degrees-of-freedom per node, and required an input of spring stiffness, k, and a coefficient of damping, c. The latter variable was set to zero due to the static nature of the analysis. The load sharing characteristics of the rear suspension system were approximated by the adjustment of spring stiffness' in each element, such that the reaction loads provided by each were similar in magnitude. The general dimensions and element mesh produced for each beam are illustrated in Appendix B.

Two variations in load distributions were considered, which included load cases one and three as defined in section 4.5.2. These load cases were chosen as representative of the most common load cases that would induce significant flexure of the chassis rails.

The first load case was distributed along the chassis rail in accordance with Load Case 1 (refer section 4.5.2). The magnitude of the load represented the maximum allowable payload. This was distributed as a uniform pressure, applied perpendicularly to the top flange along the entire length of the beam, as per Figure 7.1.

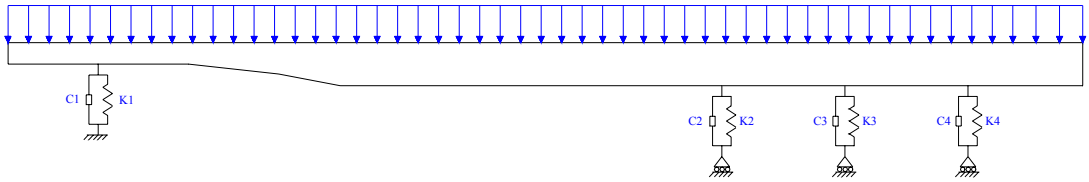

Figure 7.1 Basic Model Layout Loaded with Load Case One

The second load case was distributed along the chassis rail in accordance with Load Case Three. The magnitude of the load represented the maximum allowable payload, however this was distributed by a series of loads imposed upon nodal points over a length of six metres. The position of the load was adjusted to ensure a correct load distribution between each axle group.

Further information regarding the analysis of these beams is contained within Appendix B.

7.2.2 Results and Discussion

As previously mentioned, these two trailers possessed similar structural characteristics with respect to the ultimate strength of the deeper section of chassis rail. However, it would appear that the strength of the chassis rail sections is not the primary consideration with respect to the performance of the chassis rail. The presence of stress concentrators proved to be significant in the ultimate stress imposed on the flanges of the chassis, particularly with respect to the Lusty Allison trailer. The summarisation of the analysis results for load case one and load case three are presented in Tables 7.1(a) and (b) and 7.2(a) and (b) respectively.

These contain a comparison between the maximum stresses resulting from areas of stress concentration, and those stresses occurring in the regions of the maximum bending moment.

Table 7.1(a) Analysis Results at Highest Stress Concentration for Load Case One

	1st Principal Stress, S_1 (MPa)	Max. Tensile Stress, S_x (MPa)	Max. Comp. Stress, S_x (MPa)	Max Von Mises Stress, S_{VM} (MPa)	Max. Deflection delta (mm)
Haulmark Trailer 1992	59	59	-60	54	13
Lusty Allison Trailer 1995	140	137	-104	142	14

Table 7.1(b) Analysis Results at Chassis Rail Mid-Span for Load Case One

	1st Principal Stress, S_1 (MPa)	Max. Tensile Stress, S_x (MPa)	Max. Comp. Stress, S_x (MPa)	Max Von Mises Stress, S_{VM} (MPa)	Predicted Mid-Span Tensile Stress - Beam Theory (MPa)
Haulmark Trailer 1992	47	47	-60	47	70
Lusty Allison Trailer 1995	51	51	-104	51	62

It should be noted that only limited attempts were made to provide accuracy in the regions of high stress concentration, as this analysis was only interested in the order of magnitude of these stresses. Rather, this analysis was performed to highlight those points within the chassis rail that would appear to initiate failure, and did not account for factors such as variations in axle loading. Consequently, the values resulting from these regions should be considered purely as indicative of the stress state resulting from the effects of stress concentrators.

The predominant region of concern for the Lusty Allison trailer was shown to reside at the initial point of increase in sectional depth, as illustrated by Figure 7.2, and in Figures B.5 and B.7. While the change in beam depth is necessary to produce sufficient structural strength characteristics, the severity of the change in section represents the primary contributor to the magnitude of the stress concentration (refer section 7.5). The abrupt change present in this beam profile clearly initiates a substantial increase in localised stress, and although a small radius of approximately 50 mm was observed on the trailer in this region (and replicated within the model), this would appear to have a limited influence in the reduction of localised stress.

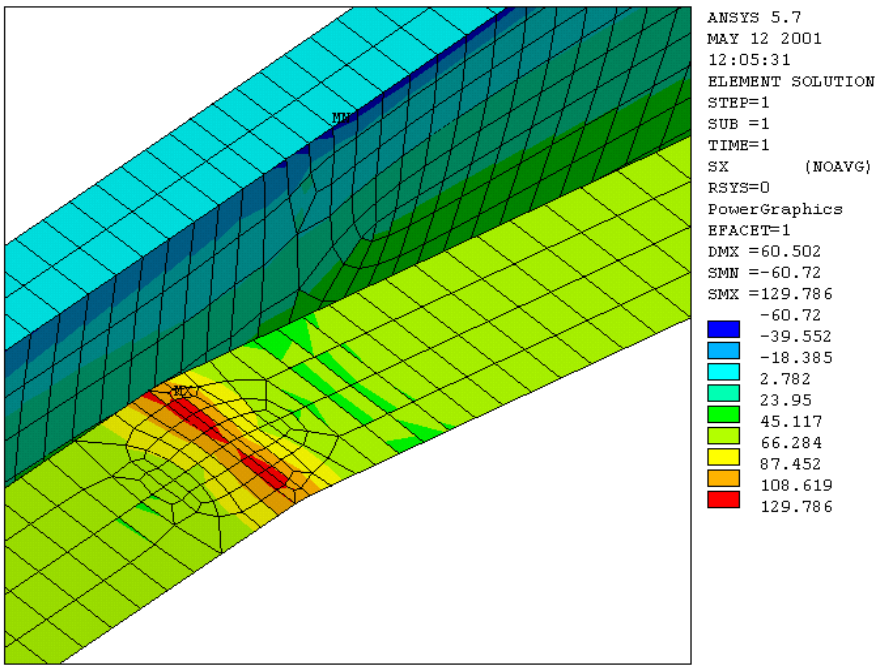

Figure 7.2 Region of Maximum Stress in Lusty Allison Trailer

In addition to this point of stress concentration, an equally abrupt change of angle is observed in the deeper end of the neck section. This also increases the localised values of stress, as illustrated by Figure B.7(c).

Table 7.2 (a) Analysis Results at Highest Stress Concentration for Load Case Three

	1st Principal Stress, S_1 (MPa)	Max. Tensile Stress, S_x (MPa)	Max. Comp. Stress, S_x (MPa)	Max Von Mises Stress, S_{VM} (MPa)	Max. Deflection delta (mm)
Haulmark Trailer 1992	172	172	-168	136	43
Lusty Allison Trailer 1995	246	240	-135	250	35

Table 7.2 (b) Analysis Results at Chassis Rail Mid-Span for Load Case Three

	1st Principal Stress, S_1 (MPa)	Max. Tensile Stress, S_x (MPa)	Max. Comp. Stress, S_x (MPa)	Max Von Mises Stress, S_{VM} (MPa)	Predicted Mid-Span Tensile Stress - Beam Theory (MPa)
Haulmark Trailer 1992	136	136	-168	136	168
Lusty Allison Trailer 1995	118	118	-135	121	148

By contrast, the Haulmark trailer exhibited significantly lower values of stress. However, the maximum stress did not result from the change in beam section, but rather from an abrupt change in flange width, as illustrated in Figures B.4 and B.6. While the reduction of flange width produces a subsequent reduction in tare mass and the avoidance of over-design, the stresses induced by this step are significant due to the already substantial tensile load imposed on the lower flange in this region. The avoidance of a stress concentration in the upper region of the neck would appear to be facilitated by the reduction of the angle of change. Further investigation of the neck region is presented in section 7.5.

The susceptibility of steel trailers to failure resulting from poor detail design and unanticipated stress concentrations (refer section 4.4.1) would appear to have been confirmed by this analysis. Further, this investigation has provided a clear indication as the points at which failure would most probably initiate.

Neglecting these points of stress concentration, the values of stress observed in the flanges of the chassis rails compare favourably with simple beam theory, which used the simplifying assumption that the triaxle group can be represented as a single pinned support. This is demonstrated by the data presented in Tables 7.1 (b) and 7.2 (b), which compare the observed stress in the lower flange of each chassis rail with that predicted using beam theory and the maximum moment anticipated by Figure 4.10.

The analysis of these steel trailers has therefore yielded useful guidance with respect to the implication of detail design. Of primary importance is the tendency of stress concentrations to form in the neck region; highlighting the need for particular consideration in relation to the FRP chassis rail design. This is addressed in detail in section 7.5.

7.3 Basic Beam Construction

Having identified the critical regions of chassis rail design with respect to steel trailers, application to an FRP chassis rail is possible. However, the basic configuration of the chassis rail must first be established in further detail to facilitate a fitting employment of the aforementioned principles. This section presents in greater detail the FRP chassis rail proposed for utilisation in the trailer.

The general construction of the proposed chassis rail comprises four sandwich panels, bonded together to form a rectangular hollow section. The accomplishment of this connection was envisaged in two forms, as illustrated by Figures 7.3 (a) and (b).

The first configuration utilises four connection pieces, which are bonded to each panel joint in two places. Two differing connection pieces are presented in the figure, in addition to two variations in sandwich panel orientation. This configuration facilitates the utilisation of plane sandwich panels, which requires no edge modification or preparation.

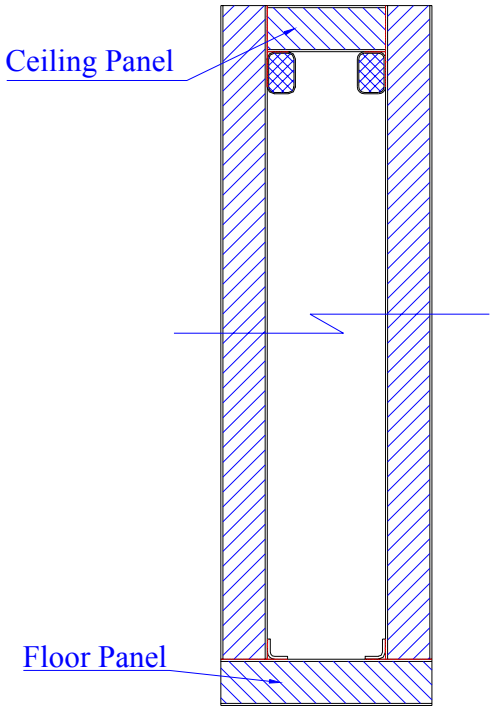

Figure 7.3 (a) Chassis Rail Cross Section Configuration – Concept One

The second concept utilises 'ceiling' and 'floor' pieces, modified to provide larger surfaces for adhesive bonding. While this configuration requires significant alteration to the upper and lower sections of the beam, the four connection pieces required for the previous concept

are not required. Two differing variations in sandwich panel configuration are illustrated in the figure.

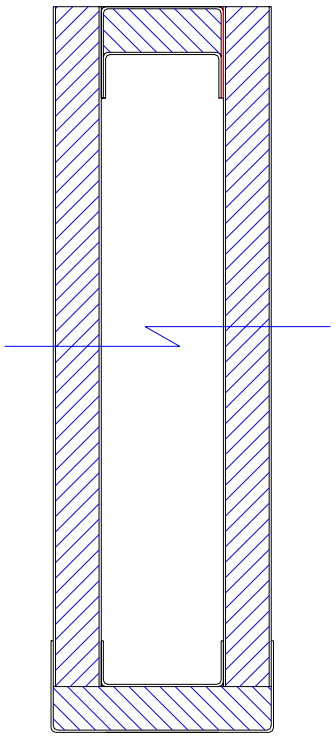

Figure 7.3 (b) Chassis Rail Cross-Section Configuration – Concept Two

The selection of the appropriate configuration was accomplished by consideration of the loads imposed on the chassis rail. In particular, the vertical compressive loading imposed on the section, as discussed in Failure Mode 14 (section 6.9.2), represented the predominant consideration with respect to cross sectional performance. As demonstrated in section 7.5, the rigidity of the connection at each corner significantly contributes to the compressive performance of the section. An observational comparison of each concept suggests that the second would provide superior joint rigidity, primarily as a result of the monocoque construction of the 'ceiling' and 'floor' sections, in addition to the superior joint integrity provided by the increase in bonding area involving the direct adhesion of two laminates. More specifically, the sandwich panel orientation denoted by the upper section of Figure 7.3 (b) would provide improved compressive and shear performance for the chassis rail. The continuation of the inner laminates through to the outer surfaces of the beam would prevent the transfer of vertical and shear loads through the core material, and provide greater flexural stiffness to the beam flanges.

The incorporation of the shear and tensile/compressive reinforcement would be accommodated as illustrated in Figure 7.3 (c). Following the assembly of the four sandwich

panels, the shear reinforcement would be applied in 'wraps', with each layer being represented by a single continuous piece of fabric which encompasses the entire circumference of the beam. The unidirectional reinforcement, used to accommodate the tensile and compressive forces produced in the flanges of the beam, is shown in the figure to be alternately dispersed between the layers of shear reinforcement. This technique, adapted from Van Erp [1], addresses a number of the potential failure modes discussed in the previous chapter. Specifically, this effectively eliminates the debonding phenomenon associated with edge effects, as all free edges of the unidirectional laminate are constrained beneath one or more layers of double bias shear reinforcement. Additionally, the intermingling of the shear and flange reinforcement allows for the effective and direct transfer of shear loading between the two reinforcements, thereby removing the need to transfer these forces through the core material. The presence of double bias layers within the flange laminates also acts to provide transverse strength, preventing the longitudinal splitting which may occur in a predominantly unidirectional laminate.

Based on the apparent strengths of this cross sectional design, this configuration was adopted for use in the preliminary investigation of the chassis rail. Exclusive application of this beam configuration was subject to confirmation of the beam cross sectional performance, as described in section 7.4.

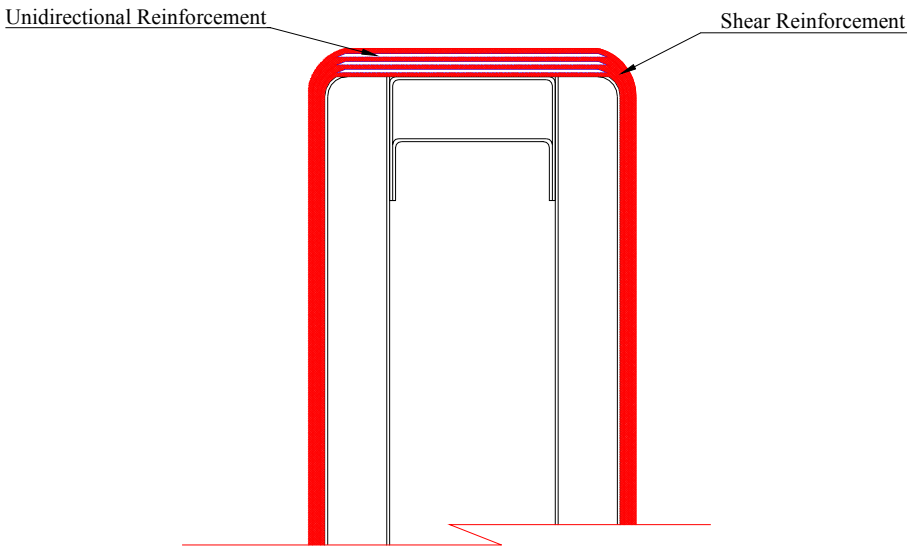

Figure 7.3 (c) Integration of the Shear and Unidirectional Reinforcement

7.4 Cross Sectional Performance Characteristics

7.4.1 Introduction

As previously outlined in section 6.9.2, the conditions inducing crushing failure of the chassis rail cross section would occur in the regions of high vertical compression. Such occurrences would typically result from the concentration of the payload directly above a support point. Specifically, a payload distribution similar to Load Case 2 (refer section 4.5.3) effectively imparts direct vertical compression to the cross section of the chassis rail in combination with the reaction force presented by the suspension system. The performance of the beam is dependent not only on the compressive properties of the wall section, but also on the ability of the wall sections to withstand global buckling.

This part of the chapter addresses the stability of the chassis rail cross section as described in Figures 7.3 (b) and (c). Finite element analysis was used to gain a basic understanding of the significant factors relating to cross sectional performance. A sample specimen was constructed and experimentally tested to illustrate the principles established by the analysis.

7.4.2 Assumptions in the Analysis of Sectional Stability

As this examination was undertaken in a preliminary context, it was not the intention of this investigation to analyse a series of cross sectional variations and experimentally verify each one. Rather, the analysis described in this section was performed in order to identify the primary contributors to cross sectional performance, while a single test piece was tested in order to provide a level of confidence in the predicted mode of failure.

A number of assumptions were made in the context of this analysis. These are summarised as follows:

1. The restraining effects of the cross members or any other ancillary attachment were ignored during the course of this analysis.
2. Sectional instability or failure is defined as the formation of cracks in the core material or laminate, or debonding/delamination of the reinforcement, which results from the excessive rotation or deflection associated with the deformation of the section under load.
3. A segment of the chassis rail, 150 mm in length, is considered in isolation. The distribution of load along the length of the chassis rail to the laminates directly

adjacent to the section in compression is ignored. Hence, it is assumed that no shear connection exists between the compressed section and the adjoining section. It is acknowledged that this assumption represents a simplification, which would yield conservative results.

4. The effect of the tensile/compressive forces carried by the upper and lower flange laminates on the compressive performance of the cross section are assumed to be small, and therefore the effects are ignored.
5. The load is uniformly distributed across the width of the beam.

Given the basic cross sectional shape as denoted by section 6.7, it is also proposed that the intended function of the reinforcement placement is as follows:

- The function of the outer wrap layers of DB E-glass is:
  - To provide restraint to the unidirectional reinforcement
  - To eliminate edge effects
  - To be capable of withstanding the entire shear load (refer section 7.7)
- The function of the laminates on the inner walls is to provide the section walls with additional stiffness, and to prevent buckling or excessive lateral deflection of the sidewalls under a compressive load. As the shear capacity of the beam is contained within the outer laminates of the sidewall, it is not necessary to incorporate shear capacity into the inner wall laminate.
- The core material was not intended to provide a significant contribution to the shear capacity of the beam, due to the comparatively low material properties of the core material. However, the primary function of the core material is to provide adequate support to the laminates to prevent local laminate buckling, wrinkling, or debonding.

The thickness of the core was decided upon as a result of a combination of factors. Primarily, it was anticipated that global buckling of the beam walls would represent the predominant failure mode. Hence, significant increases in wall stiffness could be achieved through a slight increase in the spacing of the laminates, thereby enabling a reduction in thickness of the inner laminate. Additionally, the limitations of cost and weight dictated the minimisation of all material quantities. With respect to the core, the manufacture of the PVC foam increases disproportionately with cost due to increased difficulties in maintaining consistent properties throughout the thickness. Specifically, due to the substantial quantity of core material required in each chassis rail, cost estimates provided by the manufacturer suggested that thicknesses greater than 30 mm would add an unacceptable increase in core material cost. When considered in conjunction within the

context of mass reduction, it was decided that a core thickness of 30 mm would be used in the construction of the chassis rail.

For the purposes of this analysis, a beam depth of 500 mm was chosen. As the actual depth of a given chassis rail is dependent on the constraints discussed in section 4.8, this was assumed to be a 'typical' section depth. While it could be said that a beam depth of 600 mm would represent a conservative approach by allowing an increase in the buckling length of the beam walls, it was assumed that the distribution of load along the length of the chassis rail to the laminates directly adjacent to the beam segment (which was ignored in this investigation) would adequately accommodate this in practice.

The load capacity of the section required to withstand the compressive loading was established by using information provided by RoadUser International Pty Ltd (RUI). Tests were conducted by RUI to determine the effect of dynamic wheel loading on the suspension system. These tests indicated that for a static airbag pressure of 60 psi, a peak pressure of 90 psi (with a standard deviation of 2 psi) was observed in response to a filtered random input [2]. That is, a dynamic factor of 1.5 is experienced by the suspension system, in comparison with the dynamic factor of 2.5 experienced by the chassis (in flexure). Hence, given that the maximum static load on each of the rear axles must not exceed 7.5 tonnes (refer section 4.5.1), the maximum dynamic (compressive) load transferred to the chassis rail for consideration in this investigation was calculated as:

$$\text{Load on each chassis rail} = 7.5 / 2 \text{ tonnes}$$
$$= 3.75 \text{ tonnes}$$

Therefore, given a dynamic allowance of 1.5 times the maximum static load,

$$\text{Max. Compressive Force on chassis rail} = 3750 \text{ kg} \times 9.81 \text{ m/s}^2 \times 1.5$$
$$= 55.2 \text{ kN}$$

7.4.3 Non-Linear Finite Element Analysis

Based on the stated assumptions and limitations set out in the preceding section, analysis using the finite element technique was conducted to determine the characteristic behaviour of the chassis rail cross section. A non-linear analysis was employed due to the inherent buckling nature of the problem.

A finite element program, ANSYS (v. 5.7), was used to complete the numerical analysis of each model, with 8-node plane-strain elements (PLANE 82) and 2-node compression-only

spring elements (COMBIN 14) used throughout the analysis to represent a thin 'slice' of the beam cross section and loading platforms respectively. Perfectly elastic material characteristics were assumed, and plastic deformation was not considered. Figure 7.4 shows the basic layout of the model.

The analysis considered a 2-dimensional representation of a discrete portion of the chassis rail, 150 mm in length. The primary objective of this analysis was the identification of the effects of modifications to the cross-section with respect to the stress state within the section. Additionally, it was anticipated that this analysis would enable the prediction of failure points and modes, thereby yielding a general indication of best design practice. In order to simulate the load sharing effects of the rubber mat placed between the beam and the loading platen (refer section 7.4.4), compression-only spring elements were used. These elements possessed three degrees-of-freedom per node, and required an input of spring stiffness, *k*, and a coefficient of damping, *c*. The latter variable was set to zero due to the static nature of the analysis. The general dimensions and element mesh produced for each analysis are illustrated in Appendix C.

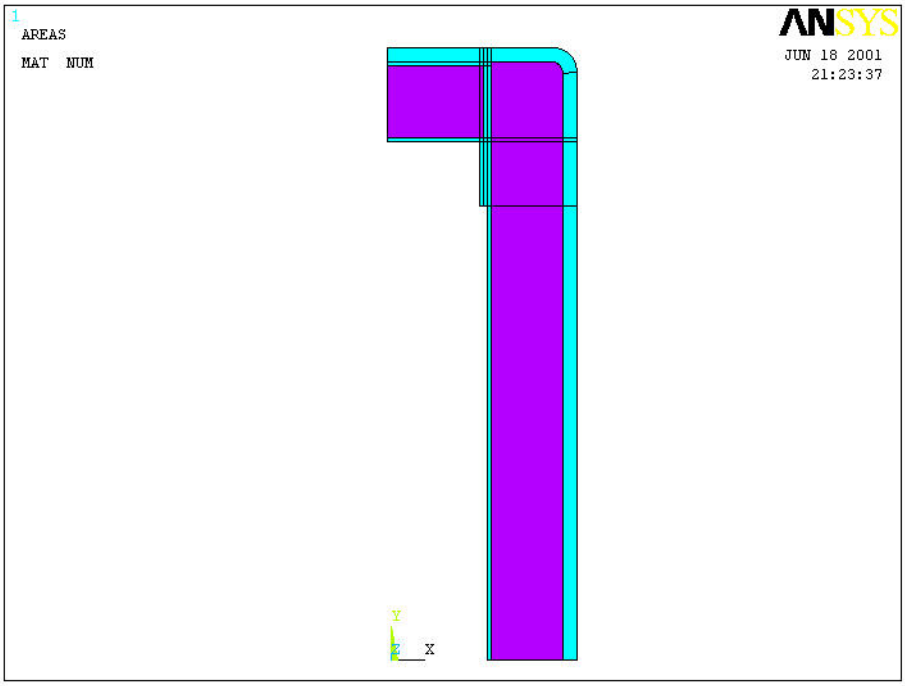

Figure 7.4 Basic Model Layout of Beam Cross Section

A number of cross-sectional variations were considered during the course of the analysis, in order to facilitate the identification of the relevant contributors to the crushing strength of

the section. Each of the iterations analysed are described as follows, and are shown in detail in Appendix C.

1. Initial Configuration

This configuration was constructed using a generic laminate lay-up sequence of [DB/0/DB] on all surfaces. Shear reinforcement (in the form of a double-bias laminate comprised of $[DB]_7$) was the only additional reinforcement added to the outside of the beam. It was anticipated that this section would yield significant sidewall deflection due to the disproportionate laminate distribution.

2. Iteration One

The first modification to the cross section involved an increase in the stiffness of the inner laminate on the sidewall. Specifically, the single layer of unidirectional E-glass was replaced with two layers of unidirectional T300 carbon fibre reinforcement. This revision was enacted to demonstrate the significance of the inner laminate stiffness.

3. Iteration Two

The second iteration comprised a reduction in the thickness of the connecting sandwich panel core, as demonstrated in Figure C.2 (d). Specifically, the core thickness was reduced from 30 mm to 10 mm, and utilised a laminate configuration identical to the original cross section. This alteration demonstrated the contribution of the stiffness of the connecting sandwich panel to cross sectional performance.

4. Iteration Three

This iteration involved an increase in the stiffness of the inner laminate of the connecting sandwich panel, replacing the single layer of unidirectional E-glass with two layers of unidirectional T300 carbon fibre reinforcement. This revision was similar to the previous, in that it demonstrated the contribution of the stiffness of the connecting sandwich panel to cross sectional performance.

5. Iteration Four

The fourth iteration represents a combination of the first and third iterations. This configuration maximises the effective stiffness of both sandwich panels, in addition to the maximisation of the joint stiffness.

6. Iteration Five

The final iteration represents a modification of the previous iteration. The thickness of all core materials was reduced from 30 mm to 10 mm, whilst maintaining the use of unidirectional carbon fibre reinforcement.

A single load case was considered, which comprised a uniformly distributed load over the entire area of the top surface. As previously mentioned, a loading platen in conjunction with compression-only spring elements were used to simulate the loading process described in section 7.4.4. A load of 35 kN was applied to the symmetric model, simulating a total load on the complete beam of 70 kN. The non-linear analysis was conducted using 10 sub-steps, and further information regarding the analysis of these beams is contained within Appendix C.

7.4.4 Fabrication and Experimentation

The beam section fabricated was representative of the original cross sectional configuration as denoted in section 7.4.3. While it can be seen from the results presented in section 7.4.5 that this configuration did not characterize the optimum solution, it was selected primarily on the basis of cost. As the purpose of this experiment was to provide only a preliminary measure of validation to the analysis, it was anticipated that the testing of any of the sections previously analysed would provide insight into the actual behaviour of the beam cross section.

The process of beam manufacture, illustrated in Appendix C, is described in an abbreviated form in this section. Polyurethane (PU) foam was used as a core material in this experiment, due to unavailability of PVC foam. As this beam section would not be exposed to long term or dynamic loading conditions, the use of PU foam is justified in this preliminary context. The E-glass reinforcement and matrix types used in this specimen were identical to those tested in Chapter 2. The hand lay-up technique (refer Chapter 2) was used throughout the beam manufacture. The construction of the beam cross section was carried out as follows:

1. Two sandwich panels were produced, comprising a 30 mm thick PU core and a laminate of [DB/0/DB] on each side. These panels were labelled as 'sidewalls'.
2. Two additional 'connecting' sandwich panels were constructed, with the addition of two laminate flanges. These flanges were oriented perpendicularly, as shown in Figure C.10 (a) and (b) in Appendix C. These panels were labelled as 'connecting' sandwich panels.
3. These flanges facilitated the adhesive bonding of the two sidewalls to the connecting sandwich panels, which was achieved through the use of an epoxy adhesive. A low clamping pressure was applied to the panels to ensure the removal of voids and produce an even glue line thickness.
4. Following the cure of the adhesive, the beam section was trimmed, and a fillet (radius 10 mm) was shaped over each corner. The fillet was necessary to allow the shear reinforcement to be adequately consolidated once laid over the corners.
5. Seven layers of DB E-glass reinforcement were wrapped around the circumference of the beam. The ends of the reinforcement were butted together in the centre of the connecting panels, with the joints being alternately staggered between the top and bottom flanges of the beam.
6. Following the ambient cure of the shear reinforcement, the beam was post cured at a temperature of 80^{0}C for the duration of 8 hours. The section was then trimmed to shape.

As previously stated, the intended purpose of this experiment was to simulate the compressive loading experienced by the chassis rail. Consequently, the beam section was placed in direct compression using an Avery Universal Testing Machine, as illustrated in Figure C.11 (a). In order to ensure that the load was evenly distributed over the surface of the beam, a rubber mat was inserted between the beam and the loading platen, as shown in Figure C.11 (b). The load was applied at a rate of 2 mm/minute, and both the load and platen deflection were measured throughout the duration of the test.

7.4.5 Results and Conclusions

a) Analysis Results

Despite the preliminary nature of this investigation, the analysis of the performance of the proposed beam cross sectional configurations yielded a number of significant facts regarding the response of the section to compressive loading.

The initial conclusions yielded by the analysis revealed a dependency of the section performance on the core material, this dependency being a function of the beam design. Specifically, a survey of the analysis results indicates that the stresses imposed on the core material are greater than those imposed on the laminates in comparison to the respective ultimate material capacities. Hence, this suggests that initial failure would occur within the core material, thereby emphasising the significance of the mechanical properties of the core. It also follows that a core material possessing a low tensile strength or poor adhesion to the laminate acts to produce premature cracking, which then contributes to extensive delamination and section failure.

Additionally, the magnitude of the stresses experienced by the core would appear to be directly related to the degree of rotation experienced at the joint of the wall to the connecting panel.

As can be seen in Table 7.3, the first iteration in the analysis resulted in a substantial decrease in core stress through stiffening of the wall panel. However, it can also be seen that the fourth iteration resulted in an increase in core stress, despite the stiffening of the connecting laminate (and therefore the joint to some degree). A typical distribution of stress throughout the core material is shown in Figure 7.5. This would suggest that the stiffness of the wall panels is a greater contributor to the reduction of joint rotation. Additionally, this indicates that it is desirable that the wall panel stiffness be greater than the stiffness of the connection panel. An over stiff connecting panel does not allow rotation of the entire joint, thereby presenting a sudden increase in stiffness (and hence a stress concentration) to the wall panel through this rotational restraint. That is to say the stiffness of the connecting panel must be such that the wall panel is able to deflect and rotate in accordance with the stiffness of wall panel, rather than the stiffness of the joint.

The above conclusion must be clarified however, in light of the results presented by the second iteration. This iteration demonstrated that a substantial reduction in the stiffness of the connecting panel (with respect to the stiffness of the wall panel) through a reduced panel thickness resulted in a significant increase in joint rotation (indicated by lateral spread in Table 7.3) and core stress. Refer to Appendix C.

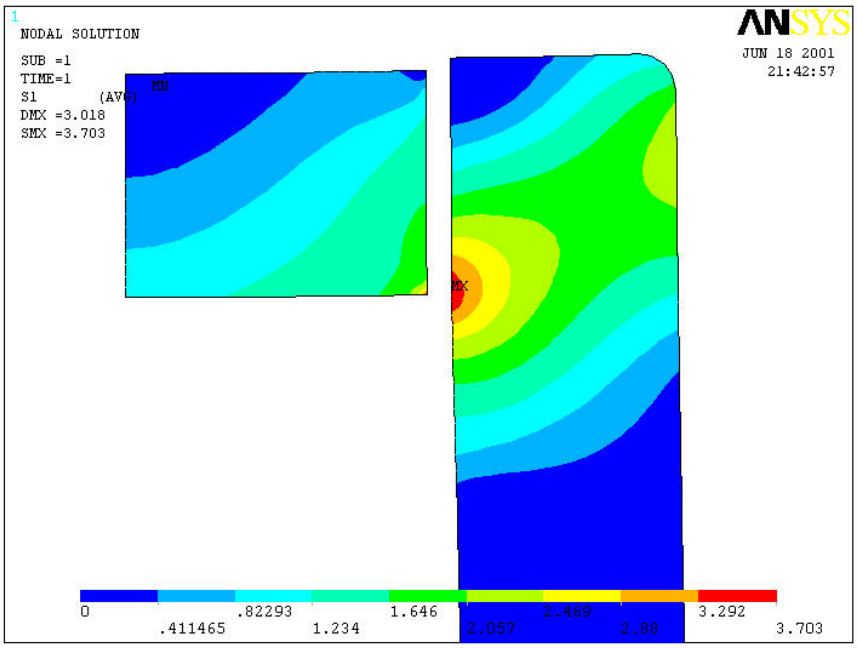

Figure 7.5 1st Principal Stress in Core of Original Section Configuration

Hence, it would appear that the minimisation of stress in the core material is achieved primarily by the stiffening of the wall panel, whilst maintaining a stiffness of the connecting panel that is less than, but comparable with, that of the wall.

Table 7.3 Summary of Analysis Results using PU Foam

Configuration No.	Total Lateral Spread (mm)	Max. Principal Core Stress (MPa)	Max. Principal Laminate Strain (%)
0	6.0	3.7	0.606
1	2.8	1.8	0.671
2	12.6	6.3	1.222
3	5.3	4.1	0.648
4	2.5	2.1	0.695
5	16.0	10.2	1.402

b) Experimental Results

As previously mentioned, a single beam cross section denoted as the 'initial configuration', was tested in preliminary verification of the analytical results. A plot of the compressive load and crosshead displacement is shown in Figure 7.6.

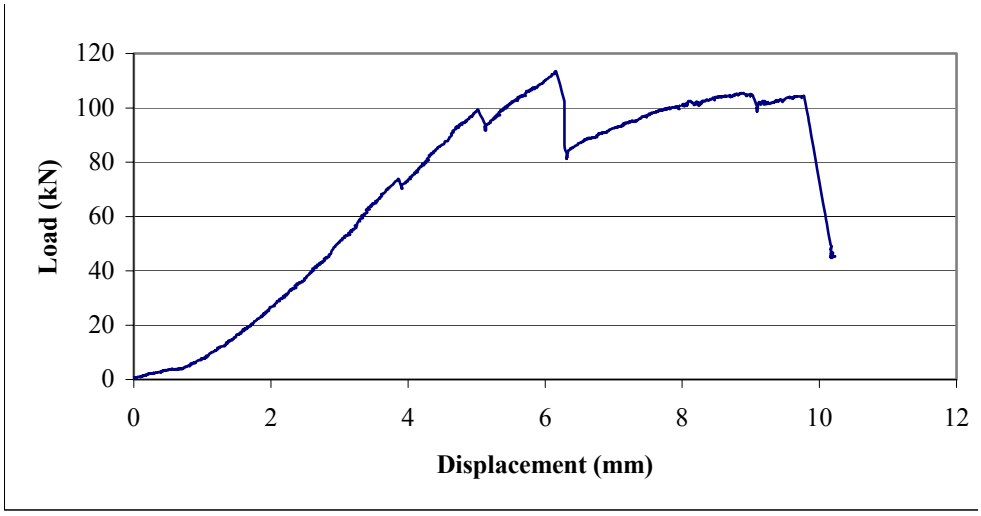

Figure 7.6 Load Vs Displacement Plot of Section Using PU Foam

As observed in the plot, initial failure occurred at a load of approximately 70 kN. This failure was manifested in the tensile failure of the core material as illustrated in Figure 7.7. The first crack occurred at the inner corner of the connecting panel, at an angle of approximately 60° to the horizontal. This is coincident with the direction of the principal stresses shown in Figure C.4 (b), which indicate a tensile failure at a similar angle. During the initial propagation of the aforementioned cracks, additional cracks formed in the core of the wall panels as predicted by the analysis in Figures C.4 (a) and (b). Continued cracking of the core resulted in the initiation of delamination in these regions, as illustrated in Figures 7.7 and C.11 (c). The test was subsequently terminated, as the structural integrity of the section was severely diminished.

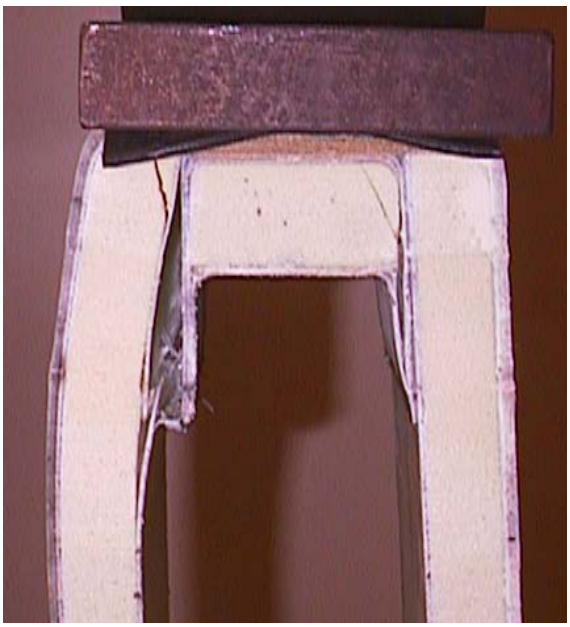

Figure 7.7 Failure of Section via Core Cracking and Delamination

c) Conclusions

The investigation described in this section was undertaken to address the sectional stability of the chassis rail cross section when subjected to compressive loading. Using finite element analysis, the significant factors relating to cross sectional performance were identified. Specifically it was concluded that, for the configurations considered, the core material represented the material in which failure first occurred. The minimisation of stress in the core material was achieved by the stiffening of the wall panels, and by maintaining a stiffness of the connecting panel that was slightly lower than that of the wall. Iteration 1 was shown to promote the lowest stresses within the core and, due to the apparent dependence of the section strength on the core material, this suggests that the first configuration possesses the greatest compressive capacity of those considered in this investigation.

A single sample of one of the variations previously analysed was experimentally tested to illustrate the principles established by the analysis. The failure observed in the specimen when subjected to a compressive force was consistent with the mode of failure predicted by the analysis. Cracking of the core was identified as the first mode of failure, and was seen to be in agreement with the analysis. The observed mode of failure clearly illustrated the significance of the core material in the performance of the cross section under compressive loading.

A direct comparison of the numerical results collected from both the analysis and the test was not performed due to the difficulties associated with reliable data collection. As measurement of the strains within the foam core or the laminates in the regions of interest was not possible, only the applied load and longitudinal deflection were recorded. Unfortunately, the inclusion of the rubber matting made the collection of accurate deflection data impossible. However, this is of minor consequence, as the objective of this investigation was only to provide verification as to the mode of failure.

The data also showed that while in-service loading reaches 55 kN, initial core cracking occurred at only 70 kN (with an ultimate capacity of 110 kN), giving a safety factor of only 1.27. However, it should be noted that the cross section tested did not represent the optimum configuration. The stresses present in the core material of Iteration 1 would suggest a significant improvement in cross sectional strength. Additionally, the assumptions made in section 7.4.2 were conservative. In particular, the effects of load

sharing via longitudinal spreading through the shear reinforcement, and the buckling restraint provided by the cross members, were ignored in these assumptions. Hence, it is anticipated that the selection of the appropriate cross sectional configuration, in addition to the inclusion of the aforementioned assistance by means of load sharing and buckling restraint, would provide ample cross sectional compressive strength to the proposed chassis rail.

7.5 Investigation of Beam Neck Area

7.5.1 Introduction

The utilisation of composite beams presents a number of unique advantages. The adaptable nature of fibre composite materials facilitates the simple addition or subtraction of reinforcement, thereby potentially enabling the matching of the beam characteristics to the moment and shear distributions within a given beam. This flexibility enables an increase in member efficiency, and a lowering of material and labour costs. However in addition to difficulties associated with shear connection between the 'web' and 'flanges' (as discussed in Section 7.3), changes in cross sectional shape and beam depth, combined with changes in required member capacity (along the length of the beam), present significant difficulties in efficient fibre composite beam design. The selection of an appropriate beam profile was determined by consideration of each of the potential profiles as follows.

Changes in chassis rail depth can be observed in the chassis of any flatbed semitrailer (refer section 3.2), with the magnitude of this change being dependent on the manufacturer. The profile alteration is necessary for a number of reasons. The moment distribution shown in Figure 4.10 illustrates the large increase in bending moment imposed on the trailer towards the midspan of the chassis rail. A relative increase in beam capacity is therefore required, this being most commonly achieved through an increase in section depth. This is readily accommodated in both the design and manufacture of steel chassis rails, and has become the accepted practice within the industry.

The centre of gravity (COG) of a trailer is also of concern. The large dimensions of some payloads, with appropriately large rotational moments of inertia, dictate low centres of gravity to maintain stability. Whilst low loaders cater for the majority of these payloads, the inevitable use of standard flatbed trailers in the transportation of oversized loads cannot be ignored. Because cornering places great demands on the suspension system and the kingpin to maintain stability, a lower COG will greatly increase the durability and capacity of a trailer, in addition to minimising the risk of overturning.

Having established the use of a ladder frame in the proposed trailer, these issues are also relevant in the determination of the appropriate profile of the FRP chassis rail. A number of possible configurations warrant consideration in the accommodation of both the strength and stability requirements previously mentioned.

Perhaps the most obvious profile considered was that as utilised in steel trailers. However, while the flexible nature of FRP structures enables the adaptation of the selected beam construction to incorporate the 'neck' section, a number of complications in this region render this configuration less attractive. In particular, the concave profile of the lower reinforcement flange presents the possibility of delamination, as previously alluded to in Failure Modes 8 and 9 in section 6.9.2.

In response to the apparent difficulties associated with the use of a distinct neck region, two alternative beam profiles that potentially avoid this problem were considered. The first alternative utilises a constant beam cross section, thereby eliminating the need to incorporate any distinct neck. Figure 7.8 shows a chassis rail comprising a constant depth along the entire length of the trailer. Variations in bending moment and shear capacity requirements are accommodated by additional reinforcement, which is added in direct proportion to the bending moment requirements shown in section 4.5.8.

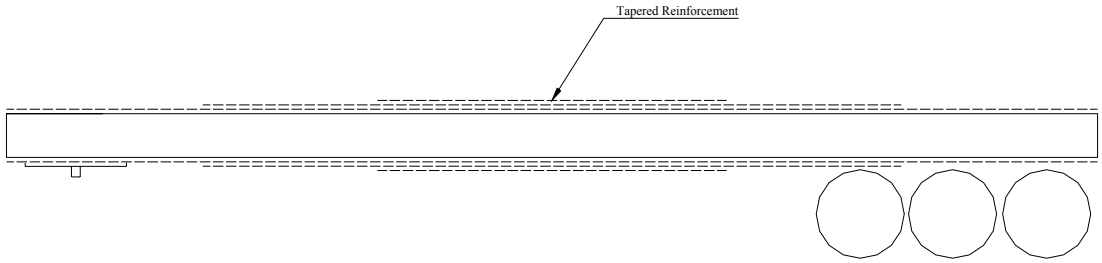

Figure 7.8 Chassis Rail of Constant Depth With Varying Reinforcement

By altering the quantity of reinforcement along the length of the beam, maximum material efficiency is achieved. However, there are a number of difficulties associated with this chassis rail profile. Increasing the COG of the payload presents a stability problem, and it is for this reason that steel chassis rails are not manufactured using a constant beam cross section. As previously mentioned in section 4.8.6, the majority of trailers currently in service are unable to withstand the recommended lateral loading limits, despite efforts to reduce the deck height. Hence, in order to conform to the recommendations regarding the lateral load limits, the adoption of a FRP chassis rail of constant cross section would necessitate a reduction in the allowable payload height. However this would effectively reduce the volume of payload that could be carried, potentially reducing the market appeal of the FRP trailer to the competitive transport industry.

In addition to issues of poor stability, the use of a beam of constant cross section presents difficulties with respect to the attainment of the optimum beam depth as presented in

section 4.8.6. Specifically, in order to reduce the COG, a particularly shallow beam depth must be adopted. However, as observed by Figure 4.15, the observance of the appropriate deflection limits would not enable the utilisation of the strength capacity of the reinforcement. In fact, this would appear to suggest that substantially greater quantities of reinforcement would be necessary to maintain the deflection limitations, thereby rendering the economic potential of the trailer void.

Further difficulties are faced in the attachment of the suspension system, as standard systems are designed to suit a particular ground clearance as found on steel trailers. The chassis rail depths suggested previously would possess an additional 200 - 300 mm in ground clearance. This, coupled with the possible increase in demand on the suspension system during cornering (due to an increased COG), may necessitate the use of an alternative suspension system not currently available.

It was therefore necessary with respect to the second possible chassis rail profile, to reduce both the quantity of reinforcement and the COG by increasing the beam depth. However, in order to avoid the difficulties associated with concave inflection in the neck region and an unsuitably high COG, a beam profile as seen in Figure 7.9 was produced. This profile avoids all re-entry angles, such that the tensile reinforcement on the underside of the beam is unable to delaminate, as illustrated in Figure 6.2 (section 6.3).

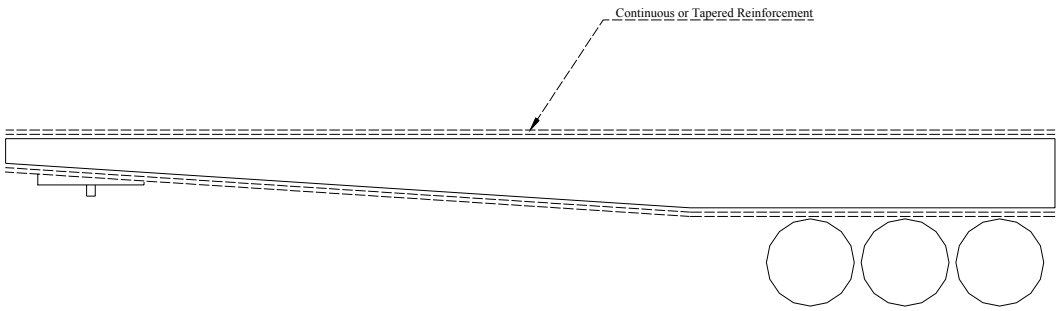

Figure 7.9 Chassis Rail of Tapered Depth

The primary difficulty associated with this profile however, pertains to the clearance between the chassis and the prime mover. This clearance is necessary in order to accommodate the relative rotation that occurs at the point of articulation. The angle of rotation, α, necessary for the clearance specified by Australian Standard AS1773 - 1996, is equal to 8°. A survey of a number of combinations of prime movers and flatbed trailers yielded that the typical distance between the kingpin and the rearward most point of the prime mover was 1500mm (refer Figure 7.10), with a minimum distance of 220mm between

the lower flange of the trailer chassis rail and the upper surface of the prime mover chassis. Hence in order to adhere to the aforementioned Australian standard, the minimum height, C, required between the lower flange of the trailer chassis rail and the upper surface of the prime mover chassis must be:

$$C = 1500 \times \tan 8°$$
$$= 211 \text{ mm}$$

This effectively implies that the chassis rail should not incorporate an increase in beam depth (relative to the depth at of the beam at the kingpin) until the point at which the chassis rail has extended past the end of the prime mover. Additionally, this implies that the distance from the front of the trailer to the kingpin should also not be greater than 1500 mm.

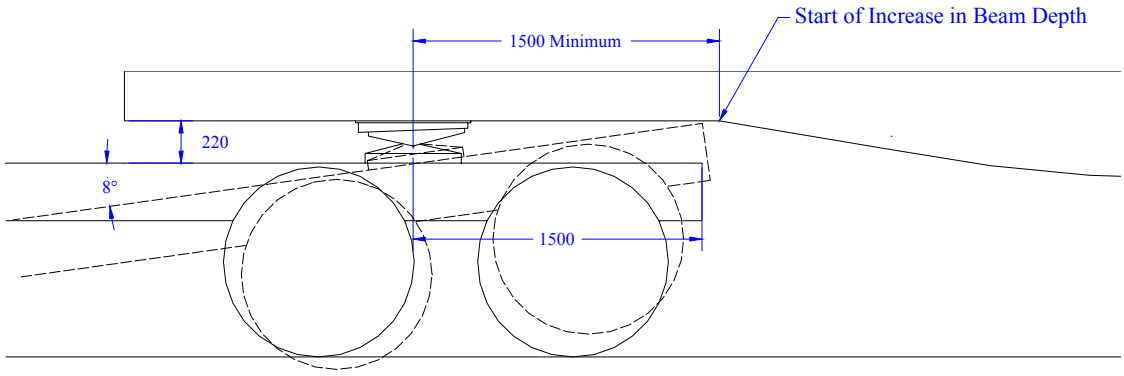

Figure 7.10 Clearance Requirements Between Prime Mover and Trailer

This figure clearly shows that it is not possible to adopt a tapered chassis rail profile, due to the restrictions imposed by the Australian standard (AS1773). Conformance to the standard would require a significant increase in depth at the shallow end of the beam in order to provide sufficient beam depth at the front edge of the trailer. In fact, the restrictions illustrated in Figure 7.10 remove this beam profile from practical consideration, despite the fact that the moment capacity requirements at the forward edge are small in comparison with the remainder of the beam. Additional complications related to this configuration reside at the kingpin, as this beam profile would require a highly modified skid plate.

It should also be noted that a number of trailers from various manufacturers did not comply with the requirements of AS1773. As seen in Appendix A, a number of the chassis rail profiles contain an increase in chassis rail depth prior to extending past the necessary

clearance point, however this is possibly due to alterations to this standard over time. Regardless of this, it was decided that the proposed FRP trailer would conform to this standard, thereby minimising the potential for damage to the flange of the chassis rail or prime mover.

Having identified other possible beam profiles and found them to be inadequate, the only viable alternative, which conforms to existing standards and components, is a beam profile similar to that observed in steel trailer design. While a number of difficulties are inherent in this profile (refer Chapter 6), this avoids the problems associated with a high COG while minimising the quantity of reinforcement required to maintain the desired beam stiffness. Potentially, the use of a double neck, as shown in Figure 7.11, could also be used in order to minimise the COG while maximising the beam depth in the region of highest moment. However, given the optimum chassis rail depths determined in Chapter 4, the large beam depth that this profile allows would not typically be required. Additionally, the inclusion of a second neck region further increases the beam complexity, thereby increasing the cost of manufacture. Hence, while this configuration does represent a possible solution, it was not considered to represent the optimum solution with respect to cost and ease of manufacture, and was abandoned in favour of a simpler beam profile.

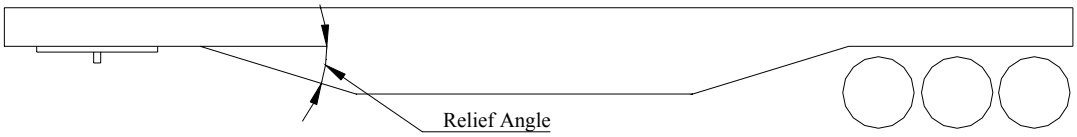

Figure 7.11 Chassis Rail Utilising a Double Neck

Given that the examination of alternate beam profiles did not yield a configuration which was clearly superior to the existing profile with respect to the restraints previously established, it was decided that the basic chassis rail profile as observed in steel trailer design would form the basis of further investigation. The elimination or minimisation of the aforementioned difficulties associated with this profile form the basis of sections 7.5.2 and 7.5.3.

7.5.2 Small-Scale Composite Neck Testing

7.5.2.1 Introduction

As illustrated in Figure 4.10, the rapid increase in bending moment observed due to specific payload configurations necessitates that the full depth of section be realised as soon as possible. The importance of stiffness in the trailer also reinforces this point, and so whilst a small relief angle would reduce stress in the neck section, a larger angle would decrease the distance from the kingpin at which the full depth would be reached.

The analysis of steel trailers (refer section 7.2) showed that the Haulmark trailer provided an acceptable compromise between the angle of change in the neck section, the associated stress concentration, and the distance along the beam to reach full depth (and hence maximum moment capacity). However this must also be balanced with respect to the clearance between the prime mover and trailer as stipulated by AS 1773.

In order to fully assess the potential of the proposed beam configuration, a series of tests, accompanied by suitable analysis, were undertaken. This investigation aimed to identify the means by which the load in the lower flange of the chassis rail could be effectively transferred from a relatively shallow section to a greater section depth. Initially, small-scale test pieces (using PFR as a core material) were used to minimise material costs and construction time. However as this section demonstrates, these tests were able to establish the principles significant to this beam profile, with these principles being transferred to the proposed beam concept previously presented.

Within the scope of this investigation, two basic beam configurations were considered. The first of the profiles was representative of the worst possible case. A relief angle of 90° was adopted to demonstrate the effect of inadequate load transfer and poor provision for the minimisation of the stress concentrations in the critical region.

The second profile included a relief angle of 15°, adapted from the Haulmark trailer. As previously mentioned, the Haulmark trailer appeared to provide a suitably low relief angle to minimise the associated stress concentration, in addition to providing adequate beam depth. The effects of several variations to this profile were also measured, as detailed in the following section.

7.5.2.2 Model Configuration

The small-scale models used in this investigation were constructed using two 'modules', (refer Figure 7.12) each comprising:

- A square section of PFR, which provided the bulk form of the member in addition to contributing to the shear capacity
- A PVC pipe, wrapped in a single layer of double bias E-glass (refer section 5.6.3 for reinforcement details), which acted as a former and reduced the quantity of PFR used in the beam
- Three layers of unidirectional E-Glass (refer section 5.6.3 for reinforcement details) were then applied to the upper and lower surfaces of the beam.

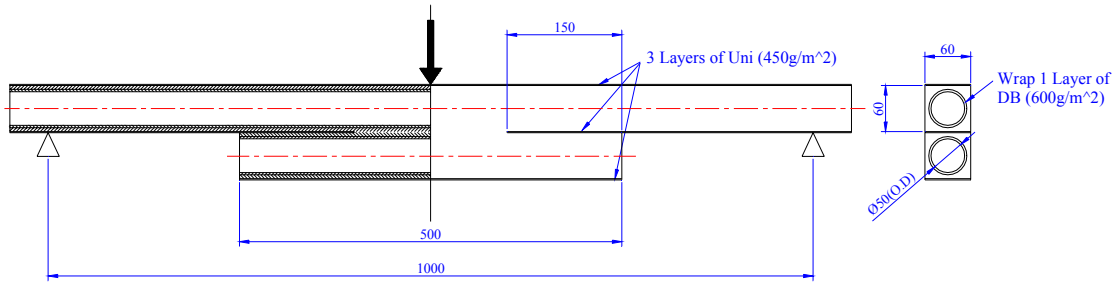

Figure 7.12 Configuration of Basic Neck Section

These members were configured to represent the approximate ratio in depth change which occurs in a given chassis rail. As can be seen from the figures in Appendix D, the reinforcement adopted two distinct orientations with respect to placement.

Initially, the unidirectional reinforcement was placed only on the outer side of the beam, as shown in Figure 7.13 (a). However, in order to facilitate a more efficient transfer of the tensile load on the lower reinforcement, the reinforcement was continued into the beam, as illustrated in Figure 7.13 (b). It was anticipated that this 'continuing reinforcement' would relieve the stress concentration, which occurred at the first point of directional change from the front of the beam. The effects of this are discussed further in both this section and also in section 7.5.3.

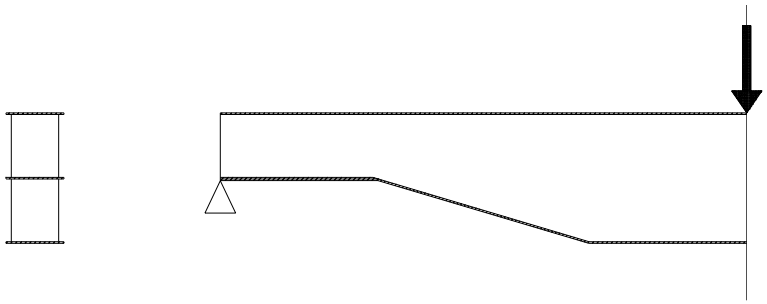

Figure 7.13 (a) Neck Region Without Continuing Reinforcement (Symmetry Used)

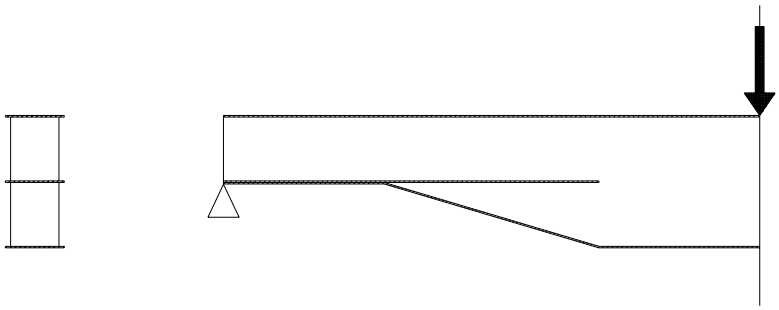

Figure 7.13 (b) Neck Region Using Continuing Reinforcement (Symmetry Used)

In order to reduce material and manufacturing costs, the span of each member was limited to 1000 mm. Additionally, as it was not economically possible to manufacture and test a large number of these specimens, each test piece was constructed such that it contained two identical neck regions, being mirrored about the beam midpoint. In this way, any anomalies associated with incorrect load placement or beam pitch would be reduced, increasing the probability of a successful test. Additionally, this configuration consumed less material, further reducing cost.

Each beam was tested in three-point-bending, with the position of the support relative to the neck region being in proportion to a full-scale chassis rail. This loading configuration also ensured that the bending moment distribution over the neck region was linear, as observed in Figure 4.10.

It should be noted that, due to the preliminary nature of this investigation, scaling effects were not taken into account in the design and construction of these specimens. However these are considered with respect to the larger test piece described in section 7.5.3.

7.5.2.3 Linear Elastic Finite Element Analysis

Numerical analysis using the finite element technique was conducted to determine the characteristic behaviour of the specimens. Given that the expected ultimate deflection was sufficiently low (<<Span/50), a linear analysis was conducted.

The objectives of this analysis are summarised as follows:

- To perform a preliminary, linear static analysis of the neck section of a small-scale, FRP chassis rail
- To investigate the performance of each chassis rail, in response to the application of loads as defined by load cases one and three.
- To enable the comparison of the structural characteristics of the various models in relation to the influence of reinforcement placement and appropriate stress concentrations reduction techniques on maximum stresses and failure modes within the beam.

A finite element program, ANSYS (v. 5.7), was used to complete the numerical analysis of each model, with 8-node plane-strain elements (PLANE 82) used throughout the analysis to represent the beam. Due to the preliminary nature of this analysis, a 2-dimensional model was chosen to reduce model complexity, particularly of the core, in addition to reducing computing resources and solution time. The use of a two-dimensional analysis was made possible through the transformation of the PVC pipe, double-bias E-Glass, and PFR core into an equivalent, homogenous core material of PFR, as illustrated in Figure 7.14. The width of the transformed core was adjusted such that this core approximation possessed identical stiffness characteristics to the actual composite core configuration. This assumption was adopted due to the anticipation that failure would occur either in the unidirectional laminate, or at the interface of this laminate and the PFR material, and was necessary to allow the use of the plane-strain element. Only half of the specimen was modelled using symmetry, further reducing model complexity. Perfectly elastic material characteristics were assumed, and plastic deformation was not considered. The general dimensions and element mesh produced for each analysis are illustrated in Appendix D.

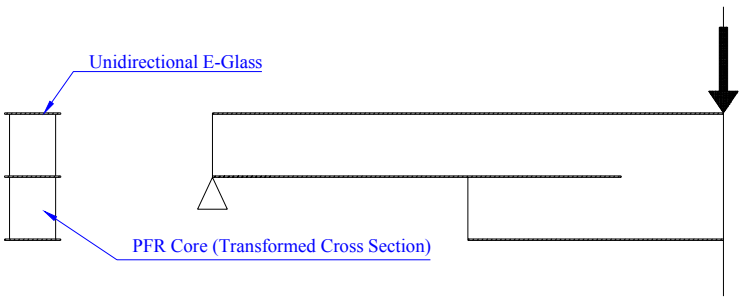

Figure 7.14 Small-Scale Neck Beam Represented with Homogeneous Core

A number of cross-sectional variations were considered during the course of the analysis, in order to facilitate the identification of the relevant contributors to the reduction of stress concentration, and improvement of load transfer through the neck region. As concluded in section 7.2, the relief angle of the neck section possesses a direct effect on the magnitude of the stress concentration in the neck region. These models were configured to examine the effect of several techniques, including:

- The reduction of the relief angle
- The use of radii in critical areas of stress concentration
- The continuing of reinforcement into the core of the beam at the neck region

An investigation into the continuation of the reinforcement into the core was initiated in order to assess the potential of this technique in stress reduction in the critical region of the neck. The continuation of the reinforcement, as illustrated in Figure 7.15, enables a significant portion of the tensile load in the reinforcement at the point of separation to be directed away from the curved reinforcement, thereby reducing the possibility of delamination of the tensile laminate from the core.

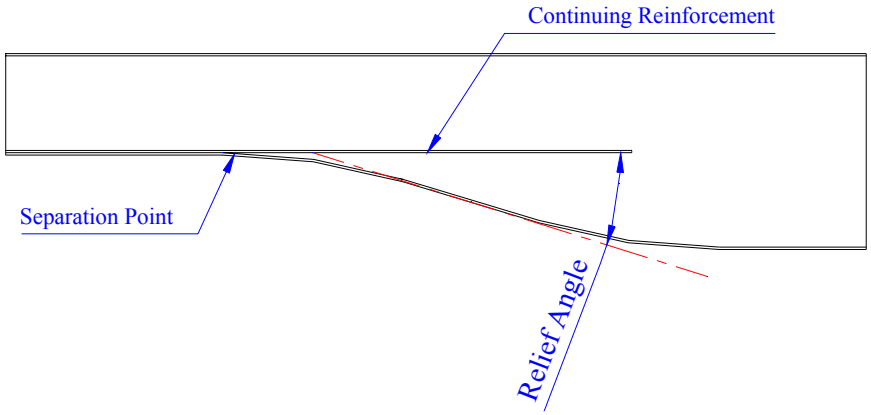

Figure 7.15 Continuation of Tensile Reinforcement in Neck Region

For the purposes of these tests, the continuing reinforcement was terminated at the point at which the laminate was positioned at the neutral axis of the beam, as it was assumed that the laminate would no longer carry any tensile load.

Seven model configurations were examined, and are summarised in Table 7.4. The 90° relief angle was included to show the full benefits of a low relief angle. Full illustration of these configurations is provided in Appendix D.

Table 7.4 Summary of Neck Section Profiles Analysed

Neck Section Number	Relief Angle (Degrees)	Reinforcement Continued Into Beam (Y/N)	Radius Size On Corners (mm)	Total Load Applied (N)
1	90	Y	0	4000
2	90	N	0	4000
3	15	Y	0	20000
4	15	N	0	20000
5	15	Y	100	20000
6	15	N	100	20000
7	15	Y	400	20000

7.5.2.4 Fabrication and Experimentation

Due to both financial and time constraints, it was not feasible to verify every configuration through experimental testing. Following an initial observation of the finite element analysis, it appeared that configurations two, three and four would provide the least relevant information regarding the reduction of stress in the neck region, and were therefore excluded. Configuration one was constructed purely to verify that the predicted failure mode associated with the high relief angle would occur, regardless of the 'continued' reinforcement. Configurations five and six were not considered for fabrication, as it was anticipated that the absence of any appreciable radii would provide a greater opportunity to gauge the effects of the presence of stress concentrations in conjunction with the continuation of the reinforcement. The seventh configuration was chosen for manufacture in order to verify the positive effects on stress reduction (refer section 7.5.2.5) of the large radii. Any conclusions reached regarding configurations two, five and six would therefore be reached solely because of the finite element analysis. Nonetheless, as this investigation was viewed as being preliminary in nature, all results were to be treated as indicative.

The process of beam manufacture, illustrated in Appendix D, is described in an abbreviated form in this section. Complete drawings of each of the test specimens are shown in Figures D.11 (e), D.12 (e), D.13 (d) and D.14 (e).

The PFR mixture used in each specimen comprised the same epoxy resin (ADR246TX/ADH160) used throughout previous experiments (refer Chapter 2), and 3MK15 glass microspheres, which were added at a ratio of 40% by volume, as prescribed by Ayers in [3]. The E-glass reinforcement and matrix types used in this specimen were

identical to those tested in Chapter 2. The hand lay-up technique (refer Chapter 2) was used throughout the beam manufacture. The following summary describes the fabrication of beam seven (refer Figure D.14 (e)), however a similar process was employed for each specimen, apart from the addition of continuing reinforcement and inclusion of fillets on the respective specimens.

1. A mould was assembled, the shape of which enabled the PFR core of each specimen to be cast lying on one side.
2. Two sections of PVC pipe were cut to the appropriate length, and the ends filled with foam to prevent the ingress of resin during submersion in the PFR.
3. A single layer of DB E-glass reinforcement, combined with epoxy resin, was wrapped around each pipe, and allowed to cure at room temperature. The surface was covered with peel-ply prior to cure, thereby eliminating the need for surface preparation prior to casting.
4. Two laminates, consisting of three layers of unidirectional E-glass [0/0/0] in epoxy resin, were then consolidated by hand lay-up, covered in peel ply, and allowed to cure at room temperature.
5. Following the application of a release agent to the mould surface, spacers were placed within the mould to ensure that the PVC pipes were correctly positioned.
6. The pipes were then placed within the mould, and restrained appropriately to prevent floating. The unidirectional laminates were then cut to size, and placed within the mould in such a way as to allow the PFR to encapsulate the required length of laminate, this being the 'continuing' reinforcement previously described.
7. The PFR was then mixed by hand and poured into the mould, and allowed to cure at room temperature.
8. Following de-moulding, the specimen was sanded to shape, and the surfaces prepared for the application of the external reinforcement.
9. Three layers of unidirectional E-glass [0/0/0] were then consolidated on both the upper and lower faces of the beam in epoxy resin, and allowed to cure at room temperature.
10. The external laminates were then sanded to shape, and the beam post-cured in an oven at 80°C for a period of 8 hours.

Subsequent to manufacture, each specimen was simply supported and subjected to three point bending. Unidirectional strain gauges were attached to the lower laminate, either at the beam midspan or at the midpoint of the angled laminate within the neck region.

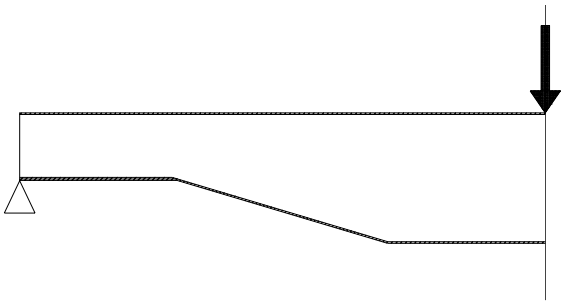

Figure 7.16 Basic Test Configuration for Small-Scale Neck Sections (Symmetry Used)

To simulate the application of a static load, the load was applied at a rate of 2 mm/minute, with the measurement of the load, strain and midspan deflection being recorded throughout the duration of each test at intervals of 0.10s. Refer to Appendix D for images of each test.

It should be noted that significant problems were encountered in achieving the desired profile of specimen seven. The primary difficulty was found in the shaping of the core to produce the desired radii (by sanding the PFR material), particularly because of the small scale of the specimen. While every effort was made to produce the correct shape, it was apparent that the final shape was not an exact representation of the analytical model. Additionally, the small scale of the specimen acted to exaggerate the influence of minor imperfection and variations on the shape of the neck section.

7.5.2.5 Results and Discussion

a) Analysis Results

The preliminary analysis conducted on the various beam configurations yielded a number of valuable results with respect to the identification of significant contributing factors to the beam performance.

A survey of the results presented in Appendix D clearly shows that the use of a low relief angle (15°) provides a significant increase in beam capacity in comparison to a high relief angle (90°). As can be seen in specimens one and two, (Figures D.4 (c) and D.5 (c)), the stresses in the core material resulting from a load of only 4 kN were comparable to the core stresses observed in the remaining specimens, to which a load of 20 kN was applied. It is assumed from this initial investigation that there exists a degree of proportionality between the relief angle and the magnitude of the stress arising from the separation point, and hence a relief angle of a lower magnitude than 15° could be expected to yield lower values of

stress at this point. Conversely, the use of a relief angle greater than 15° would yield greater stress. Hence, while quantification of the proportionality of this relationship lies outside the scope of this investigation, it can be clearly seen that the minimisation of the relief angle would yield a significant declination in beam stress. It should also be noted that the accuracy of the results gained from the analysis of specimens one and two is questionable, due to the occurrence of infinite stress concentrations present at the right - angled corner. Due to the limited scope of this analysis, no attempts were made to include the small radius that would actually be present at the separation point in the real structure, as it is not possible to accurately measure this distance.

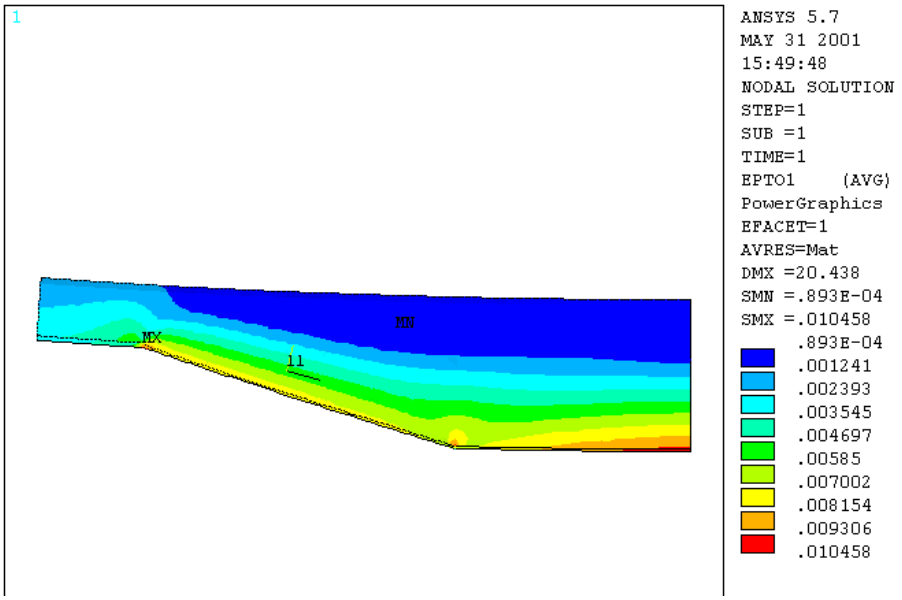

Figure 7.17 1st Principal Laminate Strain of Neck Section #4

The analysis also appears to indicate that the use of radii in both the upper and lower corners of the neck region provides assistance in the reduction of stress in these areas. At the point of separation, an abrupt change in the direction of the tensile forces within the laminate is seen to greatly increase the stresses in both the laminate and the core material in the immediate region (refer Figures 7.17 and D.7 (b)). Consequently, it follows that the use of large radii would promote the most gradual transition in the orientation of the tensile stresses within the lower laminate. This is supported by the analysis, which shows that the use of very large radii (specimen seven) yields the lowest stresses in the neck region of any other configuration.

While fundamental engineering principles attest to the observed stress reduction as a result of large radii, a comparison of the calculated laminate strain at the lower corner of specimens three (refer Figure D.6 (a) in Appendix D) and five (refer Figure 7.18) clearly

demonstrates that the use of radii at this point is also effective in stress reduction. The abrupt change in geometry observed in specimen three at the lower corner promotes a substantial localised disruption to the stress distribution in the laminate, effectively introducing a concentrated compressive force to the laminate, which acts perpendicular to the orientation of the principal stress.

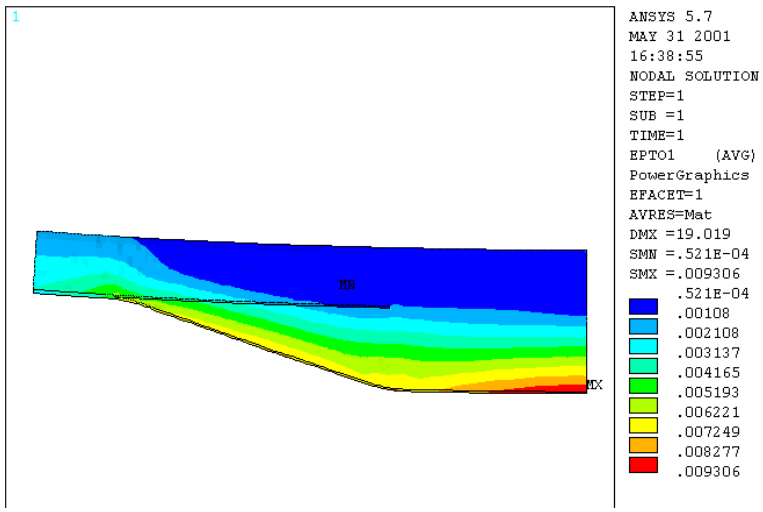

Figure 7.18 1st Principal Laminate Strain of Neck Section #5

The analysis would also appear to confirm the supposition that the continuation of the reinforcement into the beam at the 'separation point' does have a profound effect on the reduction of stress at this point. The values of maximum principal stress in the core materials of specimens one and two show a marked difference. The continuation of the reinforcement produced a reduction of more than 60% in the core stress, although this should be considered with respect to the influence of the infinite stress concentration.

With respect to remaining beams, which utilised a relief angle of 15°, a reduction of core principal stress of similar magnitudes (in comparison with specimens one and two) was not observed in those specimens in which the reinforcement was continued. Rather, the continuation of the reinforcement was effective in reducing the stress concentration at the point of separation to such a degree so as to shift the point of greatest stress away from the separation point. This effectively altered the failure mode of the beam, and significantly reduced the probability of failure at the separation point. As shown in a comparison of Figures D.6 (b) and D.7 (b), and also Figures D.8 (b) and D.9 (b), the maximum principal core stress occurs at the separation point in those specimens without the continuing reinforcement. Conversely, the highest core stresses on those specimens comprising the

continuing reinforcement reside at either the lower corner of the neck or at the beam midspan.

With respect to the prediction of the failure modes of those specimens that were fabricated, the analysis would appear to indicate that specimen one would fail at the separation point, with core cracking possibly leading to delamination of the continuing reinforcement prior to ultimate failure. The results of analysis of specimen three would indicate that failure should occur at the beam midspan, despite a minor concentration of stress in the lower corner of the neck region. However the analysis would suggest that specimen four should fail at the separation point. It is anticipated that the tensile forces within the laminate would result in delamination of the reinforcement at this point. The low stresses throughout the entire neck region of specimen seven would suggest that failure of this beam should occur at the beam midspan.

Table 7.5 Results Summary of Analysis of Small-Scale Neck Sections

Neck Section Number	Total Load (N)	Maximum E1 (uE)	Maximum S1 in Core (MPa)	Predicted Failure Point	Midspan Deflection (mm)
1	4000	9818	19.6	Concave Corner	5.3
2	4000	26962	55.0	Concave Corner	5.8
3	20000	9820	19.1	Midspan	20.6
4	20000	10458	19.8	Concave Corner	20.6
5	20000	9306	18.1	Midspan	19.2
6	20000	10723	21.6	Convex Corner	19.6
7	20000	9480	18.4	Midspan	19.5

b) Experimental Results

The testing of specimen one yielded a linear load-displacement relationship as shown in Figures D.11(c) and (d). Initial cracking was observed at a load of approximately 4.5 kN, with the specimen carrying an ultimate load of 5.9 kN. As shown in Figure 7.19, failure occurred because of delamination of the core from the continuing reinforcement, beginning at the stress concentration present at the separation point. Catastrophic failure was not observed during the initial stages of cracking, despite the brittle nature of the PFR core. However rapid crack propagation was inhibited by the partial relaxation of the load, which occurred as a result of the rapid increase in deflection during cracking. Had a dead load been used, acting under the force of gravity, it is anticipated that catastrophic failure would have occurred at a load of 4.5 kN.

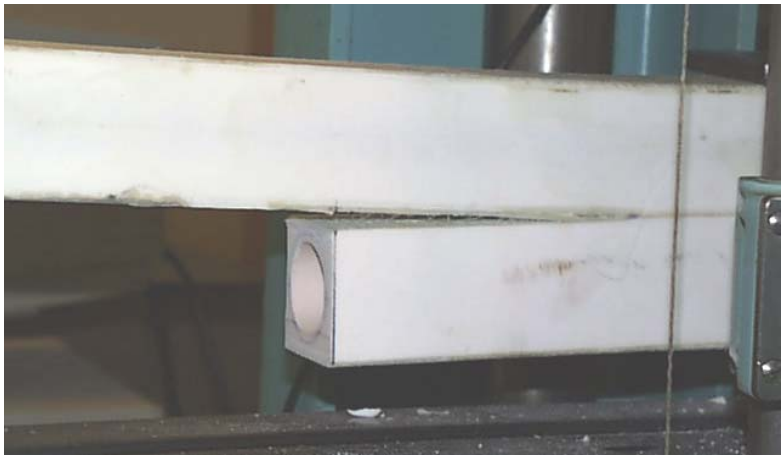

Figure 7.19 Failure of Neck Section #1

Specimen three also exhibited linear characteristics, as shown in Figures D.12 (c) and (d). While minor cracking was audible (but not visible to the observer) at a load of 18 kN, the ultimate load carried by this specimen was 27 kN. Failure of this specimen occurred at the lower corner of the neck region, as shown in Figure7.20. The nature of the failure was catastrophic, resulting from tensile rupture of the laminate. As discussed in the previous section, a stress concentration was observed in the analysis at this particular point of the neck section, however it was anticipated that the core stress at the beam midspan would be greater than that at the lower corner (refer Figure D.6 (a) and (b)). This clearly indicates that the magnitude of the stress concentration at the lower corner exceeded the values predicted by the analysis. However, it is uncertain as to whether difficulties associated with the consolidation of the laminate over the sharp bends may have contributed to the failure at this point. It should also be noted that no cracking or delamination was observed at the separation point, despite the sharp corner and the absence of radii.

Figure 7.20 Failure of Neck Section #3

In contrast to specimen three, failure of the fourth beam occurred at the separation point. As predicted, the absence of continuing reinforcement resulted in the initiation of failure at the separation point. The sudden change in direction of the tensile forces carried by the laminate at the separation point resulted in tensile rupture of the core (see Figure 7.21), thereby enabling the laminate to straighten (refer sections 6.3 and 6.9.2). As noted during the testing of specimen three, this beam exhibited audible cracking (not visible to the observer) at a load of 17 kN, with ultimate failure occurring at a load of 25 kN.

Figure 7.21 Failure of Neck Section #4

The testing of specimen seven again yielded linear behaviour, as shown in Figures D.14 (a) and (b). However, the failure of this specimen occurred in an identical fashion to that of specimen three, and at a load of 26.5 kN. The tensile failure of the laminate at the lower corner of the neck region was particularly unexpected in this case, as the utilisation of large radii was shown by the analysis to eliminate all stress concentrations in this region. This failure would appear to largely remove any possible influence introduced by difficulties in achieving the desired shape, as the radii was extremely large. However, the cause of this premature failure is apparent upon examination of the specimen cross section. As observed in Figure D.14 (e), a radius was not applied to the termination of the internal pipe. Hence, it is at this point at which a stress concentration forms within in the core material, being under compression due to the curvature of the laminate. Given that the analysis did not model the geometry of the internal pipes, the associated effects were not revealed during analysis. Following the testing of specimen seven, it was suggested that this same stress concentration might also be responsible for the mode of failure observed in specimen three. Given that specimens three and seven failed at similar loads, it would appear that the sharp pipe edge was the primary contributor to initiation of failure.

c) Comparisons and Conclusions

The investigation described in this section was undertaken to address the performance of the neck section of the chassis rail when subjected to bending. Specifically, small-scale models were used in order to ascertain the effects of various factors on the performance of the beam section.

Finite element analysis was conducted on simplified, 2-dimensional models to determine the characteristic behaviour of a variety of beam configurations. This analysis was successful in highlighting the effects of three factors, namely: variations in the relief angle, the use of radii in areas exhibiting stress concentrations, and the continuation of tensile reinforcement into the beam from the point of separation. This analysis indicated a clear correlation between the relief angle and the magnitude of the stress observed at the separation point. Further, it was observed that the introduction of radii at the separation point and the lower corner of the neck region were successful in reducing the stress at these points. However, the use of continuing reinforcement appeared to provide the greatest advantage in stress reduction, and was shown to alter the mode of failure to that of rupture of the tensile reinforcement at the beam midspan, rather than at the separation point.

The testing of several configurations was undertaken, with each specimen being loaded to failure. The failure modes observed in specimens one and four were in full agreement with the analysis, with delamination and tensile failure of the core being present in each case. However, the failure modes observed in specimens three and seven were not predicted by the analysis, which did not account for the stress concentrations introduced at the lower corner by the abrupt termination of the internal pipe. Despite this, the experimental testing clearly demonstrated the advantage provided by the use of continuing reinforcement, with the successful reduction of stress and movement of the failure point away from the separation point, as predicted by the analysis.

A comparison of the predicted and measured deflection and strain values showed that the analysis successfully modelled the member stiffness (refer Appendix D) and the distribution of load within the tensile laminate at the midpoint of the neck region and the beam midspan. A direct comparison of the numerical results collected from both the analysis and the test with respect to the failure load was not made, due to the simplifying assumptions inherent in the 2-dimensional models.

With respect to the identification of an optimum configuration, it would appear that an optimum neck section would comprise a relief angle of 15° (given that this is the minimum practical value), the incorporation of the largest practical radii at both the separation point and the lower corner of the neck region, and the utilisation of continuing reinforcement. Hence it was this configuration that was adopted for further investigation on a larger scale, with the appropriate modifications being effected to adapt to the beam cross section to that which was discussed in sections 7.3 and 7.4. The details of this investigation are presented in section 7.5.3.

7.5.3 Half-Scale Composite Neck Testing

7.5.3.1 Introduction

The preliminary investigation into the performance of the neck region yielded a number of notable results, and highlighted the significance of the neck section within the context of chassis rail design. While the elimination of stress concentrations in this region was demonstrated to have only a minor effect on the ultimate capacity of the beam, uncertainties with respect to the location and nature of the failure were eliminated. Consequently, this provides a high level of confidence with respect to the expected failure mode, resulting in greater predictability in beam performance and the maximisation of beam capacity.

However, as the previous tests utilised small-scale specimens, based on a PFR core and an alternate cross section, further testing was necessary in order to establish the validity of these conclusions with respect to the proposed chassis rail and associated section and materials. It was therefore decided that a beam comprising the cross-section presented in section 7.3 and the materials as selected in Chapter 5 should be constructed. This beam was to utilise the largest practical scale, given the available testing facilities and financial constraints.

The primary objective of this test was to demonstrate that the principles ascertained in the previous investigation were transferable to the chosen cross section, thereby establishing that the incorporation of these principles was effective in controlling the failure point of the chassis rail. It was also anticipated that the large scale of this beam specimen would enable a more detailed investigation of the beam behaviour, particularly in relation to the placement of multiple strain gauges and the associated complexity of the analytical model. While the testing of a single specimen does present difficulties with respect to probability and repeatability, it should be noted that the manufacture of the chassis rail in its present form would be facilitated by hand lay-up techniques, thereby requiring a large number of samples to form an adequate statistical data base. However, due to time and financial restrictions imposed on this study, the performance of this beam was assumed to be representative of a typical chassis rail.

7.5.3.2 Beam Configuration and Basic Design

Following an assessment of the available funds and experimental resources, it was decided that a chassis rail of one half scale of the actual beam size would be constructed. It was anticipated that any greater reduction in scale would incur an unacceptable loss of detail and practicality in manufacture, as encountered in the previous investigation utilising small-scale beams. Further, it was decided that the full length of the chassis rail was not required, as the primary objective of this investigation was to establish the performance of the neck region of the beam. Hence, the beam length was limited such that the prescribed bending moment distribution (refer section 4.5) could be adequately applied over the neck region and a suitable length of the full depth of section. The model was to be loaded in three-point bending to minimise the beam length whilst producing a linear bending moment throughout the neck region (refer Figure E.5).

In order to allow for accurate transference of the results from the half-scale model to an actual chassis rail, it was necessary to comply with a number of criteria with respect to the accurate scaling and representation of a full size structure on a smaller or larger scale. Charlton [4] states that flexural similarity, in addition to geometric similarity, is necessary for the production of a scaled model, the behaviour of which was entirely representative of the actual structure. The term 'flexural' relates to the deformation of the beam due to an applied load. The following specific criteria are specified:

1. That the deflections of the model and the actual structure satisfy the requirements of similarity by conforming to the ratio of the layout scale factor *s*, i.e.

   That is, $s\Delta' = \Delta$

   where the model is 1/s times as large as the actual structure

   Δ is the deflection of the actual structure

   Δ' is the model deflection

   Given that

   $\Delta' = 2\ d'w'\varepsilon'/3\ h'$ (for 3-point bending)

   $\Delta = 2\ d\ w\ \varepsilon\ /\ 3\ h$

   with d = beam depth

   w = beam width

   h = beam span

   And since $s = 2$

   $\varepsilon' = \varepsilon$, (as the same reinforcement types are used)

   $s.h' = h$,

$d' = d/2$,

$w' = w/2$,

it follows that:

$$\begin{aligned} LHS &= 4\, d'\, w'\varepsilon'/3\, h' \\ &= d\ w\, \varepsilon/\, 3\, (h/s) \\ &= 2\, d\, w\, \varepsilon/\, 3\, h \\ &= RHS \end{aligned}$$

Hence, the model conforms to the deflection criterion.

2. The ultimate force applied to the scaled model must conform to the following equation:

$$F_{structure} = s^2\, F_{model}\, E/E'$$

Now assuming that identical laminate materials are used in each case, and that the ratio of shear reinforcement to tensile/compressive reinforcement in the model is equal to that in the actual structure, and by neglecting the influence of the core on beam stiffness, it can be stated that

$$E = E'$$

Hence,

$$F_{model} = 0.25\, F_{structure}$$

Assuming the actual chassis rail conforms to the 'medium' trailer classification, possesses a failure strain $\varepsilon = 1.0\%$, and a maximum moment capacity $M = 12000$ kNm, then

$$F_{structure} = 1170 \text{ kN}$$

Therefore,

$$F_{model} = 292.5 \text{ kN}$$

However, it was discovered that this force was too great to be applied by the available testing equipment. Given that the scale of the beam cannot be further reduced due to the practicality issues mentioned previously, it would appear that this particular criterion could not be complied with. Consequences of this non-compliance are discussed later in this section.

3. The stress produced in the scaled model must equal that of the actual structure when the deflections are in accordance with condition one.

   That is, $\sigma_{model} = E' \sigma_{structure} / E$

   As carbon fibre was selected as the load carrying reinforcement for both the model and the proposed chassis rail, stress produced in both beams would be identical, assuming that the same type of carbon was utilised. It also follows then that the strain within the laminate of the model should be representative of that in the laminates of the actual structure.

4. The dimensionless quantity E/G should be identical for both the model and the structure in loading which induces shear

   That is, $E'/G' = E/G$

   Assuming identical materials are used in both cases, this criterion should be maintained provided the ratio of shear reinforcement to tensile/compressive reinforcement in the model is equal to that in the actual structure.

5. The 'flexibility' of both the model and the structure should be identical, where flexibility is denoted as '*a*'.

   That is, $a = E' a' / s E$

   where the flexibility, *a* is defined as

   $$a = \Delta / F$$

   Hence, $\Delta/F = \Delta'/ s F'$

   Since $\Delta = s \Delta'$

   $F' = F / s^2$

   $= 1170 / 4$ kN

   $= 292.5$ kN

   As discussed previously, the magnitude of the required force was too great for the available equipment. Therefore, it was not possible to comply with this criterion.

Given that compliance was not possible with respect to two of the specified criteria due to restrictions beyond the control of the author, it would appear that the proposed model would be insufficient to accurately represent the behaviour of the actual beam. However despite this non-conformance, it was anticipated that the results gained from the test would provide sufficient data to determine the proposed beam performance throughout the neck

region, as both the ultimate strain and failure mode of the specimen would be unaffected by the quantity of tensile/compressive reinforcement present, provided that the respect ratio of shear reinforcement was maintained. Hence based on this supposition, the half-scale beam was designed to contain a lesser quantity of reinforcement than would otherwise have been used, the actual amount being determined by a nominal ultimate failure load. An ultimate load of 90 kN was chosen in accordance with the capacity of the available testing facilities. The design process is described in detail later in this section.

The continuation of the reinforcement into the neutral axis of the beam was not achievable in the same manner as the previous small-scale neck beam specimens, as a solid core was not present in the respect region. Hence the lower connecting panel, denoted as the beam 'floor' (refer section 7.3) was thickened throughout the neck region to enable the horizontal continuation of the reinforcement, as illustrated in Figure 7.22 (and further in Figure E.5). Following the termination of the continuing reinforcement at the neutral axis, the upper floor surface was then shaped such that it returned to the correct floor panel thickness tangentially to reduce stress concentration.

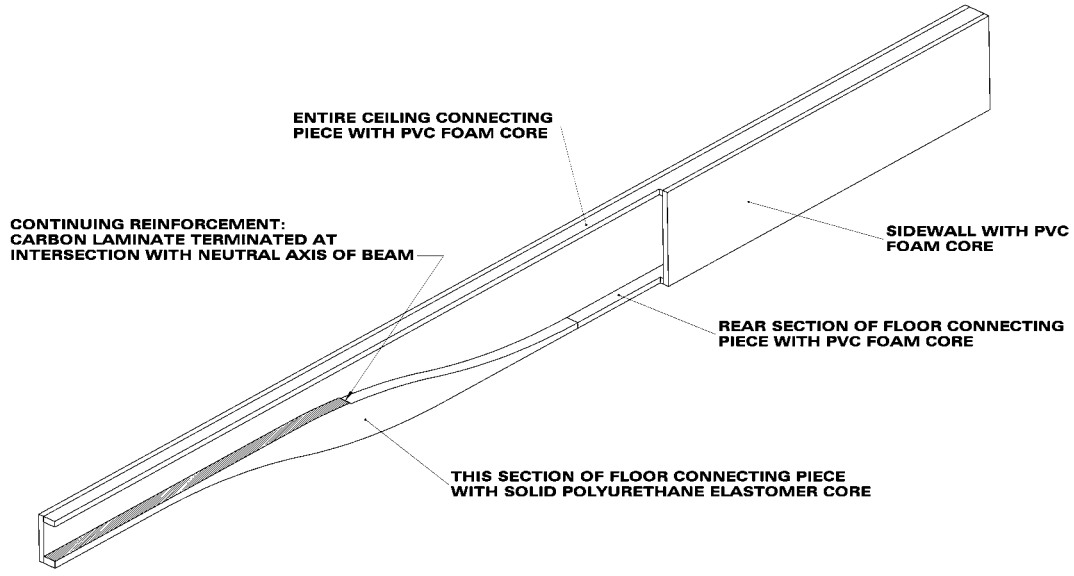

Figure 7.22 Basic Configuration of the Half-Scale Neck Beam

The core of the beam comprised two separate materials: a cross-linked PVC foam (H160 Series) by DIAB, and a cast polyurethane elastomer, RP6430, provided by Vantico Pty Ltd (for material properties refer to Appendix E). Although H200 PVC foam was specified in section 5.3 as the preferred core material, material availability dictated the use of H160 PVC foam (with a density of 160 kg/m^3). Consequently, the corresponding loss of compressive strength was compensated by the introduction of a polyurethane elastomer, which was used in place of the foam core in areas of high load concentration, which are inherent in three-point bending configurations. As this castable material was innately

flexible with respect to shape, and possessed a higher compressive strength and failure strain than both the reinforcement and the PVC foam, it was assumed that the introduction of this core material would not adversely affect the beam performance. As seen in Figures 7.22, the lower floor surface throughout the neck region was also constructed from a solid piece of polyurethane elastomer. This was introduced to reduce the probability of tensile delamination of the lower laminate; particularly as the core foam properties were lower than those originally intended. However, given that the presence of the PVC core material would result in an insignificant increase in tare weight or cost, it was adopted as part of the recommended configuration of the neck region of the actual chassis rail.

The design of the beam with respect to this investigation was similar to that envisaged for the design of the trailer chassis rails, and is discussed here in some detail to more fully explain the design process. The use of strength as the dominant design constraint was adopted for this investigation, as the beam was to be tested to failure. However, the process would be similar, should deflection (and hence strain) represent the defining criteria. Having established the fundamental beam cross-section and configuration (refer section 7.4), and specified the reinforcement and core materials, the design of the chassis rail is primarily defined with respect to the quantity and orientation of the reinforcement. This can be further simplified into the separation of the reinforcement required to carry the bending moment, and that required to carry the shear load.

Definition of the magnitude and distribution of the load represents the initial step in the design process. This process is described in detail in Chapter 4 with respect to the loads experienced by the trailer, and the classification assigned accordingly. However with respect to this investigation, a single point load of 90 kN applied as per Figure 7.23 was assigned as the nominal ultimate load case. The moment and shear distributions were then calculated, yielding a maximum moment of 70 kNm, and a maximum shear load of 51 kN.

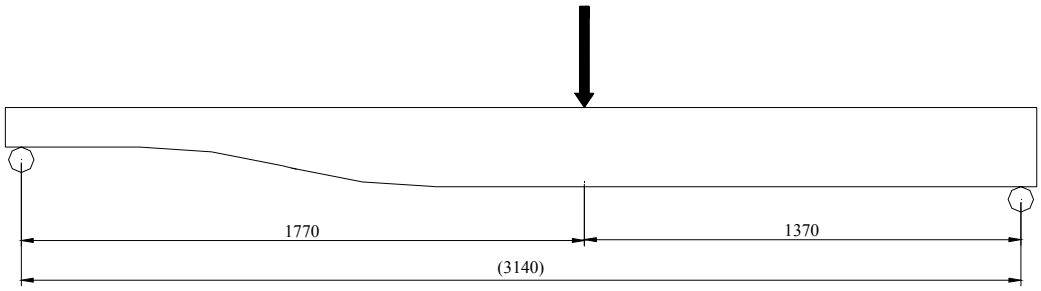

Figure 7.23 Loading Configuration for Half-Scale Neck Beam

The bending moment imposed on the beam was accommodated by unidirectional carbon fibre reinforcement, as discussed in Chapter 5. Given that the moduli and ultimate stress of the reinforcement in both tension and compression were within 4% and 7% (respectively) of each other, it was assumed that the neutral axis was located at the beam centreline. Hence, determination of the quantity of tensile/compressive reinforcement was established through the use of equations (5.2) and (5.3).

Given that

- Laminate width = 70 mm
- Fabric weight = 315 g/m^2
- Beam depth = 250 mm
- Strain at failure = 0.996% for tension, 0.87% for compression

The force to be sustained by the tensile and compressive laminates could be found:

Moment = Force x Distance

70 x 10^3 kN.mm = Force in Laminate (kN) x 250 mm

Hence,

Force in Each Laminate = 280 kN

Therefore, using equation (5.2), the number of layers, N_t, required in the tensile laminate was:

$$N_t = 280x10^3 / (1.19 \times 0.996 \times 70 \times 315)$$
$$= 10.7$$

Similarly, using equation (5.3), the number of layers, N_c, required in the compressive laminate was:

$$N_c = 280x10^3 / (1.14 \times 0.87 \times 70 \times 315)$$
$$= 12.8$$

Given the previous assumption with respect to laminate modulus, the greater number of layers required in the compressive laminate would effectively alter the position of the neutral axis. Hence, this would necessitate an iterative process in order to recalculate the distribution of force between the laminates. However, as failure of the compressive

reinforcement presented a more favourable failure mode than that of tensile failure, it was decided that the number of layers of compressive reinforcement would be reduced to equal that of the tensile reinforcement. In this way, the probability of failure in the compressive laminate was increased, thereby reducing the likelihood of catastrophic failure (refer section 6.9.2). While the reduction of the quantity of compressive reinforcement yielded an associated reduction in the ultimate beam capacity, it was decided not to increase the quantity of reinforcement, as the beam ultimate load was purely nominal. It was also anticipated that the addition of the shear reinforcement would further add to the beam capacity, and hence laminates comprising ten (10) layers of 315 g/m^2 carbon fibre reinforcement were deemed suitable for the purposes of this investigation. As a result of the redefining of the quantities of the compressive reinforcement, it was necessary to recalculate the ultimate beam load. Using the equations previously presented in this section, the ultimate load that the beam could sustain was calculated to be 71 kN, with a maximum moment of 55 kNm, and shear forces of 31 kN and 40 kN at the shallow and full depth ends respectively.

The determination of a suitable quantity of continuing reinforcement was difficult, given the limited scope of the small-scale models. Although the small-scale models utilised a quantity of continuing reinforcement equal to that of the tensile reinforcement, no conclusion were reached as to effects of a greater or lesser quantity. The significant differences between the small-scale models and the proposed half-scale model would also act to increase the uncertainty of any conclusions. Hence it was decided that, in order to minimise the usage of carbon fibre, a laminate comprising half the quantity of the tensile reinforcement would be applied to the inner surface of the floor panel as an initial estimate. It was with this quantity of continuing reinforcement that the finite element analysis was undertaken, with the results being presented in the following sections.

Consideration should also be given in the design process to the moment capacity of the shallow section of the chassis rail, as the elimination of stress concentrations in this area is of no value should the section properties of the shallow section be inadequate to sustain the imposed moment. Hence, it follows that the strain carried by the unidirectional laminates at the point of separation should be notably less than the strain imposed on the laminates at the point of maximum moment.

This condition is dependent on a number of variables, including the distance from the kingpin to the separation point, the difference in beam depth between the shallow and deep sections, and the quantity of continuing reinforcement present. While an inadequate moment capacity throughout the shallow section could be compensated by the localised

inclusion of additional reinforcement, this increases both material and manufacturing costs. Therefore, with respect to this investigation, it was decided that the strain at the separation point should not be greater than 60% of that at the maximum moment. Given the ratios of section depths between each end of the beam, and the quantity of continuing reinforcement, the distance from the support point to the separation point was set at 600 mm. Although this distance does not conform (when scaled) to the Australian standards for clearance of the prime mover (refer Figure 7.10), it can be seen that this would not invalidate any of the conclusions reached, or fail to achieve the objective of this investigation. Moreover this distance is, in reality, accurate when compared with the profiles utilised by several Haulmark trailers (refer Appendix A).

The quantity of shear reinforcement was determined using ultimate stress as a design criterion. The application of this reinforcement within the beam cross section also required consideration, as sufficient inner wall stiffness was required to avoid premature member failure due to the core cracking observed in section 7.4.

Using the mechanical properties of double bias laminates presented in section 5.6.6, the number of layers required to sustain the shear loading was calculated.

Given that

- Ultimate shear strength, S_{su} = 25 MPa
- Beam depth at shallow end = 125 mm
- Full beam depth = 250 mm
- Fabric weight = 600 g/m^2
- Thickness per layer = 0.6 mm
- Maximum shear force at shallow end = 31 kN
- Maximum shear force at full depth end = 40 kN

Assuming a constant distribution of shear stress throughout the beam depth, and the contribution of the core material to be negligible, the number of layers of double bias reinforcement at the shallow end, N_{ss}, is shown to be:

$$N_{ss} = 31 \times 10^3 / (125 \times 25 \times 0.6 \times 2)$$
$$= 8.26 \text{ per side of beam}$$

Similarly, the number of layers of double bias reinforcement required at the full depth end, N_{sf}, is shown to be:

$N_{sf} = 40x10^3 / (250 \times 25 \times 0.6 \times 2)$

$= 5.33$ layers per side of beam

However, the contribution of the core material to the shear capacity of the beam can be calculated as follows:

Given that

$G_{DB} = 3.0$ GPa

$G_{H160} = 0.73$ GPa

$\tau_{DB} = 25$ MPa

$\tau_{H160} = 2.6$ MPa

It follows that the maximum shear strain occurs at

$\gamma_{max} = 25 / 3000$

$= 0.0083$

Hence, the average shear stress in the H160 core material is

$\tau_{H160} (\gamma = 0.0083) = 73 \times 0.0083$

$= 0.608$ MPa

Therefore, the shear force sustained by the core at the beam shallow end at ultimate load is

$V_{H160\,max} = 0.608$ / Core cross-sectional area

$= 0.608 / (30 \times 125)$

$= 2.28$ kN

Similarly, the shear force sustained by the core at the full depth beam end at ultimate load is

$V_{H160\,max} = 0.608$ / Core cross-sectional area

$= 0.608 / (30 \times 250)$

$= 4.56$ kN

This effectively reduces the shear loads carried by the double bias reinforcement to 28.7 kN and 35.4 kN at the shallow and full depth ends respectively. Recalculating the number of layers required yields

N_{ssc} = 4.6 layers per side of beam
N_{sfc} = 2.8 layers per side of beam

However, in order to ensure that shear failure of the beam did not occur, this being potentially catastrophic, it was decided that the beam shear capacity should be increased, thereby augmenting the factor of safety. Hence, the number of layers specified prior to consideration of the shear contribution of the core was adopted after rounding to the nearest whole number, these being:

N_{ss} = 8 layers per side of beam
N_{sf} = 5 layers per side of beam

Following the determination of the appropriate quantity of double bias reinforcement, consideration should be given to the effect of this reinforcement on the flexural stiffness of the beam. While it is anticipated that this would be minimal with respect to the chassis rails due to the constraints relating to beam deflection and flexural strength, it should be considered in applications where deflection is critical. Using fundamental beam theory, initial hand calculations yielded an increase of 8% in the flexural stiffness of the proposed beam due to the double bias reinforcement and the foam core, increasing the calculated ultimate beam load to 76 kN. However as the quantity of shear reinforcement applied was particularly conservative, no further correction for this was considered necessary. The flexural stiffness predicted by the finite element analysis is shown in the following section, which incorporates a greater number of stiffening effects such as that imposed by the polyurethane elastomer.

The lay-up sequence used for the beam is described in detail in section 7.5.3.4, and is illustrated in Appendix E. Two layers of unidirectional E-glass reinforcement, oriented perpendicularly to the longitudinal beam axis, were also added to the inside surface of the walls. The addition of this reinforcement was calculated to increase the wall stiffness, thereby avoiding premature failure in the corner of the cross section, as described in section 7.4. However, it should be noted that the small depth of the beam, particularly at the shallow end, and the absence of direct cross sectional compression as applied in section 7.4, would suggest that the probability of premature failure in this fashion would be minimal.

7.5.3.3 Linear Elastic Finite Element Analysis

Numerical analysis using the finite element technique was conducted to determine the characteristic behaviour of the chassis rail model. Given that the expected ultimate deflection was sufficiently low (<<Span/50), a linear analysis was conducted.

The objectives of the analysis are summarised as follows:

- To produce an accurate 3-dimensional model of the proposed chassis rail model, suitable for detailed finite element analysis
- To investigate the performance of the chassis rail under load, particularly at ultimate load, and note the expected failure mode
- To allow the evaluation of the structural characteristics of the model, in particular the effectiveness of the stress-concentration reduction techniques developed through the small-scale neck investigation described in Section 7.5.2 and Appendix D.

As stated in section 7.5.2.3, ANSYS (v. 5.7) was used to complete the numerical analysis of the model. However unlike the previous instance, a 3-dimensional model was used in this analysis, utilising 20-node brick elements (SOLID95) in representation of the core material, and 8-node layered shell elements (SHELL99) in representation of the laminates. Further information on the element types can be found in Appendix E.

In order to preserve accuracy between the analysis and the actual specimen, the laminae contained within the analytical model replicated the lay-up sequences present in the actual beam, these being described in detail in section E.9. It should be noted however, that the analysis software was not capable of accurately determining the effects of changes to the lay-up sequence, particularly with respect to the confining effects of wrapping the double bias around the beam in a single piece.

To reduce the number of elements and decrease the solve time, only half of the specimen was modelled using symmetry conditions. Perfectly elastic material characteristics were assumed, and plastic deformation was not considered. The general dimensions and element mesh produced for each analysis are illustrated in Appendix E. Figure 7.24 shows the basic configuration of the model.

As seen in Figure 7.24, the load was applied over a defined area equivalent to that anticipated in the actual test. Similarly, the load at the reaction points was distributed according to the dimensions of the load spreading plates used in the experiment (refer following section). A load of 40 kN was applied to the model, this being equivalent to a

load of 80 kN applied to the full model. The response of the beam to all other load values was interpolated using the linear relationship inherent in the analysis type.

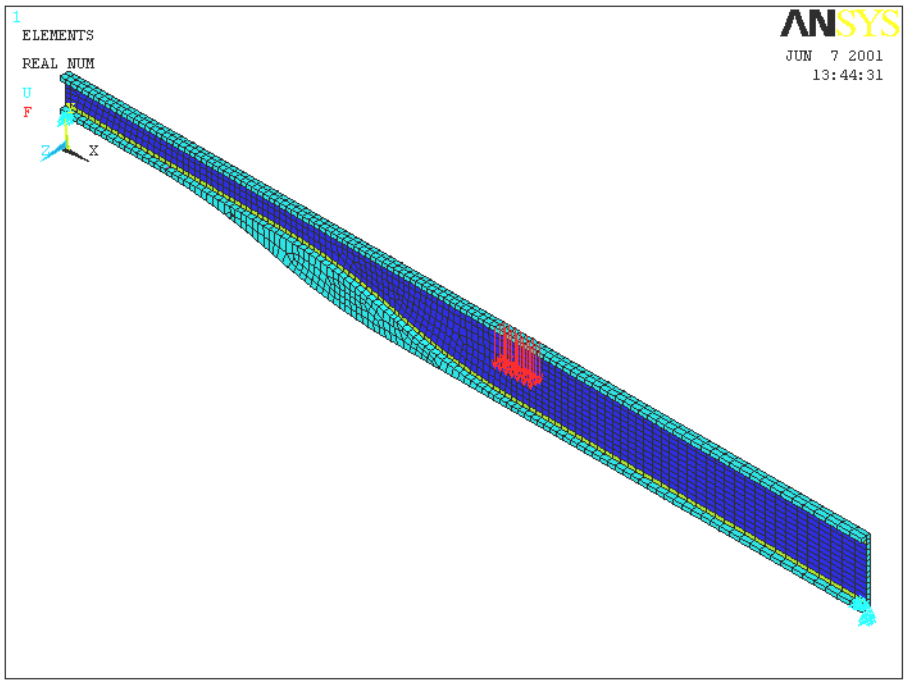

Figure 7.24 Finite Element Model of Half-Scale Neck Beam (Symmetry Used)

7.5.3.4 Fabrication and Experimentation

The process of beam manufacture, illustrated in Appendix E, is described in an abbreviated form in this section. As previously mentioned, a combination of H160 PVC foam and a polyurethane elastomer were used as core materials, the configuration of which is shown in Figure E.7. Unidirectional carbon and double bias E-glass reinforcements were used previously noted, with the reinforcement and matrix types used in this specimen possessing identical mechanical properties as those tested in Chapter 5. The hand lay-up technique (refer Chapter 2) was used throughout the beam manufacture. The construction of the beam cross section was carried out as follows:

1. The required pieces of PVC foam were cut from sheets of the appropriate thickness.
2. Two moulds were constructed to enable the casting of the polyurethane elastomer. One mould was shaped to produce flat sheets which could be cut to size, and the other mould was shaped to produce the core for the curved floor in the neck region.

3. Following preparation of the moulds, the polyurethane elastomer was cast. Once cured at room temperature for a period of 24 hours, the castings were post cured at 80° C for 16 hours.
4. The castings were then machined to the desired shape, and all core pieces were adhesively bonded together to form the four sides of the beam. Following the cure of the adhesive, all joins were sanded smooth, and the surfaces cleaned. Figure E.7 shows the core pieces prior to bonding.
5. A single layer of double bias reinforcement was laminated to the outer side of each wall piece. Following cure at room temperature for 24 hours, a laminate comprising two layers E-glass unidirectional reinforcement in combination with a single layer of double bias reinforcement, [0°/DB/0°], was laminated to the inner side of each wall piece, and allowed to cure at room temperature. A layer of peel-ply was added to the top of each laminate prior to cure to enable good secondary bonding.
6. A single layer of double bias reinforcement was laminated to each side of the floor and ceiling core pieces, as shown in Figure E.5. This required the construction of a mould, the shape of which formed the outer profile of the floor and ceiling pieces.
7. Following the cure of the floor piece, five layers of unidirectional carbon fibre reinforcement (the continuing reinforcement) were laminated on the inner side of the floor piece, as shown in Figure E.8.
8. The walls of the beam were then adhesively bonded to the floor and ceiling pieces with an epoxy adhesive. Figure E.9 shows the beam with one of the walls bonded in place. The assembled beam was then trimmed to shape and the surface cleaned in preparation for the application of the shear and unidirectional reinforcement.
9. The application of the double bias and unidirectional reinforcement is illustrated in Figure E.6. The double bias E-glass reinforcement was placed alternately between five layers of carbon fibre unidirectional reinforcement, with each layer of double bias enveloping the circumference of the beam section. The differing section sizes dictated the separation of the double bias reinforcement into three pieces, as shown in Figure E.6. An overlap of 50mm was used in the joining of adjacent pieces.
10. The beam was allowed to cure at room temperature for 24 hours, followed by post curing at 80°C for 8 hours. The ends of the beam were then trimmed where necessary. Figure E.10 shows the finished laminate at the shallow end of the beam.

As discussed in section 7.3, the wrapping of the double bias reinforcement around the beam circumference acts to perform a number of beneficial functions. However, an additional function of this wrapping is found in the restraint of the tensile concave reinforcement in the neck region. This restraint provides redundancy in the neck region, acting in

conjunction with the continuing reinforcement to further reduce the possibility of delamination of the unidirectional reinforcement. However this confining double bias reinforcement was not considered sufficient to justify the removal of the continuing reinforcement, as the double bias does not act to reduce the stress concentration present in this region. Rather, as it acts simply to confine the tensile reinforcement, any damage sustained by the confining double bias laminate may reduce its ability to confine the tensile unidirectional reinforcement, enabling delamination. Conversely, the use of unidirectional continuing reinforcement (refer Figure 7.15) effectively eliminates the stress concentration, and its internal location prevents the possibility of external influences.

It should also be noted that this method of construction was not suited to manufacture on a larger scale, primarily due to the time and difficulties associated with the hand lay-up of the reinforcement. It is anticipated that construction of a full size chassis rail would necessitate the use of a wet-out machine or resin infusion techniques to decrease production time to a suitable level. The wrapping of the double bias reinforcement is particularly sensitive to air inclusions and voids, and hence resin infusion may prove to produce the most reliable and consistent laminate.

Subsequent to manufacture, the beam was simply supported and subjected to three-point bending, as illustrated previously in Figures 7.23 and 7.24. Further detail is provided in Appendix E. A combination of steel plates and rubber matting was situated beneath the loading platen, in order to reduce the influence of the load application on the compressive laminate. Similar pieces of steel and rubber were placed between the beam and the reaction points to prevent local crushing.

A number of unidirectional strain gauges were attached to the beam, as illustrated in Figure E.11 (a). Gauge one was placed on the tensile laminate on the underside of the beam, directly beneath the load at the point of highest strain. Gauges two, three and four were placed at particular points throughout the neck region on the tensile laminate. Specifically, gauge two was placed at the lower corner of the neck region, as this had proved to be the point of failure in several of the small-scale neck specimens. Gauge three was placed mid-way along the angled laminate, in order to record the strain carried by this laminate in comparison with that carried by the continuing reinforcement. Gauge four was placed at the point of separation, in order to validate the absence of stress (and hence strain) concentrations at this point as a result of the continuing reinforcement. A fifth gauge was placed on the continuing reinforcement prior to the beam assembly at the point of predicted maximum strain on this laminate. However, this gauge was found to be inoperable at the time of testing, probably due in some part to the heat of the post curing. As it was not

possible to replace this gauge due to its internal position, no strain data was recorded on this laminate.

The measurement of the maximum compressive strain was not possible, due to the presence of the loading platen, and the difficulties associated with the accurate measurement of the complex stress field in the immediate vicinity of the concentrated load. Hence it was assumed that, neglecting the local effects of the applied load, the compressive strain was equal to that of the tensile strain.

The load was applied at a rate of 5 mm/minute, with the load, deflection (at the load point) and the aforementioned strain being recorded throughout the duration of the test at intervals of 0.10s.

7.5.3.5 Results and Discussion

a) Analysis Results

Analysis of the half-scale chassis rail yielded a number of significant results with respect to beam behaviour under load, and the validation of the stress concentration reduction techniques previously mentioned.

As shown in Figure 7.25 (and in Figures E.4 (a) and (b)), the maximum strain in the beam occurred in the compressive and tensile laminates beneath the load point. Neglecting the localised compressive effects of the loading platen, it appears that the assumption of identical strains (of opposite sign) in the tensile and compressive laminates at the load point was valid. Using these results, the strain in the compressive laminate was predicted to reach a failure strain of 0.87% (refer Chapter 5) at a load of approximately 100 kN. The shear reinforcement previously specified was shown to be adequate for this load, as indicated by the principal stress calculated within the double bias laminates.

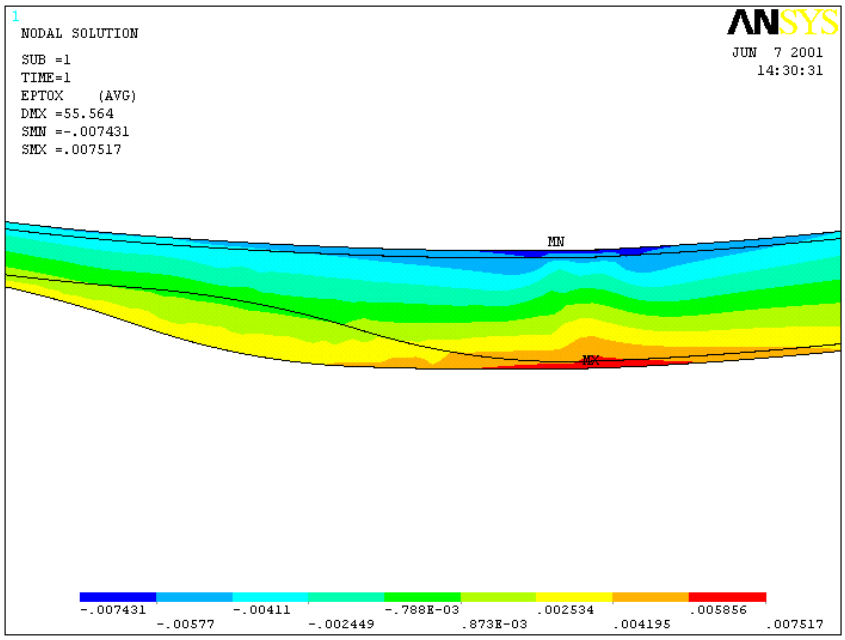

Figure 7.25 Laminate Strain Longitudinal to Half-Scale Neck Beam

A comparison of the basic design techniques presented in section 7.5.3.2 with the analysis results show that the hand calculations under predicted the beam stiffness and capacity, as shown in Figure 7.26. As previously stated, the calculated failure load of the beam was 76 kN, which is significantly lower than the failure load predicted by the finite element analysis. However, as the hand calculations did not take into account the lay-up sequence (and hence the actual distance of the fibres from the neutral axis), the double bias reinforcement surrounding the floor and ceiling pieces, or the stiffening effects of the polyurethane elastomer (in replacement of the H160 PVC foam), this discrepancy was deemed acceptable. It is assumed that the beam stiffness and capacity could be predicted with greater accuracy, if necessary, by the inclusion of the factors not considered in the previous example. However, given the complicated nature of the beam cross section and profile, and the availability of finite element software, any hand calculations with respect to chassis rail design should be considered preliminary. This comparison also highlights the conservative nature of the hand calculations, which is beneficial in reducing the probability of a beam containing insufficient reinforcement due to the absence of finite element software.

As illustrated in Figure 7.25 (and in Figures E.4 (a) and (b)), the quantity and configuration of the continuing reinforcement, in conjunction with the use of smooth transitions and large radii, was successful in eliminating all stress concentrations throughout the neck region, including the point of separation. This would appear to validate the conclusions

yielded by the small-scale investigation, and demonstrate that these principles could be effectively applied to this beam cross section. A plot of the strain carried by the continuing reinforcement is shown in Figure E.13. This demonstrates that the load imposed on this laminate is substantial, with the maximum strain (of approximately 2000με) being observed at the separation point. The strain can also be seen to reduce to a value of less than 500με at the termination of the laminate. This would appear to indicate that the load carried by the continuing reinforcement does not entirely transfer to the adjacent core material prior to termination at the beam neutral axis; however the tapering of the layers of the laminate would significantly increase the transfer of load to the core. This was incorporated into the manufacture of the test specimen.

A single stress concentration was identified in a specific area of the core, as shown in Figure E.4 (d). This was not related to the failure mode observed in the small-scale specimen number three (refer section 7.5.2.5), but rather was caused by the sudden transition between the two core materials in a region of high stress. However the magnitude of this concentration was far below the ultimate capacity of either of the core materials, and was not considered significant.

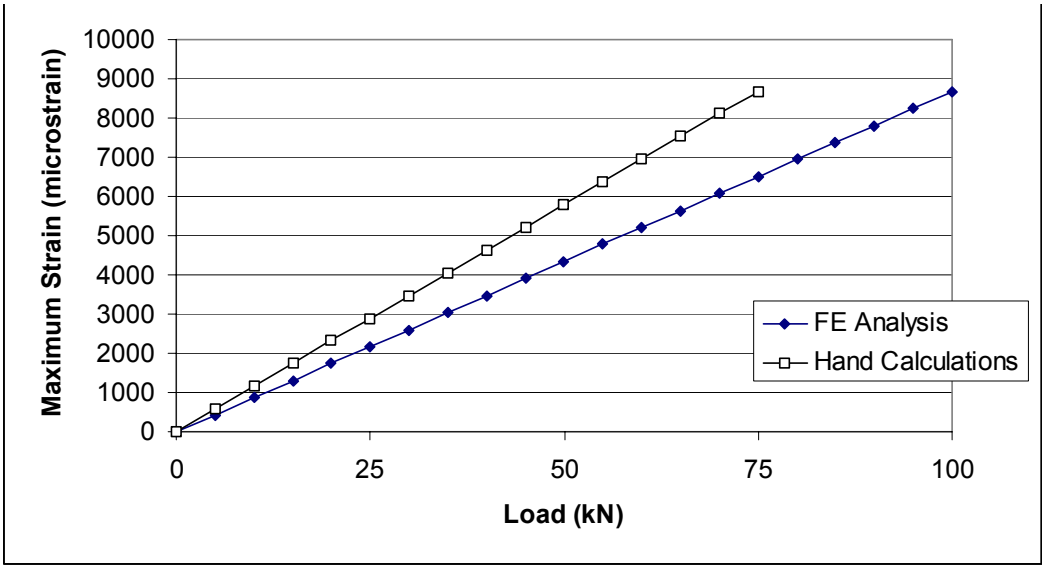

Figure 7.26 Comparison of Hand Calculations and FE Analysis of Half-Scale Neck Beam

b) Experimental Results

The results gained from the test data yielded a linear load-displacement relationship as shown in Figures E.12 (a) through (e). Minor cracking was audible immediately preceding

initial failure, which occurred at a load of 86 kN. This occurred as a result of the collapse of the compressive reinforcement, directly beneath the loading platen, as shown in Figure E.11 (c). Despite this failure, the beam retained sufficient strength to sustain further loading. At a load of 88 kN, complete failure (refer Figure 7.27 and also Figure E.11 (d)) of the beam occurred, characterised by a compressive failure of the laminate at the edge of the loading platen. However, the absence of a true dead load negated the significance of this load value, giving an actual ultimate load of 86 kN.

The maximum strain recorded prior to failure was approximately 7450 με, which was observed at gauge number one on the tensile laminate. Based on the simplifying assumption that the compressive strain under the loading platen was equal (and of opposite sign) to that of the tensile laminate, it was assumed that this was the value of compressive strain that initiated failure in the beam. However, given that the maximum strain recorded from the test was significantly lower than the ultimate compressive strain value of 8700 με (refer section 5.6.6), this would indicate that the local compressive forces imposed by the loading platen contributed significantly to the strain in the unidirectional laminate.

Figure 7.27 Beam Failure Due to Collapse of Compressive Reinforcement

The failure of the compressive reinforcement also demonstrated the failure mode of the beam in bending. As mentioned previously, the avoidance of catastrophic failure of the chassis rails was of paramount importance with respect to safety. Observations made of the

compressive nature of the beam failure, suggested that catastrophic failure would not result from a dead load (as opposed to a simulated dead load under a testing machine), despite the significant increase in beam deflection. The failure of the beam in compression also highlights the importance of the design process with respect to the capacity of the tensile and compressive unidirectional laminates. Had the compressive laminate capacity been equal to that of the tensile laminate, the probability of catastrophic failure through rupture of the tensile laminate would have been greatly increased.

However, the mode of failure observed in the test piece should also be noted in light of the influence the distribution of the load, specifically with respect to the localised compressive effects of the loading platen. A distributed load, in contrast to a concentrated 'point' load, would act to minimise any additional compressive stress local to the loaded region of the laminate. Given that a payload comprising a singular concentrated 'point' load could not actually be imposed on a trailer, and taking into consideration the load spreading provided by the deck, and a basic level of good practice with respect to load distribution on the part of the operator, it is assumed that the influences present in this test would not be relevant in a the context of an actual chassis rail.

It should also be noted that each of the strains measured throughout the neck region was consistently lower than that measured beneath the load point (gauge one). The difference in the strain measured beneath the load point and that at the separation point yielded that the later measured approximately 45% of that of the former. Similarly, the adoption of large radii on the lower corner of the neck region was effective in maintaining strains which were approximately 32% lower than that measured beneath the load point. This data clearly demonstrates the effectiveness of the techniques employed in the elimination of stress concentrations, which would typically result in the failure modes observed in the small-scale testing of the neck region.

The shear capacity of the beam was shown to be adequate, as no indication of damage to the double bias reinforcement was observed. Should the shear capacity of the double bias reinforcement been exceeded, this would have been characterised by the whitening or 'crazing' of the resin (an artificial 'yield' point), and exhibits non-linear, plastic deformation (refer section 5.6.6). Rupture of the double bias reinforcement was observed (see Figures 7.27 and E.11 (d)), however this was initiated by the compressive failure of the unidirectional laminates, which were dispersed between layers of the shear reinforcement.

c) Comparison of Results

The comparison between the strains predicted by the finite element analysis and those measured by the strain gauges on the test beam yielded favourable results. As shown in Figures E.12 (a) through (e), the laminate strains calculated by the analysis at the points corresponding to the gauge placement were extremely accurate, with the maximum relative error remaining below 10% in all cases. It would appear from these results that the analytical model successfully replicated the beam behaviour, particularly with respect to the contribution of the core and double bias laminate to the beam stiffness, as demonstrated in Figure 7.28. The accuracy of the analysis also validates the incorporation of the mechanical properties taken from the laminate testing described in Chapter 5.

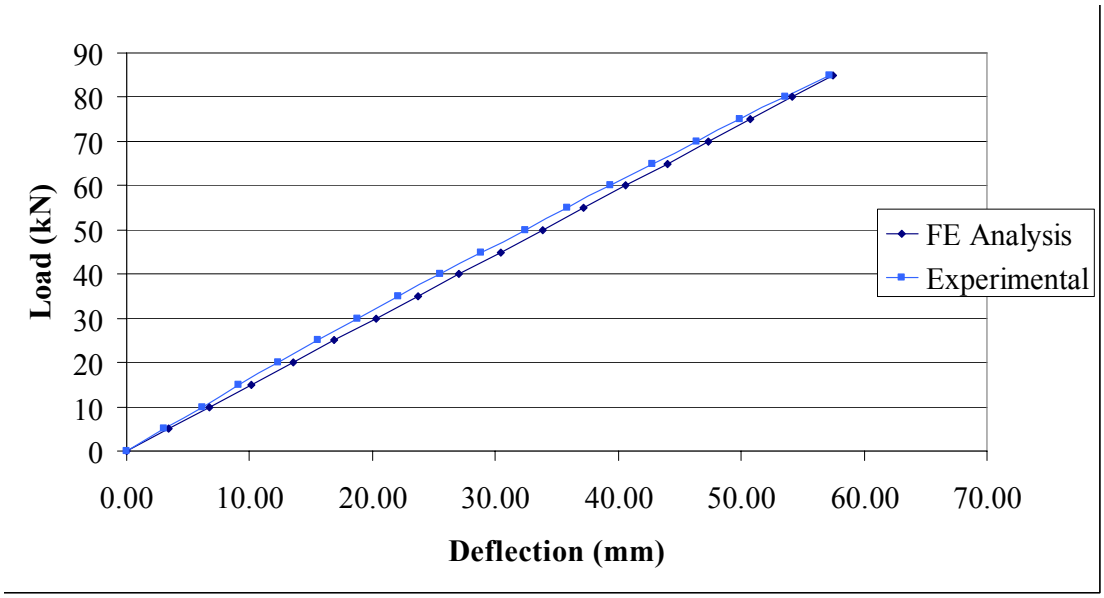

Figure 7.28 Plot of Predicted and Actual Deflection of Half-Scale Neck Beam Beneath Load Point

Although it was not possible to compare or verify the strain imposed on the continuing reinforcement due to the failure of the respective gauge, the agreement between the two data sets with respect to all other measurable quantities would lend credibility to the accuracy of the predicted strains in the continuing reinforcement. A plot of this strain is provided in Figure 7.29, this being presented as the actual strain imposed on the continuing reinforcement in the absence of experimental data.

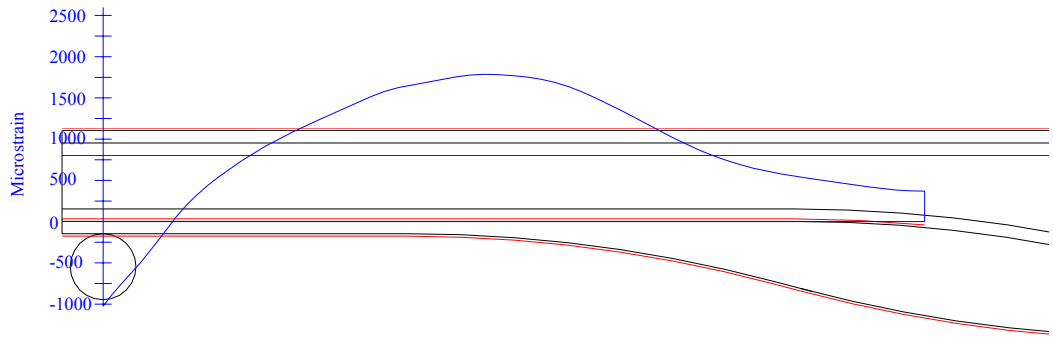

Figure 7.29 Predicted Strain In Continuing Reinforcement on Beam Inner Floor

7.5.4 Conclusions

The investigation described within this section was undertaken in order to address the difficulties associated with the accommodation of the applied loads throughout the neck region of the chassis rail. Using a combination of finite element analysis and experimental techniques, a number of factors were identified as being significant contributors to the effective transfer of the bending moment through the neck region.

Initially, a series of small-scale specimens were used to establish the fundamental principles associated with the reduction of stress in the neck region. In particular, the elimination of stress at the point of separation was investigated. Specimens of varying configurations were analysed, with several of them being tested to destruction. This investigation yielded a number of significant results. The minimisation of the relief angle was shown to be fundamental in the reduction of stress in the neck region, and an angle of 15° was shown to be the lowest practical relief angle suitable for application to this particular trailer configuration. The incorporation of continuing reinforcement to the neck region was also demonstrated as being a predominant contributor to stress reduction. This was shown to significantly reduce the magnitude of the stresses at the separation point, such that failure occurred at an alternative location on the specimen. The inclusion of large radii at both the upper and lower corners of the neck region also provided further stress reductions in these areas, however the presence of internal stress concentrations (not modelled by the 2-dimensional analysis) prevented the realisation of the full effects of the radii in the experimental specimens.

The principles ascertained through the small-scale investigation were then transferred to the proposed chassis rail and associated materials, in order to establish the validity of these conclusions within the context of the actual chassis rail. A single specimen of scale 1:2 was

analysed, constructed and experimentally tested. A direct comparison of the analytical and experimental results yielded an excellent correlation, with failure occurring in the compressive laminate beneath the load point. Measurements taken from strain gauges fixed to the specimen verified the accuracy of the model, which was then used to predict the strain imposed on the continuing reinforcement.

A preliminary design method for use in the determination of appropriate quantities of reinforcement was also demonstrated within this section. This method was intended to be purely indicative with respect to chassis rail design, with verification through finite element analysis being recommended in all cases. The use of accurate material data was necessary in order to obtain reliable results with respect to the finite element analysis.

This larger model clearly demonstrated the effectiveness of the proposed methods of stress reduction in the neck region. The strains (both predicted and measured) throughout the neck region were shown to be significantly lower than those at the point of highest bending moment, thereby confirming the objective of non-catastrophic failure of the compressive laminate. Generally, the investigation of the neck section highlighted the importance of detail design in this region. The reduction of stress concentrations was shown to significantly influence the failure mode, and provide increased reliability with respect to member capacity and structural behaviour.

7.6 Basic Cross Member Construction and Connection

7.6.1 Introduction

In the context of a ladder frame chassis, the primary function of the chassis rails is to sustain the bending moments and shear forces imposed by the payload, and transfer these to the trailer suspension and prime mover. However, the incorporation of cross members into the structure is essential for a number of reasons. Primarily, the function of the cross members is to maintain a connection between the two chassis rails, ensuring a fundamental level of structural integrity. Additionally, the cross members act to transfer load between the two chassis rails, enabling a disproportionate load to be more evenly distributed between the two members. Further, the cross members also act to provide transverse stiffness to the trailer, and transfer to the chassis rails any load that is applied to a point on the deck other than directly above the chassis rail. Torsional stiffness is also directly influenced by the characteristics of the cross members, and the rigidity of the connection to the chassis rails.

This section describes the initial development of a cross member, suitable for connection with the proposed chassis rail profile. The configuration and basic design principle associated with the selected cross member are discussed, with particular emphasis being placed on the connection of the cross member to the chassis rail. This investigation culminates in the design, analysis, and static testing of a full-scale cross member, and the behaviour of the connection to a section of chassis rail.

7.6.2 Cross Member Configuration and Preliminary Design

A survey of the cross members typically used in steel trailers (refer Appendix A) showed that standard hot-rolled I-beams represented the predominant choice in cross member selection. Specifically, it was observed that the majority of all manufacturers utilised the same cross member size. This conformity was noted to be regardless of the age of the trailer, or the capacity of the chassis rail. However, as the spacing between the cross members did vary between each trailer, it would appear that cross member choice is determined on this basis, in preference to the design and manufacture of a non-standard section.

The absence of 'standard' sections within the context of fibre composite materials removes this approach as a viable alternative. Consequently, the designation of the characteristics and properties of fibre composite cross members must be determined in combination with the selection of an appropriate spacing between the members.

Connection between the chassis rails and cross members in steel trailers is commonly performed as illustrated in Figure 7.30. A section of the web is cut from the chassis rail, and the cross member is inserted. The web of the cross member is then welded to the chassis rail, thereby minimising the potential for the degradation of the flanges of the cross member due to welding, whilst also minimising the interruption in the stress field within the flanges presented by a rigid connection to the chassis rail.

Prior to this method of insertion, a common method of connection incorporated the joining of the lower flange of the cross members to the top flange of the chassis rail. While this method was comparatively inexpensive, the centre of gravity of the payload was effectively increased, in addition to the subsequent reduction of the allowable payload height.

Despite the predominant use of I-beam and tapered flange beam sections as cross members within the context of steel trailers, alternate cross sections have been employed on occasion. An example of this is observed in a trailer produced in the United States by East Manufacturing (refer section 3.4.5). This trailer utilises tubular cross members, constructed from steel or aluminium, which are inserted through the chassis rail in a similar process to that discussed previously. Other trailers incorporate rectangular hollow tubing in a similar fashion.

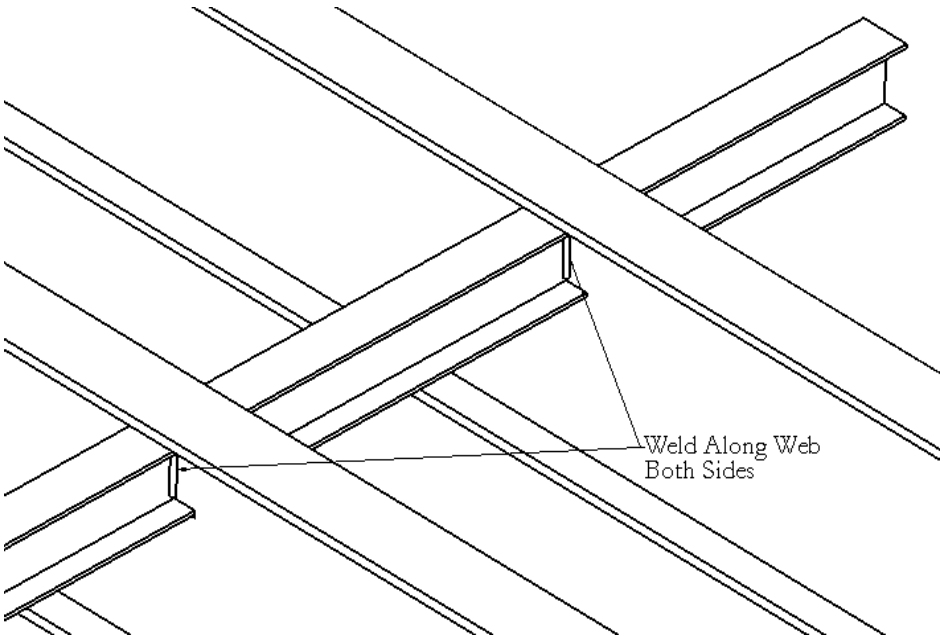

Figure 7.30 Attachment of Cross Member to Chassis Rail in Steel Trailers

With respect to the selection of an appropriate cross section for use in an FRP trailer, it has been demonstrated that the replication of a steel counterpart does not often represent the optimum solution. However due to time restrictions, an exhaustive investigation into various cross-sectional shapes was not undertaken. Determination of an appropriate cross section in this study was predominately governed by the method of connection to the chassis rails, with consideration also given to the implications of modular construction.

The minimisation of the centre of gravity of the trailer dictated that the cross members be inserted through the chassis rail. Consequently, all shear and compressive forces sustained by the cross members would be imposed on the sidewalls of the chassis rails, which emphasized the significance of the elimination of stress concentrations at the joint. This suggested the utilisation of a tubular cross section, as this would provide the greatest relief of stress concentrations in this area. Whilst this did not necessarily represent the optimum configuration with respect to member strength and stiffness in comparison to a rectangular hollow section, the minimisation of stress concentrations was considered to be of greater significance. The use of a rectangular hollow section would necessitate the incorporation of large radii (in relation to the member size) to reduce the stress concentrations present at the corners of the member, thus essentially producing an elongated circular section. Optimisation of a circular section is also possible, by ensuring the majority of the unidirectional reinforcement is placed towards the upper and lower sides of the member. The flexibility provided by the laminar construction therefore lessens the effects associated with the reduced strength and stiffness inherent in a circular section.

The modular nature of the trailer would also be assisted by the use of circular cross members, in preference to other section shapes. Should a cross member fail during the course of service, replacement of the member would inevitably involve the grinding or removal of an adhesive or fastener. If an adhesive was employed to retain the cross member, the use of a circular cutting/grinding tool of an appropriate diameter could be used to regrind the hole through the chassis rail in a single pass. Thus, the use of a circular cross member simplifies the repair process (i.e. insertion/removal), reduces downtime, and diminishes the possibility of grinding the insertion hole 'oversize'.

The design of an FRP cross member presents similar difficulties to those encountered in the design of the chassis rails. Specifically, determination of the load cases imposed on any given cross member is dependant on the distribution of the load on the member. However, the distribution of load on the cross member varies not only with the composition and form

of the payload, but also depends on the presence of other items supporting the payload, such as pallets or lengths of timber which are used to spread the load over a greater area.

The determination of appropriate strength and stiffness characteristics of an FRP cross member is aided by the presence of a notable level of conformity within steel trailers with respect to the capacity of cross members. Unlike the capacity of the chassis rails, various manufacturers of steel trailers would appear to have adopted a single member size (100 TFB), choosing instead to vary the spacing of the members to achieve the desired lateral characteristics of the trailer. However, as illustrated in Appendix B, there was relatively little difference observed in the spacing of the cross members of the later model trailers surveyed, with the distances generally varying between 600 mm and 700 mm. Hence, it would appear that the lateral characteristics of more recent trailers have remained relatively constant, being largely independent of the capacity of the chassis rails. The static moment capacity (at yield) of the 'common' cross member was noted at approximately 9 kNm, with a shear capacity of the web being 70 kN. As with the chassis rail capacity, the cross members of the Loughlin trailer (1987) represented the exception, with a moment capacity of approximately 16 kNm, and a shear capacity of 104 kN.

The widespread conformity of cross member strength enabled a more confident assessment of suitable design parameters with respect to the FRP cross member. While the large differences observed in the strength of the chassis rails promoted uncertainty with respect to realistic load cases and design factors, notable conformity of the cross member strength resulted in the deferment of a load case analysis as conducted on the chassis rails (refer Chapter 4). Rather it was decided that, using a conservative approach in light of the new nature of the proposed structure, the maximum moment capacity of the FRP cross member should be 12 kNm, at a strain level of 0.45% (refer section 4.8.6). This represents an approximate average between the two primary cross member capacities noted previously, and as the trailer proposed within this thesis was categorised as a 'medium duty' trailer (refer section 4.), this was judged to be appropriate. A preliminary investigation using basic beam theory indicated that the shear capacity of the steel cross members was far greater than necessary (in comparison with the moment capacity). Hence, assuming that the load case described in section 7.6.4 was representative of the worst case scenario, it was decided that the maximum (elastic) shear capacity of the FRP cross member should be sufficient to sustain the respective shear force; that is a maximum shear capacity of 37 kN.

The constraints on cross member design imposed by deflection limitations were not considered for a number of reasons. As discussed in chapter 4, the primary reason for limiting the deflection of the chassis rails (and the inclusion of a precamber) was concerned

with public perception. However, the same argument cannot be sustained in relation to cross members, as the magnitude of the deflections is substantially lower. The deflection of any single cross member is concealed to some degree by the deck and combing rail, and excessive load placed on a single cross member can be distributed to adjacent cross members. Additionally, it is envisaged that deflection of the cross members would promote a greater degree of direct bearing of the payload on the chassis rails in some cases. Therefore, no deflection constraints were considered in the design philosophy.

Determination of the required reinforcement quantities was not performed using a 'load per layer' approach as described in section 7.5.3.2. Rather, due to the circular shape of the cross member, and the simplifying assumption that the unidirectional reinforcement would be equally distributed around the circumference of the member, it was decided that a 'traditional' approach utilising cross sectional area of the reinforcement would be employed. This method is able to provide a valid representation of the mechanical properties of any given laminate, provided accurate data regarding laminate thickness and associated modulus are available (refer sections 2.7.3 and 5.6). Indeed, the finite element analyses employed throughout the tests described in this chapter require the input of both laminate thickness and modulus, and rely on the mechanical properties established through testing. The determination of the required quantities of shear reinforcement also utilised this method.

The proposed test configuration (refer section 7.6.5) involved the loading of the cross member in three-point-bending, with the equal application of load to two unsupported ends of the cross member, which was inserted through a restrained section of chassis rail. Consequently, each half of the cross member effectively acted as a cantilever. Assuming a free length of 700 mm, and the centroid of the applied load being 650 mm from the support, the applied force necessary to generate the prescribed moment was therefore calculated to be 18.5 kN (to be applied to each end of the cross member). Given that this load was to generate 0.45% strain within the cross member laminate, the ultimate load imposed on each cantilevered member would approximately equal 37 kN, at a failure strain of 0.9%.

Selection of an appropriate diameter for the cross member was achieved by an examination of the quantity of carbon reinforcement required to provide the desired member properties for a given diameter. Figure 7.31 shows the relationship between the approximate mass of carbon unidirectional reinforcement required to sustain a 12 kNm moment. The effects of the shear reinforcement were not considered in this calculation, which should be considered only as preliminary.

The figure indicates that to adopt a member size of 100mm, as observed in steel trailers, it would necessitate a substantial quantity of carbon reinforcement, increasing the mass and cost of the trailer. Conversely, whilst a member size of 200mm requires less than 25% of the carbon reinforcement needed for a member size of 100mm, several difficulties arise as a result of the increase in member size.

The primary difficulty relates to member stability. While the application of load to a given cross member should result in the same total member deflection regardless of the diameter, provided the quantity of reinforcement is appropriately adjusted, localised member deflection under concentrated loads is increased as the diameter increases, and as wall thickness decreases. This can lead to laminate failure that is largely independent of the load applied to the member as a whole, as the local effects on the laminate dominate the failure mode. The larger diameter also requires the removal of more material from the web of the chassis rail, further reducing the shear capacity of the chassis rail in this region.

In addition to this, a large cross member diameter increases the torsional stiffness of the chassis, and necessitates an increase in the size of the combing rails. While the torsional characteristics of a trailer chassis are not investigated in this thesis, it can be said that a large increase in the torsional stiffness of the trailer would impose additional strain on the suspension system. An increase in the size of the combing rail would also add to the cost and mass of the trailer.

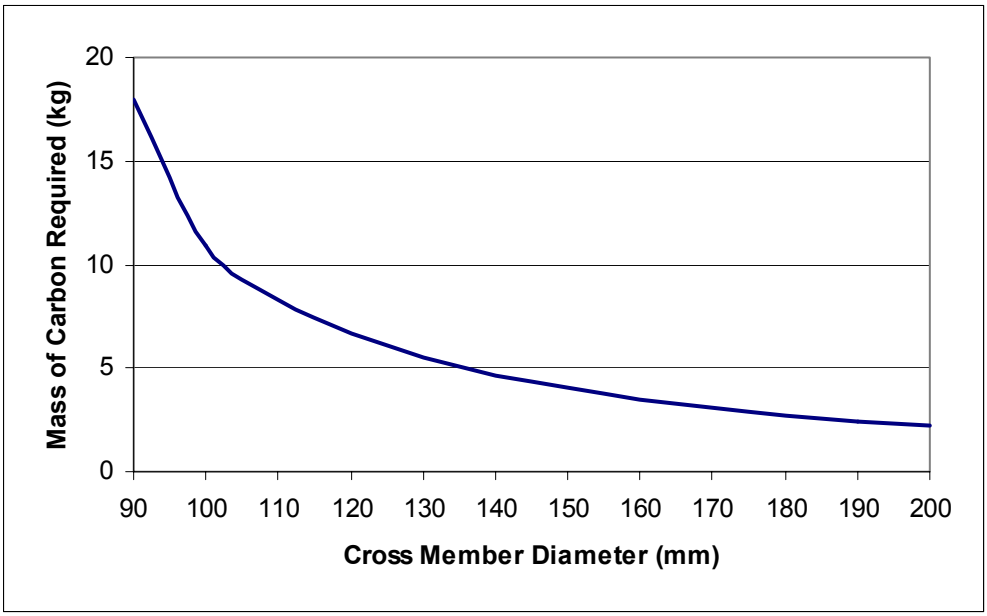

Figure 7.31 Approximate Mass of Carbon Reinforcement Required to Sustain A 12 kNm Moment for Various Cross Member Diameters

Hence, it was decided that the cross member diameter would be set to 150 mm, as this represented a reasonable compromise (see Figure 7.31) between the two member diameters previously discussed. It was noted that further detailed study into issues involving the torsional characteristics of the trailer in relation to the cross members, would be required in order to further optimise the cross member diameter.

Having determined the diameter of the cross member, a more accurate calculation of the required reinforcement was necessary. It was anticipated that the quantity of double bias reinforcement would be equal or greater than that of the unidirectional reinforcement (by mass), and hence the shear reinforcement was to be included in the determination of the total quantity of reinforcement required to sustain the moment. The quantity of shear reinforcement was therefore calculated first, by means of the basic principles described in section 7.5.3.2.

Using the mechanical properties of double bias laminates presented in section 5.6.6, the number of layers required to sustain the shear loading was calculated.

Given that

- Allowable shear strength, S_{su} = 25 MPa
- Basic Diameter = 150 mm
- Fabric weight = 600 g/m^2
- Thickness per layer = 0.6 mm
- Maximum shear force (per side) = 37 kN

As this calculation was used only to provide an initial estimate (for the finite element analysis) as to the quantities of reinforcement required, a constant distribution of shear stress throughout the beam depth was assumed. Using this assumption, the inner member diameter, R_i, is shown to be:

$$R_{in} = \left[R_{out}^2 - V/\left(S_{su} \times \pi\right)\right]^{1/2}$$

$$= \left[75^2 - 37 \times 10^3 / (25 \times \pi)\right]^{1/2}$$

$$= 71.8 \text{ mm}$$

Hence, the number of layers of double bias reinforcement, N_{scm}, is shown to be:

$$N_{scm} = (75 - 71.8) / 0.6$$
$$\approx 5.4 \text{ layers}$$

The estimate provided by this simplified calculation did not take into account the contribution to the shear capacity of the unidirectional reinforcement, or the sacrificial mandrel (refer section 7.6.3). Additional capacity within the double bias reinforcement is also available during plastic deformation. Also, it was possible that the test specimen may experience a shear force in excess of 37 kN, if the compressive strain capacity of the unidirectional carbon exceeded 0.9%. Hence, it was decided that the number of layers of double bias reinforcement be increased to six (6) for the initial estimate, to minimise the probability of shear failure of the cross member.

Calculation of the reinforcement required to sustain the bending moment included the contribution of the double bias reinforcement, in addition to that of the unidirectional carbon fibre reinforcement. A simple hand calculation was first performed to provide a basis for subsequent finite element analysis, which was used to establish the required number of carbon layers. Using the material properties gained from experimental testing in conjunction with the 'Laminator' program (refer section 5.6.6), overall mechanical properties of the 'equivalent' laminates were produced, each with varying quantities of carbon fibre reinforcement. These properties were then substituted into relevant beam equations to ascertain the maximum laminate strain produced in each laminate configuration by a moment of 12 kNm. A constant modulus in compression and tension was assumed for the equivalent laminate, with the neutral axis of the cross member located at the beam centreline. A summary of these calculations is presented in Table 7.6.

Table 7.6 Estimated Strain Values for Various Carbon Quantities

No. of Carbon Layers	Equivalent Modulus (GPa)	% Strain at Max Moment
2	19.6	0.76
3	24.2	0.57
4	26.7	0.48
5	29.5	0.41
6	31.4	0.36

This table clearly shows that a laminate including of four (4) layers of carbon fibre in combination with the double bias reinforcement would produce laminate properties closest to the desired strain value of 0.45%. Hence, it was decided that four (4) layers of 230gsm

carbon fibre reinforcement (in conjunction with the six (6) layers of double bias reinforcement) would be required to produce a cross member of sufficient capacity.

The estimate provided by this basic method formed the basis of the 3-dimensional finite element model of the cross member. This analysis provided a more accurate representation of the laminate, the contribution of each reinforcement type, and the influence of the connection to the chassis rail on the behaviour of the cross member. Details of this analysis, including the final composition of the cross member laminate, are contained in section 7.6.4 and Appendix F.

Determination of an appropriate spacing for the cross members resulted from the observations gained from steel trailer design. Discussion with several transport operators indicated that, apart from accidental damage during loading/unloading, incidence of failure of a cross member was extremely low in comparison to that of chassis rail failure. Time restrictions did not allow an investigation into the effects of cross member spacing on the structural (eg. torsional) performance of the trailer chassis. Hence, based on the experience of those in the transport industry, it was decided that for the purposes of this investigation, the cross member spacing would be set at 650 mm. Given the additional strength provided by the proposed cross members (in comparison with the typical member strength observed by the author), it was assumed that this spacing would provide a chassis of comparable strength with respect to the cross members.

With respect to the basic design of the chassis rail for application to this investigation, a number of factors were considered. The section of chassis rail considered was to replicate a full size chassis rail where possible, in particular with respect to the shear reinforcement. This was necessary in order to accurately determine the effects of the cross member on the sidewalls and points of connection. The depth of the chassis rail section was set at 600mm, which was considered representative of the maximum beam depth. Assuming a medium trailer capacity (refer Table 4.5), and using the methods outlined in section 7.5.3.2, the number of layers of double bias reinforcement required to withstand a static shear force of 70 kN (168 kN including dynamic effects) was found to be nine (9). In addition to this, it was necessary to determine the composition of the laminate on the inner surface of the sidewall. As previously mentioned in section 7.4.5, the stiffness of the laminate on the inner surface should be such that the sidewall is permitted to bow outwards to a small degree. This was achieved by the manipulation of the composition of the inner laminate, such that the neutral axis of the sidewall panel was offset towards the inside of the beam section by approximately 20% of the core thickness. This was performed using the laminate analysis program 'Laminator', and several equations based on fundamental beam theory. The

resulting inner laminate was found to consist of three layers of double bias, in conjunction with two layers of 450 gsm unidirectional E-glass, in the sequence [DB/0/DB/0/DB]. The double bias reinforcement was included in the inner laminate to provide lateral strength to the unidirectional layers, preventing longitudinal splitting. While this effectively increased the shear capacity of the beam, the quantity of shear reinforcement on the outer laminate was not recalculated to include this. Rather, the additional shear capacity provided an increased factor of safety. The floor and ceiling connecting pieces each contained two layers of double bias reinforcement on the inner side, rather than the [DB/0/DB/0/DB] lay up on the sidewall. This produced connecting panels that possessed stiffness' which were less than, but comparable with, that of the sidewalls, as recommended in section 7.4.5. Further details regarding the chassis rail are contained within the following sections.

7.6.3 Connection of Cross Member to Chassis Rail

Having established the cross sectional shape and basic dimensions of the cross members, a method of connection was required to incorporate these members into the chassis structure. As mentioned in the previous section, insertion of the cross members through the chassis rail was necessary in order to minimise the centre of gravity of the payload. While the use of a rigid connection was essential in maintaining torsional rigidity, consideration was also needed with regard to the constraints imposed by a modular construction, and the ease of repair or replacement of the cross members.

As discussed with regard to the chassis rails, the desired mode of failure resulting from the application of excessive load to a single cross member would be compressive collapse of the laminates. This mode presents a low probability of catastrophic failure, with the effects of this failure remaining localised. It was the intention of the design of this connection that failure of a cross member due to overload would be characterised purely by the failure of the cross member, without any significant effects on the chassis rail.

Two primary techniques were considered in attempting to provide a rigid connection between the intersecting members that could be easily removed. The first involved the insertion of a steel sleeve through the chassis rail. Figure 7.32 shows one of the several configurations considered, which would be inserted in the beam in two halves. Adhesive bonding formed the primary method of connection between the sleeve and all adjacent composite material, thereby avoiding the stress concentrations associated with fasteners. The transfer of load to the sidewalls was facilitated by an adhesive shear connection

between the sleeve flanges and the sidewall laminates, in addition to direct compressive bearing of the sleeve on the laminates.

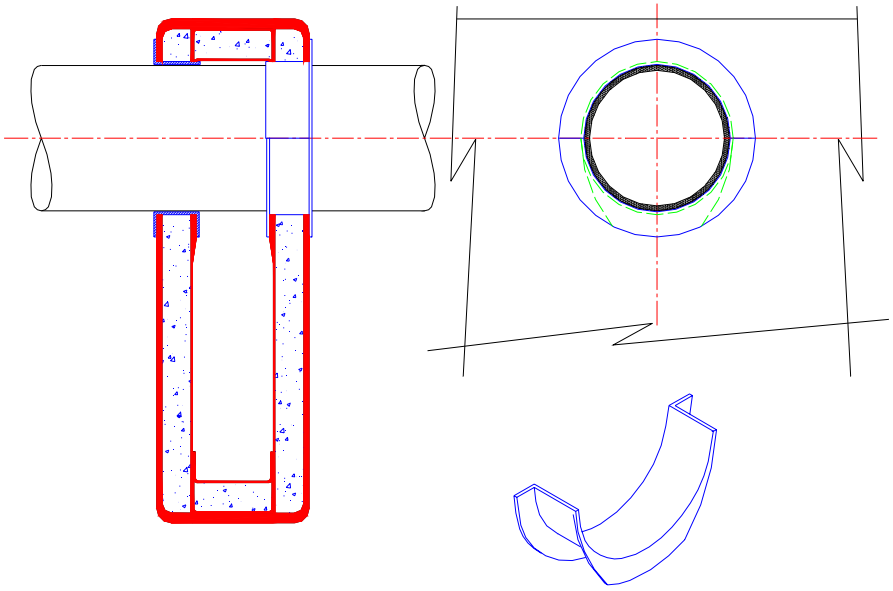

Figure 7.32 Connection of Cross Member to Chassis Rail Using Steel Sleeve

It was anticipated that a flange would be required on each side of the sidewall sandwich panel to avoid the spreading of the laminates resulting from the direct compressive force imposed by the tubular section of the sleeve. The principal difficulty associated with this method of connection involved the large disparity in strain between adjacent steel and composite materials. The intended working strains of the laminates can be as great as 0.45%, which is in excess of four times the working strain for common steels. It was anticipated that the thin adhesive layer separating this large variation in strain would be unable to accommodate such a difference whilst maintaining a rigid connection. Substitution of the steel sleeve for a material able to accommodate these strains, such as polyurethane, again reduces the rigidity of the connection through a combination of the necessary thickness of the sleeve for load distribution and a low shear modulus.

The difficulties associated with the incorporation of a separate sleeve resulted in the adoption of an alternative method of connection. This second technique involved the use of hardpoints within the core of the sidewalls. As illustrated in Figure 7.33, the hardpoints were inserted (in place of the PVC foam core) in the local region surrounding the hole through the chassis rail. The cross member was completely surrounded by the hardpoint at the connection, to ensure a secure bond on both the tension and compression sides of the cross member. The transfer of load to the sidewall laminates would be facilitated through

direct bearing on the hardpoint, which in turn would transfer the load to the laminates via the shear connection between them. An thin epoxy adhesive film would be used to connect the cross member directly to the hard points, thus eliminating the difficulties associated with any strain disparity, in addition to maintaining a rigid connection.

As shown in the figure, an additional section of hardpoint material was inserted between the two sidewalls. This section, having the same profile as that contained with the sidewalls, was included to deter delamination of the inner reinforcement in the same manner as the steel sleeve flanges, in addition to providing a greater bearing surface. It was also necessary to insert the cross member at such a position to minimise the distance between the top surface of the cross member, and the upper flange of the chassis rail. This would reduce the size and weight of spacers that would be required to connect the decking to the cross member, and decrease the depth of the combing rail. This distance was set to 30 mm.

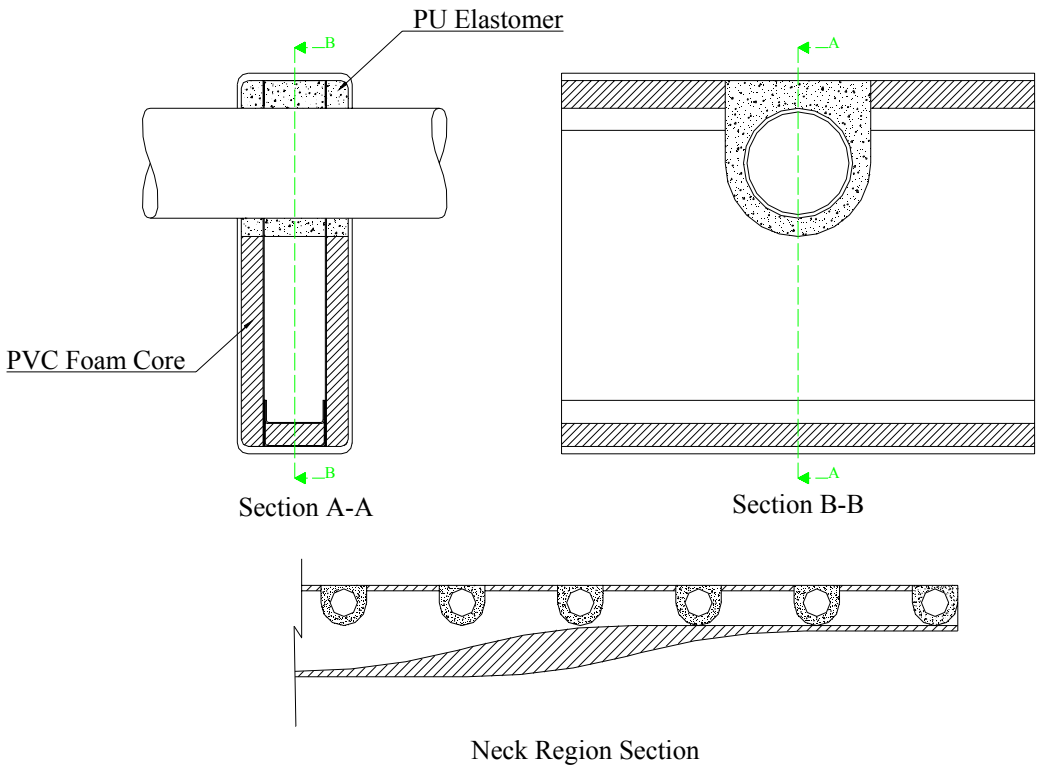

Figure 7.33 Connection of Cross Member to Chassis Rail Using Hardpoints

The unidirectional carbon reinforcement that would be present on a full-scale model on the upper and lower flanges of the chassis rail was not included in this investigation, as the test configuration effectively minimised the bending moment imposed on the section of chassis

rail considered. Rather, four (4) layers of unidirectional E-glass reinforcement (450 gsm) were added to each flange to reduce the tensile/compressive forces imposed on the double bias reinforcement due to the small bending moment imposed by the proposed test configuration. It was assumed that the absence of the quantity of carbon reinforcement which would be present in the actual structure would not adversely affect the interaction and performance of the cross member and the connection with the chassis rail.

The polyurethane elastomer employed in the half-scale chassis rail (section 7.5.3) was also selected for use as the hardpoint material in this region. The high ultimate strain capacity of this material provides compatibility with the proposed working strains. The polyurethane elastomer also possesses a modulus that is sufficiently high to act as a load-bearing surface, whilst also possessing adequate flexibility to ensure even load distribution regardless of surface roughness. Various sizes of the hardpoint were investigated during the finite element analysis to determine a suitable quantity.

The manufacture of the cross members (refer section 7.6.5) required the use of a mandrel to form the tubular section. The use of a tapered, removable mandrel was discarded in favour of the use of a sacrificial mandrel for several reasons. The costs associated with the manufacture of a suitable removable mandrel were far greater than that of the sacrificial mandrel, given that a length of PVC piping of the appropriate diameter was deemed sufficient to form the member. The inclusion of the mandrel in the final product also acted to increase the cross sectional stability of the member, particularly with respect to compressive bucking of the laminate. The weight penalty associated with these mandrels was judged to be acceptable, given the anticipated increase in sectional stability. The role of the mandrel in the member performance is discussed further in section 7.6.6.

7.6.4 Linear Elastic Finite Element Analysis

Numerical analysis using the finite element technique was conducted to determine the characteristic behaviour of the proposed cross member configuration. Linear elastic behaviour was assumed.

The objectives of the analysis are summarised as follows:

- To produce an accurate 3-dimensional model of the proposed cross member model, suitable for detailed finite element analysis
- To investigate the performance of the cross member under load, particularly at ultimate load, and note the predicted failure mode
- To allow the evaluation of the structural characteristics of the model, in particular the interaction between the cross member and the chassis rail, and the effectiveness of the hardpoint in load transference.

The reader is directed to section 7.5.3.3 and Appendix F for details regarding the software and element types used in the finite element analysis.

The analysis considered a discrete portion of the chassis rail, 650 mm in length. This section contained a single cross member, as illustrated in Figures 7.34 and 7.35. Consequently, a shear connection was used to support the model, replicating the reaction loads applied by the adjacent chassis rail. The implementation of this is discussed in the following section. The load was applied over a defined area equivalent to that anticipated in the experimental test, in representation of the worst load case. As shown in Figure F.3, a series of beam elements (of infinite stiffness) were added to the model at the end of the cross member, these being representative of a series of supporting pieces that were inserted into the end of the cross member. Insertion of these diaphragms into the open end of the member was necessary to prevent excessive local distortion, resulting from the application of the concentrated load at the free end. In the context of the actual trailer, the combing rail would fulfil this role (refer section 7.7).

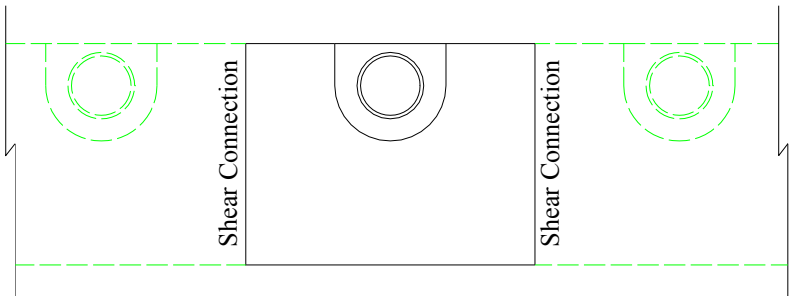

Figure 7.34 Basic Model – Section of Chassis Rail With Cross Member

A load of 21.25 kN was applied to the model, this being equivalent to a total load of 85 kN applied to the entire cross member. The response of the beam to all other load values was interpolated using the linear relationship inherent in the analysis type. No bending moment on the chassis rail was applied to simulate flexure of the member.

In order to preserve accuracy between the analysis and the actual specimen, the laminae contained within the analytical model replicated the lay-up sequences present in the actual beam, these being described in detail in section F.9. It should be noted however, that the analysis software was not capable of accurately determining the effects of changes to the lay-up sequence, particularly with respect to the confining effects of wrapping the double bias around the beam in a single piece.

In order to reduce the number of elements and decrease the solve time, one quarter of the specimen was modelled using symmetry conditions. Perfectly elastic material characteristics were assumed, and plastic deformation was not considered. The general dimensions and element mesh produced for each analysis are illustrated in Appendix F.

The analysis considered two differing sizes of the hardpoint. An initial analysis investigated the effects of a 50 mm thick 'collar' surrounding the cross member, with a second iteration investigating a collar thickness of 25 mm. As discussed in section 7.6.6, the 25 mm collar thickness proved to be satisfactory in maintaining a low level of stress in the PVC core. The laminate sequences as prescribed by the hand calculations (refer section 7.6.2) were used as initial estimates in the analysis, and were shown to adequately sustain the imposed loading. These reinforcement quantities were therefore adopted for construction. Further discussion of the analysis results is contained in section 7.6.6.

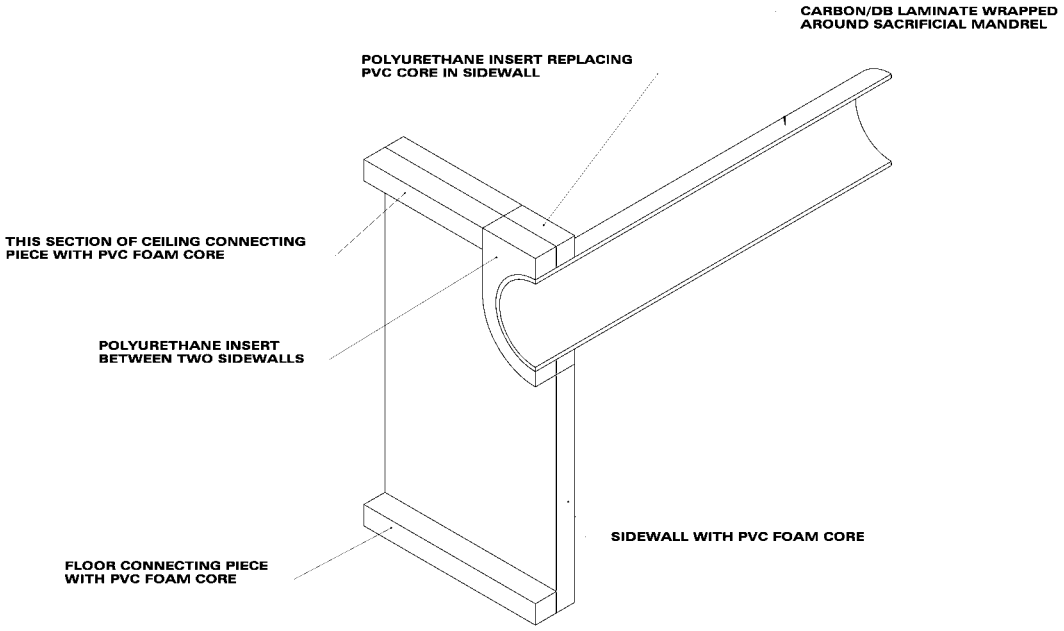

Figure 7.35 Core Material Layout of Cross Member Specimen – Quarter Model

7.6.5 Fabrication and Experimentation

The process of beam manufacture, illustrated in Appendix F, is described in an abbreviated form in this section. As previously mentioned, a combination of H200 PVC foam and a polyurethane elastomer were used as core materials, the configuration of which was illustrated in Figure 7.35 (and also in greater detail in Figures F.5 (a), (b), F.12 and F.13).

Unidirectional carbon and double bias E-glass reinforcements were used in the construction of the cross member as previously noted, with double bias and unidirectional E-glass reinforcement being utilised in the construction of the chassis rail section. It was assumed that the reinforcement and matrix types used in this test specimen possessed identical mechanical properties as those tested in Chapter 5. The hand lay-up technique (refer Chapter 2) was used throughout the beam manufacture. The construction of the beam cross section was carried out as follows:

1. A section of PVC piping, the sacrificial mandrel for the cross member, was cut to the appropriate length, and the surface cleaned.
2. Double bias E-glass and unidirectional carbon reinforcement was laminated to the pipe, in accordance with the sequence $[DB/0_{carbon}/DB/0_{carbon}/DB]_s$. The laminate was then covered in peel ply to aid in affixing of strain gauges, and the bonding of the cross member to the chassis rail.

Construction of the chassis rail section was essentially identical to that described in section 7.4.4, apart from the inclusion of the hardpoints. The variations from the procedure listed in the aforementioned section are as follows:

3. Prior to the lamination of the reinforcement onto each side of the sidewalls, a section of the PVC foam core material was removed to accommodate the hardpoint.
4. Three castings of polyurethane elastomer were produced, each containing the basic shape of the proposed hardpoint profile. An undersized hole was preformed in each casting to reduce material wastage. Once cured at room temperature for a period of 24 hours, the castings were post cured at 80° C for 16 hours. Each casting was then sanded to shape.
5. The sidewall hardpoints were inserted into the slot cut into the PVC core, and adhesively bonded using epoxy adhesive.
6. Following the atmospheric cure of the adhesive, the reinforcement was laminated to each side of the sidewalls.
7. Subsequent to the manufacture of the floor and ceiling connecting panels, the ceiling panel was divided into two parts. These panels, along with the remaining hardpoint casting, were adhesively bonded to one sidewall, as illustrated in Figure F.5 (a).
8. After allowing the adhesive to cure, the second sidewall was bonded to the specimen, as shown in Figure F.5 (b), and allowed to cure at room temperature.
9. Using a milling machine, a hole was cut through the chassis rail, concentric with the preformed holes produced in the castings. The hole was sized to provide approximately 0.75±0.25 mm of clearance, to allow penetration of the adhesive and insertion of the cross member without difficulty. The shear reinforcement was then trimmed from around the edge of the hole, to ensure that the load from the cross member was transferred to the hardpoint, rather than to the laminate. This would prevent any tendency of the outer sidewall reinforcement to delaminate at the free edge.
10. The cross member was then inserted through the chassis rail, and an epoxy adhesive was injected into the space between the two members. Care was taken in ensuring full penetration of the adhesive, and a minimum of air entrapment. The cross member was supported such that it remained concentric with the hole through the chassis rail, with an even spacing around the perimeter.

Subsequent to manufacture, the specimen was bonded to two steel supports, as illustrated in Figure F.6. Each of these supports comprised two C-section steel pieces, which were

bonded to each surface of the sidewalls using epoxy adhesive. The shear connection provided by the adhesive was representative of the shear connection between the sidewall laminates and the adjoining sections of chassis rail. It was noted that while this arrangement did provide an adequate shear connection (with an overlap length of 50 mm), it did provide a level of buckling restraint to the sidewalls that would not be present in reality. However, it was assumed that the presence of the hardpoint between the sidewalls would provide a level of buckling restraint, which would negate any effect provided by the supports. Two pieces of square hollow section (SHS) steel were also welded to the C-section pieces, and transferred the load to the ground. In this way, the shear connection provided by the bonding of the sidewalls represented the only load path from the specimen to the ground.

As illustrated in Figure F.8, timber platens in the shape of the cross member were used to distribute the load across the upper side of the member. It was envisaged that the spacers required between the cross members and the decking would adopt a similar form to the platen used in this test. Rubber matting was placed between the timber and the cross member, and a steel plate placed atop the platen to distribute the line load imposed by the loading beam (refer Figure F.8). The loading beam was pivoted at the midspan to ensure an even load distribution between each side.

A number of unidirectional strain gauges were attached to the beam to provide an indication of the strains present within the cross member. Two gauges were placed on the underside of the cross member, in close proximity to the point of connection, as shown in Figure F.7 (a). The purpose of the gauge attached to the chassis rail was to record the level of compressive strain imposed on the shear reinforcement by the cross member. A gauge was also placed at the top of each side of the cross member, as illustrated in Figure F.7 (b), to record the tensile strain within the cross member laminate. Two tensile gauges, one on each side of the member, were employed to ensure a symmetrical load distribution. It was assumed that an identical reading from the two tensile gauges would necessitate symmetry with respect to load and compressive strain.

The specimen was placed beneath an Instron testing machine (refer Figure 7.36), and loaded at a rate of 5 mm per minute (the minimum load rate available). In addition to the strain measured by the aforementioned gauges, deflection of the cross member (beneath the load point) and the magnitude of the applied load were also recorded throughout the duration of the test at intervals of 0.10s.

Figure 7.36 Completed Specimen Subjected to Loading

7.6.6 Results and Discussion

a) Analysis Results

Analysis of the section of chassis rail and corresponding cross member yielded a number of significant results with respect to the behaviour of the cross member under load, and the interaction between the cross member and chassis rail. The laminates suggested by the hand calculations were used in this analysis.

As shown in Figure 7.37 (and also in Figure F.4 (b)), the maximum strain in the cross member laminate occurred in the compressive and tensile laminates at the point of intersection between the two members. A stress concentration at the point of connection was observed, this being primarily as a result of a large change in the effective stiffness of the cross member. The magnitude of the stress in this region was also affected by the assumption of a perfectly rigid connection created within the model.

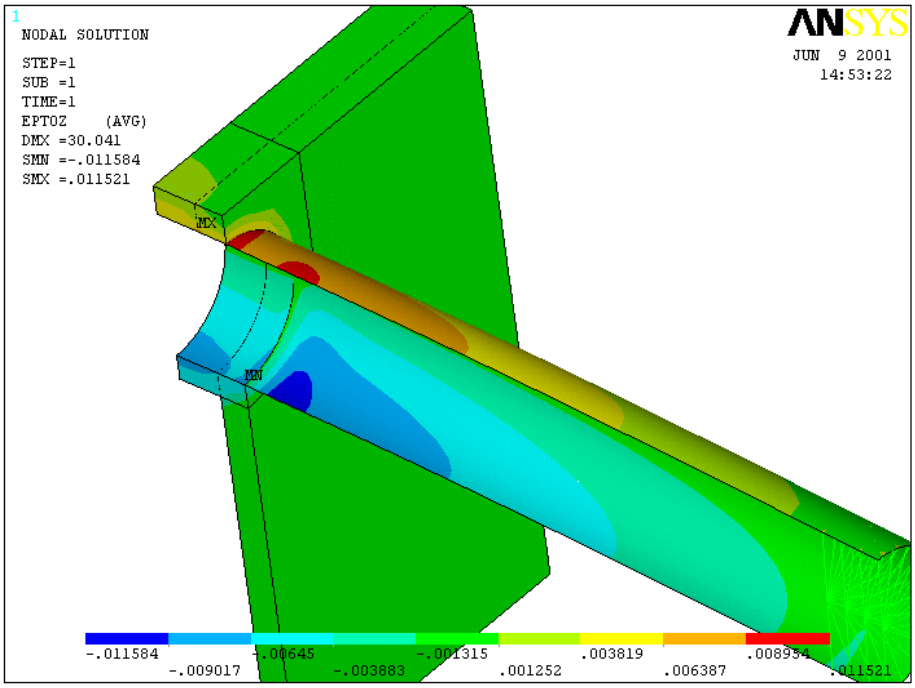

Figure 7.37 Laminate Strain in Axial Direction of Cross Member

Assuming that the magnitude of the stress predicted by the model in this region was significantly influenced by the rigidity of the connection, the respective regions of concentrated stress were neglected in the assessment of the required number of unidirectional carbon layers first predicted by the hand calculations. It was therefore found that the 1st principal strain in the cross member laminates adjacent to the region of stress concentration resulting from the applied load of 85 kN was found to be 1.02%. Using linear interpolation, a strain of 0.9% was found to correspond with a total applied load of 75 kN, or a load of 37.5 kN on each side of the cross member. This was in close agreement with the desired structural characteristics defined in section 7.6.2, which specified a maximum strain of 0.9 % corresponding to a load of 37 kN. This agreement would therefore appear to validate the method of hand calculation used to determine the required quantities of unidirectional reinforcement. The shear reinforcement previously specified was also shown to be adequate for this load, as indicated by the principal stress calculated within the double bias laminates. The laminates recommended by the hand calculations, being validated by the analysis, were therefore adopted as suitable for construction (refer section 7.6.5).

As previously mentioned, two variations were analysed with respect to the collar thickness of the hardpoint surrounding the cross member. An initial model used a collar thickness of 50 mm, however as shown in Figure 7.38, the stresses produced within the second model (with a 25 mm collar) are less than 50% of the ultimate strength of the material whilst

including the effects of the stress concentration. Figure F.4 (d) also shows that a 25 mm collar is effective in maintaining an acceptable level of stress within the PVC foam core.

Whilst further manipulation of the collar thickness could have been performed in order to minimise material usage and chassis mass, it was decided that a collar thickness of 25 mm would be sufficiently large so as to be unaffected by any misalignment or oversize drilling of the hole.

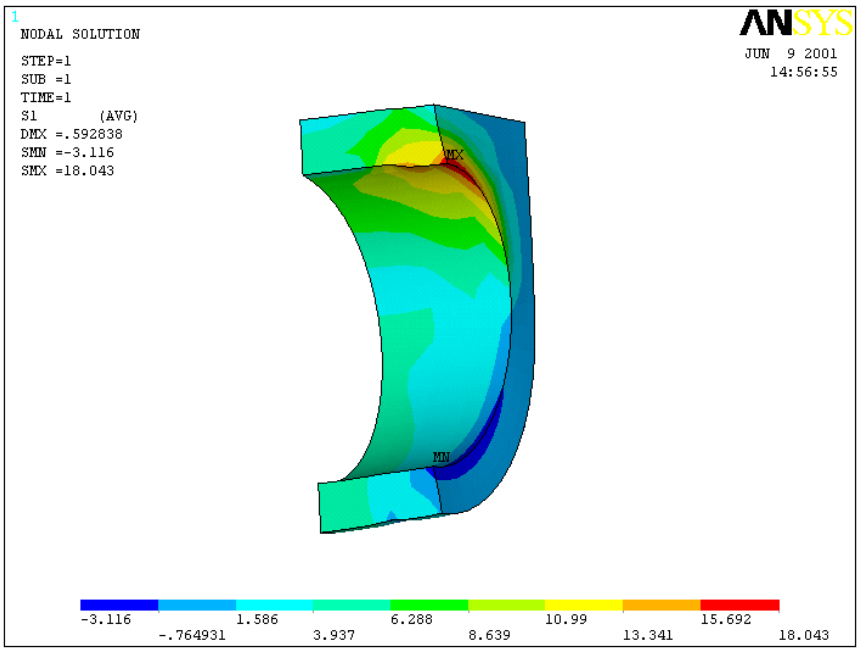

Figure 7.38 1st Principal Stress in PU Hardpoint

b) Experimental Results

The results gained from the test data yielded a linear load-displacement relationship as shown in Figures F.14 (a) through (d). Minor cracking was audible immediately preceding ultimate failure, which occurred at a load of 92 kN. This occurred as a result of collapse of the compressive reinforcement at the underside of the connection between the cross member and the chassis rail, as shown in Figure 7.39. The failure was observed to be non-catastrophic which, as previously stated, represented one of the fundamental requirements of a suitable member. Figure F.10 shows the failed member beneath the loading beam.

The maximum strain recorded prior to failure was approximately 11760 με, which was observed on the tensile laminate. Each of the tensile gauges yielded readings within 2.5% of each other, verifying the assumption of an even load distribution. The maximum

compressive strain recorded prior to failure was 10951 με. This value is significantly higher than the maximum compressive strain recorded during testing of the mechanical properties of the carbon reinforcement (refer section 5.6.6), however this can be accounted for through consideration of the difficulties mentioned in section 5.6.6 regarding specimen buckling. The presence of the PVC mandrel, in conjunction with the confining effects provided by the double bias reinforcement, would appear to have provided the additional restraint required to prevent the buckling observed during the testing of the pure carbon specimens, thereby effectively increasing the compressive capacity of the carbon reinforcement.

Subsequent to the failure of the member, the chassis rail was inspected for signs of damage. As previously discussed, it was intended that the chassis rail would not incur any damage as a result of the failure of the cross member. This inspection revealed no indications of damage to any point on the chassis rail section, demonstrating the successful nature of the proposed configuration, and providing initial validation to the analysis results, which indicated that the stresses within the core materials were well below ultimate capacity. Assuming an absence of any damage to the chassis rail in the event of an actual failure on any given trailer, replacement of the respective cross member would be therefore enabled by cutting the remaining pieces of the cross member from each of the chassis rails, and bonding a new member in its place.

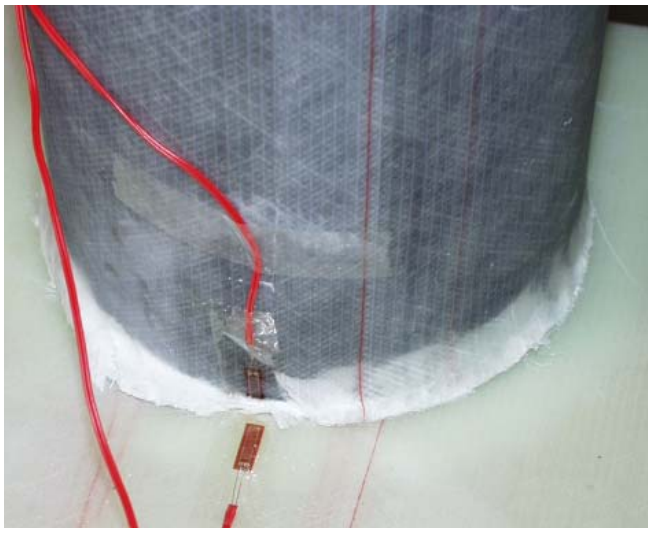

Figure 7.39 Compressive Failure of Cross Member Laminate

c) Comparison of Results

The comparison between the strains predicted by the finite element analysis and those measured by the strain gauges on the test beam yielded favourable results in most cases. As shown in Figure 7.40 (and in Figures F.14 (b) and (d)), the laminate strains calculated by the analysis at the points corresponding to the gauge placement were extremely accurate, with the maximum relative error remaining below 5% in all cases.

With respect to the third gauge which was placed on the double bias reinforcement on the chassis rail directly beneath the cross member (refer Figure F.7 (a)), the analysis predicted a linear increase in the compressive strain experienced by the shear laminate in this region. However, the experimental results indicated that very low levels of load were experienced by this laminate throughout the test, as indicated by Figure 7.41. This discrepancy can be explained by the assumptions made during the definition of the finite element model. As noted in section 7.6.5, care was taken during manufacture to ensure that the shear reinforcement was trimmed from around the edge of the hole, to ensure that the load from the cross member was transferred to the hardpoint, rather than to the laminate. The analytical model employed in this investigation did not possess sufficient complexity to incorporate this connection detail. Consequently, the rigid connection between the cross member and the shear reinforcement within the model induced compressive strains which were not present in the test specimen. The trimming of the shear reinforcement did demonstrate the effectiveness of this in reducing the probability of delamination of the free edge, instead introducing the compressive load through the shear connection with the hardpoint. The slight tensile strains imposed on the shear laminate at loads greater than 60 kN would suggest that some rotation of the side wall occurred in the local region in response to the compressive forces applied perpendicular to the sidewall plane, thereby applying a tensile strain to the outer laminate.

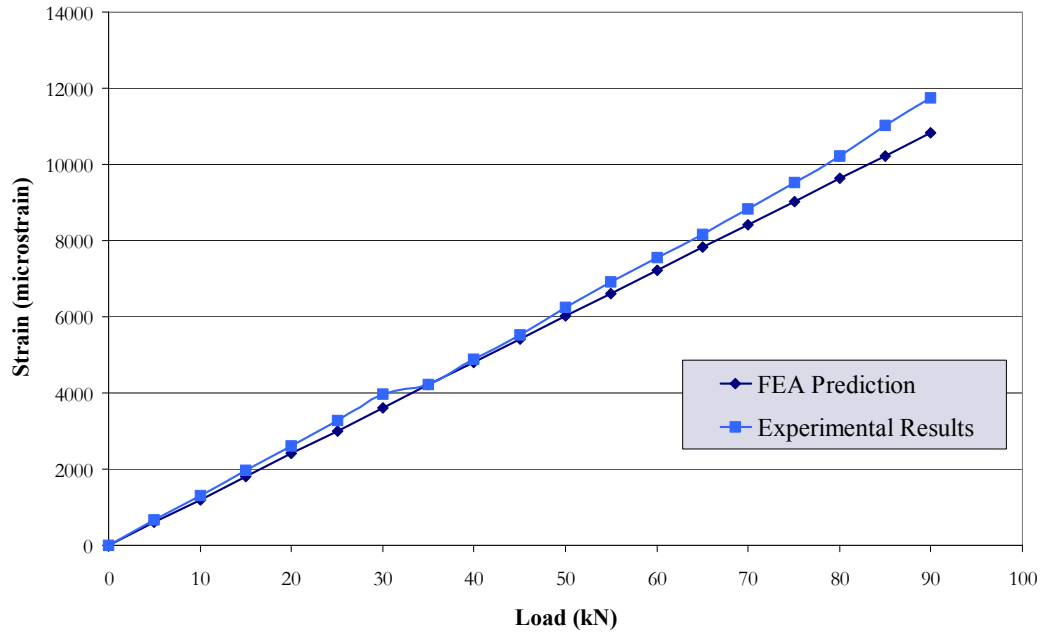

Figure 7.40 Plot of Predicted and Actual Strain at Gauge One (Tensile)

It would appear from Figure F.14 (d) that both the analytical model successfully replicated the beam behaviour with respect to the contribution of the mandrel and double bias reinforcement to the cross member stiffness. The accuracy of the analysis also further validates the incorporation of the mechanical properties taken from the laminate testing described in Chapter 5.

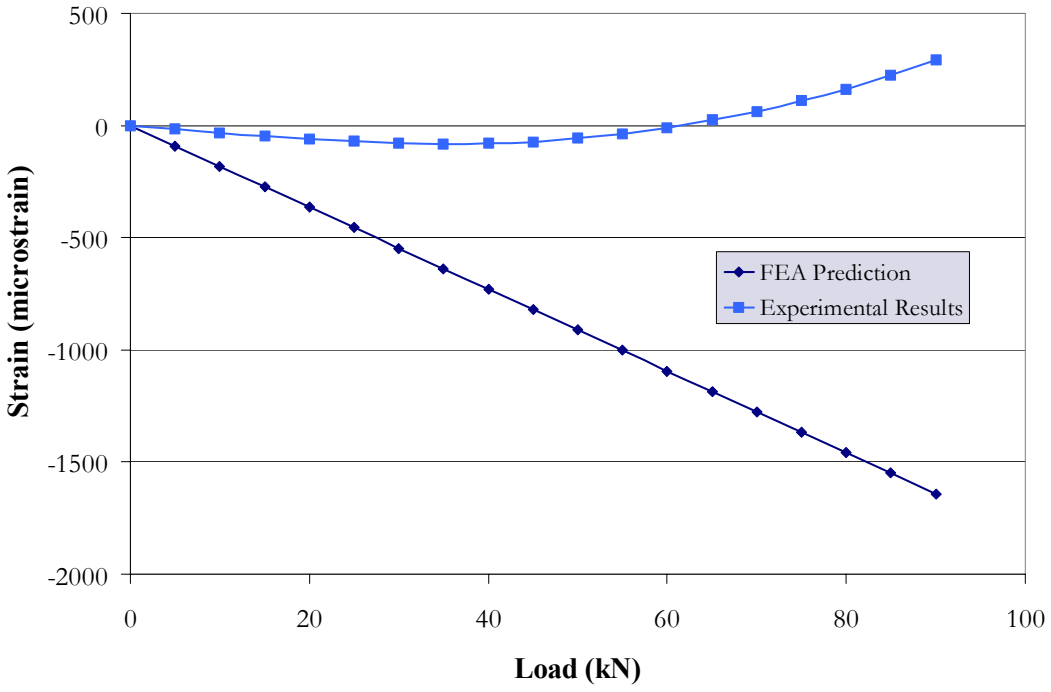

Figure 7.41 Plot of Predicted and Actual Strain at Gauge Three (Compression of Sidewall Shear Laminate)

7.6.7 Conclusions

The investigation described within this section was undertaken in order to address the design of a cross member, suitable for incorporation into the ladder frame chassis of the FRP trailer. The connection of the cross member to the chassis rails was also addressed, using a combination of finite element analysis and experimental techniques.

A preliminary design method for use in the determination of appropriate quantities of reinforcement was demonstrated within this section. The influence of strength, rather than deflection, was shown to be the predominant constraint with respect to criteria suitable for cross member design. The hand calculations were intended to be purely indicative with respect to cross member design, with verification through finite element analysis being recommended in all cases. The use of accurate material data was necessary in order to obtain reliable results with respect to the finite element analysis.

The quantities of reinforcement recommended by the hand calculations were shown to be reliable by the finite element analysis, and were adopted for use in the test specimen. A full-scale specimen, comprising a section of the chassis rail and a single cross member, was constructed and experimentally tested. A direct comparison of the analytical and experimental results yielded an excellent correlation, with failure occurring in the compressive laminate of the cross member at the point of connection. Measurements taken from strain gauges fixed to the specimen verified the accuracy of the model. A discrepancy was noted between the predicted and measured compressive strain imposed on the shear reinforcement directly beneath the cross member, however this incongruity resulted from a simplifying assumption made in the analytical model.

The failure mode observed in the test was non-catastrophic, with no damage being present on the chassis rail section as a result of the cross member failure. The compressive strain at failure was observed to be significantly higher than that which was measured during material testing, as the double bias reinforcement, in conjunction with the sacrificial mandrel, acted to prevent the premature buckling of the carbon unidirectional reinforcement that was noted during the material testing.

The significance of the connection of the cross members to the chassis rails was also subjected to a preliminary investigation. Direct transference of the compressive load from the cross member to the hardpoint was shown to effectively minimise the probability of delamination of the free edge of the shear reinforcement, with the use of a thin adhesive bond being selected to provide a rigid connection which was suited to the modular approach initially specified.

7.7 Connection of Ancillary Attachments

As previously mentioned in section 6.9, a number of failure modes were introduced addressing the attachment of ancillaries to the chassis rail. Specifically, modes 18 through 20 focused on the use and possible failure of mechanical fasteners, and the connection of items such as the kingpin, standing legs and suspension system to the chassis rail. It was envisaged that such failure would be most likely to occur as a result of emergency braking, or in the case of the standing legs, an overloaded trailer (disengaged from the prime mover) parked on uneven ground for extended periods. As stated in section 6.9, an investigation into these areas did not form part of this thesis. However, the sponsors to this project, Wagners Pty Ltd, had begun an initial investigation into the attachment of ancillaries to the proposed chassis rail. The engineer responsible for this, Mr. Peter Girgenti, completed a test involving the static and dynamic loading of a single bolt, inserted through a full-scale section of chassis rail [5]. The applied loads replicated the design loads required by the relevant Australian Standards.

Figure 7.42 Dynamic Test of Bolt Through Chassis Rail

Initial results from both the static and dynamic tests indicated that the proposed method of attachment would provide reliable service, with a static capacity greater than four times that required by the relevant Australian Standards. Further work is ongoing, particularly in relation to the design of the necessary form of the modifications required to standard ancillary components.

In addition to the attachment of major ancillary components such as those mentioned above, the design and connection of a suitable combing rail to protect and support the free ends of the cross members was also undertaken by Mr. Peter Girgenti on behalf of Wagners Pty Ltd. Several prototype rails were designed, constructed and tested to evaluate their damage tolerance and strength. Each prototype comprised all composite construction, with varying materials being substituted as protective layers in various configurations [5].

Preliminary results indicated that the use of a polyethylene coating provided the greatest resistance to the damage imposed by the tines of a forklift, the typical source of combing rail damage. Each combing rail also incorporated a means of supporting the free end section of the cross member, such that the cross sectional distortion resulting from concentrated loads (refer mode 33 - section 6.9.3 and section 7.6.4) was minimised.

Figure 7.43 Prototype Combing Rail Prepared for Collision Test

A number of other items not investigated by the author, including FRP decking and side gates are also currently under examination by Wagners Pty Ltd, with the primary focus remaining the reduction of tare mass.

7.8 Durability

This section briefly describes a number of issues relating to the durability of the proposed FRP trailer, and the highlighting of the differences present between an FRP and steel trailer with respect to maintenance. While no testing or analysis was performed by the author in relation to the implementation of protective measures, a number of issues are noted here for further consideration.

One of the primary concerns raised by many in the transportation industry is the issue of durability as it relates to the performance of the FRP trailer. It would appear that the consensus of operators remain sceptical at the prospect of a trailer without any form of protective steel framing. However, a distinction must be made between the significance of the impacts imposed on the chassis, and those imposed on the deck or combing rails. This distinction is based on the relative magnitude, frequency, and implications of the impact incidents.

With respect to the individual sections of decking or combing rail, the magnitude of the expected impact loading is sufficiently high to initiate failure of a single component. While the correct selection of laminate type in addition to the use of appropriate protective coverings will reduce the extent of the damage, the complete prevention of all damage is not economically feasible. Indeed, significant damage often occurs to the decking and combing rails of steel trailers, necessitating repair or replacement of various items subjected to impact damage. Therefore, the anticipation of periodic failure and replacement of these items suggests the use of less expensive (and possibly slightly less durable) materials, thereby reducing the economic significance of incidences of failure.

The notion of periodic failure should be kept within the greater context however, as the effects of the impact loading imposed on the deck and combing rails is not generally substantial in relation to the performance of the trailer, as a localised failure of the decking or a section of combing rail does not impede the ability of the trailer to operate effectively to any great degree.

By contrast, typical incidents of impact imposed on the chassis rails are of low magnitude, and of high frequency, resulting from the impact of road debris thrown from the tyres of the prime mover. The continual and abrasive nature of these incidents would suggest that protective coatings or shields should be employed in the exposed regions to eliminate the erosion of the laminates. Unlike damage sustained by the decking and combing rails, the

prevention of laminate abrasion is particularly significant with respect to the overall performance of the trailer, as the regions more commonly affected include the tensile reinforcement on the underside of the chassis rails in the neck region. Degradation of these laminates would greatly increase the probability of catastrophic tensile rupture of the laminate. In addition to the incorporation of protective coatings, the use of stacking sequences that increase the impact tolerance of a laminate would also be recommended.

With respect to the impact of another vehicle on the trailer, or the overturning of the trailer in the instance of a motor vehicle accident, it is envisaged that no reasonable level of protection would prevent a significant amount of damage being inflicted on the chassis of the trailer. However, such is also the case with steel trailers. Hence, although the cost of repair to the FRP trailer may then be greater than that of a steel trailer, the economic benefits associated with the reduced tare mass should negate this difference.

In response to the concerns raised by the industry operators, it should be noted that the primary objective of this trailer type is the reduction of tare mass, which implies the use of lightweight components that would not typically possess the durability of steel. Hence, these items should possess a level of durability that is balanced by the economic benefits associated with the use of lightweight materials. The adoption of new practices by operators in response to this would also assist in minimising the occurrence of accidental damage.

7.9 Conclusions

This chapter outlined the process used to apply various aspects of the design philosophy to the chassis of the FRP trailer. A number of the failure modes raised in the previous chapter were addressed, with emphasis given to the structural behaviour and performance of the chassis rails and cross members.

The structural capacity and design of two steel trailers of equal nominal capacity were investigated, using finite element analysis to determine the regions of highest stress. These results were also used to provide a comparative analysis of the two configurations. It was shown that the design of the neck region, the primary difference between the two trailers, imposed the greatest influence on the actual capacity of the chassis rails.

The cross sectional composition of the proposed FRP chassis rails was also presented, with attention given to the performance of the section under direct compressive loading. Several factors were identified as being the primary contributors to the crushing capacity of the section, with a full-scale section of the chassis rail being constructed and tested to provide verification to the finite element analysis. The profile of the proposed chassis rail was also developed, this being governed by the reduction of material costs and the centre of gravity of the payload.

In light of the results gained from the examination of steel chassis rails, a significant investigation was undertaken into the performance of the neck region of the proposed FRP chassis rail when subjected to bending. A series of small-scale beam were produced in order to ascertain the effects of various factors on the transfer of load through the neck section. A number of recommendations were produced from these tests, most notably the introduction of continuing reinforcement on the inner floor of the floor panel. A section of a half-scale chassis rail was then designed, manufactured and tested, which incorporated each of the recommendations provided by the small-scale specimens. This chassis rail was shown to perform exceptionally well, with the finite element analysis accurately predicting the beam behaviour. The mode of failure was shown to be non-catastrophic, and was not in the region of the neck section.

The design process used to determine the shape and composition of a cross member suitable for incorporation into the ladder frame chassis of the FRP trailer was also presented. The connection of the cross member to the chassis rails was addressed, using a combination of finite element analysis and experimental techniques. A full-scale specimen

incorporating a section of chassis rail connected to a cross member, was produced and tested to provide validation to the analysis. Failure of the cross member was non-catastrophic, with the compressive collapse of the cross member laminate occurring without any damage to the chassis rail. The incorporation of hardpoints into the core of the chassis rail was shown to be necessary to effectively transfer load into the sidewalls. Additionally, it was shown that the free ends of the cross member required the incorporation of internal support to prevent excessive local deformation due to concentrated loads. The modular approach to chassis construction was shown to be feasible, reducing the potential costs associated with repairs and maintenance of the chassis.

While the investigation of the various aspects of the chassis discussed within this chapter has been essentially fundamental in nature, it has aptly demonstrated the potential and feasibility of an FRP chassis suitable for a flatbed semi-trailer. This work also provides a foundation for further work, including the optimisation of the members to further reduce tare mass.

References

[1] Van Erp GM, Ayers SR, Simpson PE. Design of fibre composite structures in a civil engineering environment. Proceedings of the ACUN-2 International Composites Conference; Volume 1; 2000 Feb 14-18; UNSW, Sydney, Australia.

[2] McFarlane S. Personal communication. Melbourne: Roaduser International; 2000 October 2.

[3] Ayers SR, Van Erp GM. Development of a new structural core material for composites in civil engineering. Proceedings of the 16th Australasian Conference on the Mechanics of Structures and Materials; 1999 Dec 8-10; UNSW, Sydney, Australia.

[4] Charlton TM. Model analysis of plane structures. London: Pergamon Press Ltd; 1966: 14-16.

[5] Girgenti P. Testing of Fibre Composite Components for Semi-trailers. Unpublished internal report. Toowoomba, Queensland: University of Southern Queensland; 2000.

Chapter 8 An Investigation into the Fatigue Performance of an FRP Chassis Rail

8.1 Introduction

The assessment of the fatigue performance forms an integral part in the design process of any structure subjected to dynamic, long-term loading. The influence of fatigue with respect to heavy vehicles is significant. In particular, chassis flexure resulting from the dynamic response of the suspension to road irregularities imposes constant variations in stress on the chassis rails. Hence, inadequate consideration of the effects of fatigue can result in premature failure of the trailer. As demonstrated in section 4.4.1, fatigue failure in steel trailers often occurs as a consequence of poor detail design, and the presence of stress concentrations that initiate fatigue cracks.

The varied characteristics of fatigue damage observed in FRPs, depending on the constituents, emphasises the significance of proper consideration of FRP fatigue life. While fatigue cracks in steel can generally be repaired or the section replaced with comparatively little effort, fatigue damage in FRPs manifests itself in delamination and micro cracking throughout the full thickness of the laminate. As these forms of damage present a host of difficulties with respect to repair, the reduction or elimination of fatigue damage is of paramount importance.

This chapter addresses the role of fatigue in the design philosophy of an FRP trailer chassis, as presented in Chapter 4. Specifically, a number of parameters are defined with respect to the dynamic loading conditions imposed on a trailer, resulting in a proposed representative dynamic loading regime. Further, the fatigue testing associated with the derived load regime is described, with the implications of the results being applied to the design philosophy as set out in Chapter 4.

It should be noted that this investigation into fatigue performance was limited in its scope, primarily due to economic and time restrictions. Consequently, this chapter provides a broad insight into the fatigue performance of the proposed FRP chassis rail, with the anticipation that this would form the foundation for further research into this area, particularly with respect to the neck region and the connection of the cross members to the chassis rail.

8.2 Considerations of the Measurement of Fatigue Performance in FRPs

The use of FRP materials in fatigue applications presents a number of challenges, which must be considered when selecting the appropriate reinforcement and matrix. While the fatigue performance of commonly used steels is, in general, sufficiently documented to give reliable performance in service, the variability present in FRP laminates prevents the establishment of similarly applicable fatigue data. However, a significant volume of research into the fatigue of FRPs has been performed, in an attempt to more accurately quantify the performance of various reinforcement/matrix combinations, thereby providing indicative values to aid in the design process. Despite this, the definition of singular or general fatigue capacity for fibre composite materials is not realistic, as the variable and individualistic nature of FRP laminates produces fatigue characteristics which are equally as diverse as the static mechanical properties.

Perhaps the most direct and accurate approach is found in the actual testing of the material or structure in question, at either an elemental level utilising material testing, or at a structural level by using specimens representative of the actual structure. However, significant effort and expense is often associated with this type of testing, particularly if several configurations are to be compared. Additionally, this form of testing is extremely narrow in its application, as the results gained from the testing of a particular matrix/reinforcement combination are specific only to that particular combination of matrix and reinforcement in a given laminate stacking sequence.

In response to the difficulties associated with the prediction of fatigue performance based purely on empirical data, a substantial amount of research has been conducted into the formulation of analytical models. A large number of life prediction methods have been suggested for composite materials. These include energy criteria [2], cumulative damage [3], the derivation of fatigue modulus [4], residual strength [5] and modulus degradation [6,7], in addition to many other variations. However, a survey of this literature indicates that these models are semi-empirical, requiring varying quantities of experimental data to calculate particular parameters. While the quantity of experimental data is significantly less than that required in purely empirical approaches, the quantity of data required to produce reliable correlation is significant. For example, the strength based wear out model presented by Schaff and Davidson [1] requires that a minimum of ninety (90) specimens of various types and configurations be statically and dynamically tested to produce sufficient data for the proposed analytical model. Bond [8], in his summary of various fatigue

models, implies that the volume of testing required by the model presented in [1] is low in comparison to that required by other semi-empirical models. Such a quantity of testing lay outside the economic and time constraints present in this investigation, and therefore no attempt was made to procure data suitable for use in an analytical model.

In response to the high level of empirical data demanded by analytical models, and the non-transferable and unique nature of the mechanical properties of a given laminate and material combination, an alternative approach was adopted. The focus of this investigation was subsequently directed toward the preliminary quantification of the fatigue performance of the proposed materials, achieved solely through experimental testing. By utilising a limited number of specimens, subjected to the maximum load cases, it was anticipated that the influence of fatigue on the limiting constraints within the design philosophy would become evident.

The following section describes in detail the process used to determine the suitability of the proposed materials in relation to fatigue performance.

8.3 Elemental Fatigue Testing

8.3.1 Introduction

Evaluation of the fatigue capacity of the proposed materials was necessary to provide data which was relevant to the specific type and combination of the materials proposed for use in the FRP trailer chassis. Just as a series of static tests were performed on small specimens to determine the mechanical properties of the constituents (refer Chapter 5), a series of small test specimens were produced in order to provide a elementary level of confidence in the ability of the material to withstand the fatigue loading imposed upon it, prior to the design and construction of any large-scale test pieces.

This section describes the series of tests carried out to determine the response of the selected materials to fatigue loading. In order to remain within the financial and time restraints present, it was necessary to utilise small sample sizes exposed to extreme loading conditions. It should be noted that while these tests provide data relevant to the performance of the materials, no implications as to the structural soundness of the proposed beam configuration should be made. The fatigue performance of these materials in the context of a beam comprising the proposed configuration is considered in section 8.4.

8.3.2 Specimen Design

The available equipment determined the nature of the elemental fatigue testing. An 'Avery' fatigue machine was used, which was capable of producing a pure moment of the same or alternating sign to a dog bone specimen at a constant frequency. The magnitude of the moment was controlled by the user, with measurement of the moment being accomplished through use of calibration tables, a torsion bar and dial gauges.

The use of this apparatus necessitated the adoption of a specific specimen size and shape, as required by the machine operating manual. As shown in Figure 8.1, this comprised a dogbone shape, with a maximum thickness of ½".

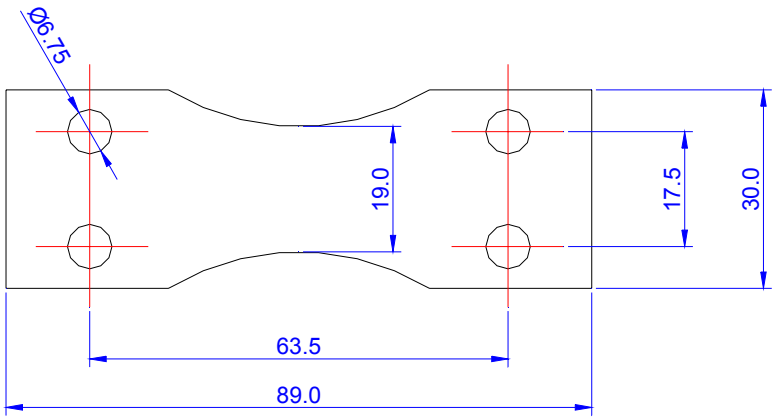

Figure 8.1 Nominal Dimensions of Dogbone Fatigue Specimens (in mm)

In order to reduce the testing time and more accurately replicate in-service conditions, it was decided that fully reversed loading conditions would not be adopted. Rather, a loading sequence was adopted which applied constant tension-tension loading to the upper face, whilst simultaneously applying compression-compression loading to the lower face. Figure 8.2 illustrates the strain imposed on the upper face. An identical loading sequence (of opposite sign) was applied to the lower face. It was assumed that the presence of the payload on the trailer would act to maintain a compressive load on the upper flange and a tensile load on the lower flange of the chassis rail at all times. It was also assumed that the dynamic 'bounce' simulated by this test did not allow a momentary release or reduction in the initial static strain imposed by the payload. Hence, the minimum applied strain was equal to that experienced by the chassis rails under a static load. The loading regime depicted in Figure 8.2 represents the application of the greatest dynamic load factor (2.5 – refer section 4.4.4) to a trailer, which has been overloaded by approximately 10%.

A number of specimen types were considered, each with varying compositions of core materials and reinforcement. The first set was comprised purely of the PFR mixture first considered as a core material (refer section 5.2). These specimens were produced in order to verify the previous assumptions made regarding the fatigue characteristics of this material. Minimal design was necessary with regard to these specimens, due to the low moment capacity of this material. Using the dimensions prescribed in Figure 8.1, and a specimen thickness of 12 mm, the applied moment on the testing apparatus was adjusted to induce the required strains on the specimen.

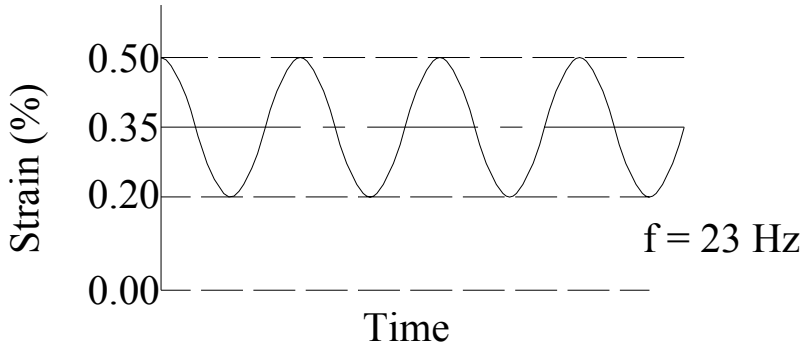

Figure 8.2 Loading Regime for Dogbone Specimens (Tensile Side of Specimen)

The second set comprised a sandwich panel consisting of a section of H200 PVC foam core, in combination with a single layer of carbon unidirectional reinforcement (230 gsm) and double bias E-glass reinforcement (600 gsm) on each side, set in epoxy resin. As these materials were proposed for use in the chassis rail, it was first necessary to test this combination of materials in an elementary context, prior to application in the full beam section. Using the dimensions prescribed in Figure 8.1, the PVC core thickness was adjusted to 8 mm to provide a total specimen thickness of 10 mm. It was not possible to increase the thickness of the PVC foam core in the specimen, due to the limited moment capacity of the testing apparatus. The lay-up chosen for this specimen was $[DB/0_{carbon}/Core/0_{carbon}/DB]$, such that the double bias reinforcement would be placed on the outer surface; as in the actual laminate sequence proposed for the beam. This ensured that any fatigue damage, which could potentially occur within the layer of double bias reinforcement, would remain visible. It was assumed that any fatigue damage sustained by the carbon would be evident through a loss of specimen stiffness, and would also be visually apparent due to delamination of the double bias layer. The combination of these materials in a single specimen would also enable a preliminary insight into the bond produced between the core material and the reinforcement.

The moment capacity of these specimens was determined using fundamental beam theory, and incorporated the contribution to the moment capacity of the double bias reinforcement. The applied moment on the testing apparatus was adjusted to induce the required strains on the specimen.

The final specimen set comprised a sandwich panel consisting of a section of polyurethane elastomer, in combination with a single layer of carbon unidirectional reinforcement (230 gsm) and double bias E-glass reinforcement (600 gsm) on each side, set in epoxy resin. As these materials were also proposed for use in the chassis rail, particularly throughout the neck region and in the collars surrounding each cross member, it was also necessary to

establish a basic level of confidence in the fatigue performance of this combination. This specimen set was identical in quantity to the second, including the lay-up sequence and thickness of the core. As the moment capacity of these specimens was only marginally higher than that of the previous set, the flexural strength of the specimens remained within the capacity of the machine.

8.3.3 Fabrication and Experimentation

The process of manufacture of the fatigue specimens is described in an abbreviated form in this section. Illustrations detailing the manufacturing process were not included in the appendices, due to the simple nature of these specimens.

The process described below details the fabrication of the third specimen set. However, a similar process was used in the manufacture of the first and second sets, apart from the addition of reinforcement to the first set. As previously mentioned, a PFR mixture was used as the sole material in the first specimen set, while H200 PVC foam and a polyurethane elastomer were utilised as core materials in the second and third specimens sets respectively. Unidirectional carbon and double bias E-glass reinforcements were also used as previously noted, with the reinforcement and matrix types used in both specimen sets possessing identical mechanical properties as those tested in Chapter 5. The hand lay-up technique (refer Chapter 2) was used throughout the specimen manufacture. The fabrication of the third specimen set was carried out as follows:

1. A single panel of polyurethane elastomer, measuring 200x300 mm, was cast. Once cured at room temperature for a period of 24 hours, the casting was post cured at 80° C for 16 hours.
2. A laminate comprising a single layer of carbon unidirectional reinforcement in combination with a single layer of double bias E-glass reinforcement, [0°/DB], was laminated to one side of the panel, and allowed to cure at room temperature. The panel was restrained to prevent warping of the panel due to contraction of the matrix during cure. A layer of peel-ply was added to the top of the laminate prior to cure to produce a smooth surface finish, reducing the probability of surface stress concentrations.
3. A second laminate, identical to the first, was laminated to the opposite side of the panel, and allowed to cure at room temperature. A layer of peel-ply was also added to the top of this laminate, prior to cure.
4. Subsequent to cure at room temperature, the panel was post cured at 80°C for 8 hours.

5. All five of the specimens were cut from the panel in rough form. The specimens were then more finely shaped by sanding, conforming to the dimensions prescribed in Figure 8.1 within ±0.5 mm.

In order to ensure that the correct levels of strain were applied, strain gauges were fitted to the specimens, thus validating the calibration of the testing apparatus (refer Figures G.2 and G.5). Observation of the strain gauge measurements was performed by slow, manual operation of the apparatus, as the sampling rate of the data recorder was insufficient when compared with the operating speed of the machine. This exercise verified the accuracy of the apparatus, and it was assumed that identical strains were imposed on the specimen during normal operation of the machine.

Following validation of the imposed strain via strain gauges, each specimen was subjected to the aforementioned loading regime at a frequency of 23 Hz. While this frequency was well in excess of that anticipated for the trailer chassis, it was not possible to alter the speed of the drive motor. As this effectively imposed a significantly higher strain rate to the specimen that would typically be experienced, it was anticipated that any hysteresis effects associated with the matrix would be revealed during this process. A counter was used to maintain a record of the number of load cycles, with each specimen being tested to failure. Testing was halted when a specimen did not fail after being subjected to a nominal count of $10x10^6$ cycles. Throughout the test stage, each specimen was inspected at intervals of $5x10^5$ cycles for the presence of fatigue cracking. The apparatus was also equipped with an auto-shut off feature, which terminated the test when a loss of flexural stiffness was detected within the specimen.

8.3.4 Results and Discussion

The testing of the first specimen set yielded a number of significant results. As shown in Table 8.1, each of the specimens failed at less than $5x10^5$ cycles as a result of fatigue cracking through the centre of specimen. Figure 8.3 shows several of the failed specimens, each exhibiting the 'beach marks' associated with fatigue failure. While the total number of specimens tested was insufficient to enable conclusive data analysis, the collected data would tend to indicate that a larger sample size would not increase the mean fatigue life of this material above $5x10^5$ cycles. The sanding of the specimen edges during the shaping process exposed a number of air bubbles entrapped within the material, these being particularly apparent around the edges of the midsection. These defects, in addition to the presence of ruptured spherical microspheres on the surface, acted to initiate the majority of the cracks present in the specimens. While is it questionable as to whether such edge

effects would be present within the actual structure, the premature failure observed in these specimens does indicate a poor fatigue capacity, with a particular susceptibility to the presence of stress concentrations. These initial results would therefore appear to validate the initial conclusions made in Chapter 5 regarding the fatigue capacity of the PFR core material.

Figure 8.3 Failures of PFR Fatigue Specimens

The results gained from the second specimen set are summarised in Table 8.1. Each of the specimens failed in an identical manner, however these failures occurred over a wide range of cycle numbers. As noted in the table, the mode of failure observed in each of these specimens was a shear failure of the foam in the region of the clamps, as illustrated in Figure 8.4.

While the machine function was to imparting a pure moment to the specimen, full restraint of the specimen was difficult. This was mainly due to concerns regarding the crushing of the panel, and other difficulties associated with the application of identical clamping forces to all specimens. Hence, the large difference in force imposed on the laminates on each side of the specimen, in combination with the variable restraint imposed by the clamps, effectively produced a longitudinal shear force throughout the core of the specimen, particularly within the region of the clamps. However, as the shear loading applied to the core would not occur within the context of the beam, these failure were not considered significant. Each of the specimens exceeded $2x10^6$ cycles, and despite a limited sample size,

it was concluded that these materials were suitable for further investigation in the context of the full-scale beam. The bond between the reinforcement and the foam was shown to be satisfactory; with delamination occurring only after shear failure of the core material had occurred.

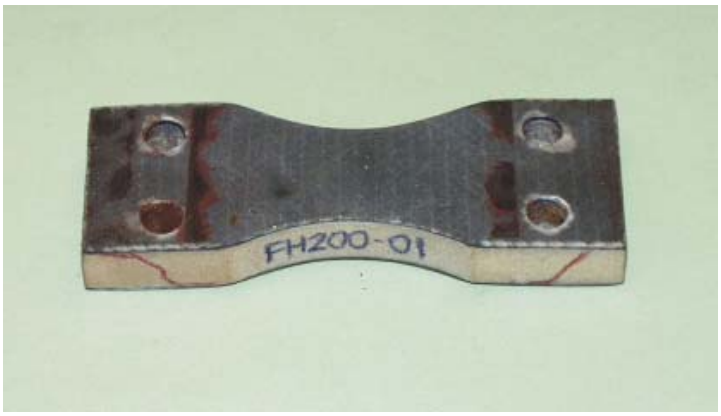

Figure 8.4 Typical Shear Failure in Specimen with PVC Foam Core (Cracks Darkened on Specimen for Clarification)

Fatigue damage was observed in the double bias laminate on a number of specimens. As shown in Figure 8.5, a number of cracks were observed in the matrix surrounding the double bias reinforcement after the completion of approximately $2x10^4$ cycles. These cracks were initiated at the free edges of the specimen, and grew toward the centre of the specimen throughout the duration of the test. The observed crack growth demonstrated the significance of fatigue at the free edge of a laminate, as previously mentioned in section 6.9.2. After monitoring this phenomenon in several specimens, it was discovered that the sanding process used to shape the specimens resulted in the initiation of a series of small delaminations within the double bias reinforcement on the free edges. Consequently, by further sanding these edges with a fine grade of sandpaper, taking care to produce a smooth edge, fatigue cracking of the double bias reinforcement was eliminated from subsequent specimens.

The outcome of the testing of the final specimen set, which incorporated the polyurethane elastomer as the core material, is also summarised in Table 8.1. Only one failure was recorded within this specimen set, which occurred at a cycle count of $19x10^6$ cycles. Upon inspection of the failed specimen, it was noted that failure had occurred because of a defect within the core material, slightly below the surface. Shear failure of the core, as observed in the PVC foam, did not occur in the polyurethane elastomer, due to the higher shear strength of this material. While a limited number of specimens were again used within this

set, it was apparent that the fatigue capacity of this combination of materials was satisfactory, given that every specimen exceeded $10x10^6$ cycles. It was therefore concluded that these materials were suitable for further investigation in the context of full-scale beam. The bond between the reinforcement and the polyurethane elastomer was also shown to be satisfactory; with delamination occurring in one specimen only after failure of the core material had occurred.

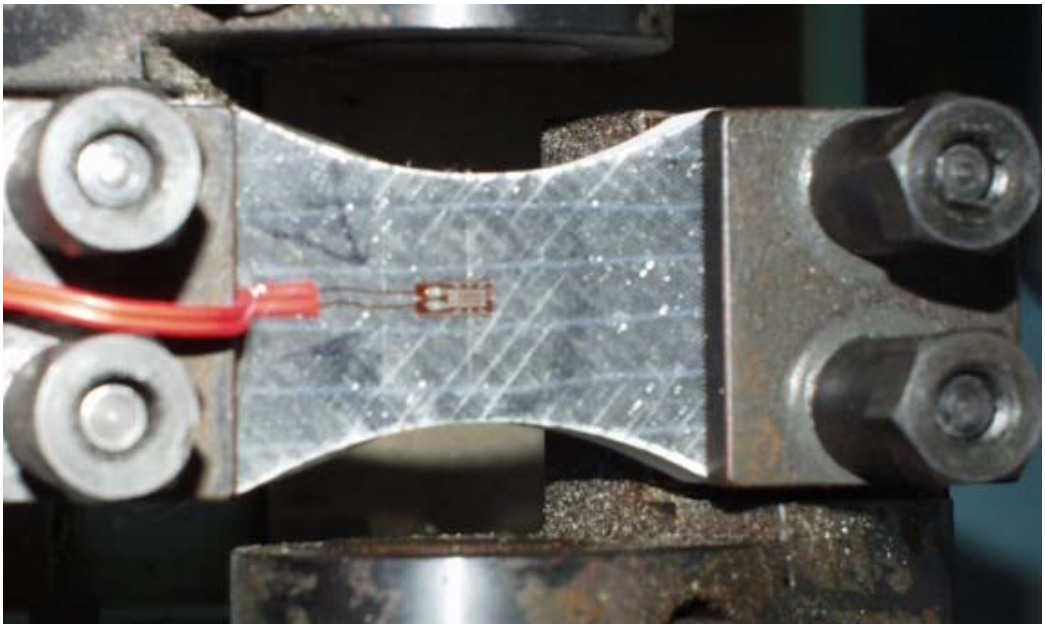

Figure 8.5 Strain Gauge Placement and Fatigue Edge Effects

8.3.5 Conclusions

The elemental fatigue testing discussed in this section was shown to be successful in validating the statements previously made regarding the fatigue performance of the PFR core material. The results provided by the second and third specimen sets were also shown to provide a sufficient level of confidence in the fatigue capacity of the chosen materials to warrant further investigation, particularly in consideration of the severe loading conditions applied to the specimens. The presence of defects and delamination at the edges of the laminate were also shown to greatly influence the fatigue life of the specimens, however this could be overcome by eliminating the presence of free edges. Therefore, the core materials and reinforcement types as specified in section 5.5 were adopted for application to the full size beam, this being detailed in the following section.

Table 8.1 Summary of Elemental Fatigue Tests

Specimen Composition	Specimen Number	Counter (1000's) Start No.	End No.	Total Cycles	Fail (Y/N)	Strain Min. (%)	Strain Max. (%)	Frequency Hz
PFR (t = 12mm)	PFR 1	9576	9621	4.5E+04	Y #	0.2	0.5	23
40% K15	PFR 2	9621	51	4.3E+05	Y #	0.2	0.5	23
ADR246TX/ADH160 Epoxy	PFR 3	51	207	1.6E+05	Y #	0.2	0.5	23
	PFR 4	207	280	7.3E+04	Y #	0.2	0.5	23
	PFR 5	280	332	5.2E+04	Y #	0.2	0.5	23
Diviny Cell H200 PVC Foam	FH200-01	2452	6773	1.4E+07	Y ^	0.2	0.5	23
(t = 8mm)	FH200-02	6773	8970	2.2E+06	Y ^	0.2	0.5	23
1 Layer 230gsm Carbon	FH200-03	8970	2472	3.5E+06	Y ^	0.2	0.5	23
1 Layer 600gsm DB Glass	FH200-04	2472	8470	6.0E+06	Y ^	0.2	0.5	23
	FH200-05	8470	415	2.0E+06	Y ^	0.2	0.5	23
PU Elastomer (t = 8mm)	PUSF01	1079	4351	1.3E+07	N	0.2	0.5	23
1 Layer 230gsm Carbon	PUSF02	7361	9215	1.2E+07	N	0.2	0.5	23
1 Layer 600gsm DB Glass	PUSF03	2370	4345	1.2E+07	Y *	0.2	0.5	23
	PUSF04	415	4180	1.4E+07	N	0.2	0.5	23
	PUSF05	4180	8236	1.4E+07	N	0.2	0.5	23

Fatigue Failure Through Crack Propagation
^ Failure of Core Material in Shear at Clamps
* Failed due to defect in specimen.

8.4 Full-Scale Beam Fatigue Testing

8.4.1 Introduction

The elemental fatigue tests described in the previous section were able to provide an initial precursor as to the typical fatigue characteristics of each material type and combination. However the size of the specimens, in addition to the inherent nature of the test procedure, render the results as purely indicative with respect to the fatigue performance of the proposed FRP chassis rail as a structure. Consequently, testing of a structure, which was representative of the actual beam, was deemed necessary in order to more accurately determine the significance of fatigue in the design philosophy.

This section details the design and construction of a full-scale section of the chassis rail, subjected to a prescribed series of dynamic loads in simulation of those that would be imposed on the chassis of a trailer. The definition of a loading regime is also detailed, this being representative of the dynamic loads imposed to a typical trailer.

Ideally, this fatigue test would incorporate both a neck region and at least one cross member, with the majority of the load being transferred to the chassis rail through the cross member. This would effectively enable the evaluation of the fatigue performance of each of the predominant aspects of the ladder frame simultaneously. However, in addition to economic limitations relating to material costs, the difficulties associated with the complexity of this test specimen would be greatly increased. Also, as a limited number of channels were available on the data-retrieving unit, the number of strain gauges necessary to effectively monitor the entire structure was judged to be insufficient. Consequently, it was decided that the scope of this test would be limited to incorporate only a section of chassis rail, thereby simplifying the monitoring process and reducing cost. This test would therefore be representative of the fatigue performance of the midsection of the chassis rail only, at which the maximum strains due to dynamic loading would occur.

8.4.2 Beam Configuration and Basic Design

A number of constraints were applied as a result of the limitations of the Instron testing machine made available for the fatigue testing. Specifically, the load capacity of the machine, in combination with the displacement and associated frequency available, dictated the use of a full-scale beam section, with a span of 2500 mm, loaded in three-point bending. This represented the only practical configuration that would enable the testing apparatus to induce the necessary strains on the beam. Ideally, a greater span would be used in order to decrease the magnitude of the shear loading in comparison with the accompanying bending moment, however, the capacity of the machine was incapable of providing further deflection at a practical frequency.

Additionally, as discussed in relation to the testing of the neck section of the chassis rail (refer section 7.5.3.2), the load capacity of the machine dictated a reduction in the quantity of unidirectional carbon reinforcement. While this further reduced the similarities between the actual FRP chassis rail and the test specimen, this simplification would still enable the application of identical strain levels to all parts of the beam section as would be present in the actual structure. Hence, any deficiency with respect to the fatigue capacity of the proposed beam cross-section would still become evident during the test.

Therefore, in accordance with the capacity of the Instron, the ultimate capacity of the beam was reduced such that the specimen possessed a failure load of 180 kN. As the magnitude of the strains experienced by the beam specimen would not exceed 4500 με (refer section 4.8.6), the maximum load applied by the Instron throughout the fatigue experiment would therefore not exceed 100 kN.

Determination of the required quantities of unidirectional and double bias reinforcement was performed in a manner similar to that described in sections 7.5.3.2 and 7.6.2, and therefore the details will not be repeated here. A single notable exception to the aforementioned design process was the incorporation of the shear reinforcement in the calculation of the stiffness characteristics and moment capacity of the specimen, due to the high proportion of shear reinforcement inherent in the aspect ratio of the beam.

Using an iterative process to manipulate the quantities of both reinforcement types to satisfy the requirements of moment and shear capacity, the laminates illustrated in Figure 8.6 were proposed for analysis. It should be noted that the ratio of carbon reinforcement to that of the double bias E-glass reinforcement was such that the shear reinforcement contributed to approximately 45% of the beam moment capacity.

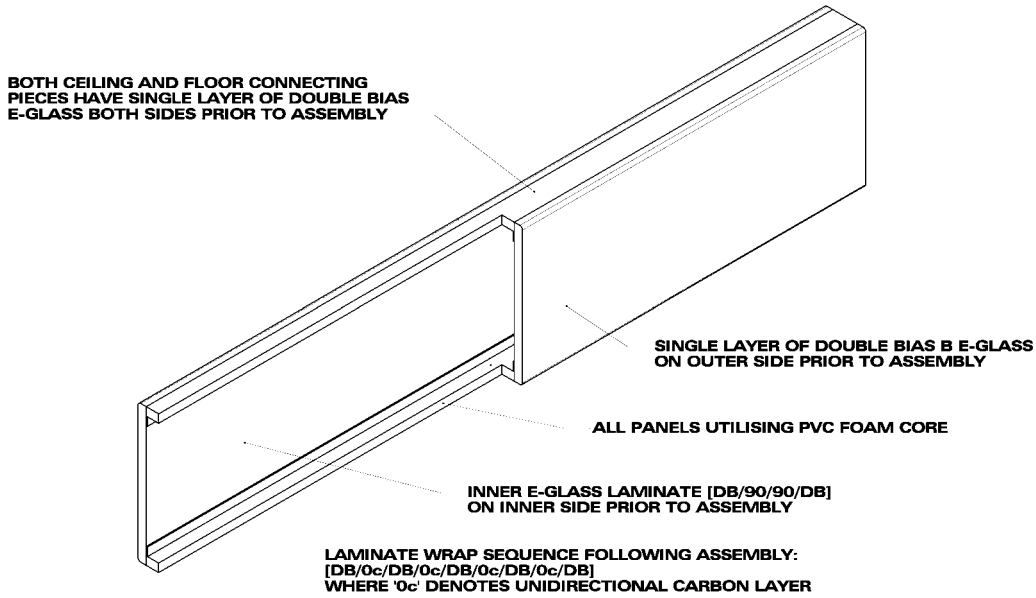

Figure 8.6 Configuration of Full-Scale Fatigue Beam

As recommended in section 5.3, H200 PVC foam was utilised as the core material for this specimen. In order to reduce material costs, it was decided that the polyurethane elastomer would not be included in this specimen, as the elemental fatigue tests indicated that the polyurethane elastomer, in combination with the selected reinforcement, possessed a fatigue capacity far in excess of that required. Hence, it was assumed that the incorporation of this material into the beam specimen would provide no additional insight into its fatigue performance, and the polyurethane elastomer could therefore be omitted. The removal of all hardpoints also provided the opportunity to assess the ability of the PVC foam core to sustain a concentrated load, as would occur along the top flange of the chassis rail in service. Further detail regarding the composition of the proposed beam specimen is contained in section G.3 of Appendix G.

8.4.3 Linear Elastic Finite Element Analysis

Limitations of the available software prohibited the prediction of fatigue or long-term performance. While this prevented the use of analytical techniques to assist in the determination of the characteristic behaviour of the beam when subjected to fatigue loading, analysis was conducted to determine the static behaviour of the section of chassis rail. Given that the expected ultimate deflection was sufficiently low (<<Span/50), a linear analysis was conducted.

The objectives of the analysis are summarised as follows:

- To produce an accurate 3-dimensional model of the proposed chassis rail section, suitable for detailed finite element analysis.
- To investigate the performance of the chassis rail under static load, particularly with respect to beam stiffness at the proposed level of loading.

The reader is directed to section 7.5.3.3 and Appendix G for details regarding the software and element types used in the finite element analysis.

In order to preserve accuracy between the analysis and the actual specimen, the laminate contained within the analytical model replicated the lay-up sequences present in the actual beam, these being described in Figure 8.6, and in further detail in section G.3.1 of Appendix G.

To reduce the number of elements and decrease the solve time, one quarter of the specimen was modelled using symmetry conditions. Perfectly elastic material characteristics were assumed, and plastic deformation was not considered. The general dimensions and element mesh produced for each analysis are illustrated in Figure 8.7, and in Appendix G.

As seen in Figure 8.7 (and in Figures G.9 (a) and (b)), the load was applied over a defined area equivalent to that anticipated in the actual test. Similarly, the load at the reaction points was distributed according to the dimensions of the load spreading plates used in the experiment (refer following section). A load of 21.5 kN was applied to the model, this being equivalent to a load of 85 kN applied to the full model. The response of the beam to all other load values was interpolated using the linear relationship inherent in the analysis type.

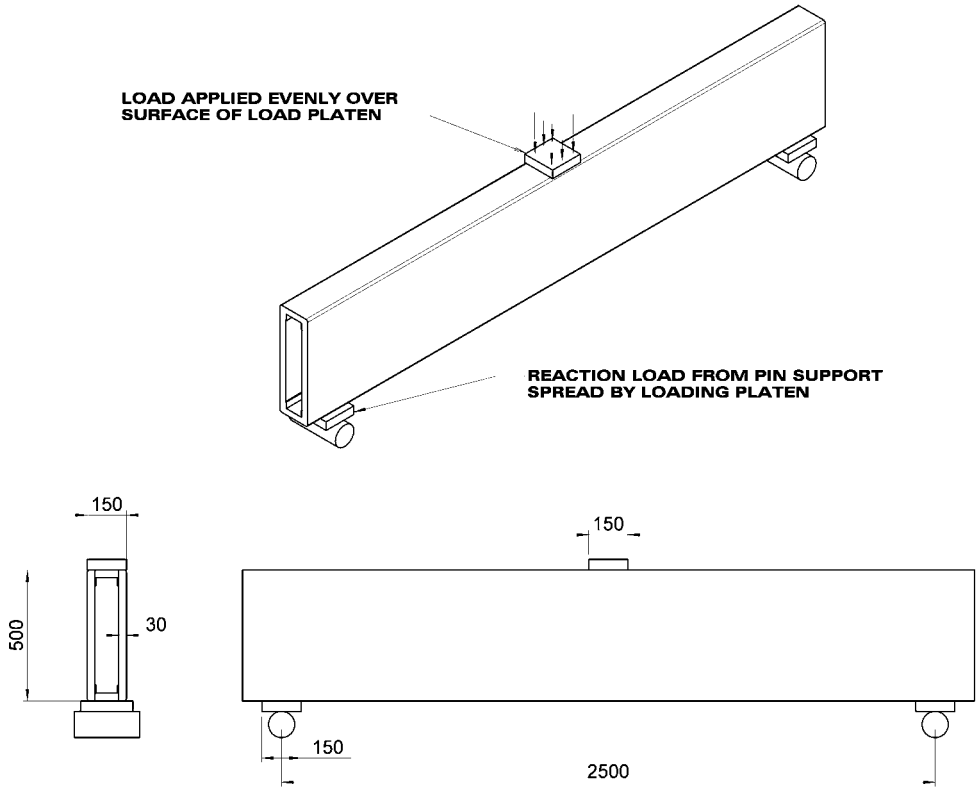

Figure 8.7 Configuration of Analytical Model of Full-Scale Fatigue Beam

8.4.4 Fabrication and Experimentation

Construction of the test beam was identical to that described in section 7.4.4, apart from the type of core material used, and the laminate sequence. As previously mentioned, H200 PVC foam was used as the only core material throughout the specimen. Also, as discussed in the previous chapter in relation to previous test specimens, unidirectional carbon and double bias E-glass reinforcements were used in the construction of the chassis rail section. Figure G.17 illustrates the composition of the laminate on the lower flange, and shows the alternating nature of the laminate sequence. The mechanical properties presented in Chapter 5 were assumed to be applicable for the reinforcement and matrix types used in this test specimen. The hand lay-up technique (refer Chapter 2) was used throughout the beam manufacture. Refer to Appendix G for further details.

Prior to the arrangement of the FRP beam in the testing apparatus, a steel beam was prepared for testing. This beam was introduced to provide a basis for calibration of the monitoring equipment, in addition to verifying the capabilities of the testing apparatus. As illustrated in Figures G.6, the beam was tested using all of the equipment proposed for use with the FRP test beam. This included a number of strain gauges, a linearly variable displacement transducer (LVDT) to measure displacement, and a load cell.

Following calibration of the equipment, the steel beam was subjected to continuous dynamic loading at various frequencies between one (1) and two (2) hertz. The magnitude of the load was sufficient to induce maximum and minimum strain values of 350 and 150 με respectively, such that the endurance limit of the beam was not exceeded, as this initial test was not designed to test fatigue capacity of the steel beam. The data was sampled at various rates to determine an appropriate resolution, with ten (10) hertz being sufficient, considering the frequencies investigated and the resulting size of the data files collected by the data recorder.

Subsequent to commencement of the test, the test was suspended once each 24-hour period, to enable the download of data from the recording equipment. A number of features contained in the data collection software were also verified for use, including an auto-shutoff feature activated by an excess of load, strain or deflection. A sample of the strains recorded at the beam midspan during this test is shown in Figure 8.8.

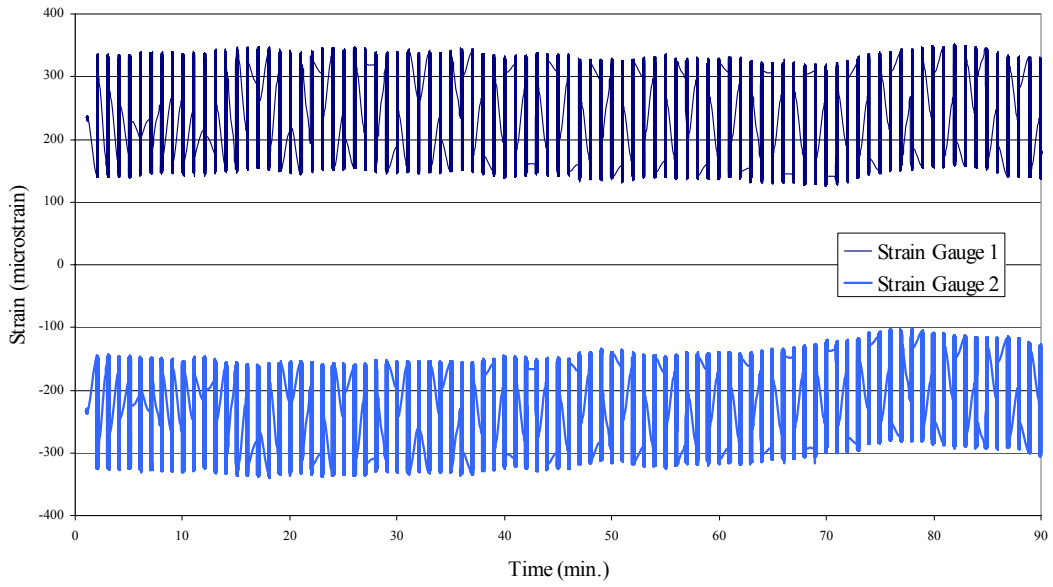

Figure 8.8 Sample of Strain Data Collected from Fatigue Test on Steel Beam

This initial test was successful in calibrating the data recording equipment, and verifying the reliability of this equipment for continuous use without constant supervision. While a number of problems were exposed with regard to the Instron machine, reliable performance was achieved following rectification. This test was therefore successful in establishing a level of confidence in the experimental apparatus and recording equipment, such that the fatigue testing of the FRP specimen could begin.

Several strain gauges were attached to the FRP beam specimen, as shown in Figure G.12. Two gauges were attached to the midspan point of the tensile flange of the beam, using two types of adhesive. This was performed under the recommendation of the manufacturer of the strain gauges, who were unsure as to the durability of the available gauges when subjected to high levels of fatigue loading. It was anticipated that should either gauge fail during the testing period, the software would automatically terminate the test, and a new gauge fitted prior to recommencement. A third gauge was attached to the shear laminate at the end of the beam, positioned such that no strain was imposed upon the gauge during typical beam loading. This gauge, acting as a temperature compensator, was inserted to record the effects of changes in ambient temperature on the readings produced by gauges one and two. While these effects were expected to be minimal with respect to the magnitude of the strains imposed by beam flexure, quantification of these effects would increase the reliability of the recorded data. As with the chassis rail specimen discussed in section 7.5.3, no strain gauge was used to measure the compressive strain, due to the presence of the loading plate at the beam midspan. As previously mentioned with regard to the steel beam, both deflection and load were also recorded using a LVDT and load cell respectively.

In order to reduce the effects of stress concentrations resulting from concentrated loading, a series of platens of various shapes, in addition to several layers of rubber matting, were inserted between the beam and the loading plate. As shown in Figure G.16, a section of timber was also used, the lower face of which was shaped to allow for the curvature of the beam under higher load. In this way, the potential stress concentrations associated with the platen edges as observed in section 7.5.3 would be minimised. As an additional safeguard to prevent overloading, several spacer plates were inserted above the timber section. These spacers were used to vertically position the loading plate such that the Instron was unable to extend the ram sufficiently to apply excessive load to the beam. Steel loading platens and rubber matting were also introduced at the support points to reduce the effects of the roller supports on the laminates. Figures G.14 and G.15 show the beam located in the test rig, prior to testing.

Preceding the commencement of dynamic loading, the beam was subjected to a static load test. In addition to providing a comparison with the finite element analysis, this test was used to establish the initial beam stiffness, thereby forming a reference point to assess the magnitude of the stiffness loss associated with fatigue damage. The beam was loaded at a rate of 5 mm/min, to a maximum load of 85 kN. The load was then removed, and the data retrieved. A comparison of these results with the finite element analysis is provided in

section 8.4.7. This process was also performed between each loading block (refer section 8.4.5), to determine the extent of any loss of beam stiffness resulting from fatigue damage.

The dynamic loading of the specimen was then initiated, with the load applied at a frequency of two (2) hertz. The magnitude and number of loading cycles applied to the beam were varied, and these are discussed in detail in the following section. Subsequent to commencement of the test, the test was suspended once each twenty-four hour period, to enable the download of data from the recording equipment. Data sampling was performed at a rate of ten (10) hertz, however due to the quantity of data acquired in twenty-four hours, the data was recorded for thirty seconds at five-minute intervals. To ensure that any notable incidents that may have occurred between the thirty-second periods were recorded, the software was configured to automatically begin continuous sampling in the event that any of the load, deflection or strain levels deviated from specified limits.

8.4.5 Determination of Dynamic Loading Regime

The definition of an appropriate loading regime, able to accurately simulate the strains imposed on both passenger and heavy vehicles during 'typical' service conditions, has formed the basis of a number of studies. Particular interest in this field has revolved around the quantification of the forces transferred to either the vehicle occupants or the payload. While success has been forthcoming in relation to the construction of an analytical model that accurately represents the vehicle structure, quantification of the loading applied to the chassis as a result of road irregularities remains a largely empirical process. Although a significant volume of research has been undertaken into the accurate description of various road surfaces and irregularities (refer section 4.3.1), a large number of variables exist that are capable of greatly influencing effects upon the chassis. Sharman [9], and Cole & Cebon [10] list a number of these variables that include, in addition to the general condition of the roads, the suspension configuration, the size and distribution of the payload and the speed of the vehicle. Each of these variables are primarily dependent on the local conditions, and the discretion of the operator. Hence, in order to provide verification to analytical models as to the accelerations and loads sustained by the vehicle, the acquisition of raw data is often undertaken. By applying measured road profiles to the analytical model, the response of the analytical and experimental models to these inputs can then be compared. Such a process is described in relation to heavy vehicles by Cole and Cebon [10] and Taylor [11], and in relation to passenger vehicles by Shibata et. al [12].

While good correlation was found by each of the above authors, a qualification of the results was added in each case, stating that small differences in the variables mentioned

previously were shown, both theoretically and experimentally, to have profound effects on the response of the vehicle. Particularly, Cole and Cebon noted that, apart from vehicle speed, the distribution of the payload represented the primary contributor to the response of a trailer. Given the variability in response arising through differences in the operating parameters, in addition to the significant differences in the configurations of trailer used in comparison with the proposed FRP trailer, the direct application of the data presented by these authors to the fatigue beam specimen was deemed inappropriate. Rather, experimental data relevant to the proposed trailer type, expected payload distribution and road conditions would be required to produce accurate data for application in this test.

An alternative approach to the definition of the dynamic loading imposed on a trailer chassis was presented by Sharman [9], which considered the frequency at which notable 'events' occurred. By correlating the number of events with the dynamic load imposed by them, an estimate regarding the fatigue life of the trailer was made. Sharman noted a distinct absence of data concerning the frequency of these events, with the relevance of the gathered data being questionable. Sidelko [13] suggested a combination of 25% smooth road and 75% rough road for operation within the United States, with the frequency of significant events being listed in Table 8.2. However, discussion of this data with a number of heavy vehicle operators suggested that the frequency of these events was underestimated, particularly in relation to the number of potholes and road irregularities encountered on roads in western Queensland.

Table 8.2 Frequencies of Significant Events Occurring Throughout Life of Trailer as Suggested by [13]

Event	Frequency (miles per event)
Tractor-trailer engagement	500
Backing into shipping dock (severe jolt)	4000
Hitting pothole or curb	1500
Tight turn up ramp	3000
Brake stop from 15 mph - hard	1000
- normal	100

As a result of these discussions, it was decided that a suitable estimate of the frequency of events applicable to the road conditions within eastern Australia would be that as shown in Table 8.3. These estimates were based on the following assumptions:

1. The trailer travels two million kilometres during its lifetime.
2. A payload of significant magnitude is carried for approximately 50% of its travelled distance (refer section 1.1).
3. The trailer is of a 'medium capacity' classification, which implies that load case three (refer section 4.4) represents the worst payload distribution.

Based on these assumptions, a number of drivers accustomed to driving several routes throughout central Queensland, were asked their opinion as to the frequency of the events listed in the table. The tabulated results represent the consensus of the drivers, highlighting the significant differences between the conditions of the roads in the United States and Australia (refer section 3.3.2). In light of the relevance of this data with respect to the intended conditions of use, which is within Australia, these event frequencies were adopted as a basis for the loading regime utilised in the fatigue testing.

Table 8.3 Frequencies of Significant Events Occurring Throughout Trailer Life as Adopted for Fatigue Test

Event	Frequency (km per event)	Dynamic Load Factor (Table 4.2)
Road irregularity	1	1.4
Hitting sizable pothole	30	1.9
Level crossing or cattle grid or equiv.	50	2.2

The application of these loads to the beam specimen presented a number of difficulties. An accurate representation of the dynamic loads imposed upon the chassis rail would include a randomised combination of each of these loads in the form of a load spectrum. However, the Instron machine was incapable of producing such a complex load output. Rather, the only available load output was that of a constant-amplitude waveform, similar to that used in the elemental fatigue testing described in section 8.3.

Due to the inadequacies and simplifications inherent in this type of loading regime, block loading was adopted to facilitate the simulation of each load event. This form of loading is completed through the discretisation of the loading spectrum, and the sequential application of each defined loading level in a prescribed order. This type of loading was within the ability of the Instron, however this would necessitate the suspension of the test to facilitate the alteration of the loading level produced by the apparatus. Block loading

techniques have been used widely in the investigation of fatigue performance, despite a tendency of the associated models to be limited in their scope of applicability [8]. In this way, it was anticipated that the frequency events producing higher dynamic loads would be in proportion to those producing lower loads, thus providing a greater level of realism than the method of testing adopted for the elementary fatigue specimens.

Based on the estimates listed in Table 8.3, the block loading sequence used in the test was as follows:

- 1 million cycles at 1.4g, simulating road irregularities
- 60,000 cycles at 1.9g, simulating potholes, sinkholes, and washouts
- 40,000 cycles at 2.2g, simulating level crossings and cattle grids.

This loading order was adopted primarily due to the difficulties associated with the suspension of the test to adjust the load level. These difficulties were discovered during the course of the loading of the steel beam, with the process requiring up to an hour of adjustment to ensure that the correct load levels were achieved.

In addition to this, it was anticipated that the application of the loading blocks in this order would maximise the quantity of data collected. This assumption was founded in the results of the elementary fatigue testing, which inferred that the lowest load level would induce little or no fatigue damage to the beam. The extent of the fatigue damage subsequent to the first loading block could then be assessed by means of a static load test (to measure beam stiffness), prior to the commencement of the second block. In this way, should failure occur during either of the two higher load blocks, a complete quota of data would already have been recorded for all previous load levels. As external restraints on the project allowed for the fabrication and testing of a single specimen, the maximisation of the quantity of data obtained was critical. It is acknowledged that this approach contains simplifications in regard to its failure to account for effects of the damage imposed by larger load levels on any subsequent loading at the lowest (and most frequent) level. The effects of the chosen load sequence were not fully known prior to the test. However, this was considered acceptable in light of the difficulties associated with the frequent alteration of the load level, and the importance of obtaining a significant portion of data from this single specimen.

As mentioned at the end of Section 8.4.4, static tests were conducted subsequent to each loading block to determine the extent of deterioration in the stiffness of the beam. This method of assessing fatigue damage, known as a stiffness-based approach, has been widely used in application to FRPs [14-18], and has been shown to obtain reasonable life

predictions for constant amplitude and two-stress amplitude loadings [18]. The periodic measurement of stiffness provides a simple means by which fatigue damage sustained by the laminate can be observed. The results pertaining to the degradation of beam stiffness are presented in the following section.

8.4.6 Results and Discussion

a) Observations from testing of Steel Beam

The only notable difficulty encountered during the course of the testing was that of minor deviations in the mean load applied to the beam over extended periods. As shown in Figure G.19, deviations in the mean load exceeding five percent were recorded. These irregularities were intermittent however, and were not considered significant. It was discovered that these irregularities were connected with fluctuations in the Instron power supply, and this was rectified using appropriate voltage filtration.

b) Finite Element Analysis

The linear static analysis conducted on the fatigue beam specimen yielded a number of notable results with respect to the predicted and observed static behaviour of the beam.

As illustrated in Figure G.10 (a), the maximum 1st principal strain was observed in the form of a stress concentration beneath the loading platen, at an orientation perpendicular to the laminate plane. While it would appear that this stress concentration increased the magnitude of laminate strain by 50%, closer investigation revealed that the high strain values were contained predominantly within the core material, and that the principal strains within the laminate were not increased by the stress concentration by more than 15%. Further, it was assumed that the impact of the stress concentration upon the compressive laminate would not be as significant as that observed on the neck beam in section 7.5.3, as the maximum strains imposed on the fatigue beam throughout the duration of the testing would not exceed 50% of the ultimate laminate capacity.

The maximum longitudinal strain occurred in the tensile laminate, and was shown to occur at the beam midspan, as shown in Figure 8.9. A comparison of the finite element analysis predictions with the hand calculations shows good correlation, and is illustrated in Figures G.11 (a) and (b). The discrepancy in the predicted beam stiffness's would suggest that the assumptions made in the hand calculations with respect to the position of the laminates relative to the neutral axis were conservative. Additionally, the hand calculations did not

account for the contribution of the vertically oriented reinforcement in the floor and ceiling connecting panels to the beam stiffness. The prediction of the midspan deflection produced by the hand calculations also showed excellent correlation, with the inclusion of shear deflection being essential in the accurate computation of total beam deflection.

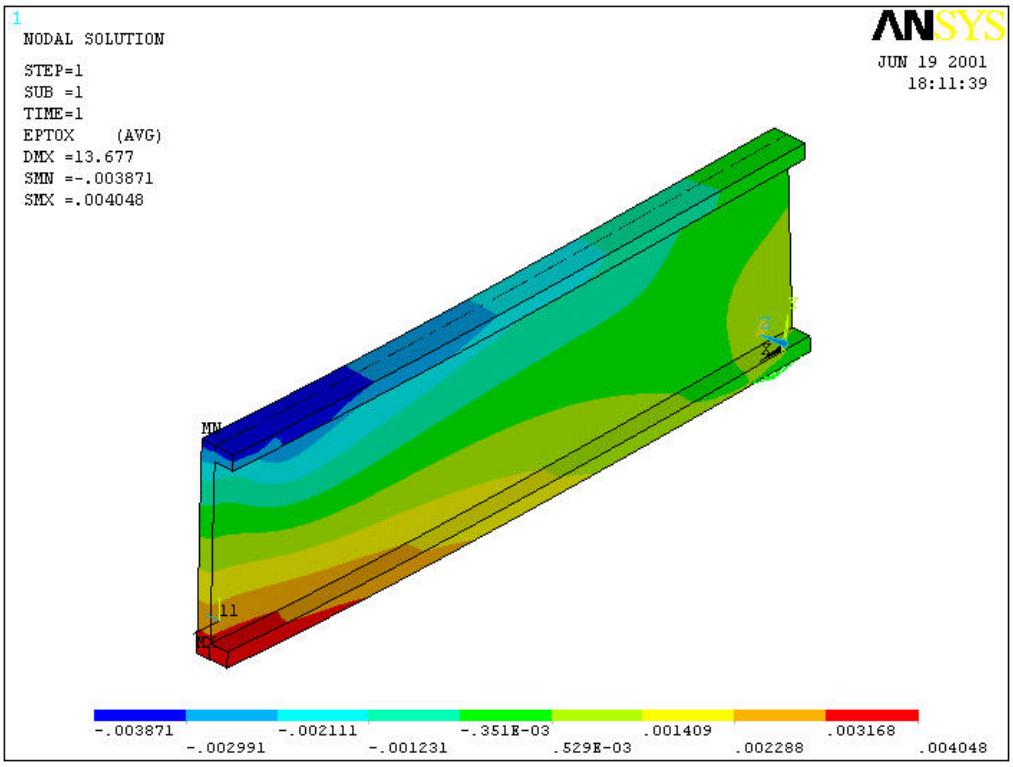

Figure 8.9 Laminate Strain in Direction of Beam Span (x-dirn)

The strains measured during the experimental testing also compared favourably with the corresponding strains predicted by the finite element analysis, as demonstrated in Appendix G (Figures G.11 (a) and (b)). These figures show that the relative error between the predicted and observed values in relation to deflection are noticeably greater that the error present in the prediction of laminate strain. This was particularly irregular, as strain and deflection are directly proportional to each other. However, this discrepancy was accounted for by the compression of the rubber matting inserted between the support points at each end of the beam, which could not be compensated for during the test procedure due to the configuration and placement of the LVDT. With respect to all further references to beam deflection, it was assumed that the compressive modulus of the rubber remained constant throughout the duration of the fatigue testing.

The accurate simulation of the beam behaviour in a static context, in combination with the results of the elemental fatigue testing, provided a level of confidence sufficient to proceed with the fatigue testing of the beam section.

c) Fatigue Testing Results of FRP Beam

The application of the first loading block to the beam specimen (refer Figure G.13) represented the fatigue loading imposed on a trailer chassis resulting from road irregularities and other minor incidents. A sample of the strain alternating between 1g and 1.4g, recorded at the gauge at the beam midspan, is shown in Figures 8.10 (with the corresponding load plot shown in G.20 in Appendix G). Due to the large number of cycles applied at this load level, the test continued continuously over a period of seven days.

Following the completion of the requisite number of loading cycles, the beam was subjected to a static loading test to determine the beam stiffness. As shown in Figure 8.11, no stiffness loss was observed because of the application of the first loading block. Consequently, in accordance with the method of assessment, it was concluded that no fatigue damage had occurred within the beam laminates.

The application of the second loading block to the beam specimen (refer Figure G.13) represented the fatigue loading imposed on a trailer chassis resulting from potholes, washouts, and incidents of equivalent severity. A sample of the applied load and corresponding strain, recorded at the beam midspan, is shown in Figures G.21 and G.22 in Appendix G. Throughout the test, it was observed that the midspan deflection corresponding to a given load remained constant. As with the first loading block, the beam did not exhibit any visual or audible signs that would indicate fatigue damage.

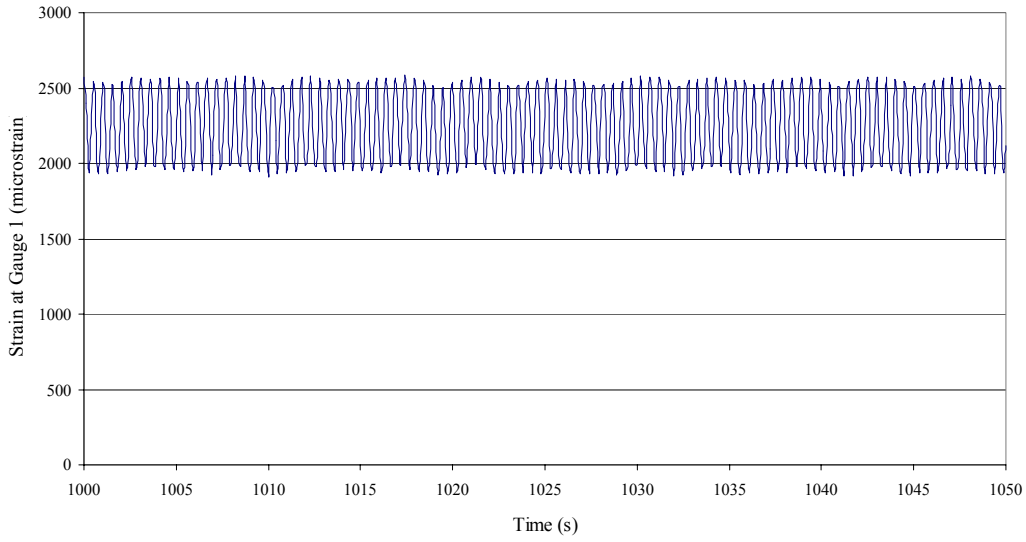

Figure 8.10 Sample of FRP Beam Strain Reading with 1g to 1.4g Loading

Following the completion of the requisite number of loading cycles, the beam was again subjected to a static loading test to determine the beam stiffness, as described previously. As shown in Figure 8.11, no stiffness loss was observed because of the application of the second loading block. Consequently, in accordance with the method of assessment, it was concluded that no fatigue damage had occurred within the beam laminates.

The application of the third loading block to the beam specimen (refer Figure G.13) represented the fatigue loading imposed on a trailer chassis resulting from level crossings, cattle grids, and other relatively infrequent incidents of a high severity. A sample of the applied load and corresponding strain, recorded at the beam midspan, is shown in Figures G.23 and G.24 in Appendix G. Throughout the test, it was observed that the midspan deflection corresponding to a given load remained constant. As with the first and second loading blocks, the beam did not exhibit any visual or audible signs that would indicate fatigue damage.

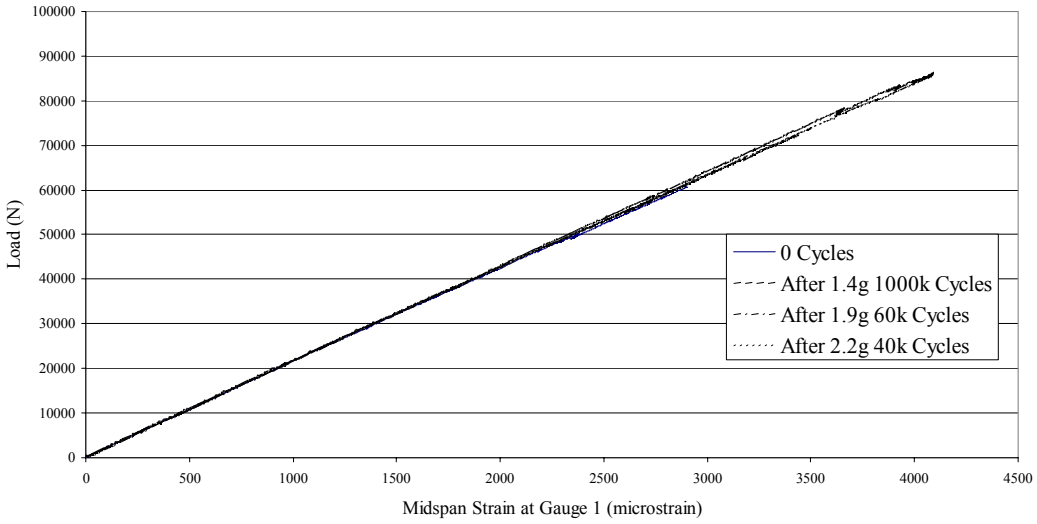

Figure 8.11 Comparison of Beam Stiffness After Each Loading Block

Following the completion of the requisite number of loading cycles, the beam was again subjected to a final static loading test to determine the beam stiffness, as described previously. As shown in Figure 8.11, no stiffness loss was observed because of the application of the third loading block. Consequently, in accordance with the method of assessment, it was concluded that no fatigue damage had occurred within the beam laminates.

The absence of any stiffness reduction within the beam would therefore appear to indicate that the fatigue loading to which the trailer would be subjected would not induce any level of fatigue damage to the chassis rails. The absence of fatigue damage from each of the loading blocks also eliminates any possible error associated with the simplifications inherent in the sequential application of each load block. It is therefore assumed that, regardless of the sequence of application, the effects of the damage imposed by larger load levels on any subsequent loading at the lowest (and most frequent) level would be inconsequential.

The results of the beam testing also demonstrate the significance of eliminating the free edges of all laminates. While edge effects influenced the elemental testing to some degree by causing premature failure in some specimens, similar failure of the beam laminates was avoided by removing all free edges in the beam design, which was accomplished through the arrangement of the laminate sequence.

8.5 Implications of Fatigue Performance on Design Philosophy

The design philosophy presented in Chapter 4 proposed a number of constraints, suitable for the determination of the structural characteristics of an FRP chassis rail. Maximisation of vehicle performance and the capacity of the reinforcement were shown to reside in a combination of the two constraints relating to beam deflection and material strength. Specifically, it was established that the maximum static and dynamic strains imposed on the laminates should not exceed 1800 με and 4500 με respectively. These constraints did not consider the effects of fatigue, or the application of reduction factors to account for possible degradation of the laminate.

The results of the experimental testing presented within this chapter would appear to indicate that the influence of fatigue on these constraints is not critical. Specifically, the absence of any observable fatigue damage to the chassis rail beam specimen when subjected to repeated loading at the strain levels defined by the previous constraints would clearly suggest that consideration need not be given to the influence of fatigue in relation to the determination of appropriate beam characteristics. That is, any constraints imposed by the effects of fatigue do not displace those determined by deflection and strength constraints as presented in Chapter 4.

Consideration should be given to the influence of fatigue on joint design, and other areas comprising potential stress concentrations. However, the exceptional performance observed in the static tests of both the neck beam section and the cross member test specimen, in addition to the excellent fatigue capacity observed in the polyurethane elastomer through elemental fatigue testing, suggests that the fatigue performance of the entire chassis would not impose any additional strength reduction factors on the strain levels previously determined. In practice, validation of this assumption could only be achieved experimentally.

8.6 Conclusions

This chapter has described the initial investigation undertaken to determine the fatigue characteristics of the proposed chassis rail section. This was performed primarily to establish the effects of the beam fatigue capacity on the design constraints suggested in the design philosophy presented in Chapter 4.

The determination of the fatigue performance of the proposed materials was limited to the response of the materials to the strain levels predicted in-service. This was achieved through the use of elemental specimens subjected to a pure moment, inducing strain levels equivalent to the maximum levels proposed by the design philosophy in Chapter 4. These elemental tests clearly demonstrated the poor fatigue capacity of the PFR core material, validating the exclusion of the PFR as a possible core material. Conversely, both the PVC foam core and the polyurethane elastomer exhibited adequate fatigue performance, with the polyurethane elastomer exceeding the required fatigue life by a significant margin. The carbon and E-glass reinforcements also exhibited adequate fatigue performance, with the laminate maintaining integrity throughout each test. The influence of 'Edge effects' was also demonstrated, reinforcing the importance of eliminating free edges in the chassis rail construction.

In light of the observed fatigue performance of the proposed materials on an elemental level, the process used for design, construction, and experimental validation of the FRP chassis rail was presented. Having reduced the quantity of reinforcement due to limitations of the experimental apparatus, the beam was subjected to a series of loading blocks. These loading blocks were representative of the dynamic forces of various magnitudes resulting from significant 'events', which occur throughout the duration of service of a trailer. The magnitude and frequency of these events was established through examination of previous work, and consultation with industry operators.

Through periodic measurement of the beam stiffness, it was shown that the beam did not sustain any damage as a result of the fatigue loading. The absence of any observable fatigue damage to the specimen demonstrated the soundness of the proposed beam section, and confirmed the results of the elemental fatigue testing. Due to the simplified nature of the beam specimen, no conclusions could be made with regard to the effects of the cross members and neck section on the fatigue performance of the chassis. However, the fundamental approach adopted with respect to fatigue throughout this chapter was

successful in demonstrating the potential of the proposed cross section (refer Section 7.4) to withstand the fatigue loading imposed on an FRP trailer.

The tests presented within this chapter also demonstrated that fatigue did not represent an influential constraint in the design of the chassis rail capacity. Rather, the constraints imposed by member deflection and the allowable strain within the reinforcement would remain the dominant constraints in the design process.

References

[1] Schaff JR, Davidson BD. Life prediction methodology for composite structures. Part II – spectrum fatigue. J. of Composite Materials 1997; 31(2): 1997.

[2] Kliman V. Fatigue life estimation under random loading using the energy criterion. International Journal of Fatigue1985; 7 (1): 39-44.

[3] Ben-Amoz M. Cumulative damage theory for fatigue life prediction. Engineering Fracture Mechanics 1990; 37 (2): 341-347.

[4] Hwang W, Han KS. Fatigue of composites – fatigue modulus concept and life prediction. Journal of Composite Materials 1986; 20 (2): 154-165.

[5] Rotem A. Residual strength after fatigue loading. International Journal of Fatigue 1988; 10 (1): 27-31.

[6] Mai YW, Diao X, Ye L. A statistical model of residual strength and fatigue life of composite laminates. Composites Science Technology1995; 54 (3): 329-336.

[7] Lee LJ, Yang JN, Sheu DY. Prediction of fatigue life for matrix-dominated composite laminates. Composites Science Technology1993; 46 (1): 21-28.

[8] Bond IP. Fatigue life prediction for grp subjected to variable amplitude loading. Composites: Part A 1999; 30: 961-970.

[9] Sharman PW. The use of dynamic strain records to estimate the fatigue life of a semi-trailer chassis. IEEE Conference Record of Annual Conference of Electrical Engineering Problems in the Rubber and Plastics Industries, Inst. of Phys, Stress Anal Group, Annual Conference, Stress, Vibration and Noise Analysis in Vehicles 1975; Birmingham, England; New York: John Wiley and Sons; 1975: 461 – 471.

[10] Cole DJ, Cebon D. Validation of an articulated vehicle simulation. Vehicle System Dynamics 1992; 21: 197-223.

[11] Taylor C. Fabrication and testing of high-strength, high capacity, weight optimised trailers. Proceeding of the 5th Annual International Conference on High Level Radioactive Waste Management; 1994 May; Las Vegas, Nevada; 2: 931-933.

[12] Shibata T, Miyajima M, Tani M, Yoneda E. Laboratory system endurance testing of major car components. Int. J. of Vehicle Design1984; 5 (3): 374-388.

[13] Sidelko WJ. An objective approach to highway truck frame design. SAE Paper No. SP 276. Warrendale, PA: Society of Automotive Engineers; 1965.

[14] Yang JN, Jones DL, Yand SH, Meskini A. A stiffness degradation model for graphite epoxy laminates. J. Composite Materials 1990; 24: 753–769.

[15] Yang JN, Yang SH, Jones DL. A stiffness-based statistical model for predicting the fatigue life of graphite/epoxy laminates. J. Composite Technology 1989; 11: 129–134.

[16] Hwang W, Han KS. Cumulative damage models and multi-stress fatigue life prediction. J. of Composite Materials1986; 20: 125-153.

[17] Poursartip A, Beaumont PWR. The fatigue damage mechanics of a carbon fibre composite laminate: Part II – life prediction. Composites Science and Technology 1985; 25: 283-299.

[18] Schaff JR, Davidson BD. Life prediction methodology for composite structures: Part I – constant amplitude and two-stress level fatigue. J. of Composite Materials 1997: 128-157.

Chapter 9 Conclusions

9.1 Review of Research

The incorporation of fibre composite materials into heavy vehicle structures provides significant advantages with respect to the reduction of tare mass, leading to increases in productivity and efficiency. However, it was discovered that the acceptance and utilisation of these materials into the heavy vehicle industry required the examination of several fundamental areas.

In addition to a limited understanding within the industry in regard to FRPs, the absence of any design philosophy relevant to either steel or fibre composite trailer chassis' presented the greatest hindrance to the application of FRPs to flatbed semi-trailer chassis'. This PhD study has addressed the assessment of the potential of FRPs in application to semi-trailers, with the significant issues being divided into two areas:

- The development of a design philosophy, intended specifically to address the application of FRPs to semi-trailers.
- The design, analysis and experimental validation of a new type of FRP trailer chassis, utilising the aforementioned design philosophy.

9.2 Major Outcomes and Key Findings

1. The Definition of Significant Load Cases and Trailer Classifications

Flatbed trailers continue to be utilised in the transportation of payloads that vary greatly with respect to size, mass, and the distribution of the payload to the chassis. An overview of current industry practice highlighted the need for industry guidelines in design. The substantial variations in the structural capacity of flat bed semi-trailers did not enable the immediate selection of the most efficient structural characteristics. These variations highlighted the independent nature of trailer design, in which each manufacturer determines it's own design in accordance with experience. Therefore, six significant load cases were defined as being characteristic of typical distributions of the payload. Using these load cases, this study proposed a method of trailer classification that was categorised by variations in load distribution, and was suggested to assist in design optimisation and the reduction of trailer overloading caused by incorrect payload distribution. This provided a basis for optimisation of the chassis of a trailer with respect to its intended use. This system of classification also reduces the probability of overloading resulting from incorrect payload distribution. Details of this system of classification have been presented in Chapter 4.

2. Development of a Design Philosophy Suited Specifically to FRP Semi-trailers

The extent of published research into vehicle dynamics revealed a clear focus on the prediction of the dynamic response and behaviour of semi-trailers, as well as the impact of heavy vehicles on roads. However, a survey of the literature revealed a distinct absence in the quantification of the dynamic behaviour of a trailer chassis. Specifically, it was shown that the magnitude of the dynamic load factors, which should be applied to the appropriate static load cases, had not been sufficiently defined to enable reliable application to trailers suitable for Australian conditions. Consequently this study presented a dynamic design factor for application to the proposed design philosophy, based on a combination of experimental findings and the experience of the trailer manufacturing industry. The designation of a dynamic design factor (DDF) included data extracted from both research and industry sources. A common factor of 2.5 was identified and applied throughout this study.

The use of design constraints suitable for application to FRP structures was shown to present a number of differences with respect to the design of steel trailers. In addition to the use of strength as a design constraint, the influence of deflection in FRP trailer design was shown to be significant. These design constraints were compared in order to determine the critical or dominant constraint. The constraints on deflection and strength were shown to be necessary in terms of public perception, and the preservation of acceptable factors of safety with respect to the FRP. For a prescribed range of precamber values, it was shown that an optimum value could be identified which utilised the upper limits of each constraint. Outside the prescribed range of precamber values, the deflection constraint was shown to be dominant for lower values of precamber, while the laminate strength constraints were shown to dominate when the values of precamber were high. Therefore, this study was successful in presenting a method whereby the optimum solution with respect to trailer performance could be found for any specified value of precamber.

Details of the design philosophy and the establishment of the dynamic design factors have been presented in Chapter 4.

3. Establishment of a selection criteria which identifies appropriate FRP materials for use in this application

While a large range of fibre composite materials is available, not all are suitable for application to trailers. By examining a range of fibre composite materials that were commonly available, the desired material characteristics were selected on the basis of their significance with respect to the project aims and the expected operational conditions. On the basis of these comparisons, suitable composite materials were selected for further investigation and application.

The selection process identified two suitable core materials of similar properties. The H200 PVC foam was selected due to greater availability. Three commonly available fibre types were also subjected to a comparison with respect to several key characteristics, with carbon fibre selected as the primary reinforcement type reinforcement as a result of superior performance in almost every category. The low cost and availability of E-glass double bias fabric were the primary factors in the selection of this form of reinforcement for the accommodation of the shear loads to which the chassis is subjected.

The uncertainty associated with published laminate properties prompted the limited testing of each of the reinforcement types used within this research. Specifically, the tensile and

compressive properties of the unidirectional carbon, unidirectional E-glass, and double-bias E-glass laminates used within this project were established, in addition to the proposal of a general equation designed to provide an accurate estimation of the strength characteristics and capacity of a unidirectional carbon laminate.

Details concerning the selection of suitable materials, and the determination of the mechanical properties of the reinforcement have been presented in Chapter 5.

4. Development of a New Type of FRP Chassis for a Flatbed Semi-trailer

The application of the selected materials to a specific trailer configuration was accomplished through the development of a series of conceptual designs, which included a number of material types and manufacturing techniques. The various concepts considered comprised monocoque and ladder frame configurations, the latter of which being essentially modular. The presented range of conceptual designs was intended as representative, rather than exhaustive, of the structural configurations possible using FRP materials. All monocoque structures, in addition to one of the ladder frame structures, utilised the casting nature of PFR for use as a high strength core. The use of a structural foam core, in addition to the lower material volume provided by the ladder frame configuration, provided large reductions in tare mass to concepts one and five in comparison with the monocoque structures consisting of PFR.

By evaluating each concept in relation to key parameters, a single concept was selected and investigated more closely. It was the conclusion of this study that a ladder-frame chassis construction would most aptly accommodate the specifications noted earlier, and was therefore subjected to further investigation.

The possible failure modes associated with the final concept were briefly summarised, being separated into those applicable to the chassis rail or cross members, with the critical modes identified further investigation. Details of the selection process and discussion regarding the anticipated failure modes were presented in Chapter 6.

5. Validation of the Design Philosophy through Experimental Testing

The proposal of a design philosophy and the selection of a trailer configuration provide a purely hypothetical basis for the assessment of FRPs in application to flatbed semitrailers. Hence, this PhD study described a series of experimental tests, incorporating scaled models, which were representative of the significant sections of the proposed chassis. A number of the expected failure modes were addressed, with emphasis given to the structural behaviour and performance of the chassis rails and cross members.

A cross sectional composition of the proposed FRP chassis rails was presented, the primary requirement being the performance of the section under direct compressive loading. Several factors were identified as being the primary contributors to the crushing capacity of the section, with a full-scale section of the chassis rail being constructed and tested to provide verification to the finite element analysis.

Having examined common points of failure and high stress in the chassis rails of steel trailers, an investigation was undertaken into the performance of the neck region of the proposed FRP chassis rail when subjected to bending. A number of recommendations were produced from a series of tests utilising small-scale beam segments, including the introduction of continuing reinforcement on the inner floor of the bottom panel. The design, construction and testing of a section of chassis rail (half-scale), which incorporated each of the recommendations provided by the small-scale specimens, was shown to perform exceptionally well, with the finite element analysis accurately predicting the beam behaviour. The mode of failure was shown to be non-catastrophic, and was not in the region of the neck section.

The design process used to determine the shape and composition of a cross member suitable for incorporation into the ladder frame chassis of the FRP trailer was also presented. The connection of the cross member to the chassis rails was addressed, using a combination of finite element analysis and experimental techniques. A full-scale specimen incorporating a section of chassis rail connected to a cross member, was produced and tested to provide validation to the analysis. Failure of the cross member was non-catastrophic, with the compressive collapse of the cross member laminate occurring without any damage to the chassis rail. The incorporation of hardpoints into the core of the chassis rail was shown to be necessary to effectively transfer load into the sidewalls. Additionally, it was shown that the free ends of the cross member required the incorporation of internal support to prevent excessive local deformation due to

concentrated loads. The modular approach to chassis construction was shown to be feasible, reducing the potential costs associated with repairs and maintenance of the chassis.

Through a series of static tests, it was shown that the conceptual frame possessed adequate structural characteristics to perform the required functions of the chassis, and that several of the key failure modes could be accurately predicted. Through experimental fatigue testing on both elemental and large scale models, it was shown that fatigue loading did not impose any additional limitations on the design constraints, simplifying the design process.

Further investigations were undertaken to determine the fatigue characteristics of the proposed chassis rail section. This was performed primarily to establish the effects of the beam fatigue capacity on the design constraints suggested in the design philosophy.

The determination of the fatigue performance of the proposed materials was limited to the response of the materials to the strain levels predicted in-service. This was achieved by initially using small elemental specimens, followed by full experimental validation of the FRP chassis rail using a full-scale section of chassis rail. The elemental specimen tests provided validation for the choice of core material and reinforcement type, with all materials recommended by the selection process (refer Chapter 5) exhibiting adequate fatigue performance. The influence of 'edge effects' was also demonstrated, reinforcing the importance of eliminating free edges in the chassis rail construction.

The full-scale test beam was subjected to a series of loading blocks, these being representative of the dynamic forces of various magnitudes resulting from significant 'events' which occur throughout the duration of service of a trailer. The magnitude and frequency of these events was established through examination of previous work, and consultation with industry operators. Through periodic measurement of the beam stiffness, it was shown that the beam did not sustain any damage as a result of the fatigue loading. The absence of any observable fatigue damage to the specimen demonstrated the soundness of the proposed beam section, and confirmed the results of the elemental fatigue testing. These tests also demonstrated that fatigue did not represent an influential constraint in the design of the chassis rail capacity. Rather, the constraints imposed by member deflection and the allowable strain within the reinforcement would remain the dominant constraints in the design process.

Therefore, having used the design philosophy as a guideline in the design of the specimens in experimental program, the successful demonstration of the experimental tests provided

validation of the major aspects of the design philosophy. Details regarding the experimental program have been presented in Chapters 7 and 8.

6. Affirmation of the Potential of FRPs in Application to Flatbed Semi-trailers

The consolidation of the design philosophy through testing clearly demonstrated that FRPs possess significant advantages over traditional materials within this context. Using the chassis configuration proposed in this study, it is estimated that a tare mass reduction of up to 30% is possible, providing a distinct economic advantage over steel trailers.

This study has presented only limited discussion regarding the cost of manufacture, due to the large number of variables relating to the method of manufacture, production volumes, fluctuations in material prices, and the willingness of the industry to pay increased capital costs to reduce tare mass. Increasing use of these materials into civil applications suggests that FRPs are becoming increasingly competitive with traditional materials. Hence, the achievement of significant mass reduction and the degree of success achieved in determining the behaviour of the proposed structure under the prescribed conditions, has confirmed the potential of FRPs, identifying them as feasible for further application in this area.

9.3 Recommendations for Further Research

Through the course of this PhD study it has become increasingly clear that the level of knowledge present within the academic and industrial communities is somewhat deficient with respect to the development and implementation of design standards, the classification of trailer capacities, and the incorporation of alternate materials such as FRPs into the heavy transport industry. Contained below is a summary of key topics that have been identified for further research and application.

Trailer Chassis Behaviour

- An investigation into the dynamic behaviour of a ladder frame chassis, subjected to Australian road conditions. Specifically, a dynamic load factor describing the dynamic flexure of the chassis rails should be investigated, including the influence of:

  - Trailer length
  - Chassis stiffness
  - Suspension type
  - Vehicle speed
  - Payload distribution

- An investigation into the torsional performance of the chassis, including the influence of:

  - Flexibility of connections on trailer performance
  - Fatigue loading on connection integrity

- The development of design guidelines and standards, for both steel and FRP trailers, with a particular focus on the design of chassis rails. Investigation should also be performed into the advantages and practicality of the adoption of trailer classifications.

Variations to Chassis Configuration

- Investigation into the structural characteristics of alternative chassis configurations. While a ladder frame was considered in this study due to the focus on modular construction, other variations in configuration should also be considered if alternate objectives are identified.

Fatigue Testing

- A detailed investigation into the fatigue performance of the chassis, focused specifically at:

  - The interaction of the cross members with the chassis rail
  - The fatigue performance of the neck section
  - The influence of shear fatigue on the design of shear reinforcement.

- Further investigation into the interaction of the suspension and kingpin components with the chassis rail, particularly in a dynamic environment.

Implications of Tare Reduction

- The reduction of tare mass through use of FRPs introduces a number of characteristics that require attention. These include:

  - Practical assessment of the durability of the proposed trailer, including the quantification of environmental effects encountered during service, and evaluation of the effects of various impact events on the life and performance of the trailer.
  - Investigation in the effects of tare reduction on the towing, turning and braking characteristics of the trailer, including the consequences of overturning (whilst laden or unladen), and the response of trailer when subjected to collision with another vehicle.

Detail Design

- Further development of the proposed concept is required in order to produce a complete, full-scale prototype, and to provide further information regarding the suitability of composite materials within this genre. Areas suggested for further development include:

  - Investigation into the development of lightweight ancillary components, including suspension components and standing legs.
  - Detailed cost analysis of the trailer, which will be primarily dependent on the manufacturing method adopted.
  - Completion of minor detail design, including the attachment of an FRP decking and combing rails.

Appendix A – Characteristics of Existing Steel Trailers

A.1 McGrath Trailer 1980

Table A.1 Chassis Characteristics of McGrath Trailer (1980)

Manufacturer	McGrath	**Suspension**	Spring
Year	1980	**Axle Config.**	Tri-axle
	Chassis Rails		**Cross Members**
	Section B-B (mm)	Section A-A (mm)	(mm)
Top Flange **Flange Thickness** Bottom Flange	16 25	16 25	4
Web Thickness	6	6	4
Web Depth	190	390	92
Flange Width	100	100	58
Member Spacing	1000	1000	640
Y Bar	100	190	46
I_{xx} (mm^4)	4.7E+07	2.0E+08	1.2E+06
Moment Capacity (kNm)	166	364	8.7
Shear Capacity (kN)	228	468	74

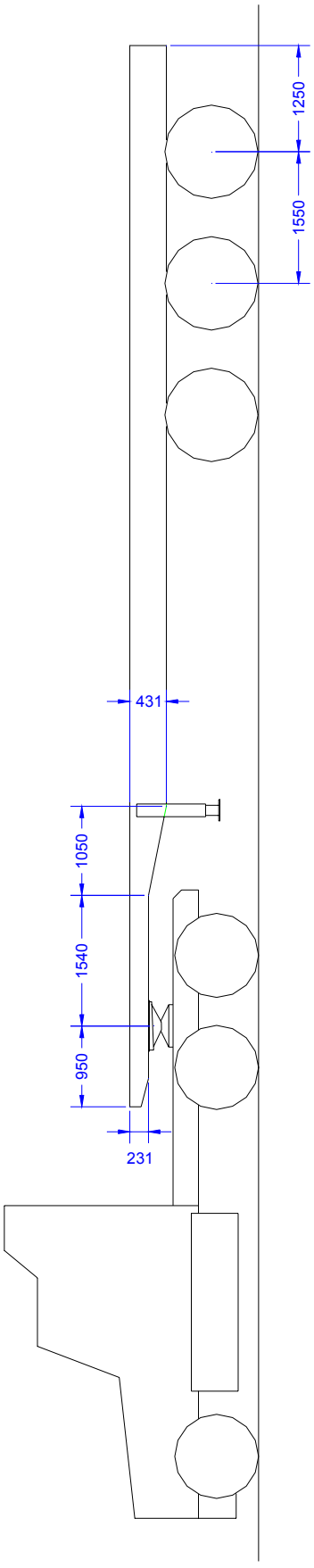

Figure A.1 Basic Chassis Rail Profile of McGrath Trailer (1980)

A.2 Haulmark Trailer 1982

Table A.2 Chassis Characteristics of Haulmark Trailer (1982)

Manufacturer	Haulmark	**Suspension**	Spring
Year	1982	**Axle Config.**	Tri-axle
	Chassis Rails		**Cross Members**
	Section B-B (mm)	Section A-A (mm)	(mm)
Top Flange **Flange Thickness** Bottom Flange	20 20	10 10	6
Web Thickness	10	10	4
Web Depth	230	410	88
Flange Width	100	150	45
Member Spacing	900	900	480
Y Bar	135	215	44
I_{xx} (mm^4)	7.3E+07	1.9E+08	1.3E+06
Moment Capacity (kNm)	189	309	8.9
Shear Capacity (kN)	460	820	70

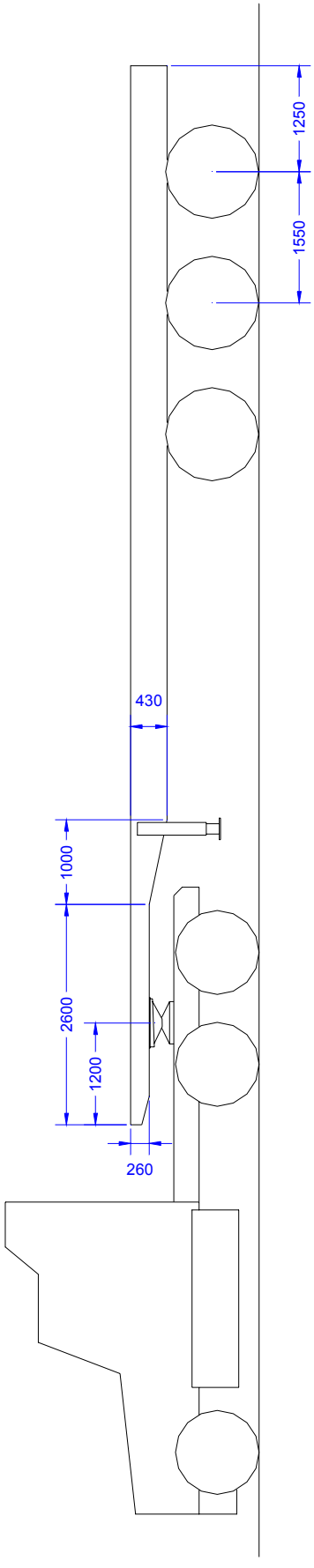

Figure A.2 Basic Chassis Rail Profile of Haulmark Trailer

A.3 Fruehauf Trailer 1985

Table A.3 Chassis Characteristics of Fruehauf Trailer (1985)

Manufacturer	Fruehauf	**Suspension**	Spring
Year	1985	**Axle Config.**	Tri-axle
	Chassis Rails		**Cross Members**
	Section B-B (mm)	Section A-A (mm)	(mm)
Top Flange **Flange Thickness** Bottom Flange	15 15	10 10	6
Web Thickness	15	10	4
Web Depth	220	405	88
Flange Width	100	150	45
Member Spacing	900	900	480
Y Bar	125	213	44
I_{xx} (mm^4)	5.5E+07	1.8E+08	1.3E+06
Moment Capacity (kNm)	153	304	8.9
Shear Capacity (kN)	660	810	70

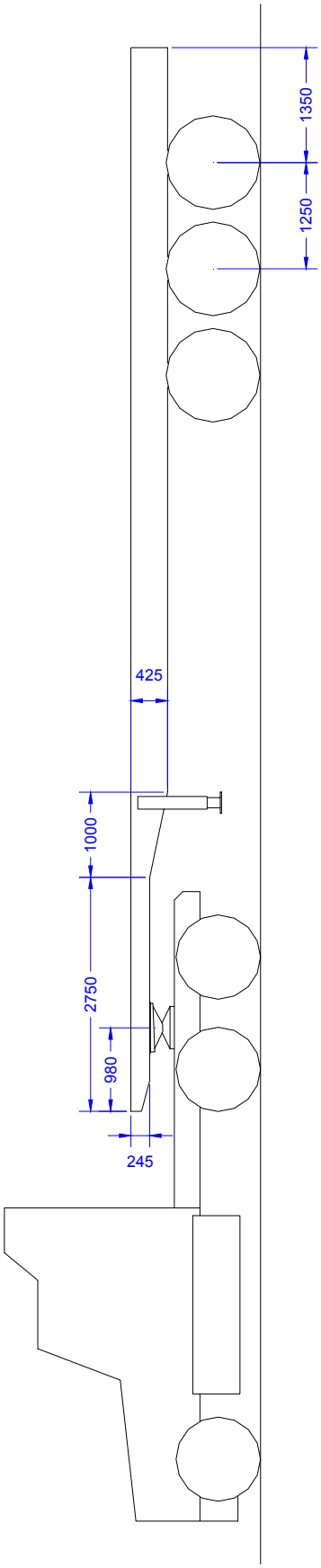

Figure A.3 Basic Chassis Rail Profile of Fruehauf Trailer (1985)

A.4 Loughlin Trailer 1987

Table A.4 Chassis Characteristics of Loughlin Trailer (1987)

Manufacturer	Loughlin	**Suspension**	Spring
Year	1987	**Axle Config.**	Tri-axle
	Chassis Rails		**Cross Members**
	Section B-B (mm)	Section A-A (mm)	(mm)
Top Flange **Flange Thickness** Bottom Flange	12 20	12 20	5
Web Thickness	10	10	4
Web Depth	268	568	130
Flange Width	130	130	60
Member Spacing	1030	1030	600
Y Bar	131	272	65
I_{xx} (mm^4)	9.7E+07	5.0E+08	3.3E+06
Moment Capacity (kNm)	259	641	16.3
Shear Capacity (kN)	536	1136	104

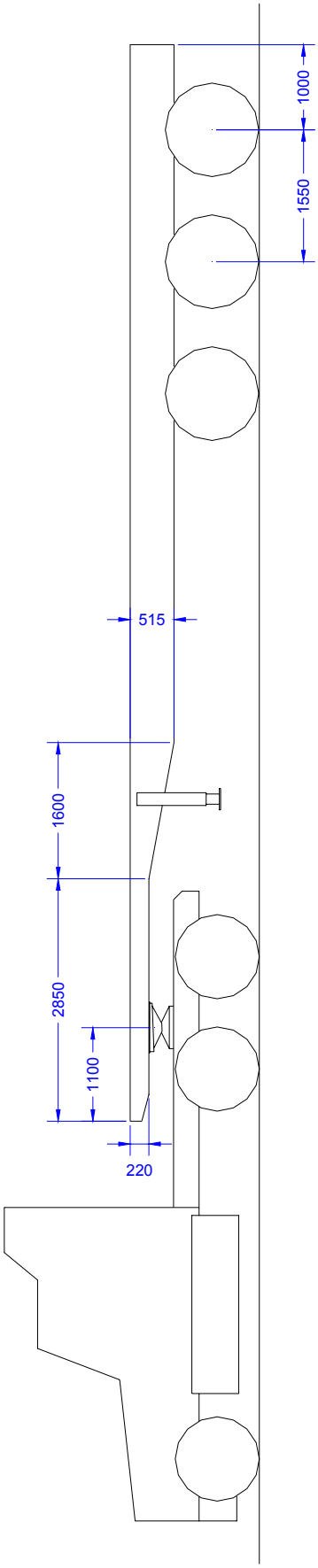

Figure A.4 Basic Chassis Rail Profile of Loughlin Trailer (1987)

A.5 Loughlin Trailer 1989

Table A.5 Chassis Characteristics of Loughlin Trailer (1989)

Manufacturer	Loughlin	**Suspension**	Spring
Year	1989	**Axle Config.**	Tri-axle
	Chassis Rails		**Cross Members**
	Section B-B (mm)	Section A-A (mm)	(mm)
Top Flange **Flange Thickness** Bottom Flange	12 16	12 16	6
Web Thickness	6	6	4
Web Depth	270	580	88
Flange Width	130	130	45
Member Spacing	970	970	480
Y Bar	136	284	44
I_{xx} (mm^4)	8.2E+07	4.2E+08	1.3E+06
Moment Capacity (kNm)	211	512	8.9
Shear Capacity (kN)	324	696	70

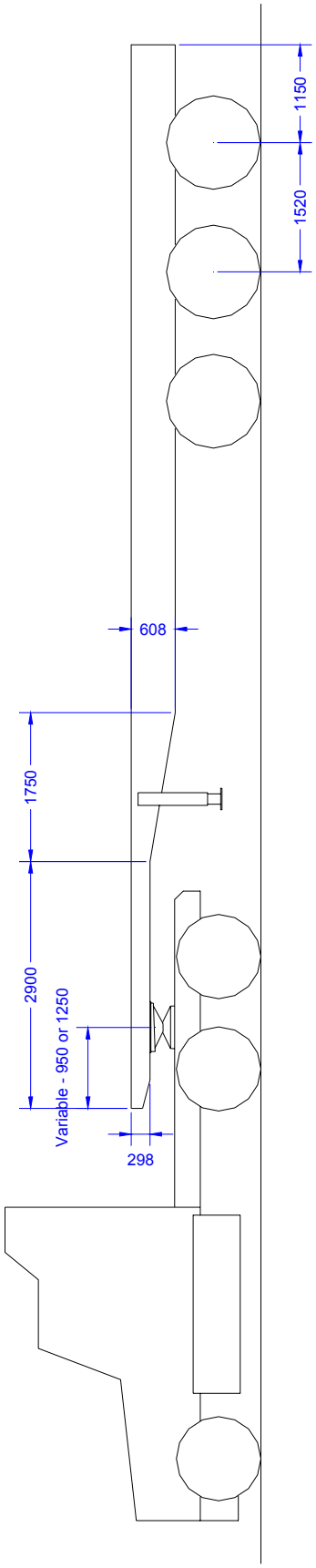

Figure A.5 Basic Chassir Rail Profile of Loughlin Trailer (1989)

A.6 Haulmark Trailer 1992

Table A.6 Chassis Characteristics of Haulmark Trailer (1992)

Manufacturer	Haulmark	**Suspension**	Spring
Year	1992	**Axle Config.**	Tri-axle
	Chassis Rails		**Cross Members**
	Section B-B (mm)	Section A-A (mm)	(mm)
Top Flange **Flange Thickness** Bottom Flange	12 20	12 20	6
Web Thickness	8	8	4
Web Depth	228	488	88
Flange Width	150	100	45
Member Spacing	960	960	480
Y Bar	110	235	44
I_{xx} (mm^4)	7.6E+07	2.8E+08	1.3E+06
Moment Capacity (kNm)	242	411	8.9
Shear Capacity (kN)	365	781	70

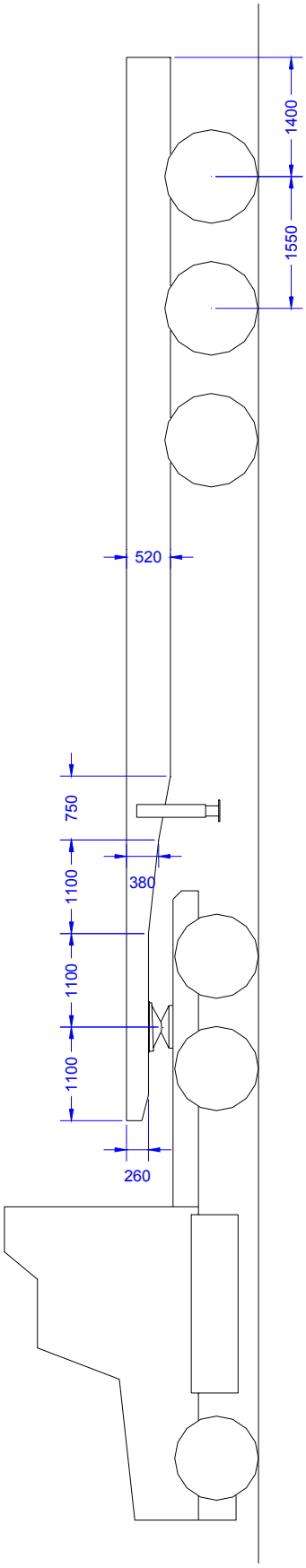

Figure A.6 Basic Chassis Rail Profile of Haulmark Trailer (1992)

A.7 Lusty Allison Trailer 1995

Table A.7 Chassis Characteristics of Lusty Allison Trailer (1995)

Manufacturer	Lusty Allison	**Suspension**	Spring
Year	1995	**Axle Config.**	Tri-axle
	Chassis Rails		**Cross Members**
	Section B-B (mm)	Section A-A (mm)	(mm)
Top Flange **Flange Thickness** Bottom Flange	20 20	20 20	6
Web Thickness	4	4	4
Web Depth	210	475	88
Flange Width	130	130	45
Member Spacing	890	890	480
Y Bar	125	258	44
I_{xx} (mm^4)	7.2E+07	3.5E+08	1.3E+06
Moment Capacity (kNm)	202	482	8.9
Shear Capacity (kN)	168	380	70

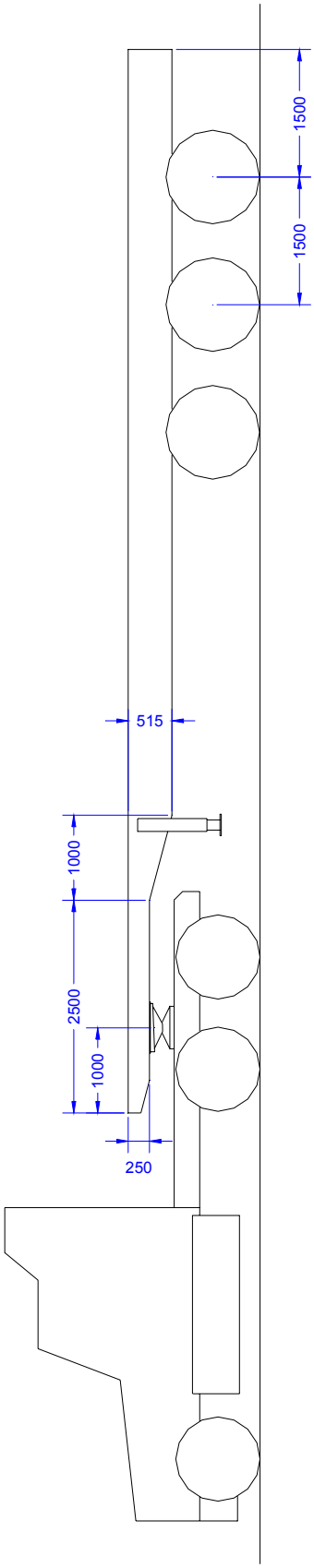

Figure A.7 Basic Chassis Rail Profile of Lusty Allison Trailer

A.8 Haulmark Trailer 1996

Table A.8 Chassis Characteristics of Haulmark Trailer (1996)

Manufacturer	Haulmark	**Suspension**	Spring
Year	1996	**Axle Config.**	Tri-axle
	Chassis Rails		**Cross Members**
	Section B-B (mm)	Section A-A (mm)	(mm)
Top Flange **Flange Thickness** Bottom Flange	12 20	12 20	6
Web Thickness	8	8	4
Web Depth	248	498	88
Flange Width	100	100	45
Member Spacing	950	950	480
Y Bar	122	239	44
I_{xx} (mm^4)	6.4E+07	2.9E+08	1.3E+06
Moment Capacity (kNm)	183	421	8.9
Shear Capacity (kN)	397	797	70

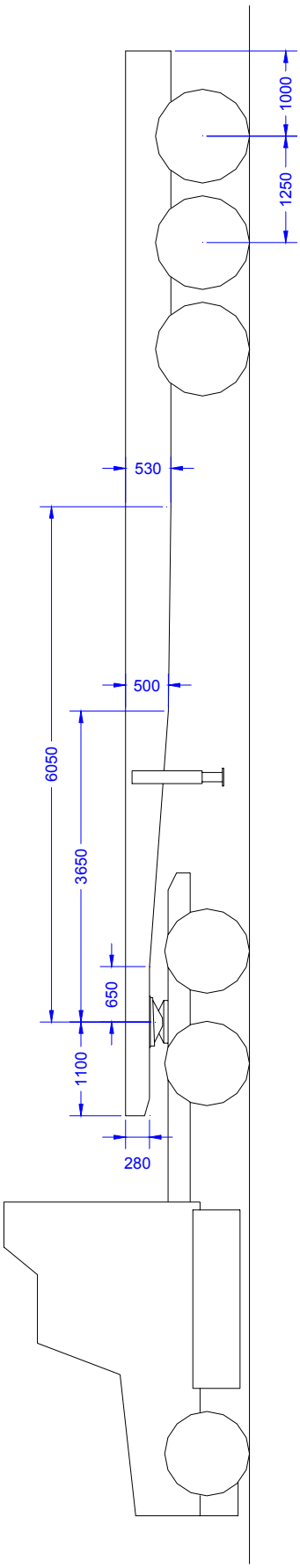

Figure A.8 Basic Chassis Rail Profile of Haulmark Trailer (1996)

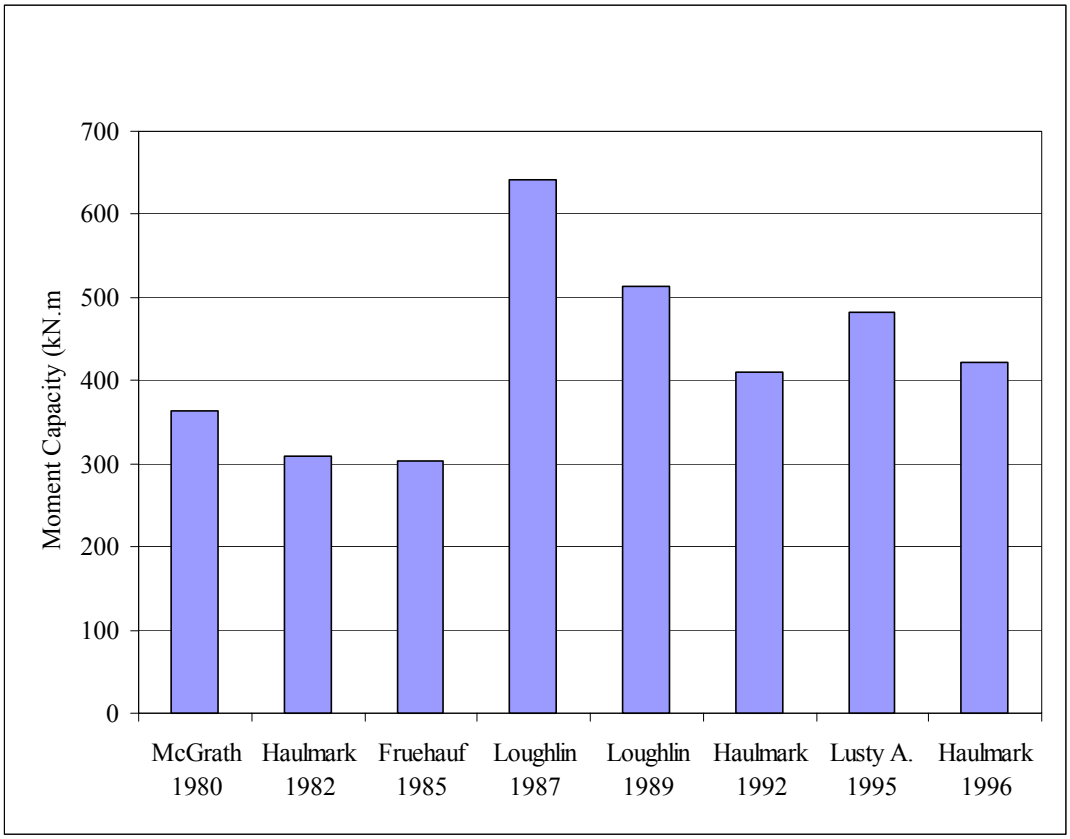

Figure A.9 Moment Capacity at Yield of Various Flatbed Trailers

Appendix B – Steel Flatbed Trailer Analysis

B.1 Analysis Identification

1992 Haulmark Trailer	HM01 / HM01Lc3
1995 Lusty Allison Trailer	LA03 / LA03Lc3

B.2 Aim of Analysis

- To perform a linear static analysis of the chassis rails of two steel trailers of comparable ultimate strength.
- To investigate the performance of each chassis rail, in response to the application of loads as defined by load cases one and three.
- To allow the comparison of the structural characteristics of the two chassis rails in relation to the influence of beam profile on maximum stress.

B.3 Model Form

The layout of each model is depicted in Figures D.1 and D.2, which were taken from the basic dimensions of each chassis rail presented in Appendix B.

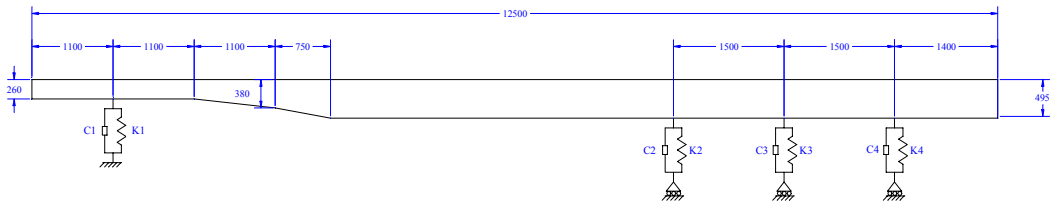

Figure B.1 (a) Basic Model Layout of Haulmark Trailer

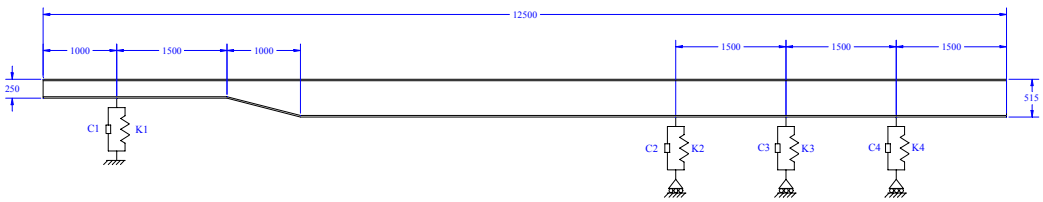

Figure B.1 (b) Basic Model Layout of Lusty Allison Trailer

B.4 Material Properties

The material used in these trailers was assumed to be mild steel (350 Grade), as denoted by the trailer manufacturer's, and was modelled as isotropic, and perfectly elastic.

Young's Modulus, E : 200 GPa

Poisson's Ratio, γ : 0.29

B.5 Analysis Program

Analysis program:	ANSYS 5.7
Computer:	Intell 266MMX
	128MB Ram
	Win98
Analysis type:	Linear static

B.6 Mesh Details

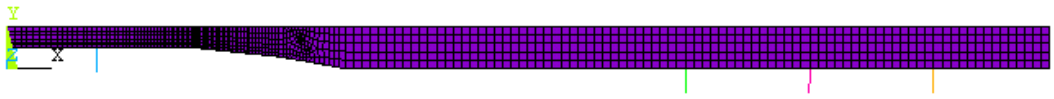

Figure B.2 (a) Mesh Used for Haulmark Trailer

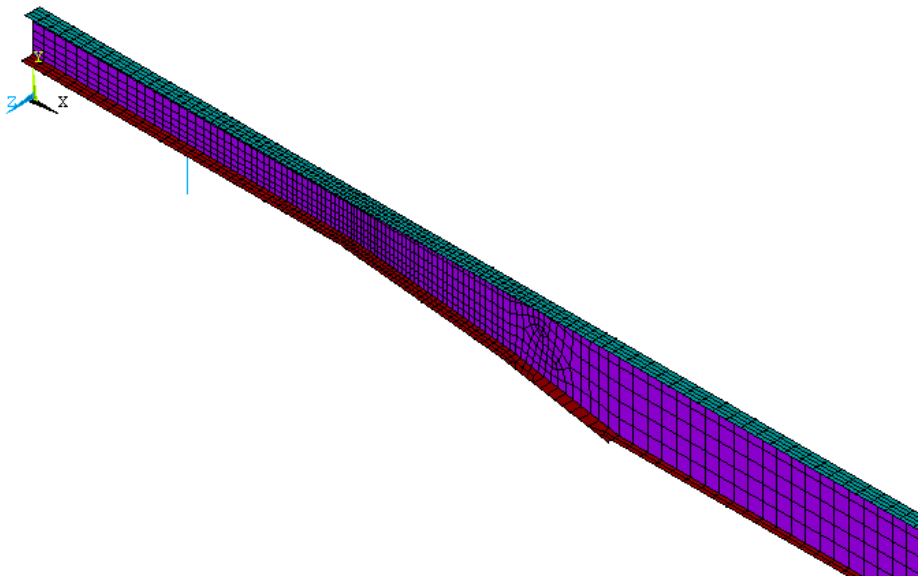

Figure B.2 (b) Mesh in Neck Area of Haulmark Trailer

Figure B.3 (a) Mesh Used for Lusty Allison Trailer

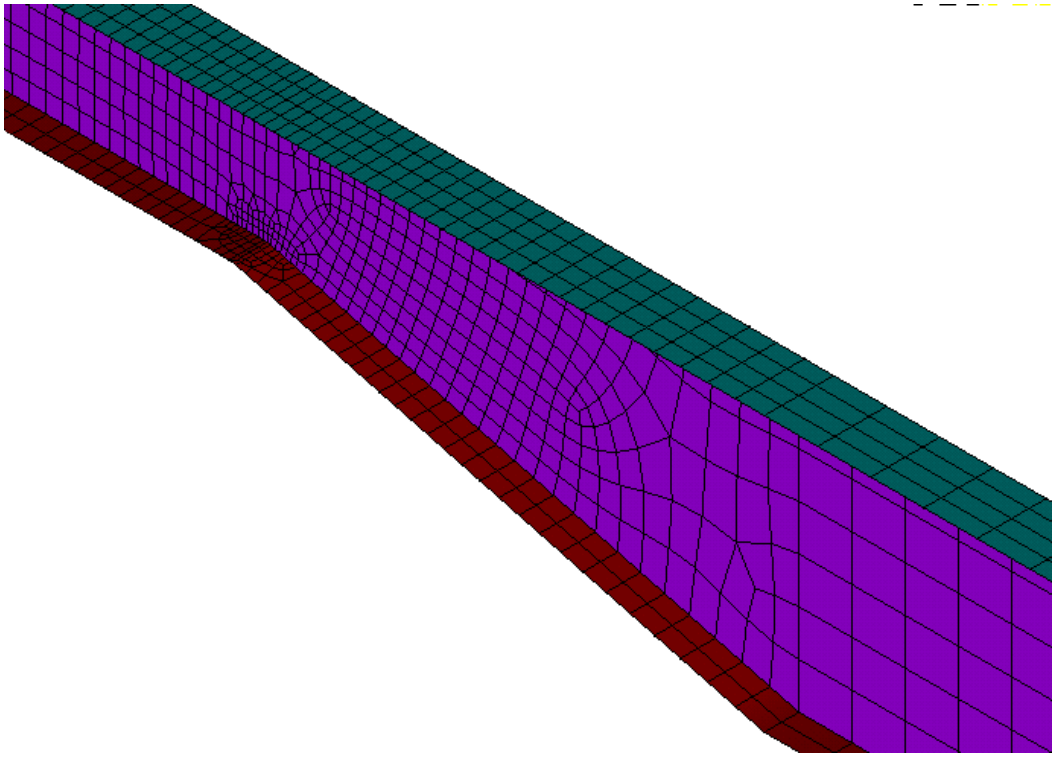

Figure B.3 (b) Mesh in Neck Area of Lusty Allison Trailer

Element Type:

1. SHELL 63 Has both bending and membrane capabilities. Both in-plane and normal loads are permitted. The element has six degrees of freedom at each node: translations in the nodal x, y, and z directions and rotations about the nodal x, y, and z-axes. Stress stiffening and large deflection capabilities are included. Refer ANSYS manual for further details.
2. COMBIN 14 Has longitudinal or torsional capability in one, two, or three-dimensional applications. The longitudinal spring-damper option is a uniaxial tension-compression element with up to three degrees of freedom at each node: translations in the nodal x, y, and z directions. No bending or torsion is considered. Refer ANSYS manual for further details.

B.7 Application of Boundary Conditions

The magnitude and position of the applied load was in accordance with the configuration specified by Load Case Three, section 4.5.4.

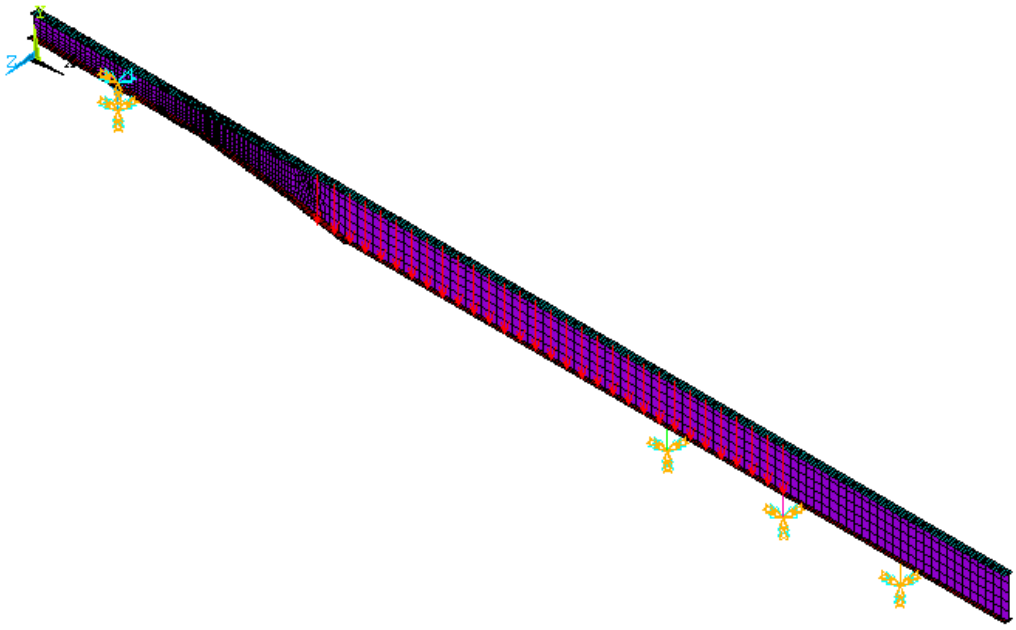

Figure B.4 (a) Boundary Conditions for Load Case Three on Haulmark Trailer

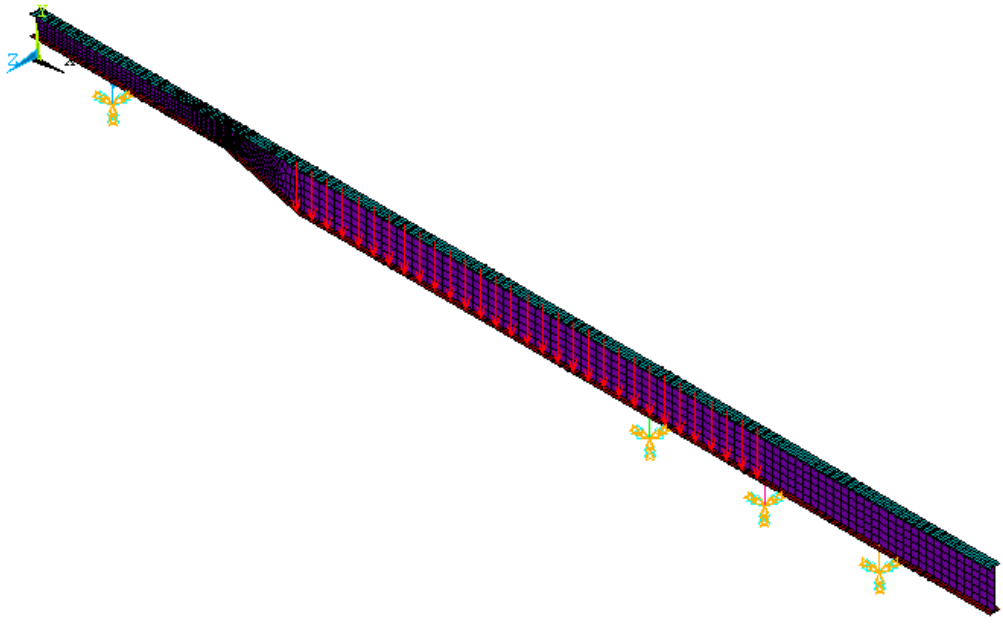

Figure B.4 (b) Boundary Conditions for Load Case Three on Lusty Allison Trailer

Table B.1 presents a summary of the real constants applied to each of the element groups:

Table B.1 Real Constant Values Used in Analysis

Real Constant	Notation	Haulmark Trailer		Lusty Allison Trailer	
		Load Case 1	Load Case 3	Load Case 1	Load Case 3
SET 1	Upper Flange Thickness	12	12	20	20
SET 2	Web Thickness	8	8	4	4
SET 3	Lower Flange Thickness	20	20	20	20
SET 4	K1	1500	1500	1200	1500
SET 5	K3	580	580	560	580
SET 6	K2	560	500	550	500
SET 7	K4	600	800	560	700

B.8 Load Case One Results

B.8.1 Haulmark Trailer

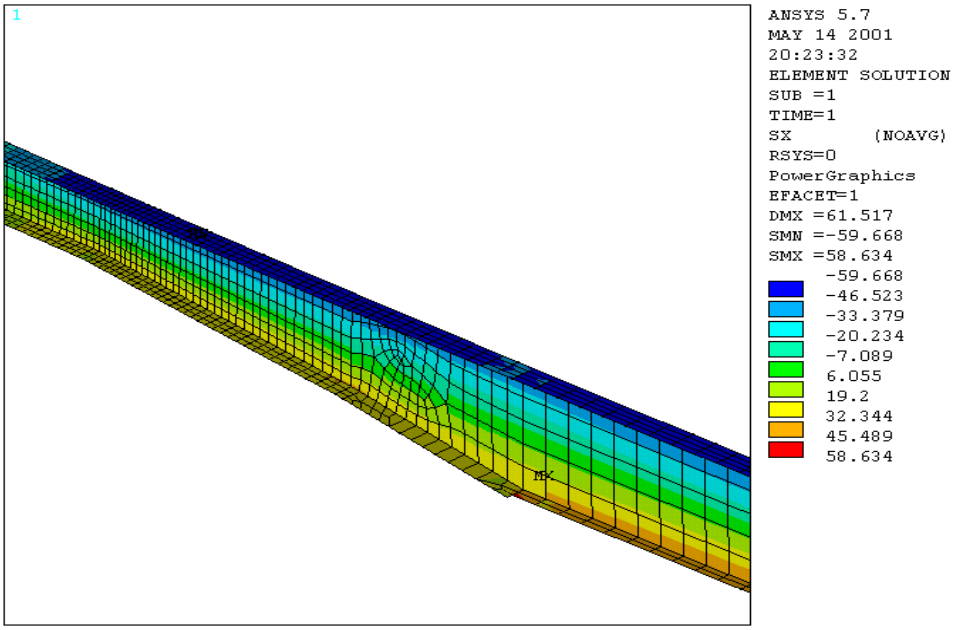

Figure B.5 (a) Maximum Stress in X-Direction Under Load Case One – Haulmark Trailer

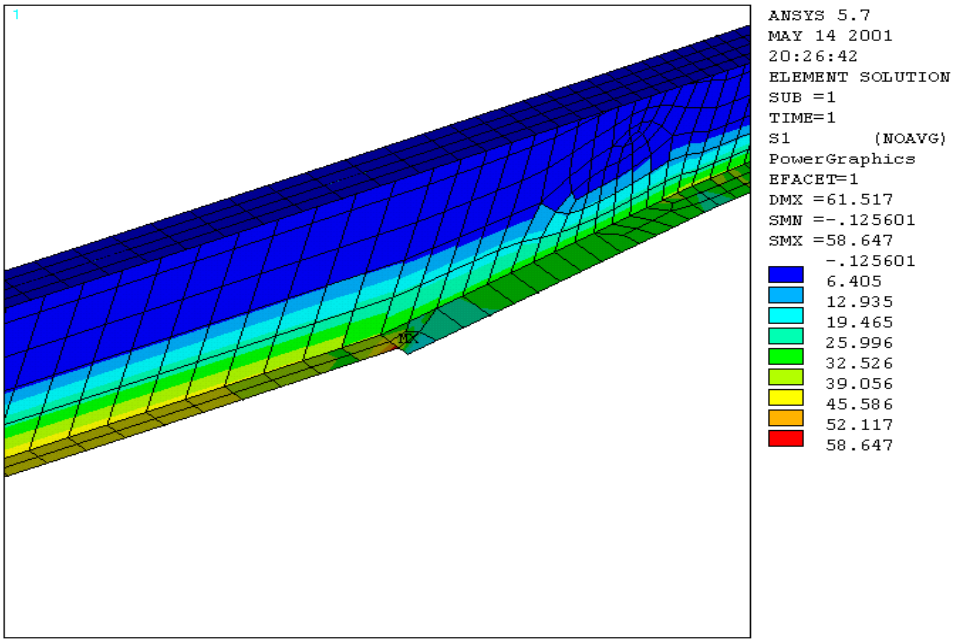

Figure B.5 (b) Maximum Principal Stress Under Load Case One – Haulmark Trailer

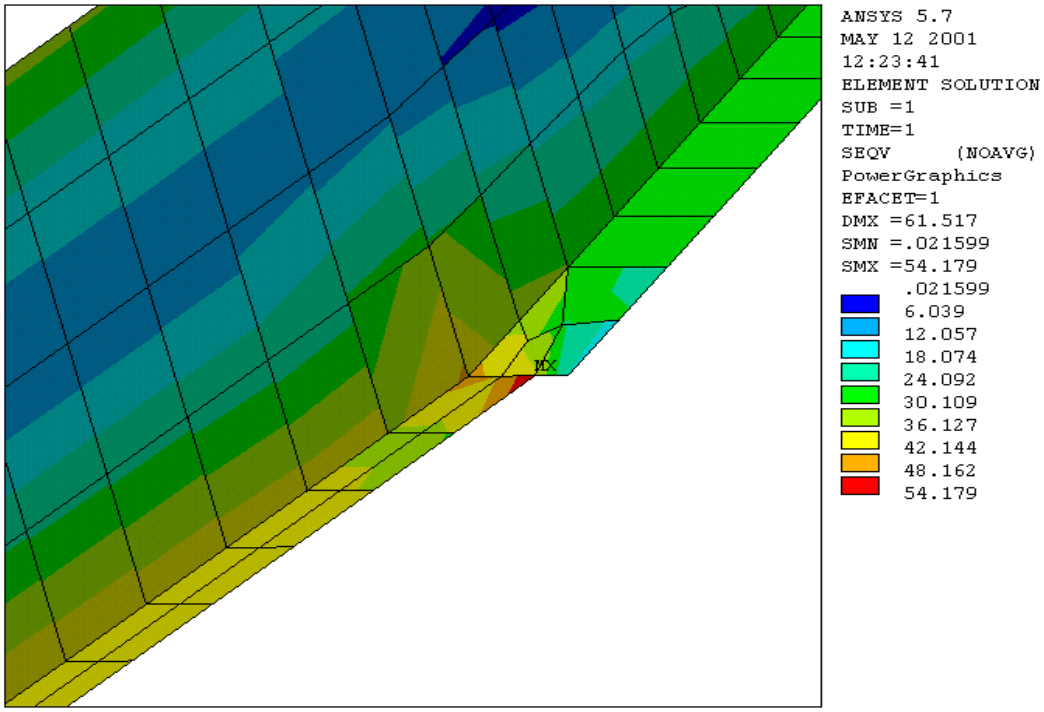

Figure B.5 (c) Maximum Von Mises Stress Under Load Case One – Haulmark Trailer

B.8.2 Lusty Allison Trailer

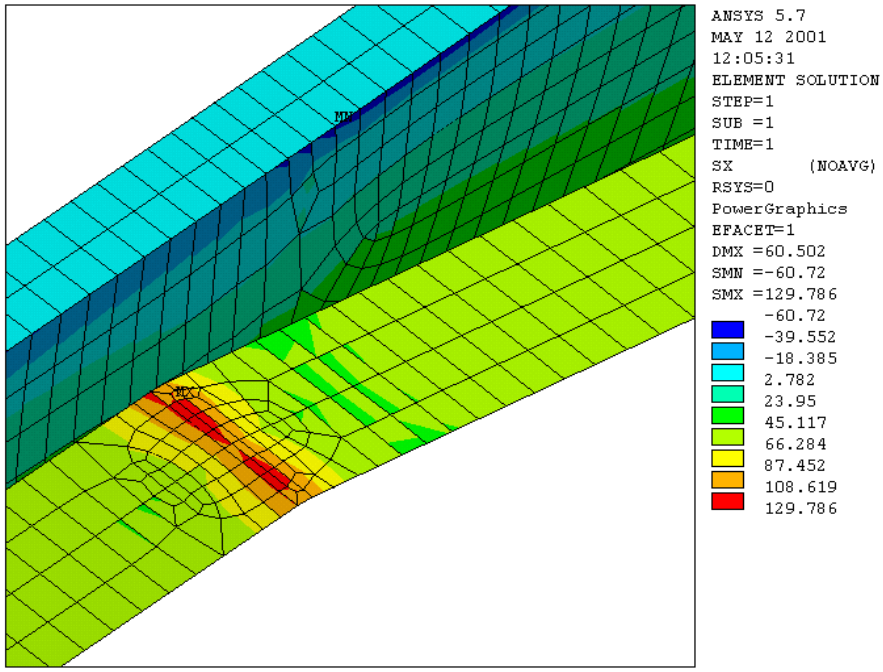

Figure B.6 (a) Maximum Stress in X-Direction Under Load Case One – Lusty Allison Trailer

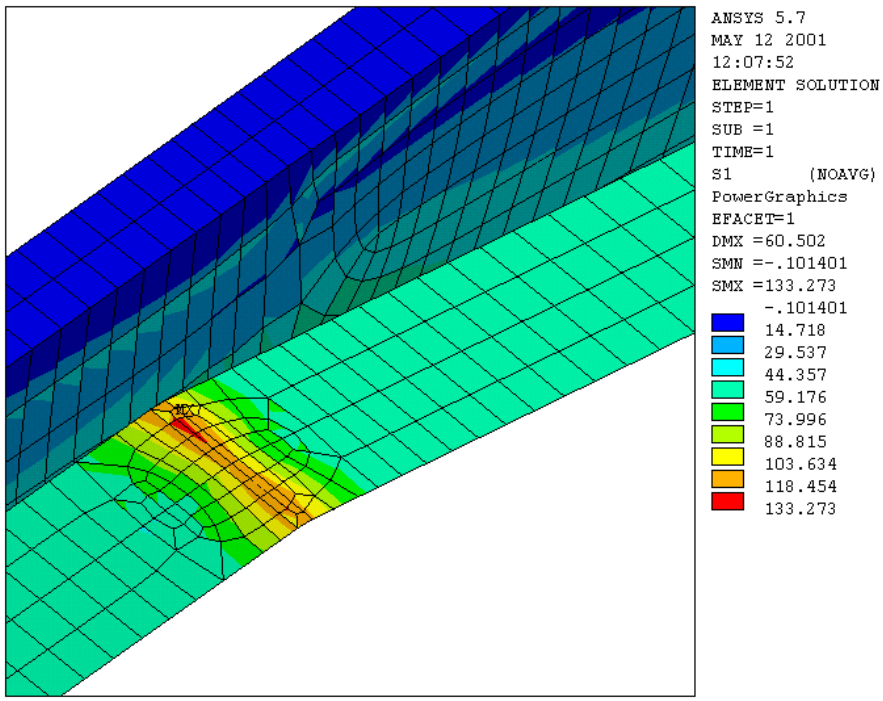

Figure B.6 (b) Maximum Principal Stress Under Load Case One – Lusty Allison Trailer

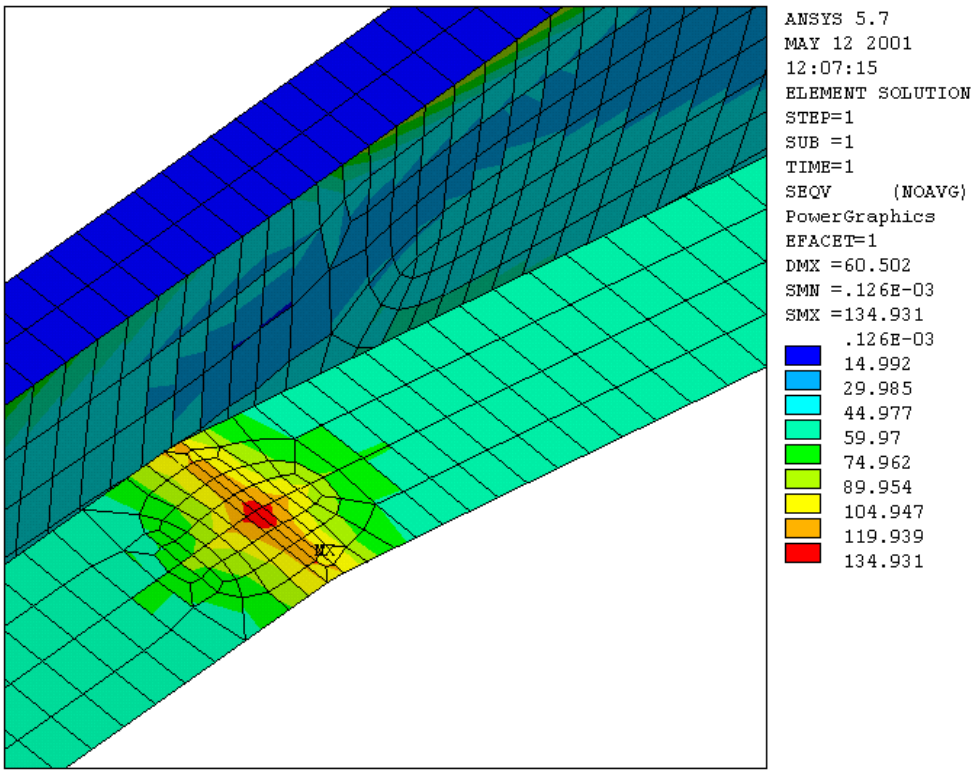

Figure B.6 (c) Maximum Von Mises Stress Under Load Case One – Lusty Allison Trailer

B.9 Load Case Three Results

B.9.1 Haulmark Trailer

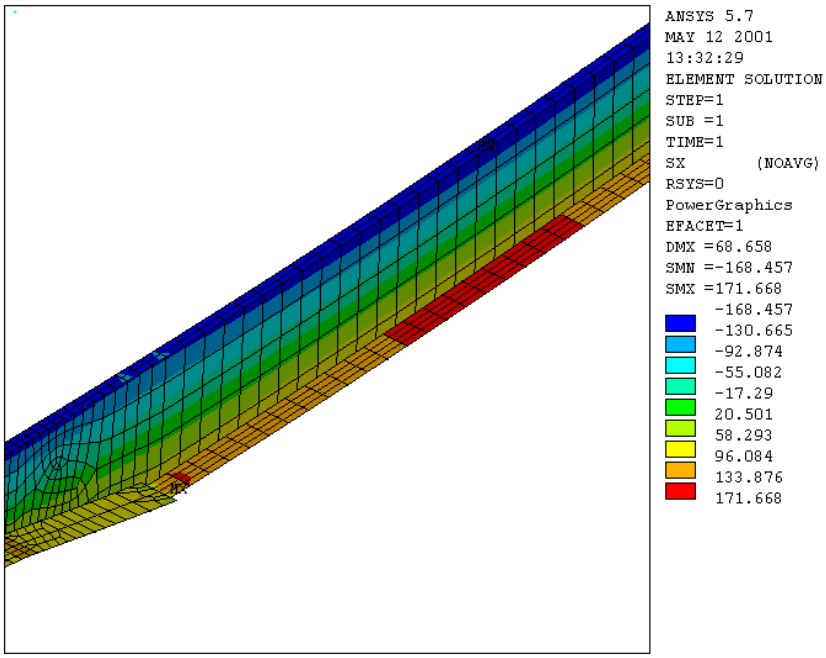

Figure B.7 (a) Maximum Stress in X-Direction Under Load Case Three – Haulmark Trailer

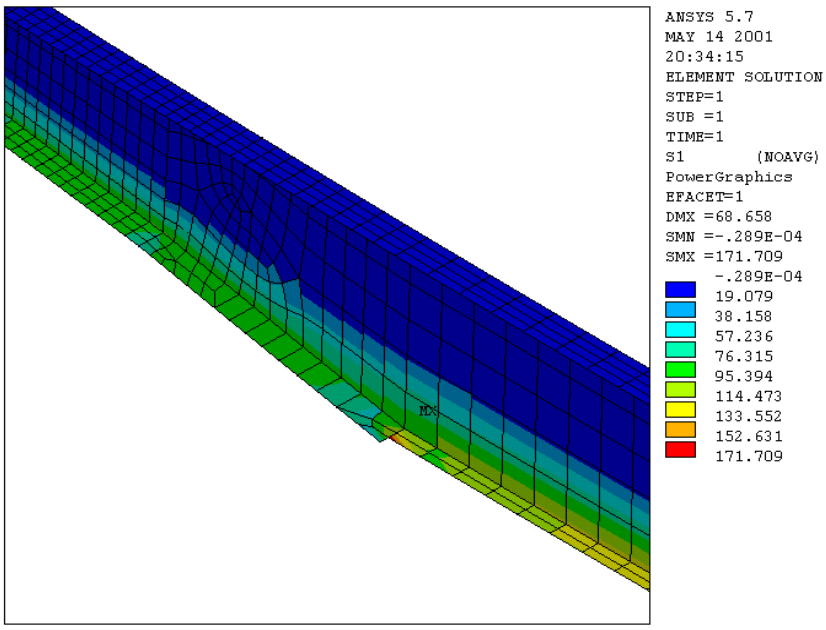

Figure B.7 (b) Maximum Principal Stress Under Load Case Three – Haulmark Trailer

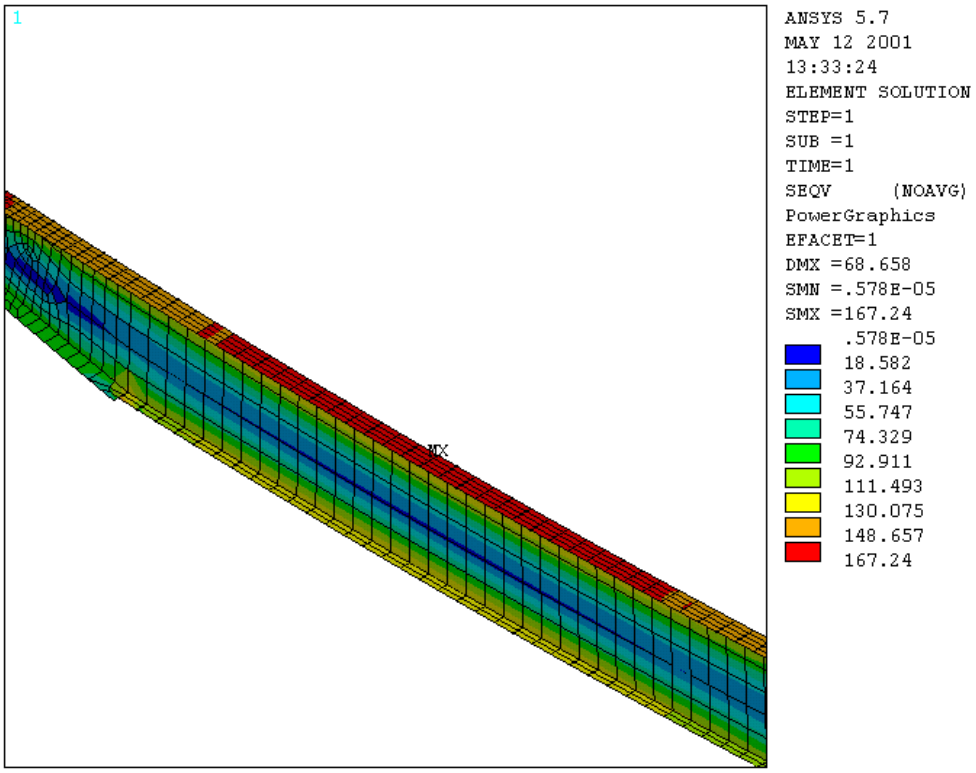

Figure B.7 (c) Maximum Von Mises Stress Under Load Case Three – Haulmark Trailer

B.9.2 Lusty Allison Trailer

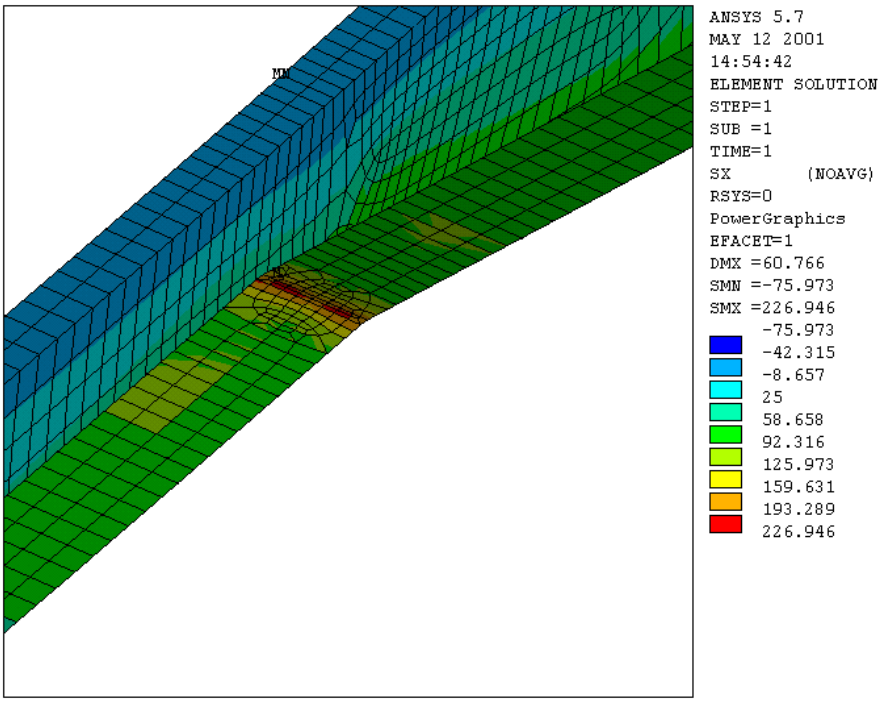

Figure B.8 (a) Maximum Stress in X-Direction Under Load Case Three – Lusty Allison Trailer

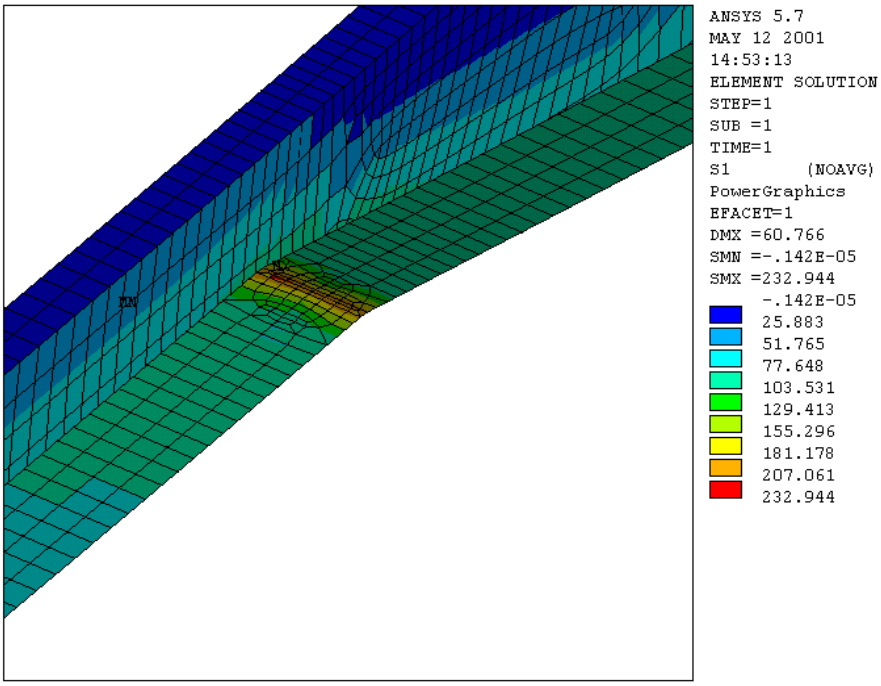

Figure B.8 (b) Maximum Principal Stress Under Load Case Three – Lusty Allison Trailer

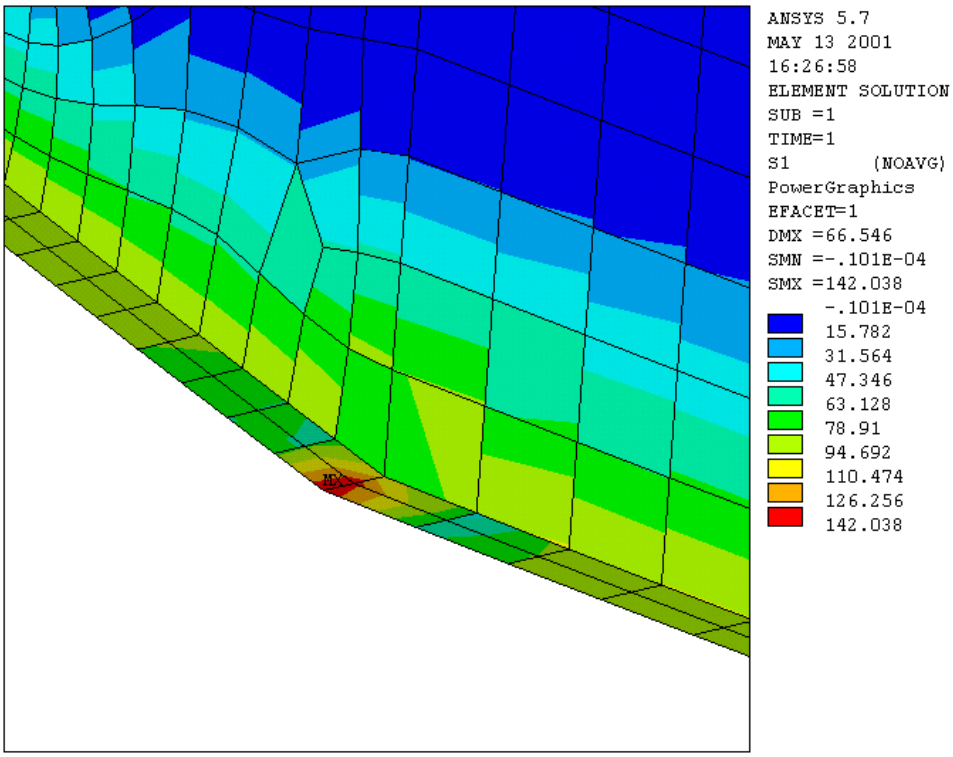

Figure B.8 (c) Principal Stress at Second Stress Concentration Under Load Case Three – Lusty Allison Trailer

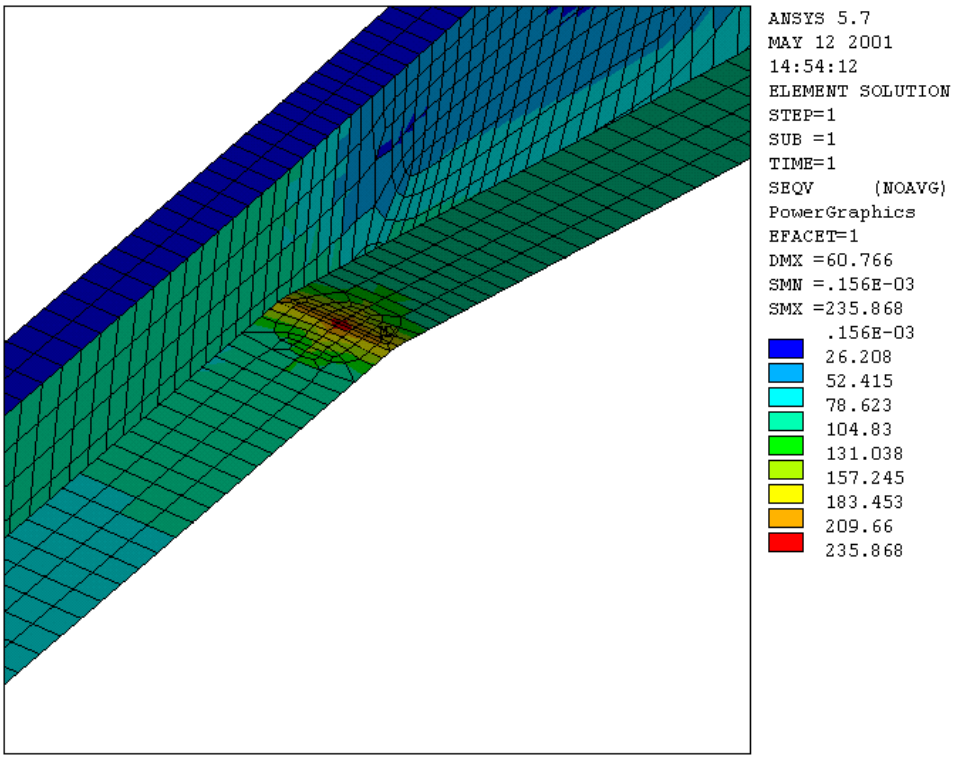

Figure B.8 (d) Maximum Von Mises Stress Under Load Case Three – Lusty Allison Trailer

Appendix C – Cross Sectional Analysis

C.1 Analysis Identification

Poly Urethane Foam Core crush2DorigPU.txt, crush2Diter1-5PU

C.2 Aim of Analysis

To perform a linear static analysis of the chassis rails of two steel trailers of comparable ultimate strength.

- To investigate the performance of each chassis rail, in response to the application of loads as defined by load cases one and three.
- To allow the comparison of the structural characteristics of the two chassis rails in relation to the influence of beam profile on maximum stress.

C.3 Model Form

The layout of the model is depicted in Figure C.1, which was taken from the basic dimensions of the chassis rail presented in section 7.3. An identical model was used for both cross sections, with the exception of material properties of the core material. A steel plate was placed atop the cross section, supported by elastic spring elements, in order to provide an even and distributed load, as experienced by the test pieces.

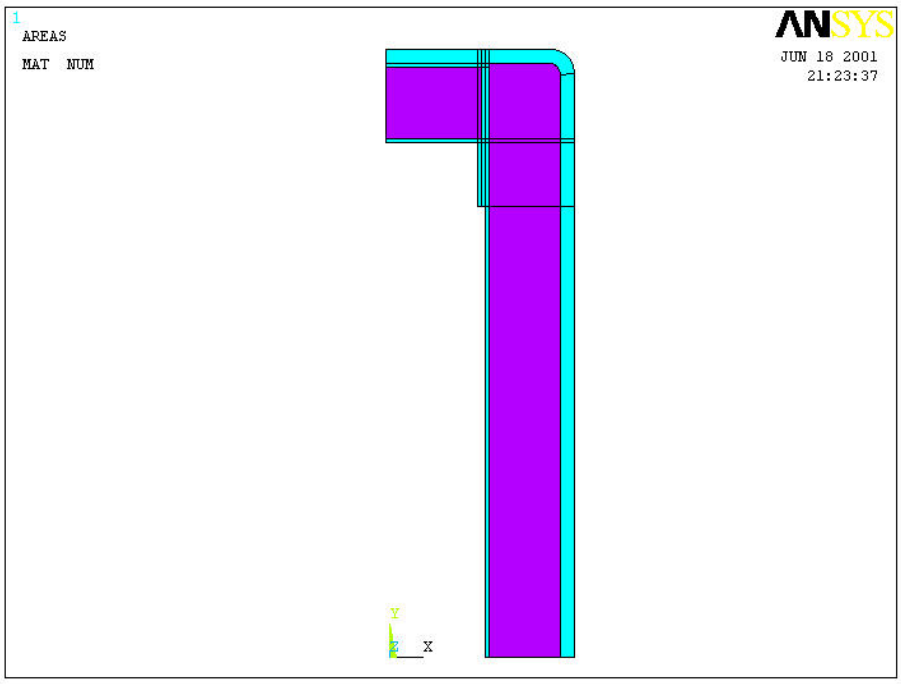

Figure C.1 Basic Model Layout Beam Cross Section

C.4 Material Properties

Both unidirectional and double bias (DB) fabrics were used in this beam. An orthotropic material represented the unidirectional laminates, with the x-direction of each element being oriented according to the global model x-axis. The double bias fabric was represented by two uni-directional laminates, oriented at $\pm 45^0$, as discussed in section 5.6.6. The material properties, taken from section 5.6.6 and other sources where appropriate, were input into the model as follows:

1. Properties of E-glass Uni-directional reinforcement (300 g/m^2):

Young's Modulus, E_1 : 28624 MPa

E_2 : 7404 MPa

Poisson's Ratio, γ_{xy} : 0.322

Shear Modulus, G_{xy} : 2986 MPa

T'ness per layer of t_{UD} : 0.3 mm

Unidirectional E-glass (300 g/m^2)

T'ness per layer of t_{DB} : 0.6 mm

Double Bias Fabric (600 g/m^2)

2. Properties of T300 Carbon Fibre Uni-directional reinforcement (315 g/m^2):

Young's Modulus, E_1 : 64973 MPa

	E_2 :	7404 MPa
Poisson's Ratio,	γ_{xy} :	0.23
Shear Modulus,	G_{xy} :	6000 MPa
Thickness per layer.	t_{UD} :	0.53 mm

3. Properties of Polyurethane Foam

Young's Modulus,	E_1 :	250 MPa
Poisson's Ratio,	γ_{xy} :	0.32

Laminate Stacking Sequences:

The laminate stacking sequences used for each configuration of the basic model are described in section 7.4.3.

C.5 Analysis Program

Analysis program:	ANSYS 5.7
Computer:	Intell 266MMX
	128MB Ram
	Win98
Analysis type:	Non-Linear static (Large Displacement Static)
No. of Sub-steps:	10

C.6 Mesh Details

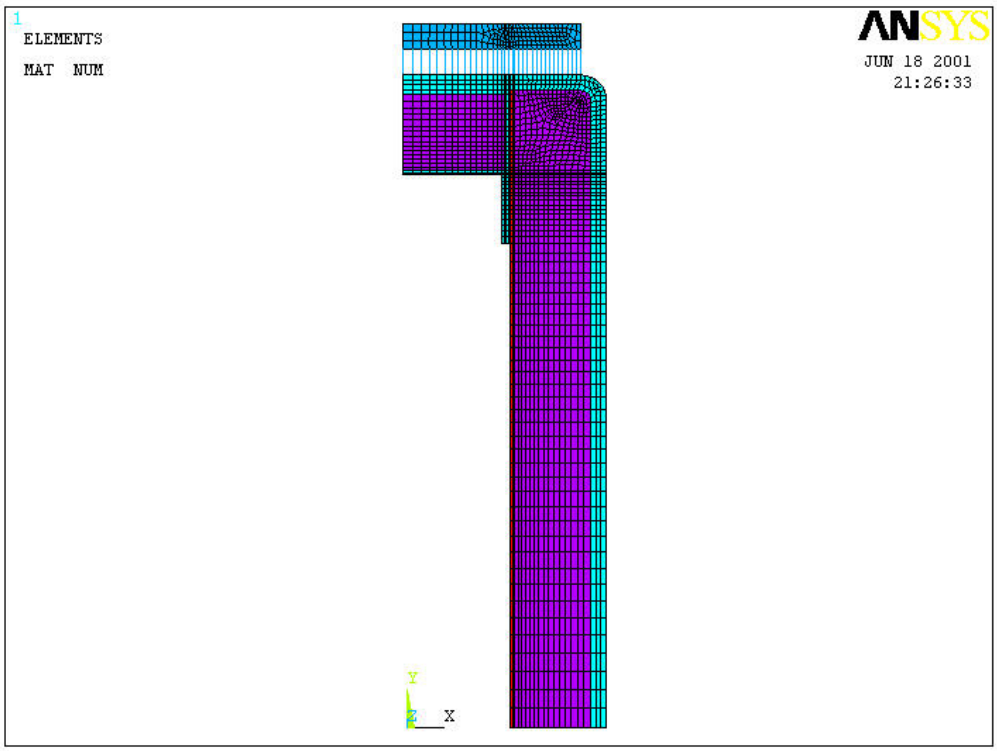

Figure C.2 (a) Mesh Used for Cross Section Analysis – Original Form

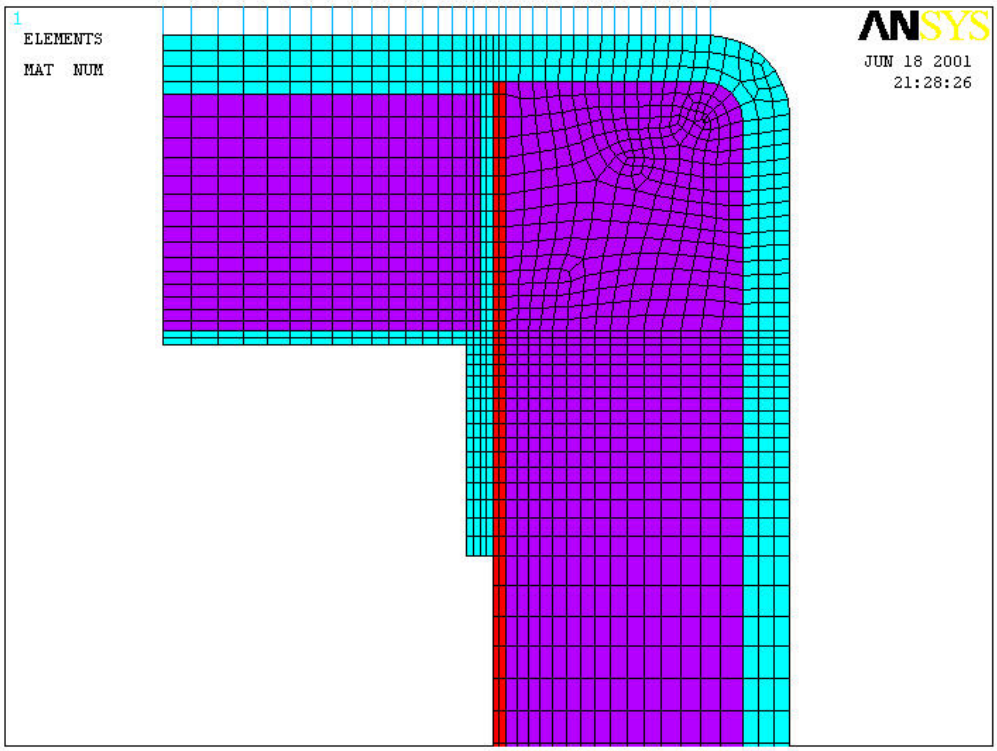

Figure C.2 (b) Magnified View of Original Mesh

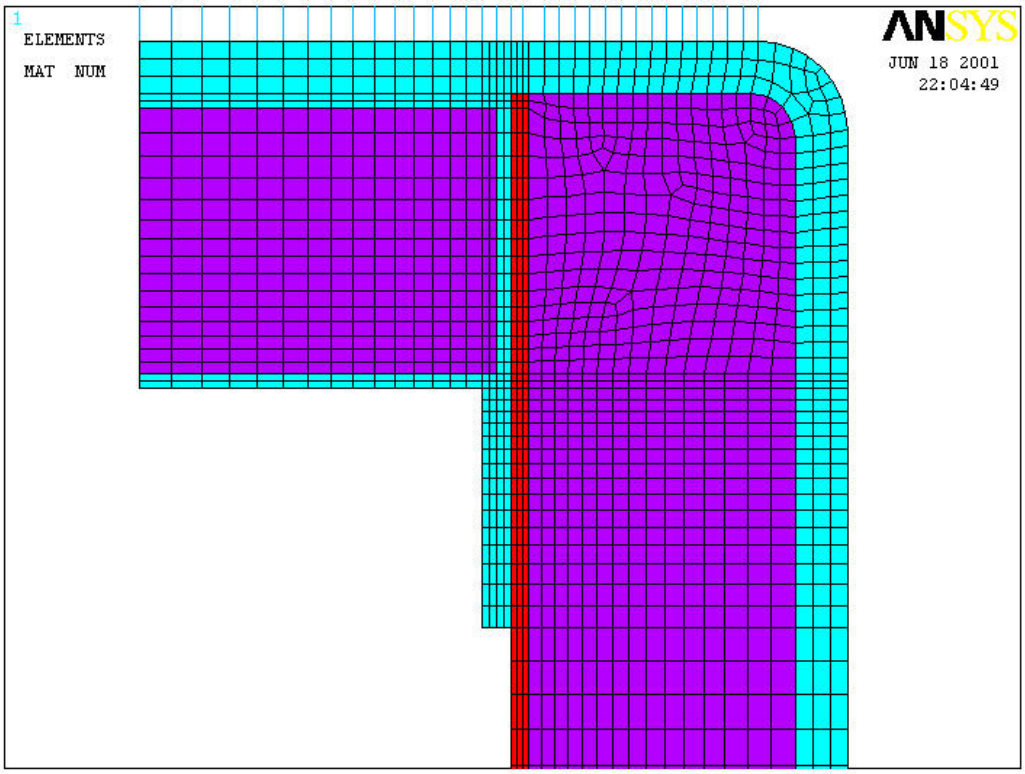

Figure C.2 (c) Mesh Used for Cross Section Analysis – Iteration #1

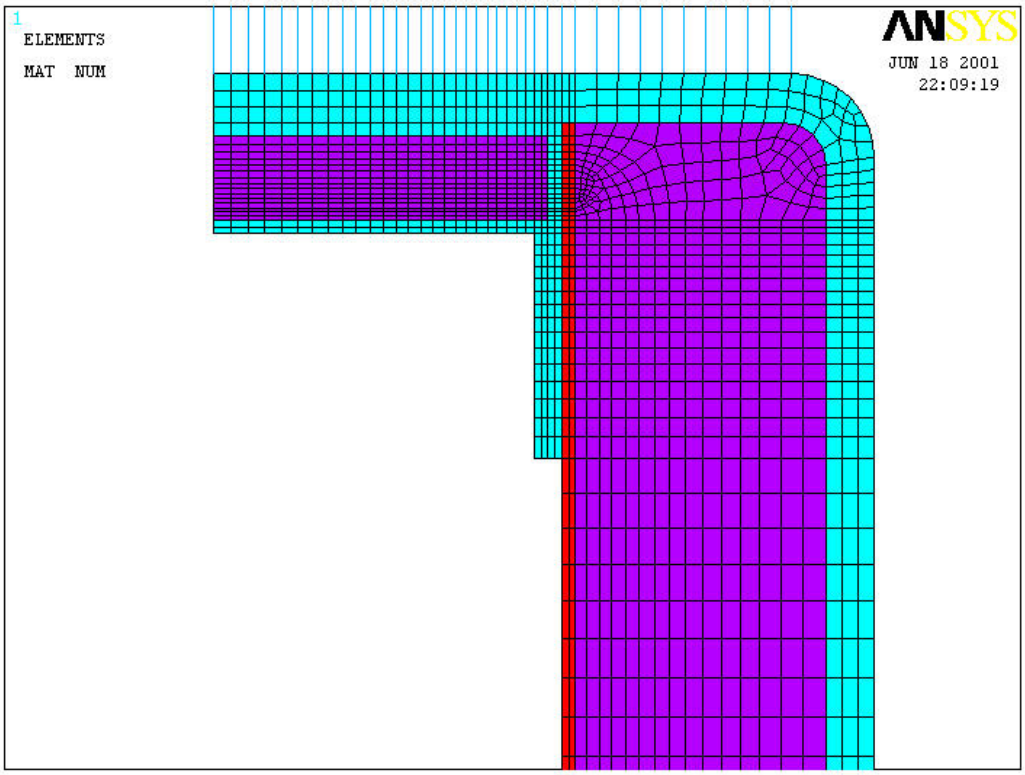

Figure C.2 (d) Mesh Used for Cross Section Analysis – Iteration #2

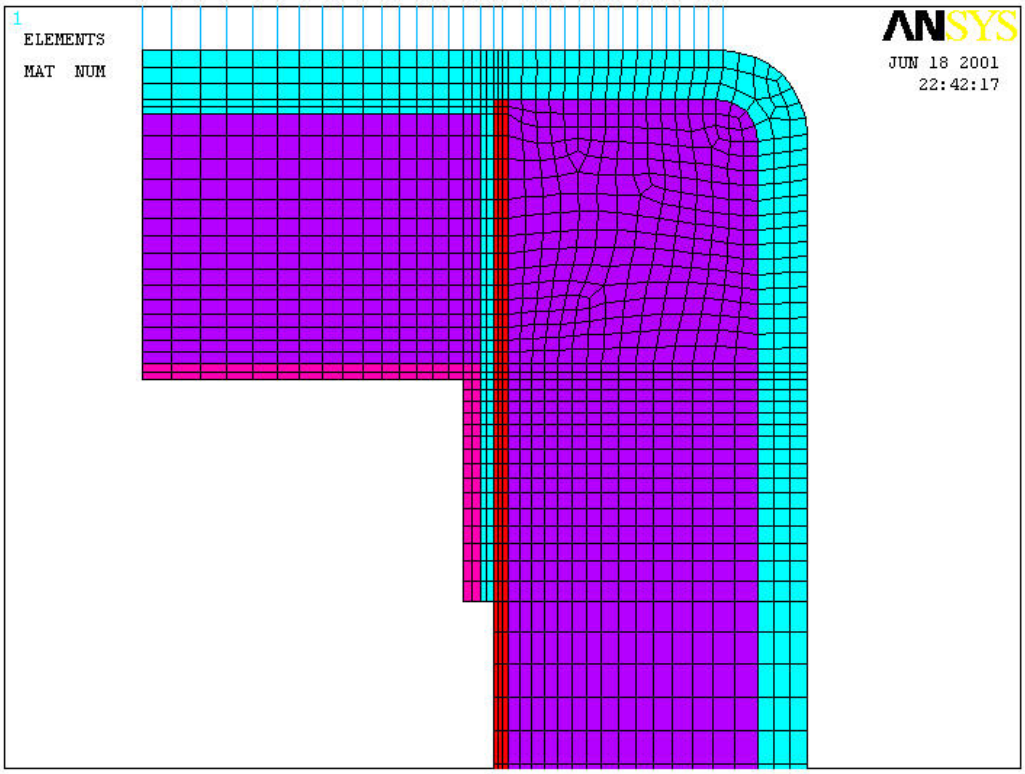

Figure C.2 (e) Mesh Used for Cross Section Analysis – Iteration #3

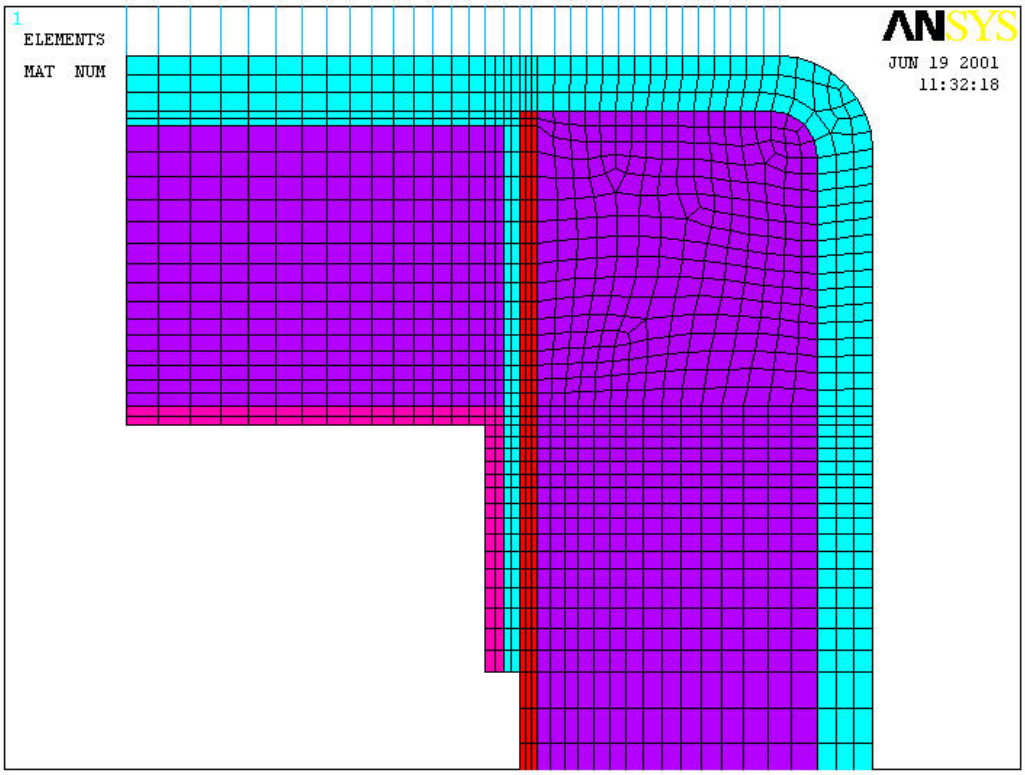

Figure C.2 (f) Mesh Used for Cross Section Analysis – Iteration #4

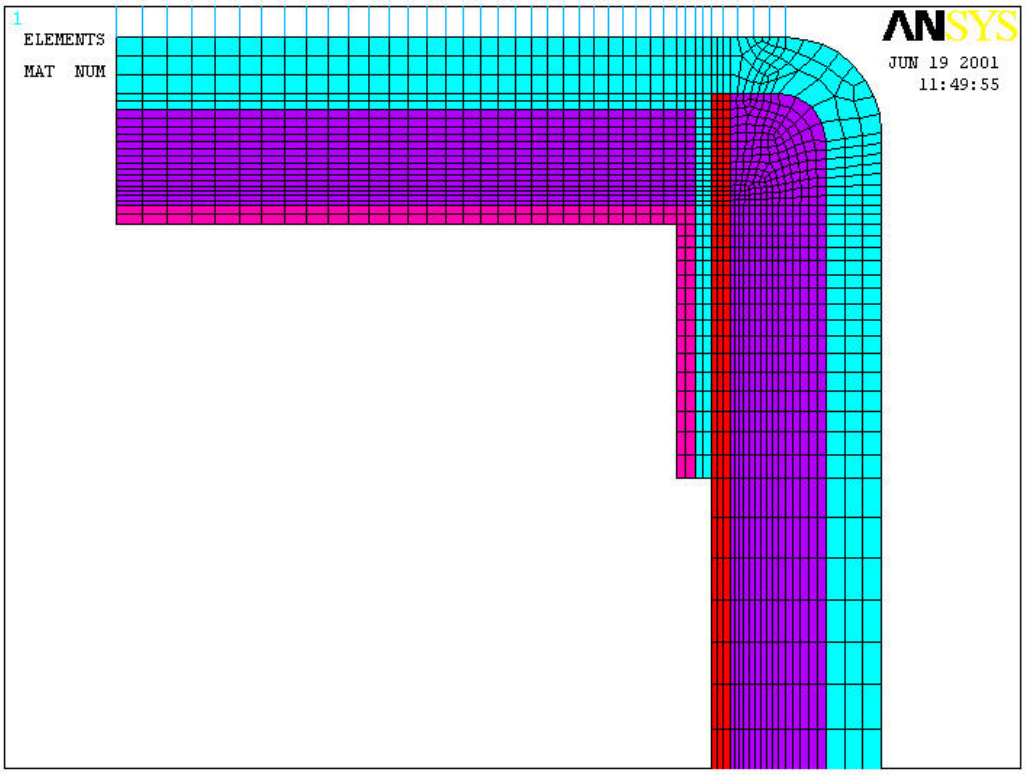

Figure C.2 (g) Mesh Used for Cross Section Analysis – Iteration #5

Element Type:

1. PLANE 82 Has both bending and membrane capabilities. Both in-plane and normal loads are permitted. The element has six degrees of freedom at each node: translations in the nodal x, y, and z directions and rotations about the nodal x, y, and z-axes. Stress stiffening and large deflection capabilities are included. Refer ANSYS manual for further details.
2. COMBIN 14 Has longitudinal or torsional capability in one, two, or three-dimensional applications. The longitudinal spring-damper option is a uniaxial tension-compression element with up to three degrees of freedom at each node: translations in the nodal x, y, and z directions. No bending or torsion is considered. Refer ANSYS manual for further details.

C.7 Application of Boundary Conditions

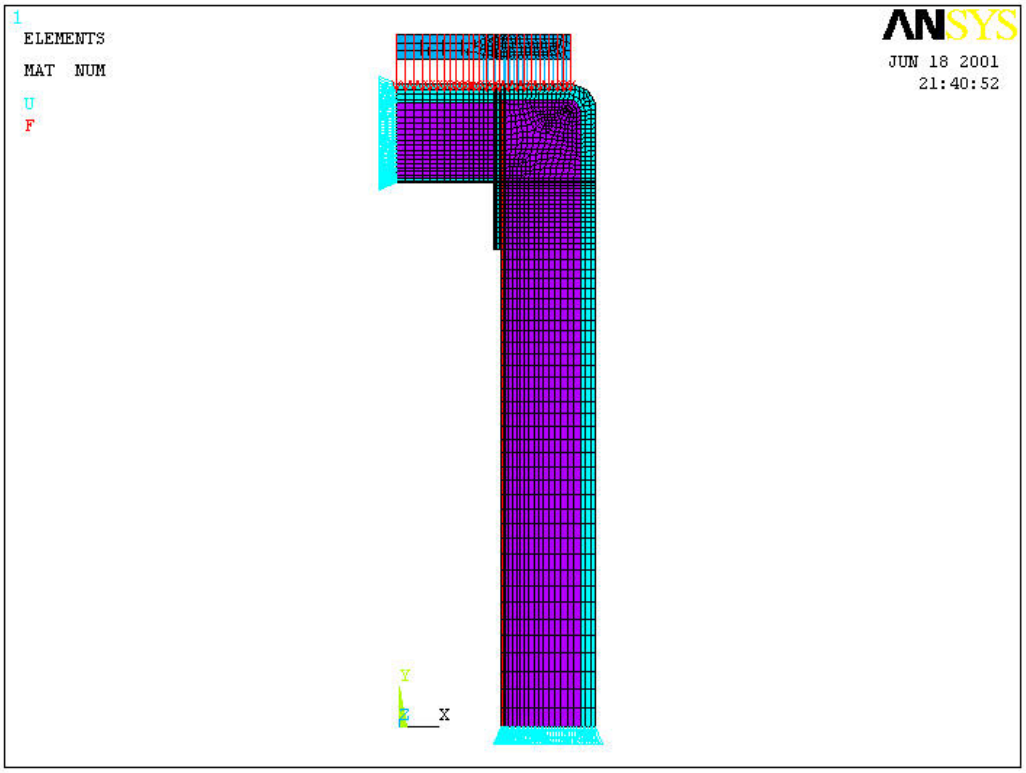

Figure C.3 (a) Boundary Conditions Applied to Each Beam Section

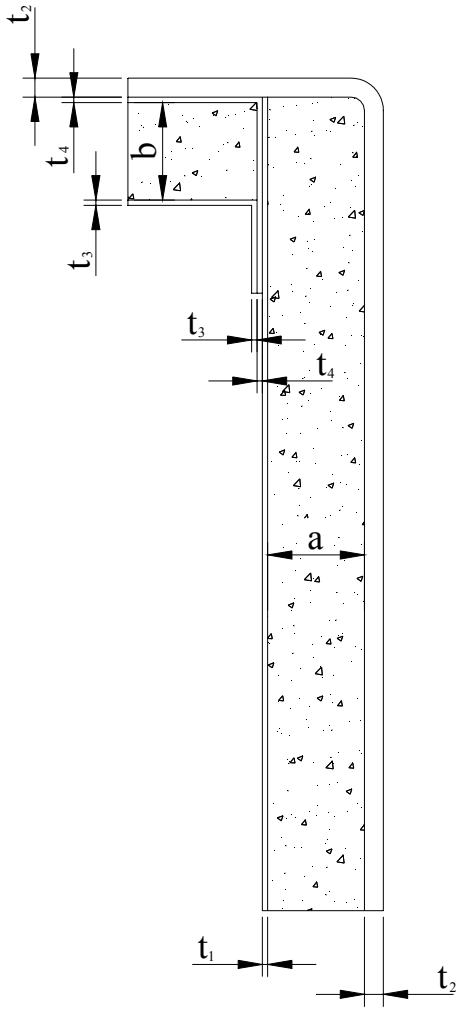

Figure C.3 (b) Denotation of Section Dimensions

Table C.1 presents a summary of the real constants applied to each of the element groups:

Table C.1 Real Constant Values Used in Analysis

REAL CONSTANT	Notation	HAULMARK TRAILER		LUSTY ALLISON TRAILER	
		Load Case 1	Load Case 3	Load Case 1	Load Case 3
SET 1	Upper Flange Thickness	12	12	20	20
SET 2	Web Thickness	8	8	4	4
SET 3	Lower Flange Thickness	20	20	20	20
SET 4	K1	1500	1500	1200	1500
SET 5	K3	580	580	560	580
SET 6	K2	560	500	550	500
SET 7	K4	600	800	560	700

C.8 Original Configuration Results

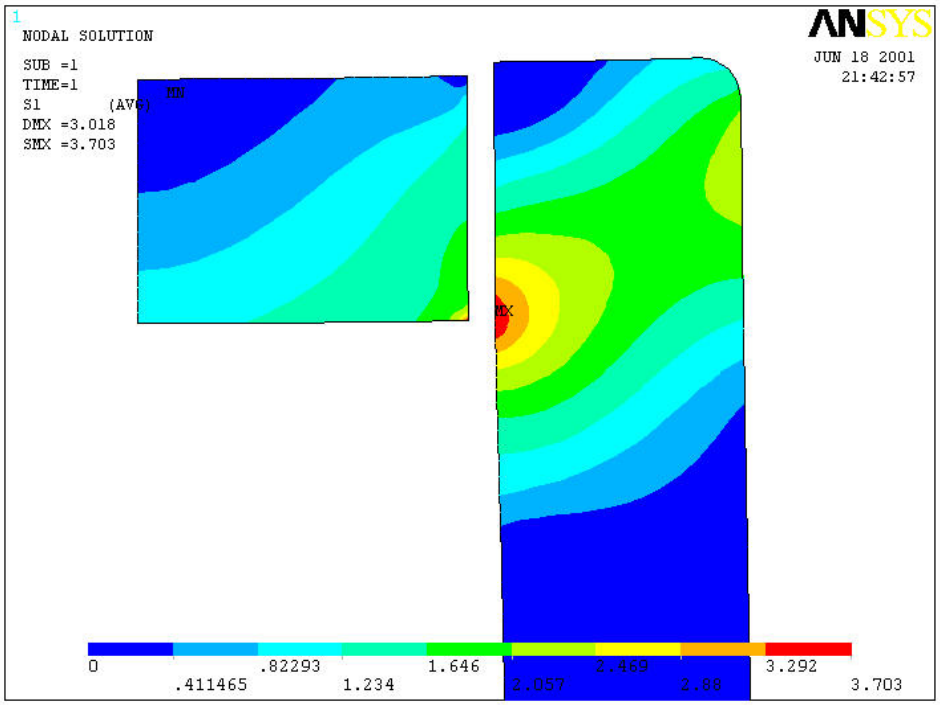

Figure C.4 (a) 1st Principal Stress In Core Material – Original Configuration

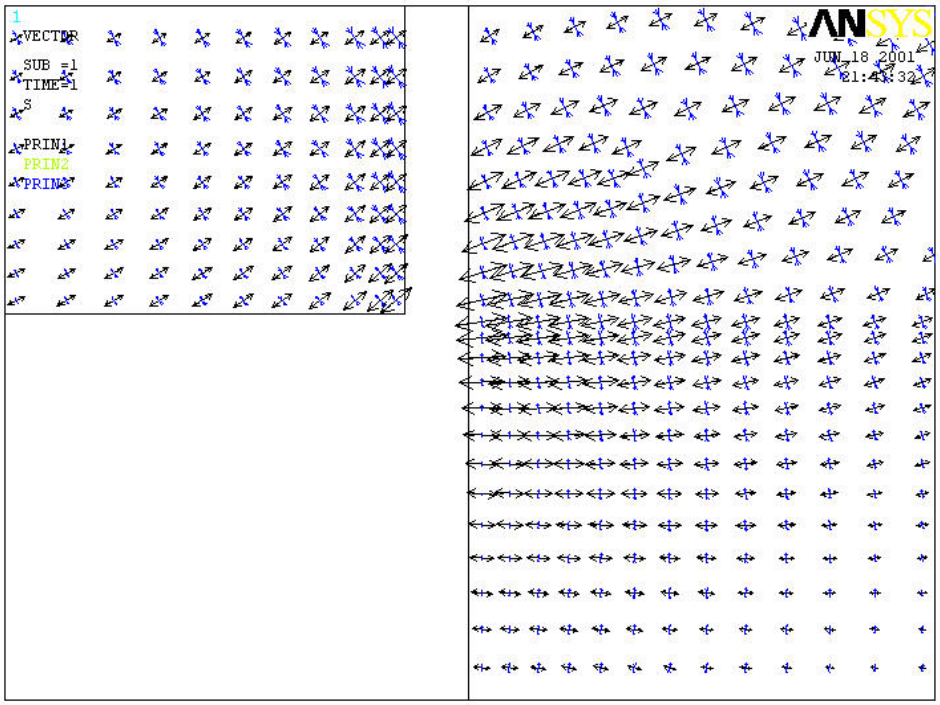

Figure C.4 (b) Vector Plot of Principal Stress In Core Material – Original Configuration

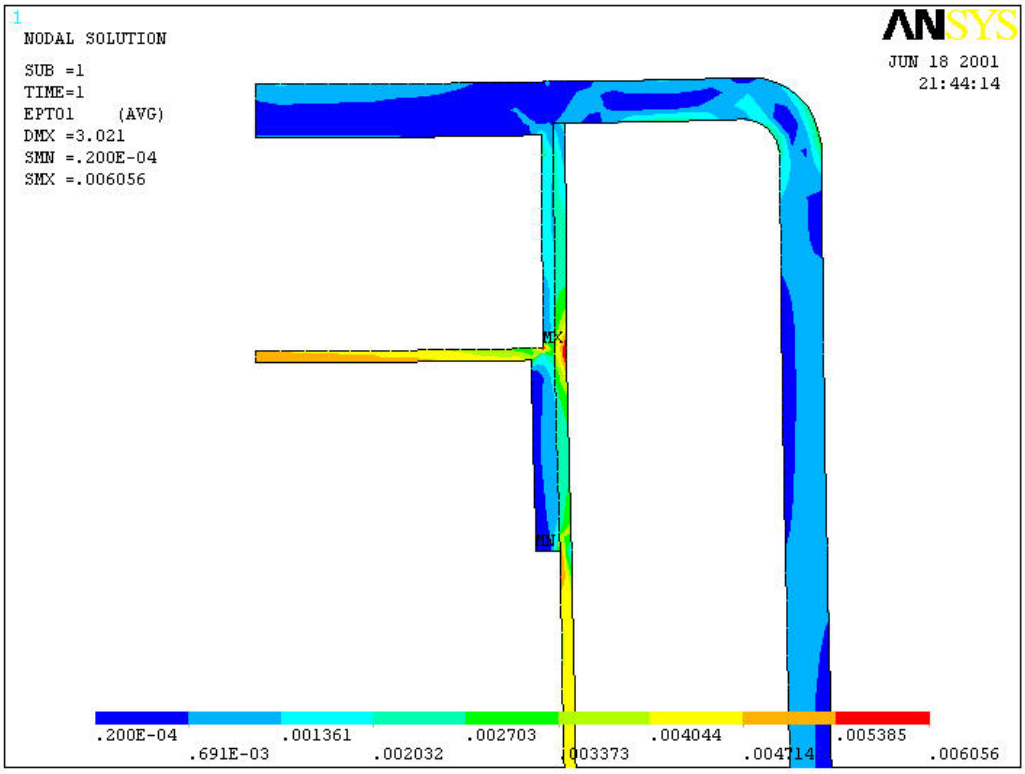

Figure C.4 (c) 1st Principal Strain in Laminates – Original Configuration

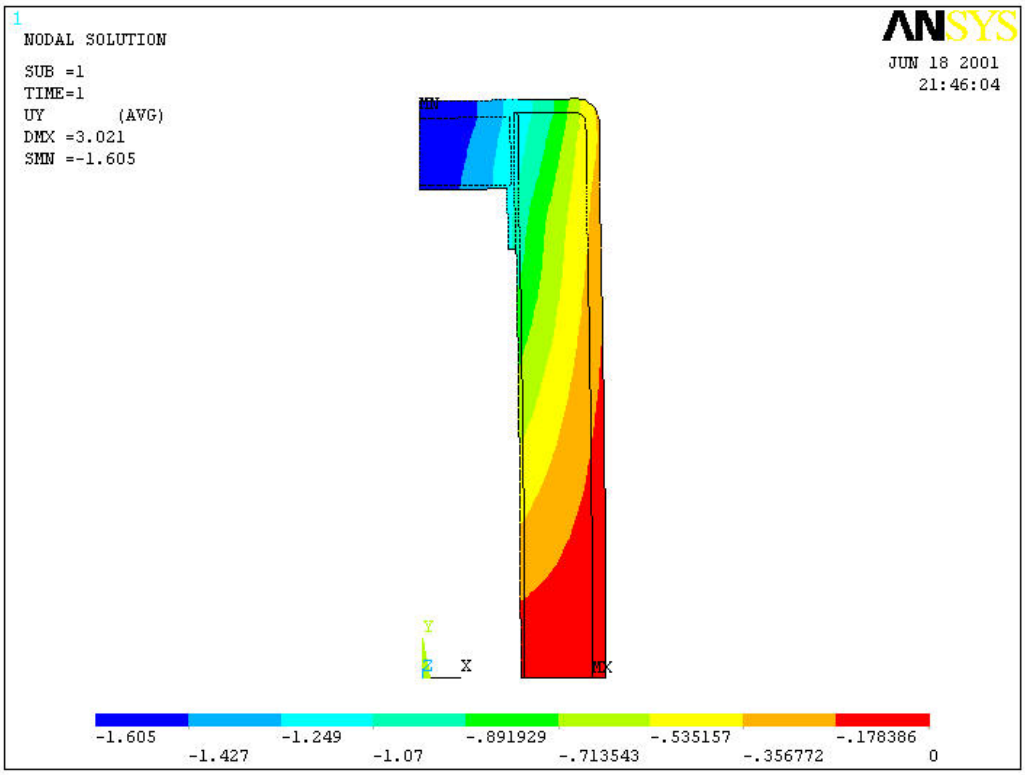

Figure C.4 (d) Vertical Deflection of Cross Section – Original Configuration

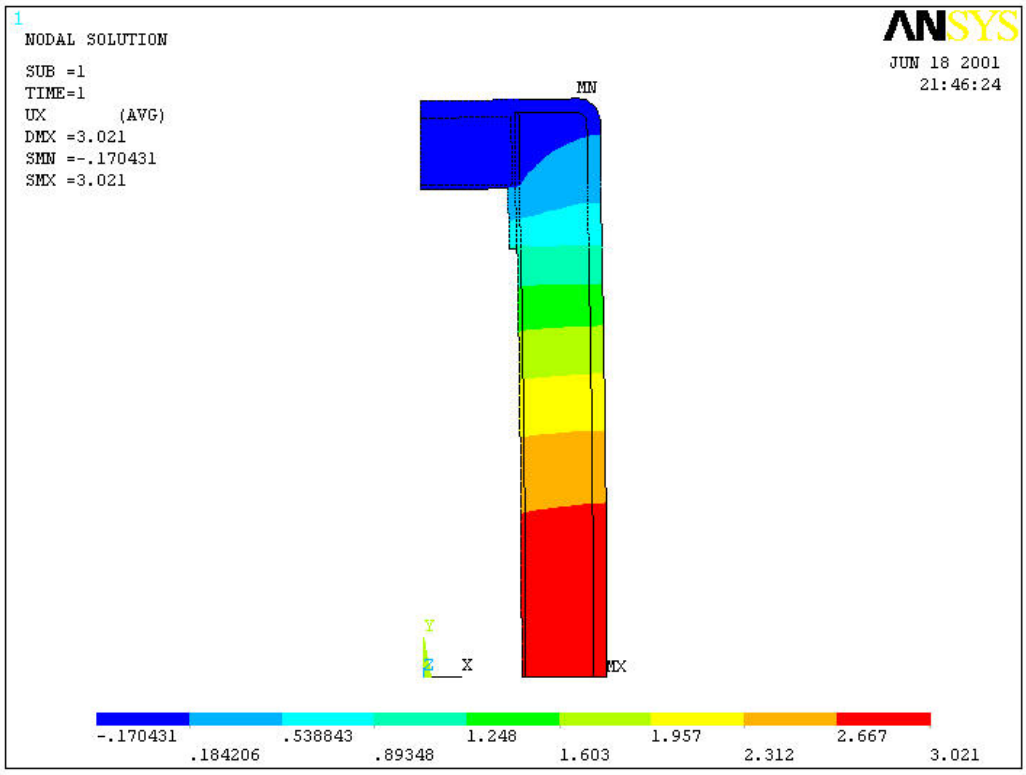

Figure C.4 (e) Lateral Deflection of Section Walls – Original Configuration

C.9 Iteration #1 Results

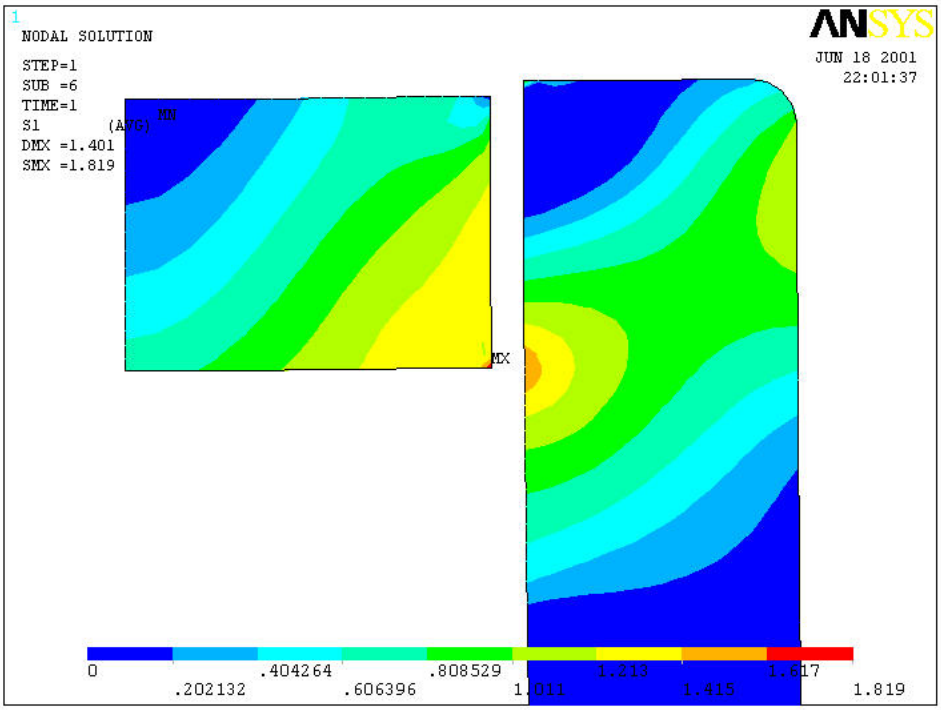

Figure C.5 (a) 1st Principal Stress In Core Material – Iteration #1

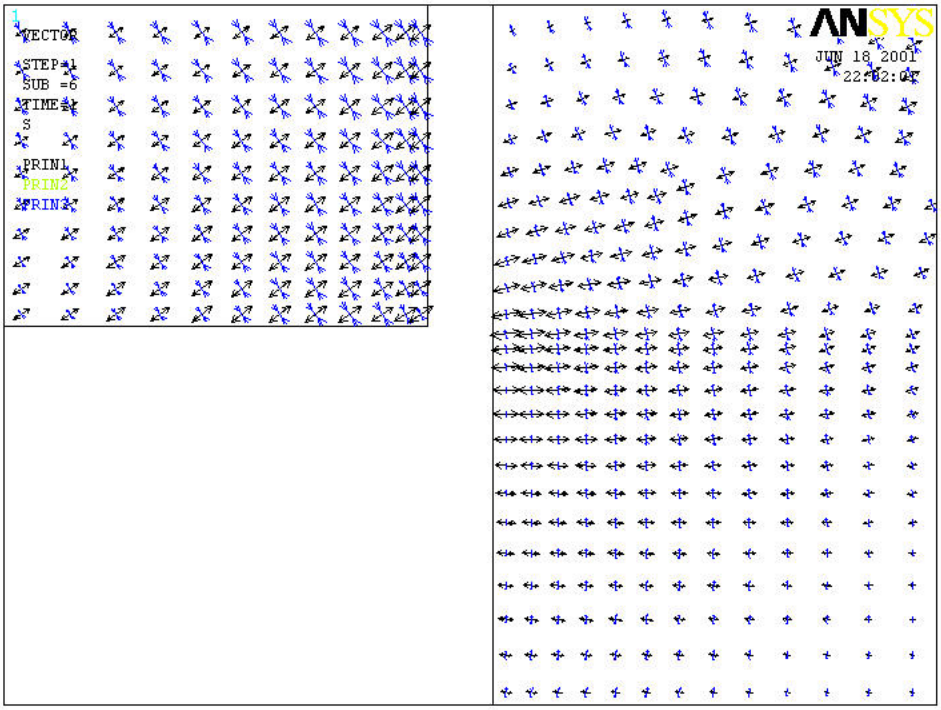

Figure C.5 (b) Vector Plot of Principal Stress In Core Material – Iteration #1

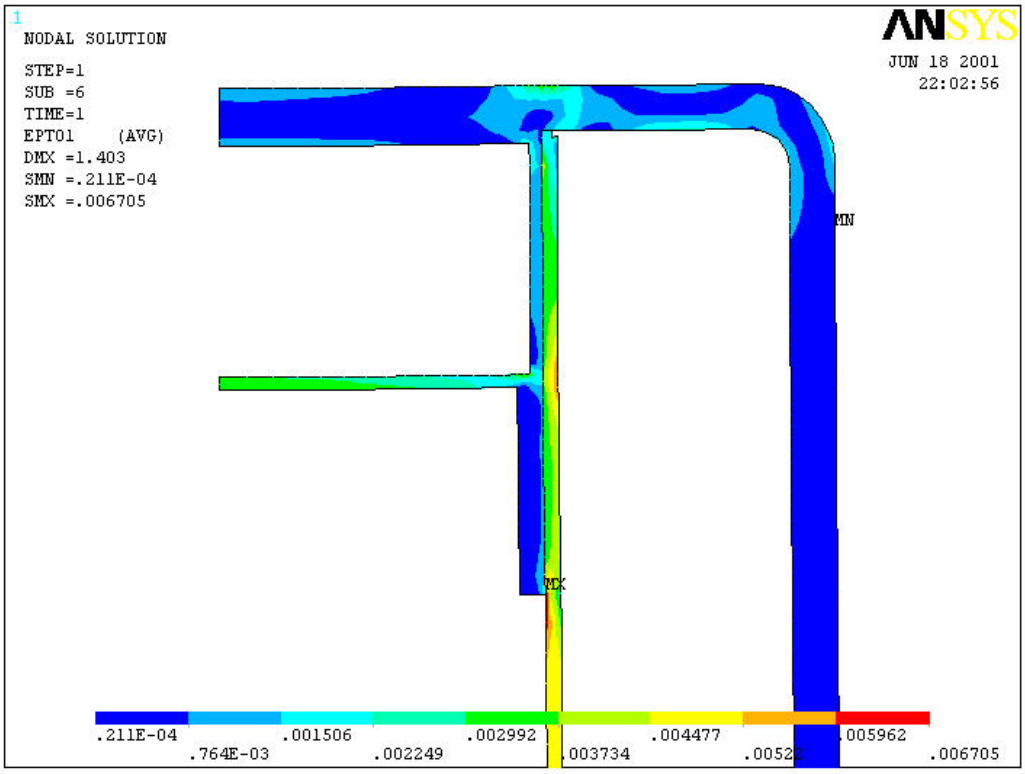

Figure C.5 (c) 1st Principal Strain in Laminates – Iteration #1

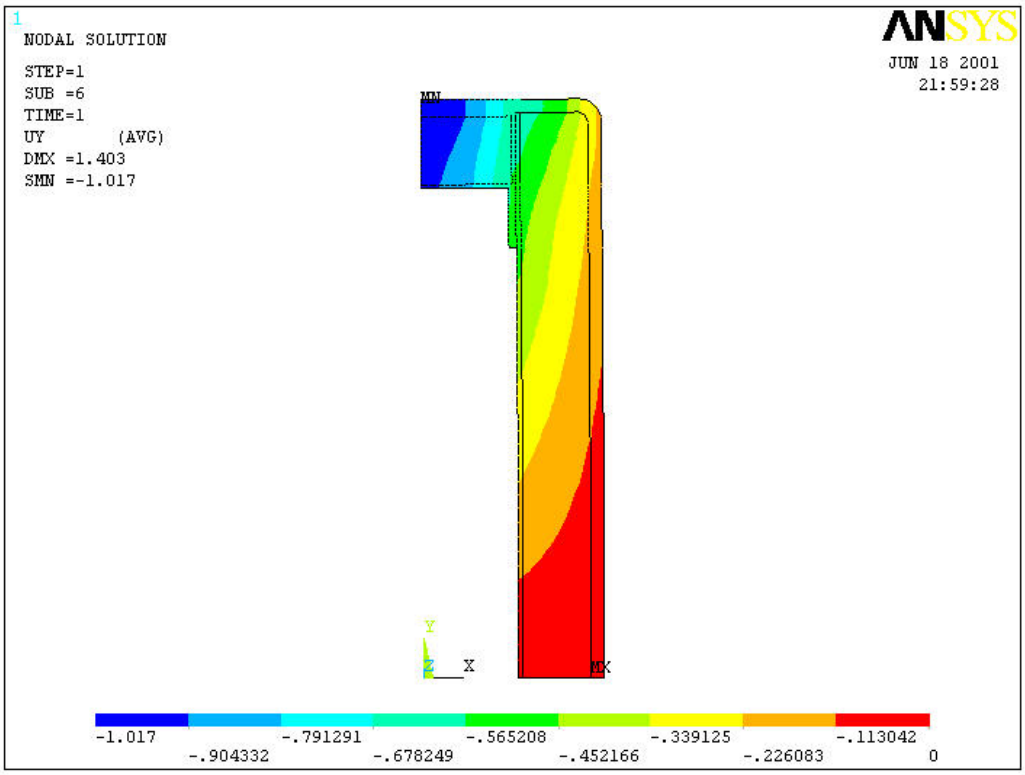

Figure C.5 (d) Vertical Deflection of Cross Section – Iteration #1

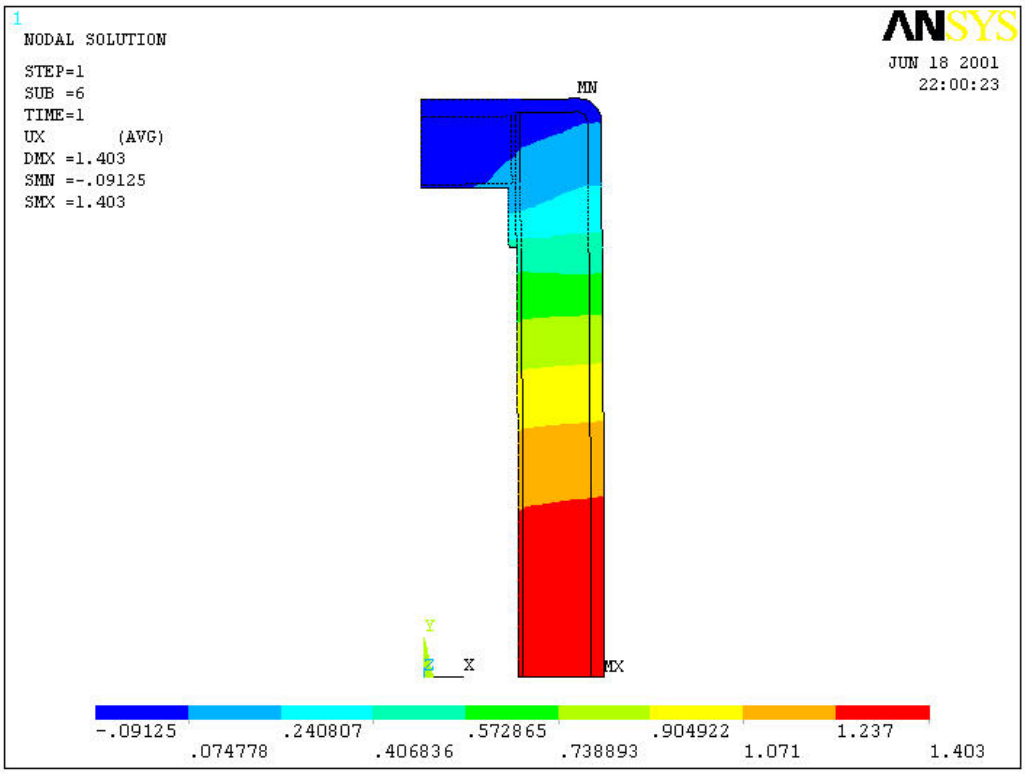

Figure C.5 (e) Lateral Deflection of Section Walls – Iteration #1

C.10 Iteration #2 Results

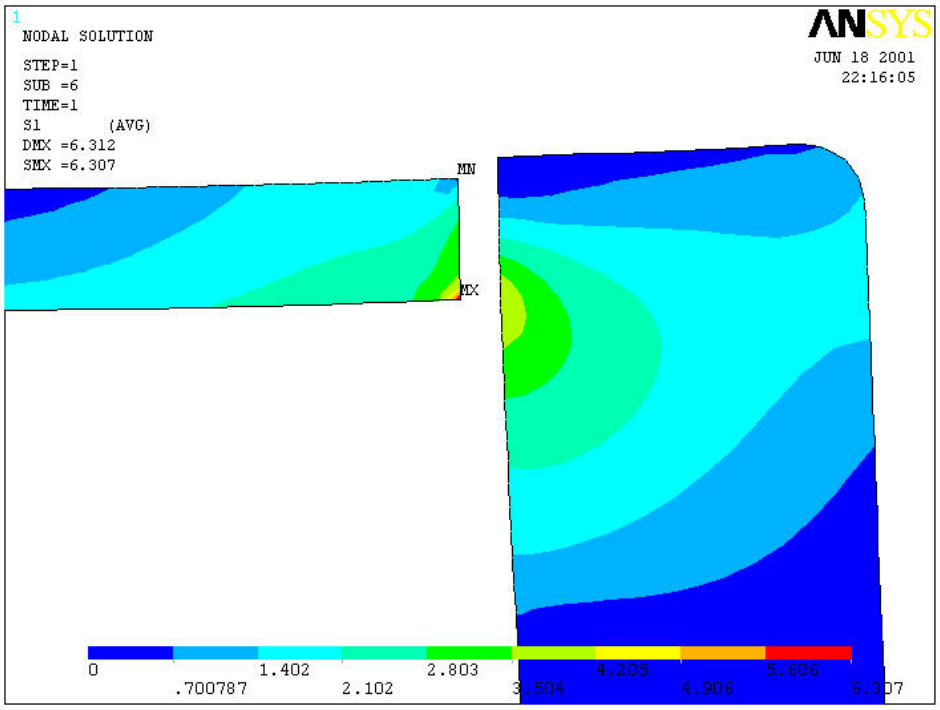

Figure C.6 (a) 1st Principal Stress In Core Material – Iteration #2

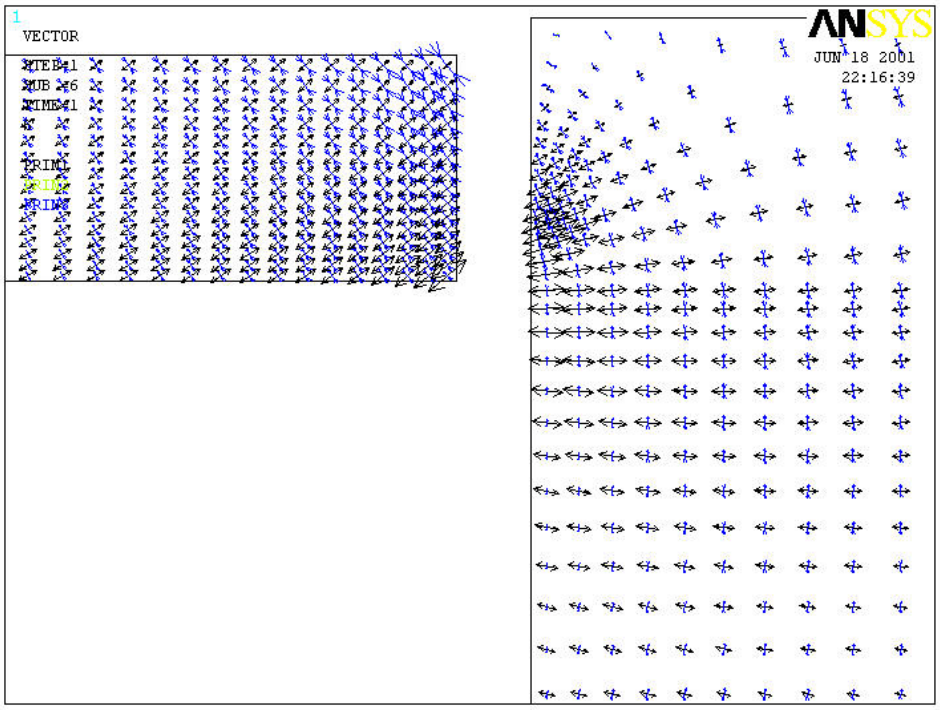

Figure C.6 (b) Vector Plot of Principal Stress In Core Material – Iteration #2

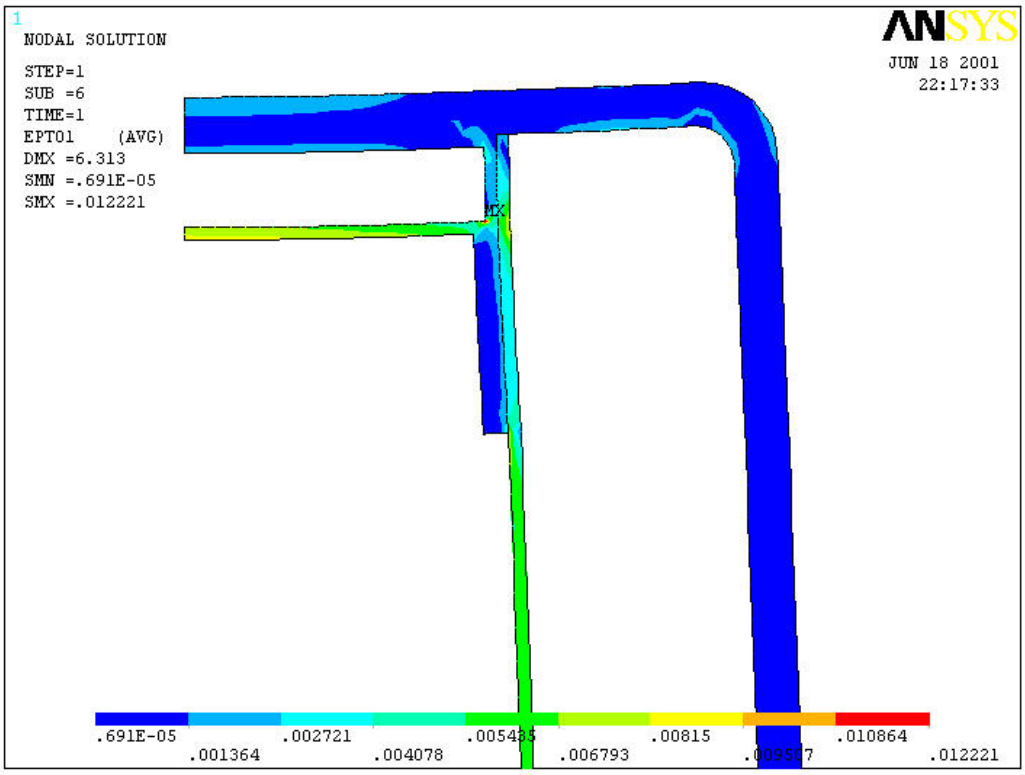

Figure C.6 (c) 1st Principal Strain in Laminates – Iteration #2

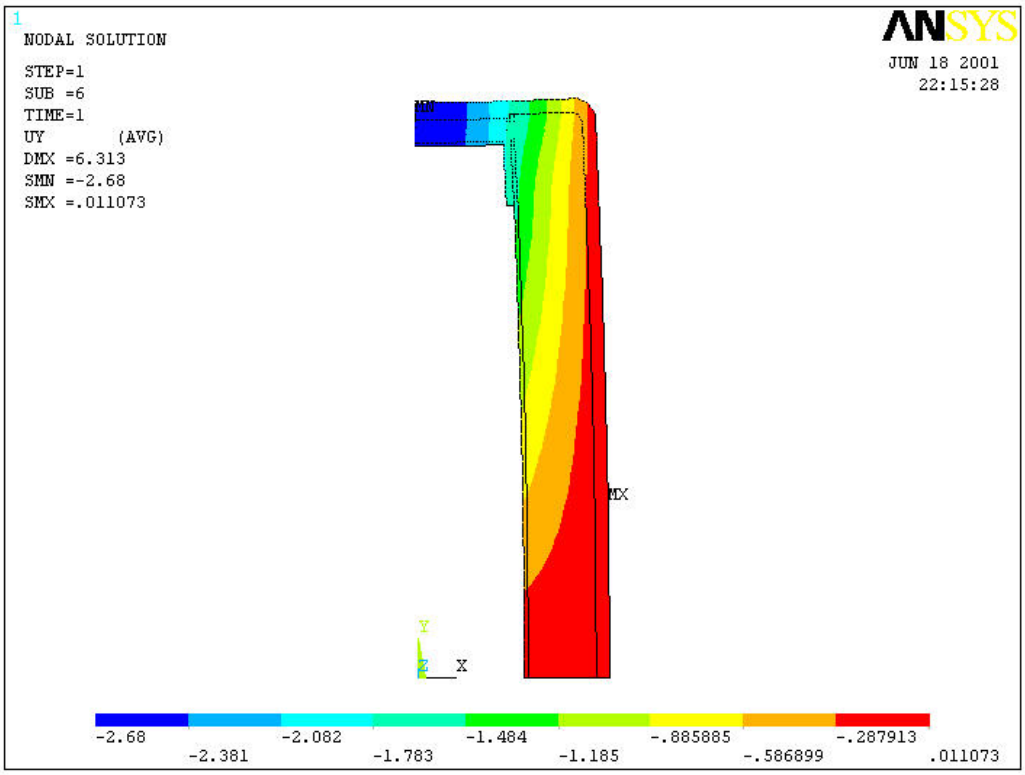

Figure C.6 (d) Vertical Deflection of Cross Section – Iteration #2

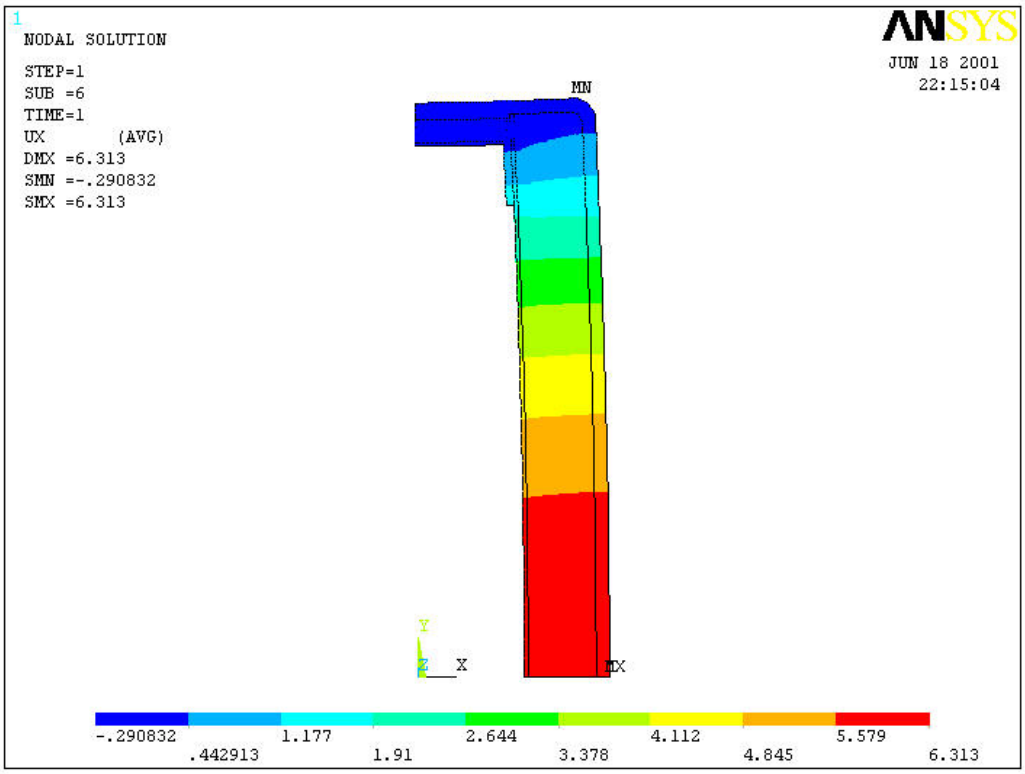

Figure C.6 (e) Lateral Deflection of Section Walls – Iteration #2

C.11 Iteration #3 Results

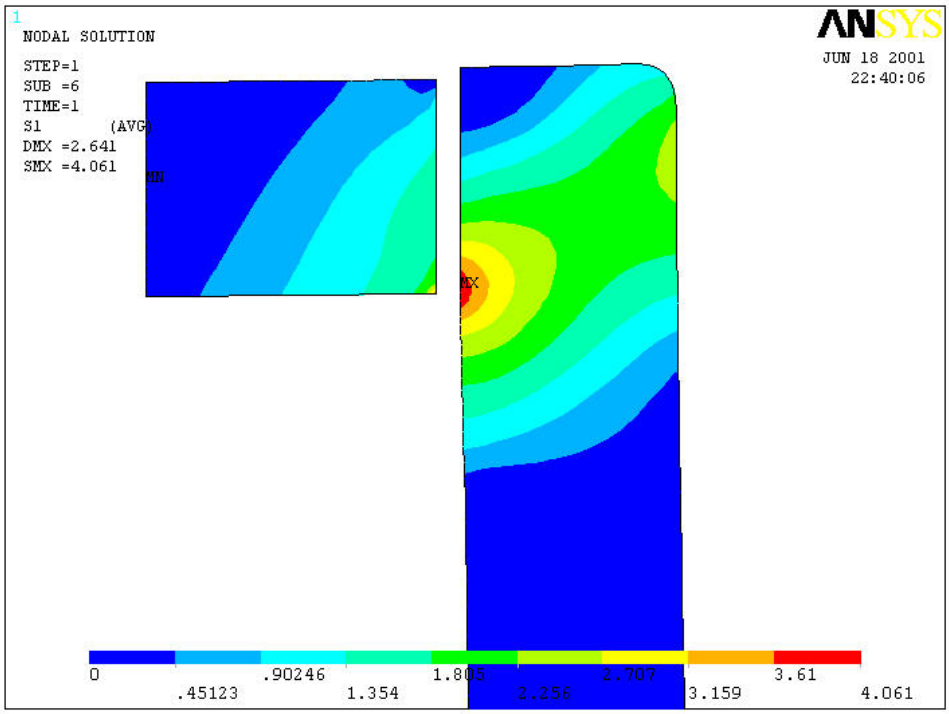

Figure C.7 (a) 1st Principal Stress In Core Material – Iteration #3

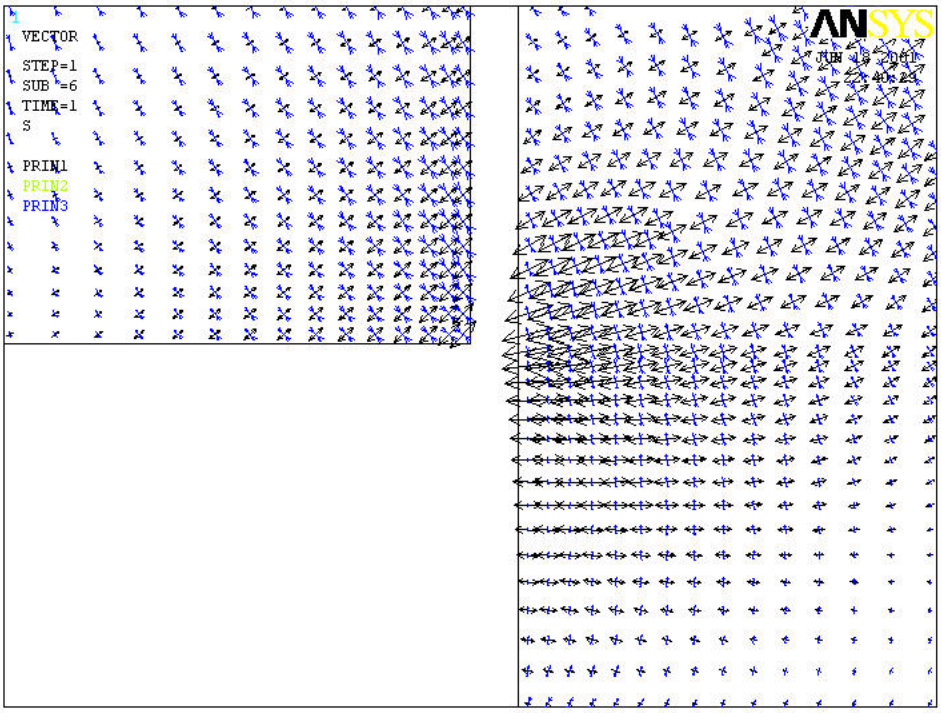

Figure C.7 (b) Vector Plot of Principal Stress In Core Material – Iteration #3

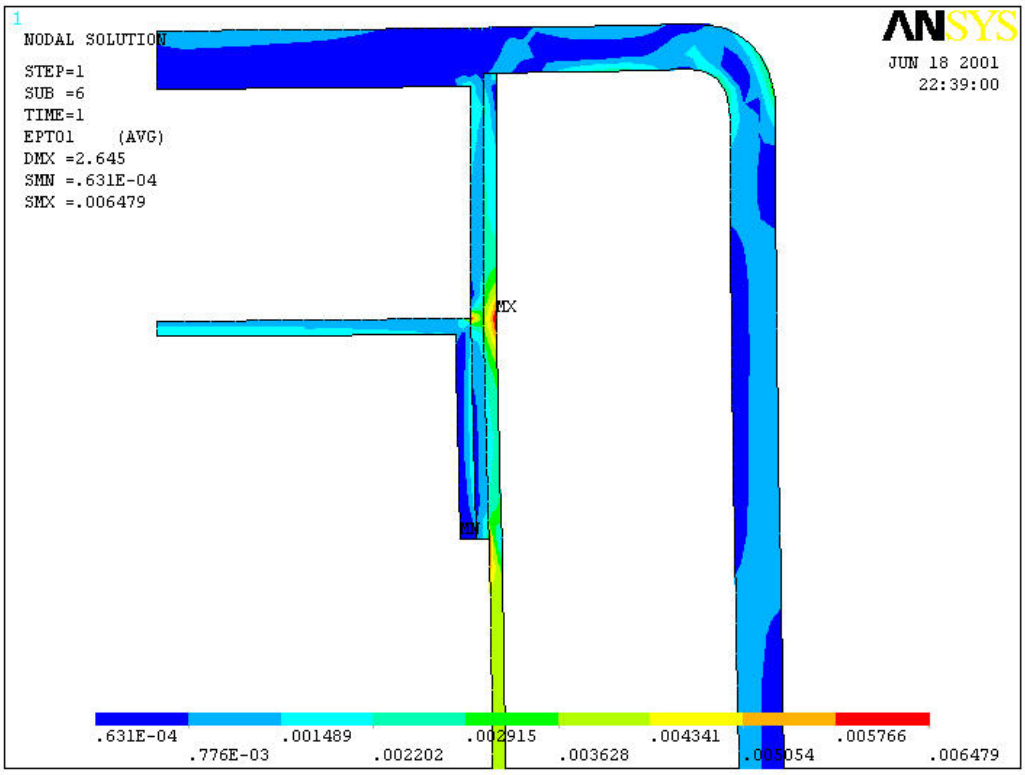

Figure C.7 (c) 1st Principal Strain in Laminates – Iteration #3

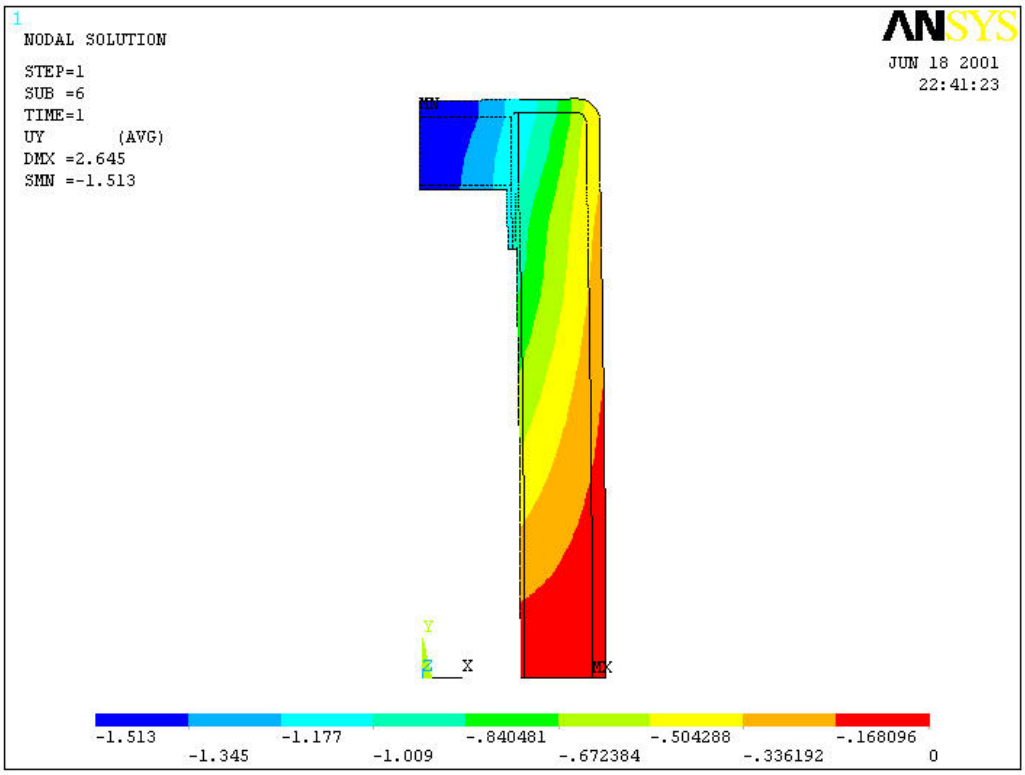

Figure C.7 (d) Vertical Deflection of Cross Section – Iteration #3

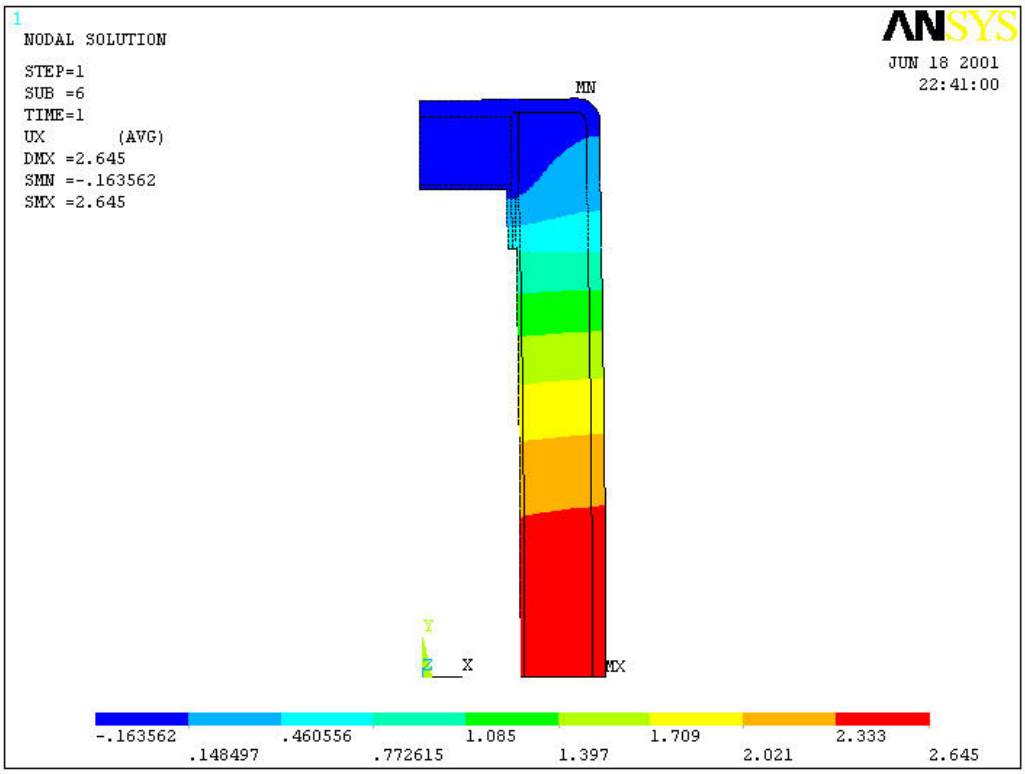

Figure C.7 (e) Lateral Deflection of Section Walls – Iteration #3

C.12 Iteration #4 Results

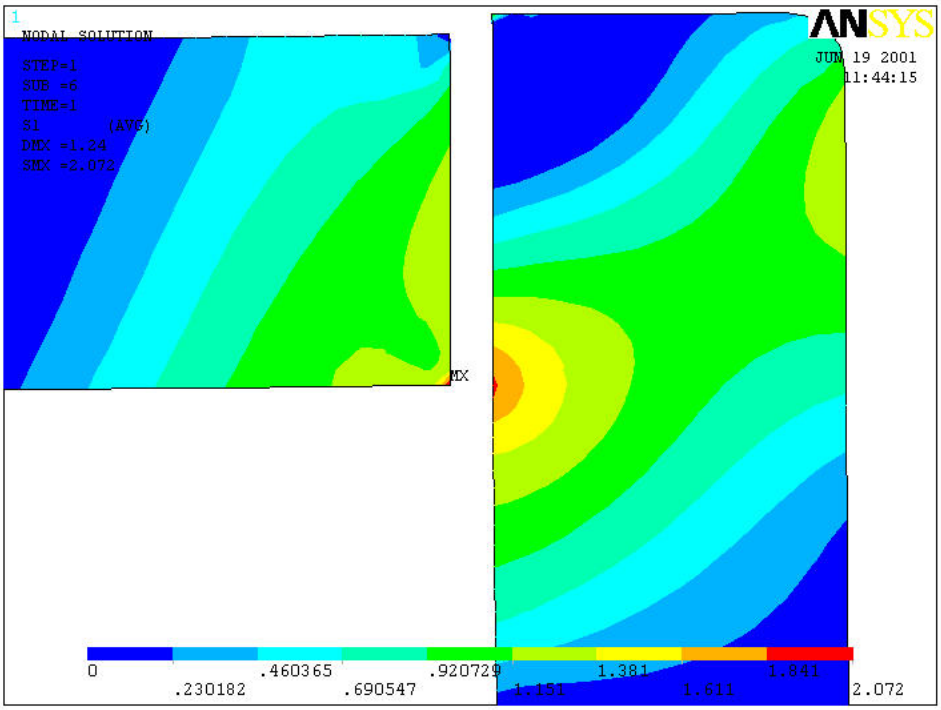

Figure C.8 (a) 1st Principal Stress In Core Material – Iteration #4

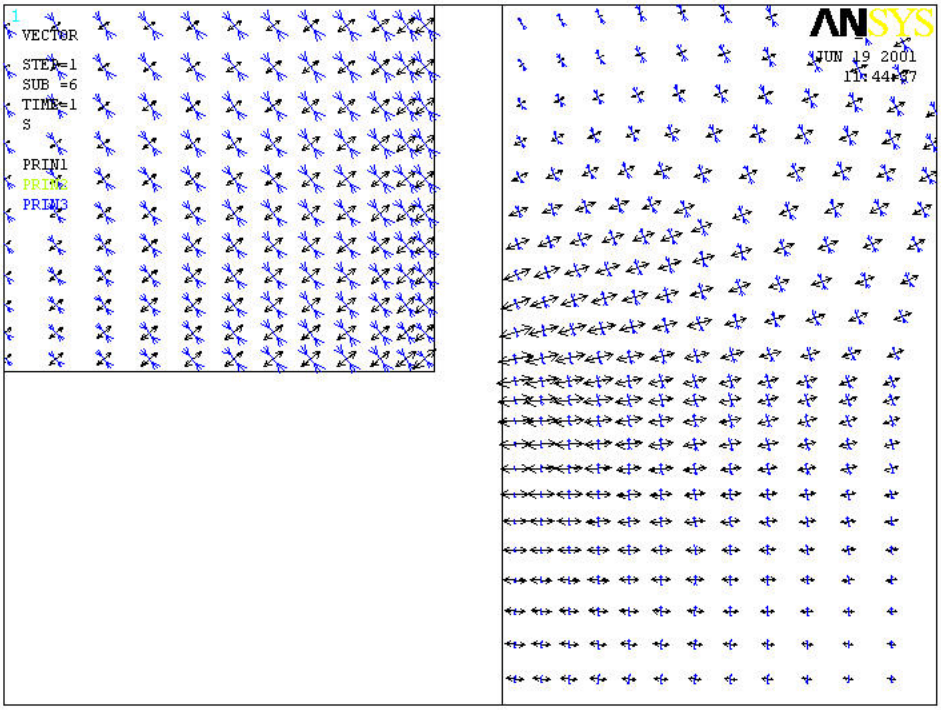

Figure C.8 (b) Vector Plot of Principal Stress In Core Material – Iteration #4

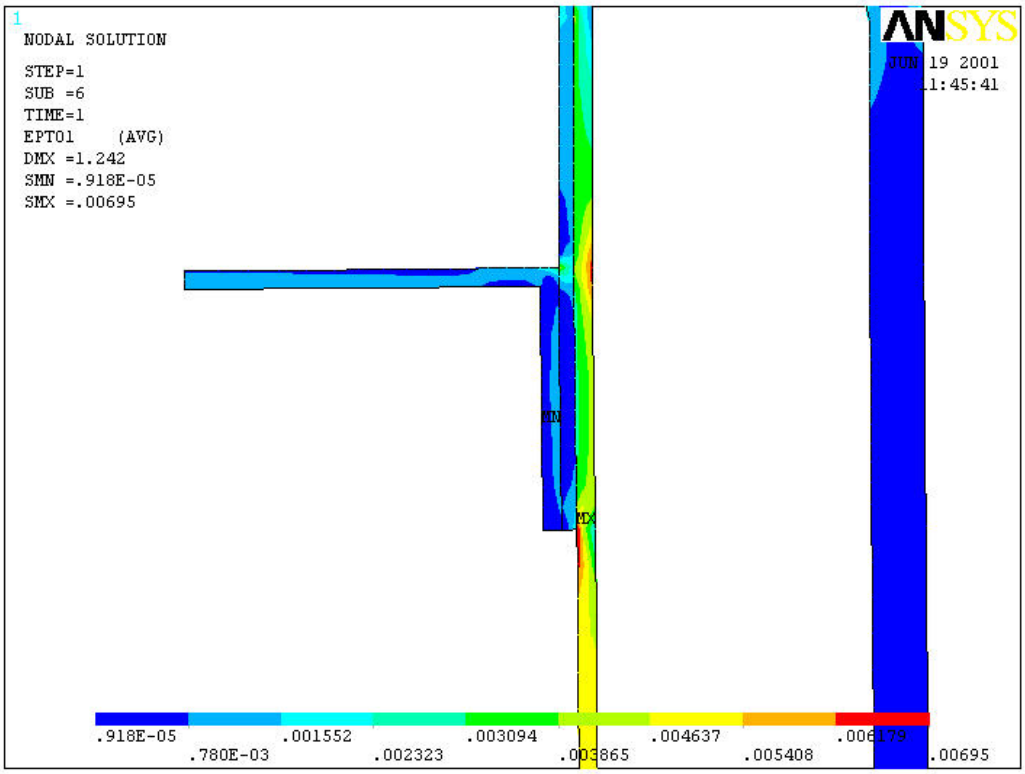

Figure C.8 (c) 1st Principal Strain in Laminates – Iteration #4

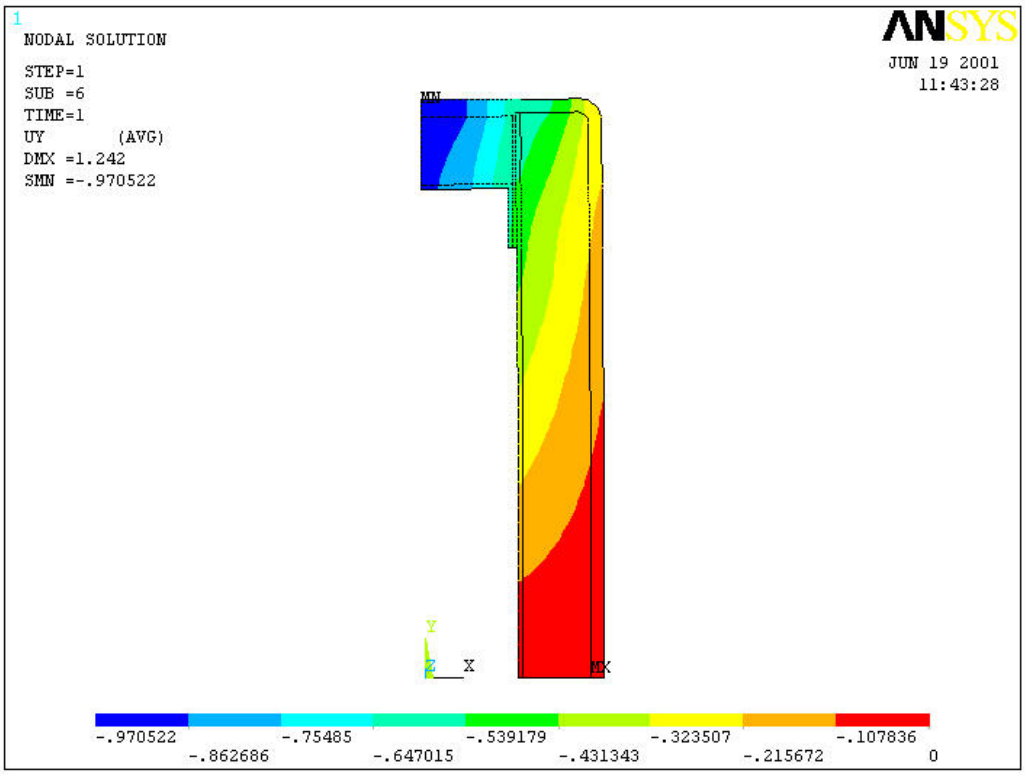

Figure C.8 (d) Vertical Deflection of Cross Section – Iteration #4

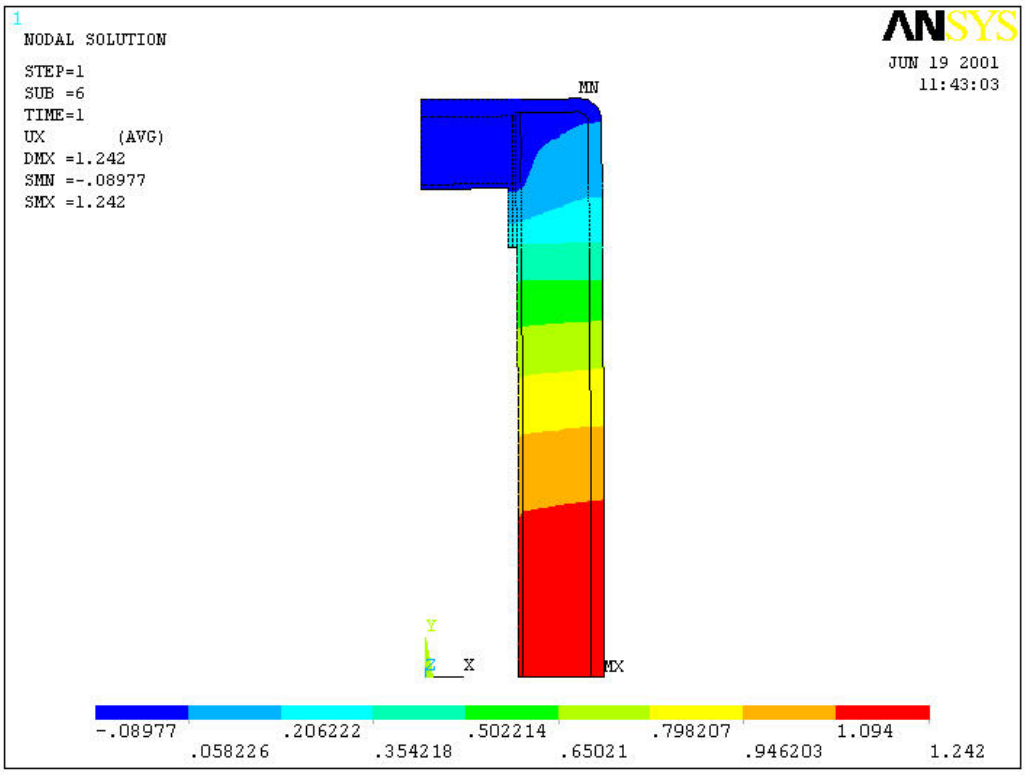

Figure C.8 (e) Lateral Deflection of Section Walls – Iteration #4

C.13 Iteration #5 Results

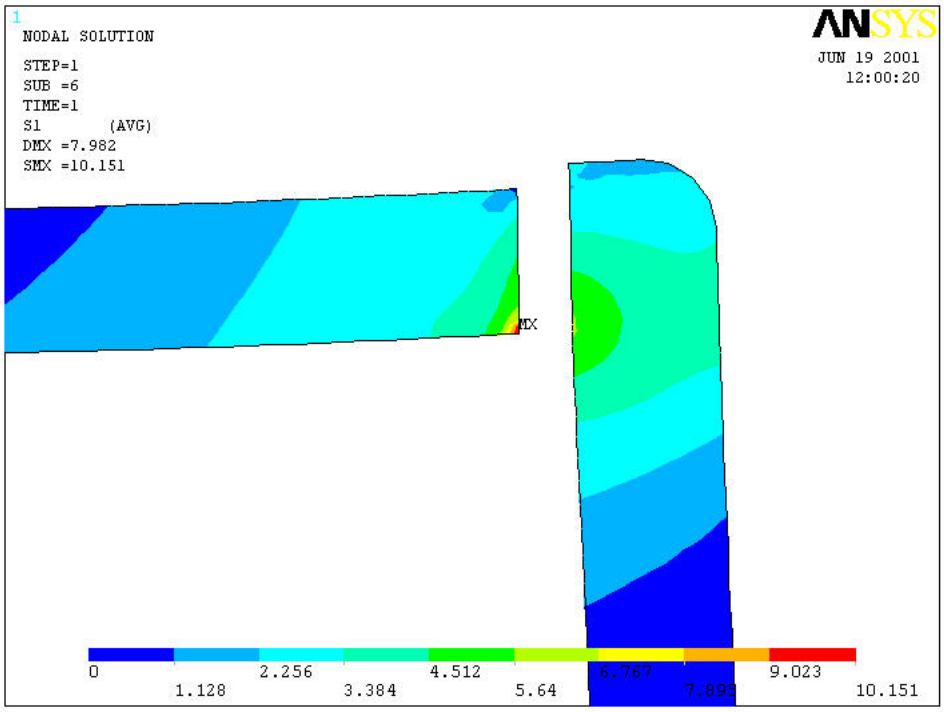

Figure C.9 (a) 1st Principal Stress In Core Material – Iteration #5

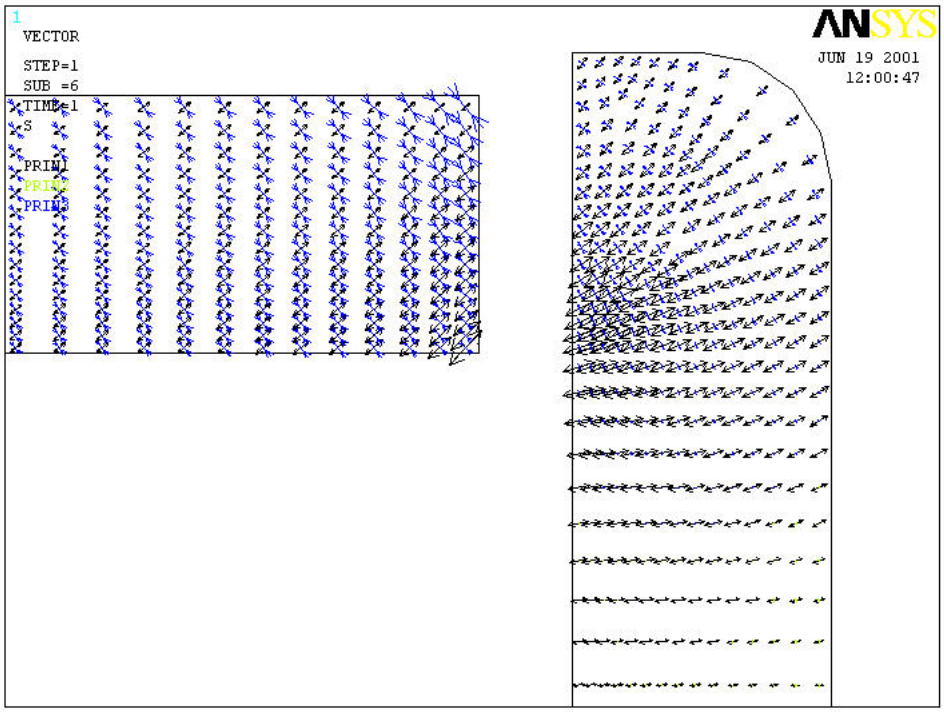

Figure C.9 (b) Vector Plot of Principal Stress In Core Material – Iteration #5

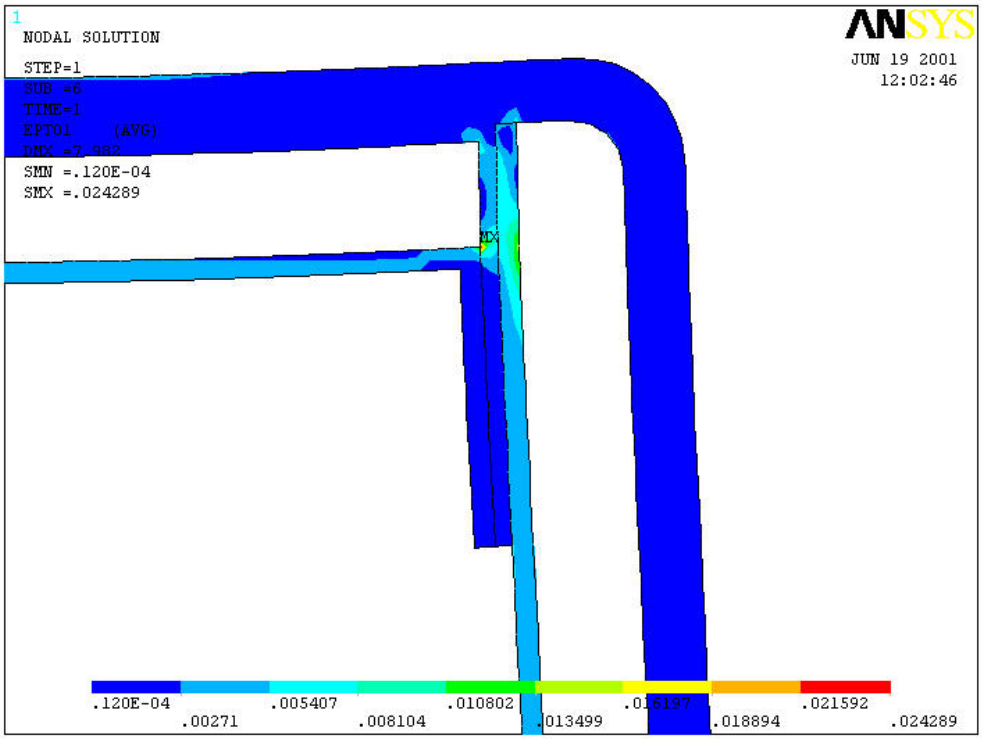

Figure C.9 (c) 1st Principal Strain in Laminates Including Infinite Stress Concentration – Iteration #5

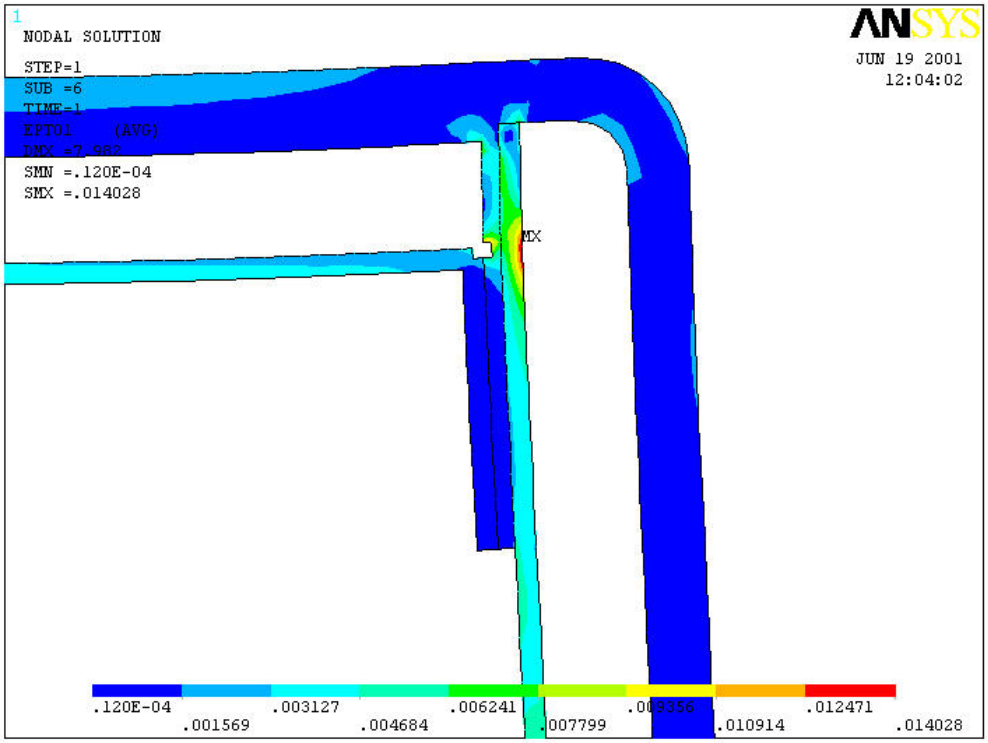

Figure C.9 (d) 1st Principal Strain in Laminates Without Infinite Stress Concentration – Iteration #5

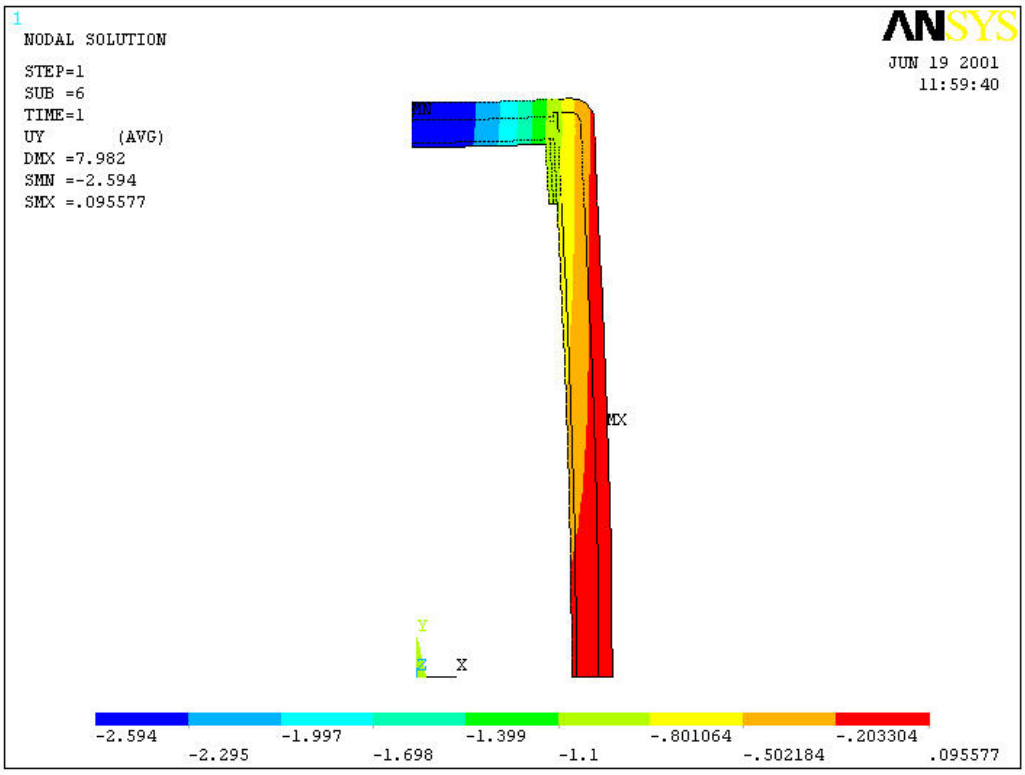

Figure C.9 (e) Vertical Deflection of Cross Section – Iteration #5

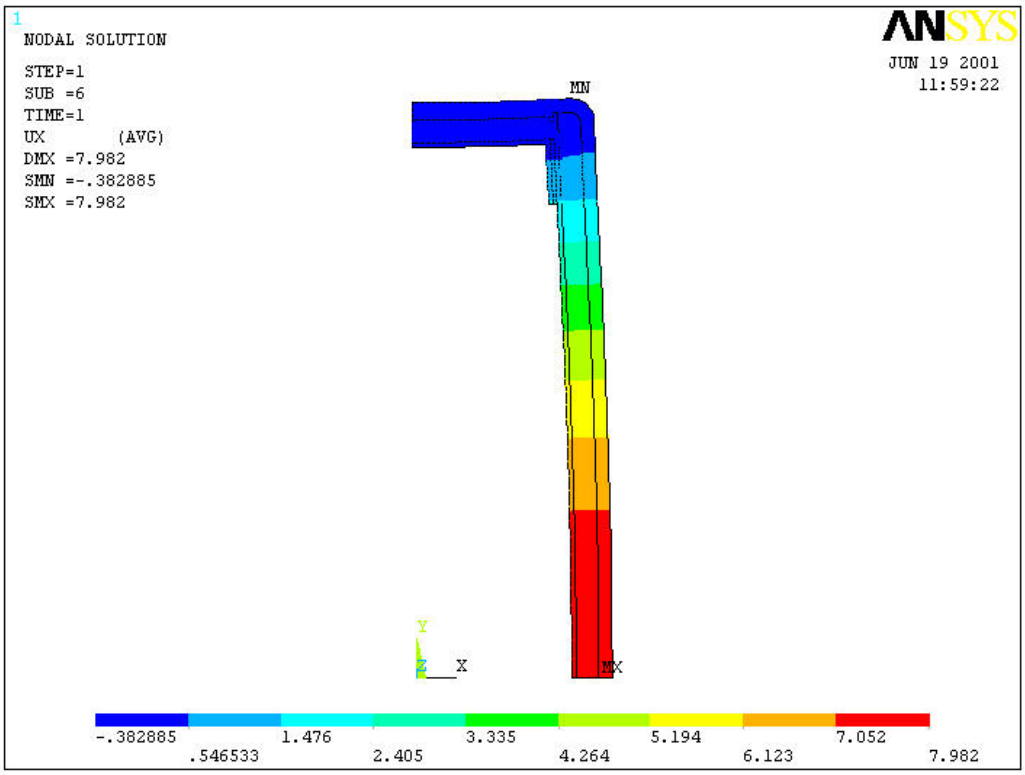

Figure C.9 (f) Lateral Deflection of Section Walls – Iteration #5

C.14 Experimental Results

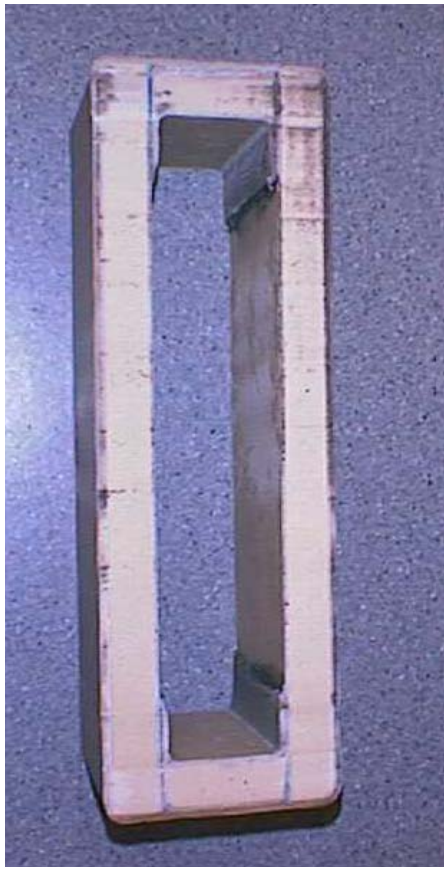

Figure C.10 (a) Completed Beam Section With PU Core

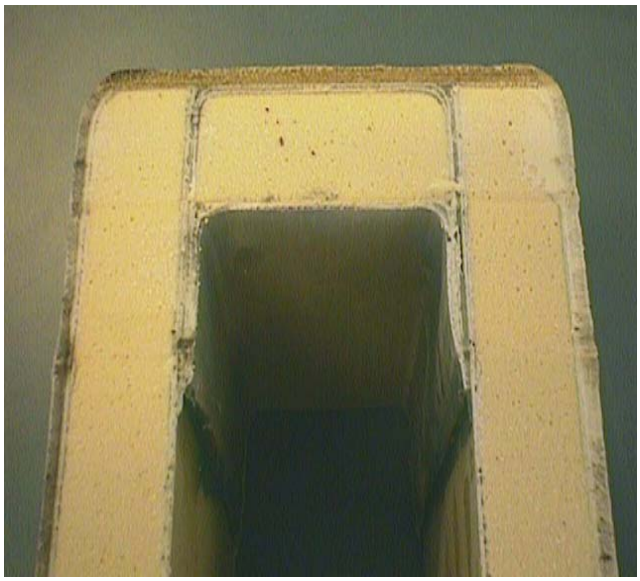

Figure C.10 (b) Joining Detail Of Beam Section

Figure C.11 (a) PU Section With First Core Crack (Top Right Side)

Figure C.11 (b) Ultimate Cross Sectional Failure through Delamination

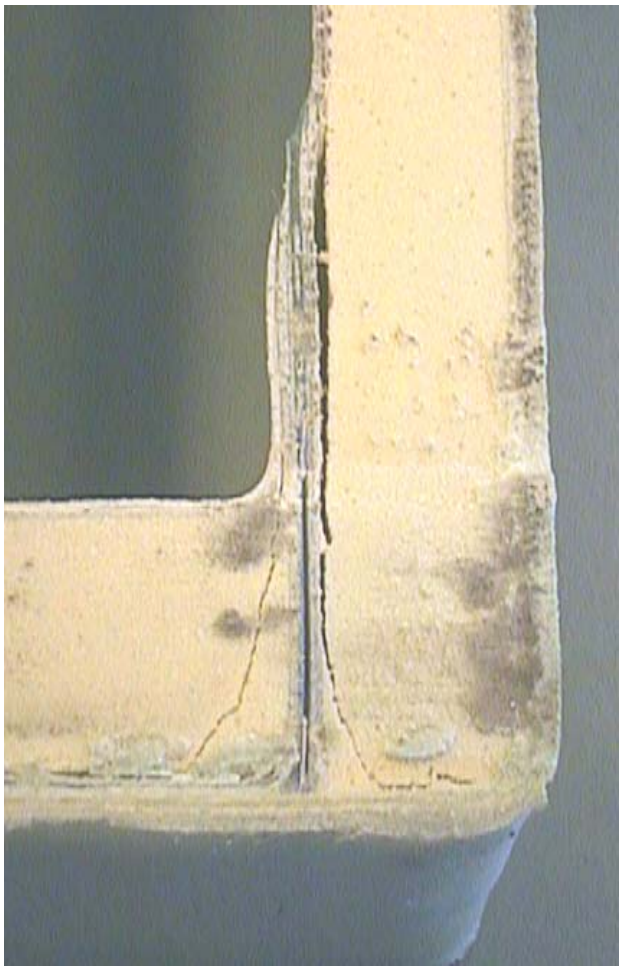

Figure C.11 (c) Crack Location in Joint

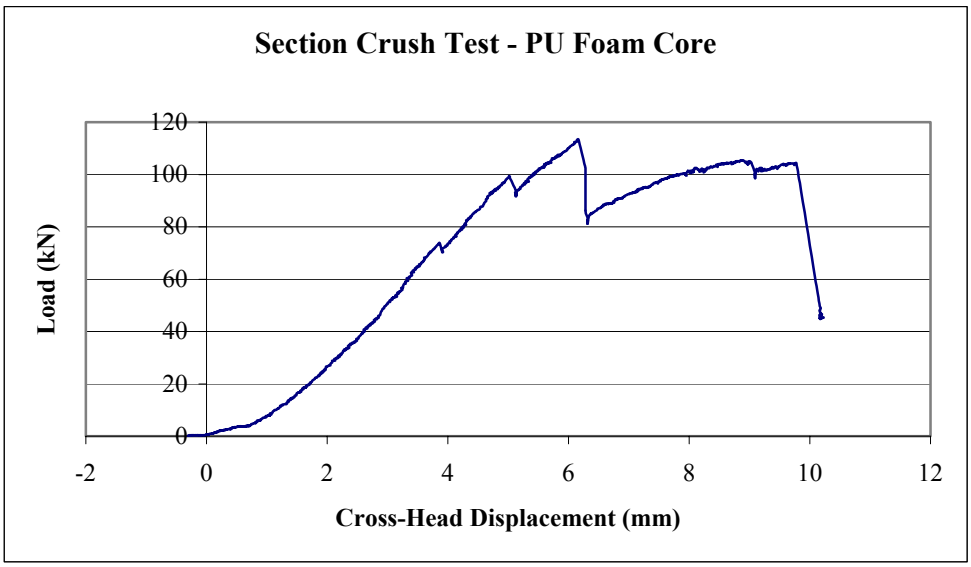

Figure C.12 Load-Displacement Plot for PU Cored Cross Section

Appendix D – Small-Scale Neck Analysis and Testing Results

D.1 Analysis Identification

Model 1	Right-angle joint – reinforcement continued [NECK1.db]
Model 2	Right-angle joint – reinforcement NOT continued [NECK1c.db]
Model 3	15 degree – no fillet – reinforcement continued [NECK9b.db]
Model 4	15 degree–no fillet– reinforcement NOT continued [NECK9.db]
Model 5	15-degree 100 mm top and bottom fillet – reinforcement continued [NECK7c.db]
Model 6	15-degree 100 mm top and bottom fillet - reinforcement NOT continued [NECK7d.db]
Model 7	15 degree 400 mm fillets top and bottom – reinforcement continued [NECK 11.db]

D.2 Aim of Analysis

- To perform a preliminary, linear static analysis of the neck section of an FRP chassis rail on a small scale
- To investigate the performance of each chassis rail, in response to the application of loads as defined by load cases one and three.
- To allow the comparison of the structural characteristics of the various models in relation to the influence of reinforcement placement and appropriate stress concentrations reduction techniques on maximum stresses and failure modes within the beam.

D.3 Model Form

The layout of each 2-dimensional model is depicted in Figures D.1 (a)-(g). These include two relief angles, various radii and two different forms of reinforcement placement, as discussed in section 7.5.2. As each beam was to be tested using three-point bending, with the load placed at midspan, symmetry was used to reduce solution time and computing resources.

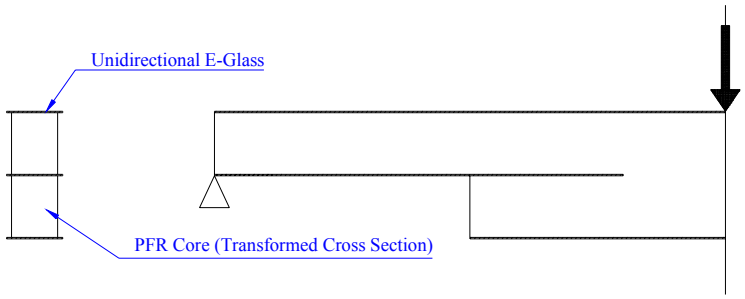

Figure D.1 (a) Basic Model Layout Neck Section #1

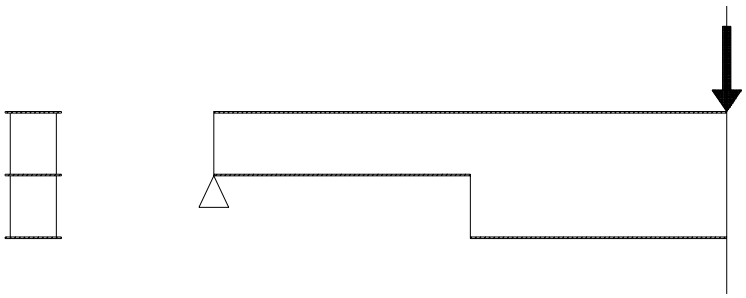

Figure D.1 (b) Basic Model Layout Neck Section #2

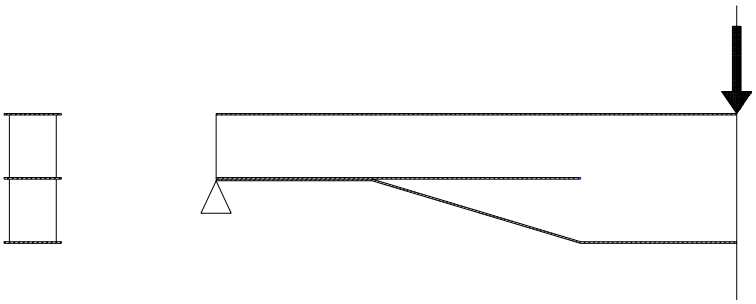

Figure D.1 (c) Basic Model Layout Neck Section #3

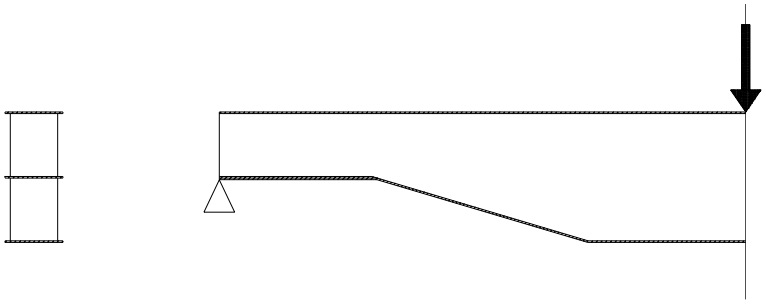

Figure D.1 (d) Basic Model Layout Neck Section #4

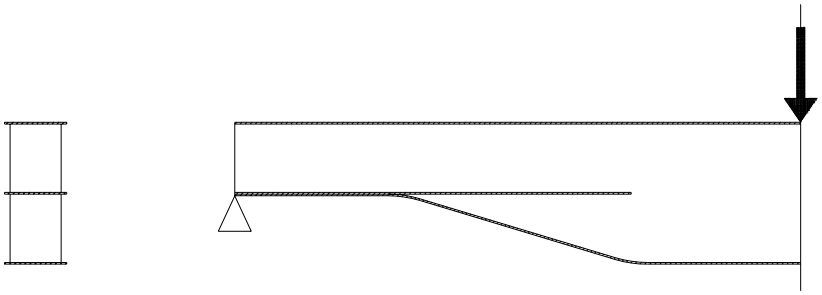

Figure D.1 (e) Basic Model Layout Neck Section #5

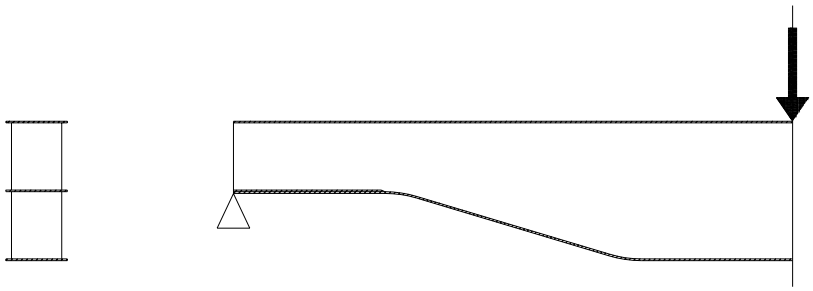

Figure D.1 (f) Basic Model Layout Neck Section #6

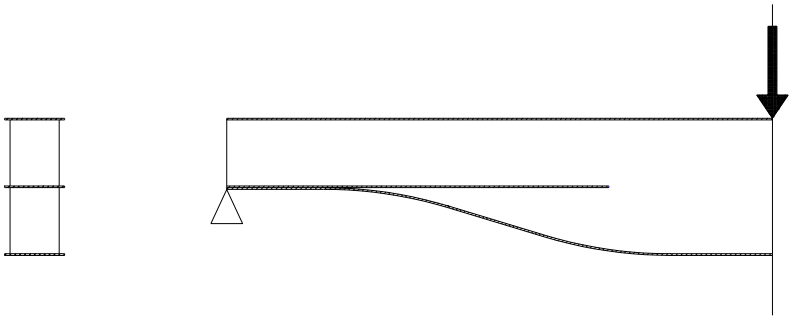

Figure D.1 (g) Basic Model Layout Neck Section #7

D.4 Material Properties

An orthotropic material represented the unidirectional laminates, with the x-direction of each element being oriented according to the local x-direction axis, parallel to the joining line between the core and laminate.

1. Properties of E-glass Uni-directional reinforcement:

Young's Modulus,	E_1 :	28624 MPa
	E_2 :	7404 MPa
Poisson's Ratio,	γ_{xy} :	0.322
Shear Modulus,	G_{xy} :	2986 MPa
Thickness in y-direction:		1.5 mm
Thickness in z-direction:		55 mm

The PFR core material, consisting of a mixture of epoxy resin (ADR246TX & ADH160) and 3MK15 glass microspheres (40% by volume) was assumed isotropic. As mentioned in section 7.5.2, the circular void and wrap of double bias were replaced with a transformed solid PFR section, using the protocol of transformed cross section. The effective stiffness of the beam would therefore be maintained.

2. Properties of PFR core material:

Young's Modulus,	E_1 :	2000 MPa
Poisson's Ratio,	γ :	0.1
Thickness in z-direction, t:		45 mm

D.5 Analysis Program

Analysis program:	ANSYS 5.7
Computer:	Intell 266MMX
	128MB Ram
	Win98
Analysis type:	Linear static (Assumed Small Displacement)

D.6 Mesh Details

The meshes used for some neck sections were the same whether or not there was reinforcement carried through – the properties of the respective elements were simply changed.

Element Type:

1. PLANE 82 The 8-node element is defined by eight nodes having two degrees of freedom at each node: translations in the nodal x and y directions. The element may be used as a plane element or as an axi-symmetric element. The element has plasticity, creep, swelling, stress stiffening, large deflection, and large strain capabilities. Refer ANSYS manual for further details.

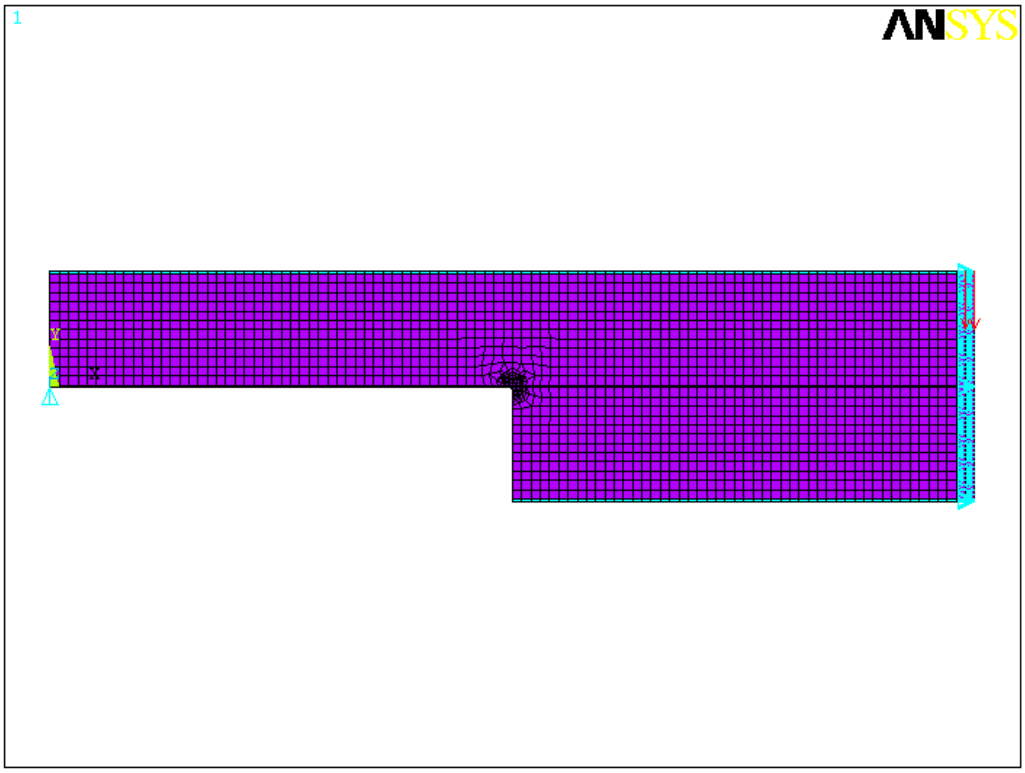

Figure D.2 (a) Mesh Used for Neck Sections #1 and #2

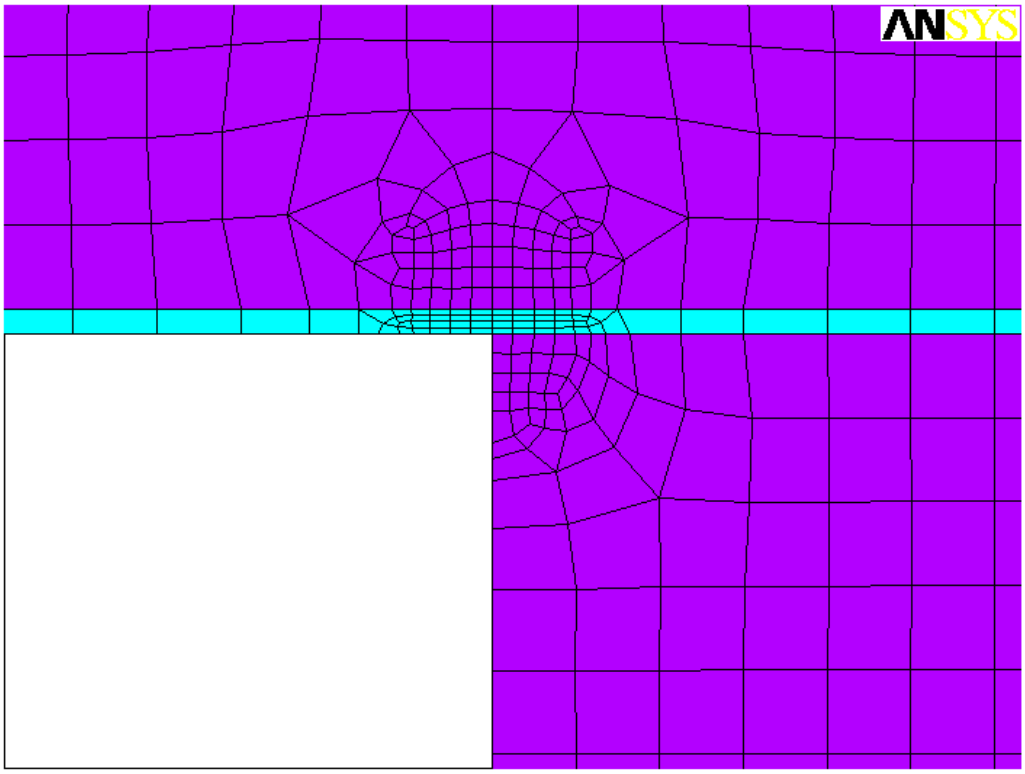

Figure D.2 (b) Magnified View of Element Divisions in Corner

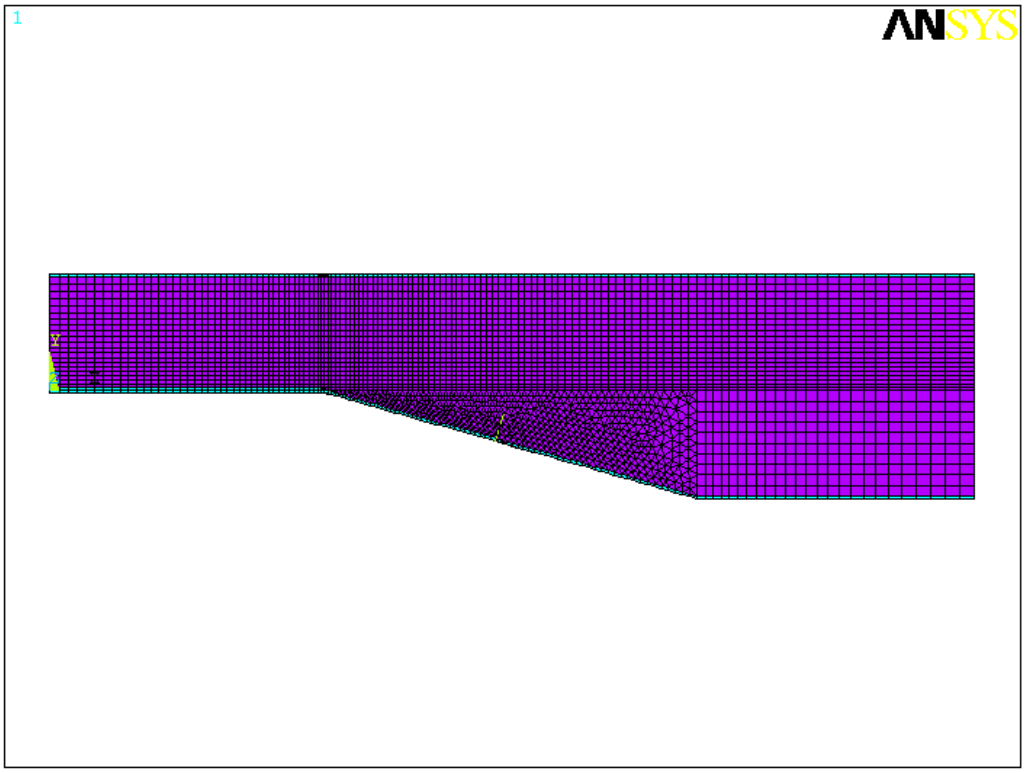

Figure D.2 (c) Mesh Used for Neck Sections #3 and #4

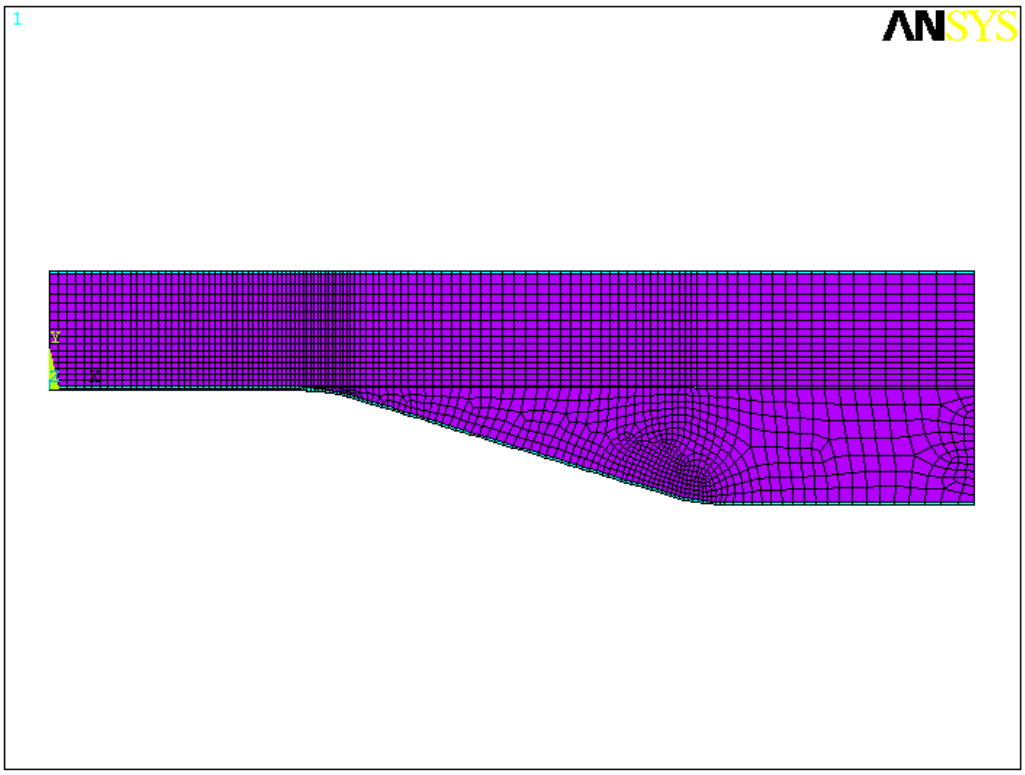

Figure D.2 (d) Mesh Used for Neck Sections #5 and #6

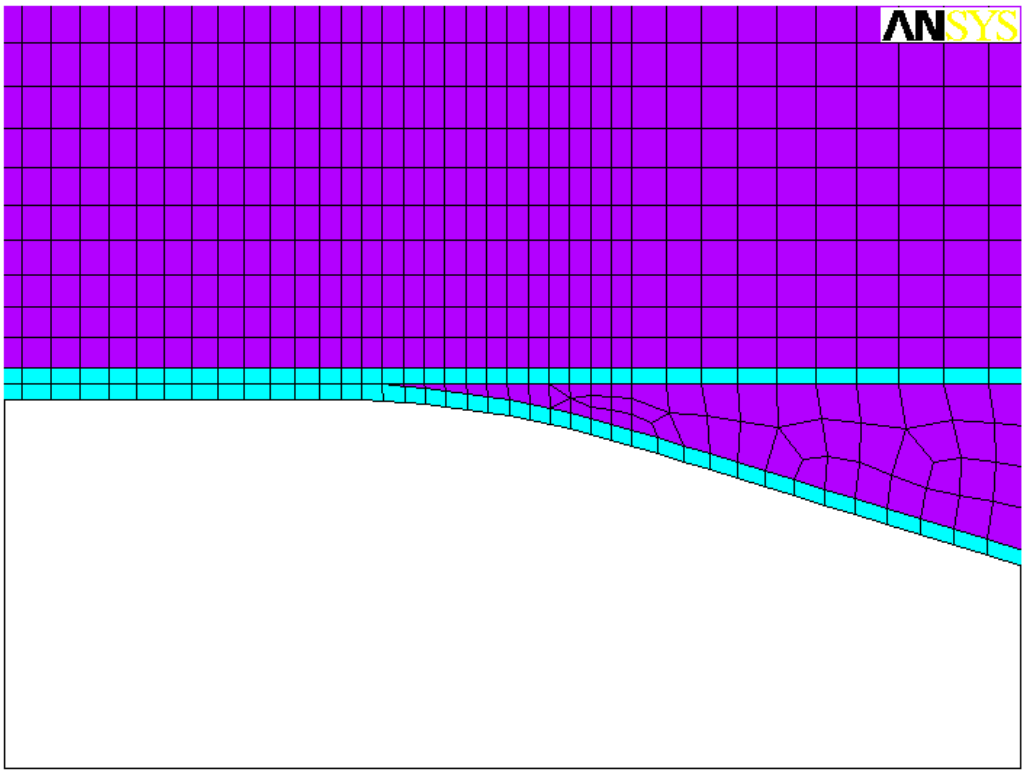

Figure D.2 (e) Example of Continuation of Reinforcement

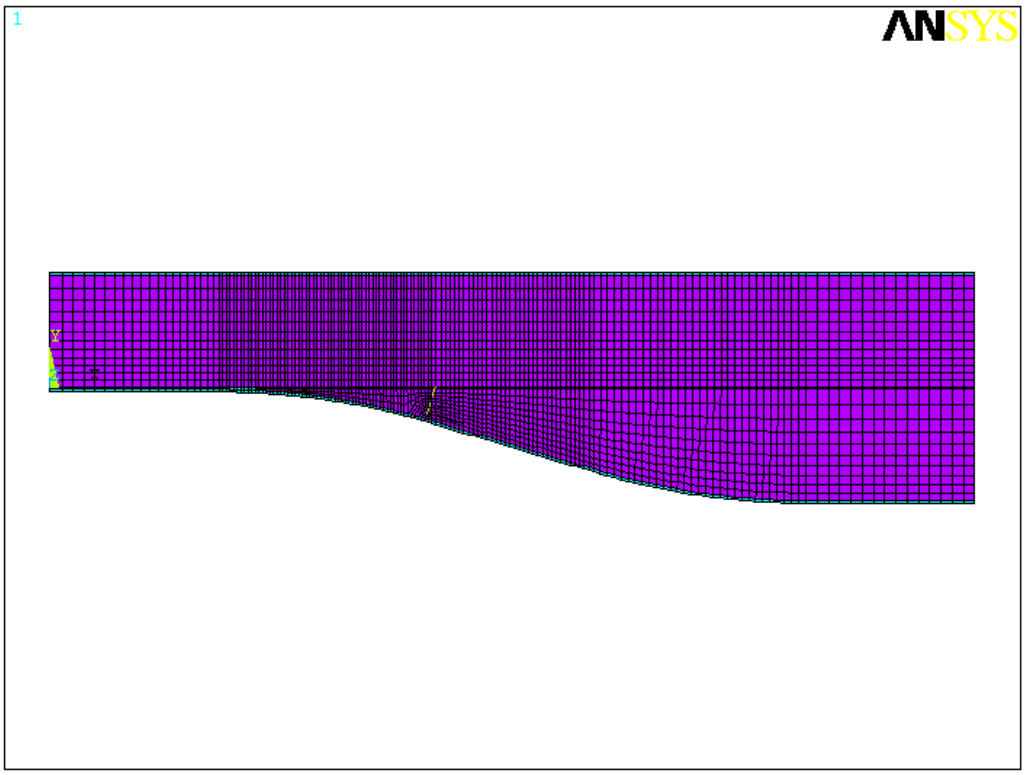

Figure D.2 (f) Mesh Used for Neck Section #7

D.7 Application of Boundary Conditions

The boundary conditions applied to each model were identical, apart from the magnitude of the load applied. Symmetry conditions were applied along the line of symmetry, and a load applied over the two nodes closest to this line. The opposite end of the beam was supported in the vertical direction only.

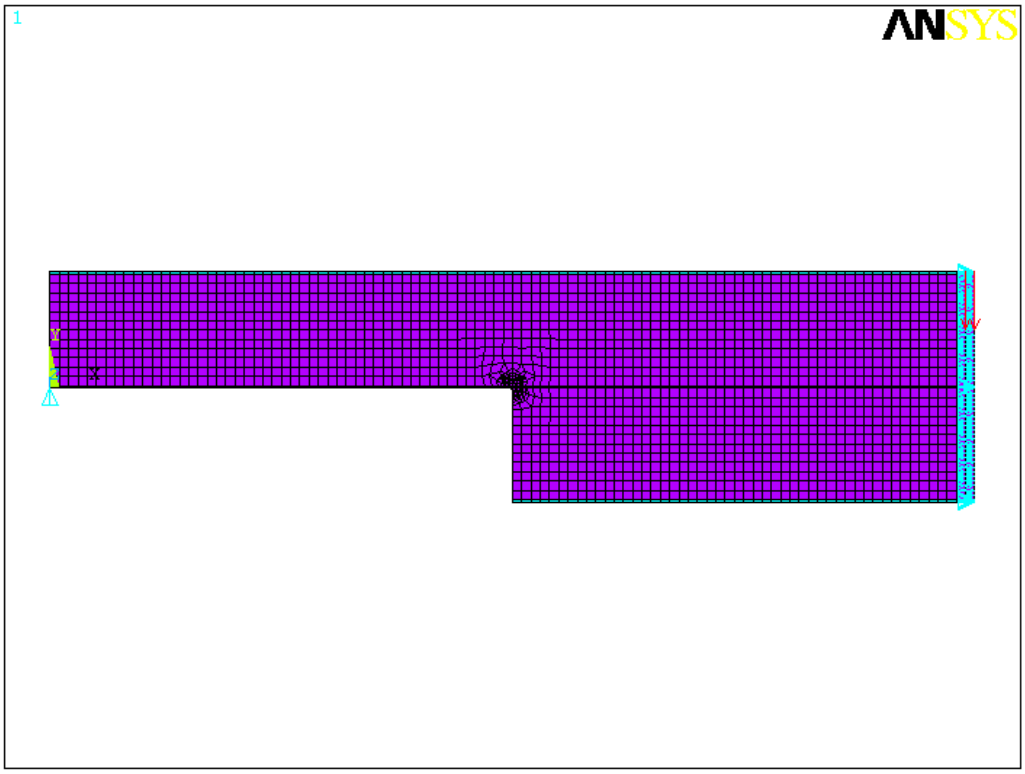

Figure D.3 Boundary Conditions Imposed on Each Model

Total equivalent load of 4 kN was applied to neck sections one and two, as this was the estimated failure load.

The remaining neck sections were loaded with a total equivalent load of 20 kN, as these beam types were likely to sustain a greater load. Also, an identical loading on each of the beam configurations would allow direct comparison as to the highest values of stress and strain, and provide a direct comparison, highlighting the superior configuration. Table D.1 presents a summary of the boundary conditions and real constants applied to each of the models.

Table D.1 Summary of Neck Section Profiles Analysed

Neck Section Number	Relief Angle (Degrees)	Reinforcement Continued Into Beam (Y/N)	Radius Size On Corners (mm)	Total Load Applied (N)	Reinforcement Thickness (mm)	Reinforcement Width (mm)	Core Width (mm)
1	90	Y	0	4000	1.5	55	45
2	90	N	0	4000	1.5	55	45
3	15	Y	0	20000	1.5	55	45
4	15	N	0	20000	1.5	55	45
5	15	Y	100	20000	1.5	55	45
6	15	N	100	20000	1.5	55	45
7	15	Y	400	20000	1.5	55	45

D.8 Neck Section #1 Results

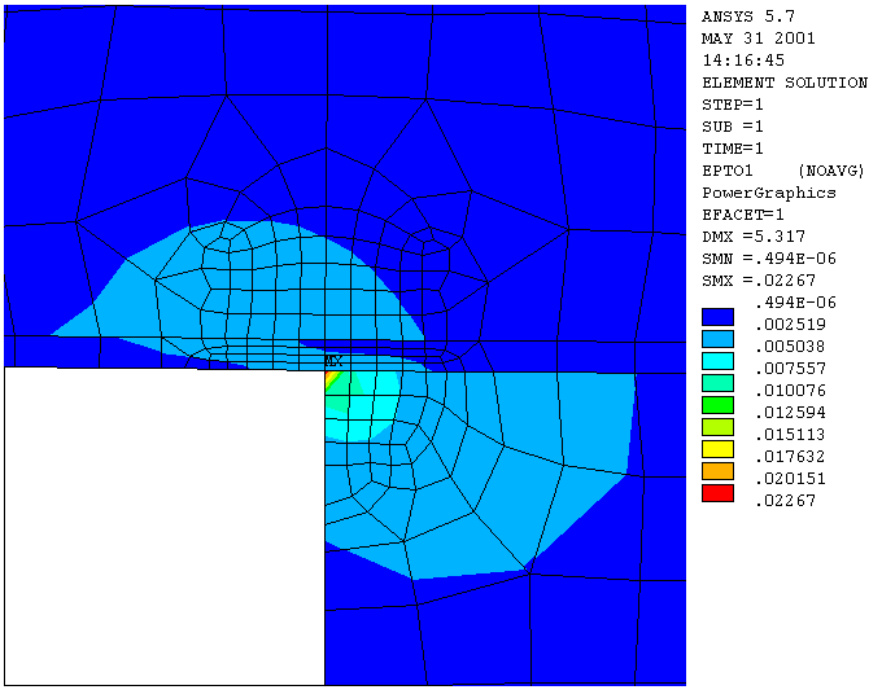

Figure D.4 (a) 1st Principal Strain Including Infinite Stress Concentration – Neck Section #1

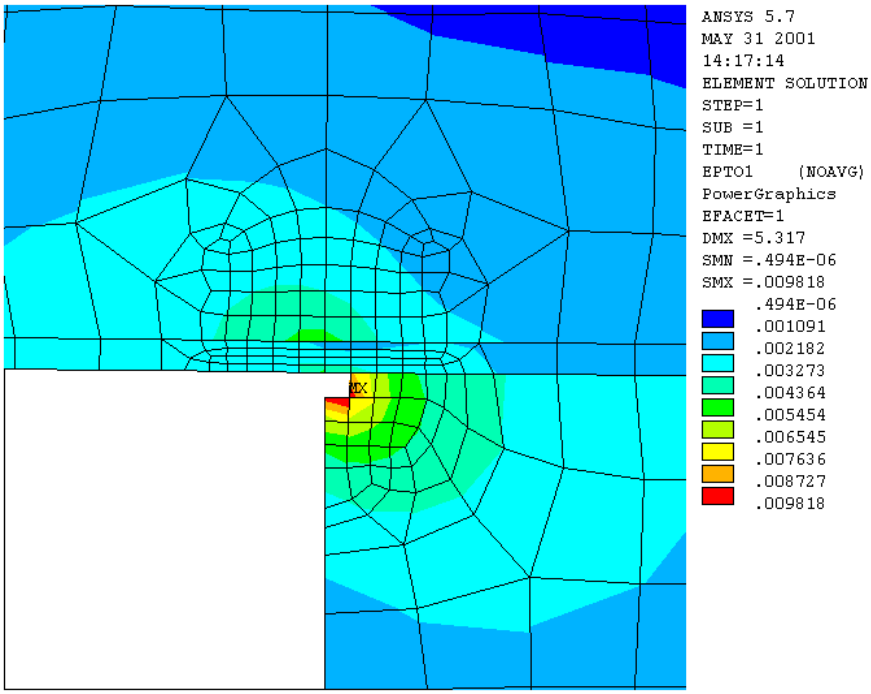

Figure D.4 (b) 1st Principal Strain Neglecting Element Containing Infinite Stress Concentration – Neck Section #1

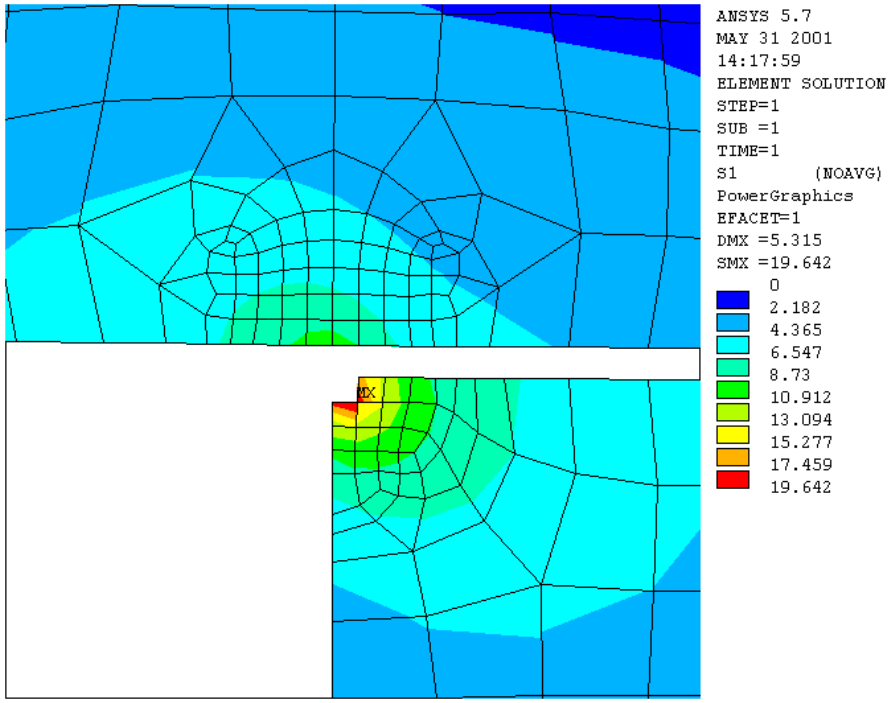

Figure D.4 (c) 1st Principal Stress in Core Material Neglecting Element Containing Infinite Stress Concentration – Neck Section #1

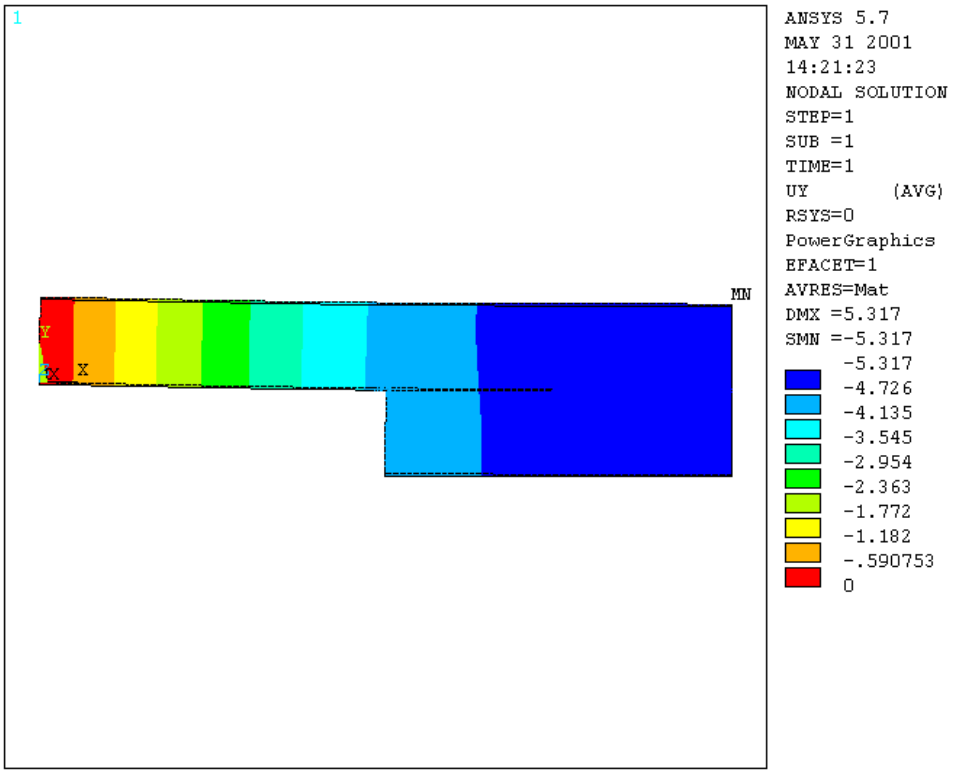

Figure D.4 (d) Neck Section #1 Deflection

D.9 Neck Section #2 Results

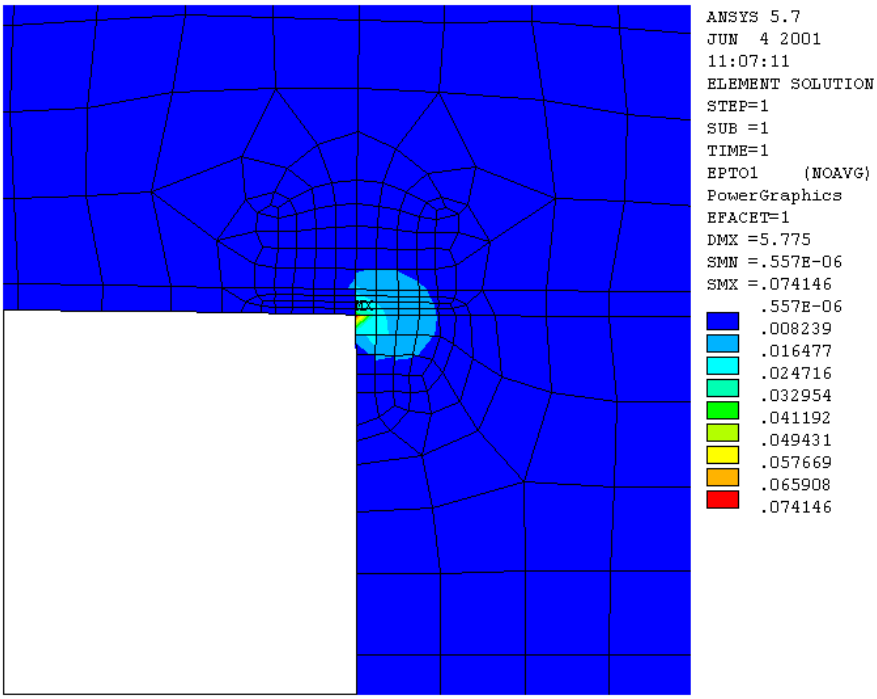

Figure D.5 (a) 1st Principal Strain Including Infinite Stress Concentration – Neck Section #2

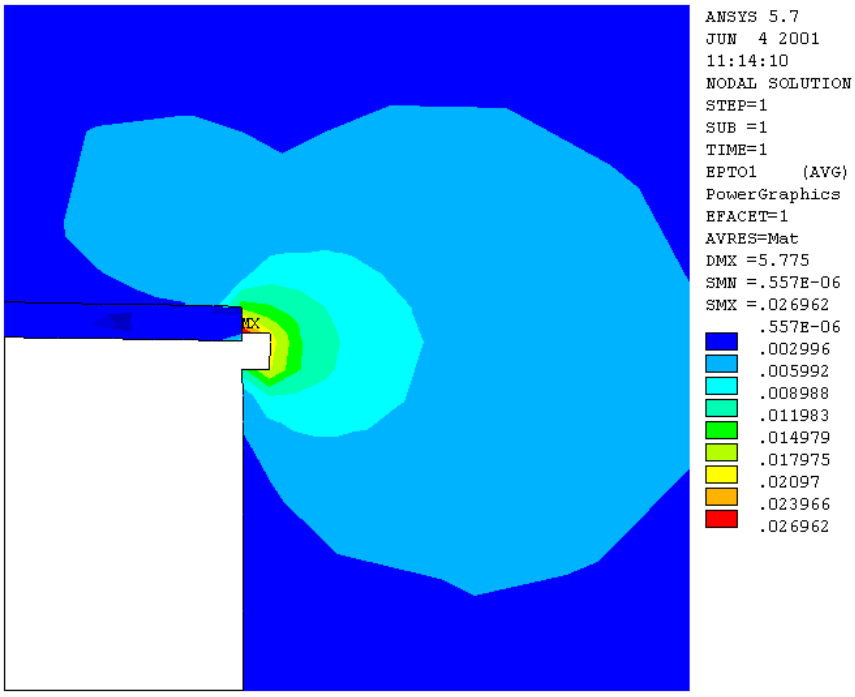

Figure D.5 (b) 1st Principal Strain Neglecting Element Containing Infinite Stress Concentration – Neck Section #2

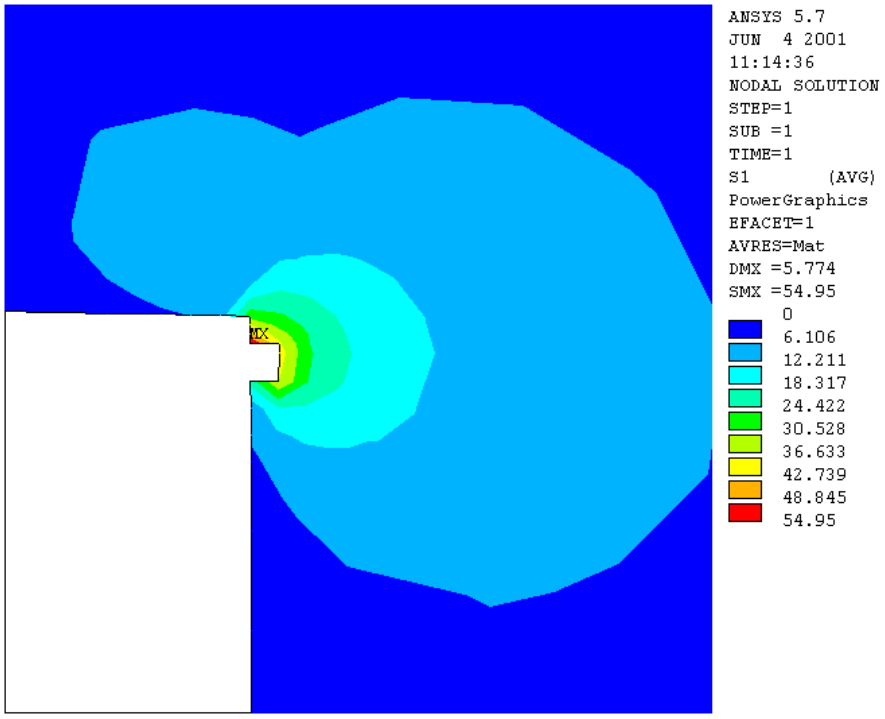

Figure D.5 (c) 1st Principal Stress in Core Material Neglecting Element Containing Infinite Stress Concentration – Neck Section #2

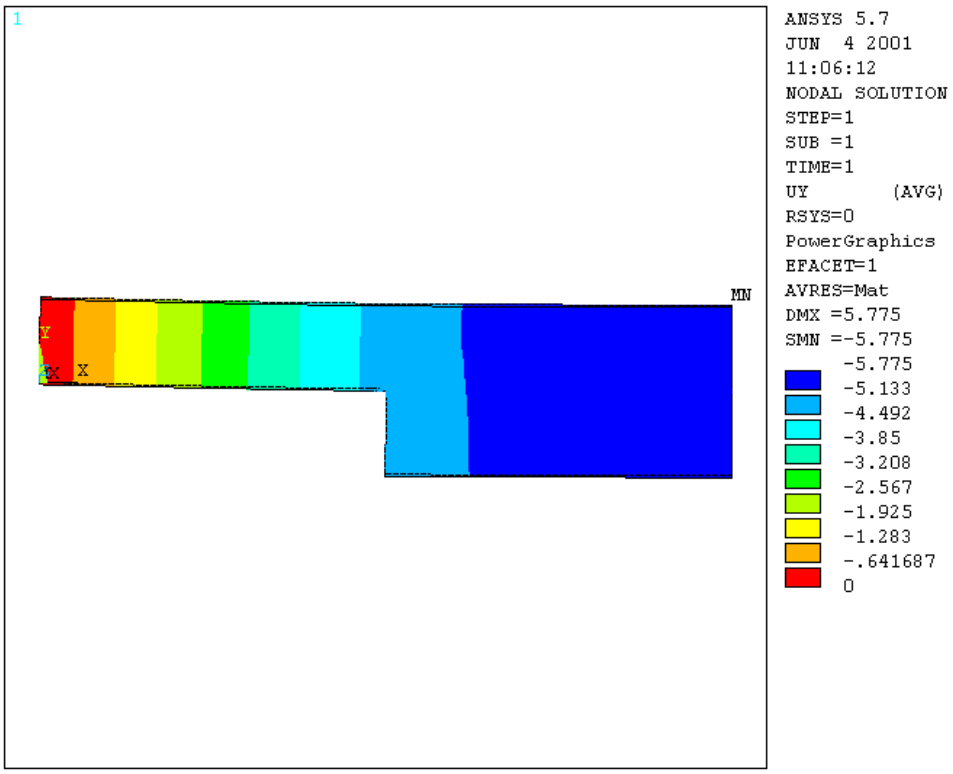

Figure D.5 (d) Neck Section #2 Deflection

D.10 Neck Section #3 Results

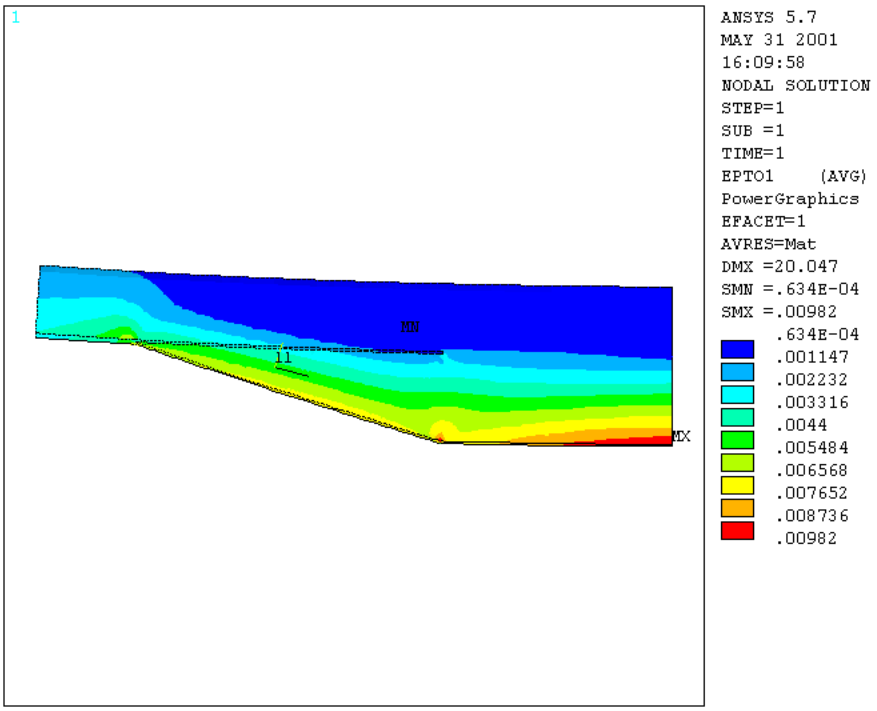

Figure D.6 (a) 1st Principal Strain – Neck Section #3

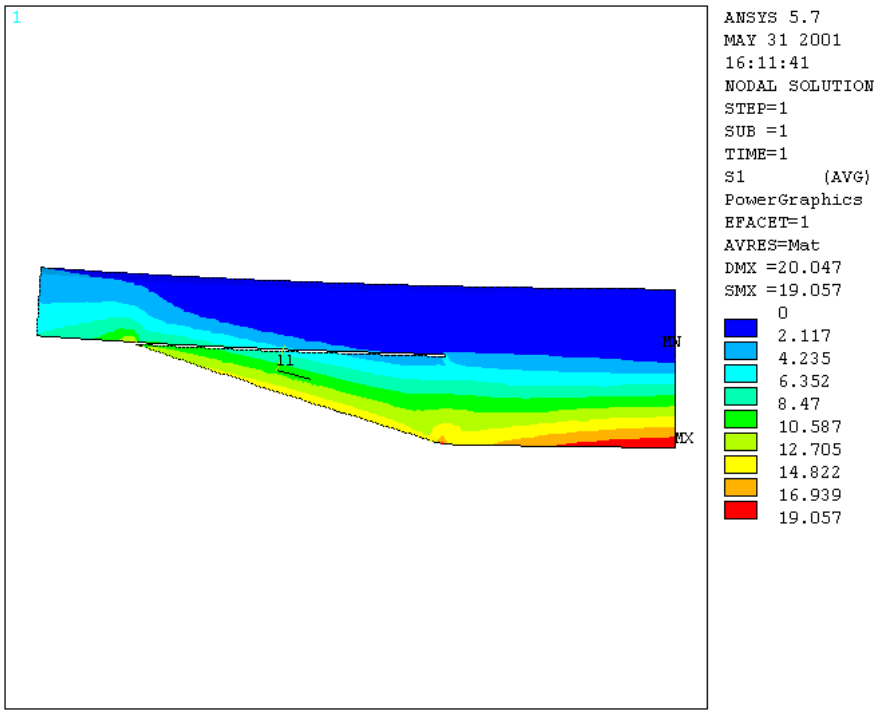

Figure D.6 (b) 1st Principal Stress of Core Material – Neck Section #3

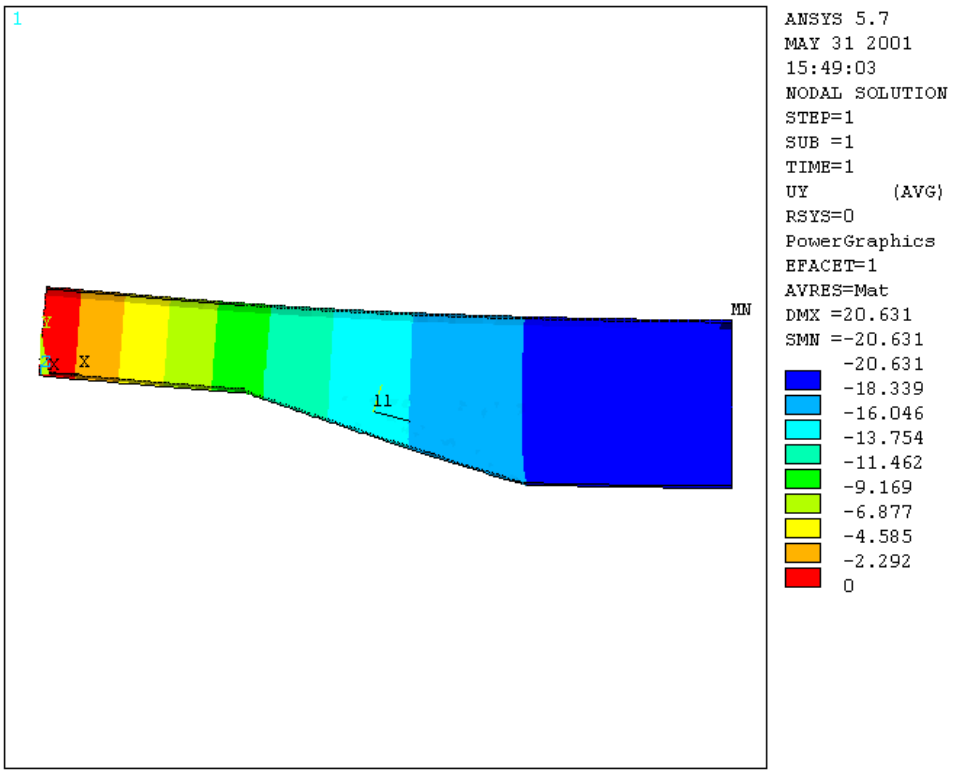

Figure D.6 (c) Neck Section #3 Deflection

D.11 Neck Section #4 Results

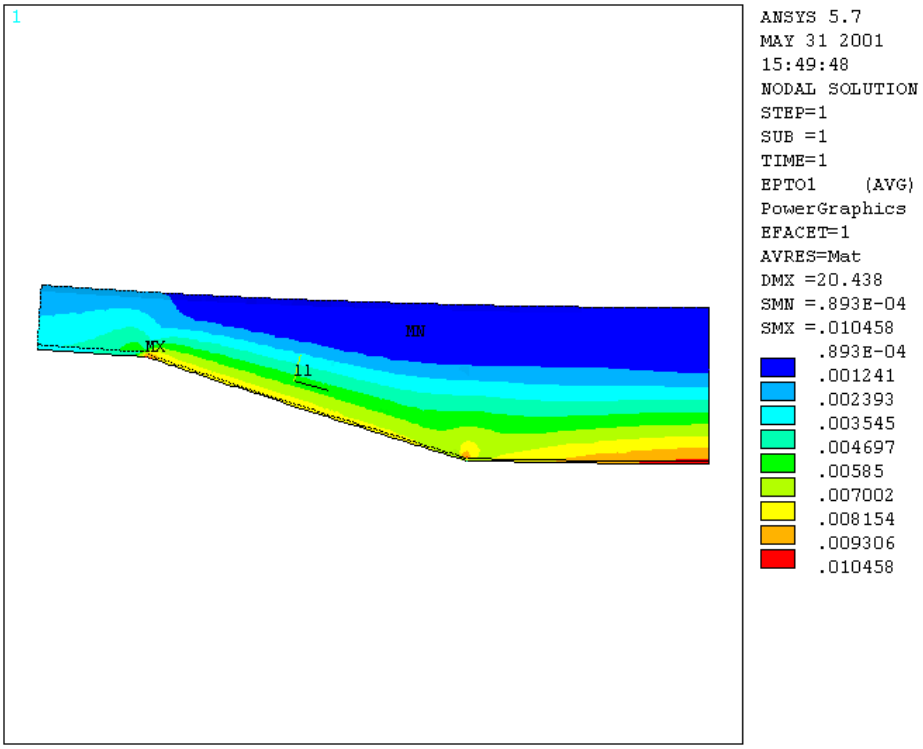

Figure D.7 (a) 1st Principal Strain – Neck Section #4

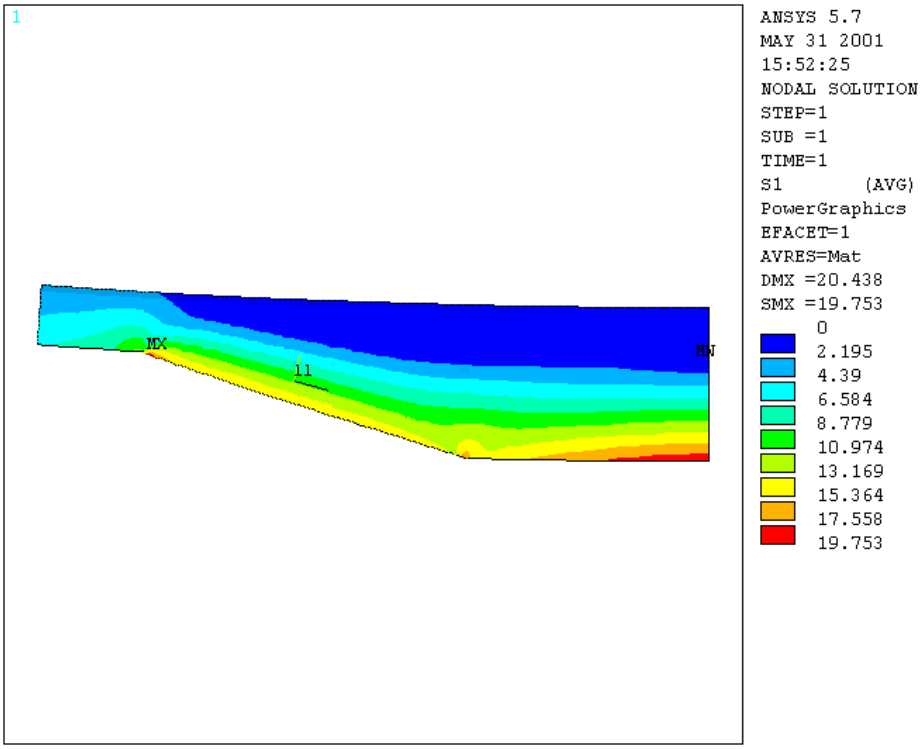

Figure D.7 (b) 1st Principal Stress of Core Material – Neck Section #4

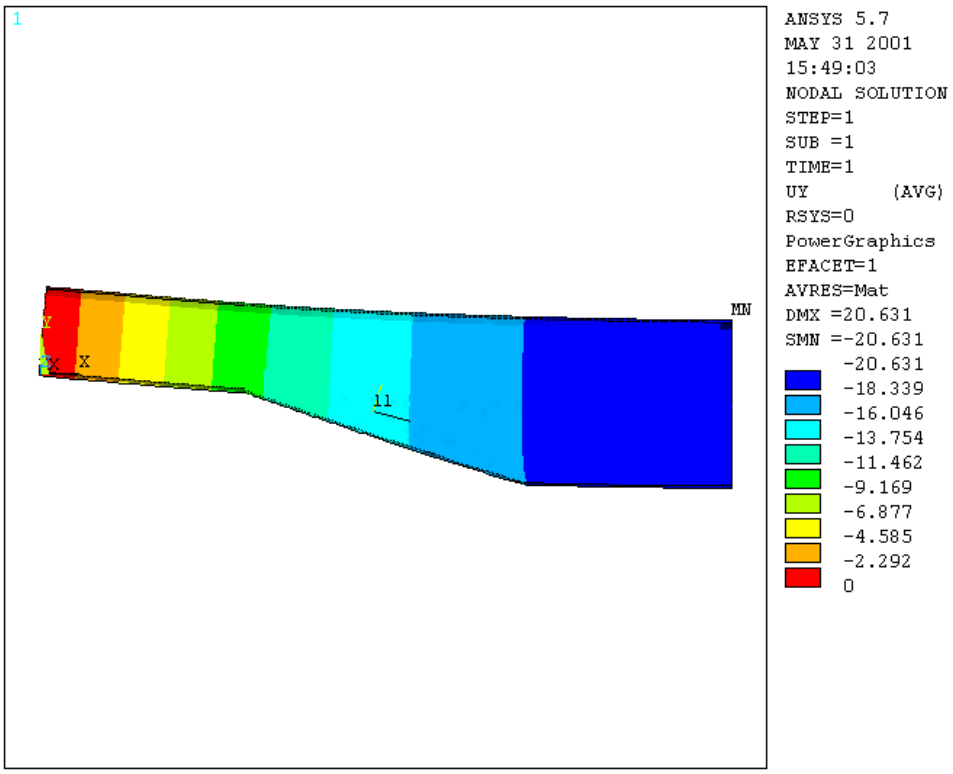

Figure D.7 (c) Neck Section #4 Deflection

D.12 Neck Section #5 Results

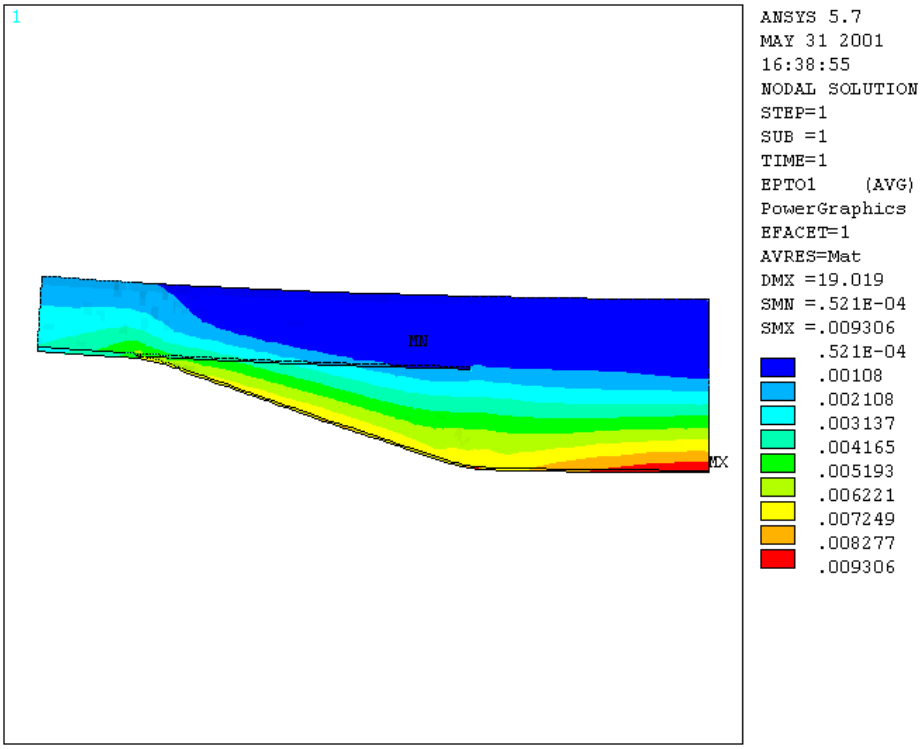

Figure D.8 (a) 1st Principal Strain – Neck Section #5

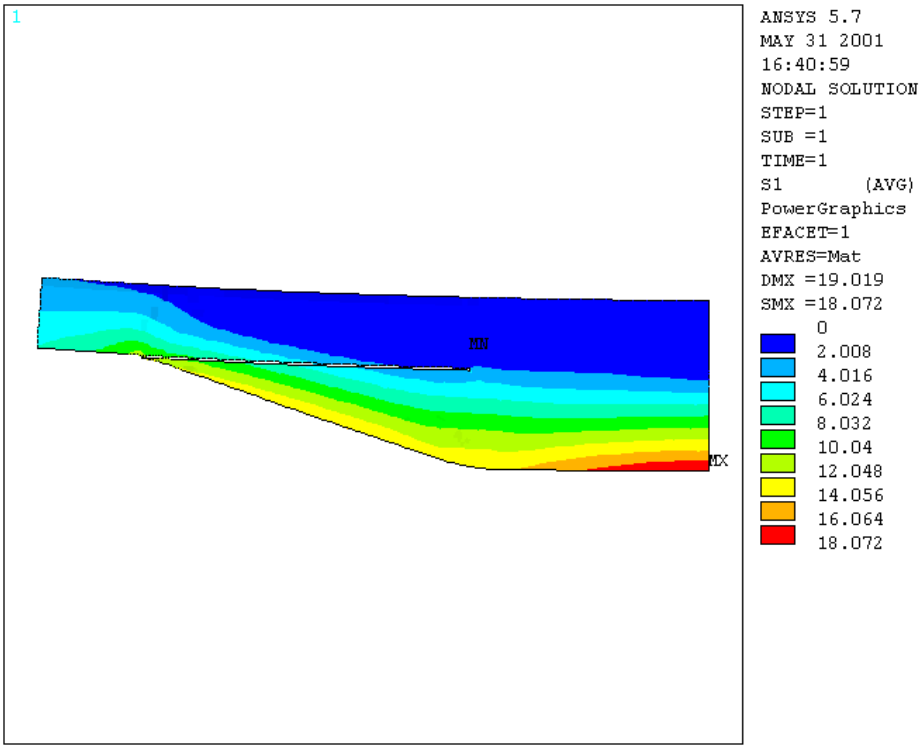

Figure D.8 (b) 1st Principal Stress of Core Material – Neck Section #5

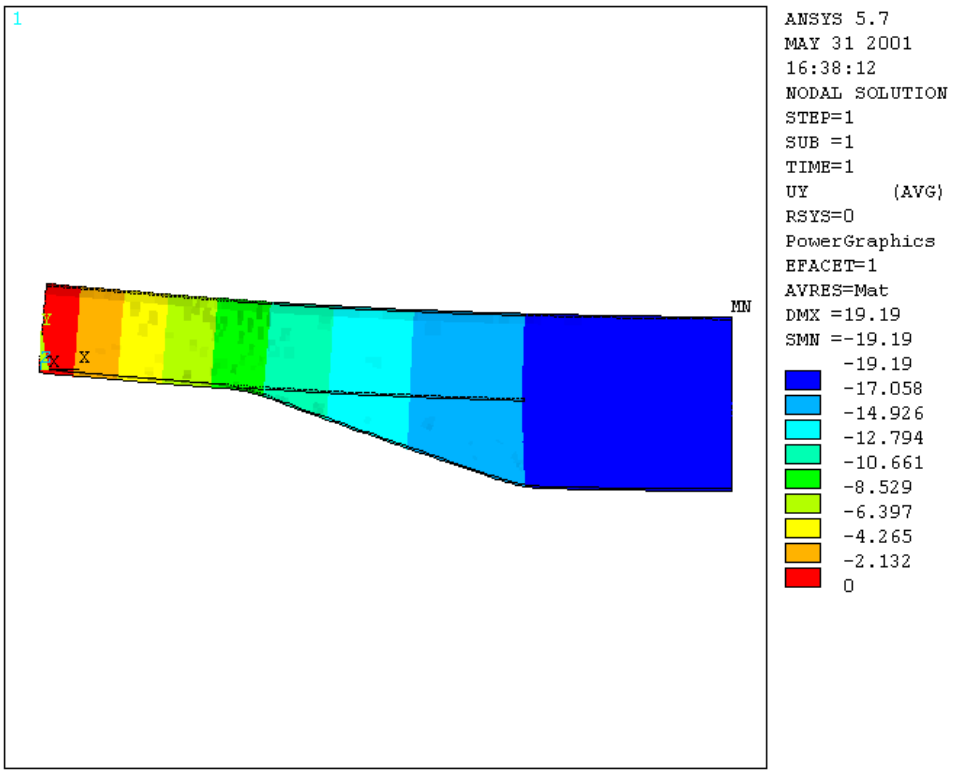

Figure D.8 (c) Neck Section #5 Deflection

D.13 Neck Section #6 Results

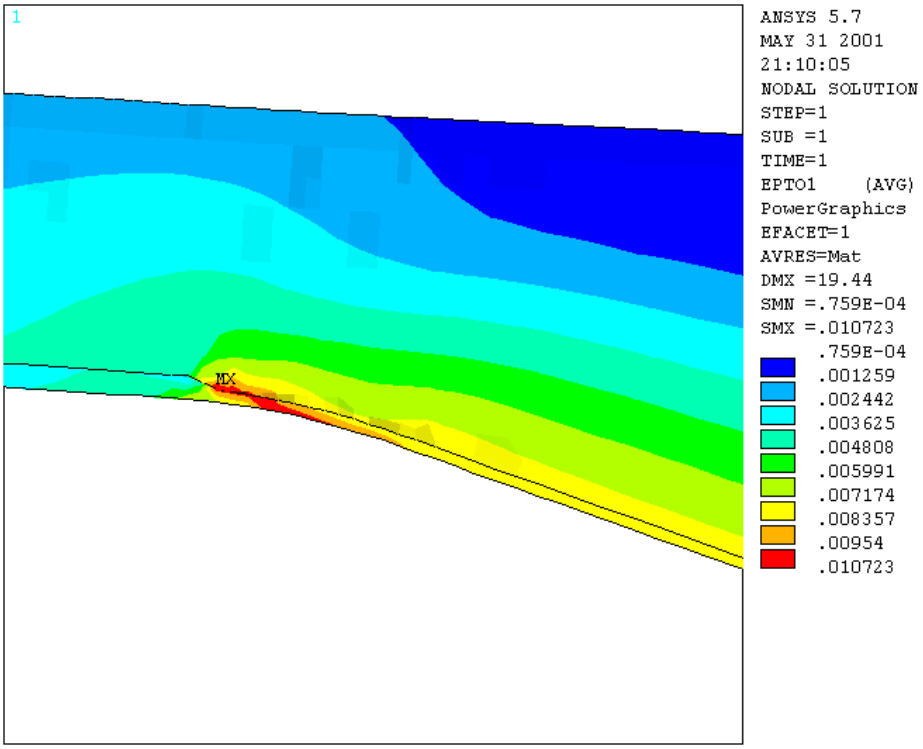

Figure D.9 (a) 1st Principal Strain – Neck Section #6

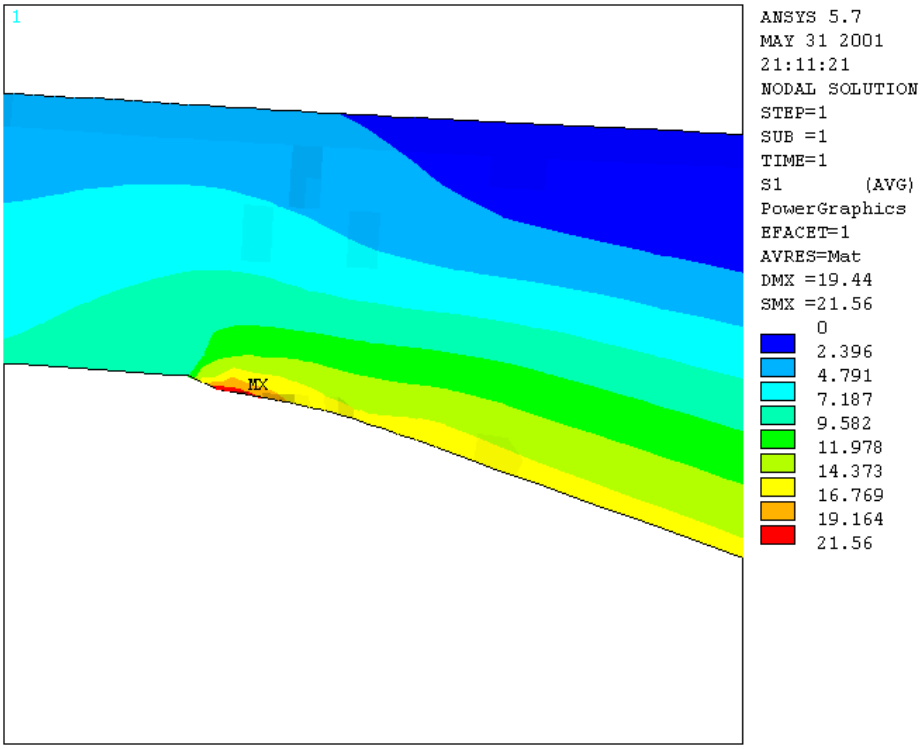

Figure D.9 (b) 1st Principal Stress of Core Material – Neck Section #6

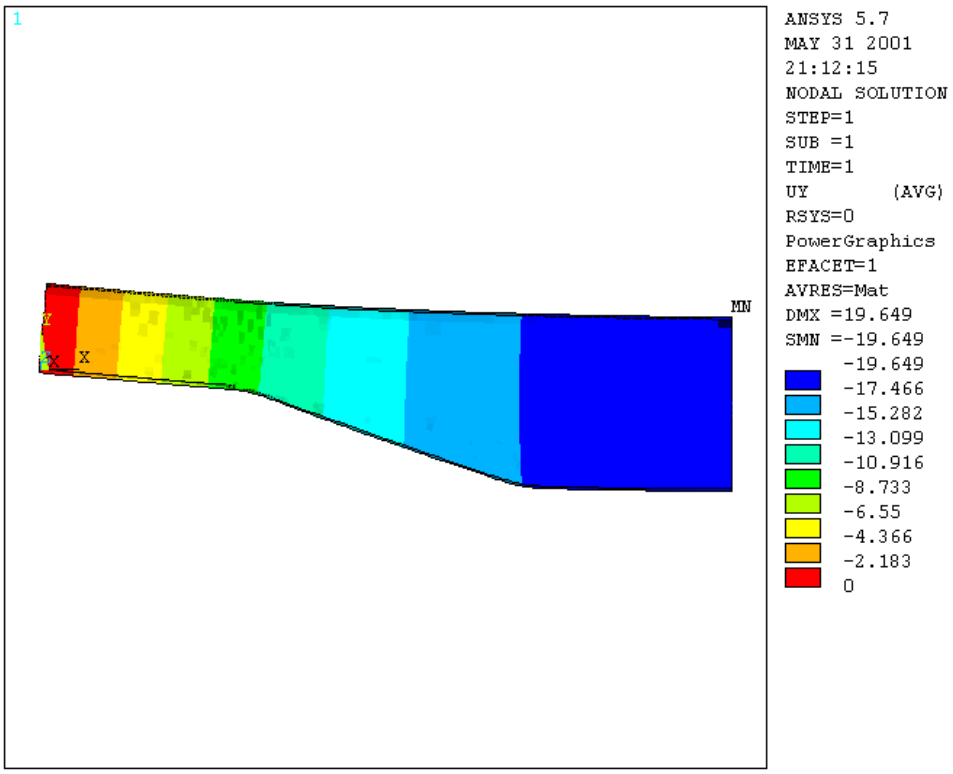

Figure D.9 (c) Neck Section #6 Deflection

D.13 Neck Section #7 Results

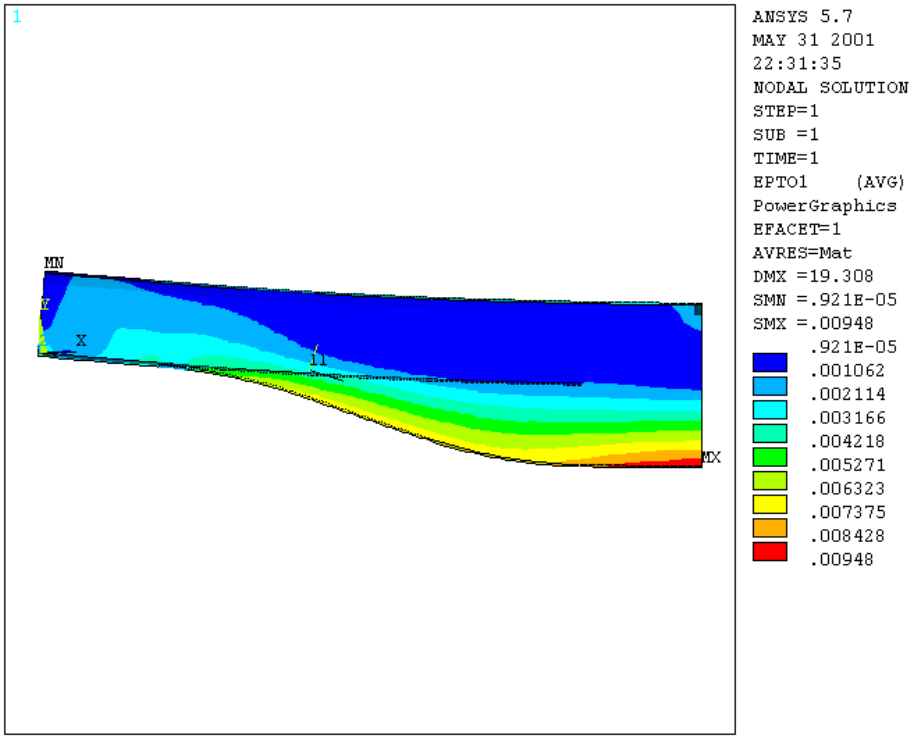

Figure D.10 (a) 1st Principal Strain – Neck Section #7

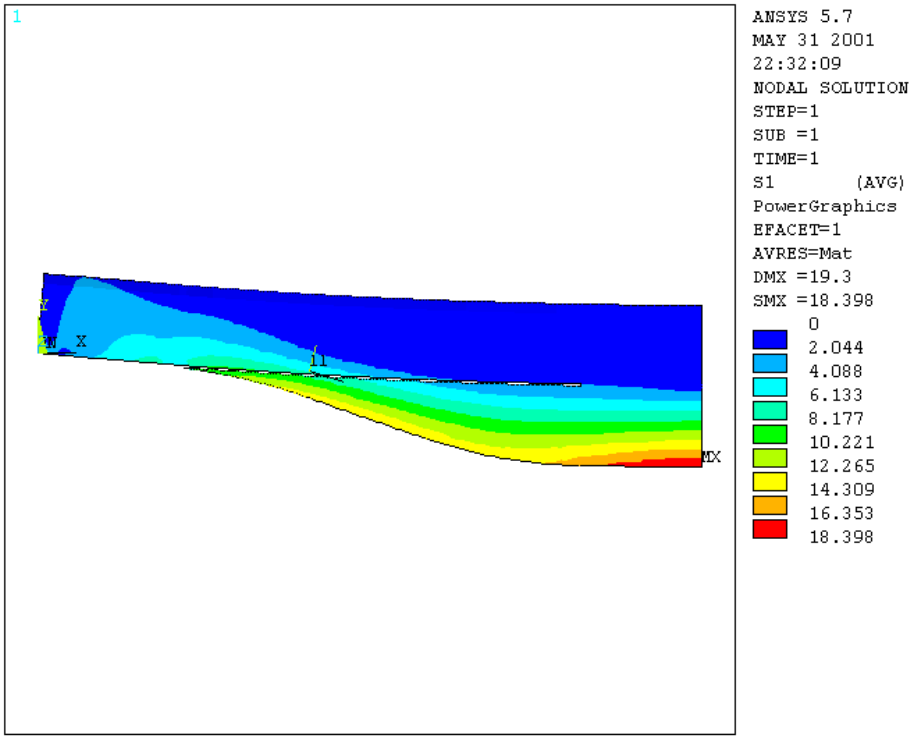

Figure D.10 (b) 1st Principal Stress of Core Material – Neck Section #7

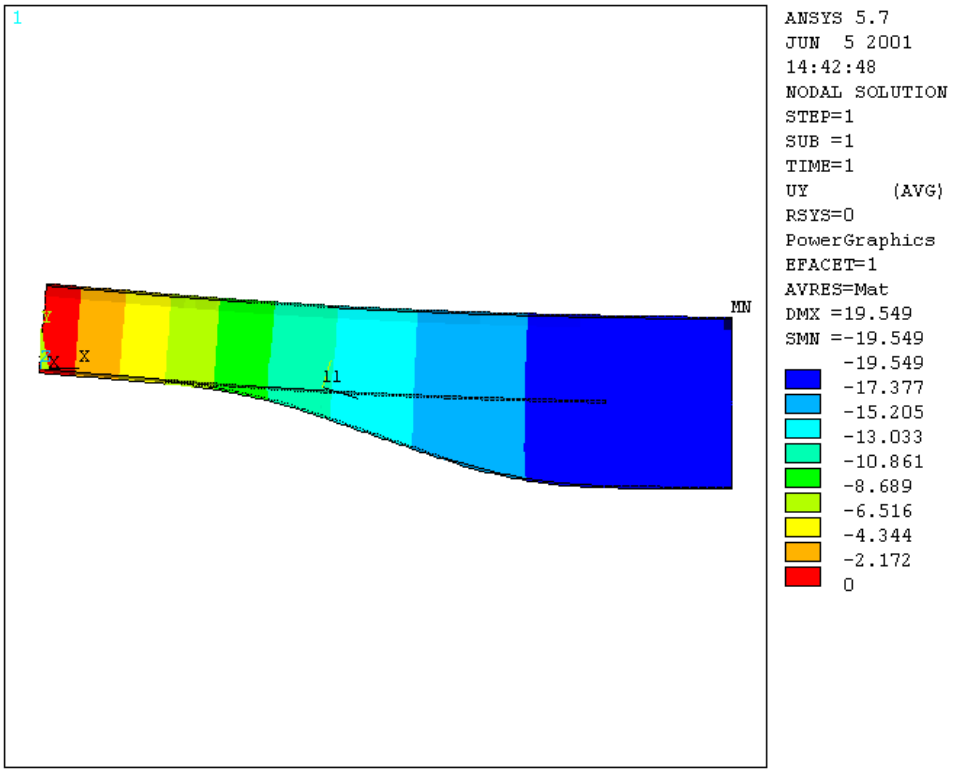

Figure D.10 (c) Neck Section #7 Deflection

Table D.2 Results Summary of Analysis

Neck Section Number	Total Load (N)	Maximum E1 (uE)	Maximum S1 in Core (MPa)	Predicted Failure Point	Midspan Deflection (mm)
1	4000	9818	19.6	Concave Corner	5.3
2	4000	26962	55.0	Concave Corner	5.8
3	20000	9820	19.1	Midspan	20.6
4	20000	10458	19.8	Concave Corner	20.6
5	20000	9306	18.1	Midspan	19.2
6	20000	10723	21.6	Convex Corner	19.6
7	20000	9480	18.4	Midspan	19.5

D.14 Experimental Results

D.14.1 Neck Section #1

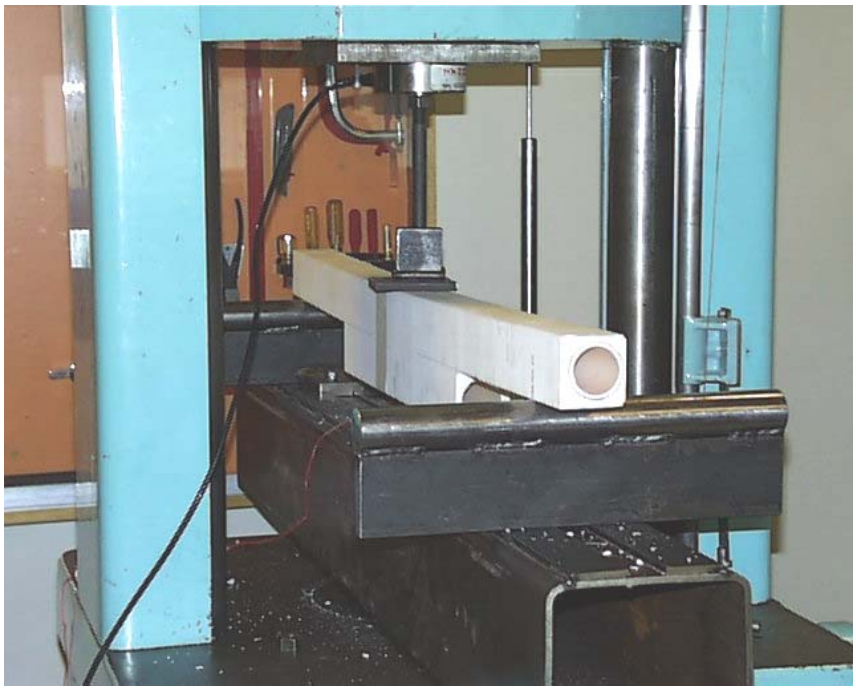

Figure D.11 (a) Neck Section #1 In Test Rig

Figure D.11 (b) Failure of Neck Section #1

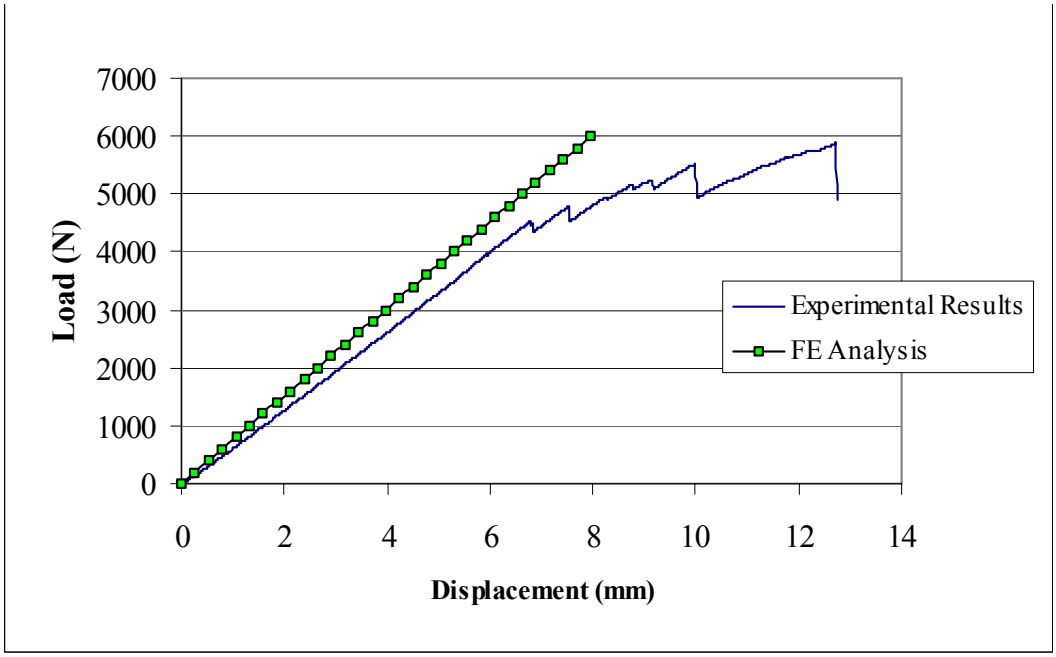

Figure D.11 (c) Load Vs Displacement Curve For Neck Section #1

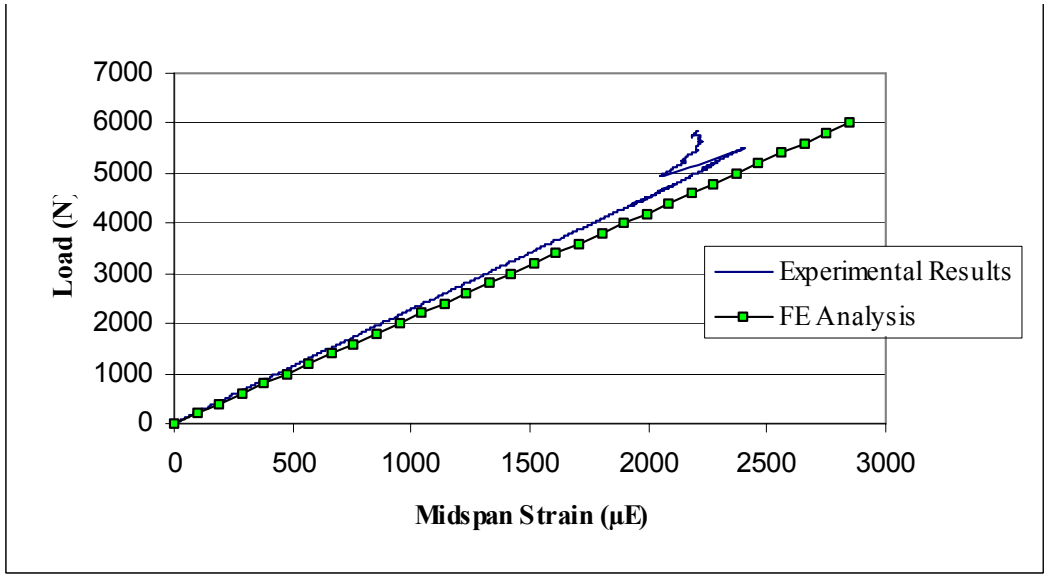

Figure D.11 (d) Load Vs Strain at Midspan For Neck Section #1

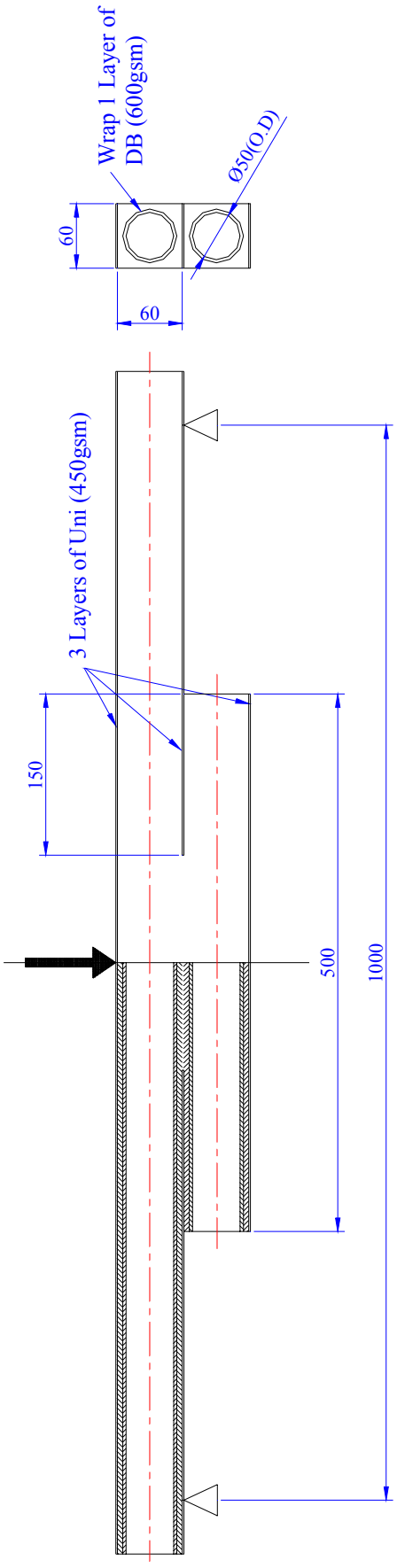

Figure D.11 (e) Configuration of Neck Section #1

D.14.2 Neck Section #3

Figure D.12 (a) Neck Section #3 In Test Rig

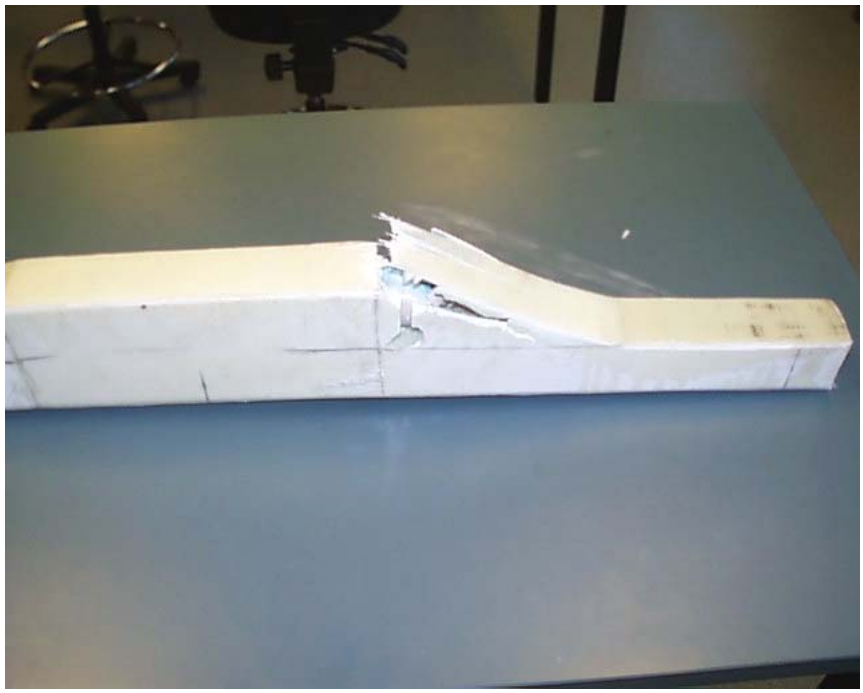

Figure D.12 (b) Failure of Neck Section #3

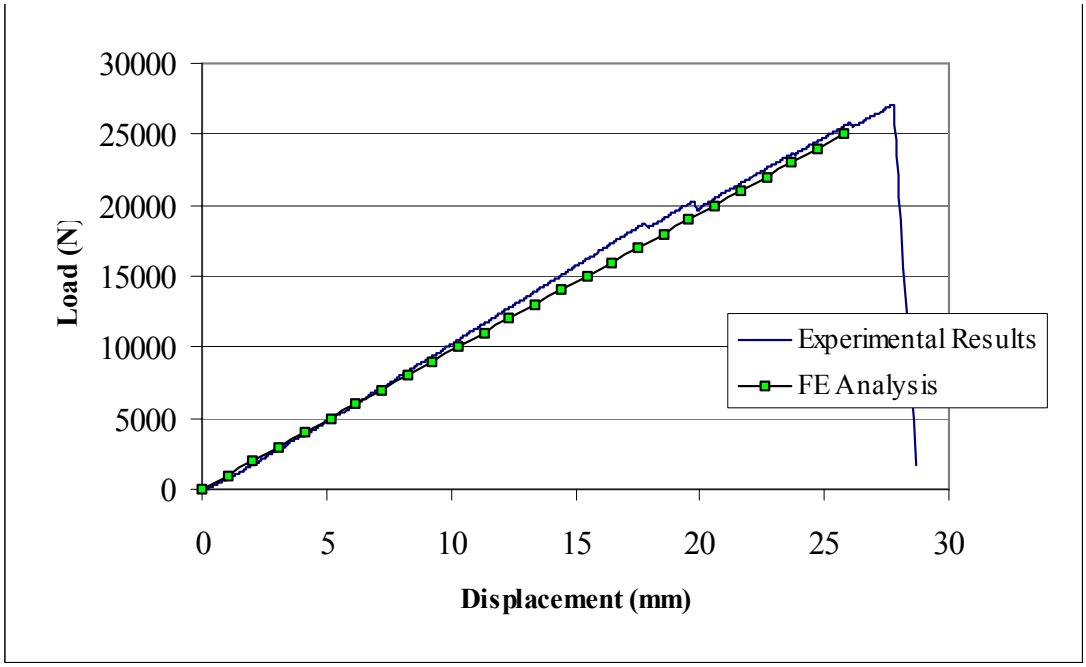

Figure D.12 (c) Load Vs Displacement Curve For Neck Section #3

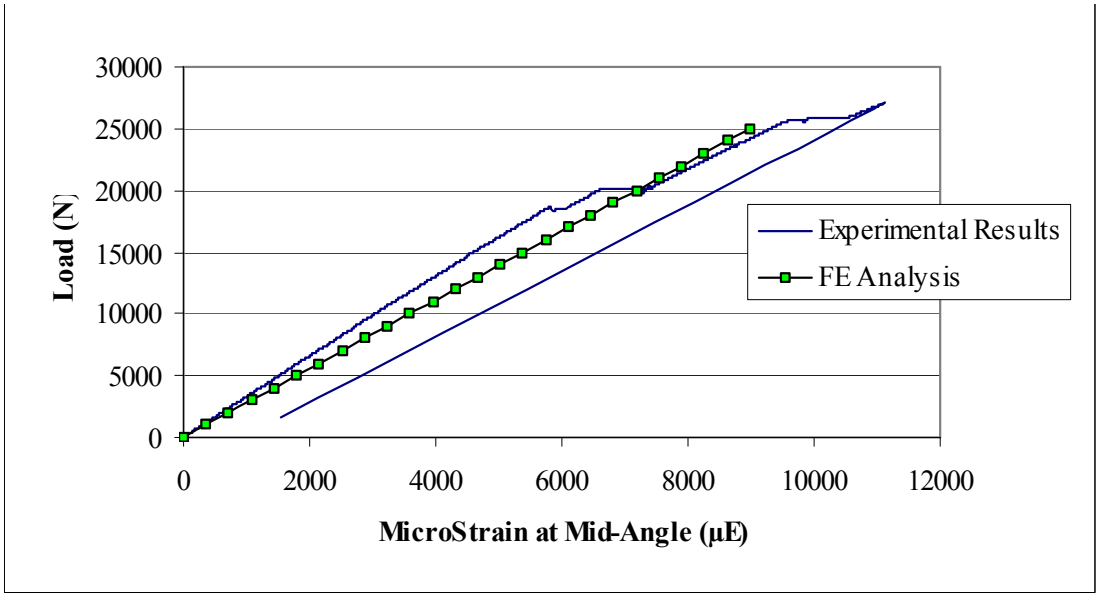

Figure D.12 (d) Load Vs Strain at Midangle For Neck Section #3

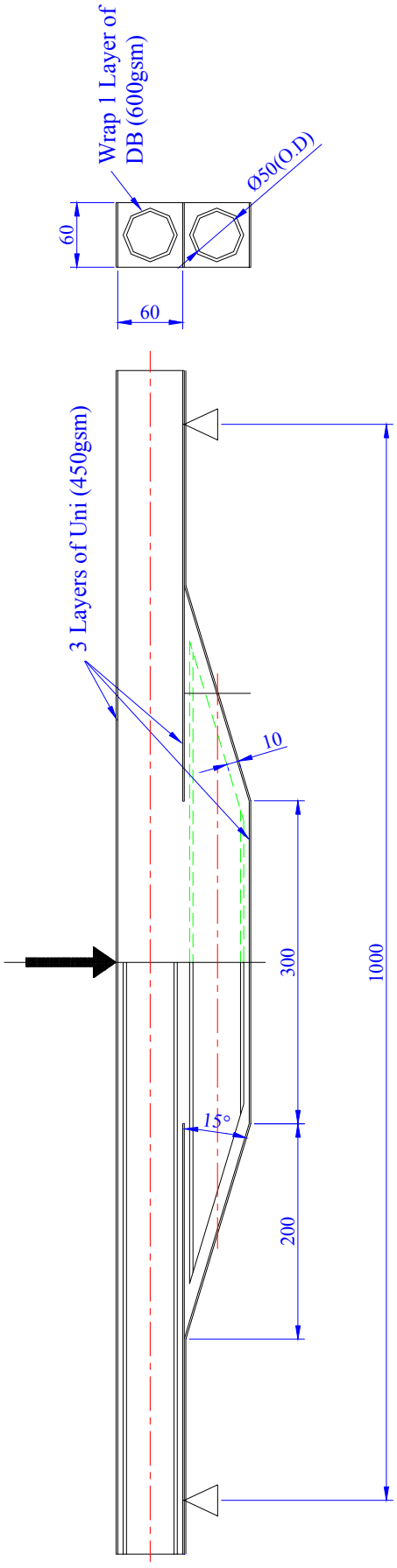

Figure D.12(e) Configuration of Neck Section #3

D.14.3 Neck Section #4

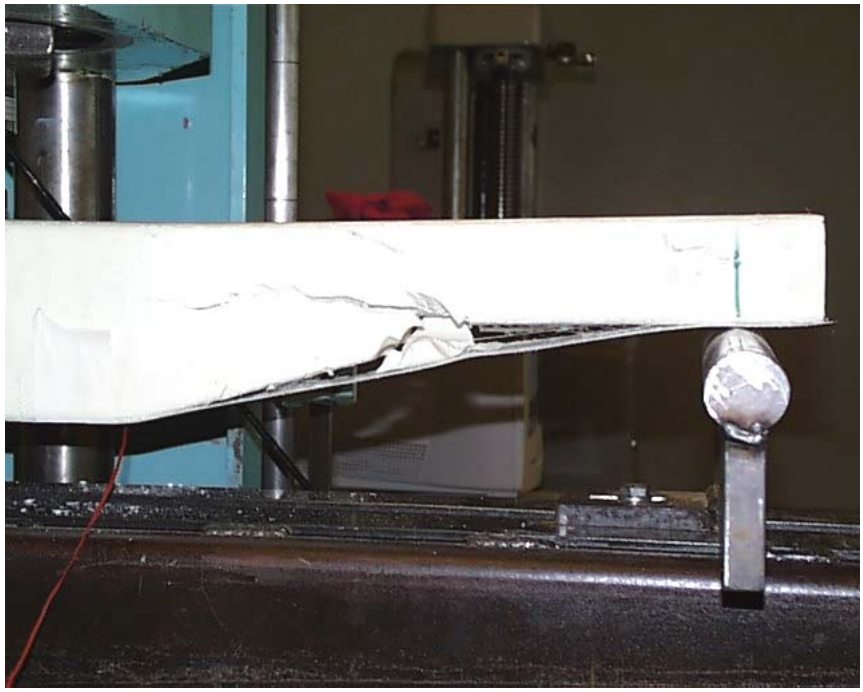

Figure D.13 (a) Failure of Neck Section #4

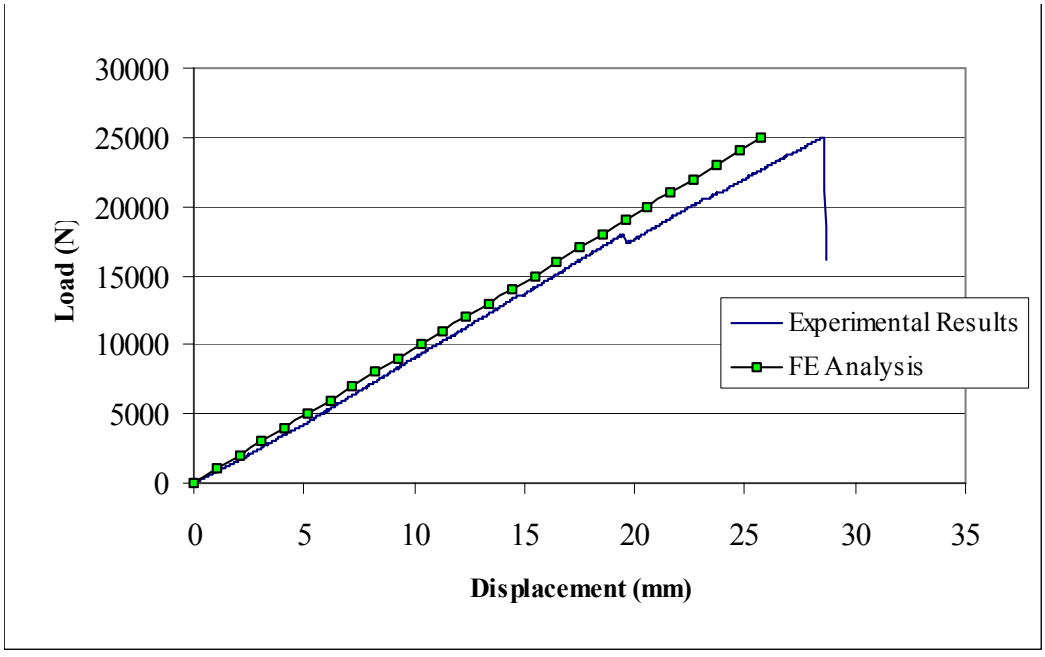

Figure D.13 (b) Load Vs Displacement Curve For Neck Section #4

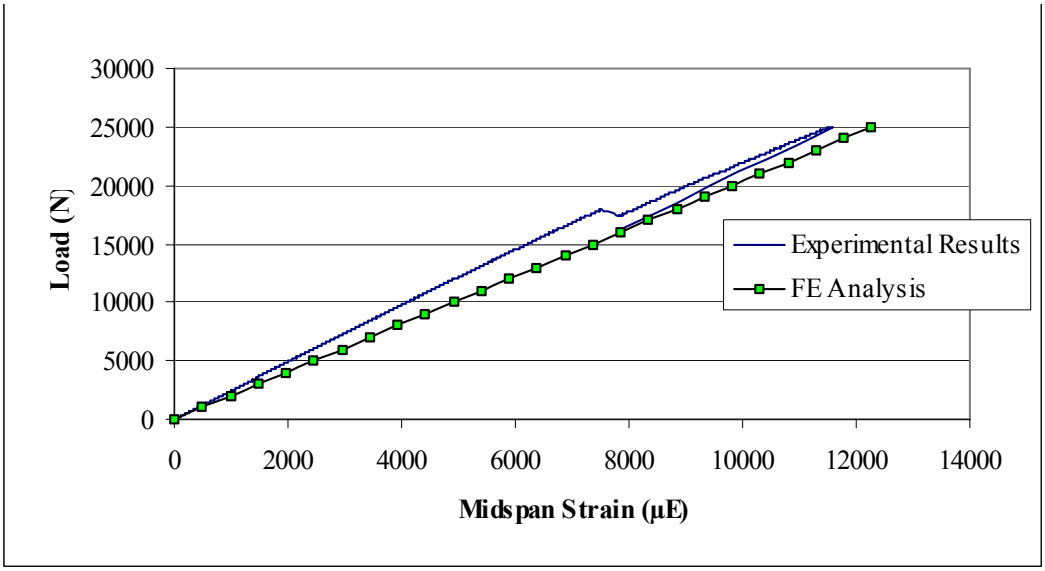

Figure D.13 (c) Load Vs Strain at Midspan For Neck Section #4

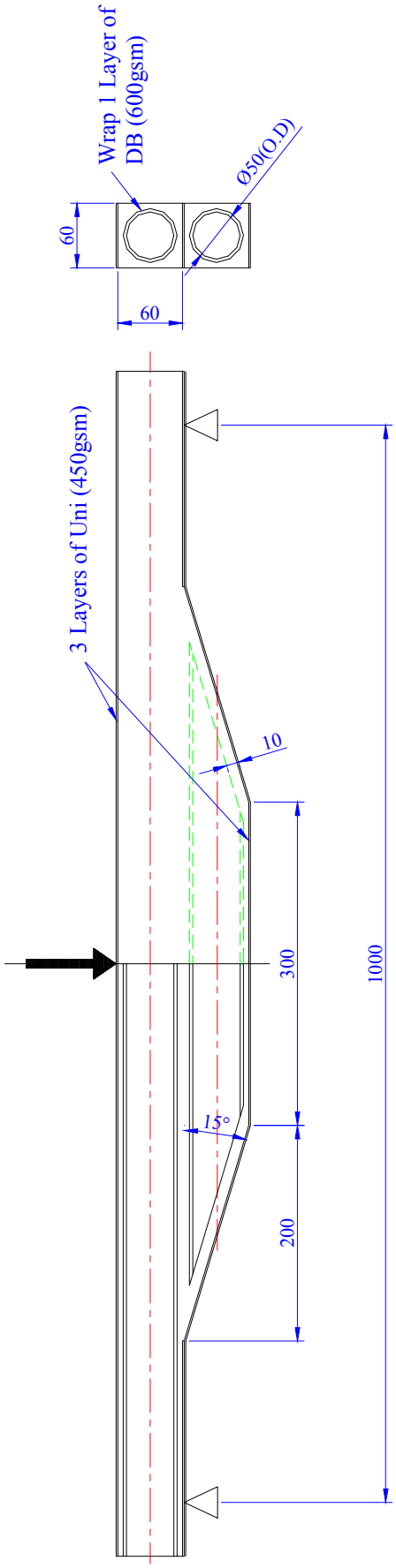

Figure D.13 (d) Configuration of Neck Section #4

D.14.4 Neck Section #5

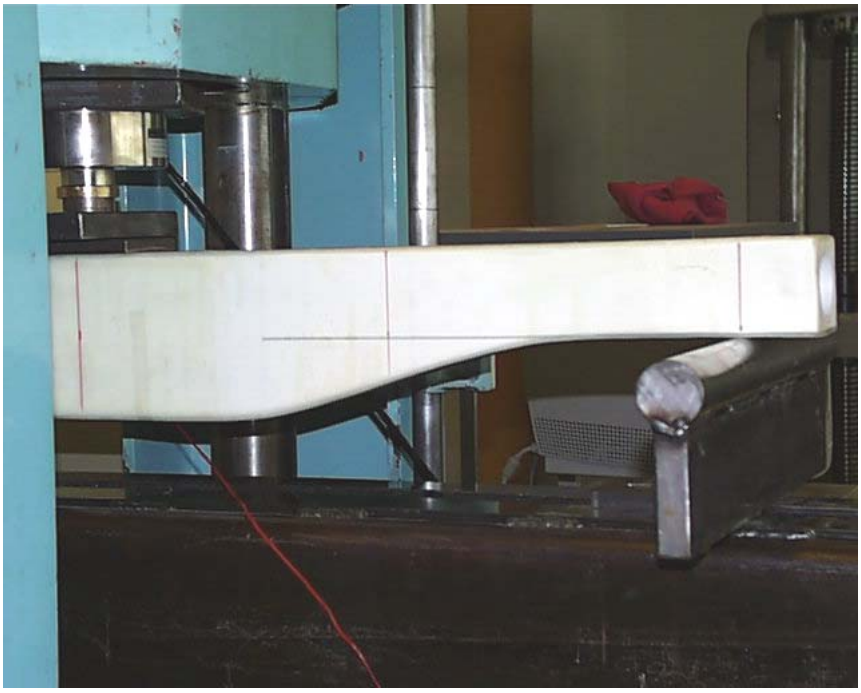

Figure D.14 (a) Neck Section #5 In Test Rig

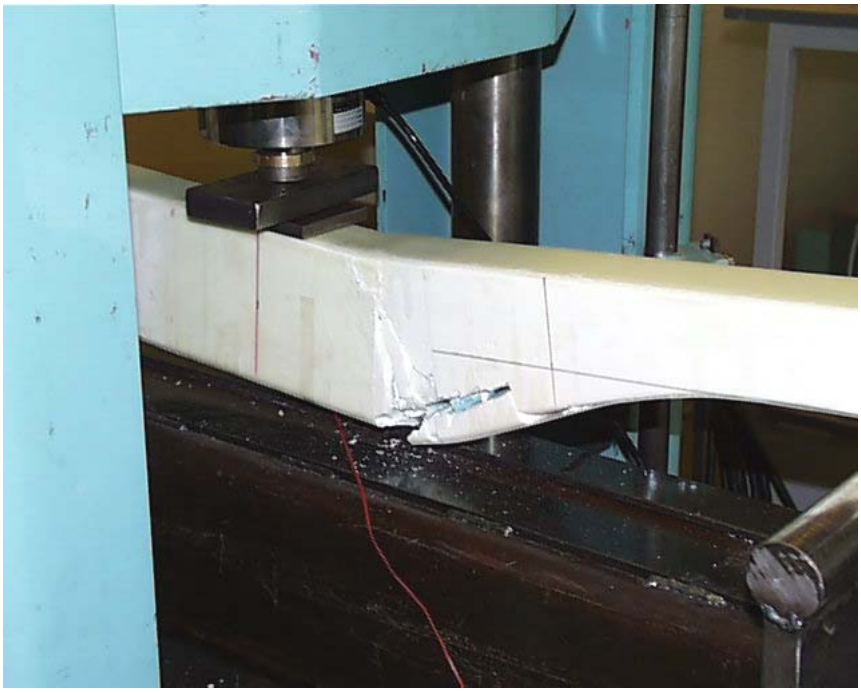

Figure D.14 (b) Failure of Neck Section #5

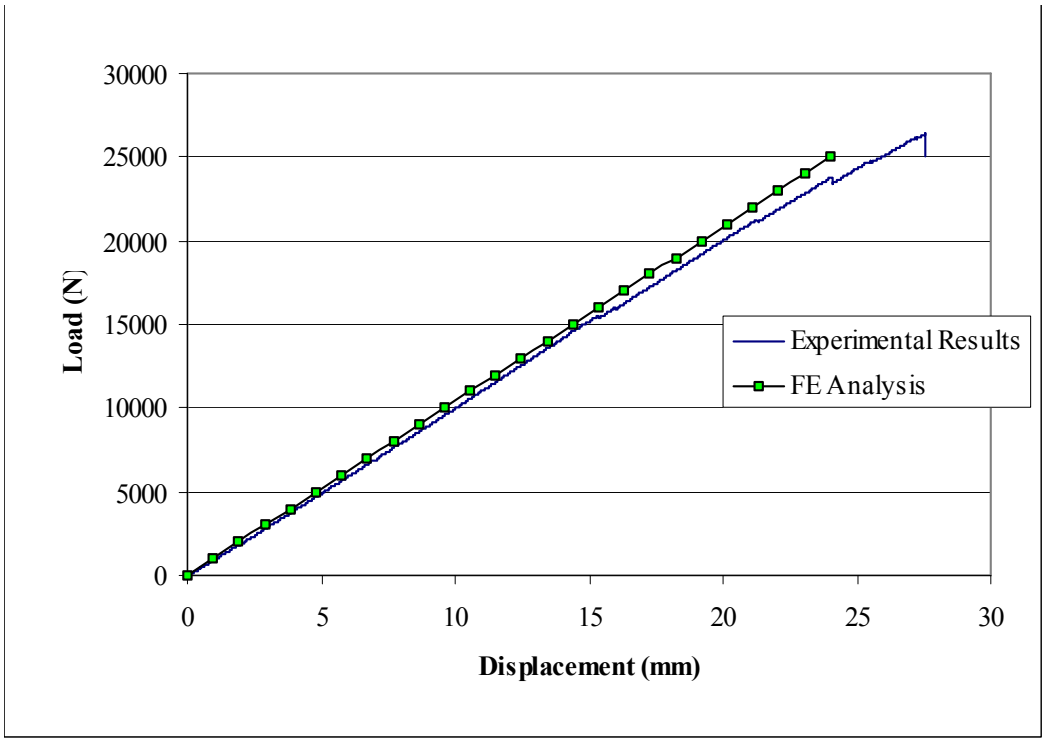

Figure D.14 (c) Load Vs Displacement Curve For Neck Section #5

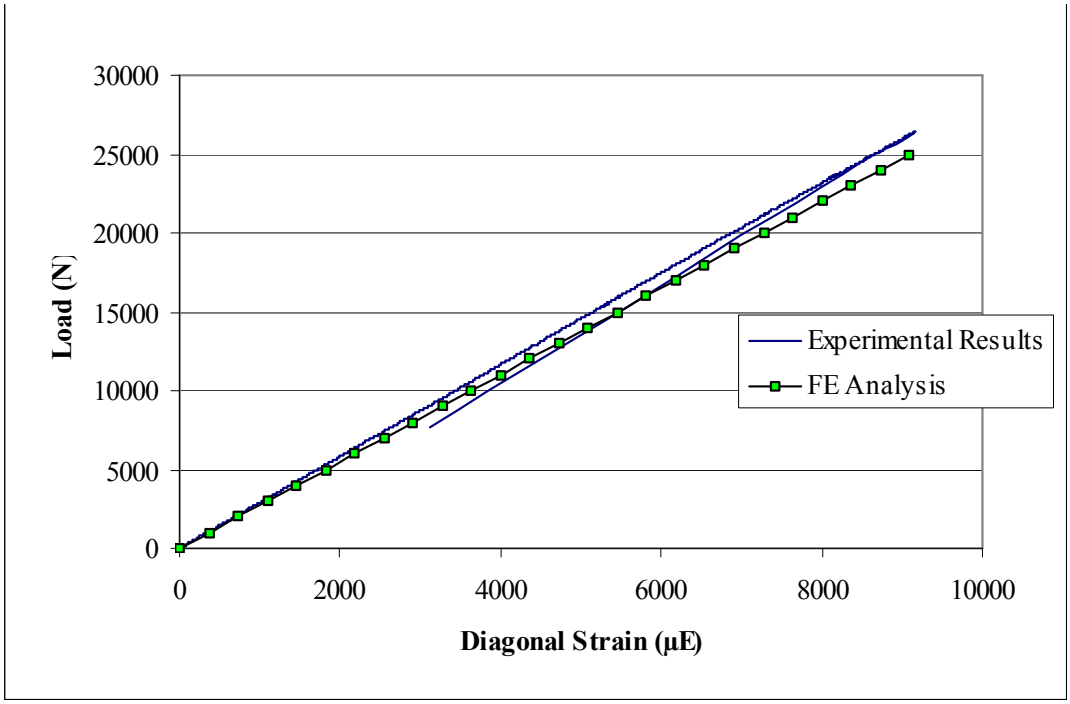

Figure D.14 (d) Load Vs Strain at Midangle For Neck Section #5

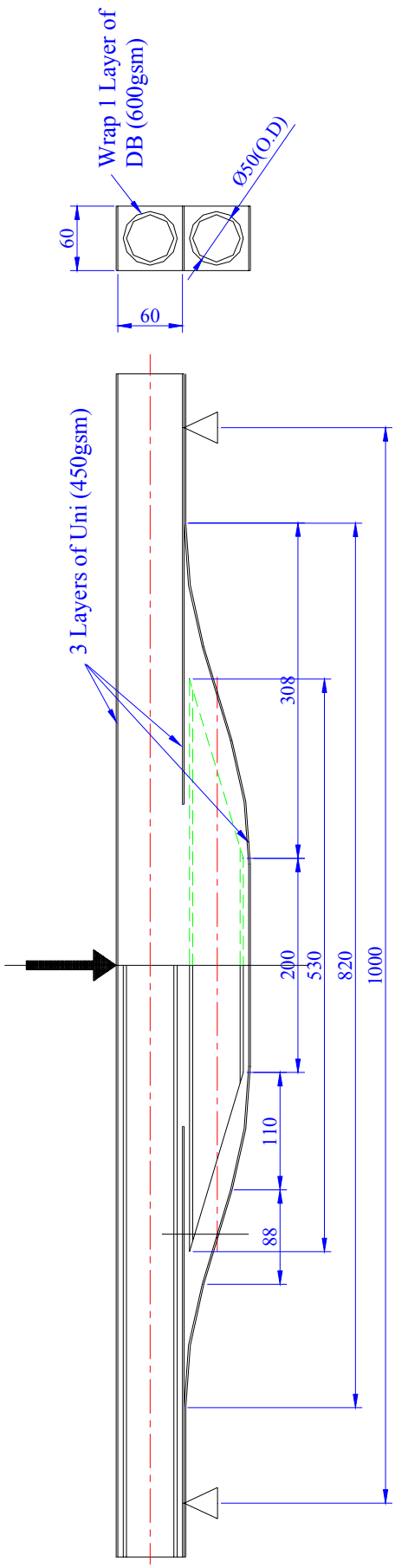

Figure D.14 (e) Configuration of Neck Section #5

Appendix E – Half-Scale Neck Analysis and Testing Results

E.1 Analysis Identification

Model 1 scaleneck3d.db

E.2 Aim of Analysis

- To perform a linear static analysis of the neck section of an FRP chassis rail
- To investigate the performance of each chassis rail under load, particularly at ultimate load, and observe the expected failure modes

To allow the evaluation of the structural characteristics of the model, in particular the effectiveness of the stress concentration reduction techniques developed through the small-scale neck investigation described in Section 7.5.2 and Appendix D.

E.3 Model Form

This 3-dimensional model was intended to replicate the real structure with as much detail as was deemed practical. Figures E.1 (a) and (b) show the basic form of the model, which utilises symmetry in order to reduce solution time and computing resources.

E.4 Material Properties and Laminate Stacking

Both unidirectional and double bias (DB) fabrics were used in this beam. An orthotropic material represented the unidirectional laminates, with the x-direction of each element being oriented according to the global model x-axis. The double bias fabric was represented by two uni-directional laminates, oriented at $\pm 45^{0}$, as discussed in section 5.6.6. The material properties, taken from section 5.6.6 and other sources where appropriate, were input into the model as follows:

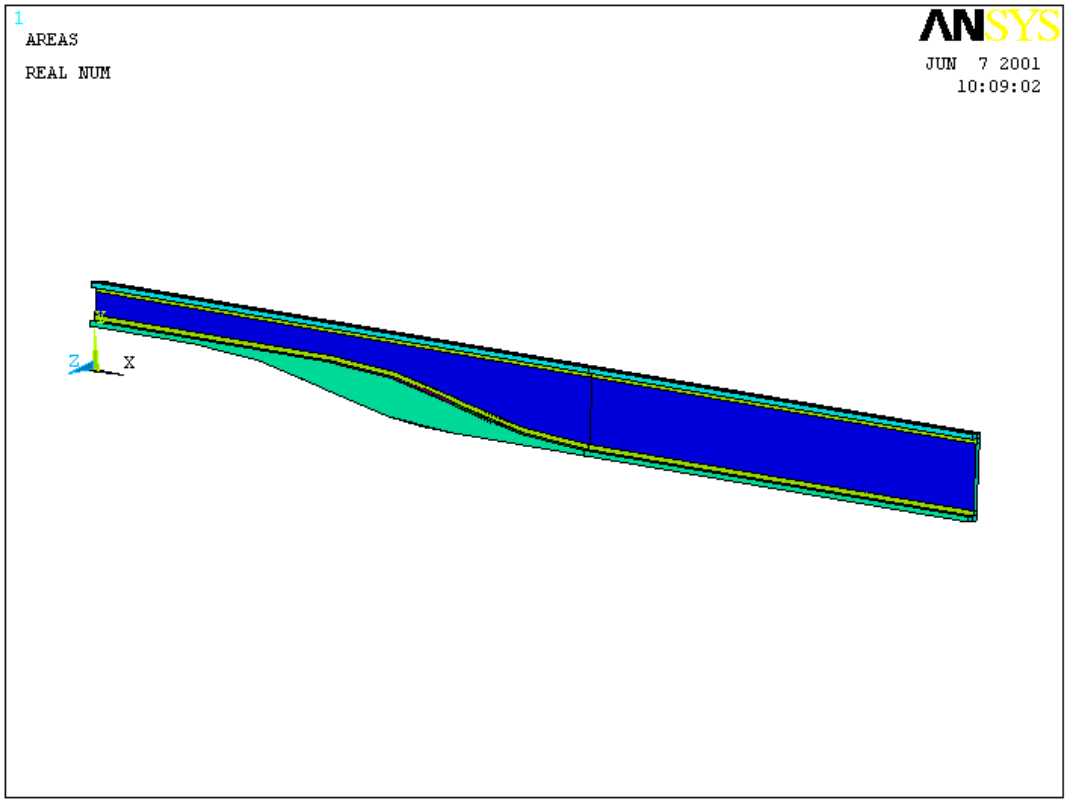

Figure E.1 (a) Basic Model Layout

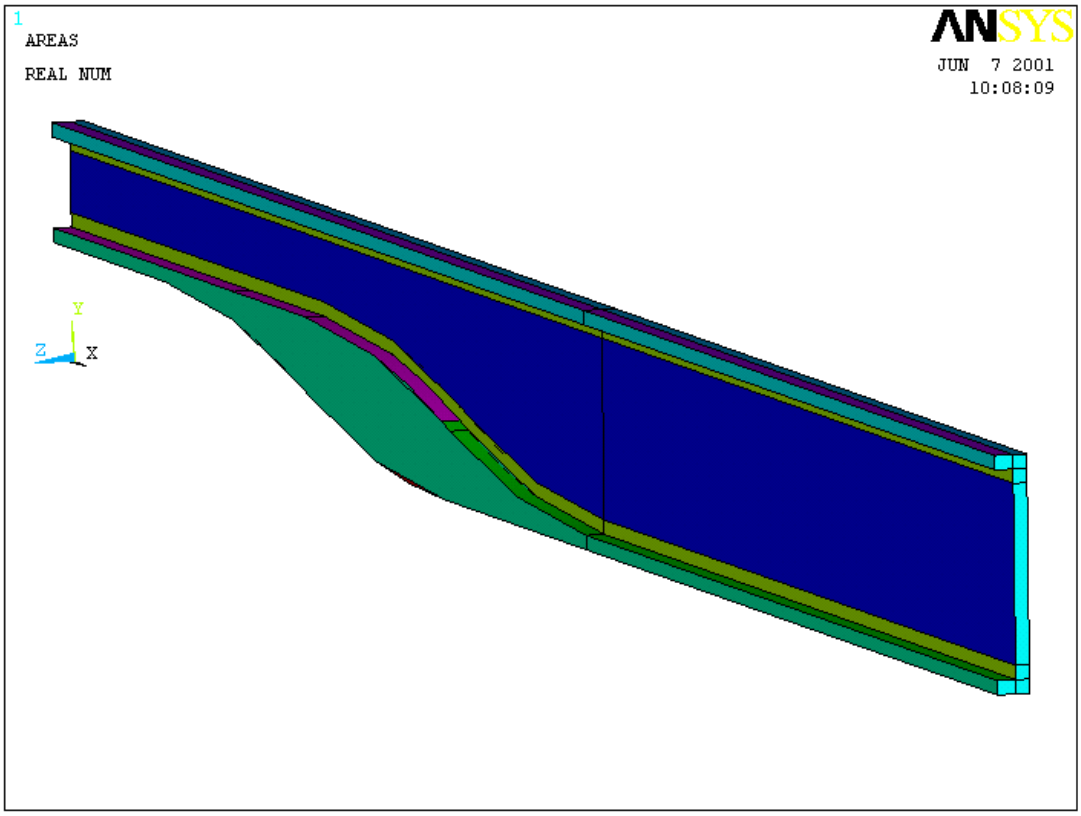

Figure E.1 (b) Basic Model Layout

1. Properties of E-glass Uni-directional reinforcement (300 g/m^2):

Young's Modulus, E_1 : 28624 MPa

E_2 : 7404 MPa

Poisson's Ratio, γ_{xy} : 0.322

Shear Modulus, G_{xy} : 2986 MPa

T'ness per layer of t_{UD} : 0.3 mm

Unidirectional E-glass (300 g/m^2)

T'ness per layer of t_{DB} : 0.6 mm

Double Bias Fabric (600 g/m^2)

2. Properties of T300 Carbon Fibre Uni-directional reinforcement (315 g/m^2):

Young's Modulus, E_1 : 64973 MPa

E_2 : 7404 MPa

Poisson's Ratio, γ_{xy} : 0.23

Shear Modulus, G_{xy} : 6000 MPa

Thickness per layer. t_{UD} : 0.53 mm

3. Properties of H200 PVC Foam supplied by DIAB Pty Ltd (ρ = 200 kg/m^3):

Young's Modulus, E_1 : 250 MPa

Poisson's Ratio, γ_{xy} : 0.32

4. Properties of PU Elastomer, RP6430, supplied by Vantico Pty Ltd:

Young's Modulus, E_1 : 1500 MPa

Poisson's Ratio, γ_{xy} : 0.25

Laminate Stacking Sequences:

The laminae contained within the model replicated the layup sequences present in the actual beam. The layup sequences are described in detail in E.9.

E.5 Analysis Program

Analysis program:	ANSYS 5.7
Computer:	Intell 266MMX
	128MB Ram
	Win98
Analysis type:	Linear static (Assumed Small Displacement)

E.6 Mesh Details

The mesh used in the analysis is shown in Figures E.2 (a) and (b). This mesh was designed to provide a relatively high level of accuracy throughout the neck section, although no particular region warranted further element refinement due to the absence of significant stress concentrations as demonstrated in section E.8.

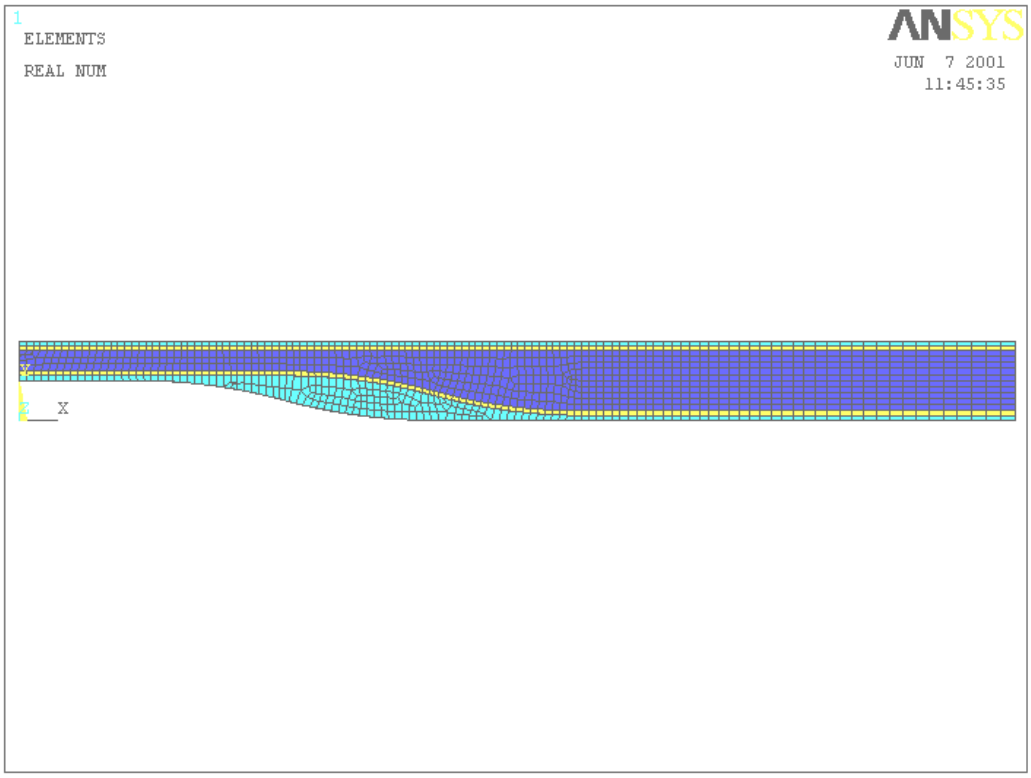

Figure E.2 (a) Mesh Used for Neck Sections

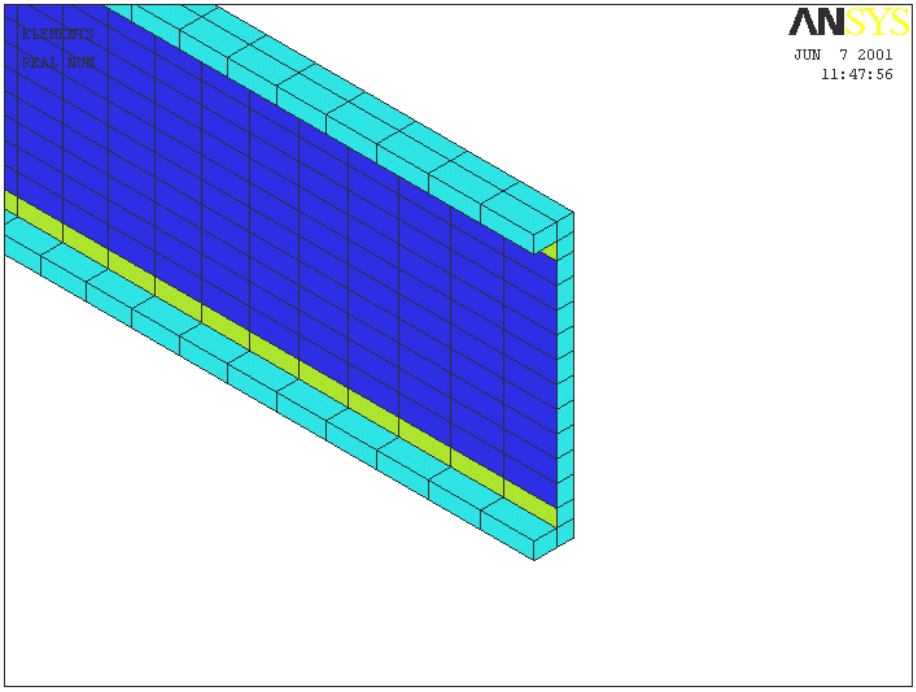

Figure E.2 (b) Magnified View of Beam Representation

Element Type:

1. SHELL 99 May be used for layered applications of a structural shell model. Allows up to 250 layers. If more than 250 layers are required, a user-input constitutive matrix is available. The element has six degrees of freedom at each node: translations in the nodal x, y, and z directions and rotations about the nodal x, y, and z-axes. Refer ANSYS manual for further details.

2. SOLID 95 It can tolerate irregular shapes without as much loss of accuracy. Have compatible displacement shapes and are well suited to model curved boundaries. The element is defined by 20 nodes, having three degrees of freedom per node, and translations in the nodal x, y, and z directions. The element may have any spatial orientation. This element has plasticity, creep, stress stiffening, large deflection, and large strain capabilities. Refer ANSYS manual for further details.

E.7 Application of Boundary Conditions

The model was loaded in three-point bending, being simply supported. Consequently, one end was restrained in the global y-direction, while the other was restrained in both the x- and y-directions. Appropriate symmetry conditions were applied along the line of symmetry.

The load was applied approximately 200 mm from the beam midspan, as illustrated in Figure E.3. A magnitude of 40 kN was applied to the model (equivalent to 80 kN on full beam), and the response of the beam to all other load values was interpolated using the linear relationship inherent in the analysis type.

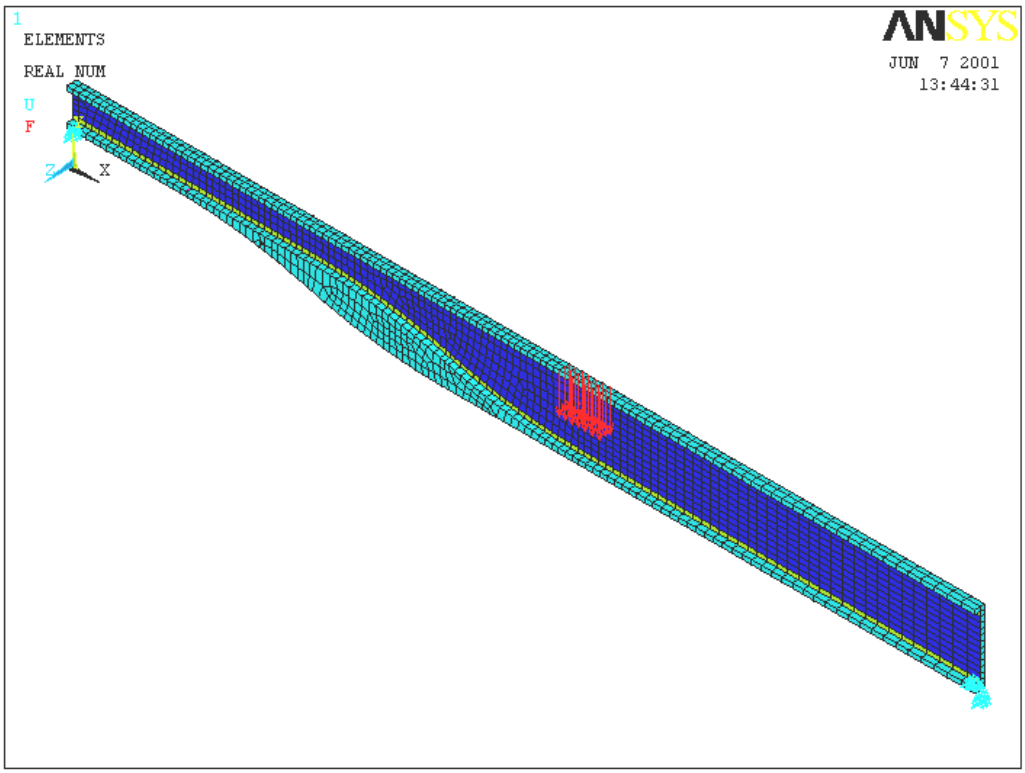

Figure E.3 Boundary Conditions Imposed on Model

E.8 Analysis Results

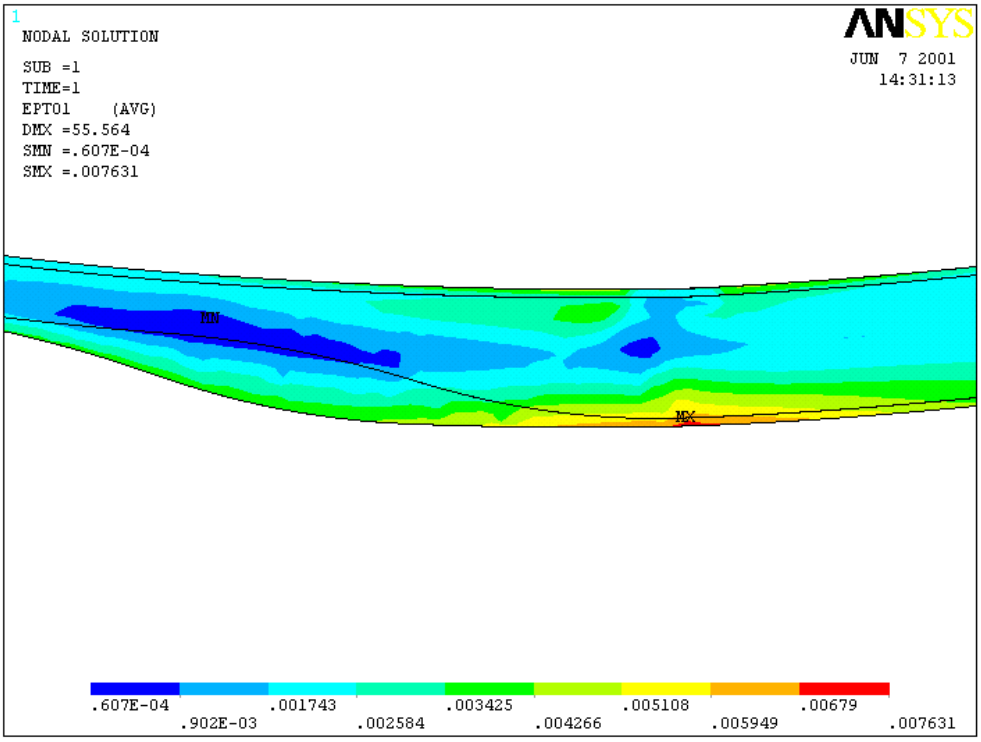

Figure E.4 (a) 1st Principal Strain In Laminate

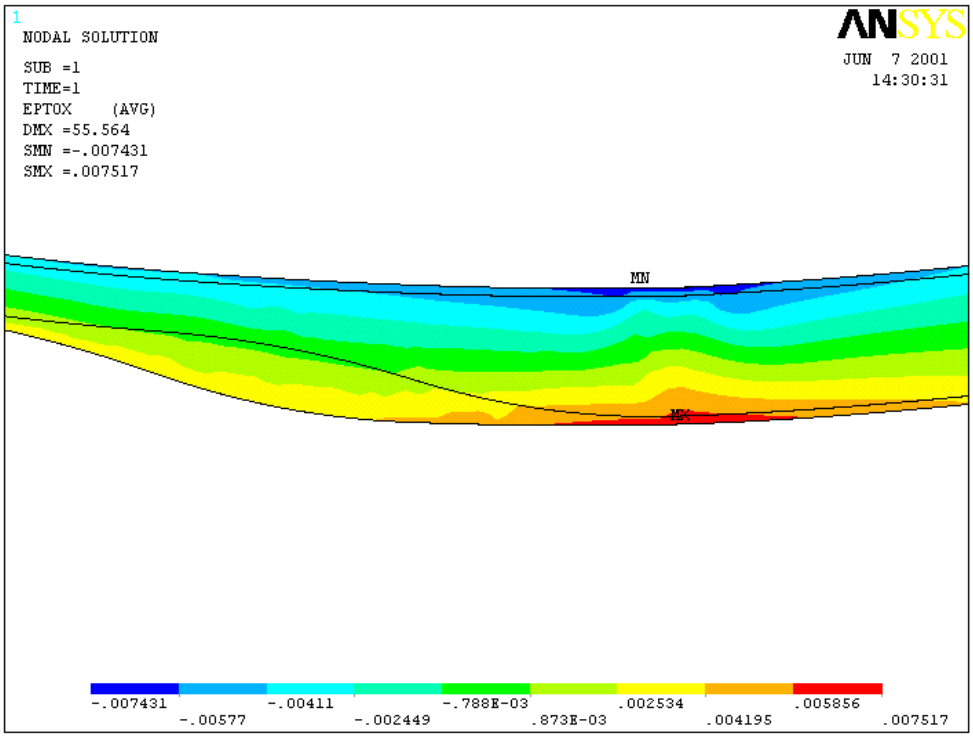

Figure E.4 (b) Laminate Strain in X-direction

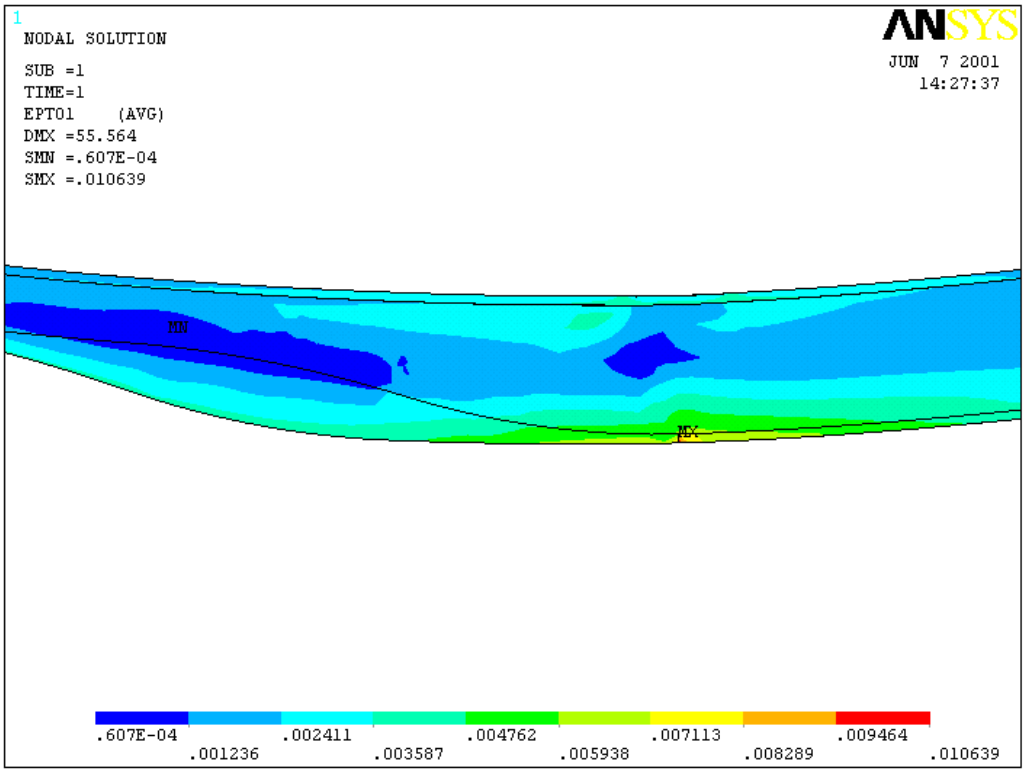

Figure E.4 (c) 1st Principal Strain In Core Materials

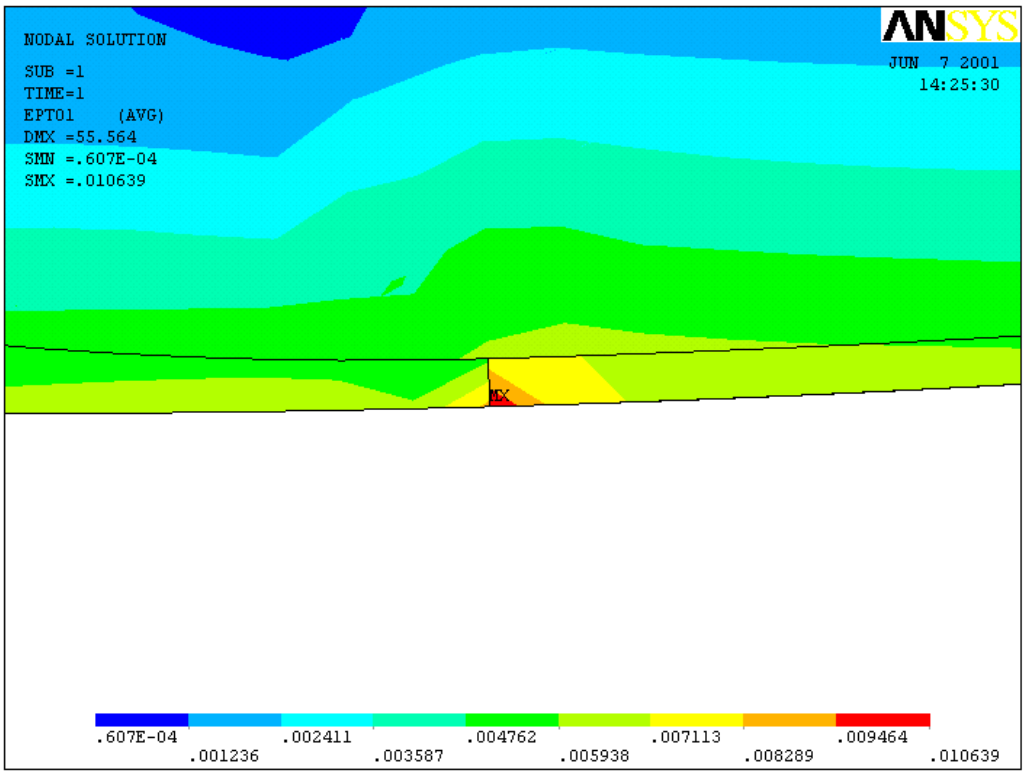

Figure E.4 (d) Magnified View of Stress Concentration at Join of Core Materials

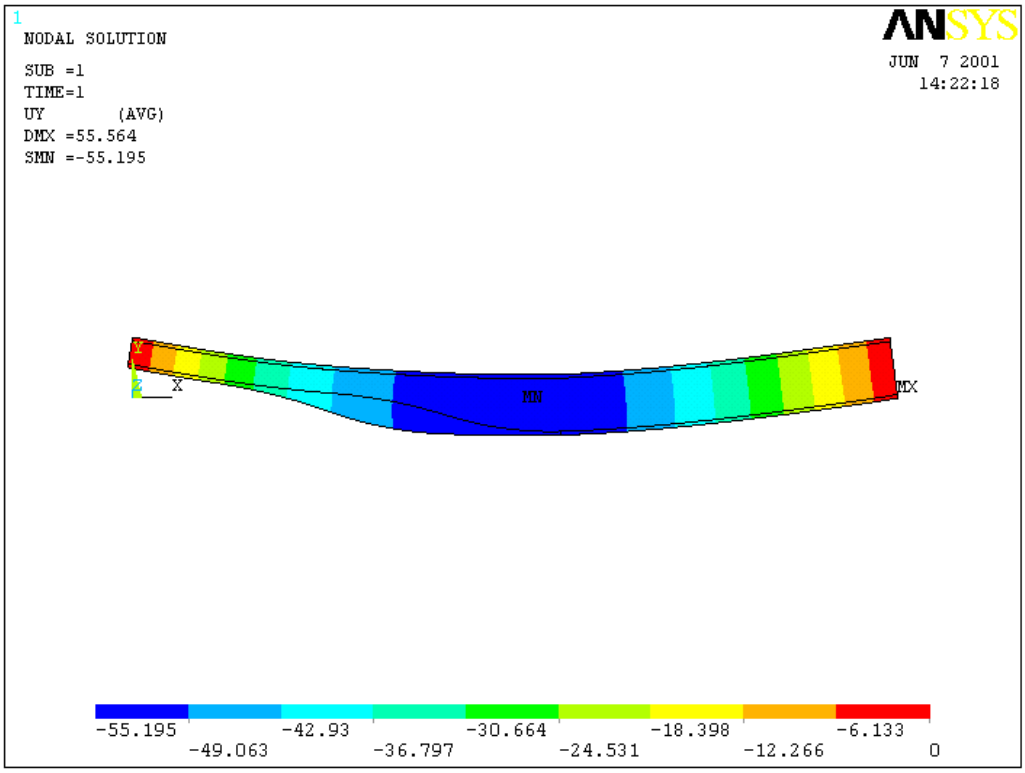

Figure E.4 (e) Neck Beam Deflection

NOTE:

Strain value results from analysis corresponding with the positions of the strain gauges are shown in section E.10

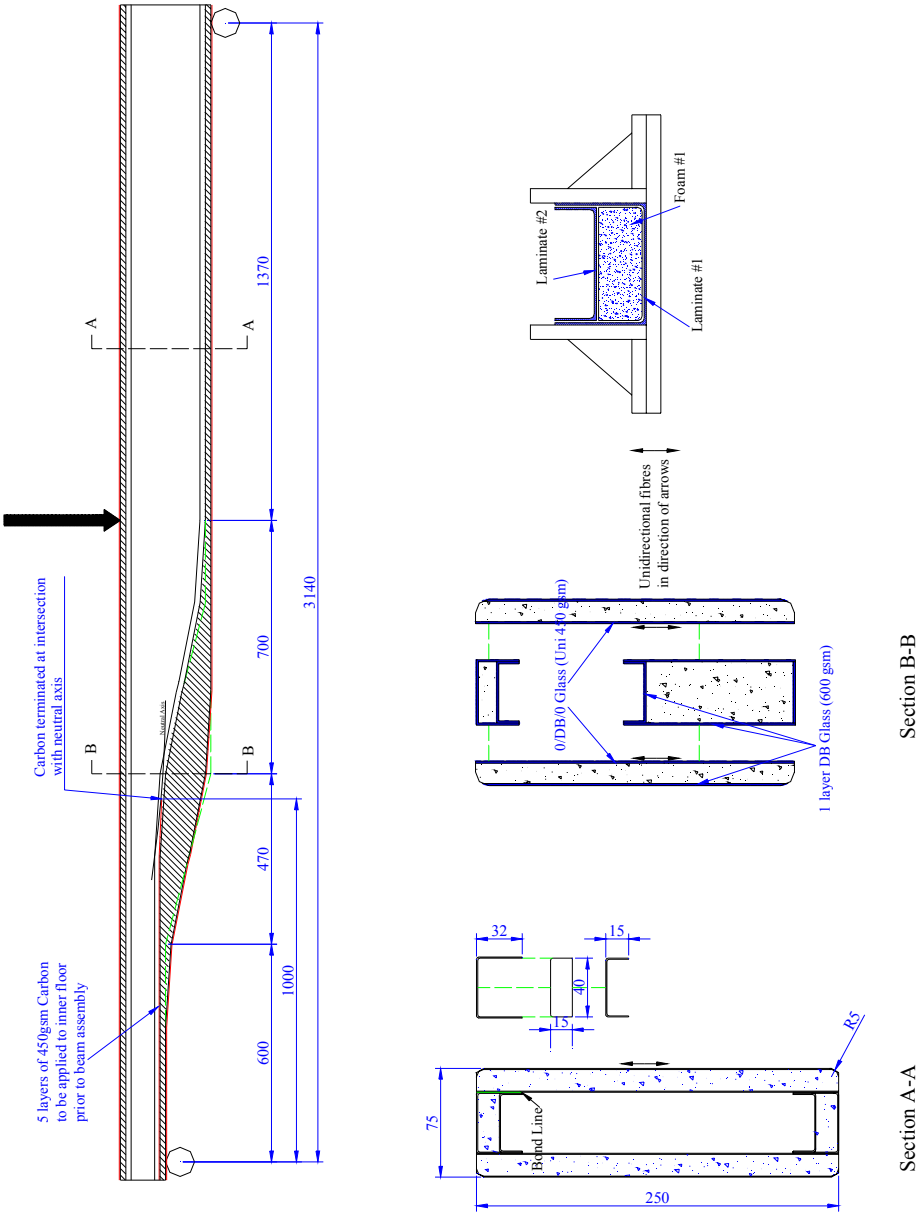

Figure E.5 Detail Drawing of Neck Beam

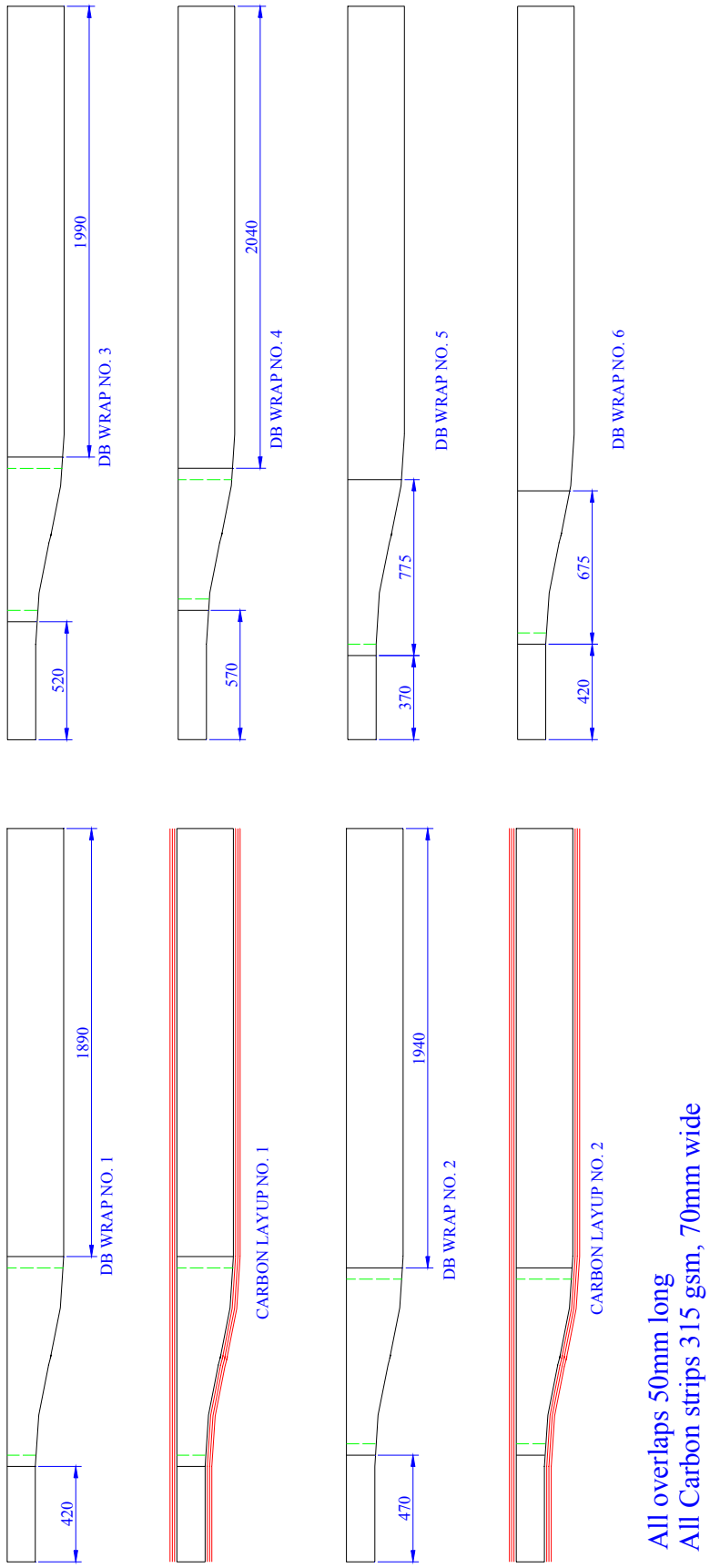

Figure E.6 Sequence for Wrapping Reinforcement

E.9 Fabrication of Neck Section

The dimensions of the beam section are shown in Figure E.5, including detail regarding the basic laminate configurations that were initially applied to the sandwich panels before assembly. The proposed wrapping sequence used to apply the primary carbon fibre and DB shear reinforcement is shown in Figure E.6.

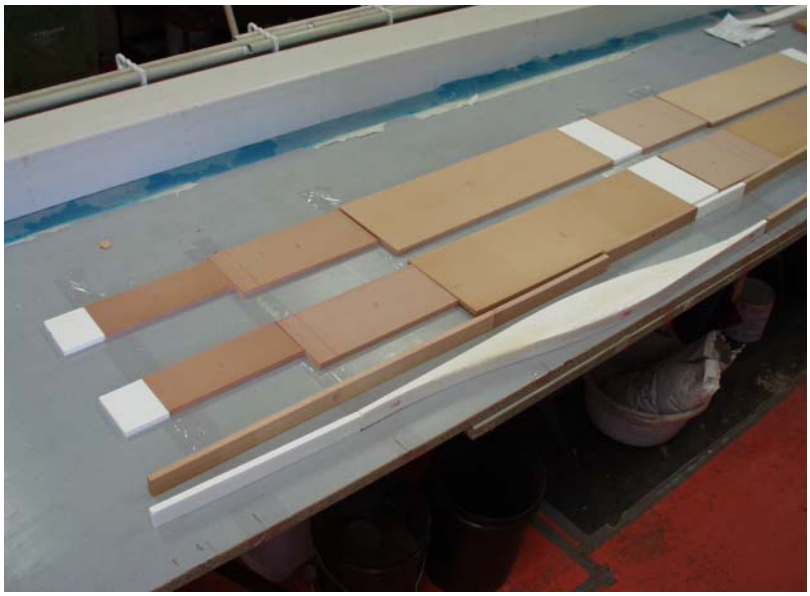

Figure E.7 Core Materials Prior To Joining

Figure E.8 Carbon Reinforcement Laminated to Inner Floor

Figure E.9 Neck Beam Partially Assembled

Figure E.10 Completed Beam Showing Laminate Wrap Sequence

E.10 Experimental Testing and Results

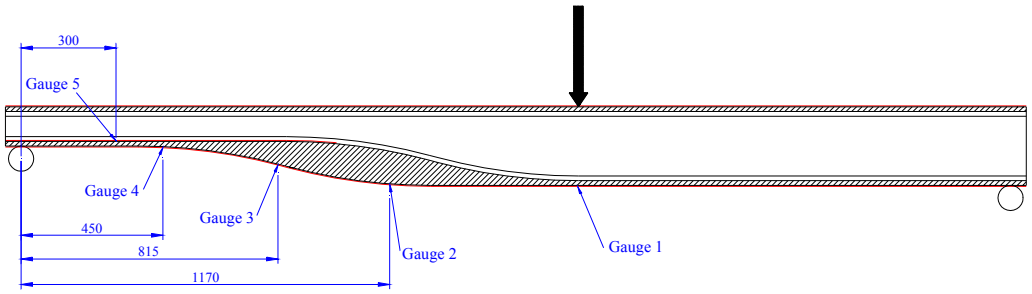

Figure E.11 (a) Placement of Strain Gages

Figure E.11 (b) Neck Beam In Testing Rig

Figure E.11 (c) Initial Failure Point Beneath Load Pad

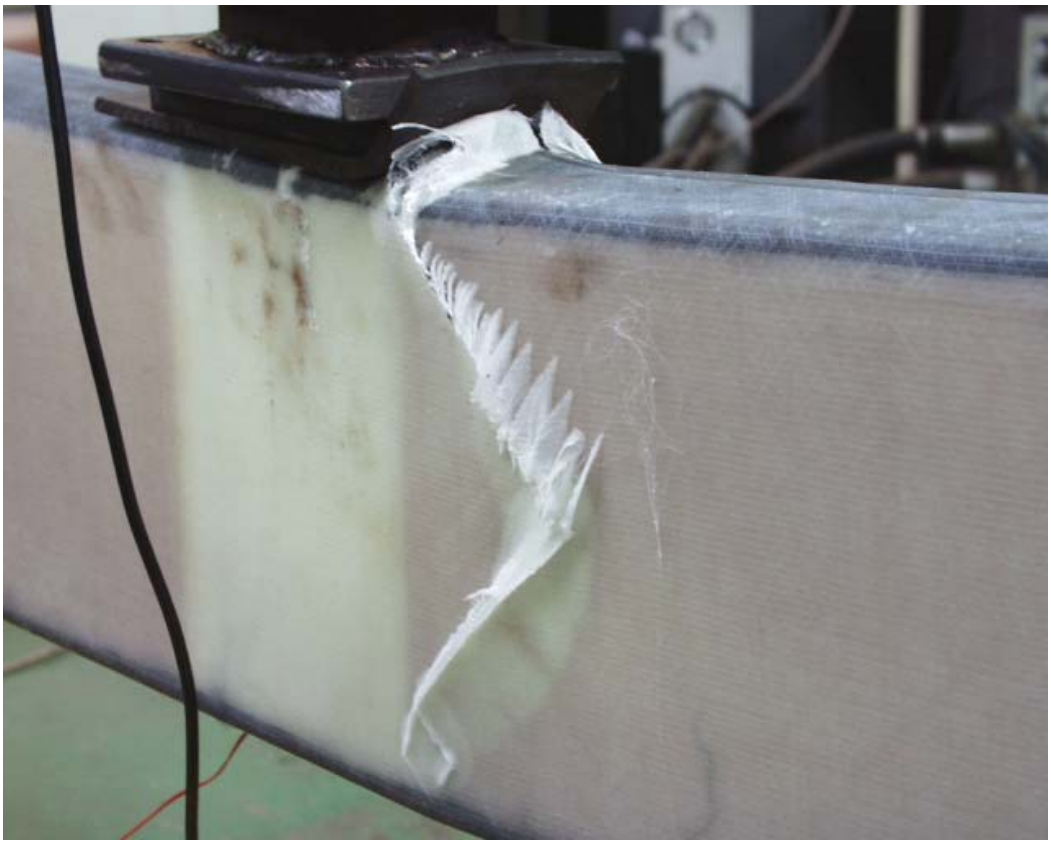

Figure E.11 (d) Final Failure Initiated Beside Load Pad

Figure E.11 (e) Both Failure Points with Load Pad Removed

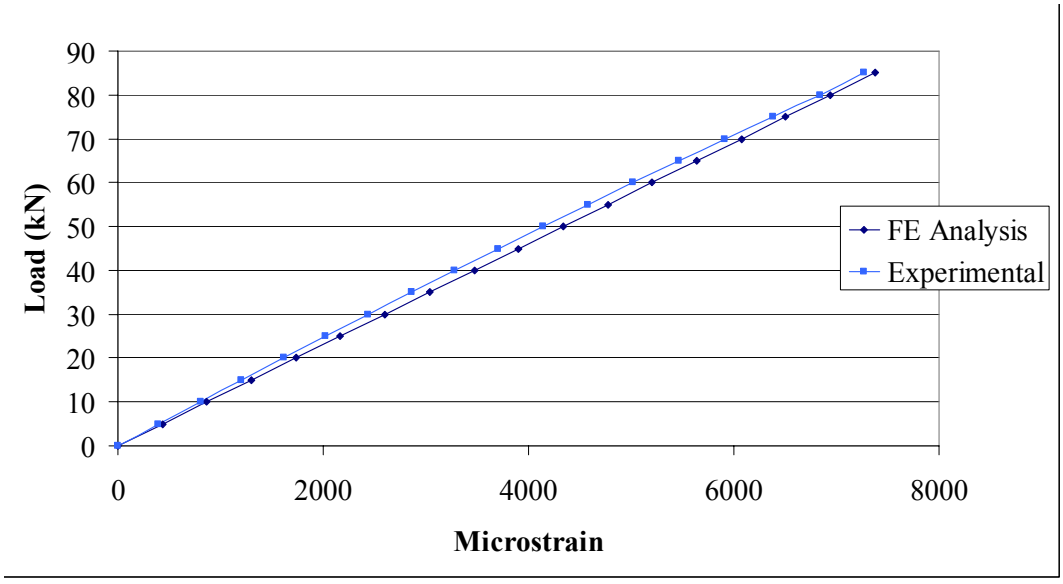

Figure E.12 (a) Plot of Predicted and Actual Strain at Gauge 1

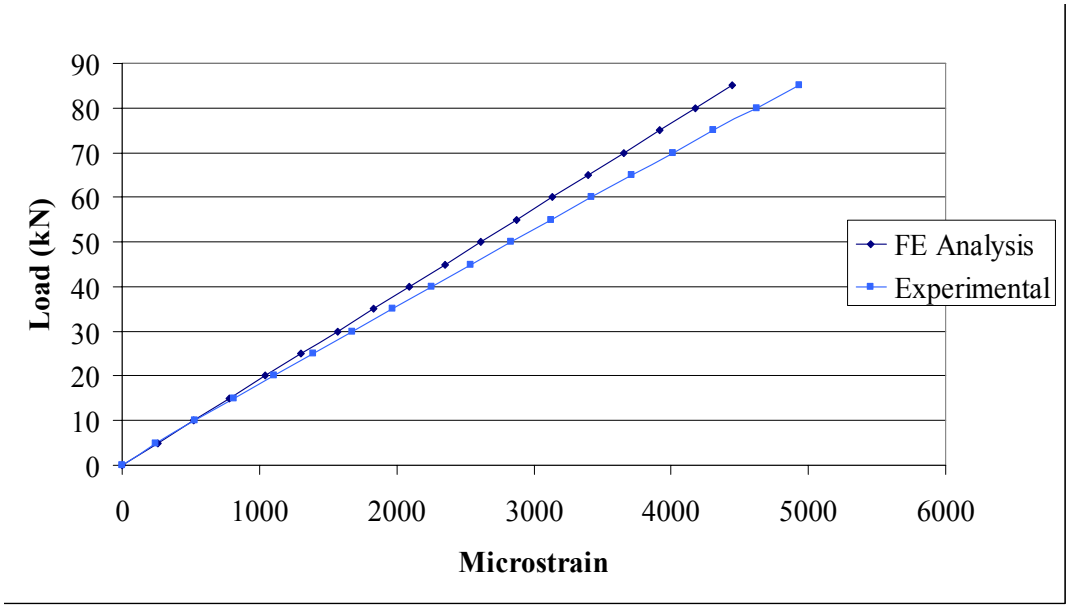

Figure E.12 (b) Plot of Predicted and Actual Strain at Gauge 2

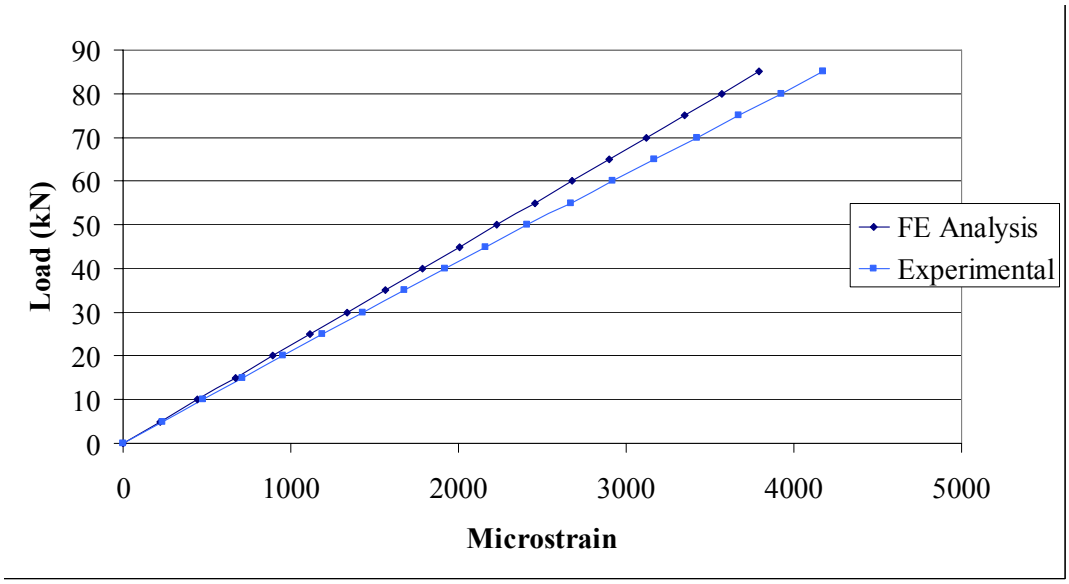

Figure E.12 (c) Plot of Predicted and Actual Strain at Gauge 3

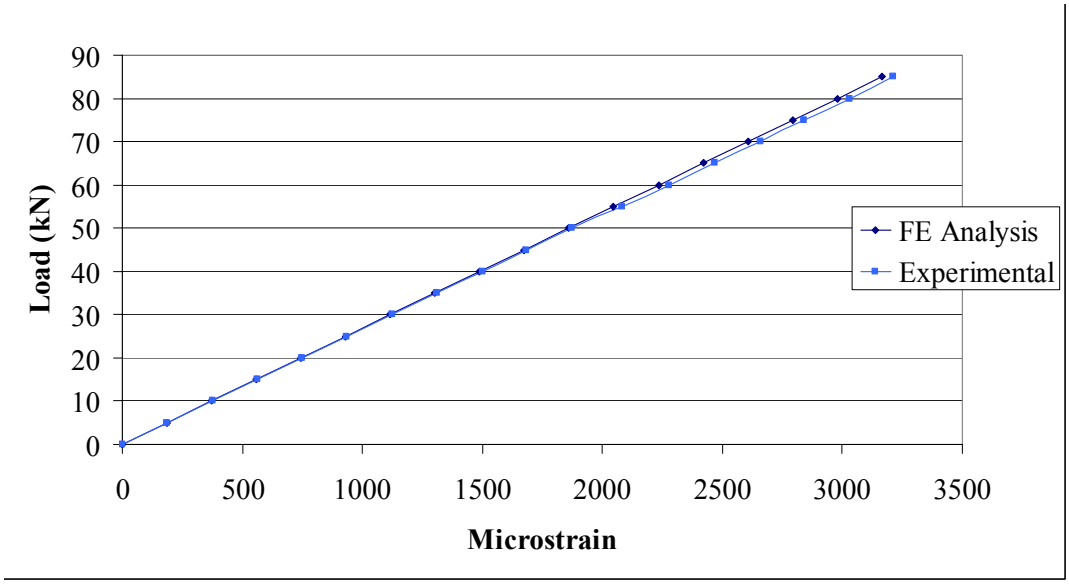

Figure E.12 (d) Plot of Predicted and Actual Strain at Gauge 4

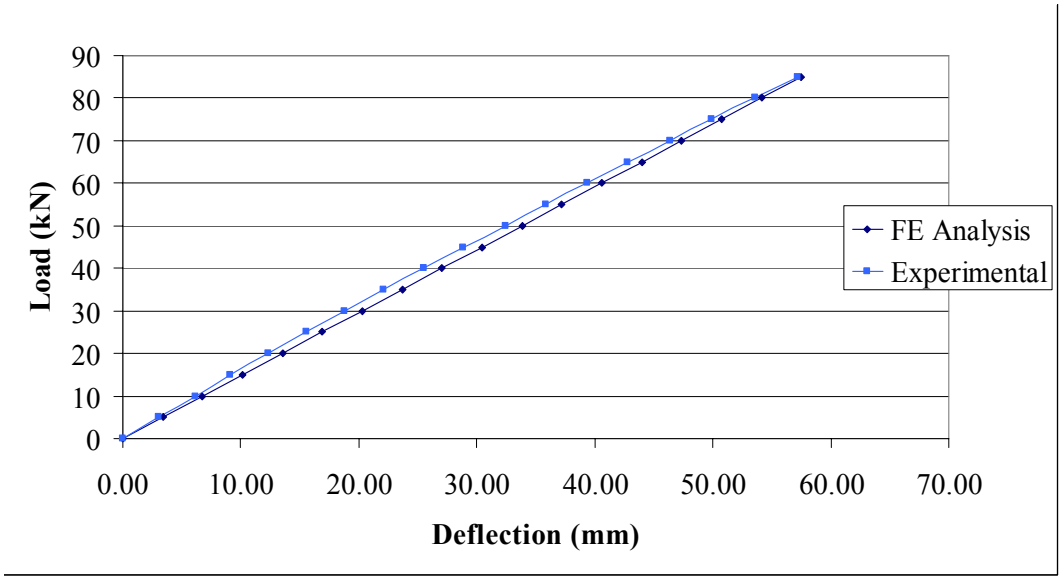

Figure E.12 (e) Plot of Predicted and Actual Deflection At Load Point

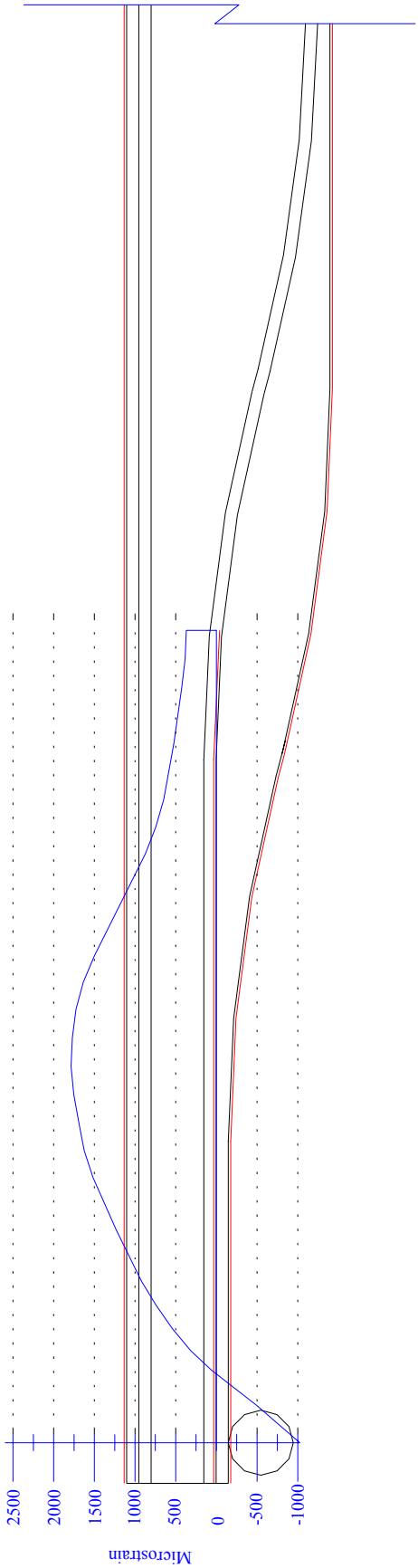

Figure E.13 Predicted Strain In Carbon Laminate on Inner Floor

Appendix F – Cross Member Analysis and Testing Results

F.1 Analysis Identification

Model 1 Xmem25mm.db

F.2 Aim of Analysis

Purpose of analysis was:

To determine the static behaviour of the system

- To investigate the performance of each cross member and joint under load, particularly at ultimate load, and observe the expected failure modes

F.3 Model Form

This 3-dimensional model was intended to replicate the real structure with as much detail as was deemed practical. Figures F.1 (a) and (b) show the basic form of the model, which utilises symmetry in order to reduce solution time and computing resources.

F.4 Material Properties and Laminate Sequence

Both unidirectional and double bias (DB) fabrics were used in this beam. An orthotropic material represented the unidirectional laminates, with the x-direction of each element being oriented according to the global model x-axis. The double bias fabric was represented by two uni-directional laminates, oriented at $\pm 45^0$, as discussed in section 5.6.6. The material properties, taken from section 5.6.6 and other sources where appropriate, were input into the model as follows:

1. Properties of E-glass Uni-directional reinforcement (460 g/m^2):

Young's Modulus,	E_1 :	28624 MPa
	E_2 :	7404 MPa
Poisson's Ratio,	γ_{xy} :	0.322
Shear Modulus,	G_{xy} :	2986 MPa
T'ness per layer of	t_{UD} :	0.46 mm

Unidirectional E-glass (460 g/m^2)

T'ness per layer of Double Bias Fabric (600 g/m²) t_{DB} : 0.6 mm

2. Properties of T300 Carbon Fibre Uni-directional reinforcement (315 g/m²):

Young's Modulus, E_1 : 64973 MPa

E_2 : 7404 MPa

Poisson's Ratio, γ_{xy} : 0.23

Shear Modulus, G_{xy} : 6000 MPa

Thickness per layer. t_{UD} : 0.53 mm

3. Properties of H200 PVC Foam supplied by DIAB Pty Ltd (ρ = 200 kg/m³):

Young's Modulus, E_1 : 250 MPa

Poisson's Ratio, γ_{xy} : 0.32

4. Properties of PU Elastomer, RP6430, supplied by Vantico Pty Ltd:

Young's Modulus, E_1 : 1500 MPa

Poisson's Ratio, γ_{xy} : 0.25

Laminate Sequences:

The laminae contained within the model replicated the layup sequences present in the actual beam. The layup sequences are described in detail in section F.9.

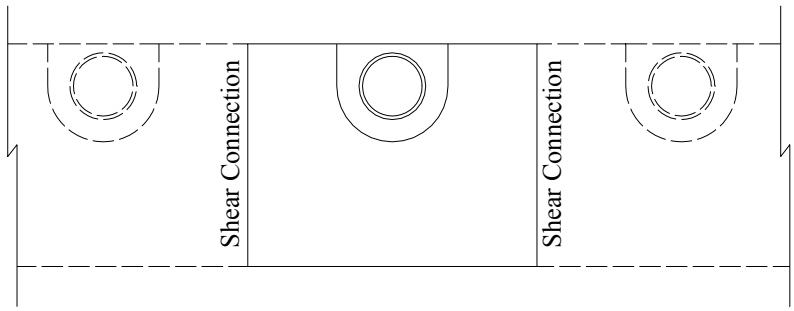

Figure F.1 (a) Basic Model – Section of Chassis Rail With Cross Member

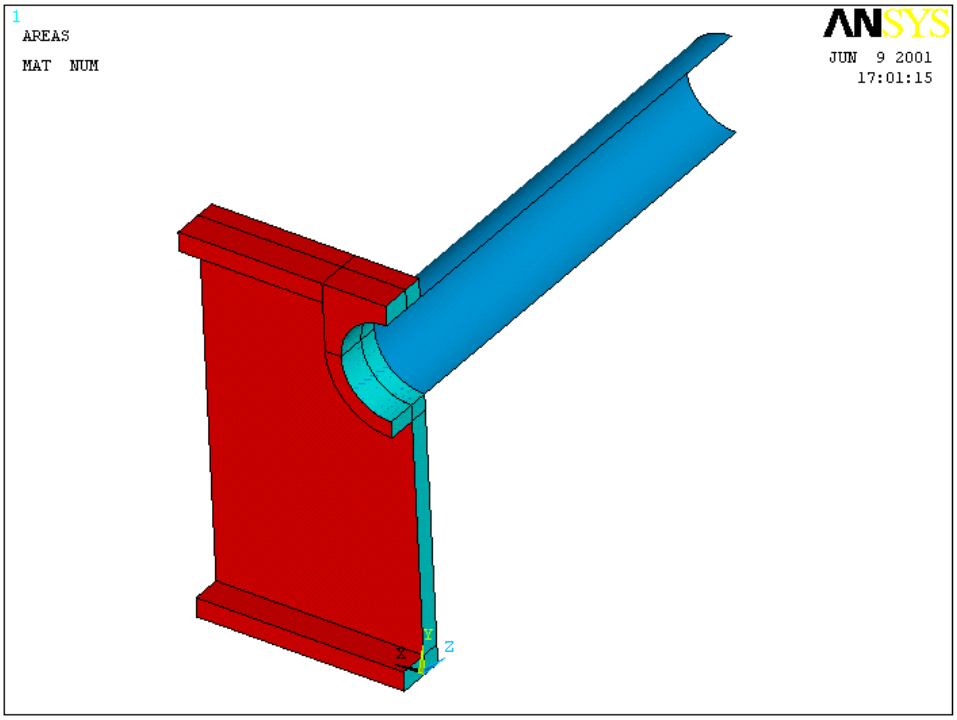

Figure F.1 (b) Basic Quarter Model of Cross Member Connection

F.5 Analysis Program

Analysis program:	ANSYS 5.7
Computer:	Intell 266MMX
	128MB Ram
	Win98
Analysis type:	Linear static (Assumed Small Displacement)

F.6 Mesh Details

The mesh used in the analysis is shown in Figures F.2 (a) and (b). This mesh was designed to provide the most accurate analysis detail throughout the cross member and in the region directly surrounding the cross member at the point of connection. This was done as the performance of the cross member and the interaction with the chassis rail in the immediately surrounding region was of primary interest in this analysis.

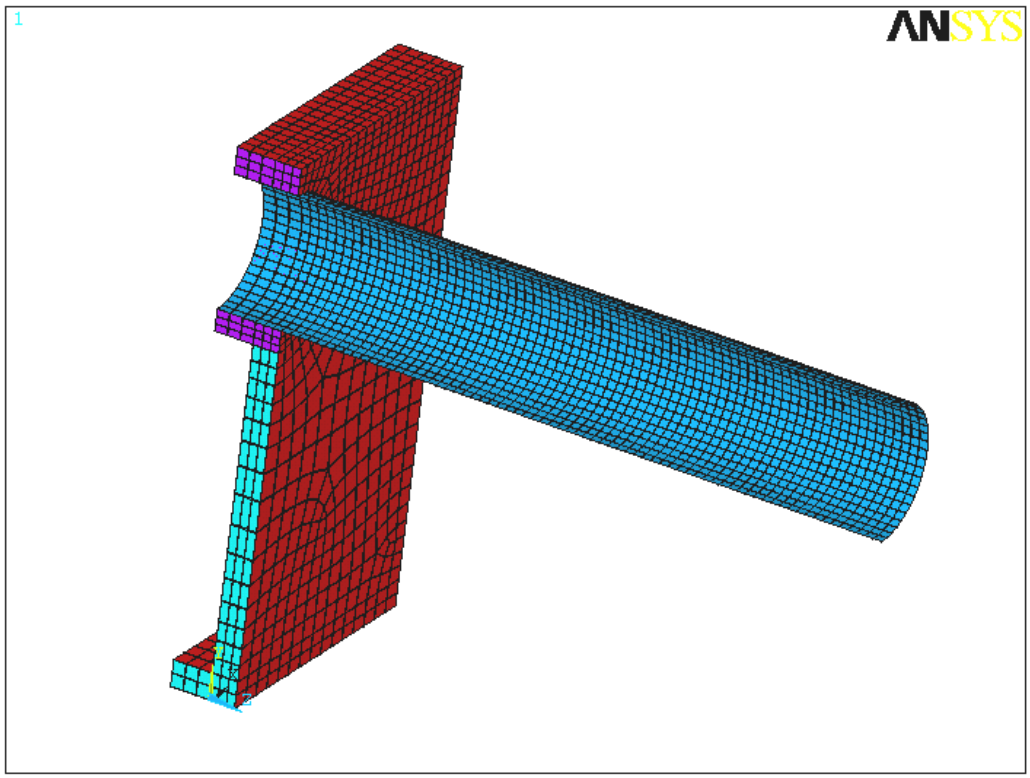

Figure F.2 (a) Element Mesh Used for Analysis

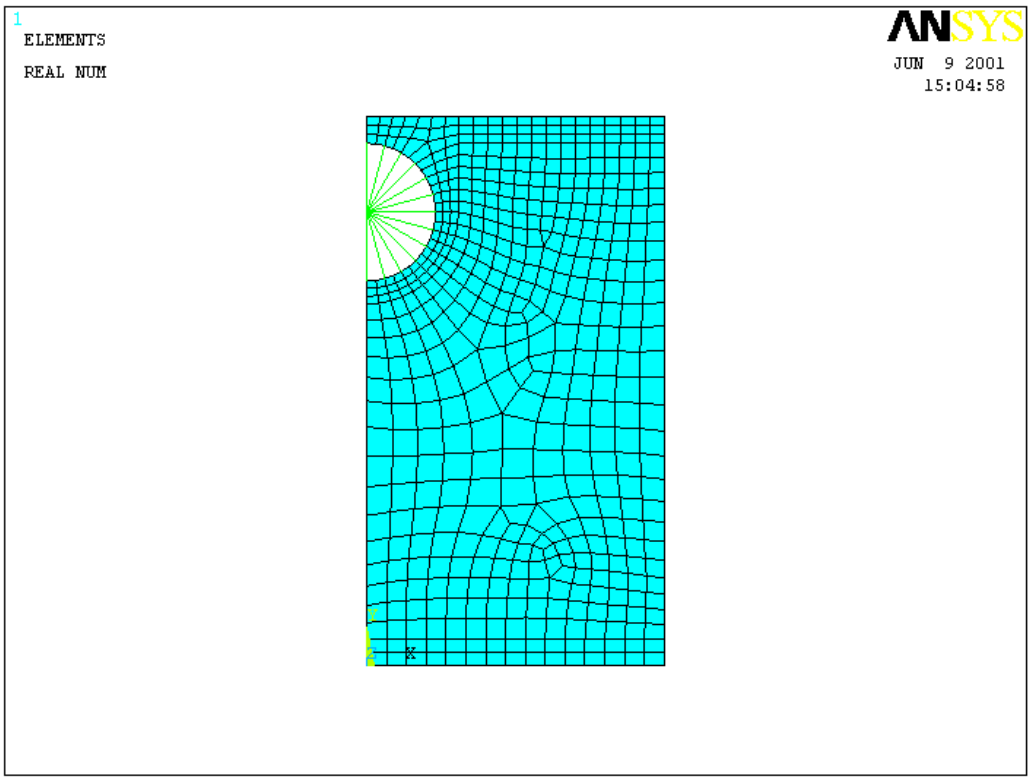

Figure F.2 (b) Element Mesh for Chassis Rail Walls

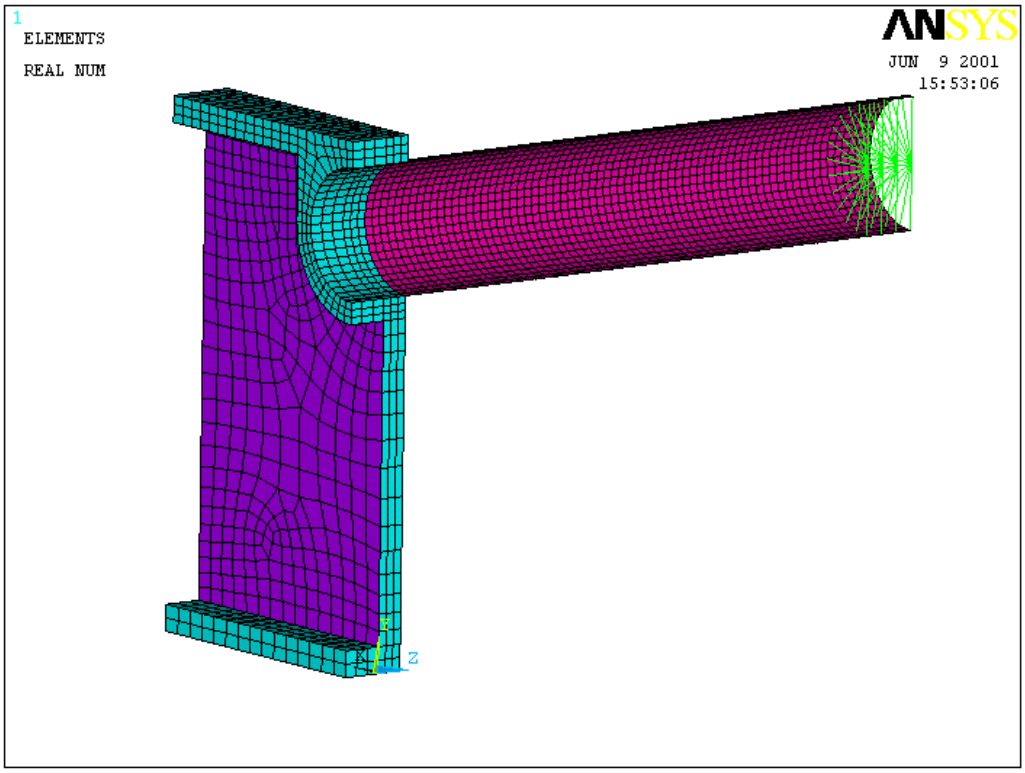

Figure F.2 (c) Alternate View of Mesh Including Load Spreading Elements

Element Type:

1. SHELL 99 May be used for layered applications of a structural shell model. Allows up to 250 layers. If more than 250 layers are required, a user-input constitutive matrix is available. The element has six degrees of freedom at each node: translations in the nodal x, y, and z directions and rotations about the nodal x, y, and z-axes. Refer ANSYS manual for further details.

2. SOLID 95 It can tolerate irregular shapes without as much loss of accuracy. Have compatible displacement shapes and are well suited to model curved boundaries. The element is defined by 20 nodes, having three degrees of freedom per node, and translations in the nodal x, y, and z directions. The element may have any spatial orientation. This element has plasticity, creep, stress stiffening, large deflection, and large strain capabilities. Refer ANSYS manual for further details.

F.7 Application of Boundary Conditions

Relevant restraining conditions were applied to all nodes adjoining the lines of symmetry. The nodes on the end edges of the chassis rail were restrained to simulate the connection of this section to the adjoining chassis rails (refer Figure F.1 (a)), thus ensuring that the load was carried by the shear reinforcement on the sidewalls of the beam, rather than the unidirectional reinforcement on the upper and lower surfaces.

The load was distributed over a number of nodes at the end of the cross member, as illustrated in Figure F.3. The load was applied over a distance of approximately 100 mm from the end of the cross member, as illustrated in Figure F.3. A magnitude of 21.25 kN was applied to the model (equivalent to a total load of 85 kN on the complete structure), and the response of the structure to all other load values was interpolated using the linear relationship inherent in the analysis type.

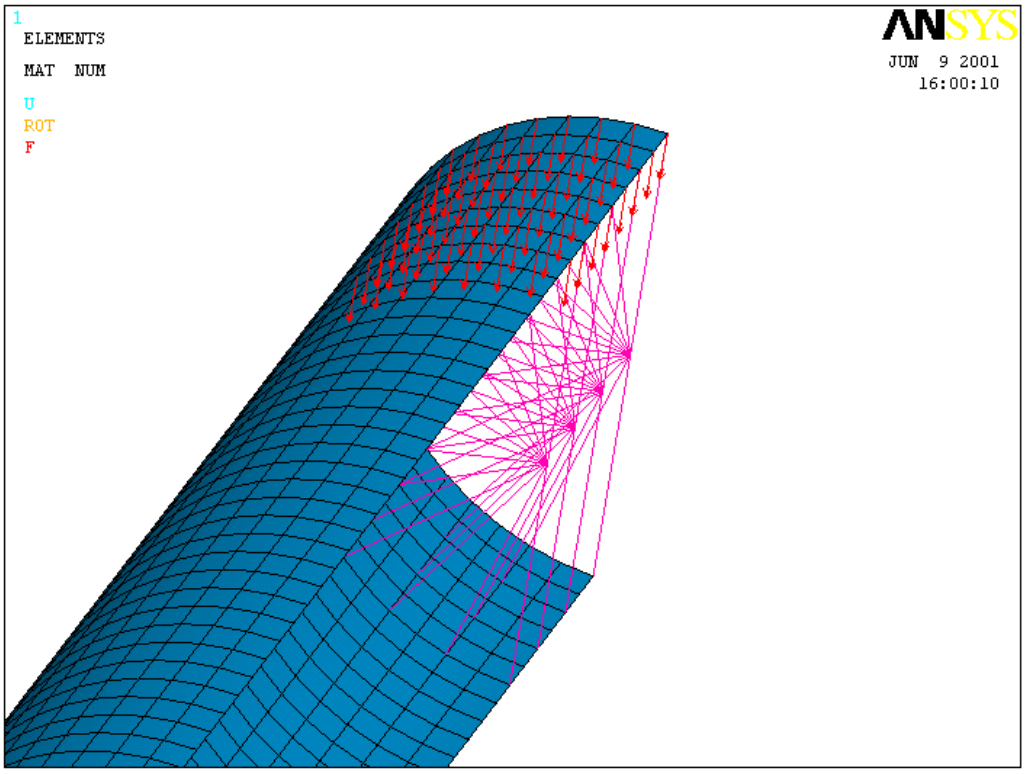

Figure F.3 Nodal Loading Imposed on Model

F.8 Analysis Results

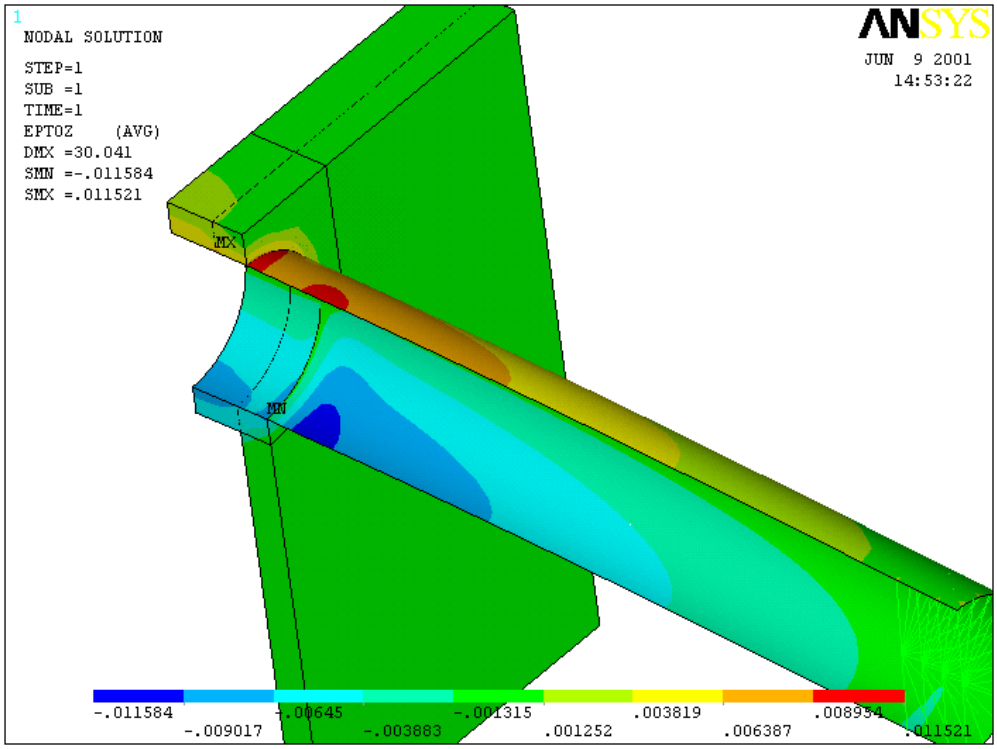

Figure F.4 (a) Laminate Strain In Axial Direction of Cross Member (z-axis)

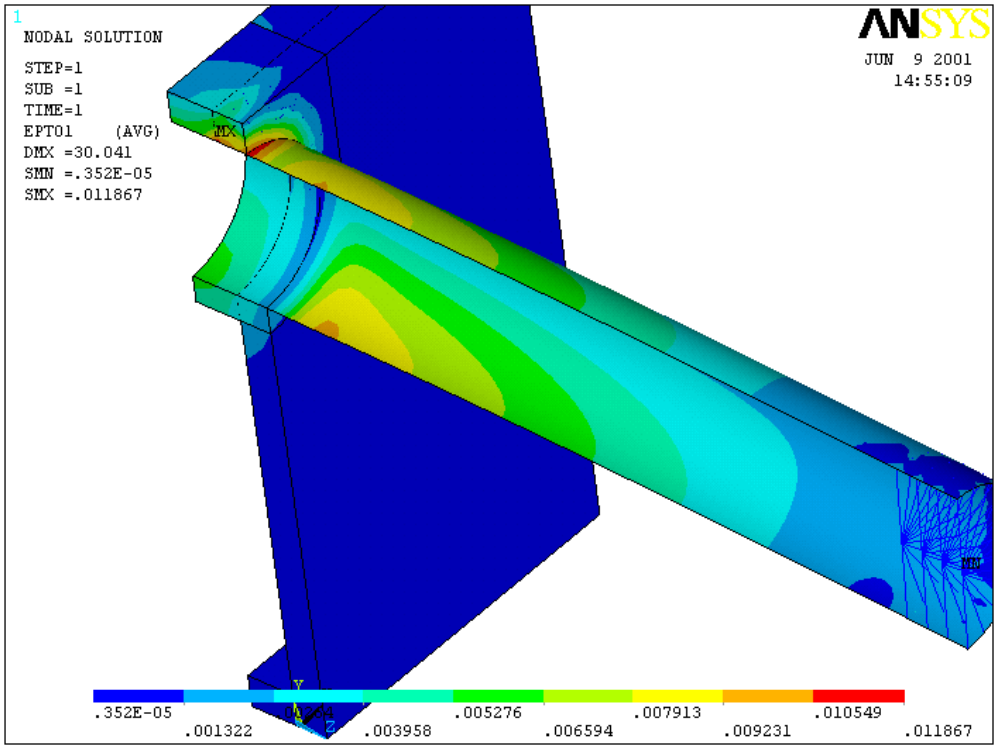

Figure F.4 (b) 1st Principal Strain in Cross Member

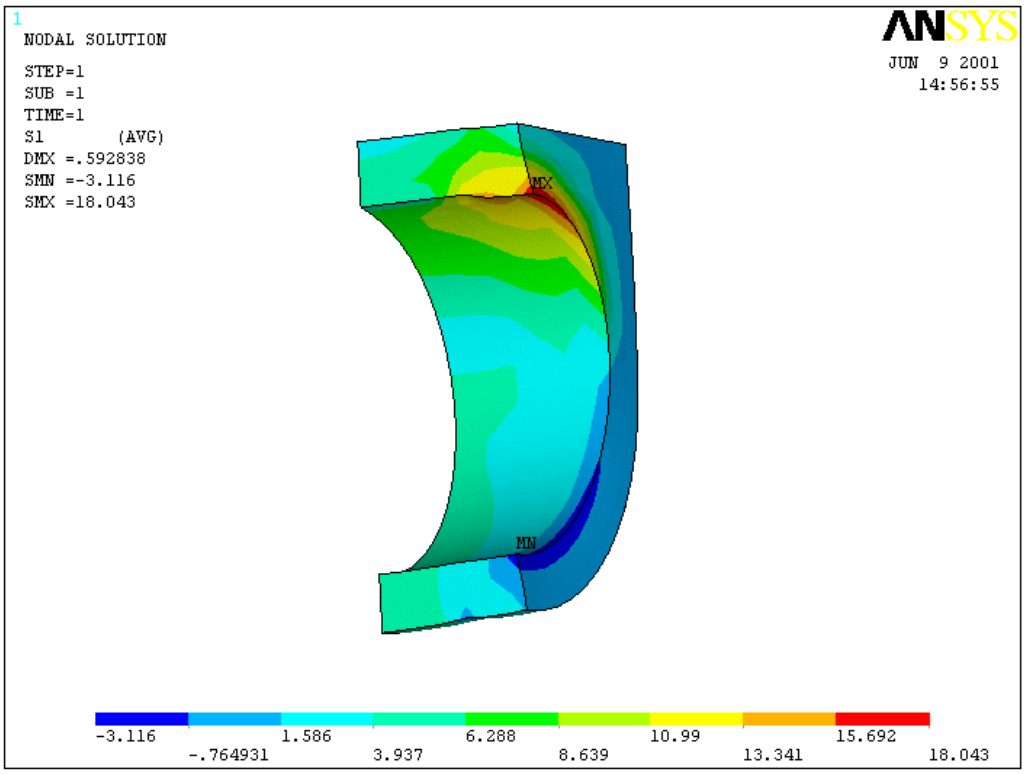

Figure F.4 (c) 1st Principal Stress In PU Elastomer Hardpoint

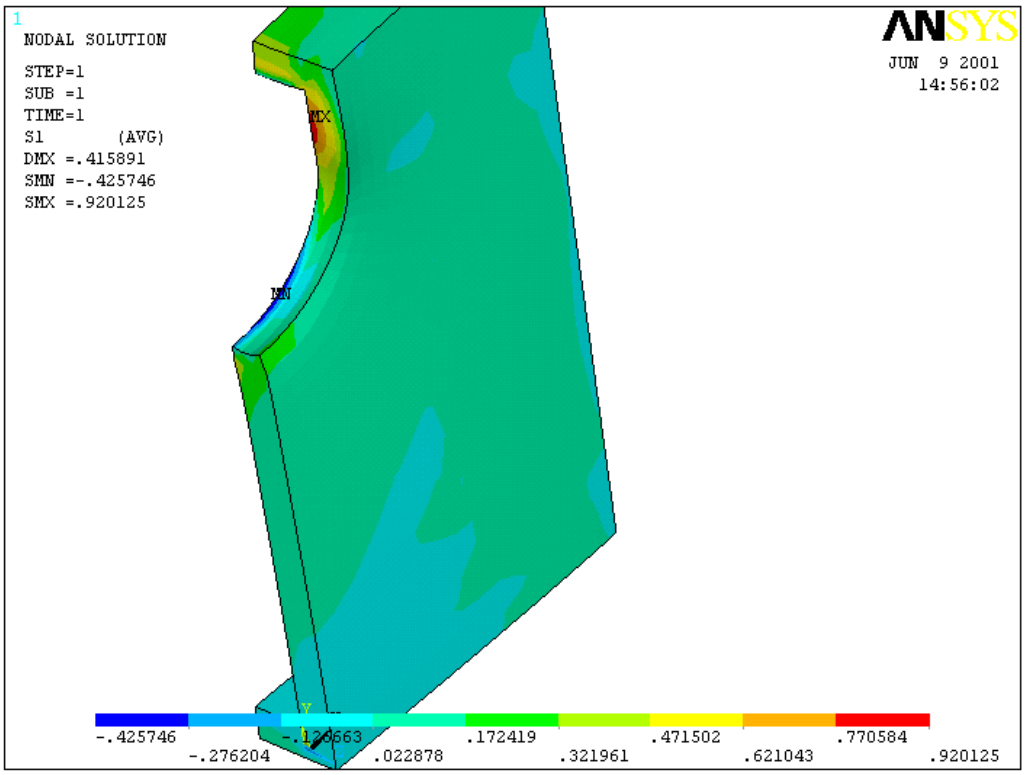

Figure F.4 (d) 1st Principal Stress In PVC Foam Core

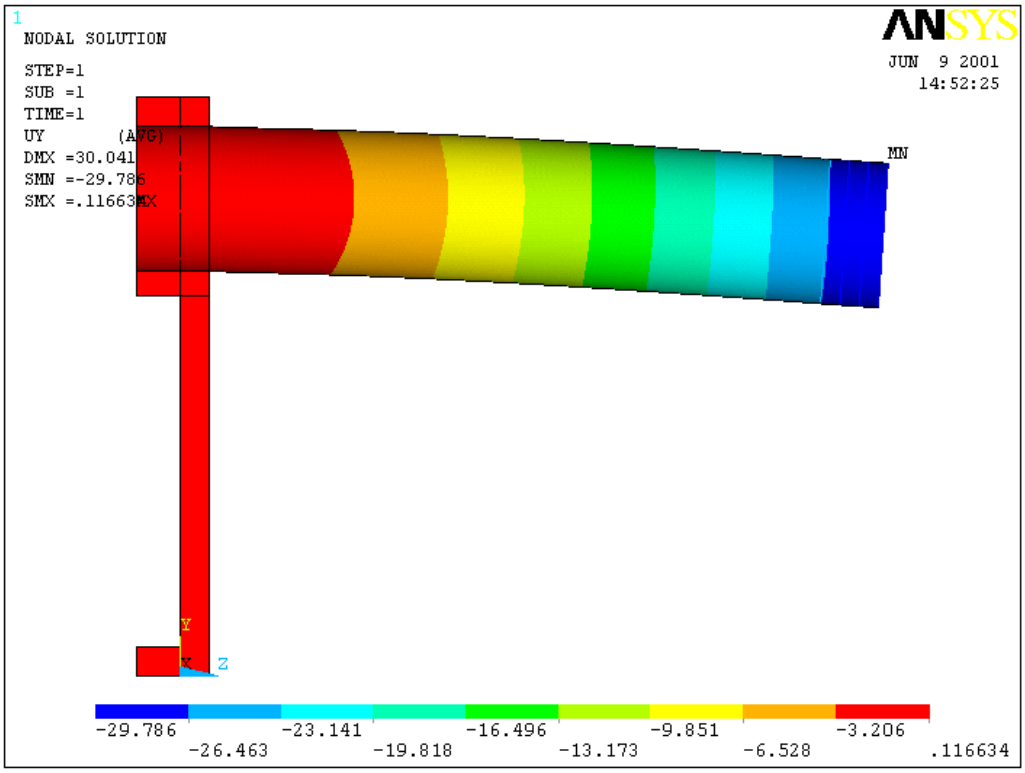

Figure F.4 (e) Cross Member Deflection

NOTE:

Strain value results from analysis corresponding with the positions of the strain gauges are shown in section F.10

F.9 Fabrication of Neck Section

The dimensions of the beam section are shown in Figure F.12, including detail regarding the basic laminate configurations that were initially applied to the sandwich panels before assembly. The proposed wrapping sequence used to apply the primary carbon fibre and DB shear reinforcement is shown in Figure F.13.

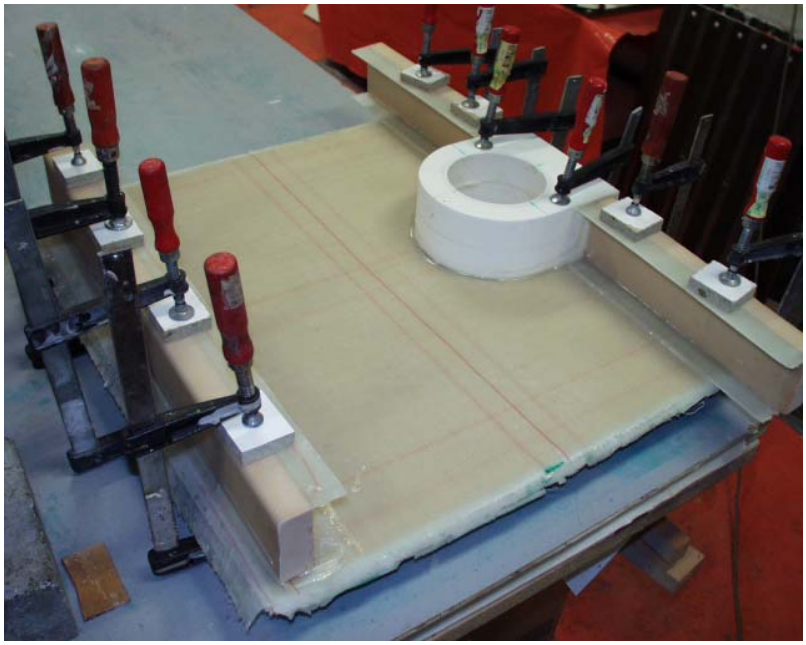

Figure F.5 (a) Bonding of Ceiling, Floor and Hardpoint Insert to Sidewall

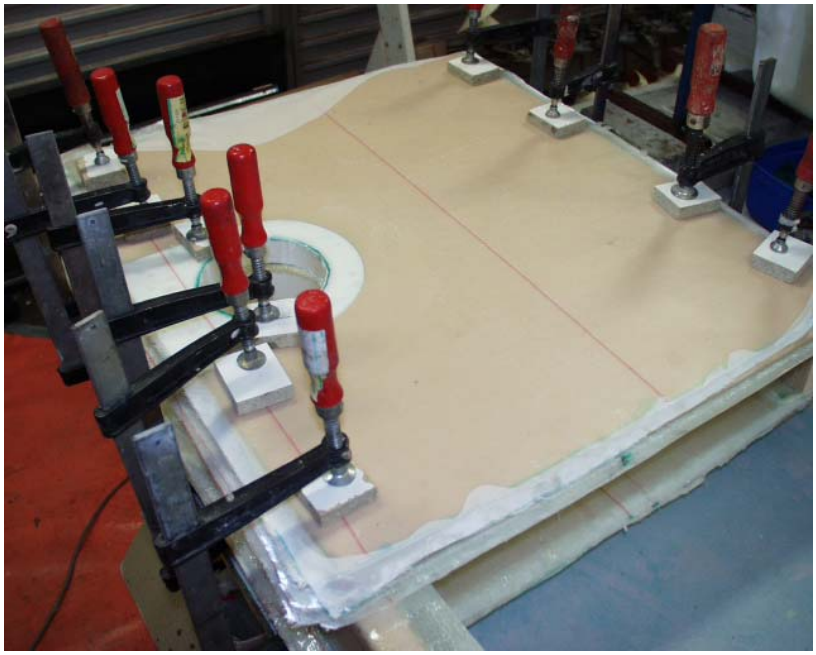

Figure F.5 (b) Bonding of Second Sidewall

Figure F.6 Completed Test Piece Bonded to Steel Frame

F.10 Experimental Results

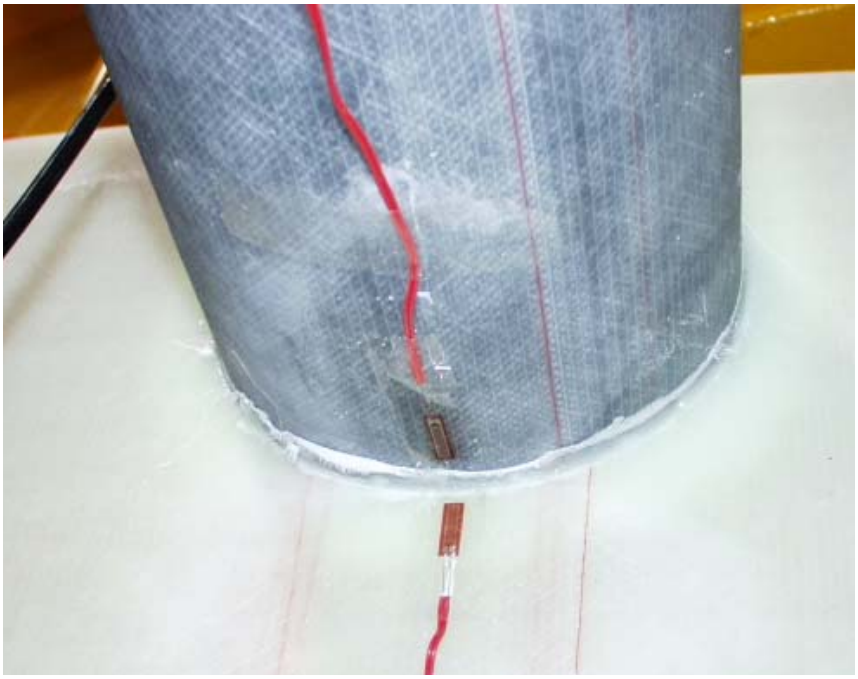

Figure F.7 (a) Strain Gauges Two and Three Placed on Underside of Cross Member

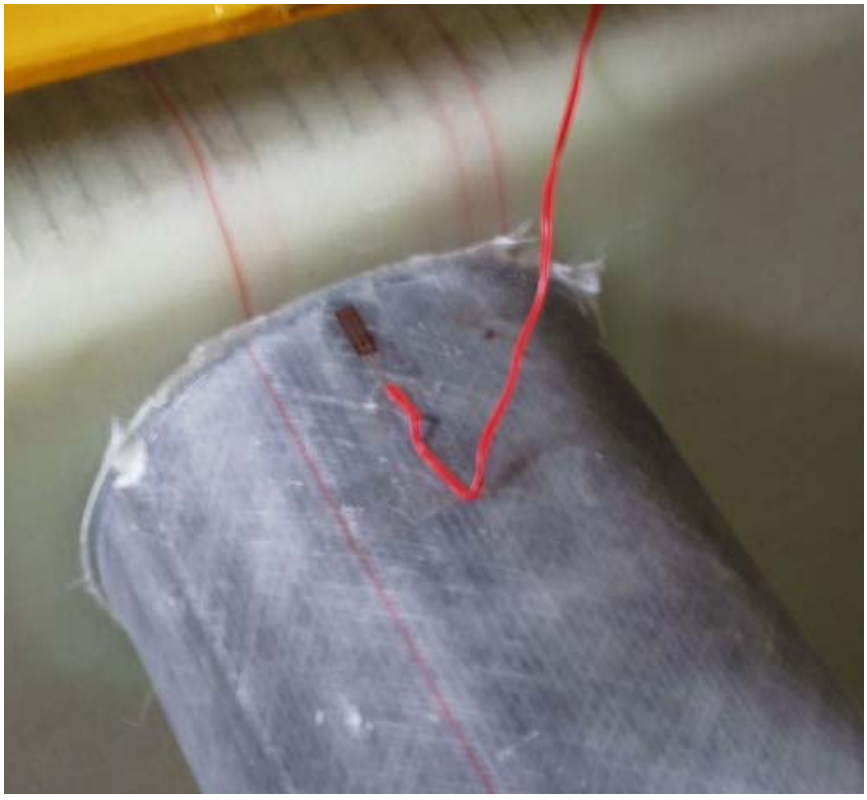

Figure F.7 (b) Strain Gauge One Placement on Upper Side of Cross Member

Figure F.8 Loading Platform and LVDT Placement

Figure F.9 Flexure of Cross Member during Testing

Figure F.10 Failure of Cross Member

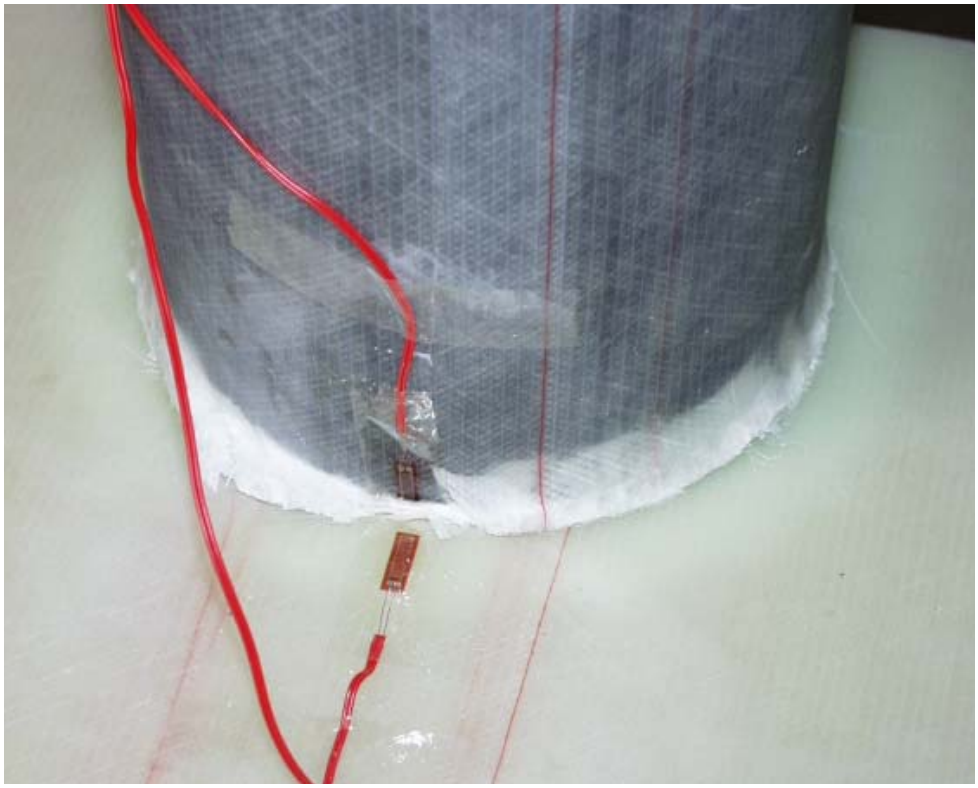

Figure F.11 Compressive Failure of Cross Member Laminate

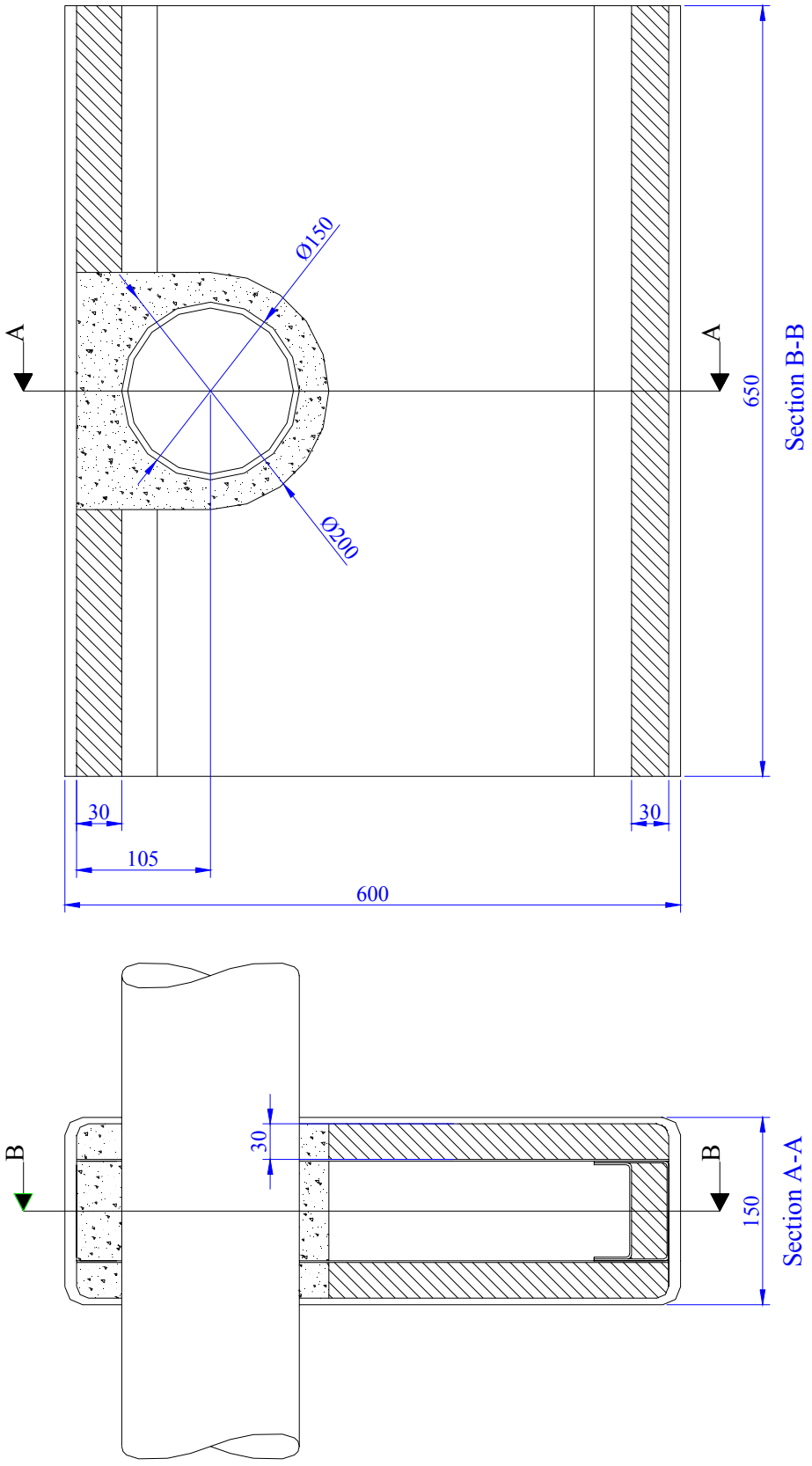

Figure F.12 Cross Member Test Piece Dimensions

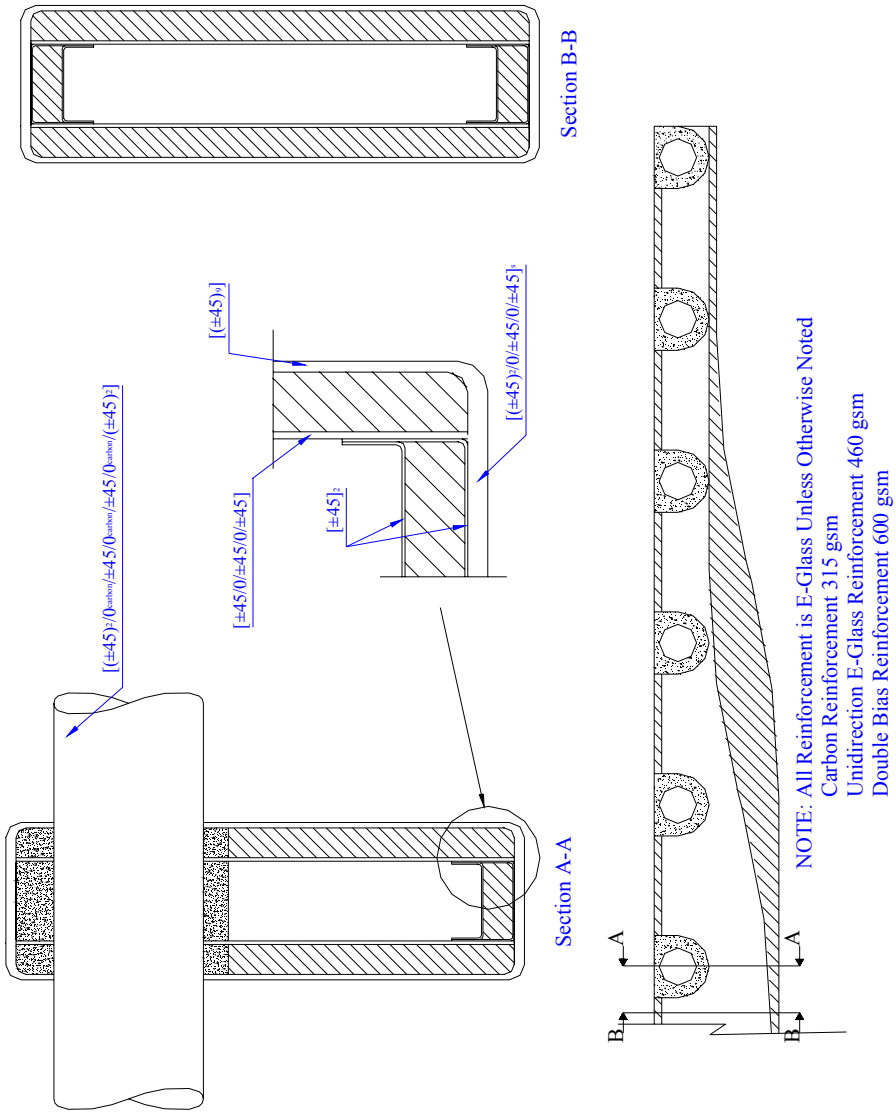

Figure F.13 Layup Sequence Details of Cross Member Test Piece

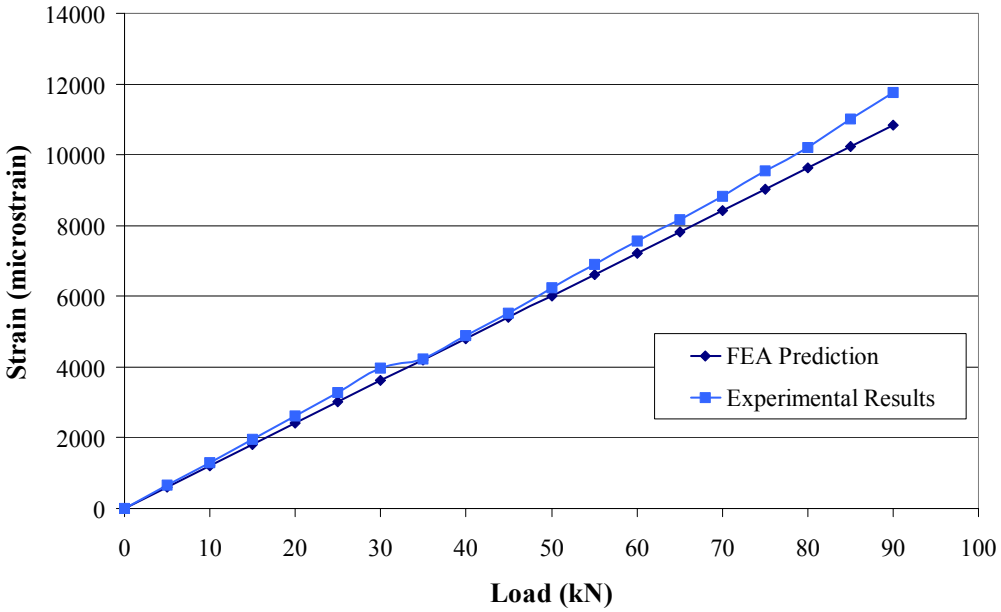

Figure F.14 (a) Plot of Predicted and Actual Strain at Gauge 1

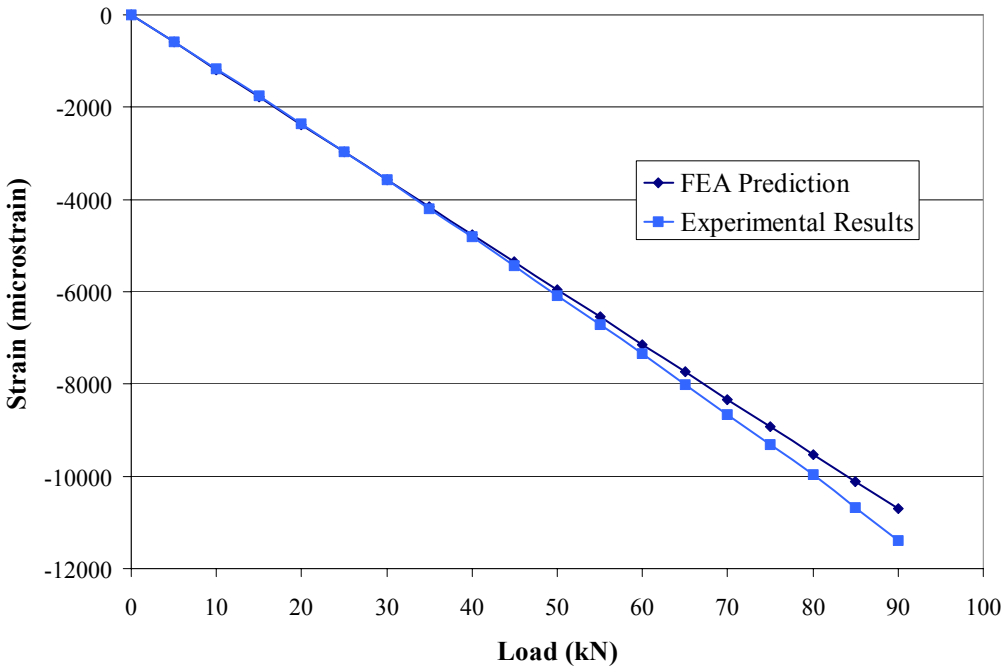

Figure F.14 (b) Plot of Predicted and Actual Strain at Gauge 2

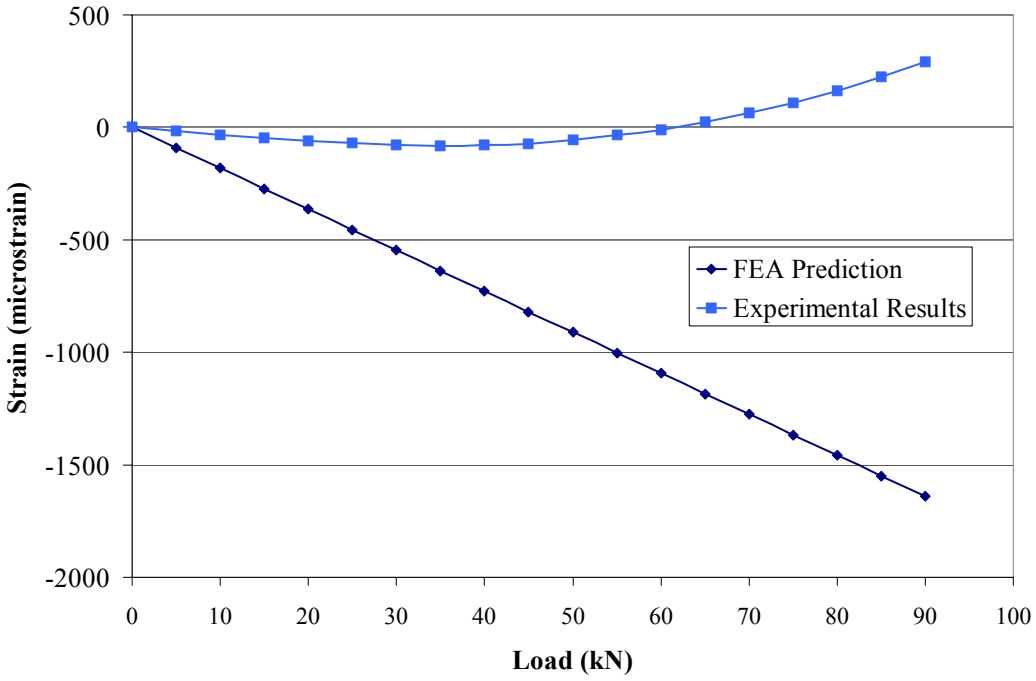

Figure F.14 (c) Plot of Predicted and Actual Strain at Gauge 3

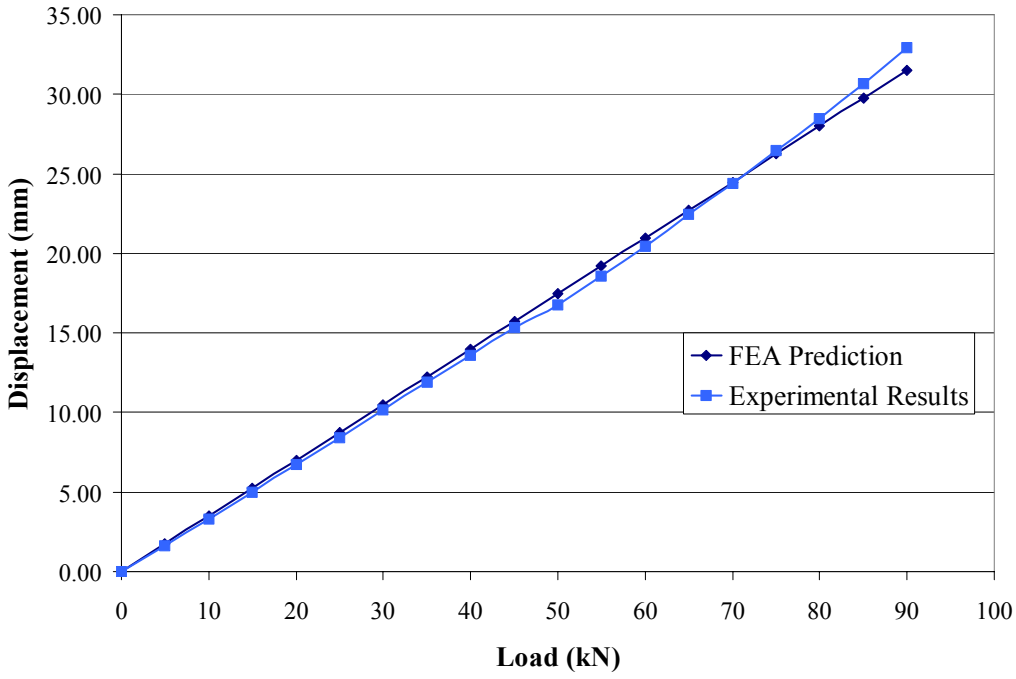

Figure F.14 (d) Plot of Predicted and Actual Deflection At Load Point

Appendix G – Fatigue Testing Data

G.1 Elemental Fatigue Testing

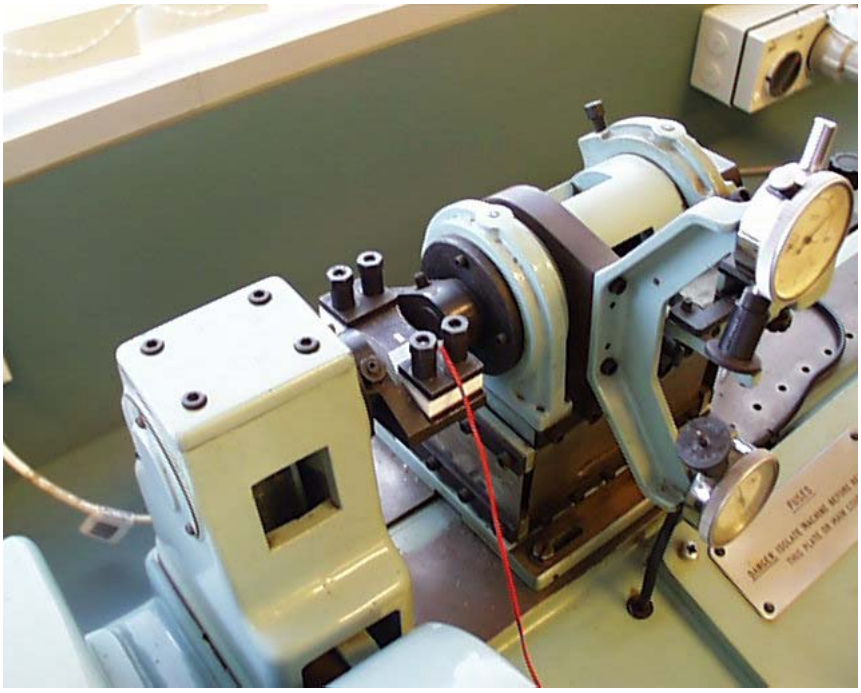

Figure G.1 Specimen In Fatigue Testing Machine

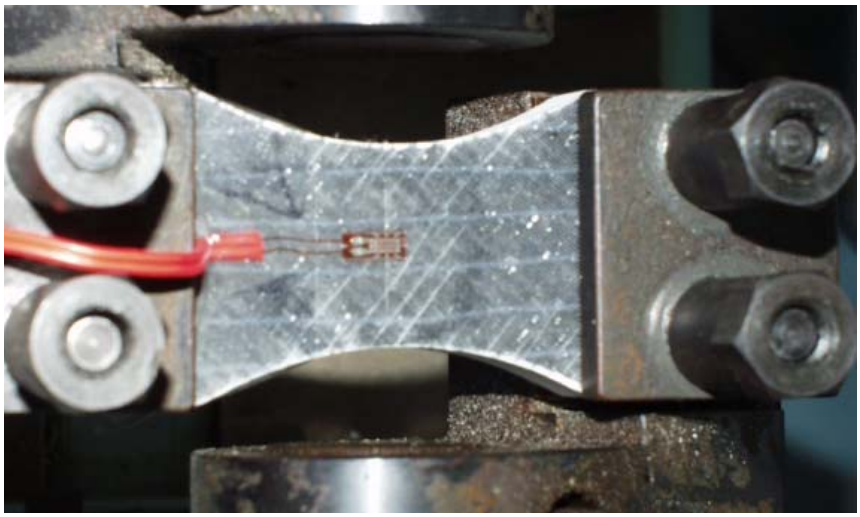

Figure G.2 Strain Gauge Placement and Fatigue Edge Effects

Figure G.3 Failure of Several PFR Fatigue Specimens

Figure G.4 Typical Shear Failure in Specimens with PVC Foam Core

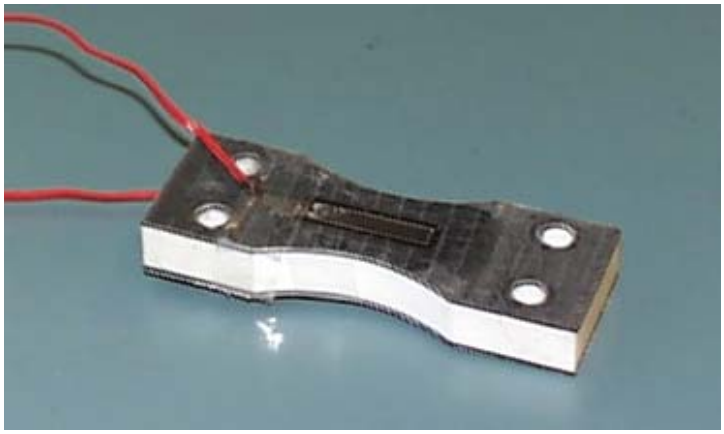

Figure G.5 Fatigue Specimen with PU Elastomer Core

Table G.1 Summary of Elemental Fatigue Testing Results

Specimen Composition	Specimen Number	Counter (1000's) Start No.	Counter (1000's) End No.	Total Cycles	Fail (Y/N)	Strain Min. (%)	Strain Max. (%)	Frequency Hz
PFR (t = 12mm)	PFR 1	9576	9621	4.5E+04	Y#	0.2	0.5	23
40% K15	PFR 2	9621	51	4.3E+05	Y#	0.2	0.5	23
ADR246TX/ADH160 Epoxy	PFR 3	51	207	1.6E+05	Y#	0.2	0.5	23
	PFR 4	207	280	7.3E+04	Y#	0.2	0.5	23
	PFR 5	280	332	5.2E+04	Y#	0.2	0.5	23
Diviny Cell H200 PVC Foam	FH200-01	2452	6773	1.4E+07	Y^	0.2	0.5	23
(t = 8mm)	FH200-02	6773	8970	2.2E+06	Y^	0.2	0.5	23
1 Layer 230gsm Carbon	FH200-03	8970	2472	3.5E+06	Y^	0.2	0.5	23
1 Layer 600gsm DB Glass	FH200-04	2472	8470	6.0E+06	Y^	0.2	0.5	23
	FH200-05	8470	415	2.0E+06	Y^	0.2	0.5	23
PU Elastomer (t = 8mm)	PUSF01	1079	4351	1.3E+07	N	0.2	0.5	23
1 Layer 230gsm Carbon	PUSF02	7361	9215	1.2E+07	N	0.2	0.5	23
1 Layer 600gsm DB Glass	PUSF03	2370	4345	1.2E+07	Y*	0.2	0.5	23
	PUSF04	415	4180	1.4E+07	N	0.2	0.5	23
	PUSF05	4180	8236	1.4E+07	N	0.2	0.5	23

Fatigue Failure Through Crack Propagation
^ Failure of Core Material in Shear at Clamps
* Failed due to defect in specimen.

G.2 Fatigue Testing of Steel Beam

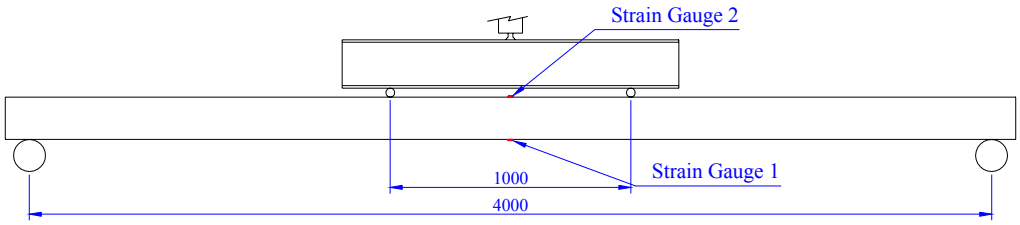

Figure G.6 Basic Layout of Fatigue Test on Steel Beam

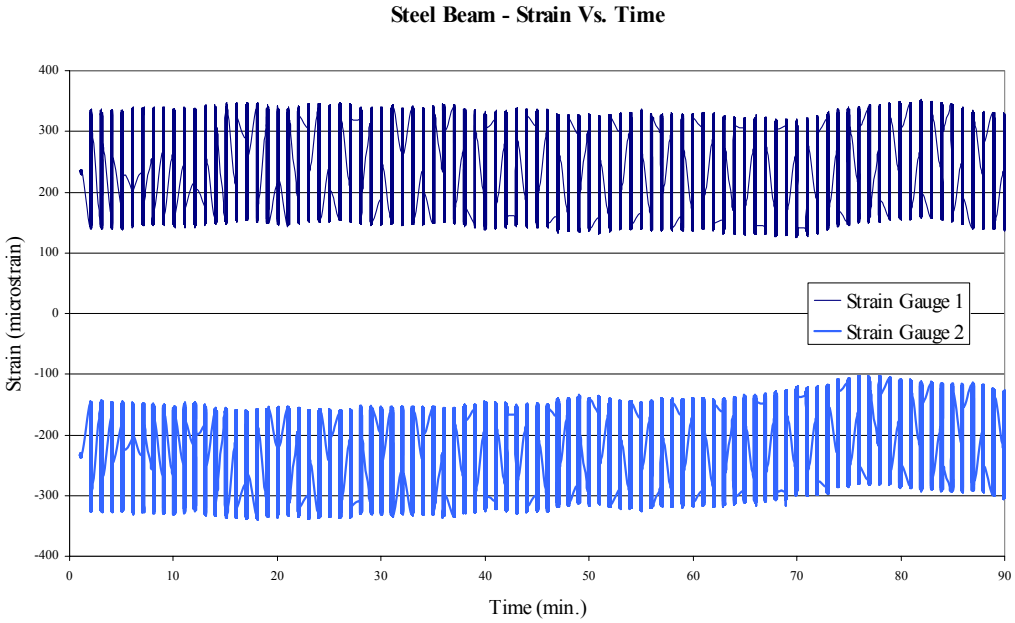

Figure G.7 Sample of Strain Data from Fatigue Test on Steel Beam

G.3 Fatigue Testing of Chassis Rail

G.3.1 Finite Element Analysis

G.3.1.1 Analysis Identification

Model 1 Fatiguebeam.db

G.3.1.2 Aim of Analysis

To produce an accurate 3-dimensional model of the proposed chassis rail section, suitable for detailed finite element analysis.

- To investigate the performance of the chassis rail under static load, particularly with respect to beam stiffness at the proposed level of loading.

G.3.1.3 Model Form

This 3-dimensional model was intended to replicate the real structure with as much detail as was deemed practical. Figures G.8 and G.9 (a) and (b) illustrate the basic form of the model, which utilises symmetry in order to reduce solution time and computing resources.

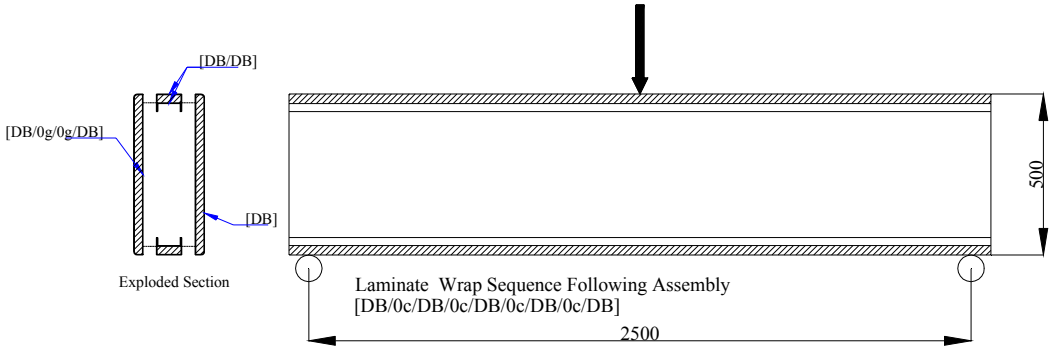

Figure G.8 Fatigue Beam Configuration

G.3.1.4 Material Properties and Laminate Stacking

Both unidirectional and double bias (DB) fabrics were used in this beam. An orthotropic material represented the unidirectional laminates, with the x-direction of each element being oriented according to the global model x-axis. The double bias fabric was represented by two uni-directional laminates, oriented at 645^0, as discussed in section

5.6.6. The material properties, taken from section 5.6.6 and other sources where appropriate, were input into the model as follows:

1. Properties of E-glass Uni-directional reinforcement (300 g/m^2):

Young's Modulus, E_1 : 28624 MPa
E_2 : 7404 MPa
Poisson's Ratio, γ_{xy} : 0.322
Shear Modulus, G_{xy} : 2986 MPa
T'ness per layer of t_{UD} : 0.3 mm
Unidirectional E-glass (300 g/m^2)
T'ness per layer of t_{DB} : 0.6 mm
Double Bias Fabric (600 g/m^2)

2. Properties of T300 Carbon Fibre Uni-directional reinforcement (315 g/m^2):

Young's Modulus, E_1 : 64973 MPa
E_2 : 7404 MPa
Poisson's Ratio, γ_{xy} : 0.23
Shear Modulus, G_{xy} : 6000 MPa
Thickness per layer. t_{UD} : 0.53 mm

3. Properties of H200 PVC Foam supplied by DIAB Pty Ltd (ρ = 200 kg/m^3):

Young's Modulus, E_1 : 250 MPa
Poisson's Ratio, γ_{xy} : 0.32

4. Properties of PU Elastomer, RP6430, supplied by Vantico Pty Ltd:

Young's Modulus, E_1 : 1500 MPa
Poisson's Ratio, γ_{xy} : 0.25

Laminate Stacking Sequences:
The laminae contained within the model replicated the layup sequences present in the actual beam. The layup sequences are described in Figure G.8.

G.3.1.5 Analysis Program

Analysis program: ANSYS 5.7
Computer: Intell 266MMX
128MB Ram

Win98

Analysis type: Linear static (Assumed Small Displacement)

G.3.1.6 Mesh Details

The mesh used in the analysis is shown in Figures G.9 (a) and (b). This mesh was designed to provide a relatively high level of accuracy throughout the entire beam section, although no particular region warranted further element refinement due to the absence of significant stress concentrations.

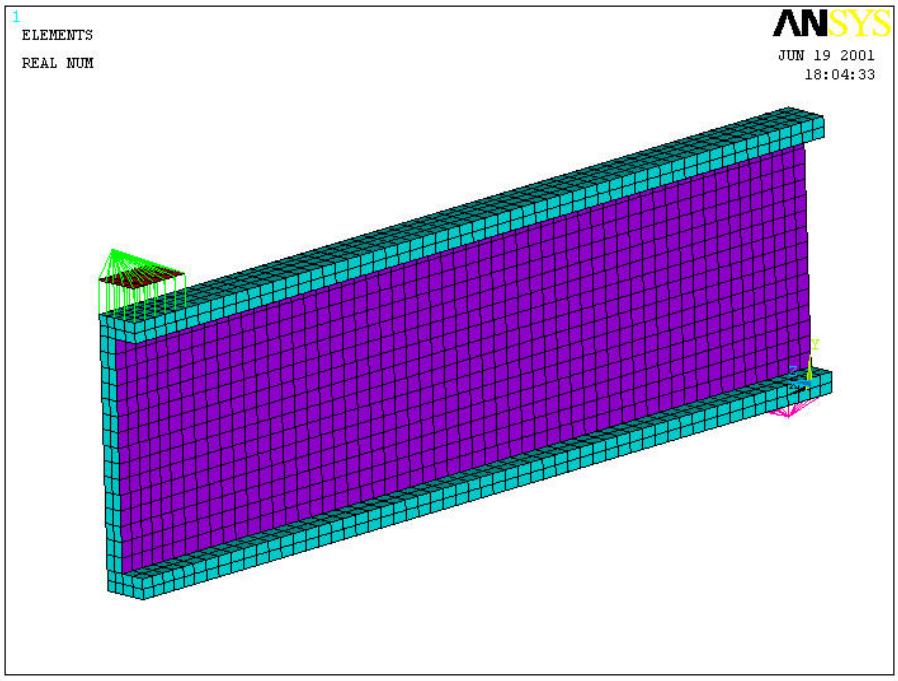

Figure G.9 (a) Element Mesh for Fatigue Beam Model

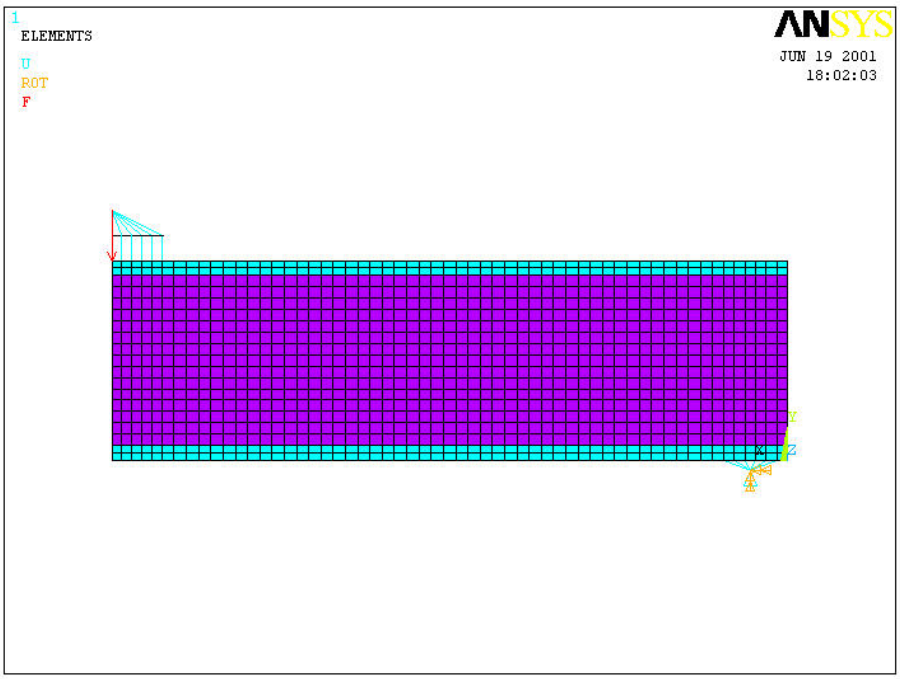

Figure G.9 (b) Mesh and Boundary Conditions Imposed on Fatigue Beam

G.3.1.7 Application of Boundary Conditions

The model was loaded in three-point bending, being simply supported. Consequently, one end was restrained in the global y-direction, while the other was restrained in both the x- and y-directions. Appropriate symmetry conditions were applied along the line of symmetry.

The load was applied at the beam midspan, as illustrated in Figure G.9 (b). A load magnitude of 21.5 kN was applied to the model (equivalent to 85 kN on full beam), and the response of the beam to all other load values was interpolated using the linear relationship inherent in the analysis type.

G.3.1.8 Analysis Results

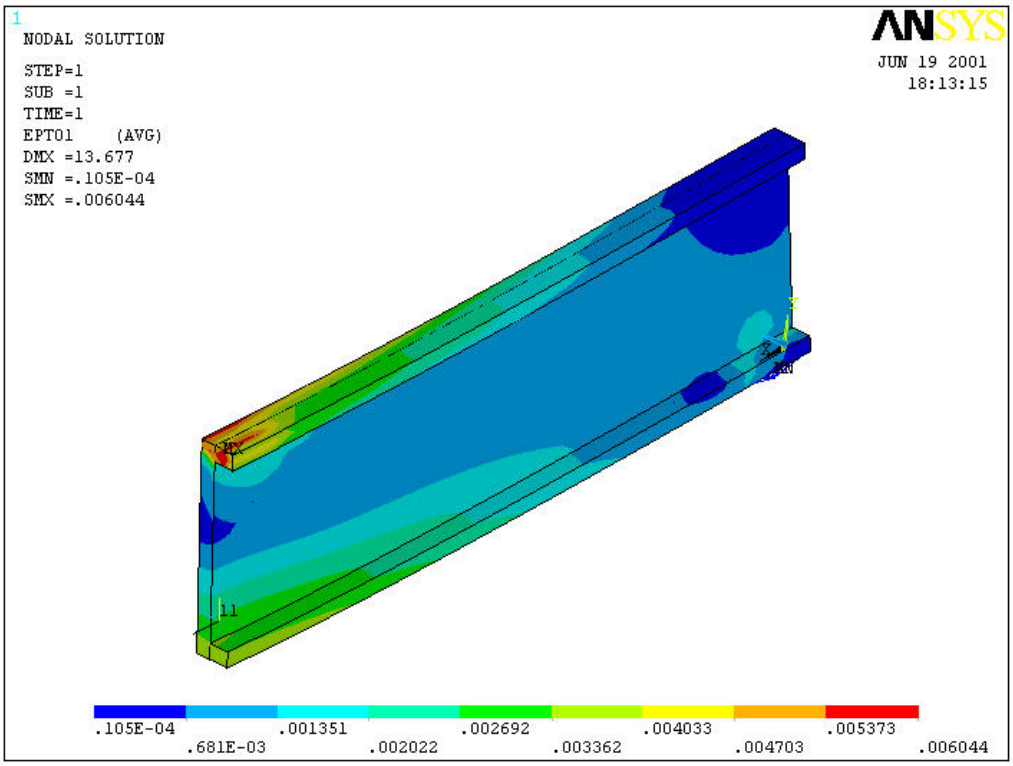

Figure G.10 (a) 1st Principal Strain In Laminates Of Fatigue Beam

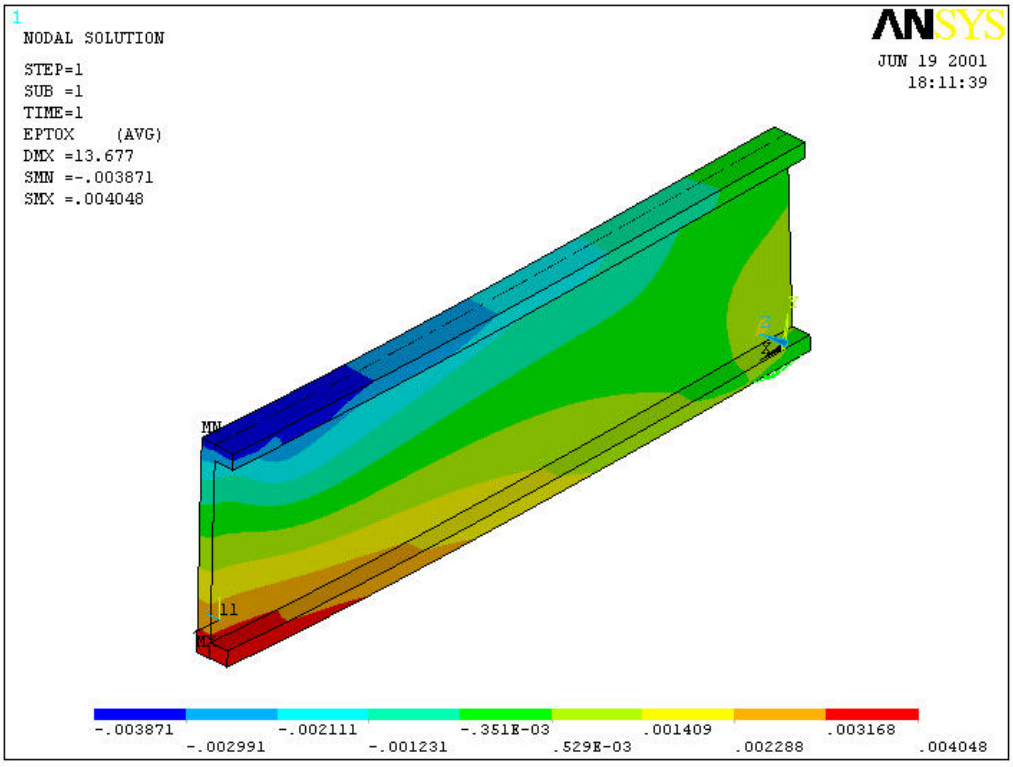

Figure G.10 (b) Laminate Strain in Direction of Beam Span (x-dirn)

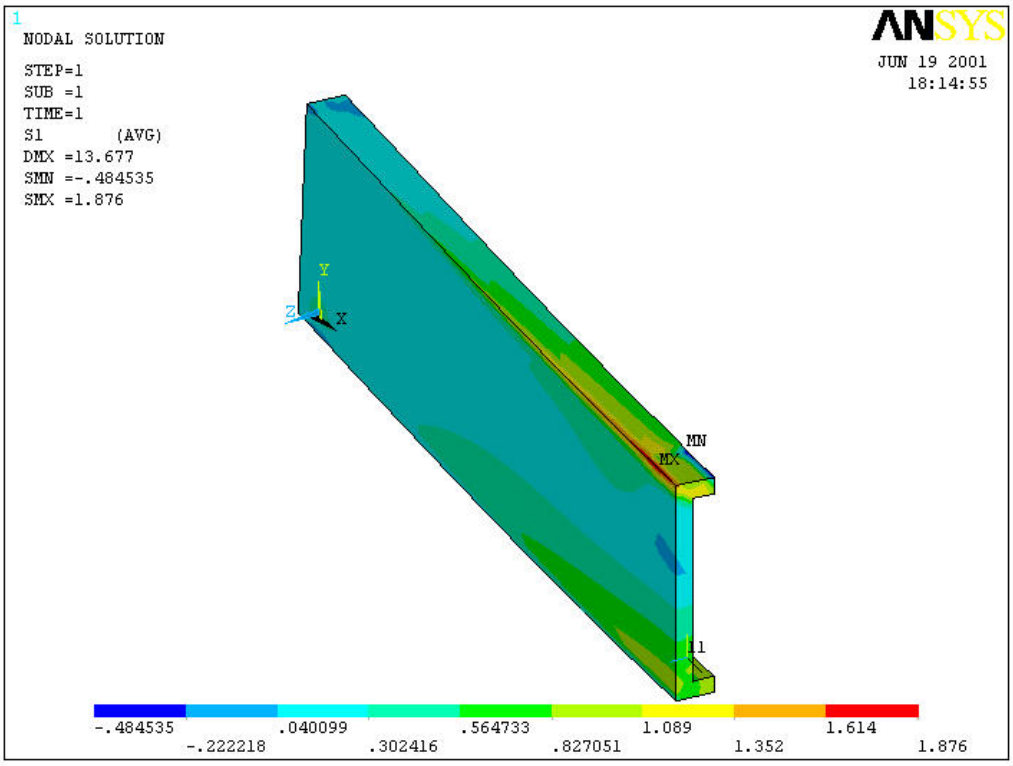

Figure G.10 (c) 1st Principal Stress on Core Material of Fatigue Beam

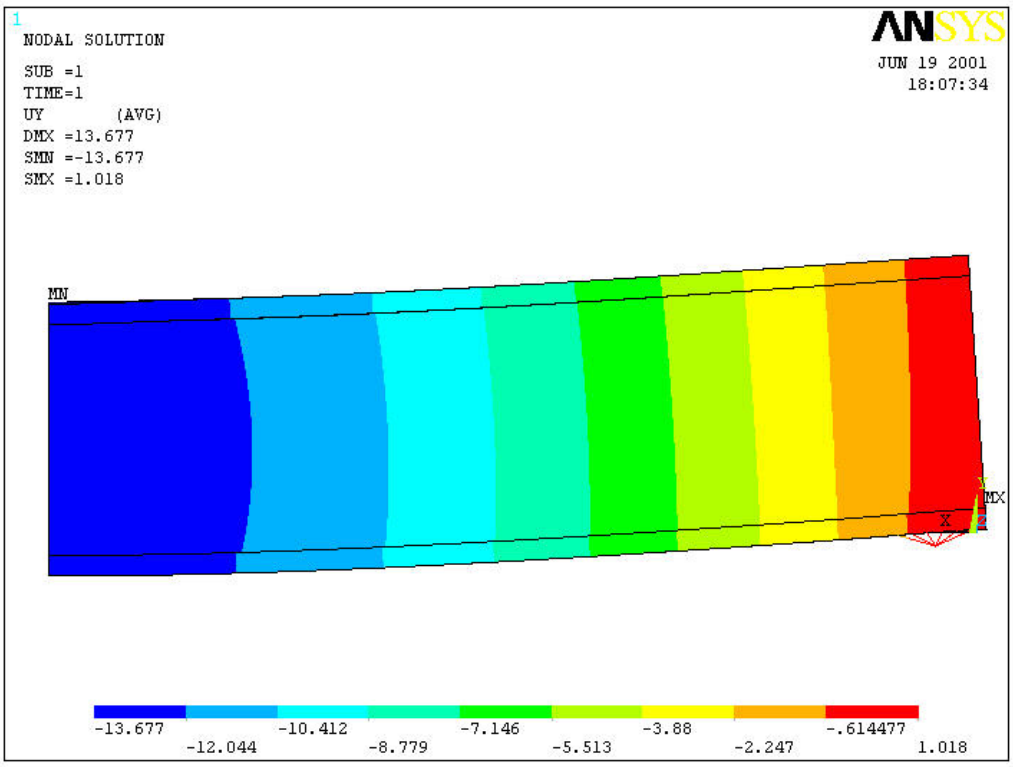

Figure G.10 (d) Deflection of Fatigue Beam

G.3.2 Experimental Results of Static Test

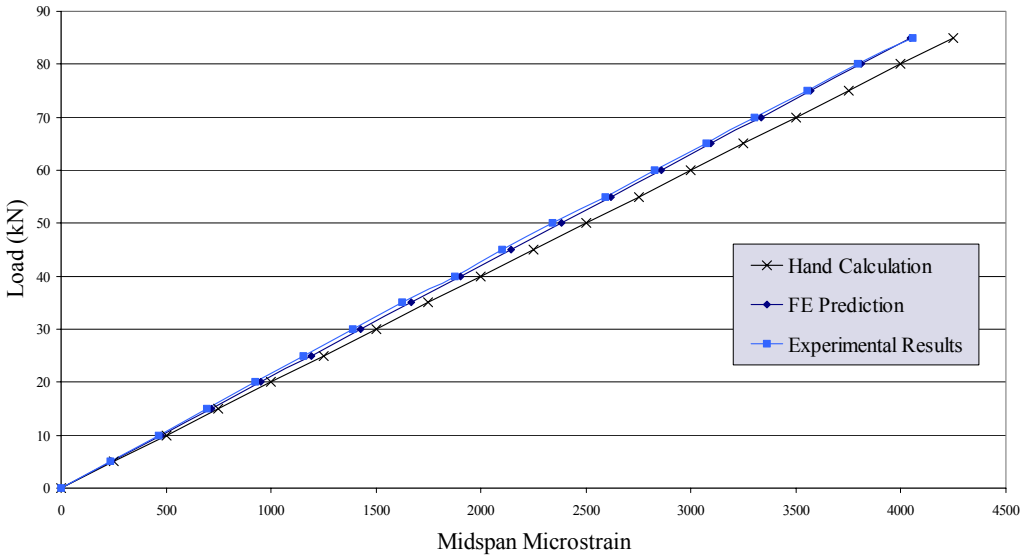

Figure G.11 (a) Comparison of Static Beam Strain – Analysis Vs. Experimental

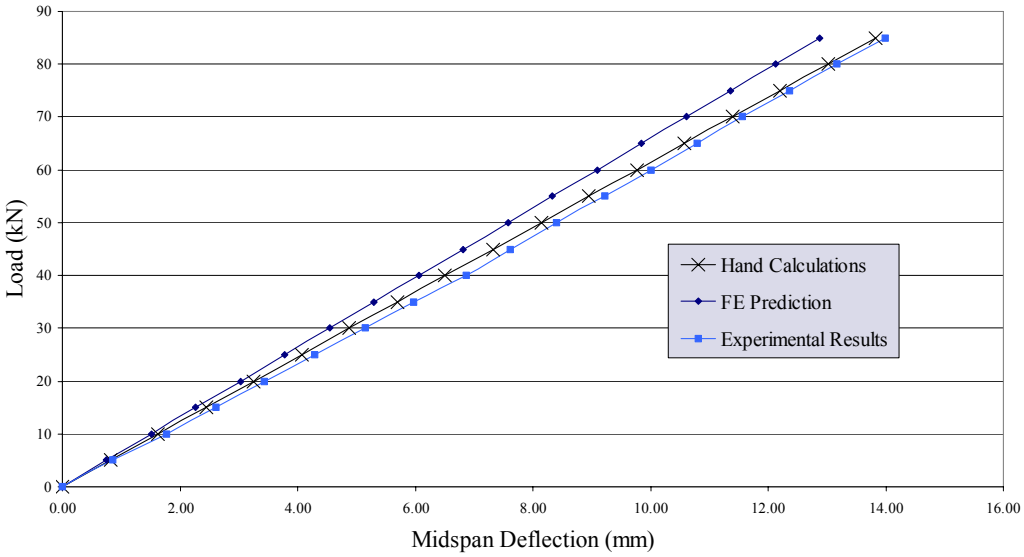

Figure G.11 (b) Comparison of Static Beam Deflection – Analysis Vs. Experimental

G.3.3 Experimental Procedure of Fatigue Testing

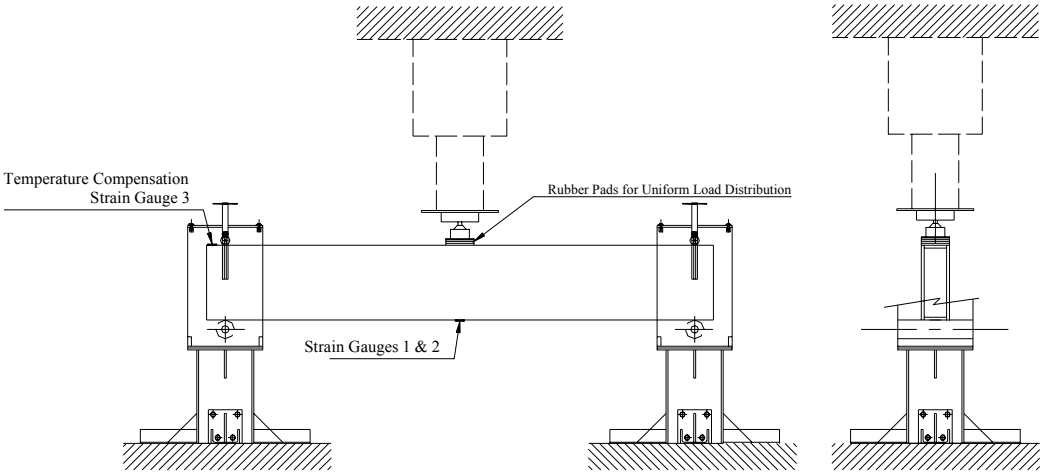

Figure G.12 Basic Test Layout of FRP Fatigue Beam Test

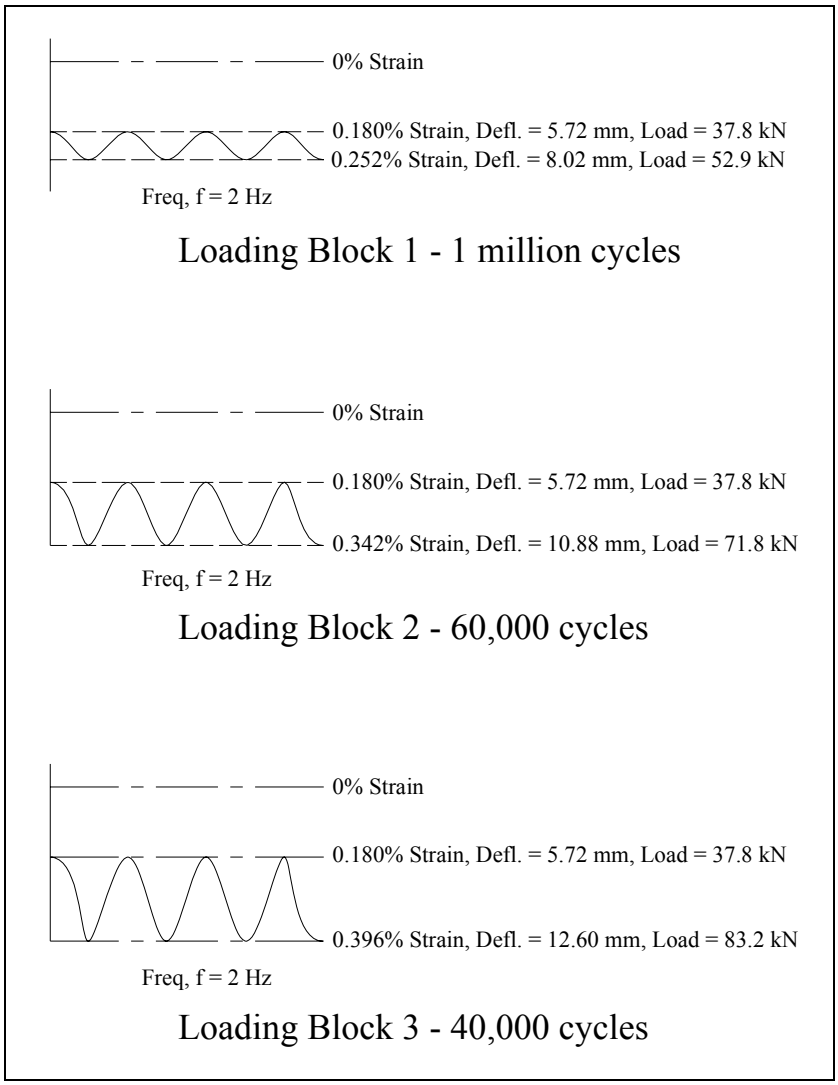

Figure G.13 Summary of Loading Regimes for Fatigue Beam

Figure G.14 FRP Chassis Rail in Test Rig

Figure G.15 Alternate View of Chassis Rail in Test Rig

Figure G.16 Steel Spacers and Rubber Matting Used to Transfer and Distribute Load

Figure G.17 Magnified View of Beam Construction Including Hybrid Laminate

G.3.4 Experimental Results of Fatigue Testing

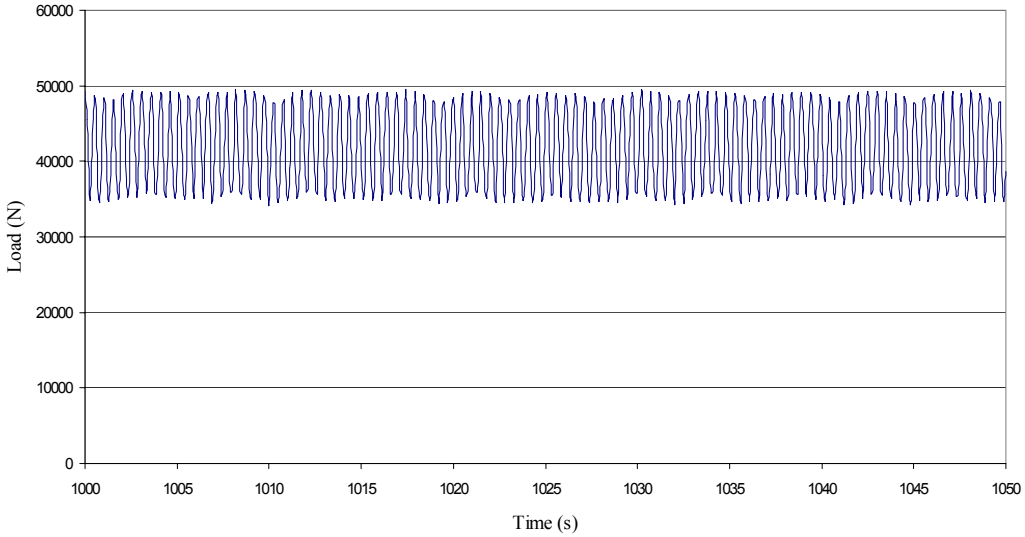

Figure G.18 Sample of FRP Beam Fatigue Loading – 1.4g

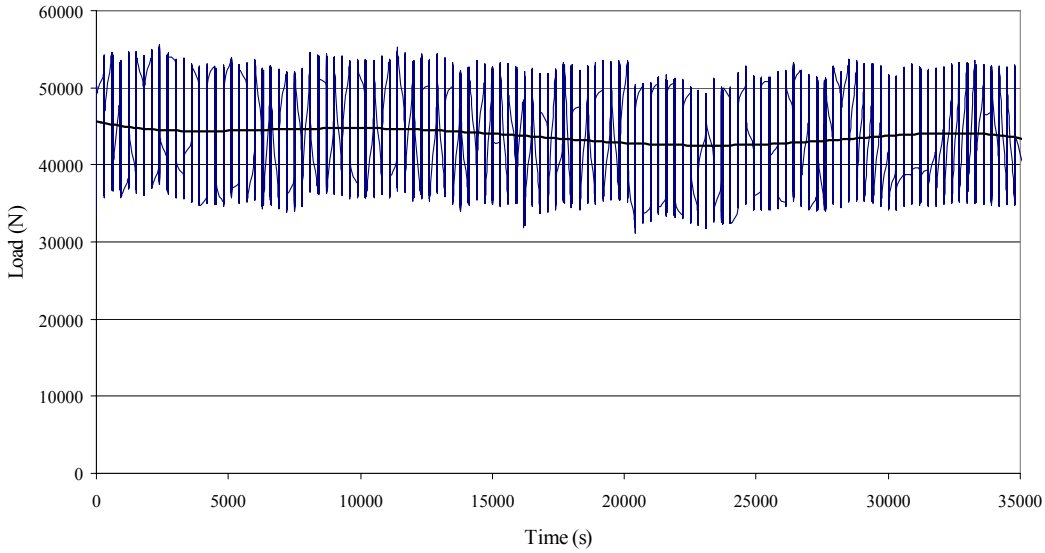

Figure G.19 Typical Irregularities in Load Control

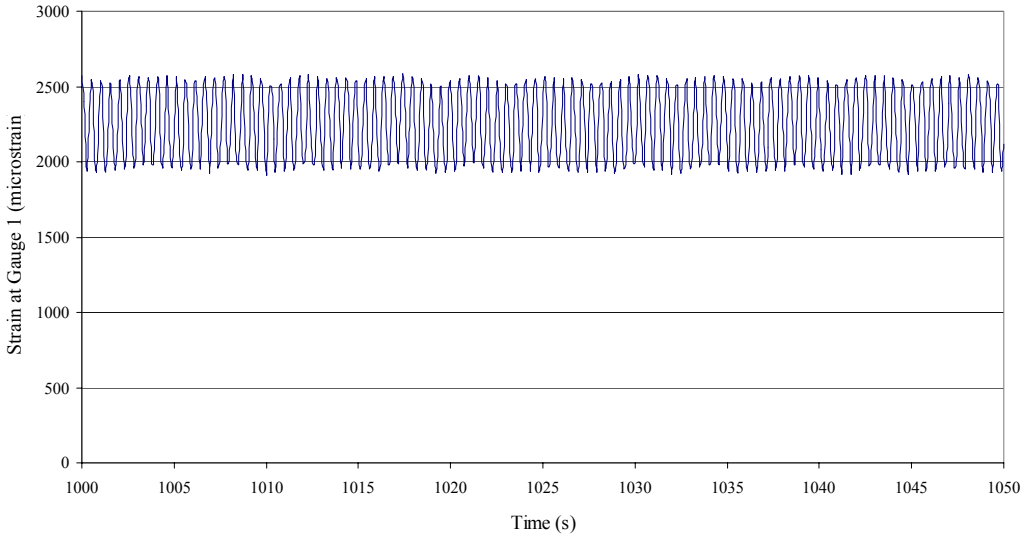

Figure G.20 Sample of Strain at Gauge #1 – 1.4g

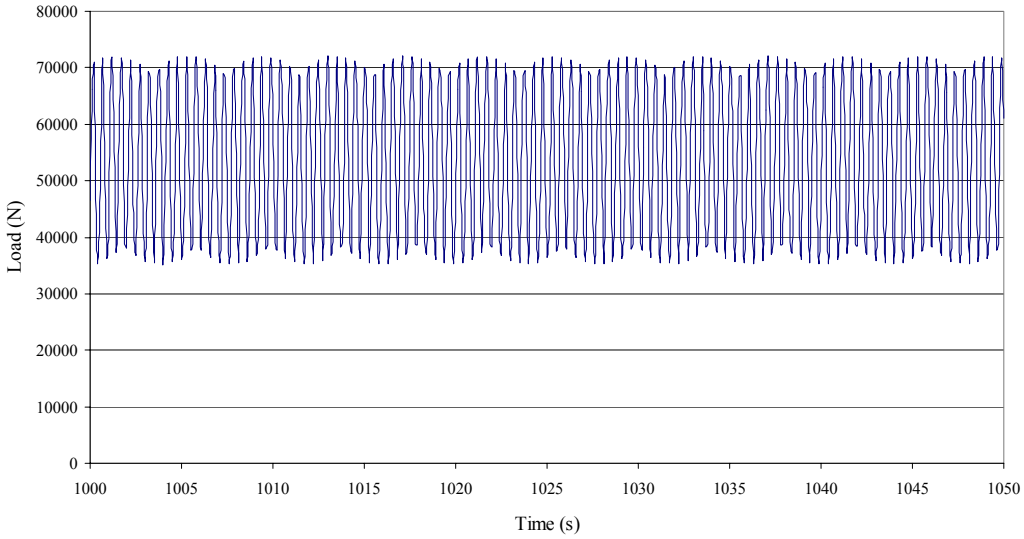

Figure G.21 Sample of FRP Beam Fatigue Loading – 1.9g

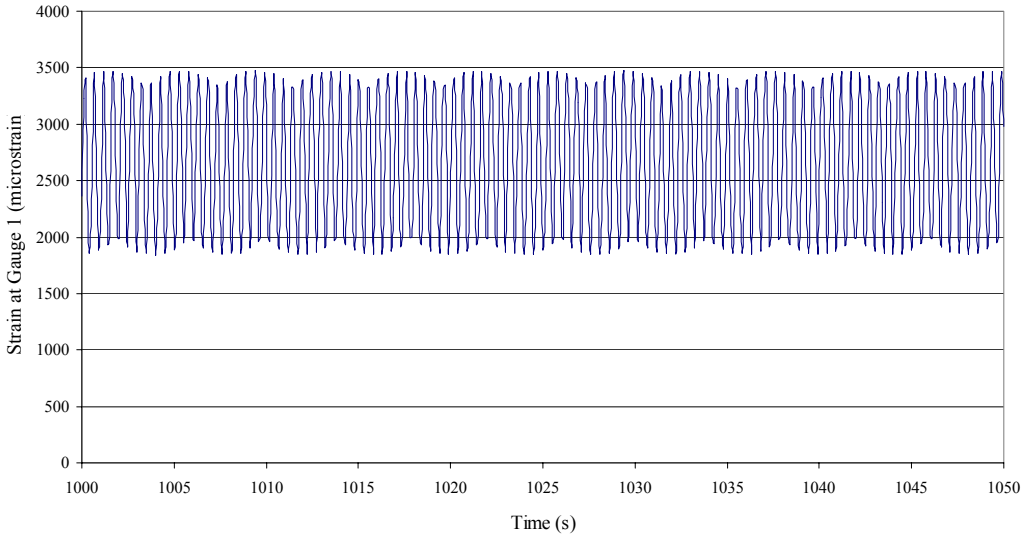

Figure G.22 Sample of Strain at Gauge #1 – 1.9g

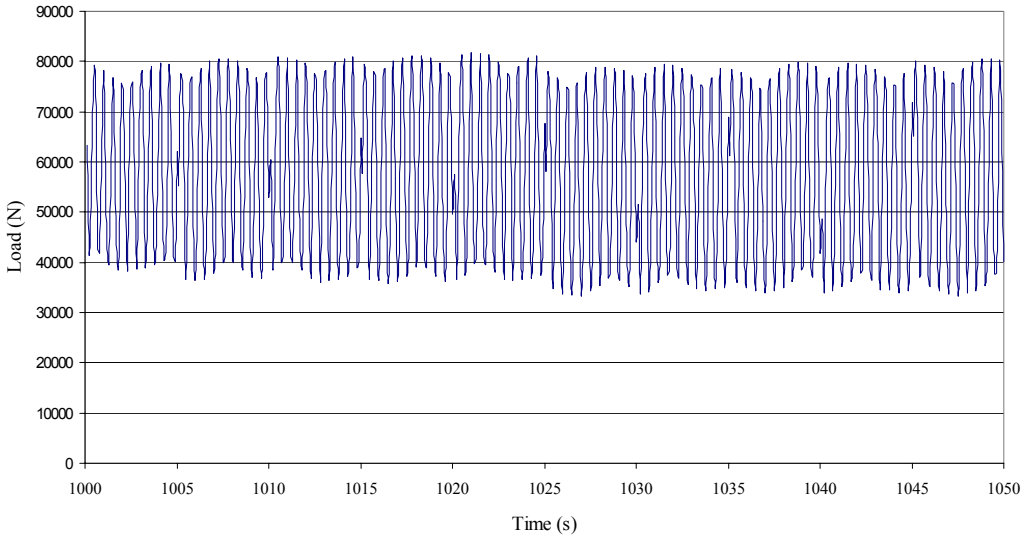

Figure G.23 Sample of FRP Beam Fatigue Loading – 2.2g

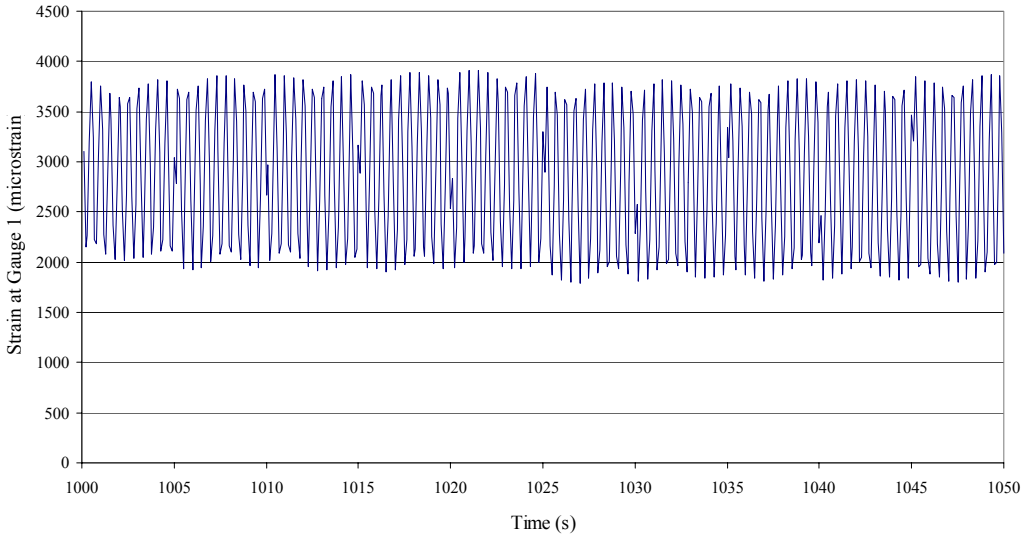

Figure G.24 Sample of Strain at Gauge #1 – 2.2g

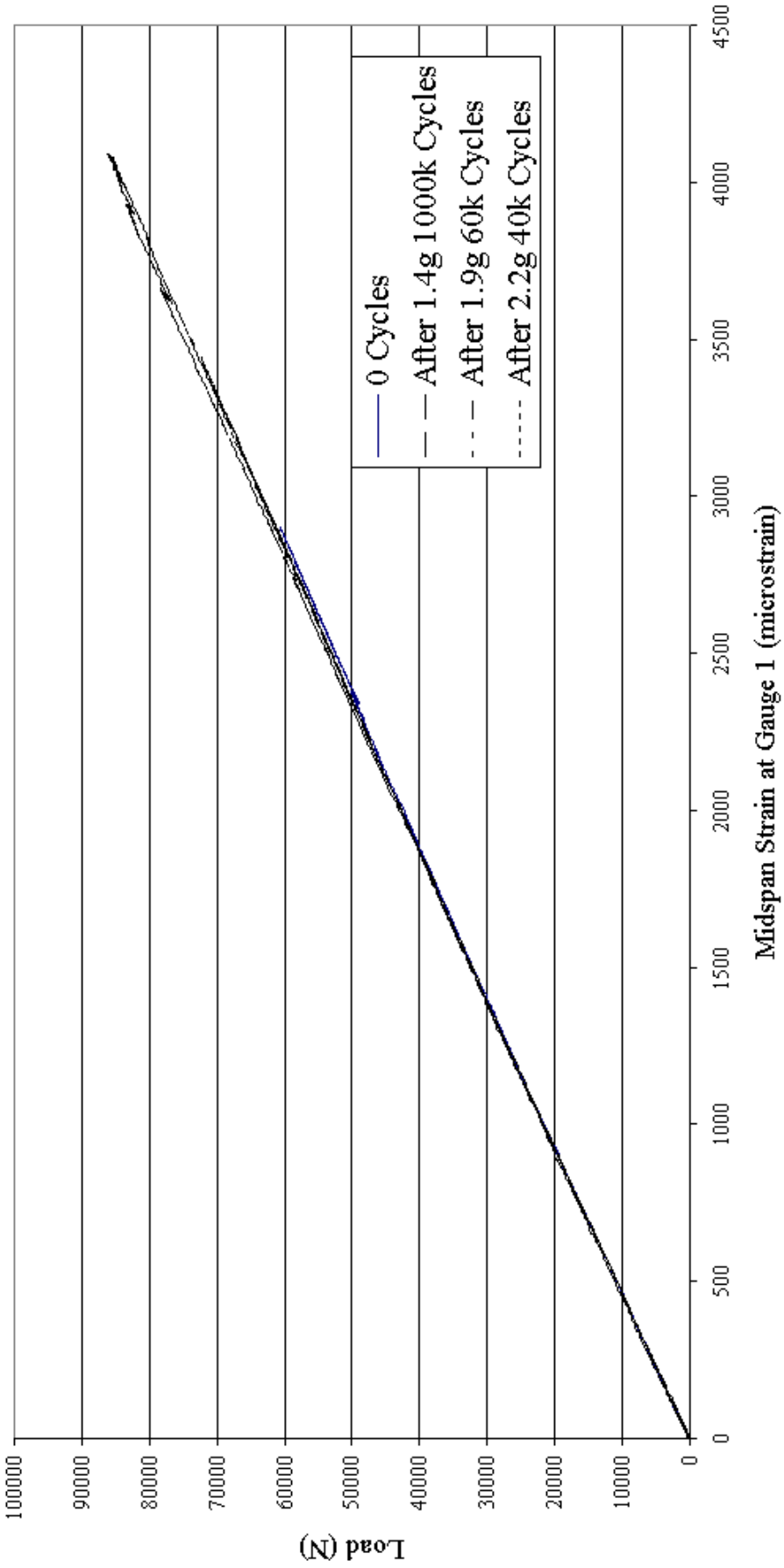

Figure G.25 Comparison of Beam Stiffness at Various Times in Fatigue Loading Cycles